Model Calibration Report for the Lower East Coast Subregional Model – North Palm Version

September 2018

Anushi Obeysekera, Jefferson Giddings, and Uditha Bandara, P.E.

South Florida Water Management District | 3301 Gun Club Road | West Palm Beach, FL 33406

TABLE OF CONTENTS

List of Tables iii
List of Figures iv
Acronyms and Abbreviations vii
1. Introduction 1
1.1 Scope 2
1.2 LECSR-NP History 2
2. Model Conceptualization 2
2.1 Study Area 2
2.2 Climate 6
2.2.1 Rainfall 7
2.2.2 Evapotranspiration 13
2.3 Land Use and Soil 17
2.4 Surface Water System 20
2.5 Hydrogeology 21
2.6 Water Use 27
3. Simulation of the Flow System 28
3.1 Computer Code Selection 28
3.2 Evapotranspiration and Recharge 29
3.3. Model Design 39
3.3.1 Spatial and Temporal Discretization 39
3.3.2 Groundwater Flow System 39
3.4 Water Use 61
3.4.1 Public Water Supply 61
3.4.2 Non-Public Water Supply 61
4. Model Calibration and Verification 62
4.1 Methodology 62
4.2 Calibration Criteria 63
4.2.1 Flow Discharges 63
4.2.2 Water Level Elevations 64
4.2.3 Qualitative Analysis 67
4.3 Calibration Results 69
4.3.1 Flow Discharges 69
4.3.2 Water Level Elevations 77
4.3.3 Wetland Rapid Assessment Procedure (WRAP) Cells 83
4.3.4 Water Budgets 85

4.4 Model Verification 87
4.4.1 Flow Discharges 87
4.4.2 Water Level Elevations 94
4.5 Sensitivity Analysis 99
4.5.1 Parameters and Methodology 99
4.5.2 Sensitivity Results 99
5. Conclusions 106
5.1 Limitations 106
6. Literature Cited 107
Appendix A: Groundwater Wells A-1
Appendix B: Wetland Gauges B-1
Appendix C: WRAP Cells C-1
Appendix D: Water Budgets D-1
Appendix E: Verification Results E-1

LIST OF TABLES

Table 1. Percent of total area by land use types in the LECSR-NP active model area. 17
Table 2. Aquifer properties from slug tests for screen interval from 95 to 100 feet within the Mecca property. 23
Table 3. Aquifer properties from slug tests for screen interval from 40 to 45 feet within the Mecca property. 23
Table 4. Aquifer properties from slug tests for screen interval from 10 to 15 feet within the Mecca property. 23
Table 5. Aquifer properties from slug tests within the Mecca property..... 24
Table 6. Aquifer properties from aquifer performance tests within the Mecca property..... 24
Table 7. Aquifer parameters at Corbett Wildlife Management Area. 25
Table 8. Aquifer properties at the White Fences and Deer Run communities. 25
Table 9. Aquifer properties at the L-8 Flow Equalization Basin. 26
Table 10. Aquifer properties within the L-8 FEB. 27
Table 11. Average groundwater withdrawals (in mgd) in the LECSR-NP active model area, including surface water withdrawals for the City of West Palm Beach..... 27
Table 12. MODFLOW add-on packages used in the LECSR-NP. 29
Table 13. Monthly averaged percent seepage losses between the Control 2 and Control 3 pump stations. 58
Table 14. Flow discharge statistics for the calibration period (2006 – 2014). 69
Table 15. Groundwater monitoring well statistics for the calibration period (2006 – 2014). 77
Table 16. Wetland gauge statistics for the calibration period (2006 – 2014)..... 79
Table 17. Statistics for sequestered locations for the calibration period (2006 – 2014). 81
Table 18. Field estimated and simulated inundation for Wetland Rapid Assessment Procedure cells. 83
Table 19. Description of MODFLOW terminology used in water budget schematics. 85
Table 20. Flow structure statistics for the verification period (2000 – 2005). 87
Table 21. Groundwater monitoring well statistics for the verification period (2000 – 2005)..... 96
Table 22. Wetland gauge statistics for the verification period (2000 – 2005). 97
Table 23. Parameters and multipliers of sensitivity analysis for the LECSR-NP. 99
Table 24. Frequency distribution of mean head residuals based on 58 groundwater monitoring wells and 61 wetland gauges..... 101
Table 25. Coefficient of determination (R^2) values for sensitivity runs at seven discharge locations. 103

LIST OF FIGURES

Figure 1. Boundaries of the LECSR-NP active model domain. 3
Figure 2. Elevation within the LECSR-NP active model domain. 5
Figure 3. AMO Index from 1948 through 2013. 6
Figure 4. Spatial distribution of NEXRAD-generated rainfall across the LECSR-NP active model area in 2011 (a representative dry year). 8
Figure 5. Spatial distribution of NEXRAD-generated rainfall across the LECSR-NP active model area in 2013 (a representative wet year) 9
Figure 6. Average annual rainfall in the LECSR-NP active model area (2006 to 2014). 10
Figure 7. Average monthly rainfall in the LECSR-NP active model area (2006 to 2014). 10
Figure 8. Map of NOAA climate divisions in Florida. 11
Figure 9. 12-month SPI patterns for District 5, District 6, and the average for 2006 to 2014 12
Figure 10. 12-month SPI patterns for District 5, District 6, and the average for 1965 to 2005 13
Figure 11. Spatial distribution of NLDAS-generated reference ET across the LECSR-NP active model area in 2011 (a representative dry year). 14
Figure 12. Spatial distribution of NLDAS-generated reference ET across the LECSR-NP active model area in 2013 (a representative wet year) 15
Figure 13. Average annual reference evapotranspiration for the LECSR-NP active model area (2006 to 2014). 16
Figure 14. Average monthly reference evapotranspiration for the LECSR-NP active model area (2006 to 2014). 16
Figure 15. Land use/land cover in the LECSR-NP active model area. 18
Figure 16. Hydrologic soil types in the LECSR-NP active model area. 19
Figure 17. Locations of new aquifer performance test data used in the LECSR-NP. 22
Figure 18. Water use by type applied in the LECSR-NP. 28
Figure 19. General schematic of the Agricultural Field Scale Irrigation Requirement Simulations program. 30
Figure 20. MODFLOW and Evapotranspiration-Recharge tool calibration flow chart. 31
Figure 21. Spatial distribution of runoff derived from the Evapotranspiration-Recharge program for 2011. 32
Figure 22. Spatial distribution of runoff derived from the Evapotranspiration-Recharge program for 2013. 33
Figure 23. Spatial distribution of unsaturated zone evapotranspiration derived from the Evapotranspiration-Recharge program for 2011. 34
Figure 24. Spatial distribution of unsaturated zone evapotranspiration derived from the Evapotranspiration-Recharge program for 2013. 35
Figure 25. Spatial distribution of maximum potential groundwater evapotranspiration derived from the Evapotranspiration-Recharge program for 2011. 36
Figure 26. Spatial distribution of maximum potential groundwater evapotranspiration derived from the Evapotranspiration-Recharge program for 2013. 37
Figure 27. Spatial distribution of extinction depths across the LECSR-NP active model area. 38
Figure 28. Model layering scheme and typical materials, average elevations, and thickness ranges. 40
Figure 29. Transmissivity of the surficial aquifer system for the LECSR-NP. 41
Figure 30. Spatial distribution of groundwater recharge derived from the Evapotranspiration-Recharge-Runoff program across the LECSR-NP active model area in 2011 42
Figure 31. Spatial distribution of groundwater recharge derived from the Evapotranspiration-Recharge-Runoff program across the LECSR-NP active model area in 2013 43

Figure 32. Spatial distribution of saturated zone evapotranspiration derived from the Evapotranspiration-Recharge-Runoff program across the LECSR-NP active model area in 2011. 44
Figure 33. Spatial distribution of saturated zone evapotranspiration derived from the Evapotranspiration-Recharge-Runoff program across the LECSR-NP active model area in 2013. 45
Figure 34. Spatial distribution of wetland cells across the LECSR-NP active model area. 47
Figure 35. Spatial distribution of drain cells across the LECSR-NP active model area. 48
Figure 36. Spatial distribution of river cells across the LECSR-NP active model area. 49
Figure 37. Spatial distribution of Diversion sink cells across the LECSR-NP active model area. 50
Figure 38. Spatial distribution of Diversion source cells across the LECSR-NP active model area. 51
Figure 39. Spatial distribution of Reinjection Drain Flow sink locations across the LECSR-NP active model area. 52
Figure 40. Spatial distribution of Reinjection Drain Flow source cells across the LECSR-NP active model area. 53
Figure 41. Historical releases before June 2009 at G-160 during the dry season. 55
Figure 42. Historical releases before June 2009 at G-160 during the wet season. 55
Figure 43. Historical releases after June 2009 at G-160 during the dry season. 56
Figure 44. Historical releases after June 2009 at G-160 during the wet season. 56
Figure 45. Monthly averaged seepage losses between the Control 2 and Control 3 pump stations from 2006 to 2014. 58
Figure 46. Spatial distribution of General Head Boundary cells across the LECSR-NP active model area. 60
Figure 47. Water use distribution for non-public water supply permits. 62
Figure 48. Flow discharge locations used in LECSR-NP calibration. 64
Figure 49. Groundwater monitoring well locations used in LECSR-NP model calibration. 65
Figure 50. Wetland gauge locations used in LECSR-NP model calibration. 66
Figure 51. Wetland Rapid Assessment Procedure (WRAP) cells and indicator regions used for LECSR-NP model calibration. 67
Figure 52. Water budget basin boundaries for the LECSR-NP. 68
Figure 53. Simulated and historical monthly flow hydrograph for the C-18 weir from 2006 to 2014. 70
Figure 54. Simulated and historical cumulative monthly flow curve for the C-18 weir from 2006 to 2014. 70
Figure 55. Simulated and historical monthly flow hydrograph for Lainhart Dam from 2006 to 2014. 71
Figure 56. Simulated and historical cumulative monthly flow curve for Lainhart Dam from 2006 to 2014. 71
Figure 57. Simulated and historical monthly flow hydrograph for S-46 from 2006 to 2014. 72
Figure 58. Simulated and historical cumulative monthly flow curve for S-46 from 2006 to 2014. 72
Figure 59. Simulated and historical monthly flow hydrograph for G-92 from 2006 to 2014. 73
Figure 60. Simulated and historical cumulative monthly flow curve for G-92 from 2006 to 2014. 73
Figure 61. Simulated and historical monthly flow hydrograph for G-160 from 2006 to 2014. 74
Figure 62. Simulated and historical cumulative monthly flow curve for G-160 from 2006 to 2014. 74
Figure 63. Simulated and historical monthly flow hydrograph for Cypress Creek and Hobe Grove Ditch from 2006 to 2014. 75
Figure 64. Simulated and historical cumulative monthly flow curve for Cypress Creek and Hobe Grove Ditch from 2006 to 2009. 75
Figure 65. Simulated and historical monthly flow hydrograph for Kitching Creek from 2006 to 2014. 76

Figure 66. Simulated and historical cumulative monthly flow curve for Kitching Creek from 2006 to 2009 76
Figure 67. Calibration status and mean absolute error for groundwater monitoring wells used in LECSR-NP calibration. 82
Figure 68. Calibration status and mean absolute error of wetland gauges used in LECSR-NP calibration 82
Figure 69. Simulated and historical monthly flow hydrograph for the C-18 weir from 2000 to 2005. 88
Figure 70. Simulated and historical cumulative monthly flow curve for the C-18 weir from 2000 to 2005. 88
Figure 71. Simulated and historical monthly flow hydrograph for Lainhart Dam from 2000 to 2005. 89
Figure 72. Simulated and historical cumulative monthly flow curve for Lainhart Dam from 2000 to 2005. 89
Figure 73. Simulated and historical monthly flow hydrograph for S-46 from 2000 to 2005. 90
Figure 74. Simulated and historical cumulative monthly flow curve for S-46 from 2000 to 2005. 90
Figure 75. Simulated and historical monthly flow hydrograph for G-92 from 2000 to 2005. 91
Figure 76. Simulated and historical cumulative monthly flow curve for G-92 from 2000 to 2005. 91
Figure 77. Simulated and historical monthly flow hydrograph for Cypress Creek and Hobe Grove Ditch from 2000 to 2005. 92
Figure 78. Simulated and historical cumulative monthly flow curve for Cypress Creek and Hobe Grove Ditch from 2002 to 2005. 92
Figure 79. Simulated and historical monthly flow hydrograph for Kitching Creek from 2000 to 2005. 93
Figure 80. Simulated and historical cumulative monthly flow curve for Kitching Creek from 2000 to 2005. 93
Figure 81. Groundwater monitoring wells used in LECSR-NP verification. 94
Figure 82. Wetland gauges used in LECSR-NP verification. 95
Figure 83. Status and mean absolute error for groundwater monitoring wells used in LECSR-NP verification. 98
Figure 84. Status and mean absolute error for wetland gauges used in LECSR-NP verification. 98
Figure 85. Sensitivity of simulated heads to changes in horizontal hydraulic conductivity in groundwater monitoring wells. 105
Figure 86. Sensitivity of simulated heads to global changes in drain conductance in wetland gauges. 105
Figure 87. Sensitivity of simulated heads to global changes in general head boundary conductance in groundwater monitoring wells. 106

ACRONYMS AND ABBREVIATIONS

AFSIRS	Agricultural Field Scale Irrigation Requirements Simulation
AMO	Atlantic Multidecadal Oscillation
bls	below land surface
cfs	cubic feet per second
DV	deviation of volume
ENSO	El Niño Southern Oscillation
ET	evapotranspiration
FEB	flow equalization basin
GHB	general head boundary
GWP	Grassy Waters Preserve
LECSR	Lower East Coast Subregional Model
LECSR-NP	Lower East Coast Subregional Model – North Palm
LiDAR	Light Detection and Ranging
LRWRP	Loxahatchee River Watershed Restoration Plan
MAE	mean absolute error
mgd	million gallons per day
NEXRAD	Next Generations Radar
NGVD29	National Geodetic Vertical Datum of 1929
NLDAS	North American Land Data Assimilations Systems
NOAA	National Oceanic and Atmospheric Administration
NS	Nash-Sutcliffe coefficient
PWS	public water supply
R^2	coefficient of determination
RDF	reinjection drain flow
SAS	surficial aquifer system
SFWMD	South Florida Water Management District
SPI	Standardized Precipitation Index
USACE	United States Army Corps of Engineers
USGS	United States Geological Survey
WRAP	Wetland Rapid Assessment Procedure

1. INTRODUCTION

This document describes the calibration of the Lower East Coast Subregional Model – North Palm (LECSR-NP) version. This numerical model is based on the United States Geological Survey (USGS) MODFLOW (Harbaugh et al., 2000) computer code, designed to simulate groundwater flow and limited surface water features. The model was used to support analysis and development of the Loxahatchee River Watershed Restoration Project (LRWRP) Project Implementation Report, one of the components of the Comprehensive Everglades Restoration Plan (CERP), which is jointly implemented by the United States Army Corps of Engineers (USACE) and the South Florida Water Management District (SFWMD).

The study area focuses on the northern portion of the SFWMD's Lower East Coast Water Supply Planning Area and the southern portion of the Upper East Coast Water Supply Planning Area. The study area covers approximately 700 square miles of freshwater lakes, wetlands, estuaries, uplands, agricultural operations, extensive urban areas, and coastal ecosystems within a highly managed system of canals, structures, and levees that control water levels in the surficial aquifer system (SAS). These canal systems control water levels to minimize flooding during extreme rain events and to maintain aquifer levels along the coast in order to prevent saltwater intrusion, recharge coastal wellfields, and provide surface water during droughts. Additional population growth and agricultural development in the area continues to increase water demands, which must be balanced with the needs of the environment.

The Loxahatchee River is a federally designated Wild and Scenic River in northeastern Palm Beach and southeastern Martin County, Florida. Several tributaries contribute water to the river, including the North Fork, Wilson Creek, and Kitching Creek, which flow out of Jonathan Dickinson State Park. Hobe Grove Ditch and the Cypress Creek Canal provide water to the northwestern portion of the river from urban and agricultural operations in Martin County and the Pal Mar wetland area. However, the primary source of water to the river flows over Lainhart Dam.

The contributing basins that provide water to Lainhart Dam include an extensive area of urban and wetland systems. Historically, agricultural operations in the area also provided water to the river, but most of these land-use types have or are in the process of being converted to wetland restoration areas or urban development. The contributing basins to Lainhart Dam include the urban areas of Jupiter Farms, Calusa, PGA National and surrounding golf course communities, Loxahatchee Slough, and the northern portion of Grassy Waters Preserve (GWP). To the west, a combination of wetland restoration projects, the Pratt and Whitney facility, the Mecca property, the Avenir proposed development and other private properties, and the eastern portion of the Corbett Wildlife Management Area contribute to Lainhart Dam. The Town of Jupiter and Seacoast Utilities SAS wellfields are east of Loxahatchee Slough.

Flows to the Loxahatchee River have diminished over time, resulting in a shift in vegetation from freshwater to brackish/marine vegetation at the lower reaches of the river (Florida Department of Environmental Protection and SFWMD, 2010). As a result, the SFWMD adopted a Minimum Flow and Minimum Water Level (MFL) for the river to stabilize conditions (SFWMD, 2002). The USACE and SFWMD subsequently developed a comprehensive restoration plan for South Florida that included potential restoration projects for the Loxahatchee River (USACE and SFWMD, 1999). This project was designed to develop a groundwater modeling tool with limited surface water capabilities that can simulate projects that intend to improve flows to the river and restore wetland systems in the watershed while retaining the capability to evaluate potential impacts the proposed projects may have on existing legal users in the area.

1.1 Scope

The scope of this document covers the development of the LECSR-NP, following a standard protocol for model development as outlined by Anderson and Woessnar (1992). The report is separated into five sections, including the introduction, scope, and history presently being discussed. **Section 2** will discuss the development of the conceptual model, including data collection, hydrology, hydrogeology, water use, and other physical factors affecting model construction. Simulation of the flow system, including code selection and model design, are discussed in **Section 3**. The ability of the tool to simulate observed field conditions are discussed in the calibration, verification, and sensitivity portions of **Section 4**. **Section 5** concludes the report with a discussion on model capabilities, limitations, and general recommendations.

1.2 LECSR-NP History

Original development of the LECSR-NP was undertaken by Montoya et al. (2010) to support ongoing water supply management and ecosystem restoration efforts in northern Palm Beach County within the Loxahatchee River watershed. That version of the model originated from the Lower East Coast Subregional Model (LECSR) (Giddings et al., 2006).

Since the 2010 modeling effort, regional land use/land cover and topography data have been updated. Additionally, monitor wells and geotechnical borings recently were completed within the L-8 and C-18 basins. The SFWMD also conducted a water availability assessment for the proposed Mecca Impoundment, which indicated the movement of water within the C-18 Basin was different than what was conceptualized previously (Montoya and Kuebler, 2016). Lastly, several monitoring wells and wetland gauges with historical data have been identified and data provided to the modeling team for model calibration purposes.

This revised version of the LECSR-NP was modified specifically for the LRWRP to develop and evaluate the plan, incorporate additional and updated information as indicated above, and address comments received from the USACE and the Interagency Modeling Center regarding model conceptualization and development.

2. MODEL CONCEPTUALIZATION

2.1 Study Area

The original LECSR active model domain included the entire southeastern coast of Florida from the City of Stuart in Martin County south to Florida Bay in Miami-Dade and Monroe counties. For this project, the area was refined to address specific questions with existing and proposed features in northern Palm Beach and southern Martin counties (**Figure 1**). The eastern boundary coincides with the Atlantic Ocean and follows the brackish intracoastal waterway, which serves as a stable physical boundary. The St. Lucie (C-44) Canal from the St. Lucie Estuary west to Lake Okeechobee is the northern boundary. The C-44 Canal is a primary canal managed by the USACE within the regional surface water management system. Lake Okeechobee, in the northwestern corner of the study area, is a managed lake and the primary surface water supplier for southeastern Florida. The southern model boundary is the physical boundary of the L-10, L-12, and C-51 canals in central Palm Beach County. The LECSR-NP simulates overland flow through wetland systems, the general operations of the canal network, and the SAS flow regime.

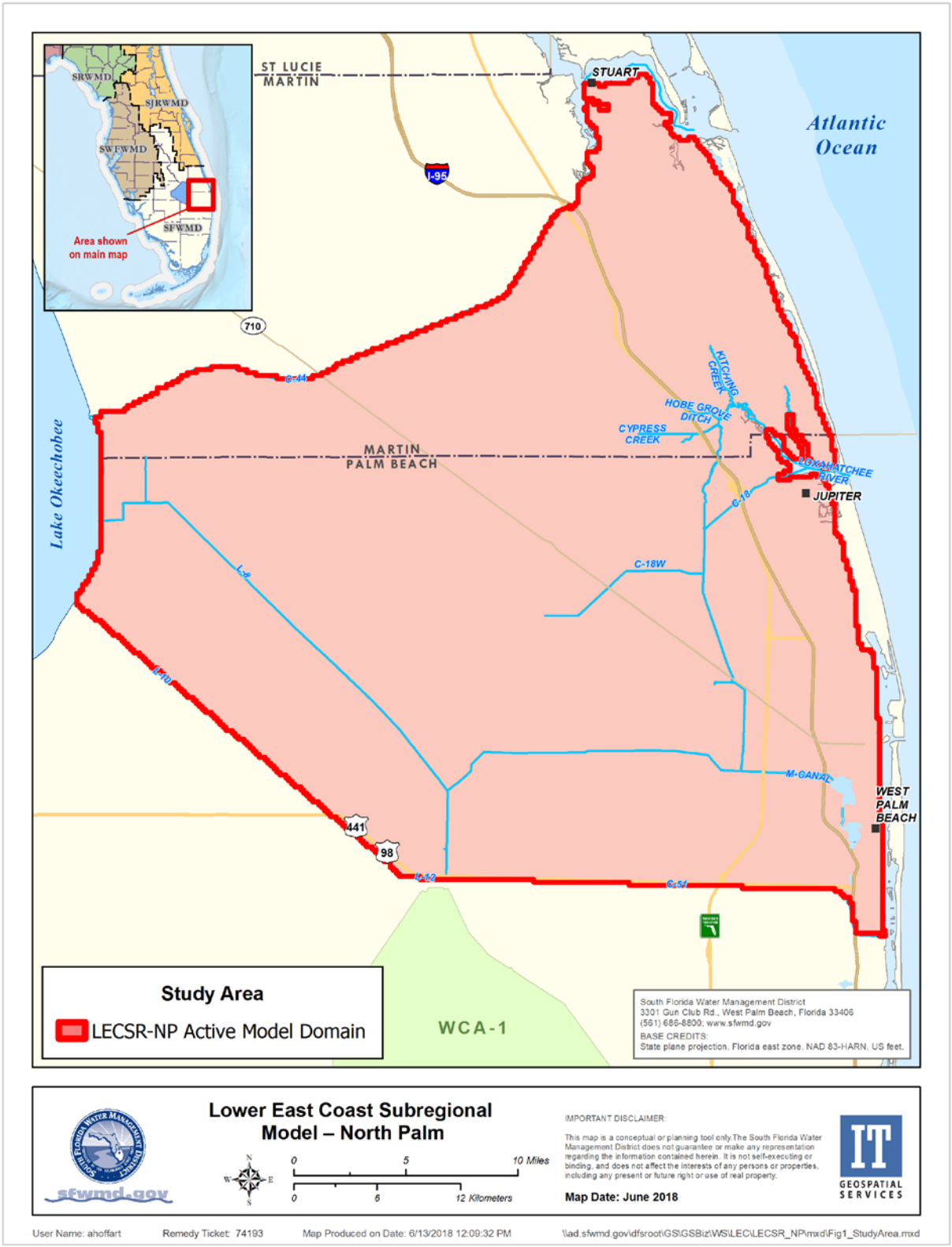

Figure 1. Boundaries of the LECSR-NP active model domain.

Three physiographic regions are present in the study area: the Atlantic Coastal Ridge, the Eastern or Sandy Flatlands, and the Everglades-Lake Okeechobee Basin. The Atlantic Coastal Ridge extends along the eastern portion of the study area parallel to the coastline. It is generally 3 to 4 miles wide and has the largest topographic relief, with elevations ranging from sea level to more than 80 feet in Jonathan Dickinson State Park. The ridge is composed of fine- to medium-grained sands with occasional underlying limestone resulting in relatively good underground drainage. The only large natural cut across the ridge occurs where the Loxahatchee River empties into the Indian River Lagoon and Atlantic Ocean at Jupiter inlet.

The Eastern Flatlands is the largest physiographic region within the study area and stretches from approximately Interstate 95 on the east to near Lake Okeechobee on the west. Elevations generally are flat, ranging from approximately 15 to 25 feet National Geodetic Vertical Datum of 1929 (NGVD29). In developed areas, drainage is controlled by numerous primary and secondary canal systems that ultimately discharge into the ocean. The Everglades-Lake Okeechobee Basin is the smallest of the physiographic regions and includes lands west of the L-8 Canal, including the Everglades Agricultural Area. The area is almost exclusively agriculture and is underlain by organic peat and muck soils.

In South Florida, very small changes in topography can substantially affect the hydrologic response. Topographic data are from the SFWMD's South Florida Merged Topography coverage. The coverage is a 5-foot cell size, high-resolution digital elevation model composed of more than 40 separate sources of data, including Light Detection and Ranging (LiDAR) data sets, photogrammetry, Everglades global positioning system (GPS), contours, and spot elevations. The coverage was created in April 2016 and uses the best available data for the model domain. Topographic data are standardized to NGVD29, and zonal statistics were used to create mean elevation coverage for each 704 × 704-foot model cell. Elevation data for the LECSR-NP active model area are displayed in **Figure 2**.

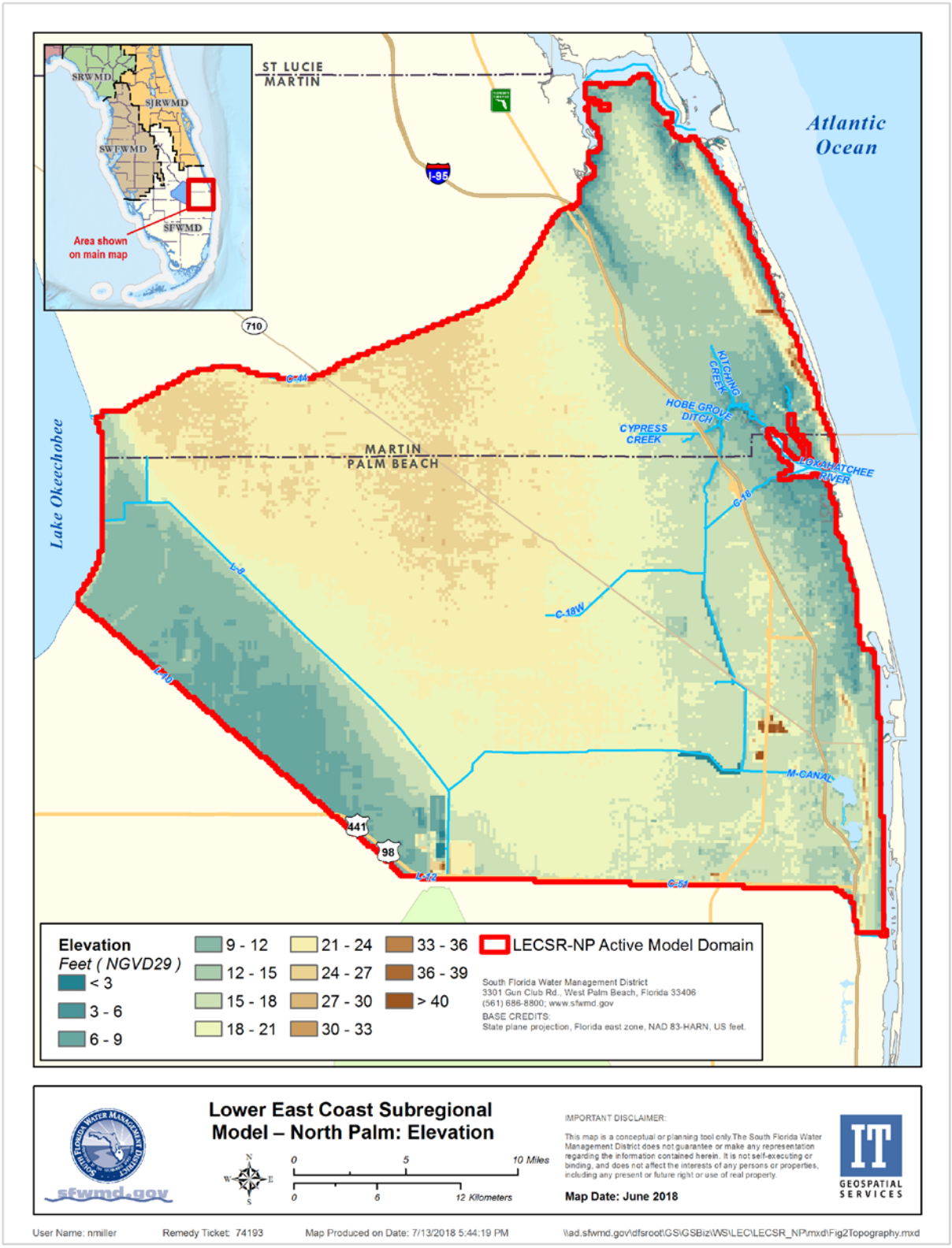

Figure 2. Elevation within the LECSR-NP active model domain.

2.2 Climate

Martin and Palm Beach counties are in southeastern Florida, which is considered a tropical climate. Proximity to the Gulf Stream current tends to moderate air temperatures in the study area. In West Palm Beach, the average temperature is 75.4°F, with highs near 90°F in July and August and lows near 50°F in January and February. Annual average rainfall is 61.38 inches per year (based on data from 1939 through 2017 at the Palm Beach International Airport), and the reference evapotranspiration (ET) for the region averages approximately 59 inches per year (a net surplus of fresh water). Approximately 75 percent of rainfall occurs during the wet season, which extends from mid-May through mid-October.

The South Florida climate is highly variable, predominantly due to naturally occurring phenomena such as the Atlantic Multidecadal Oscillation (AMO) and El Niño Southern Oscillation (ENSO). These oscillations relate to temperatures on the surface of the Atlantic and Pacific Oceans, respectively. Deviations from the mean surface temperature indicate whether the oscillation is in the positive or negative phase, with the changes in phase resulting in climate variability in South Florida.

The AMO focuses on sea surface temperature within the North Atlantic Basin. The AMO notably influences the climate in South Florida during the wet season, especially from August through September (SFWMD, 2011). **Figure 3** shows the Kaplan SST V2 AMO Index data provided by the National Oceanic and Atmospheric Administration (NOAA) for 1948 through 2013. Data from 2013 through 2014 currently is unavailable. Based on the data, the AMO was in a warm phase from 1948 through 1969, a cold phase from 1970 through 1994, and another warm phase from 1995 through 2013. The warm phase of the AMO represents wetter conditions during the wet season, while the cold phase of the AMO represents drier conditions during the wet season. The period of record for the LECSR-NP calibration is from 2006 to 2014, which coincides with a warm phase of the AMO, indicating the calibration period would have wetter conditions during the wet seasons. This is important to consider given the LECSR-NP will be used to support selection of a recommended plan for the LRWRP, which has a simulation period of record (1965 through 2005) longer than the calibration period. The LRWRP simulation period of record would have high climate variability, and the LECSR-NP calibration period does not coincide with the AMO cold phase (1970 through 1994).

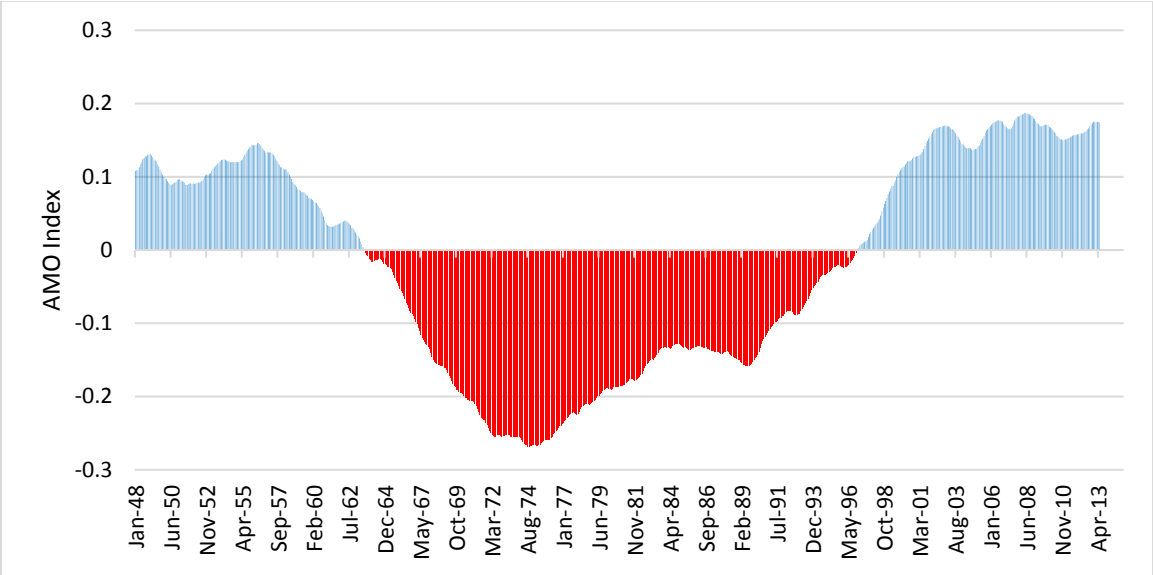

Figure 3. AMO Index from 1948 through 2013 (Data from: https://www.esrl.noaa.gov/psd/data/timeseries/AMO/).

ENSO is a naturally occurring climate variability pattern where the easterly trade winds near the coast of South America push warm water away from the coastline, allowing cooler water to upwell, which causes the sea surface temperature to be cooler than average. If the easterly trade winds are stronger than normal, the sea surface temperature is cooler than normal; this phenomenon is known as La Niña. If the easterly trade winds are weaker than normal, the sea surface temperature is warmer; this is known as El Niño. The transition period between El Niño and La Niña typically is 3 to 7 years. Unlike the AMO, which impacts the wet season in South Florida, ENSO impacts the dry season months, especially during winter. When ENSO is in an El Niño phase, the dry season typically is wetter than normal, and when ENSO is in a La Niña phase, the dry season typically is drier than normal (SFWMD, 2011).

2.2.1 Rainfall

Rainfall represents the largest input of water into the hydrologic system and can vary substantially between years. Between 1939 and 2017, the minimum annual rainfall at the Palm Beach International Airport was 37 inches in 1955 and the maximum rainfall was 109 inches in 1947. In recent years, more than 90 inches of rain was recorded in 1994 and less than 43 inches occurred in 2000. In the summer, rainfall can vary drastically across the region based on the distribution of afternoon thunderstorms, generally along the sea breeze front. Rainfall is provided by thunderstorms and tropical systems in the summer and early fall and from passing cold fronts in other months.

Rainfall data from 2006 to 2014 were derived from Next Generations Radar (NEXRAD) (Brown, 2014). NEXRAD data provide complete spatial coverage of rainfall amounts using a predetermined grid resolution (2 km by 2 km). Four NEXRAD sites operated by the National Weather Service cover the LECSR-NP active model area: KBYX in Key West, KAMX in Miami, KMLB in Melbourne, and KBTW in Tampa. **Figures 4** and **5** show the spatial distribution of rainfall derived from NEXRAD data for the LECSR-NP active model area in 2011 (a dry year) and 2013 (a wet year), respectively.

Average annual rainfall data from 2006 to 2014 for the LECSR-NP active model area are shown in **Figure 6**. The driest year recorded was 2006, with 40 inches of rainfall, and 2011 was the second driest year. The wettest year recorded was 2008, with 57 inches of rainfall, and 2012 through 2014 also were consistently wet years. Average annual rainfall during this period was approximately 52 inches.

Rainfall distribution can vary substantially across the region on a daily or weekly basis. This is especially true during summer when warmer temperatures create scattered afternoon thunderstorms, referred to as convective rainfall. **Figure 7** shows the monthly variation of rainfall from 2006 to 2014 for the LECSR-NP active model area. Approximately 70 percent of the rain received falls during the wet season (May through October).

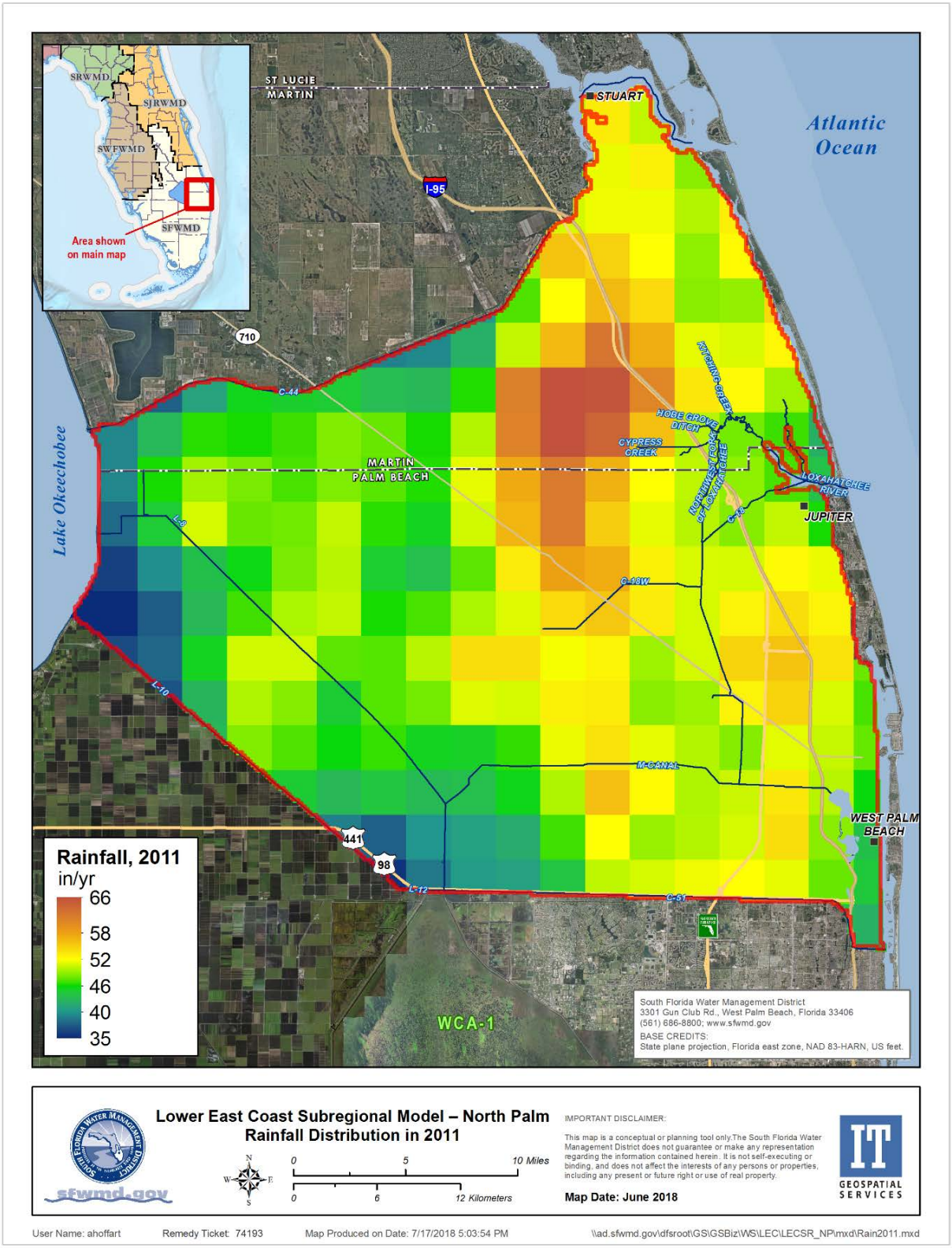

Figure 4. Spatial distribution of NEXRAD-generated rainfall across the LECSR-NP active model area in 2011 (a representative dry year).

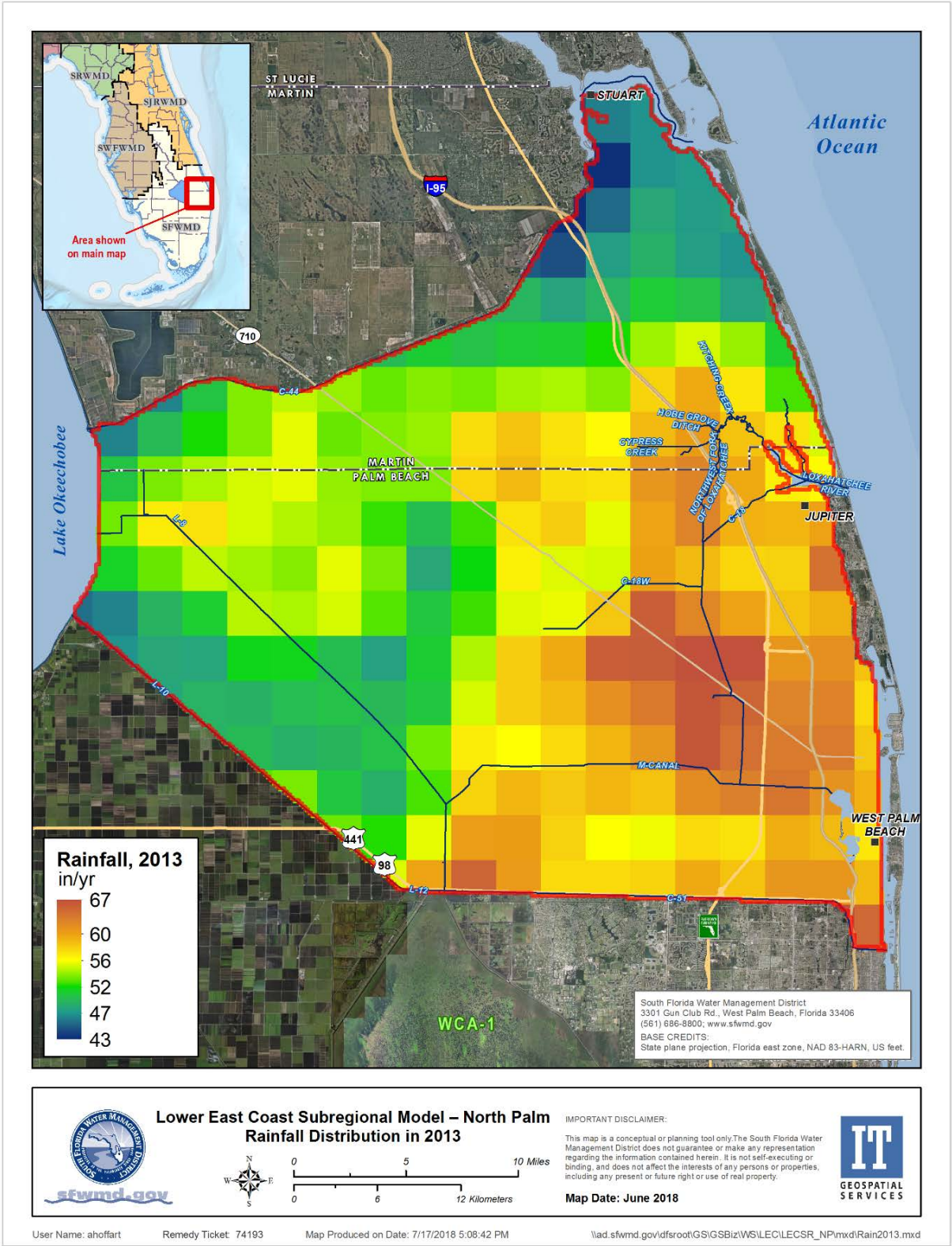

Figure 5. Spatial distribution of NEXRAD-generated rainfall across the LECSR-NP active model area in 2013 (a representative wet year).

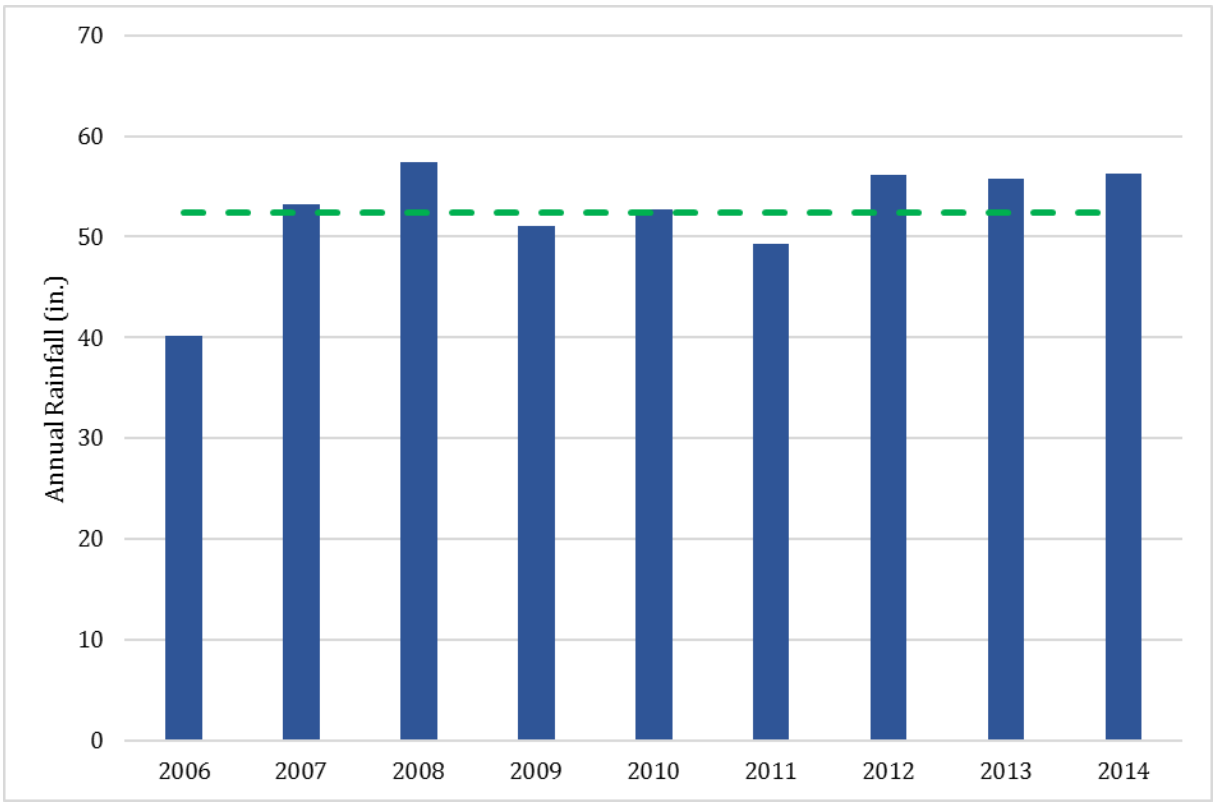

Figure 6. Average annual rainfall in the LECSR-NP active model area (2006 to 2014).

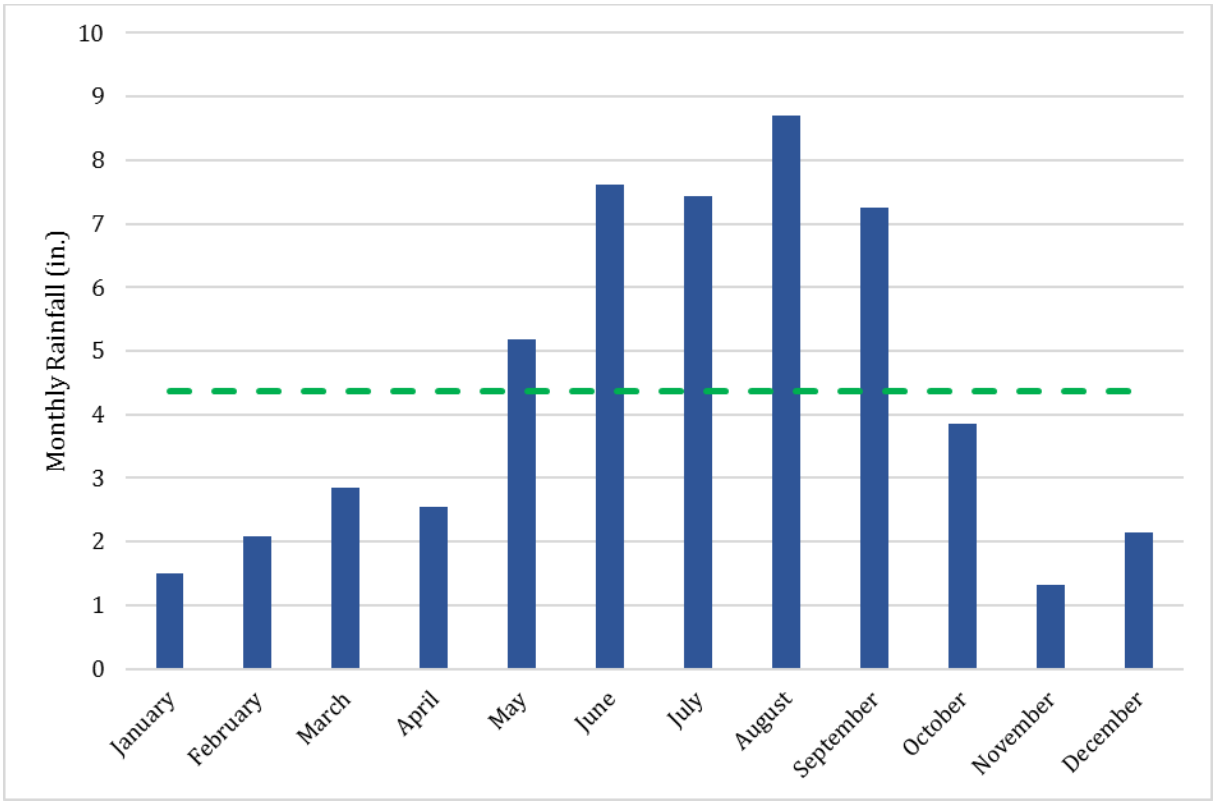

Figure 7. Average monthly rainfall in the LECSR-NP active model area (2006 to 2014).

Variations in rainfall over time can lead to drought or flooding, which can have serious impacts to the region's water resources. Periods of high water conditions may require the SFWMD to discharge large quantities of water to the coastal estuaries, which may cause localized environmental problems. Conversely, periods of prolonged rainfall deficit may result in water shortage restrictions and saltwater intrusion into coastal aquifers. In order to standardize rainfall patterns, the Standardized Precipitation Index (SPI) was developed to assess the severity of drought conditions (McKee, 1993). The SPI is a normalized index based upon the number of standard deviations the observed cumulative precipitation deviates from the climatological average. Although originally designed to measure the degree of a drought, it also can be used to evaluate average and wet conditions and is useful in understanding and quantifying climatic conditions for long-term, transient groundwater model simulations.

NOAA Climate Division SPI 12-month values were downloaded for Florida Climate Divisions 5 and 6 (**Figure 8**). SPI data were available from 1965 to 2014, allowing for comparisons to be made between rainfall patterns within the LECSR-NP calibration period (2006 to 2014), the model validation period (2000 to 2005), and the LRWRP simulation period (1965 to 2005). Thus, the model was introduced to similar extremes and patterns in rainfall during the calibration period. Standardized Precipitation Index 12-month values for Divisions 5 and 6 were averaged. Plots were produced for the calibration period and simulation period for Division 5, Division 6, and the average SPI.

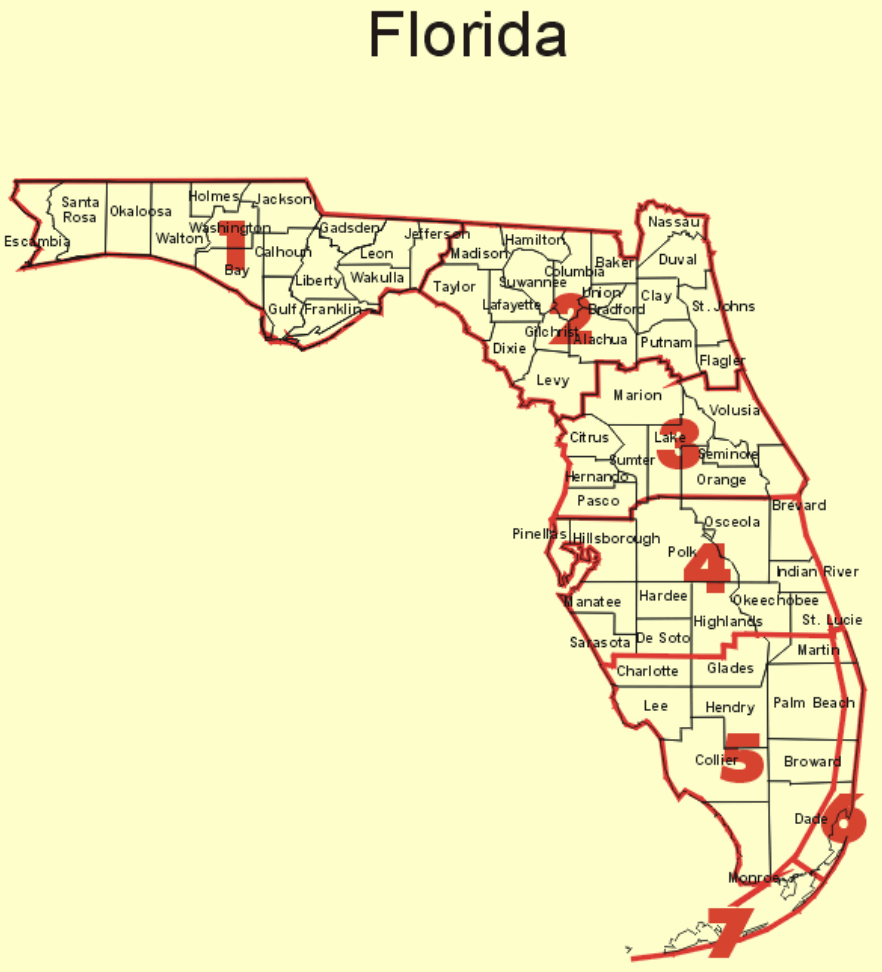

Figure 8. Map of NOAA climate divisions in Florida (Map from: http://www.cpc.ncep.noaa.gov/products/analysis_monitoring/regional_monitoring/CLIM_DIVS/florida.gif).

Figure 9 shows the climate variability based on the SPI 12-month calculation for the calibration and verification period (2006 to 2014). Although there was some variability between the two divisions in 2008 and 2013, overall, they have very similar SPI 12-month values. Based on the average SPI value, dry years occurred in 2007, 2009, and 2011. The minimum SPI 12-month value was -1.7, which occurred in 2011. Based on the average SPI value, wet years occurred in 2010, 2012, and 2013. The maximum SPI 12-month value was 1.1, which occurred in 2012. The average SPI 12-month value over the entire calibration period was -0.2, which indicates the calibration period is slightly drier than average conditions.

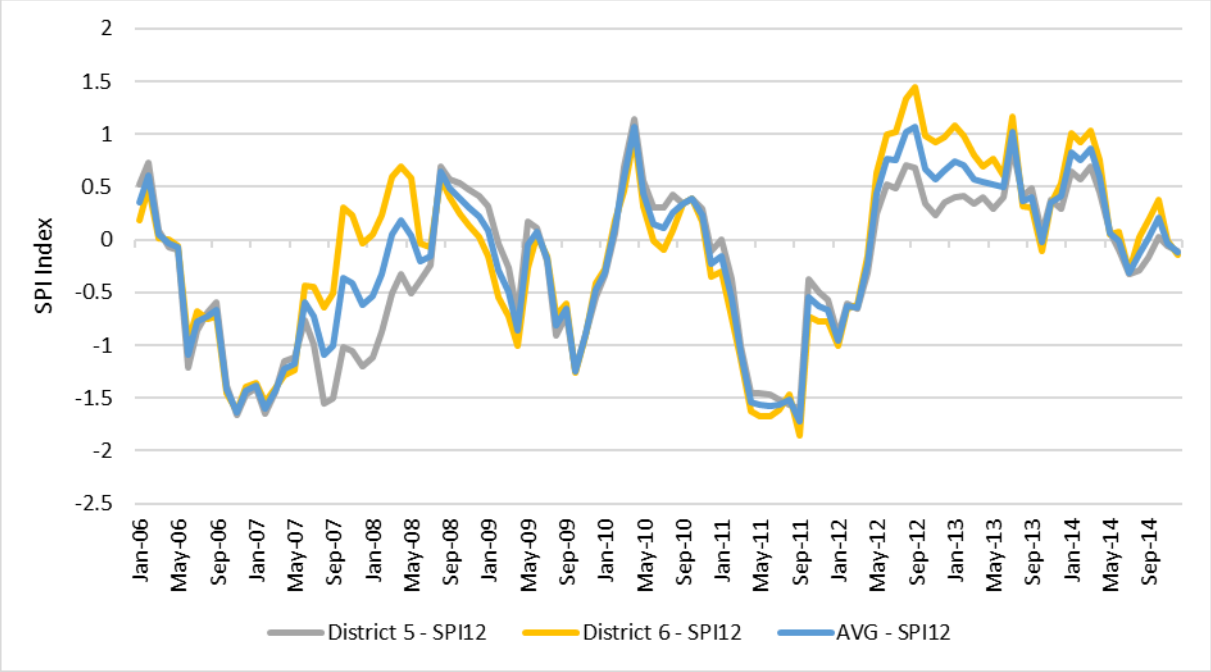

Figure 9. 12-month SPI patterns for District 5, District 6, and the average for 2006 to 2014.

Figure 10 shows the climate variability based on the SPI 12-month calculation for the simulation period (1965 to 2005). Although there was some variability between the two divisions in 1975, 1989, and 2001, overall, they have very similar SPI 12-month values. Based on the average SPI value, dry years occurred in 1971, 1975, 1981, 1989, 1990, and 2001. The minimum SPI 12-month value was -2.33, which occurred in 1971. Based on the average SPI value, wet years occurred in 1966, 1968, 1970, 1983, 1994, 1995, 1996, and 1999. The maximum SPI 12-month value was 2.535, which occurred in 1995. The average SPI 12-month value over the entire simulation period was 0.06, which indicates the simulation period represents average conditions.

Comparing the calibration period to the simulation period, the calibration period generally is drier than the simulation period. Although both periods have wet and dry years, the extreme events typically occurred during the simulation period. Therefore, for model verification, a period will be selected that includes extreme dry, extreme wet, and average conditions.

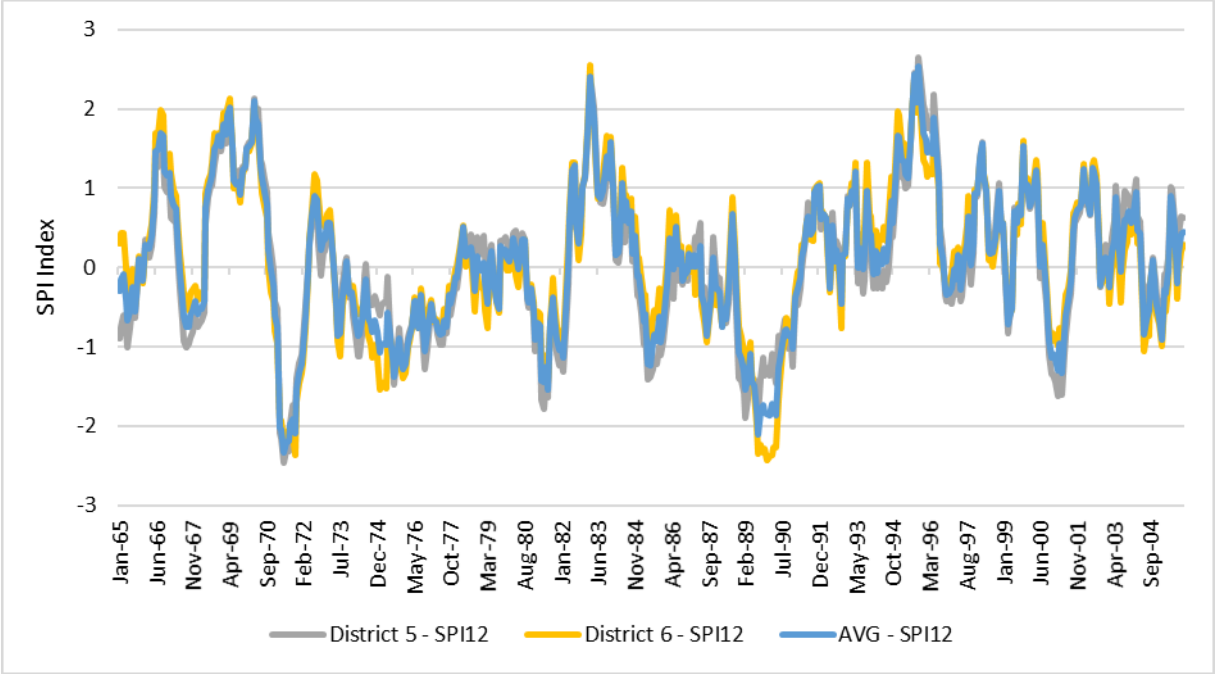

Figure 10. 12-month SPI patterns for District 5, District 6, and the average for 1965 to 2005.

2.2.2 Evapotranspiration

Evapotranspiration (ET) is the physical process by which water is lost to the atmosphere by evaporation from water bodies and by transpiration from plants. ET plays a major role in the hydrologic cycle in South Florida because the water table is near land surface throughout the year. Reference ET is defined as the rate of ET from a hypothetical crop—which in South Florida is grass—that has an assumed height, a fixed canopy resistance, and an albedo that resembles ET from an extensive surface of green grass cover of uniform height, actively growing, completely shading the ground, and not short of water (Food and Agriculture Organization of the United Nations, 1990). The reference crop should be taken as a hypothetical crop with fixed parameters and resistance coefficients. These crop coefficients are complex empirical factors derived from experimental data and encompass all characteristics of the crop that differ from those of the reference crop. These coefficients quantify how soil and crop conditions affect actual ET.

Reference ET data from 2006 to 2014 were derived from North American Land Data Assimilations Systems (NLDAS) data, which provide complete spatial coverage of reference ET amounts using a predetermined grid resolution (2 km by 2 km; Brown, 2013). **Figures 11** and **12** show the spatial distribution of reference ET derived from NLDAS data for the LECSR-NP active model area in 2011 (a dry year) and 2013 (a wet year), respectively.

ET can represent the greatest water loss from the system. In general, reference ET is approximately 59 inches per year between 2006 and 2014 for the reference crop (**Figure 13**). The highest ET rate was approximately 62 inches in 2009, while the lowest ET rate was less than 57 inches in 2014.

In general, the monthly distribution of reference ET follows the solar radiation curve (**Figure 14**). Over the period of record, May, June, and July have the highest maximum ET rates. Reference ET is lowest during December.

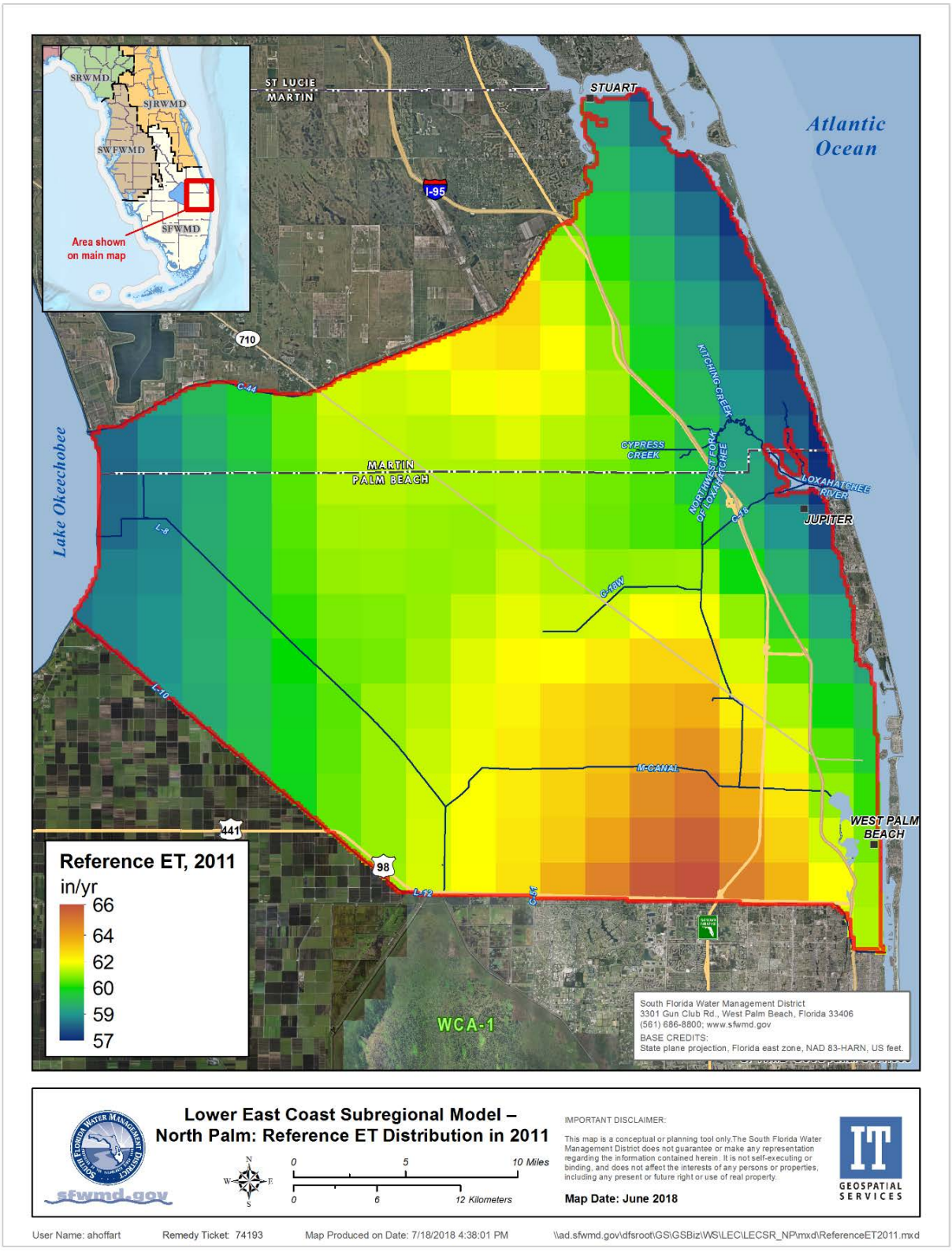

Figure 11. Spatial distribution of NLDAS-generated reference ET across the LECSR-NP active model area in 2011 (a representative dry year).

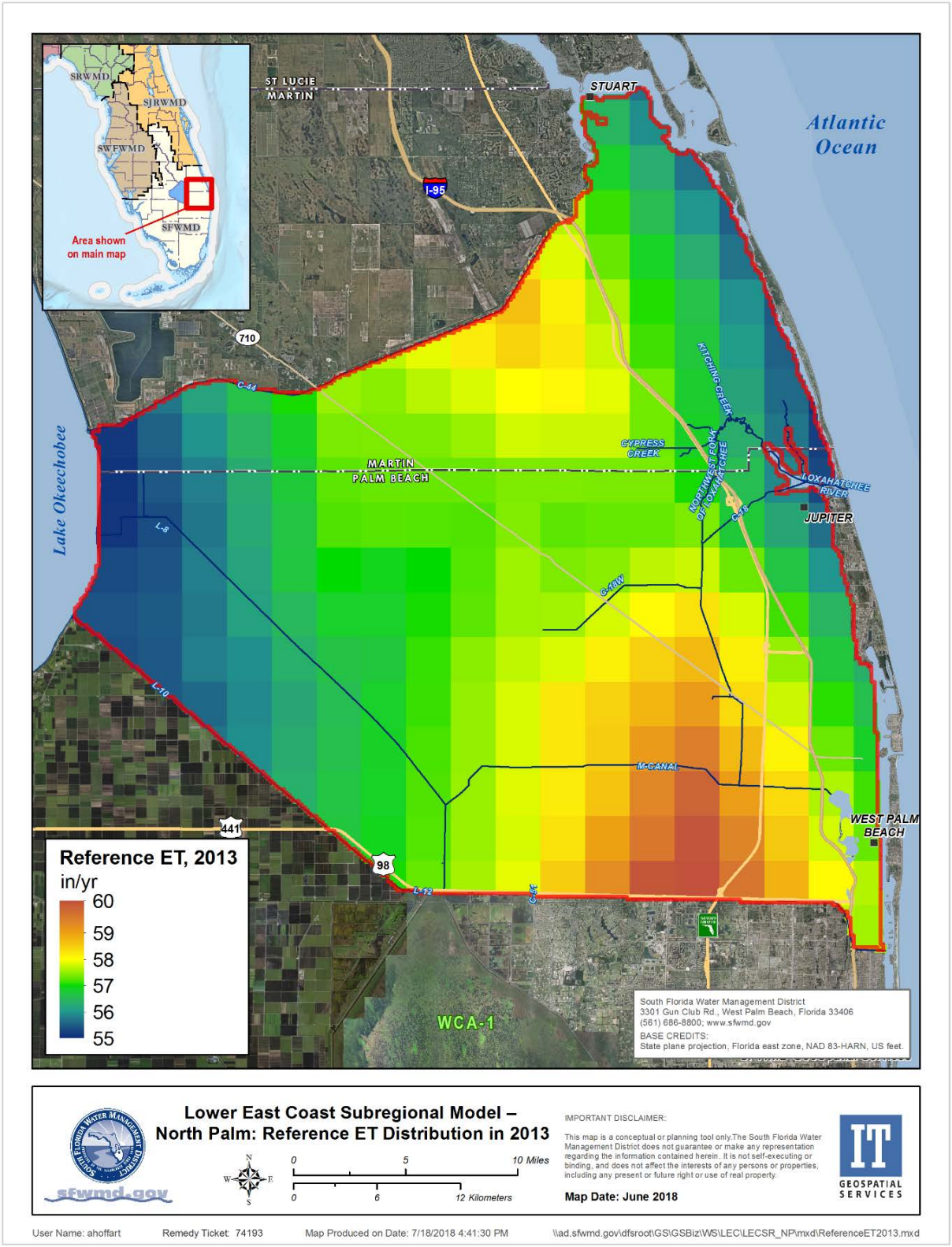

Figure 12. Spatial distribution of NLDAS-generated reference ET across the LECSR-NP active model area in 2013 (a representative wet year).

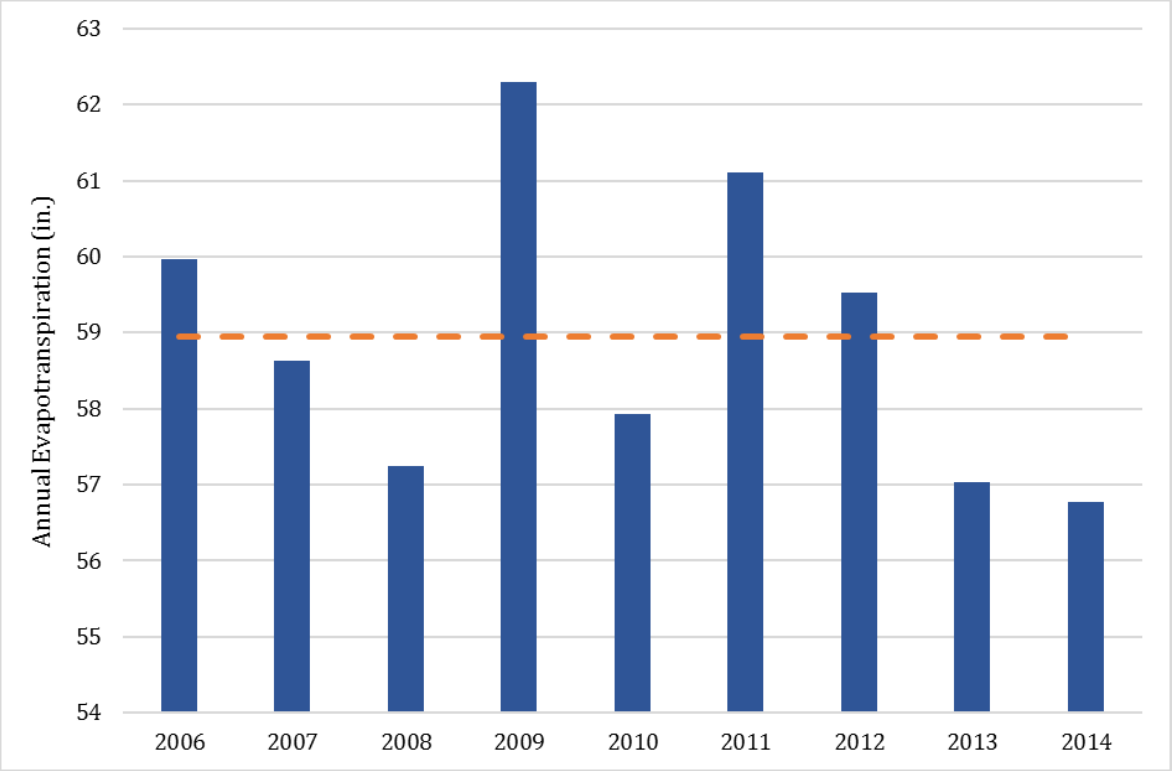

Figure 13. Average annual reference evapotranspiration for the LECSR-NP active model area (2006 to 2014).

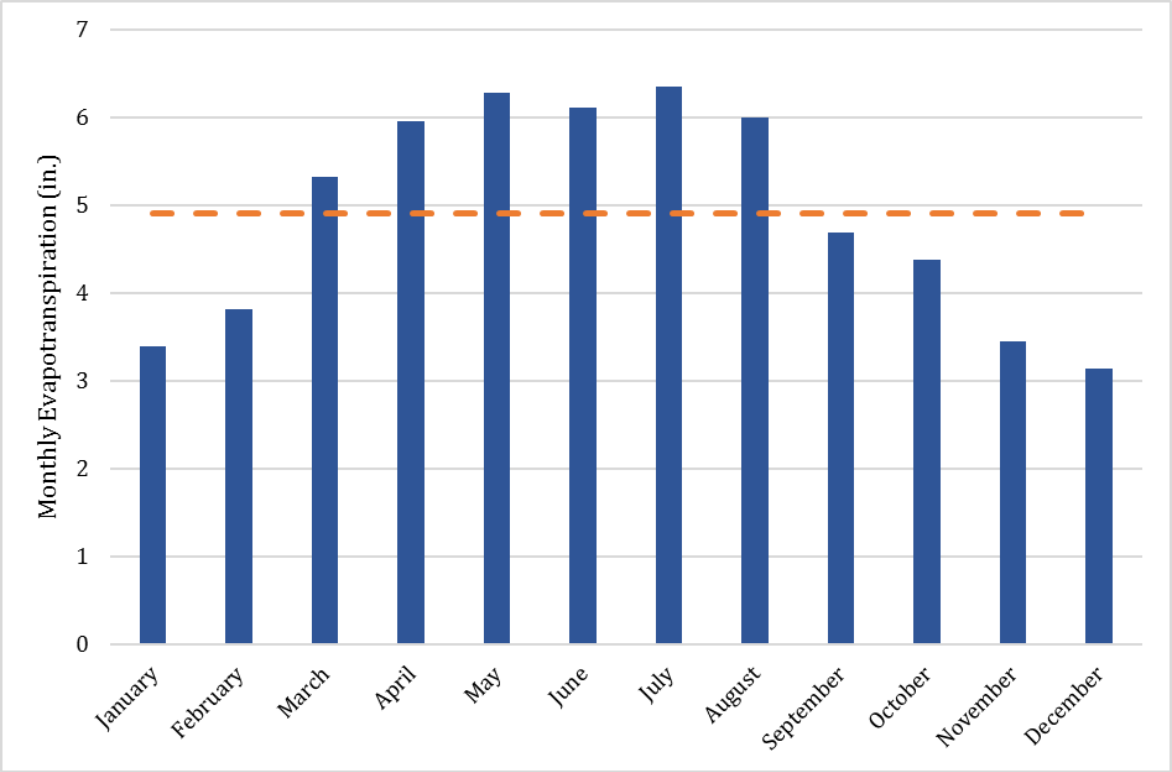

Figure 14. Average monthly reference evapotranspiration for the LECSR-NP active model area (2006 to 2014).

2.3 Land Use and Soil

Land use for the LECSR-NP is a combination of the best available land use/land cover data from the Upper East Coast 2012 update and the SFWMD's 2014 land use update. The 2012 update covers the portion of the active model domain in Martin County and northern Palm Beach County, and the 2014 land use update covered the southern portion of the active model domain. Land use classification includes several levels that detail the type of use. **Figure 15** shows a partially aggregated level 3 classification (data obtained from medium-altitude photography flown between 10,000 and 40,000 ft) for the LECSR-NP active model area. The largest land use classification is urban areas, covering 26 percent of the active model area. Most urban areas are along the coast and in the southern L-8 and C-51 basins. The second largest land use classification is wetlands, covering 23 percent of the LECSR-NP active model area (**Table 1**). Wetland areas include expansive systems such as those in Jonathan Dickinson State Park, Pal Mar, Corbett Wildlife Management Area, and Loxahatchee Slough. Agricultural land uses cover approximately 21 percent of the active model area.

Table 1. Percent of total area by land use types in the LECSR-NP active model area.

Land Use Type	Acres	Percent
Wetlands	126,727	23%
Water	24,924	5%
Urban and Built-up	138,660	26%
Transportation and Communications	13,921	3%
Barren Land	5,129	1%
Sugar Cane	71,566	13%
Agriculture Crops	11,455	2%
Other Agriculture	33,438	6%
Improved Pasture	19,503	4%
Unimproved Pasture	3,867	1%
Upland Non-Forested	17,122	3%
Upland Forest	75,236	14%

The LECSR-NP active model area encompasses nearly 700 square miles (approximately 441,000 acres). Historically, much of this landscape was covered with wetland marshes, swamps, and flood-tolerant upland species such as pines and palmettos. Due to the flat, low-lying topography and relatively limited access to the ocean for surface water discharge, much of the region is poorly drained and prone to flooding.

Soil characteristics reflect the complex interaction among topography, climate, vegetation, hydrology, and parent material. Soil classification data from the Soil Survey Geographic Database (SSURGO) for the LECSR-NP active model area are presented in **Figure 16**. In the LECSR-NP active model area, the predominant soil types are sand depression, flatwood soils, and flat soils. Sand depression is a poorly drained hydric soil mostly consisting of sand marine sediments with occasional mucky or loamy sand. Flatwood soils are poorly drained nonhydric upland soils, which also predominantly have sandy marine sediments. Similar to sand depression, flat soils are poorly drained hydric soils with sandy marine sediments (Zahina et al., 2001).

Various soil types have different runoff and recharge potentials and typically are classified into hydrologic groups. There are four hydrologic groups for soils that can be combined to create dual hydrologic soil groups. Dual hydrologic soil groups are assigned when the water table is within 60 centimeters of the surface, but water may be able to travel through the soil. Dual hydrologic soil groups are A/D, B/D, and

C/D. Group A soils have low runoff potential when thoroughly wet and water is being transmitted freely through the soil. Group A soils typically consist of more than 90 percent sand with less than 10 percent clay. Group B soils have moderately low runoff potential when wet. These soils typically consist of 50 to 90 percent sand with 10 to 20 percent clay. Group C soils have moderately high runoff potential when thoroughly wet, with water transmission being somewhat impeded. These soils typically are 20 to 40 percent clay and less than 50 percent sand. Group D soils have high runoff potential when thoroughly wet. Water movement through Group D soil is very restricted. Group D soils typically are more than 40 percent clay and less than 50 percent sand (United States Department of Agriculture, 2007). The predominant grouping within the LECSR-NP active model area is hydrologic group A/D, indicating the soils are predominantly sand with low runoff potential when saturated, where the water table exists within 60 centimeters from the surface.

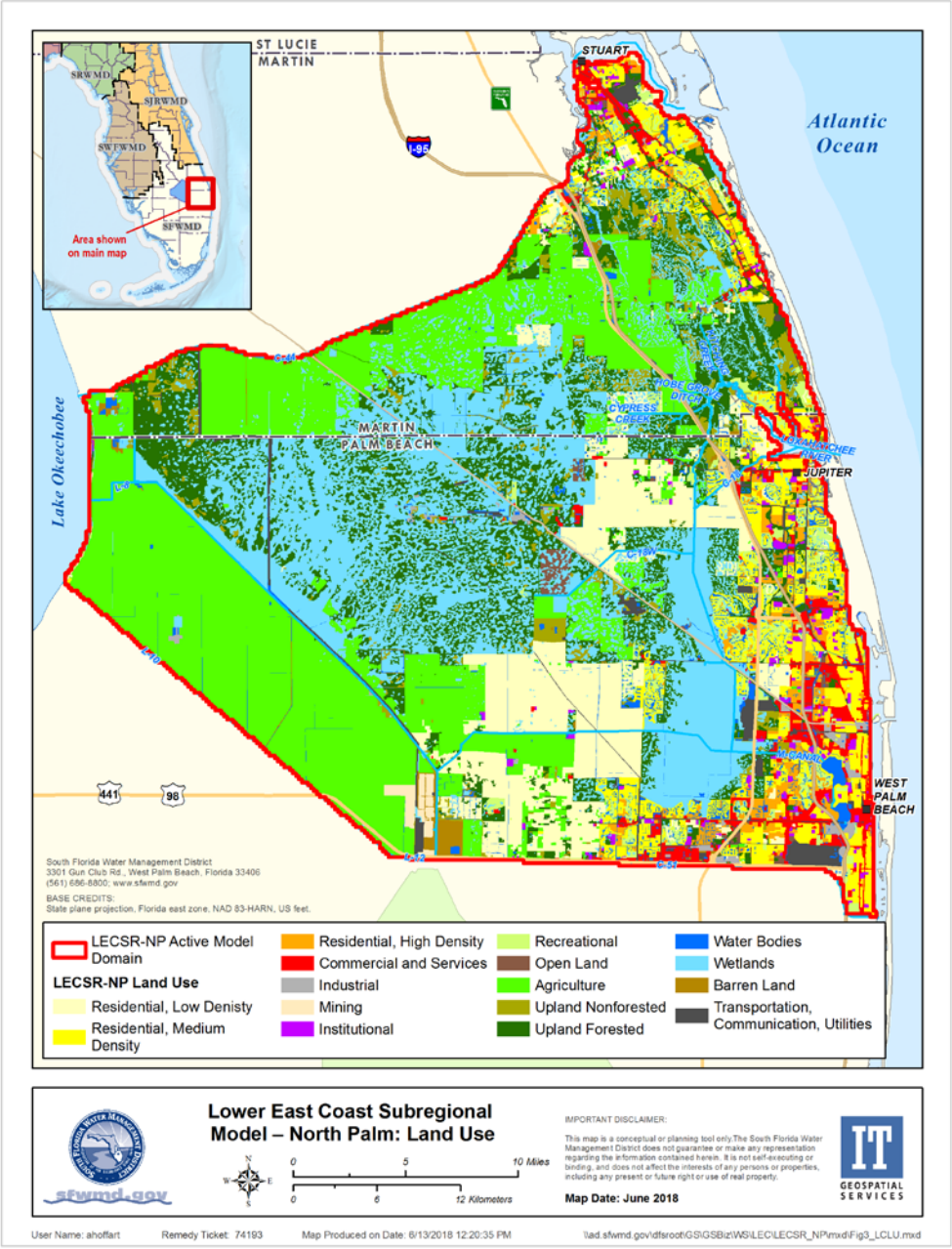

Figure 15. Land use/land cover in the LECSR-NP active model area.

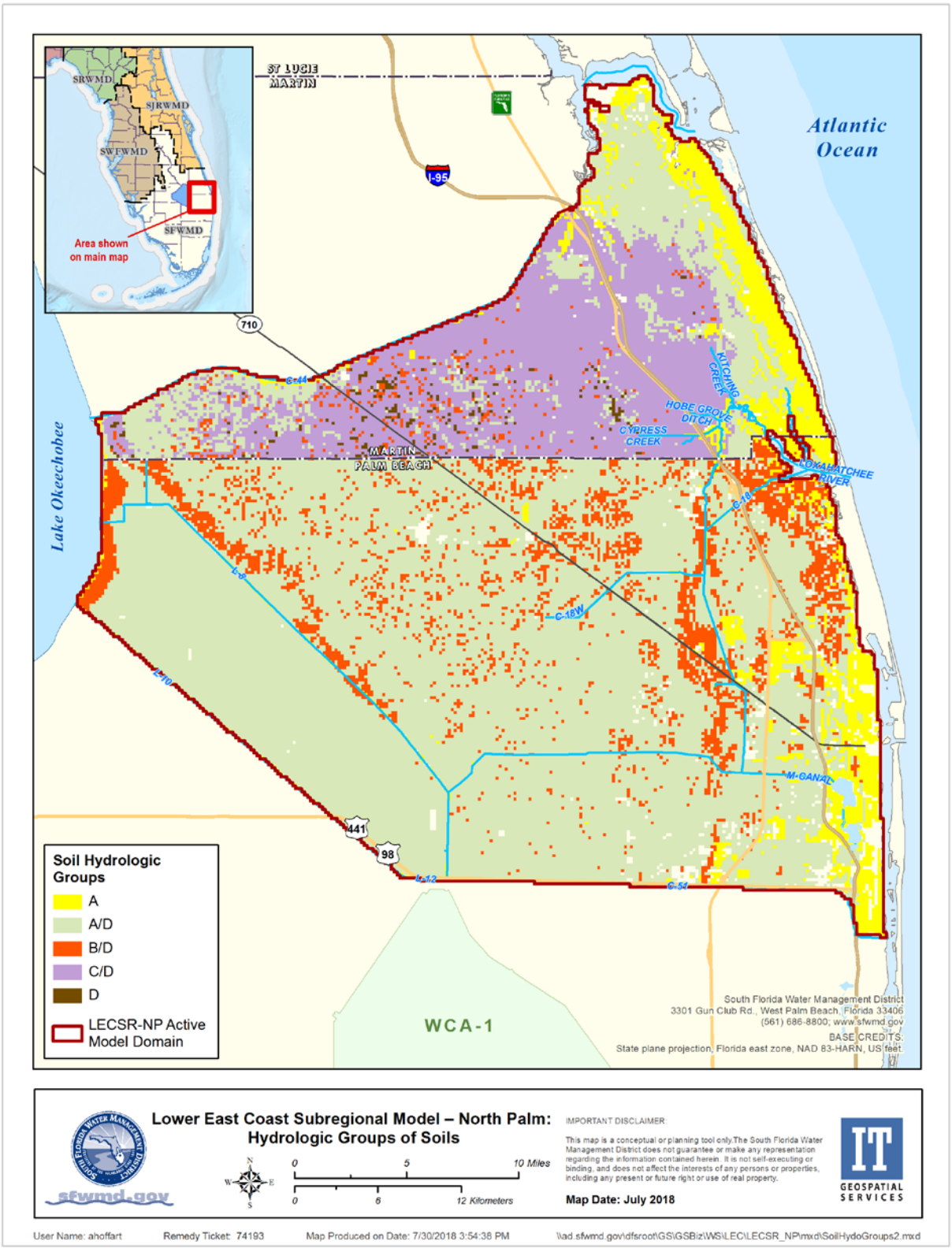

Figure 16. Hydrologic soil types in the LECSR-NP active model area.

2.4 Surface Water System

Surface water systems within the active model area include Lake Okeechobee to the west and the Indian River and Lake Worth lagoons to the east. Numerous wetland systems, canals, mining areas, smaller lakes, and the Wild and Scenic Loxahatchee River with its tributaries exist within the study area. Lake Okeechobee is the largest freshwater lake in Florida and is heavily managed to meet multiple objectives. As it relates to the active model area, Lake Okeechobee provides surface water to meet the irrigation demands of the Everglades Agricultural Area and the City of West Palm Beach's public water supply (PWS). Flood control releases from the lake can be made through the C-44 Canal along the northern boundary of the active model area and water supply releases are made to coastal communities via the C-51 Canal along the southern boundary of the study area. In addition to the C-44 and C-51 canals, two additional primary canals exist within the active model area and are managed by the SFWMD or USACE. The C-18 Canal is a major canal system in the center of the active model area and is controlled by the S-46, C-18 weir, and G-160 structures for flood control and environmental purposes. The C-17 Canal is used to control water levels for flood control in West Palm Beach, North Palm Beach, and Riviera Beach coastal communities.

Local (secondary) canal systems in South Florida are maintained and operated by cities, counties, and water control districts (also known as 298 Districts for the chapter of Florida Statutes that outlines their responsibilities). These secondary canal systems receive runoff from the areas they manage and store excess water or move it to the SFWMD primary canal system. There are several 298 Districts within the active model area, including the Lake Worth Drainage District, Loxahatchee Groves Water Control District, Pal Mar Water Control District, Northern Palm Beach County Improvement District, South Indian River Water Control District, Hobe St. Lucie Conservancy District, and Indian Trail Improvement District. In addition to routing runoff away from developments and into the primary canal network, several 298 Districts take water from the primary canal network or other major SFWMD features to provide water for local irrigation, agricultural, and urban needs. Tertiary canals are the smaller swales, ditches, and ponds designed to remove stormwater or provide irrigation at the local level.

The City of West Palm Beach uses surface water from Clear Lake as its source of water for the PWS system. Water is brought into Clear Lake through the M-Canal from GWP to the west. GWP and Clear Lake are augmented from the SFWMD regional system via the M-Canal, which connects to the L-8 Canal near the Everglades Agricultural Area. The City of West Palm Beach operates a pump station, CS-2, at the L-8 Canal that sends regional system water approximately 8.5 miles east into GWP, then to the CS-3 pump station, and ultimately to Clear Lake. The stretch of the M-Canal from CS-2 to CS-3 is maintained at a higher elevation than the surrounding canal system operated by Indian Trail Improvement District. This head difference (in addition to several constrictions in the M-Canal from a bridge crossing and canal width) results in noticeable seepage loss across this section of the canal reach. Unpublished work conducted by Lal (2015) and the SFWMD (2015) attempted to quantify these seepage losses. Both works clearly identified major obstacles with the bridge crossing in the canals and noticeable head losses at these obstructions. Pumpage by the City of West Palm Beach at CS-2 can exceed 150 cubic feet per second (cfs) and potentially 200 cfs before the canal and bridge constraints cause issues. As a result of this relatively large volume of pumped water, the SFWMD (2015) conducted a seepage test along the canal reach and concluded that up to 7 percent of the water pumped may be lost to seepage. Lal (2015) expanded on the study and concluded that a loss of approximately 6 percent can occur at higher pumping rates. However, seepage loss can increase substantially when the CS-2 pump station discharges at reduced rates. Cutting through the central portion of the study area is a large expanse of relatively undeveloped upland and wetland systems stretching from near Lake Okeechobee to the west to the Jupiter Inlet to the east. These upland and wetland systems include the DuPuis Management Area, Corbett Wildlife Management Area, Pal Mar Water Control District, Loxahatchee Slough region, Loxahatchee River region, GWP, Nine Gems and Gulfstream Grove area, and Jonathan Dickinson State Park.

2.5 Hydrogeology

The active model area in South Florida is underlain by approximately 20,000 feet of continuous carbonates, evaporites, and clastic sediments deposited relatively uninterrupted throughout the Cenozoic era (Smith and Lord, 1997). The primary geologic formations under the study area include the Cedar Keys, Oldsmar, Avon Park, Ocala Limestone, and Hawthorn Group. The Pliocene/Pleistocene deposits include the Tamiami, Fort Thompson, and Anastasia formations, which form the basis of the SAS in northern Palm Beach and Martin counties. The SAS is the only aquifer system considered in this study. A detailed discussion on the general geology, hydrostratigraphy, and water-bearing units in the study area can be found in Giddings et al. (2006).

Since the development of the original LECSR, additional hydrogeologic investigations of the SAS have been undertaken in the study area (**Figure 17**). Areas of recent detailed hydrogeologic investigations include the L-8 Flow Equalization Basin (FEB) in the eastern part of the Everglades Agricultural Area (Gannett Fleming, 2015), the Mecca property adjacent at the western end of the C-18 Canal (Arcadis, 2015), and eastern Corbett Wildlife Management Area (Gannett Fleming, 2016). A general compilation of data in Palm Beach County by Reese and Wacker (2009) and the mapping of the Ochopee Limestone member of the Tamiami Formation in Palm Beach County (Reese and Wacker, 2007) was reviewed but provided minimal insight for the refinement of the LECSR-NP. Collins et al. (2016) assessed surface water and groundwater conditions in Loxahatchee Slough as a result of the construction and operation of the G-160 control structure. Hydrologic, geophysical, and geotechnical information was collected at the White Fences and Deer Run communities by Gannett Fleming (2015).

Collins et al. (2016) evaluated the effects of changing seasonal control elevations of the G-160 structure located on the C-18 Canal. The G-160 structure was constructed in 2003 and began limited operations in 2004. Prior to construction, the southern leg of the C-18 Canal was controlled by the S-46 structure, which discharged to the ocean when water levels in the canal approached 14.9 feet NGVD29. The purpose of the G-160 structure was to increase water levels in the southern leg of the C-18 Canal to improve hydroperiods in adjacent wetlands and provide a source of water for the Loxahatchee River while still maintaining flood control capabilities for the surrounding urban developments and roads. Collins et al. (2016) constructed 14 monitor wells equipped with recorders in Loxahatchee Slough to provide critical long-term information regarding water levels in the slough. In addition to the well installation, Collins et al. (2016) evaluated general horizontal and vertical flow direction, and the results were somewhat inconclusive. Vertical flow generally was downward in areas away from canals and upward near canals; horizontal flow was towards the C-18 Canal or adjacent major wellfields.

The constructed monitor wells were completed between 20 and 70 feet below land surface (bls) with split-spoon samples collected at 2-foot intervals. The lithology of the upper portion of the SAS in the study area consists of unconsolidated sands and shells that range in thickness from 20 to 70 feet bls. Several wells encountered limestones, marls, and coquina layers from 40 to 70 feet bls, suggesting the presence of the Anastasia Formation, Caloosahatchee Marl, and/or Fort Thompson Formation. These layers could indicate the presence of the northern extent of the Biscayne aquifer, although no aquifer testing was conducted for this study to confirm a zone of high hydraulic conductivity (greater than 1,000 feet/day), which defines the Biscayne aquifer.

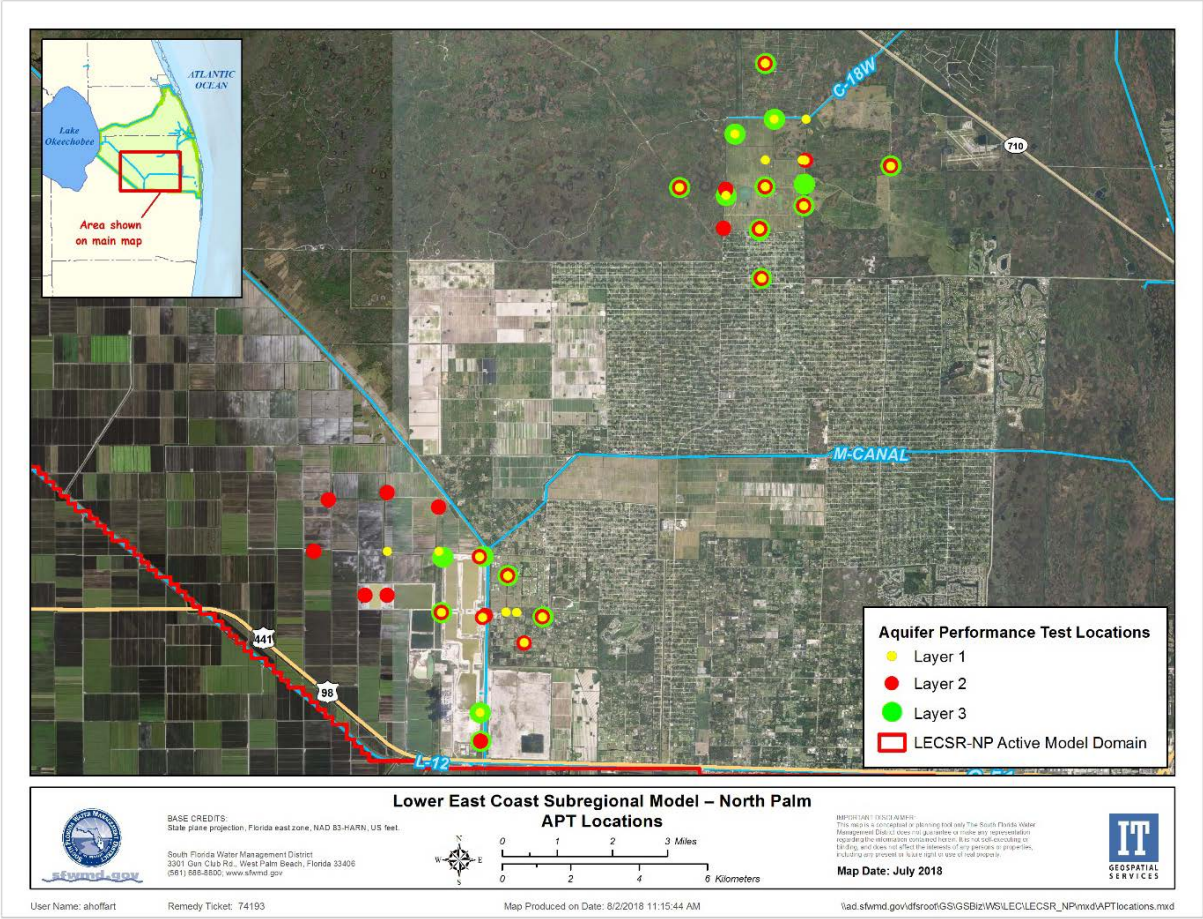

Figure 17. Locations of new aquifer performance test data used in the LECSR-NP.

At the western end of the C-18 Canal is the Mecca property, purchased by Palm Beach County and the SFWMD. Arcadis (2015) conducted a site-specific evaluation of the Mecca property involving the drilling, installation, and testing of 24 wells. The lithology at the site is relatively uniform. The maximum penetration of the geologic wells was 100 feet bls. In general, the entire thickness was a medium-dense gray sand that became denser with depth on the western side of the property. Several minor limestone/shell layers were encountered at approximately 45, 60, and 80 feet bls in central and eastern areas of the property. The aquifer properties at the site were estimated using slug-tests, constant-head permeability tests and two constant-rate aquifer performance tests. The results of the aquifer tests indicate hydraulic conductivities (Kh) generally are typical for South Florida sands, ranging from 1.0 to 25.0 feet/day. The results of the various tests are presented in **Tables 2** to **6**.

Table 2. Aquifer properties from slug tests for screen interval from 95 to 100 feet within the Mecca property (From: Arcadis, 2015).

Well ID	Screen (feet)	Constant Head	Slug In #1	Slug In #2	Slug Out #1	Slug Out #2	Average
		Hydraulic Conductivity (Kh) (feet/day)					
MFEB1-GW1	95-100	46.10	19.00	25.00	24.00	24.00	27.62
MFEB2-GW1	95-100	1.20	1.50		1.60		1.43
MFEB3-GW1	95-100	24.30	19.00	21.00	5.90	9.70	15.98
MFEB4-GW1	95-100	9.70	11.00	9.10	8.80	7.30	9.18
MFEB5-GW1	95-100	4.70	5.50	3.60	1.90	2.00	3.54
MFEB6-GW1	95-100	29.30	63.00	21.00	24.00	28.00	33.06
MFEB7-GW1	95-100	86.90	19.00	17.00	17.00	21.00	32.18
MFEB8-GW1	95-100	7.00	10.00	8.30	2.50	1.90	5.94

Table 3. Aquifer properties from slug tests for screen interval from 40 to 45 feet within the Mecca property (From: Arcadis, 2015).

Well ID	Screen (feet)	Constant Head	Slug in #1	Slug in #2	Slug Out #1	Slug Out #2	Average
		Hydraulic Conductivity (Kh) (feet/day)					
MFEB1-GW2	40-45	22.20	11.00	11.00	8.10	8.70	12.20
MFEB2-GW2	40-45	33.50	27.00	28.00	27.00	29.00	28.90
MFEB3-GW2	40-45	2.10	1.80	1.60	1.90	1.70	1.82
MFEB4-GW2	40-45	18.70	97.00	120.00	43.00	40.00	63.74
MFEB5-GW2	40-45	2.20	1.50	1.50	2.00	1.60	1.76
MFEB6-GW2	40-45	12.70	8.20	9.70	7.30	7.80	9.14
MFEB7-GW2	40-45	87.20	61.00	26.00	35.00	23.00	46.44
MFEB8-GW2	40-45	6.60	6.60	5.80	6.20	6.10	6.26

Table 4. Aquifer properties from slug tests for screen interval from 10 to 15 feet within the Mecca property (From: Arcadis, 2015).

Well ID	Screen (feet)	Constant Head	Slug in #1	Slug in #2	Slug Out #1	Slug Out #2	Average
		Hydraulic Conductivity (Kh) (feet/day)					
MFEB1-GW3	10-15	2.60	30.00	39.00	19.00	19.00	21.92
MFEB2-GW3	10-15	0.60	0.90		1.20		0.90
MFEB3-GW3	10-15	13.30	5.60	5.60	5.50	5.60	7.12
MFEB4-GW3	10-15	3.00	1.80	1.70	1.70	2.00	2.04
MFEB5-GW3	10-15	1.30	24.00	16.00	22.00	30.00	18.66
MFEB6-GW3	10-15	49.10	140.00	93.00	93.00	180.00	111.02
MFEB7-GW3	10-15	7.30	3.20		3.00		4.50
MFEB8-GW3	10-15	6.40	4.40	4.00	4.30	4.10	4.64

Table 5. Aquifer properties from slug tests within the Mecca property (From: Arcadis, 2015).

Well ID	Screen (feet)	Constant Head	Slug in #1	Slug in #2	Slug Out #1	Slug Out #2	Average
		Hydraulic Conductivity (Kh) (feet/day)					
MFET01-PZ1	20-25	19.90	12.00	14.00	12.00	12.00	13.98
MFET02-PZ1	10-30	12.90	11.00	7.30	10.00	7.90	9.82
MFET03-PZ1	25-30	13.90	9.30	9.50	8.00	8.60	9.86
MFET04-PZ1	55-60	4.60	3.60	3.70	3.50	3.60	3.80
MFET05-PZ1	40-60	4.70	3.20	3.20	3.40	3.20	3.54
MFET07-PZ1	65-70	3.50	2.50	2.70	1.30	1.50	2.30
MFET07-PZ2	20-25	4.80	2.70	2.70	2.60	2.80	3.12
MFET08-PZ1	20-25	3.50	2.40	2.40	2.40	2.30	2.60
MFET09-PZ1	20-25	10.00	4.30	4.10	4.00	3.80	5.24
MFET10-PZ1	45-50	7.20	9.40	9.30	7.00	7.30	8.04
MFET11-PZ1	25-30	4.40	3.30	2.70	3.20	3.20	3.36

Table 6. Aquifer properties from aquifer performance tests within the Mecca property (From: Arcadis, 2015).

Observation Well	Distance (feet)	Cooper-Jacob*	Theis Recovery	Moench	Moench	Average	
		Kh (feet/day)			Storage	Kh (feet/day)	T (feet^2/day)
MFET01-PZ1	250	28.00	45.00	29.00	6.30E-04	34.00	3,400.00
MFET03-PZ1	65	14.00	27.00	17.00	9.00E-04	19.33	1,933.33
MFEB3-GW2	116	14.00	24.00	16.00	5.50E-04	18.00	1,800.00
MFEB3-GW3	114	12.00	28.00	10.00	3.30E-04	16.67	1,666.67
MFET04-PZ1	150	14.00	23.00	17.00	3.00E-04	18.00	1,800.00

Kh = hydraulic conductivity; T = transmissivity.
* Cooper and Jacob (1946).

West of the Mecca property is the Corbett Wildlife Management Area, a large natural area in northern Palm Beach County. Gannett Fleming (2016) conducted a site-specific evaluation of the aquifer at a single location in the eastern portion of the wildlife management area. The work included construction of a tri-zone monitor well with standard penetration test borings, geophysical logs, and aquifer testing. The results of the boring indicted the upper 32 feet were composed of a loose to moderately dense-grain, dark gray sand with some shell fragments. From 33 to 60 feet bls, this fine, dark gray sand became dense to very dense, and from 60 to 100 feet bls, it transitioned into a medium-dense to dense, silty gray, fine sand. Both slug tests and short-term single-well aquifer tests were conducted at three intervals in the SAS. The results suggest extremely low hydraulic conductivity values for the SAS compared to other sites in the region. The test intervals were 10 to 15 feet bls, 34 to 39 feet bls, and 95 to 100 feet bls. The results are presented in **Table 7**.

Table 7. Aquifer parameters at Corbett Wildlife Management Area (From: Gannett Fleming, 2016).

Observation Well	Depth (feet bls)	Estimated Aquifer Thickness (feet)	Single Well Pump Test – Duration 1 Hour					Slug Test
			Rate (gpm)	Hantush Method - Kh (feet/day)	Newman-Witherspoon Method - Kh (feet/day)	Average Kh (feet/day)	Average Transmissivity (feet^2/day)	Kh (feet/day)
MFEB9-GW1	10-15	40.0	6.5	0.75	0.68	0.72	28.60	42.68
MFEB9-GW2	34-39	39.3	5.9	0.40	0.41	0.41	15.92	10.17
MFEB9-GW3	95-100	39.3	2.3	0.60	0.45	0.53	20.63	6.89

bls = below land surface; gpm = gallons per minute; Kh = hydraulic conductivity.

The White Fences and Deer Run communities are east of the L-8 FEB in western Palm Beach County. Gannett Fleming (2015) conducted a site-specific evaluation of the aquifer at these communities. Of specific interest to this study are the findings from the installation and testing of three monitor well clusters. Continuous lithologic data were collected to a depth of 100 feet bls, and three aquifer tests were conducted at each site to determine the aquifer parameters at various depths. The boring results indicted a layer of sand rests on a 10-foot thick limestone layer approximately 10 feet bls. Below the limestone layer is 75 feet of medium to very dense gray fine sand, with some shell fragments. In two of the borings (95 to 100 ft bls), a tan sand was encountered, suggesting the top of the Tamiami Formation may have been penetrated. Short-term single-well aquifer tests were conducted at three intervals in the SAS for each site: 20 feet bls, 50 feet bls, and 90 feet bls. The results are presented in **Table 8**.

Table 8. Aquifer properties at the White Fences and Deer Run communities (Modified from: Gannett Fleming, 2015).

Well ID	Screened Interval (feet)	Hantush	Theis	Hantush	Theis	Average	Average
		Kh (feet/day)		T (feet^2/day)		Kh (feet/day)	T (feet^2/day)
L8DR1U	22-32	6.21	16.06	1,024.80	2,810.10	11.13	1,917.45
L8DR1M	38-54	3.26	13.78	537.60	2,412.30	8.52	1,474.95
L8DR1L	70-80	0.11	0.62	18.00	107.80	0.36	62.90
L8DR2U	8-18	8.80	16.46	1,452.00	2,880.00	12.63	2,166.00
L8DR2M	46-56	4.19	25.80	691.20	4,514.40	14.99	2,602.80
L8DR2L	90-100	5.64	19.68	931.20	3,443.50	12.66	2,187.35
L8WF1U	18-28	3.53	8.97	582.40	1,568.90	6.25	1,075.65
L8WF1M	56-66	12.41	43.60	2,047.20	7,629.60	28.00	4,838.40
L8WF1L	80-90	8.81	60.01	1,454.00	10,500.90	34.41	5,977.45

The L-8 FEB originally was a mining operation and now is owned and operated by the SFWMD to provide supplemental water to Stormwater Treatment Area 1 and to support the State of Florida's Restoration Strategies plan. The site is somewhat unique for a southeastern Florida mining operation in that the mine was able to operate in relatively dry conditions within minimal dewatering pumping capacity even though the operation was drawn down tens of feet below the existing water table. The general lithology at the site is peat/fill/sand at the surface underlain by approximately 30 feet of limestone and sands. A medium to fine sand with intermittent limestone extends an additional 70 feet. Underlying this is a fine sand that extends to the base of the SAS. Gannett Fleming (2015) conducted several aquifer tests on the monitor wells installed surrounding the L-8 FEB. The results are provided in **Table 9**.

Mining operations exist near the L-8 FEB. Dunkelberger Engineering and Testing, Inc. (2009) investigated a potential mining site northwest of the L-8 FEB at the proposed C-51 Reservoir Phases I and II site. Nine borings were drilled to 50 feet bls, with geologic samples collected at 5-foot intervals. Upon completion of the boring, permeability tests were conducted at 10-foot intervals to determine aquifer parameters at each site. The lithology consisted of a 4- to 24-foot layer of sand with varying amounts of silt, shell, muck, fill, and limestone. Below this sand was an approximately 20-foot layer of silty, sandy limestone to a maximum depth of 38 feet bls. The bottom portion of each boring was a brown to gray, clean to slightly silty sand with some shell fragments. Results are provided in **Table 10**.

The above referenced reports do not encompass all investigations that have occurred in the study area over recent years; however, the results provide a more thorough understanding of the aquifer properties in the central and western portions of northern Palm Beach County. The results from these studies suggest a slightly less productive aquifer than previously anticipated for the area.

Table 9. Aquifer properties at the L-8 Flow Equalization Basin (Modified from: Gannett Fleming, 2015).

Well ID	Screened Interval (feet)	Hantush	Theis	Observation Well	Average	Observation Well	Average	Slug Test
		Kh (feet/day)				Specific Yield	T (feet^2/day)	Kh (feet/day)
L8FEB1U	49-54			1.49	1.49	0.14	261	13.47
L8FEB1M	77-82			19.02	19.02	0.14	3,329	
L8FEB1L	136-146	0.54	0.56		0.55		96	
L8FEB2U	52-57			18.79	18.79	0.10	3,120	34.00
L8FEB2M	82-87			38.91	38.91	0.16	6,460	30.19
L8FEB2L	130-140	30.43	39.08		34.75		5,769	
L8FEB3U	66-71			24.92	24.92	0.30	4,561	
L8FEB3M	93-98	6.77	6.31		6.54		1,197	
L8FEB3L	128-138			24.95	24.95	0.19	4,566	30.78
L8FEB4U	37-42	19.68	17.30		18.49		3,088	
L8FEB4M	62-67			23.78	23.78	0.04	3,971	10.40
L8FEB4L	106-116			7.36	7.36	0.13	1,229	48.93
L8FEB5U	38-43			22.84	22.84	0.01	4,089	26.09
L8FEB5M	57-62	7.01	11.04		9.03		1,616	
L8FEB5L	106-116			38.64	38.64	0.14	6,916	31.32
L8FEB6U	10-15			32.42	32.42	0.05	6,063	11.02
L8FEB6L	30-35	9.85	17.40		13.63		2,549	
L8FEB7U	8-13	1.53	6.62		4.08		110	
L8FEB7L	29-34			34.44	34.44	0.15	930	47.39
L8PZ5B	33-38			211.28	211.28	0.15	36,340	
L8PZ5C	53-58			39.90	39.90	0.22	6,864	
L8PZ5D	73-78	3.23	3.51		3.37		580	

Note: Where information was not available, cells were left blank.
Kh = hydraulic conductivity; T = transmissivity.

Table 10. Aquifer properties within the L-8 FEB (From: Dunkelberger Engineering and Testing, Inc., 2009).

Observation Well	Pumping Rate (cfs)	5-10 foot Interval	15-20 foot Interval	25-30 foot Interval	35-40 foot Interval	45-50 foot Interval	**Average**
		Hydraulic Conductivity (Kh) (feet/day)					
TMW-101	5.0-10.0		20.20	20.50	7.80	8.40	**14.23**
TMW-102	0.5-15.0	1.90	21.40	42.40	5.50	22.00	**18.64**
TMW-103	1.0-10.0	3.70	27.10	14.00	4.50	3.70	**10.60**
TMW-104	1.3-15.0	4.30	77.30	9.90	7.20	4.60	**20.66**
TMW-105	0.1-10.0	0.40	14.70	7.30	6.00	26.90	**11.06**
TMW-106	0.5-10.0	2.10	29.70	4.90	2.70	18.90	**11.66**
TMW-108	5.0-10.0	17.50	22.20	8.00	12.30	10.20	**14.04**
TMW-110	5.0-10.0	16.80	25.20	8.90	7.60	13.70	**14.44**
	Average	**6.67**	**29.73**	**14.49**	**6.70**	**13.55**	**14.42**

cfs = cubic feet per second.

2.6 Water Use

Within the LECSR-NP active model area, groundwater and surface water withdrawals for PWS, industrial use (including power plants), landscaping, and recreational water use (including golf courses) were identified from the SFWMD permit database. Permits were screened to exclude those withdrawing from sources other than the SAS (e.g., surface water, the Floridan aquifer system), except for the City of West Palm Beach's PWS permit, which lists surface water as the primary source of water. Permits were grouped into several water use categories such as nursery irrigation, agriculture purposes, golf course irrigation, and landscape purposes. A total of 121 permits were used: 17 PWS permits, 2 nursery permits, 54 landscape permits, 7 industrial permits, 34 golf course permits, and 7 agriculture permits.

Water use totals and average annual water use per county for withdrawals from the SAS in the active model area are shown in **Table 11**. During the calibration period (2006 to 2014), permitted PWS withdrawals averaged approximately 98 million gallons per day (mgd), with 91 mgd withdrawn in Palm Beach County and only a small portion of that water used in Martin County. The largest PWS users were the City of West Palm Beach, Palm Beach County Water Utilities Department, and Seacoast Utility Authority. In Martin County, golf courses are the second largest use type, closely followed by agricultural users. On average, during the calibration period, landscape, industrial, and nursery water users within Martin County use less than 1 mgd each. In Palm Beach County, the second largest user is landscape irrigation, followed by golf courses and industrial permits. On average, agricultural users and nurseries used less than 0.5 mgd during the calibration period.

Table 11. Average groundwater withdrawals (in mgd) in the LECSR-NP active model area, including surface water withdrawals for the City of West Palm Beach.

County	Agriculture	Golf Courses	Industrial	Landscape	Nurseries	Public Water Supply	**Total**
Martin	2.70	3.12	0.64	0.75	0.16	6.45	**13.82**
Palm Beach	0.30	6.58	1.33	8.37	0.09	91.20	**107.87**
Total	**3.00**	**9.70**	**1.97**	**9.12**	**0.25**	**97.65**	**121.69**

Note: Industrial and Public Water Supply values are actual reported values; all other types are estimated values based on the Agricultural Field-Scale Irrigation Requirements Simulation (AFSIRS).

Figure 18 shows the distribution of simulated SAS average water use across the LECSR-NP active model area. Values are for the SAS and do not account for surface water or other aquifer withdrawals, except the City of West Palm Beach. Approximately 80 percent of total water use is for PWS. Golf courses are the second largest user; however, golf courses only account for 8 percent of the water withdrawn from the SAS. Water use for landscape permits are only slightly less than golf courses. Agriculture, industrial, and nursery permits make up the remaining water use categories modeled in the LECSR-NP.

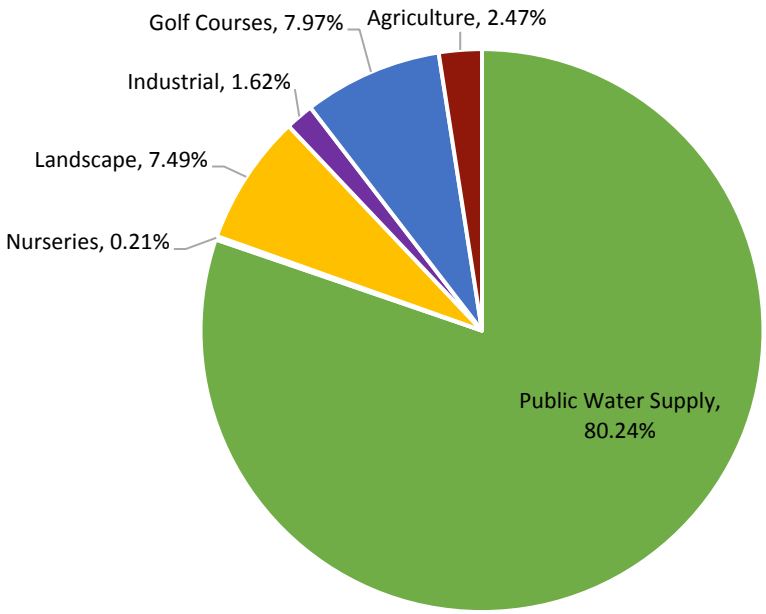

Figure 18. Water use by type applied in the LECSR-NP.

3. SIMULATION OF THE FLOW SYSTEM

3.1 Computer Code Selection

MODFLOW (Harbaugh et al., 2000), a code created and updated by the USGS, was used for this modeling effort. MODFLOW has been widely accepted in the groundwater modeling profession for many years, it is in the public domain, and its modular structure allows for additional hydrologic functionality.

MODFLOW simulates groundwater flow in aquifer systems using the finite difference method. The aquifer system is divided into rectangular or quasi-rectangular blocks (called cells) by a grid. The cells are organized by rows, columns, and layers. MODFLOW allows the user to specify which cells are within the groundwater flow system (i.e., are active) and which cells are outside of the groundwater flow system (i.e., are inactive). For each active cell, the user must specify aquifer properties and information related to wells, canals, and other hydrologic features.

The MODFLOW model code consists of a main program and a series of independent subroutines called modules. The modules are grouped into packages that address a particular hydrologic process or solution algorithm. For the LECSR-NP, the following MODFLOW version 2000 standard packages were used: Basic (BAS6), Block-Centered Flow (BCF6), Drain (DRN), River (RIV), General Head Boundary (GHB), Recharge (RCH), Evapotranspiration (EVT), and Strongly Implicit Procedure (SIP).

Numerous MODFLOW packages have been developed specifically for the SFWMD to simulate additional hydrologic functionality. Some packages were used for the LECSR-NP (**Table 12**) and are discussed in greater detail in Giddings et al. (2006).

Table 12. MODFLOW add-on packages used in the LECSR-NP.

Package	Author(s)	Description
Utility Generation (UGEN)	Restrepo et al. (2003)	Creates input files during model execution by linking static (time invariant) data with time series (variant) data.
Wetland (WTL)	Restrepo et al. (1998)	Simulates overland flow in wetlands using the uppermost model layer and barriers to flow.
Reinjection Drain Flow (RDF)	Jones (1999)	Similar to the Drain package, but it allows water to be redirected to another location instead of being permanently removed from the model.
Diversion (DIV)	Restrepo et al. (1998)	Simulates the effects of water control structures (e.g., pump stations, gravity flow drains, weirs) on water levels.
Trigger (TRG)	Randall (1992)	Simulates wellfield withdrawal cutbacks as a function of water level in trigger cells and in Lake Okeechobee; simulates Lower East Coast water shortage policy associated with saltwater intrusion.
Multiple Wells (WEL)	Rodberg (1999)	Simulates withdrawals from wells by reading multiple input files.
Output Control Summation (OC)	Welter (1999)	Sums cell-by-cell flows to reduce output size.
Multibud (BUD)	Ecology and Environment, Inc. (2004a)	Outputs an internal water budget for a set of specified cells at a given frequency to reduce output size.

3.2 Evapotranspiration and Recharge

Standard MODFLOW recharge (RCH) and evapotranspiration (EVT) packages were used to simulate recharge and ET rates, respectively, in the model. These packages require estimated maximum recharge and ET rates for each cell that could intersect with the water table. In South Florida, rainfall typically does not directly equal the recharge that could reach the aquifer based on unsaturated zone uptake from storage and ET as well as from surface water runoff. To account for losses, a pre-processor was developed to better estimate these rates (Restrepo and Giddings, 1994). The ET and recharge estimates are calculated using the Agricultural Field Scale Irrigation Requirement Simulations program (AFSIRS) developed at the University of Florida (Smajstrla, 1990) coupled with the standard National Resources Conservation Service curve number approach for determining event-based runoff (United States Department of Agriculture, 1986). An iterative calibration approach is implemented between the ET-Recharge parameters and the MODFLOW model parameters. An updated version of this processor, which went through USACE Agency Technical Review, was utilized for this study (Bandara, 2018).

The AFSIRS program is a daily root-zone water balance model that uses daily rainfall, potential ET (PET), land use, soil type, crop coefficients, and irrigation rates, system type, and efficiency. The program originally was developed to estimate irrigation demands and was adapted to simulate non-irrigated areas as well. **Figure 19** shows various irrigated root zone processes considered in the AFSIRS program. AFSIRS calculates soil water content (STO), net irrigation requirement (NIR), net drainage (DR), and ET deficit terms for the root zone. This drainage term, or the volume of water that passes through the unsaturated zone to the water table, is the daily maximum input rate applied to the MODFLOW Recharge package. When

applying the tool to a diverse land use environment, three distinct recharge and ET areas emerge; irrigated areas, non-irrigated areas, and open water areas. In non-irrigated areas, vegetation uses the available water in the unsaturated zone and supplements the additional demands from the water table, if the extinction depth of the plant is greater than the depth to the water table. Thus, the potential groundwater ET becomes the potential ET minus the unsaturated zone ET, as calculated from the AFSIRS program. The potential ET for any crop type is equal to the reference ET multiplied by the crop coefficient, Kc (Potential ET = Reference ET × Kc). The reference ET is the rate at which water would be removed from the soil and plant surface of actively grown grass. The crop type is determined by the land use designation. The potential groundwater ET is then passed to MODFLOW, which calculates the actual groundwater ET based on the distance from the ET surface to the water table and on the extinction depth of the crop. In irrigated areas, the crop demand is met first from rainfall and available soil moisture content and then supplemented from an irrigation source. This results in the net saturated zone ET approaching zero. Conversely—for open water areas such as lakes, rivers, and other areas where the water table surface is exposed—recharge will equal rainfall and the ET will equal or be close to the potential ET rates.

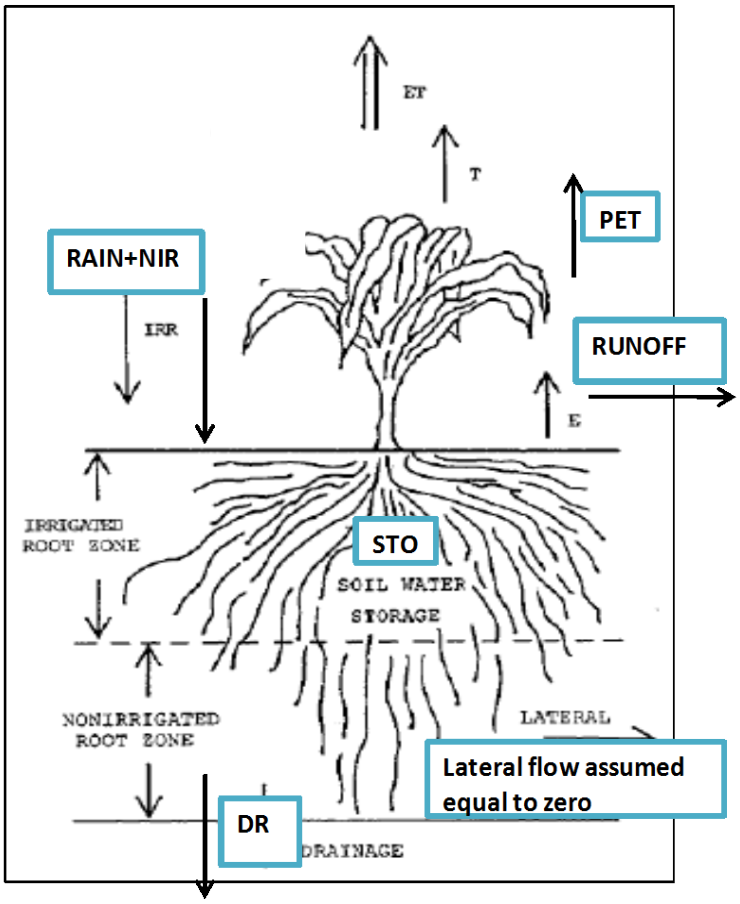

Figure 19. General schematic of the Agricultural Field Scale Irrigation Requirement Simulations program (Modified from: Smajstrla, 1990).

The main input requirements for the ET-Recharge-Runoff program include daily rainfall and reference ET data. Surface water basin delineations are required to calibrate the structure flows and follow the USGS hydrologic unit code (HUC) subdivisions. The Florida Land Use Cover Classification Systems (FLUCCS) codes were used to delineate the land use classifications of which the percent pervious and the crop type are defined. Crop information includes the crops normally grown in South Florida, their crop coefficients, whether the crop is irrigated or not, the growing season, the root zone depth, and the irrigation type and

efficiency. The final input requirement is the hydrologic soil data based on the four main types and combinations (A, B, C, D, A/D, B/D, and C/D), defined by the United States Department of Agriculture (1986). Runoff curve numbers depend on the Florida Land Use Cover Classification Systems code and the soil type.

An iterative approach between the ET-Recharge-Runoff program and MODFLOW was implemented during the calibration process to address surface water structure flows as well as surface and groundwater stages. The National Resources Conservation Service curve number method assumes runoff occurs instantaneously, which is not the case in the LECSR-NP study area. To overcome this, the Muskingum method (Cunge, 1969) was used to route the direct runoff produced from the ET-Recharge-Runoff program, which applies the time lag and attenuates the peaks in the runoff hydrograph. The first iteration of the process was to run the MODFLOW model with the initial ET and recharge estimates and compare the observed stream flow hydrograph with the simulated flows and the simulated versus observed stages from the monitoring network. Because the curve numbers were estimated for normal conditions, adjustments were made to the curve numbers to account for the antecedent moisture content on a running 5-day cumulative rainfall for wet and dry season conditions using the method outlined by Chow et al. (1988). After review of the model results, a second iteration was conducted where the curve number, Muskingum routing parameters, extinction depths, and river and/or drain conductance were adjusted to achieve a better match between the observed and simulated flows and heads. The second process was repeated until reasonable matches and statistics were achieved. **Figure 20** shows the various input data used and output data produced by the ET-Recharge-Runoff program and how the different model components fit together in the iterative calibration process.

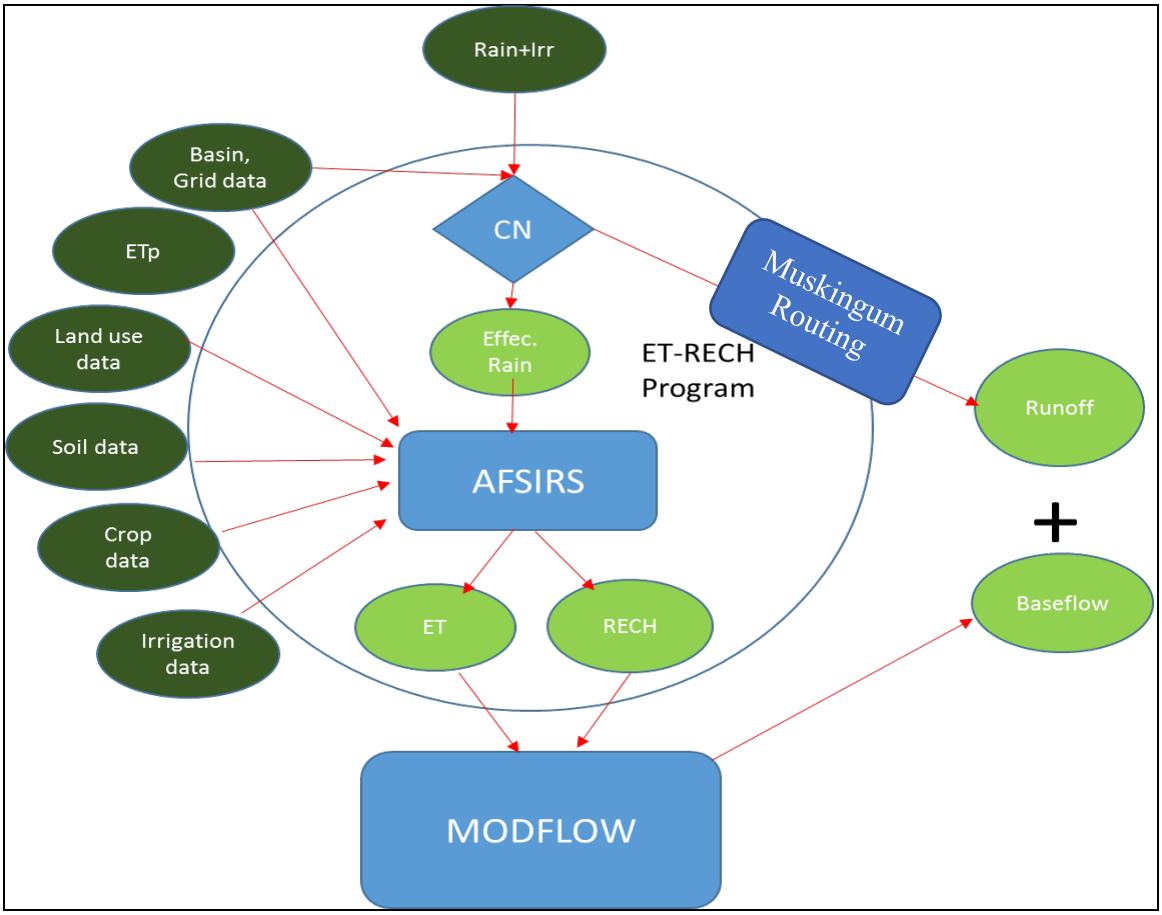

Figure 20. MODFLOW and Evapotranspiration-Recharge tool calibration flow chart.

Outputs from the ET-Recharge-Runoff package are shown in **Figures 21** to **27**. For each output, graphics were developed for 2011 and 2013 to represent conditions during a dry year (2011) and a wet year (2013). **Figures 21** and **22** show the spatial distribution of runoff for 2011 and 2013, respectively. The dark green areas in these figures represent wetlands where recharge equals rainfall and there is zero runoff. **Figures 23** and **24** show the spatial distribution of unsaturated zone ET rates for 2011 and 2013, respectively. Because wetland areas are considered saturated, these areas have values near zero for the unsaturated zone ET rate. **Figures 25** and **26** show the spatial distribution of maximum potential ET from the saturated zone for 2011 and 2013, respectively. **Figure 27** shows the spatial distribution of the extinction depths used in the LECSR-NP active model area.

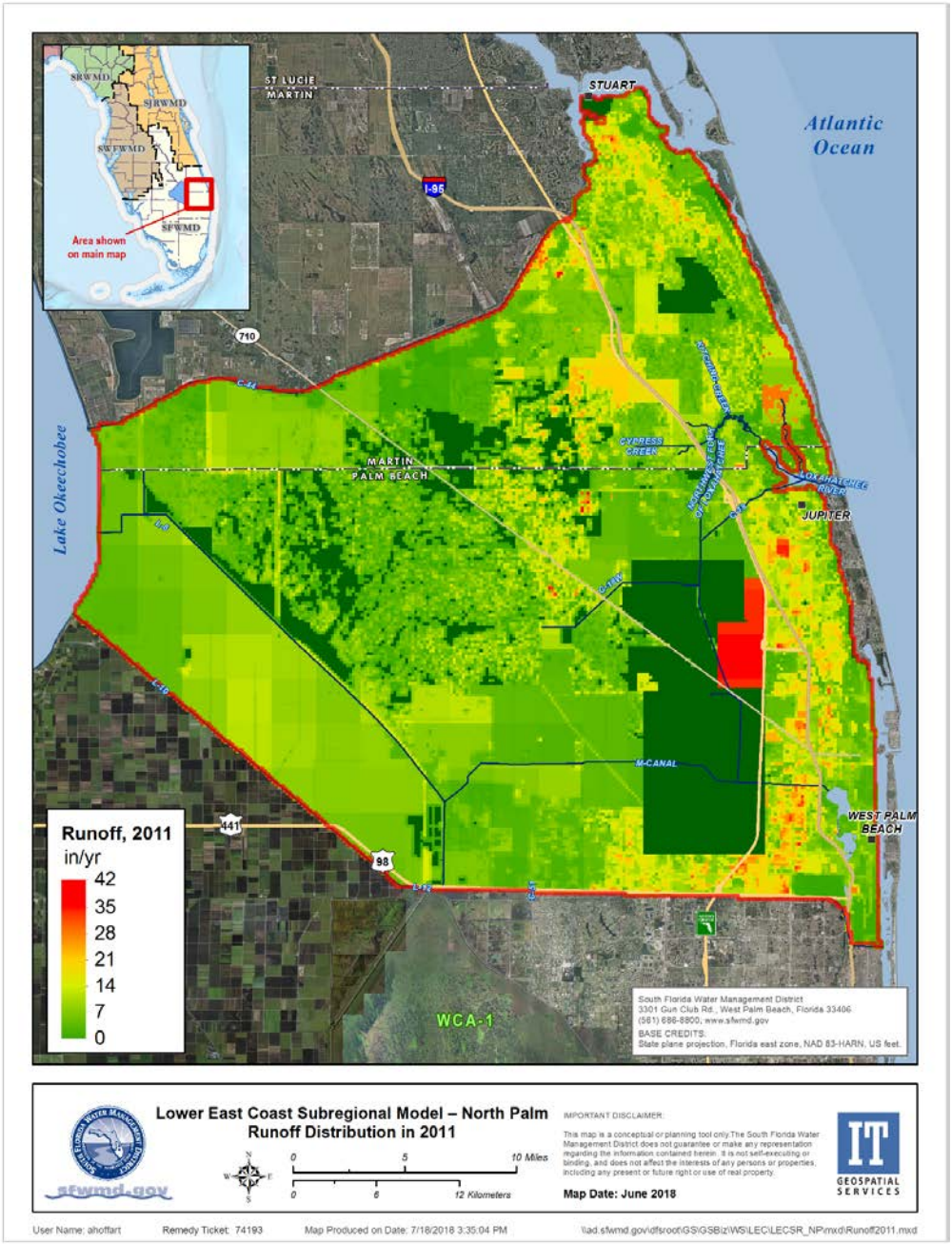

Figure 21. Spatial distribution of runoff derived from the Evapotranspiration-Recharge program for 2011.

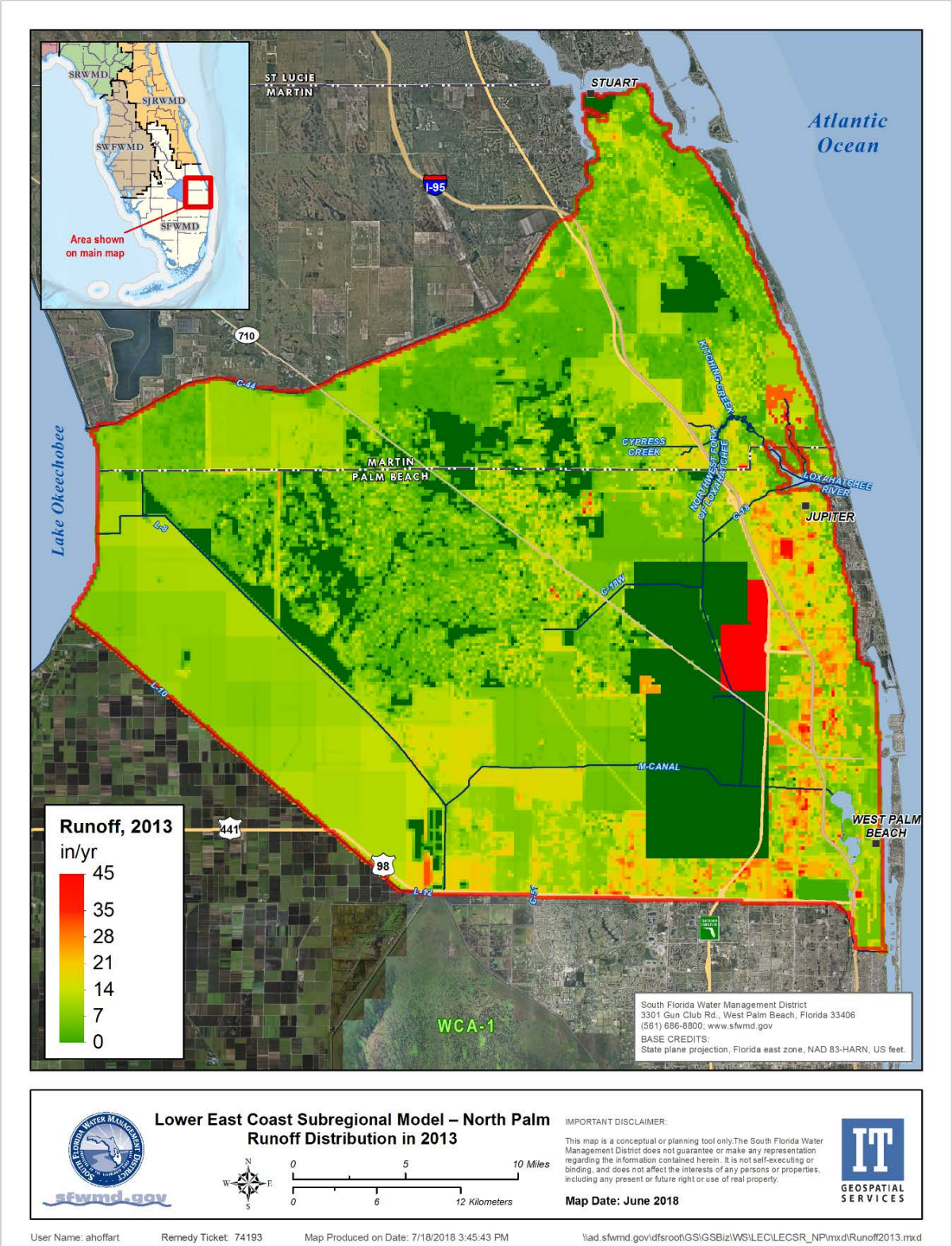

Figure 22. Spatial distribution of runoff derived from the Evapotranspiration-Recharge program for 2013.

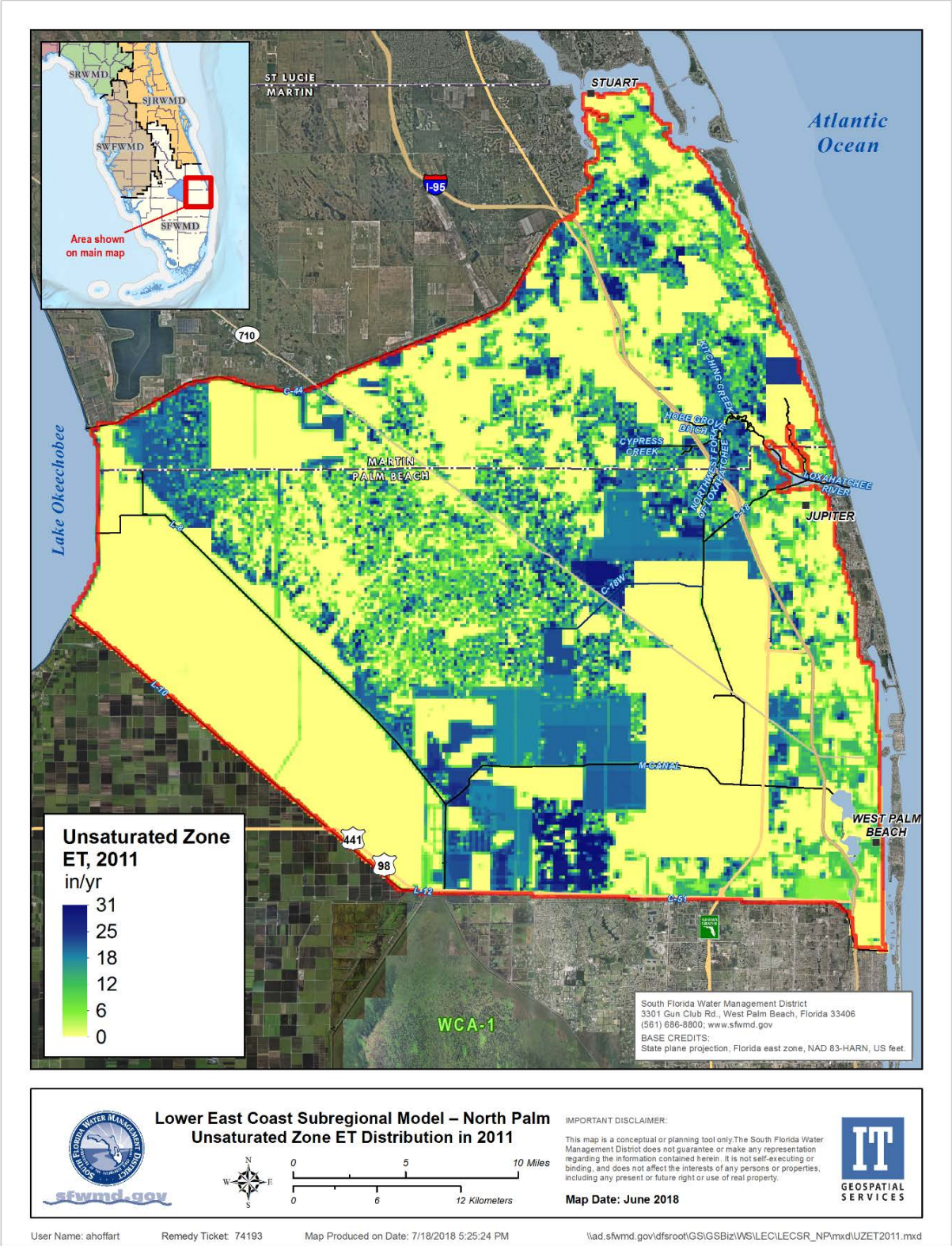

Figure 23. Spatial distribution of unsaturated zone evapotranspiration derived from the Evapotranspiration-Recharge program for 2011.

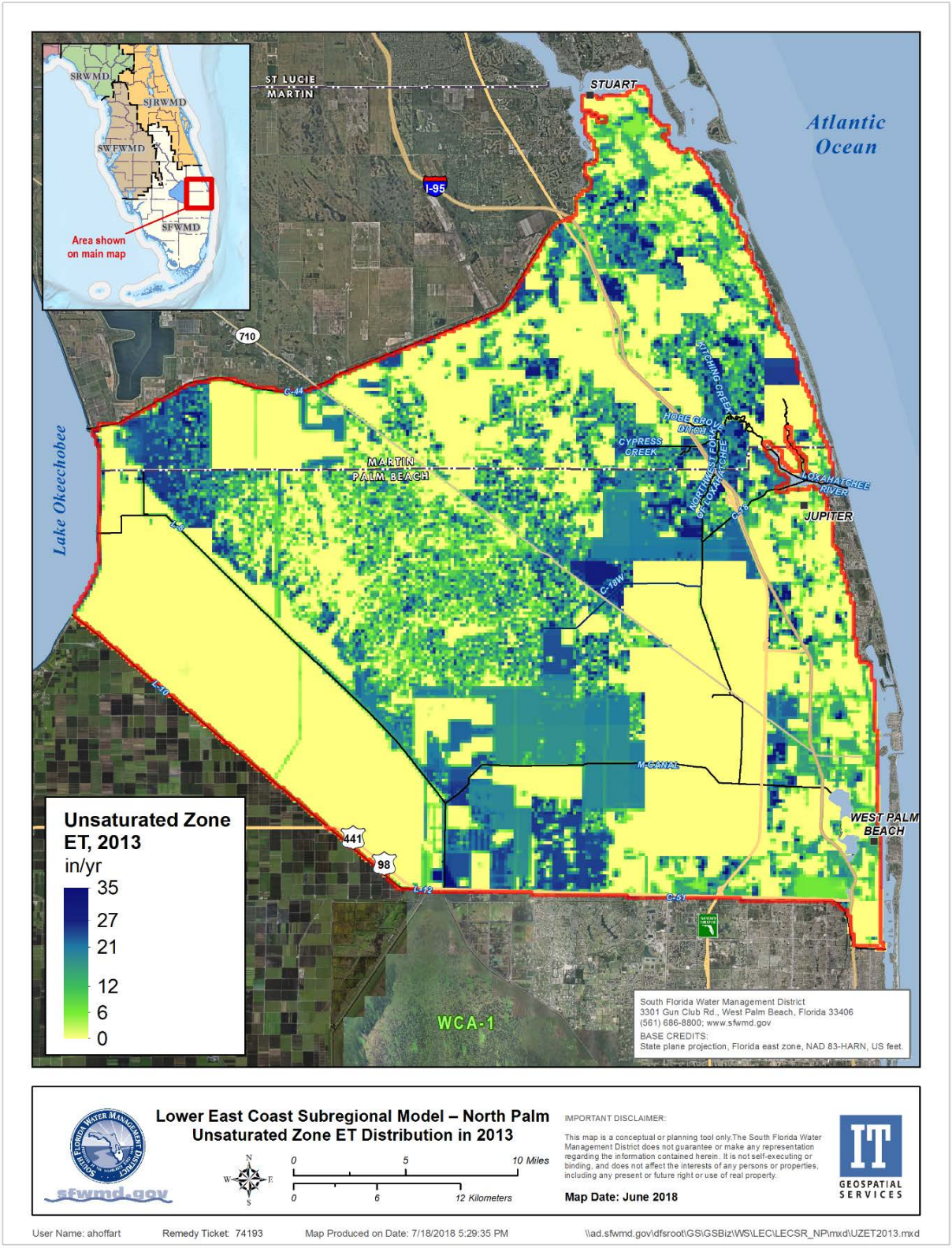

Figure 24. Spatial distribution of unsaturated zone evapotranspiration derived from the Evapotranspiration-Recharge program for 2013.

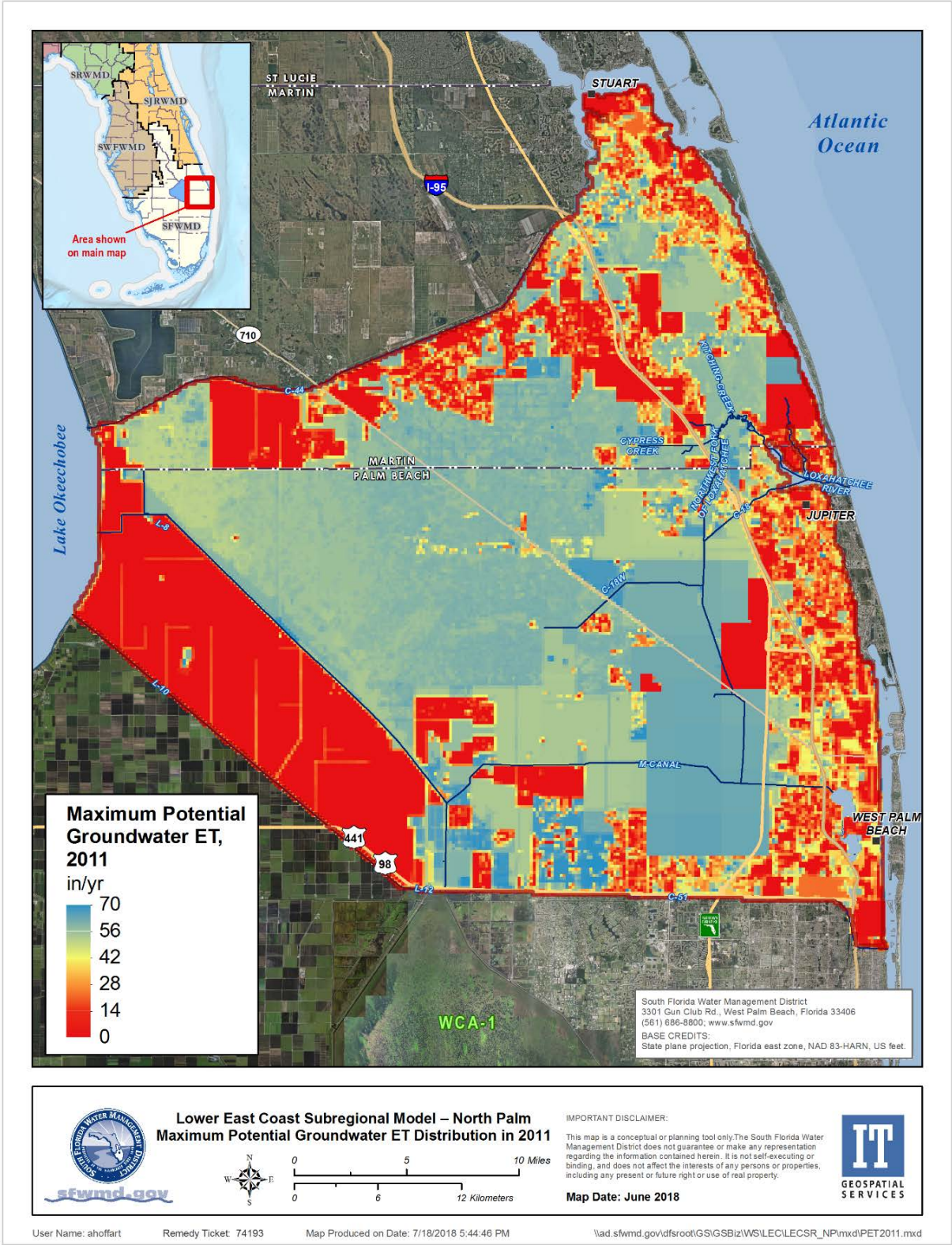

Figure 25. Spatial distribution of maximum potential groundwater evapotranspiration derived from the Evapotranspiration-Recharge program for 2011.

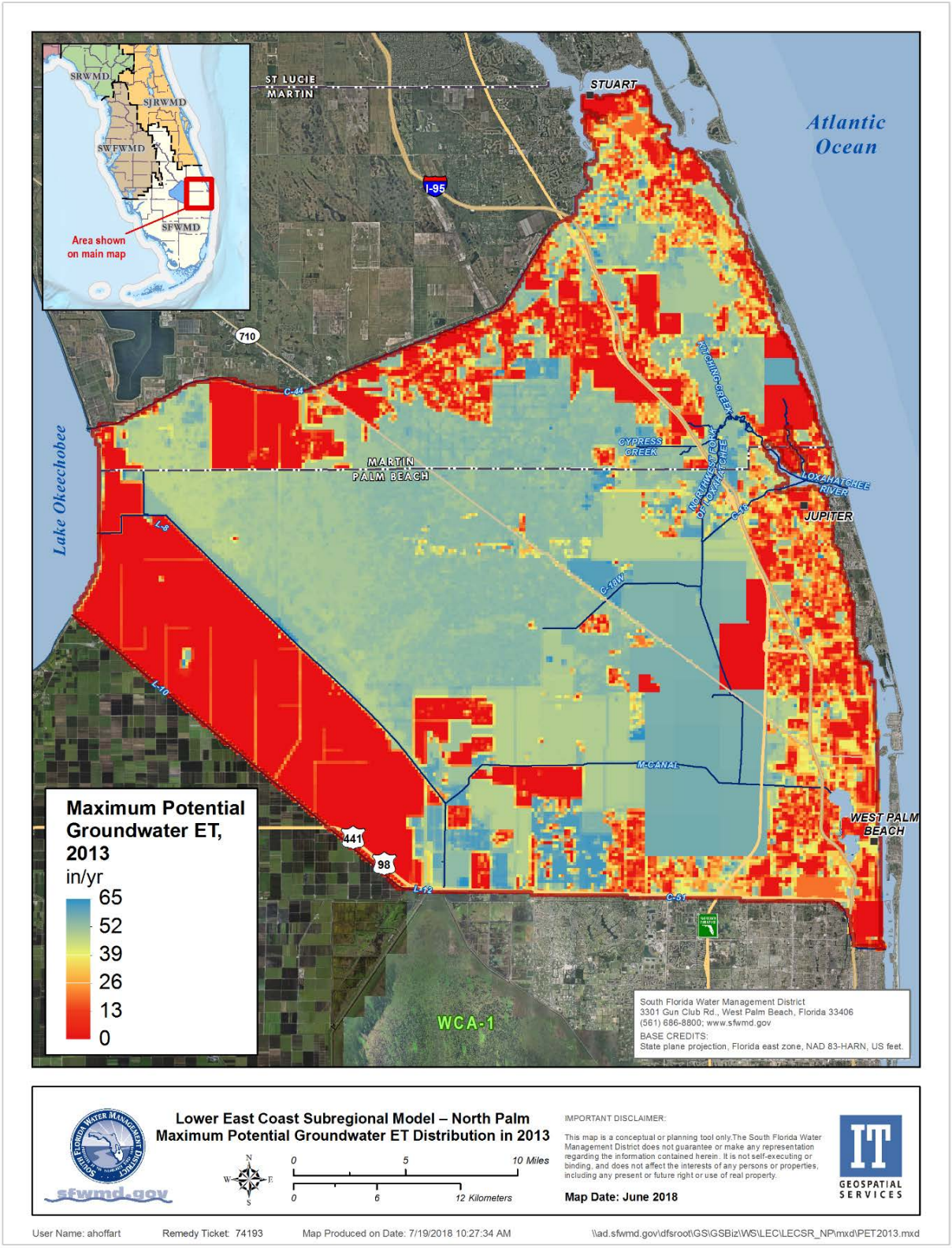

Figure 26. Spatial distribution of maximum potential groundwater evapotranspiration derived from the Evapotranspiration-Recharge program for 2013.

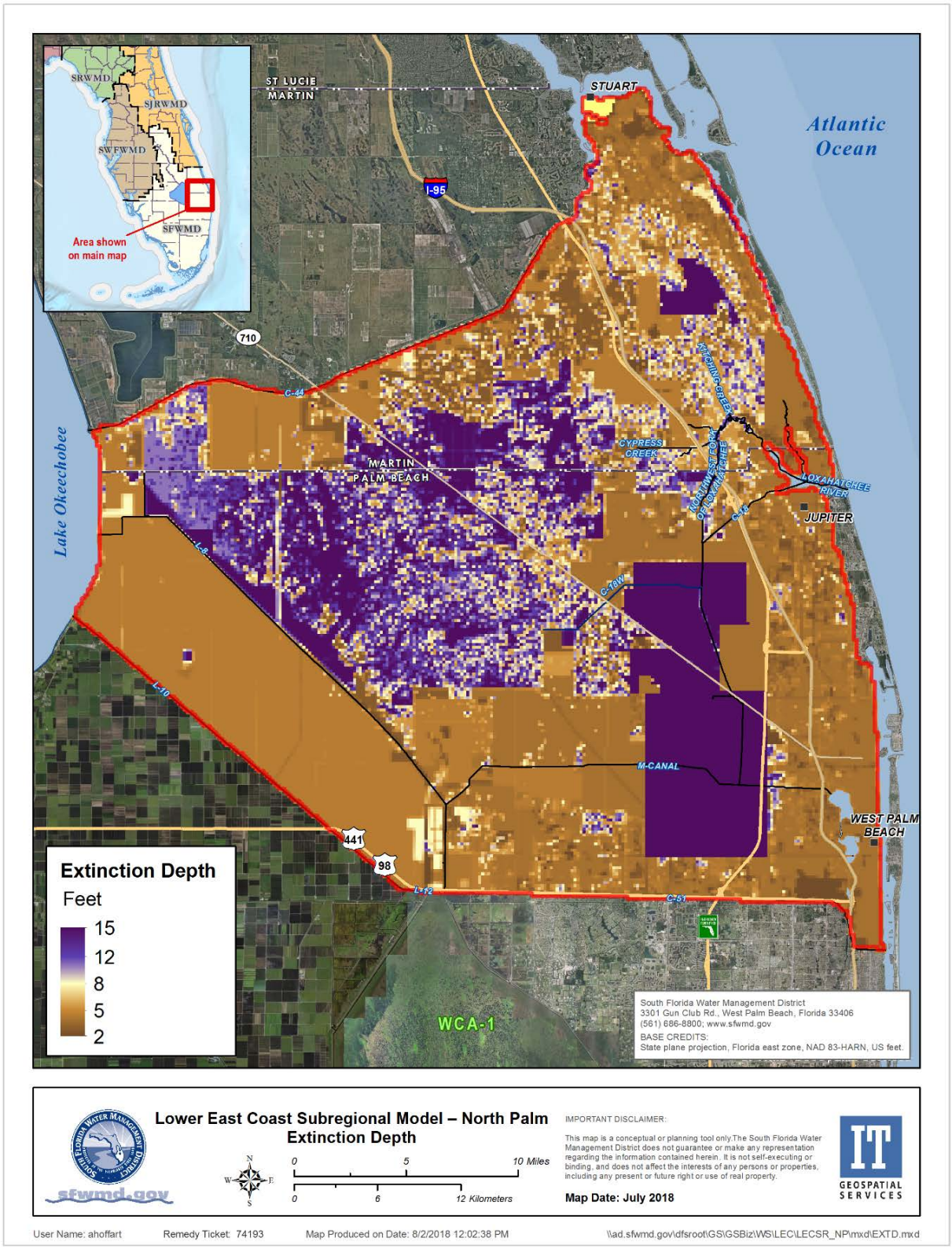

Figure 27. Spatial distribution of extinction depths across the LECSR-NP active model area.

3.3. Model Design

3.3.1 Spatial and Temporal Discretization

The LECSR-NP uses the same model grid as the LECSR, except the area south of the study area is inactivated. Therefore, model execution time and disk storage are reduced substantially. The grid cells are 704 feet by 704 feet (each cell covering approximately 11 acres) with 292 rows and 408 columns, resulting in a full grid of 119,136 cells per layer. The grid limits of the LECSR-NP, from the lower left corner node coordinates (x_{min}, y_{min}) are given as (680961.0, 839750.0) in U.S. State Plane, Florida East Zone, NAD83. Selecting the cell size was a compromise between the regional (i.e., large nodal spacing) and local (i.e., small nodal spacing) hydraulic gradients present in South Florida.

The LECSR-NP was developed for transient conditions. A temporal discretization of one day was chosen. This discretization was applied as a daily time step in a daily stress period. Daily input data were available to construct the hydrologic packages (e.g., ET, Recharge, River, Drain, GHB, Reinjection Drain Flow [RDF], Diversion), except in the case of pumping stresses. Average monthly pumping rates (fluxes) were used to generate daily withdrawals because pumping records are compiled monthly. This uniform grid and daily stress period allowed for an adequate level of subregional accuracy with manageable run and post-processing times.

3.3.2 Groundwater Flow System

3.3.2.1 Vertical Discretization

The LECSR-NP is divided into three vertical layers based on hydrostratigraphic subdivisions. The uppermost layer (Layer 1) generally consists of the sands and lower permeable limestone and sandstone units deposited during the end of the Pleistocene and Holocene. Layer 2 composes the early and middle Pleistocene and Pliocene deposits for the Fort Thompson, Anastasia, and Caloosahatchee formations, which generally are the more productive units of the SAS in the study area. Layer 3 is the Tamiami Formation, consisting of the Pinecrest sands and Ochopee limestone. A complete discussion of the vertical discretization of the model can be found in Giddings et al. (2006), which has been updated with the recent boring information discussed in the **Section 2.5**. **Figure 28** shows the general modeling layering, elevations, and thickness ranges.

3.3.2.2 Aquifer Properties

The hydraulic conductivities used in the LECSR-NP were obtained from multiple sources and use the existing LECSR as a basis. Aquifer parameters were updated with recent information collected at the sites identified in the **Section 2.5**. Noticeable changes mainly occurred near the L-8 Canal close to the mining operations where the properties of the upper portion of the SAS are substantially lower than previously estimated. A composite transmissivity of the SAS is presented in **Figure 29**.

3.3.2.3 Initial Conditions

To develop the initial conditions for the LECSR-NP, an initial set of model input parameters and hydrologic inputs were used to create a pseudo-steady-state run. The output from the pseudo-steady-state run was compared to observed historical data. If the results from the run were vastly different from observed historical heads, modifications were made to the initial conditions and the run was repeated. This process was repeated until the first 30 stress periods were stable.

Series	Lithostratigraphic Units			Approximate Thickness (feet)	Lithology	Hydrologic Unit	Approximate Thickness (feet)	Model Layer
Holocene	Undifferentiated Soil and Sand	H	Undifferentiated	0-5	Marl, peat, organic soil, quartz sand	Surficial Aquifer System	0-200	1
Pleistocene	Pamlico Sand	H-Q5		0-50	Quartz sand			
	Fort Thompson Formation	Q5-Q4		0-100	Marine limestone and minor gastropod-rich freshwater limestone			
	Anastasia Formation	Q5-Q4		0-200	Coquina, quartz sand and sandy limestone			
	Fort Thompson Formation	Q3-Q1		0-100	Marine limestone and minor gastropod-rich freshwater limestone			2
	Anastasia Formation	Q3-Q1		0-200	Coquina, quartz sand and sandy limestone	Biscayne Aquifer		
	Pinecrest Sand Member	T2	Tamiami Formation	0-90	Quartz sand, pelecypod-rich quartz sandstone, terrigenous mudstone	Upper Semiconfining to Confining Unit	0-130	3
Pliocene	Ochopee Limestone Member	T1		0-130	Pelecypod lime rudstone and floatstone, pelecypod-rich quartz sand, moldic quartz sandstone	Gray Limestone or Lower Tamiami Aquifer		

Figure 28. Model layering scheme and typical materials, average elevations, and thickness ranges.

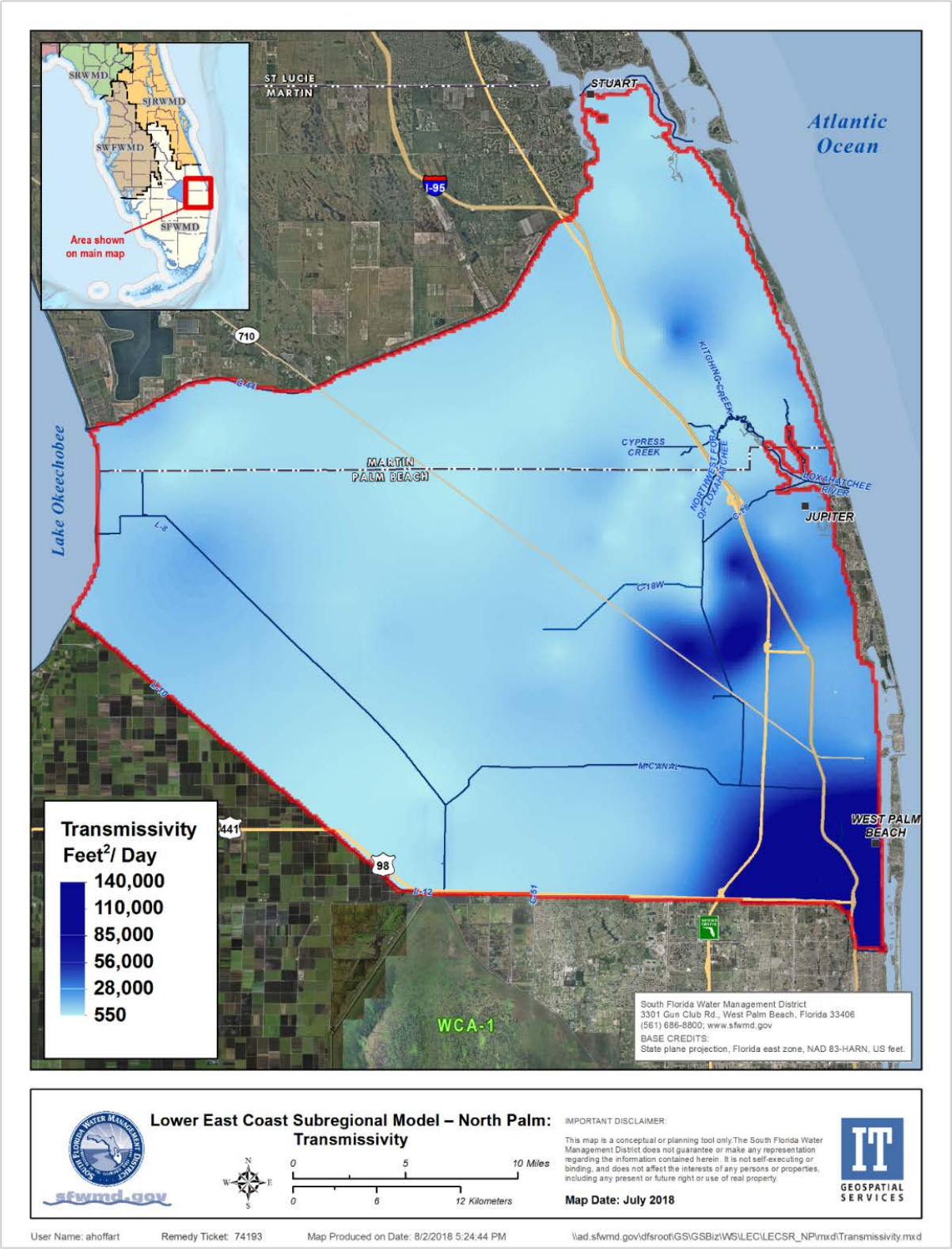

Figure 29. Transmissivity of the surficial aquifer system for the LECSR-NP.

3.3.2.4 Groundwater Recharge and Saturated Zone Evapotranspiration

Groundwater recharge and saturated zone ET were derived from the ET-Recharge-Runoff program. **Figures 30** and **31** show the spatial distribution for groundwater recharge in 2011 and 2013, which are representative of a dry year and a wet year, respectively. **Figures 32** and **33** show the spatial distribution for the saturated zone ET in 2011 and 2013, respectively.

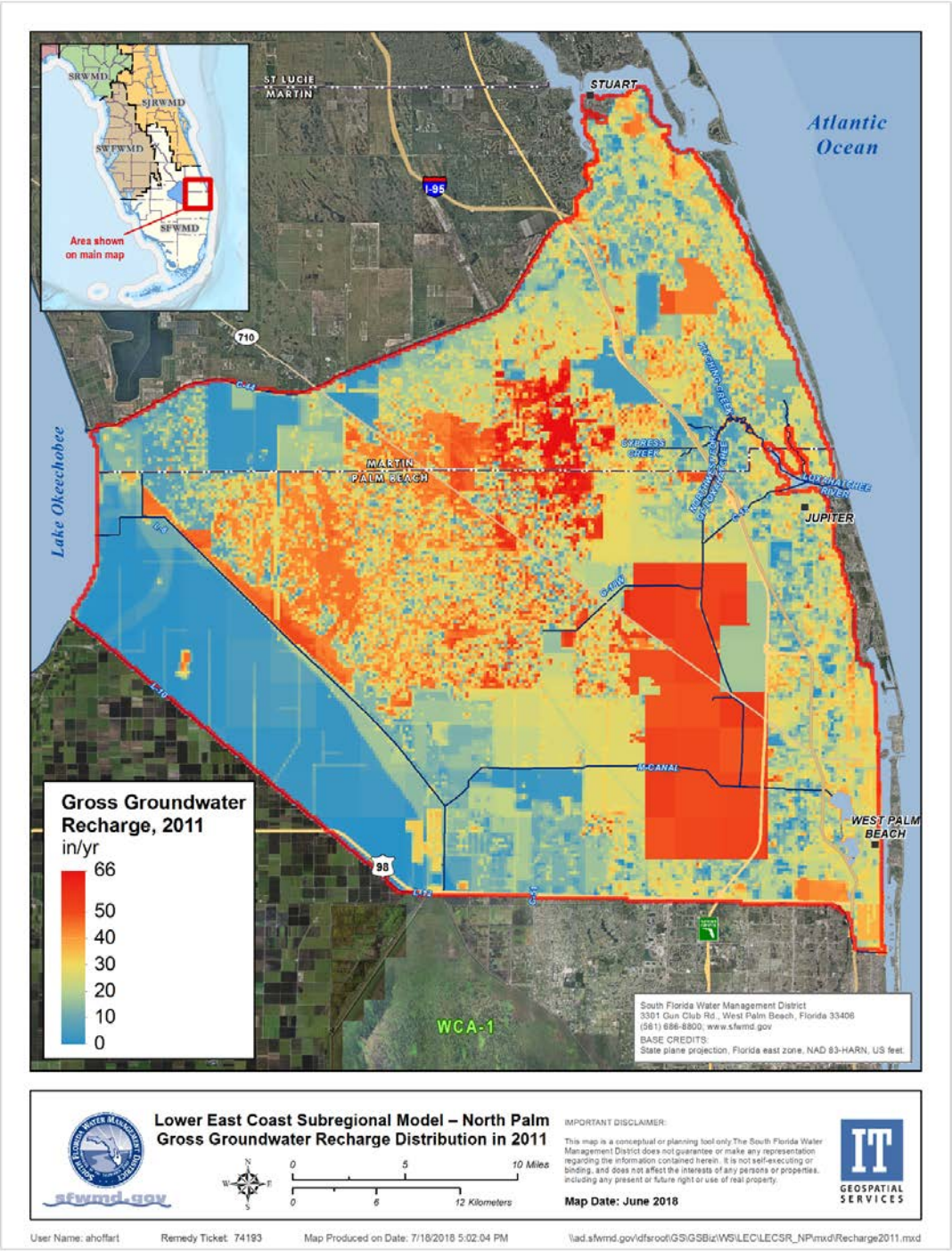

Figure 30. Spatial distribution of groundwater recharge derived from the Evapotranspiration-Recharge-Runoff program across the LECSR-NP active model area in 2011.

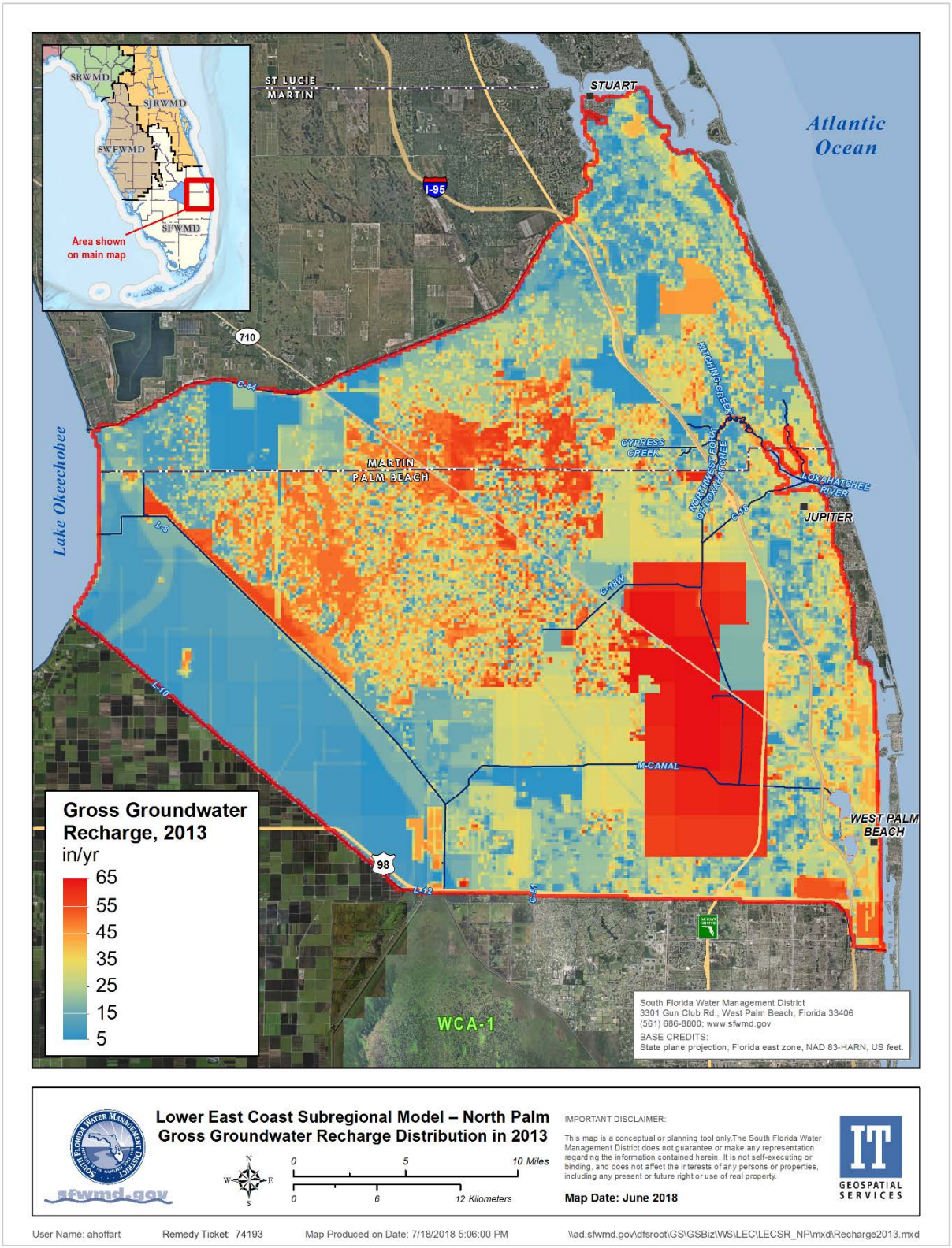

Figure 31. Spatial distribution of groundwater recharge derived from the Evapotranspiration-Recharge-Runoff program across the LECSR-NP active model area in 2013.

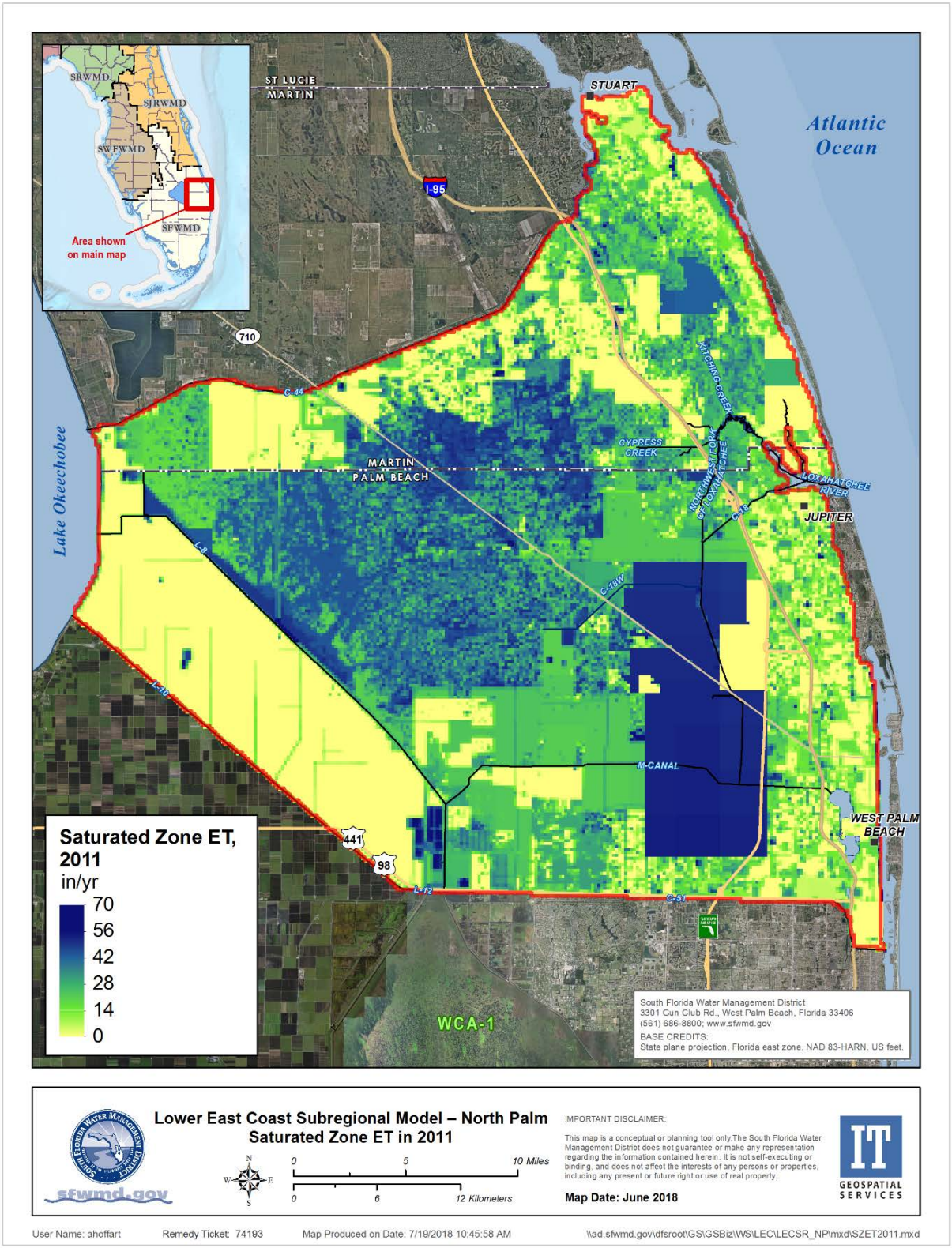

Figure 32. Spatial distribution of saturated zone evapotranspiration derived from the Evapotranspiration-Recharge-Runoff program across the LECSR-NP active model area in 2011.

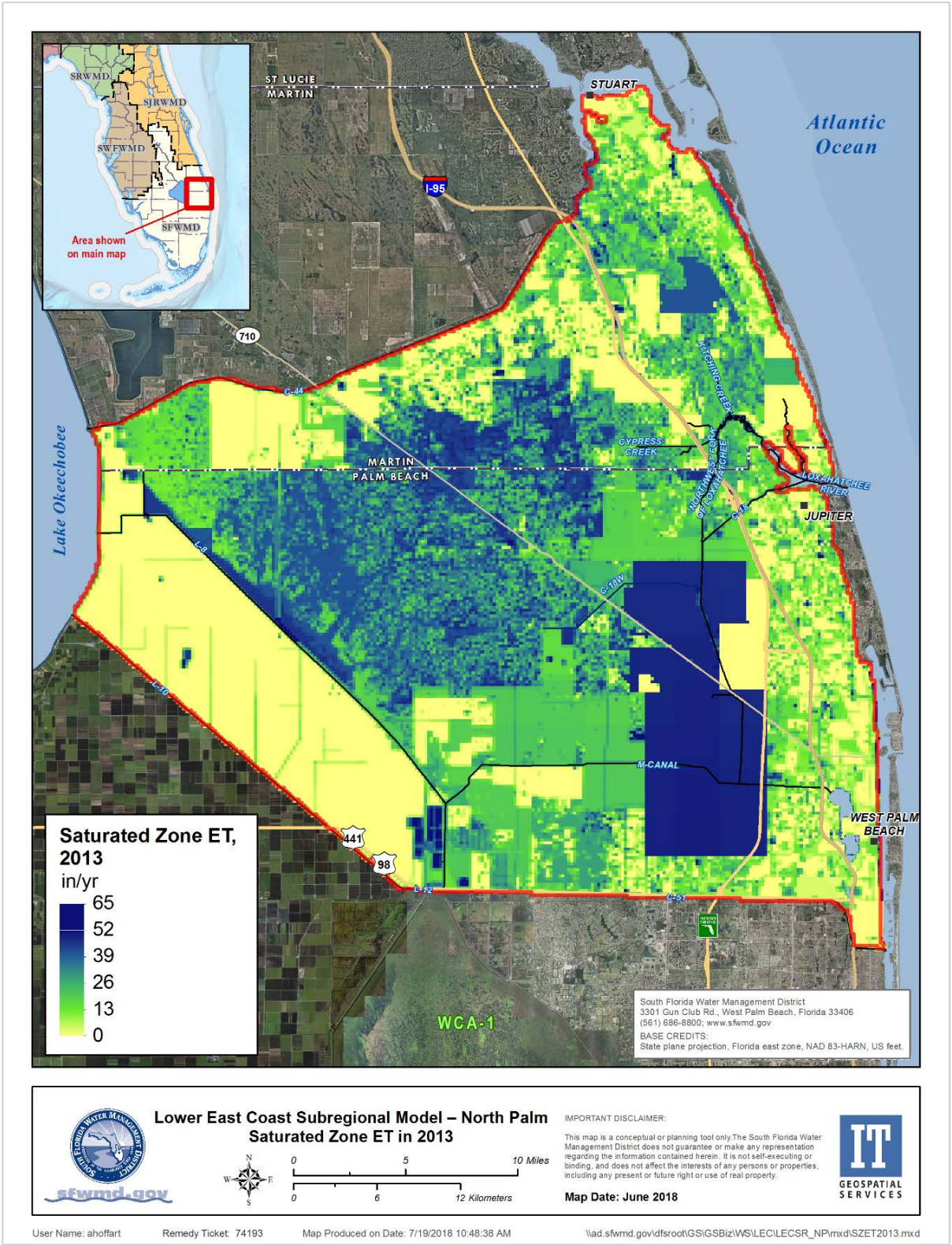

Figure 33. Spatial distribution of saturated zone evapotranspiration derived from the Evapotranspiration-Recharge-Runoff program across the LECSR-NP active model area in 2013.

3.3.2.5 Surface Water Flow System

Several MODFLOW packages were used to simulate the surface water flow system. **Figures 34** to **40** show the spatial distribution of the cells for each package. **Figure 34** shows the spatial distribution of the cells classified as wetlands. The Wetland package was used to simulate overland flow using the Kadlec (1990) equation:

$$q = K\, h^{\beta} S_f^{\alpha}$$

For areas classified as wetlands, runoff was not calculated by the ET-Recharge program and was set to zero. In addition to simulating areas classified as wetlands according to the most recent land use/land cover data, the Wetland package can be used to simulate barriers to flow, such as seepage barriers and levees. For the LECSR-NP, a barrier is simulated in Flow-way 3 along Pine Glades, where Palm Beach County placed a seepage barrier during restoration efforts.

Figure 35 shows the spatial distribution of the drains simulated in the model domain. The Drain package was used to simulate any existing drainage canals at their control elevation and effectively removes this water from the model area once the control elevation is reached. If the existing drainage canals typically route water from one area to the next, the network was simulated with the Diversion or RDF package.

Figure 36 shows the spatial distribution of the river segments simulated in the model domain. The River package was used to simulate primary canals with a known historical stage, such as the L-8 Canal. When water needs to be routed through the canal using stages and flows, either the Diversion or RDF package was used.

Figures 37 and **38** show the spatial distribution of the source and sink cells used in the Diversion package, respectively. The Diversion package introduces routed runoff from the ET-Recharge program into the model. The Diversion package also simulates the movement of water using set stage criteria for the source and sink cells, along with a flow volume, which is sent only when the model cells have met the stage criteria.

Figures 39 and **40** show the spatial distribution of the source and sink cells used in the RDF package, respectively. The RDF package is used when a daily stage constraint is used to move water from one cell to another cell. The use of the RDF and Diversion packages accounts for the amount of water that is moved from one area of the model to another.

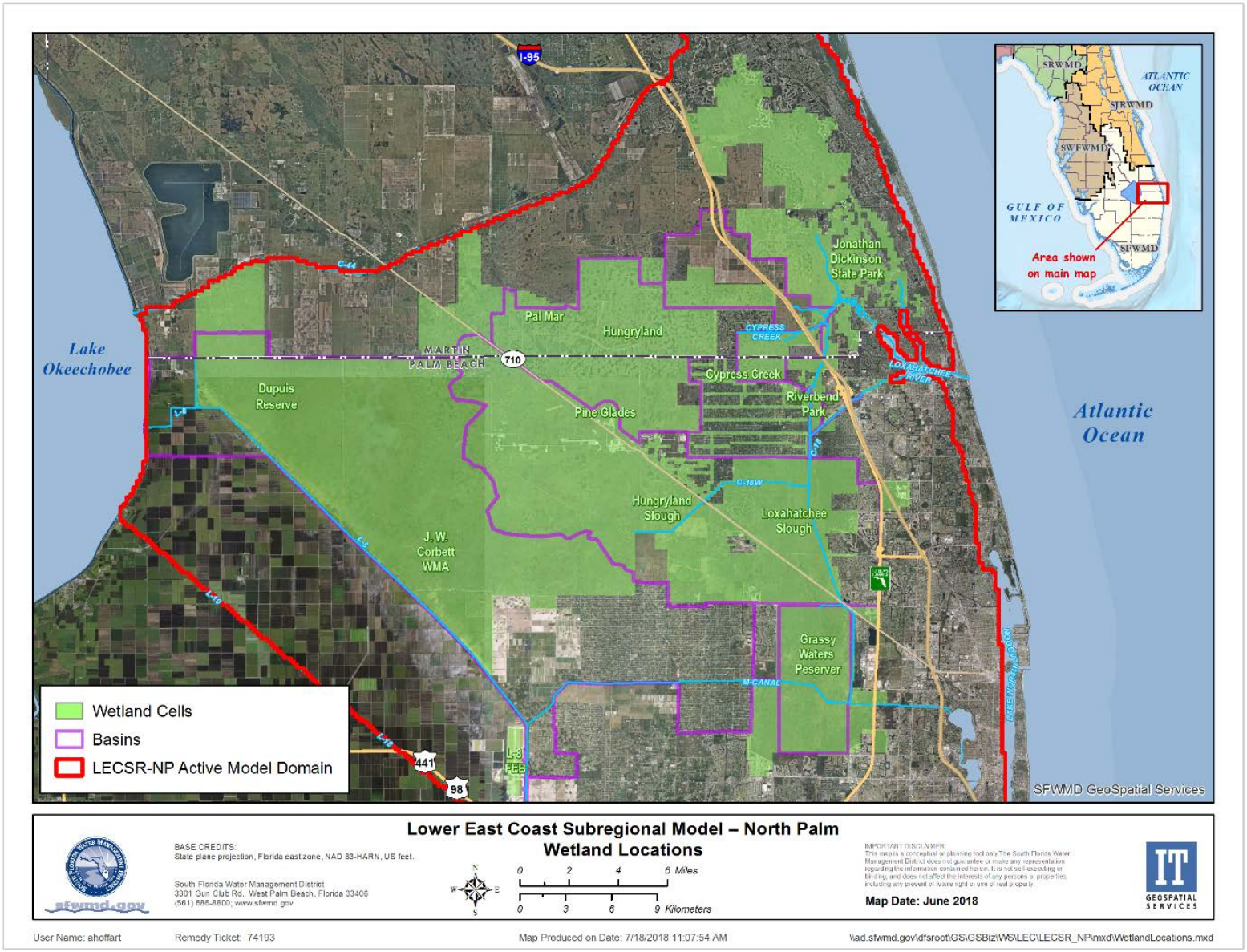

Figure 34. Spatial distribution of wetland cells across the LECSR-NP active model area.

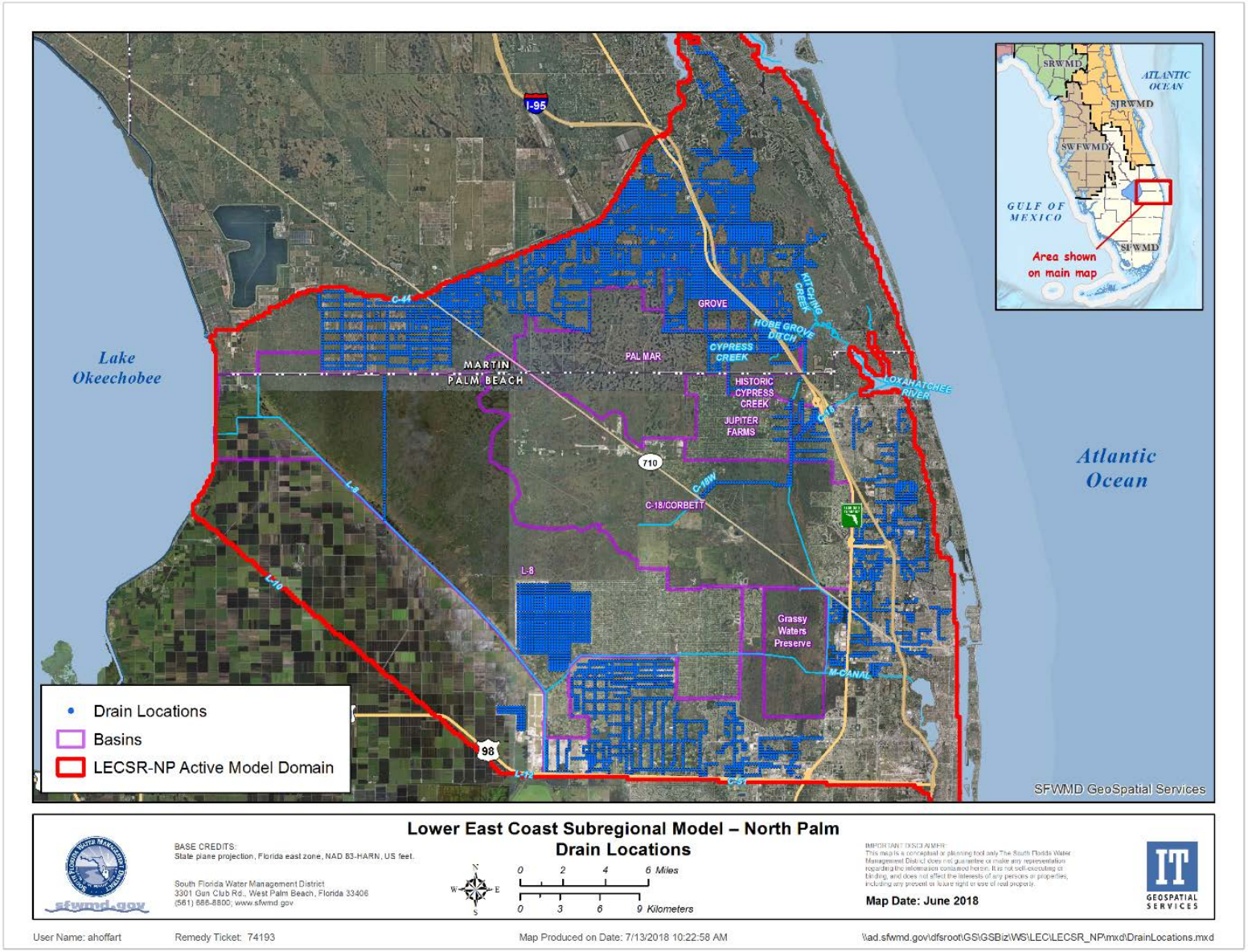

Figure 35. Spatial distribution of drain cells across the LECSR-NP active model area.

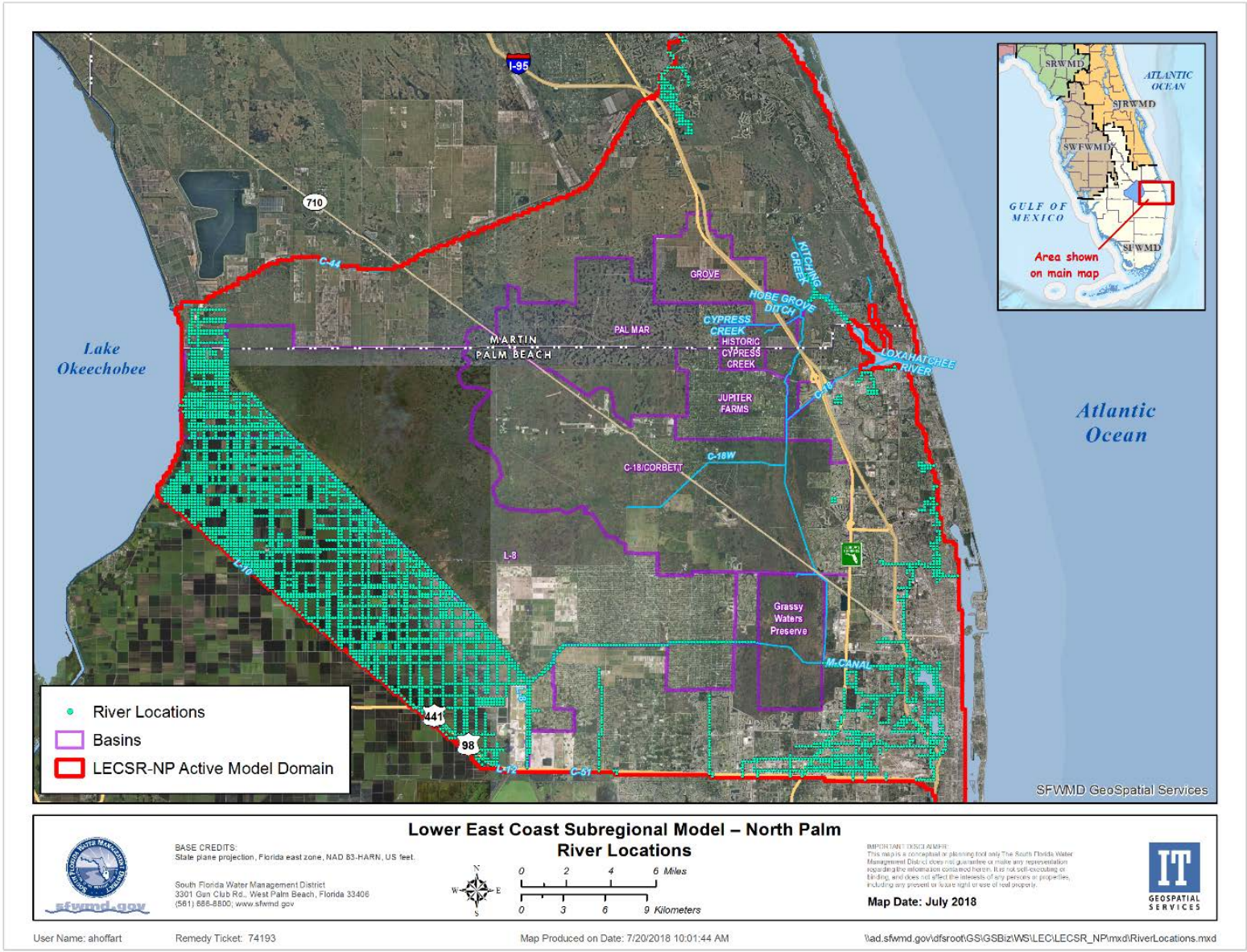

Figure 36. Spatial distribution of river cells across the LECSR-NP active model area.

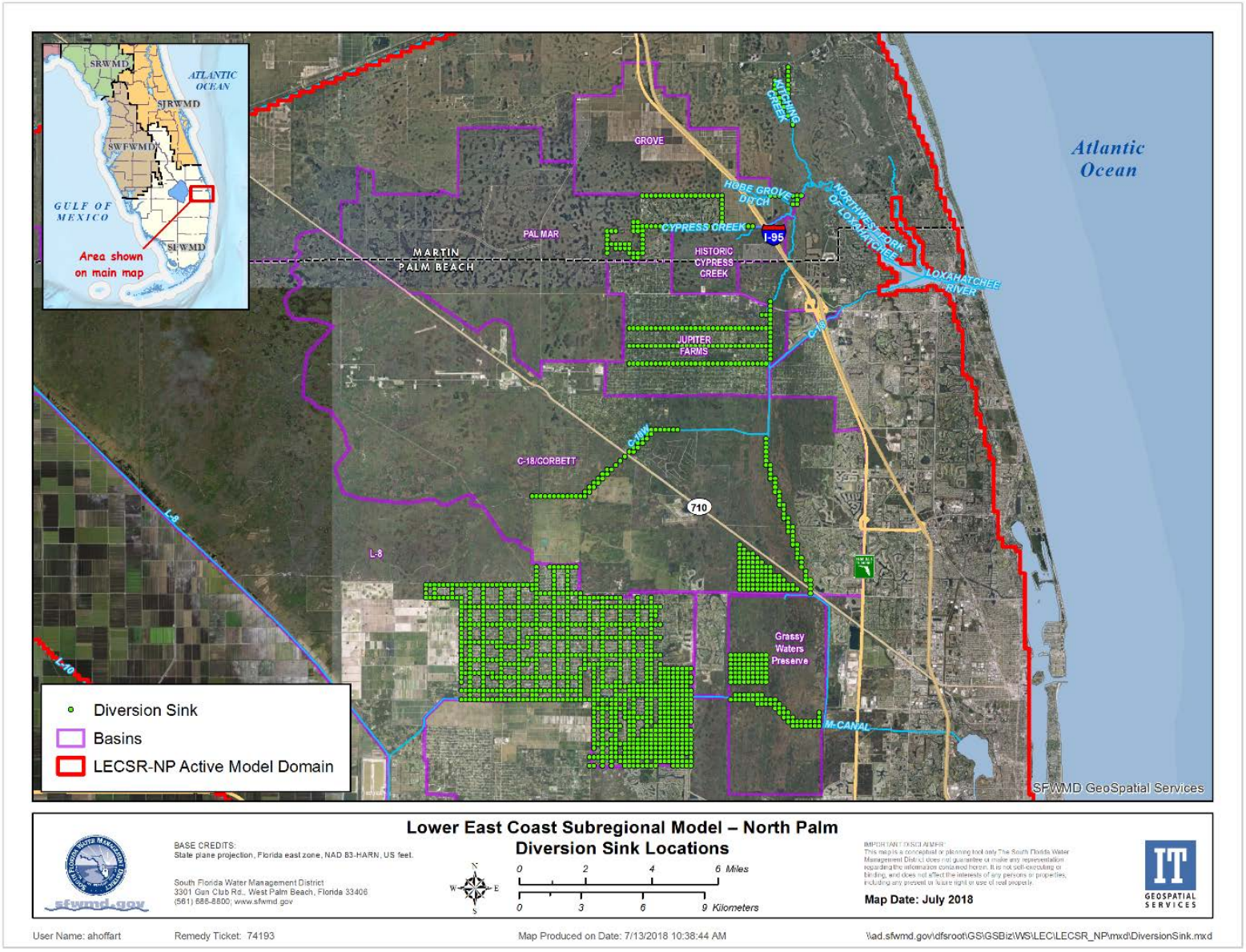

Figure 37. Spatial distribution of Diversion sink cells across the LECSR-NP active model area.

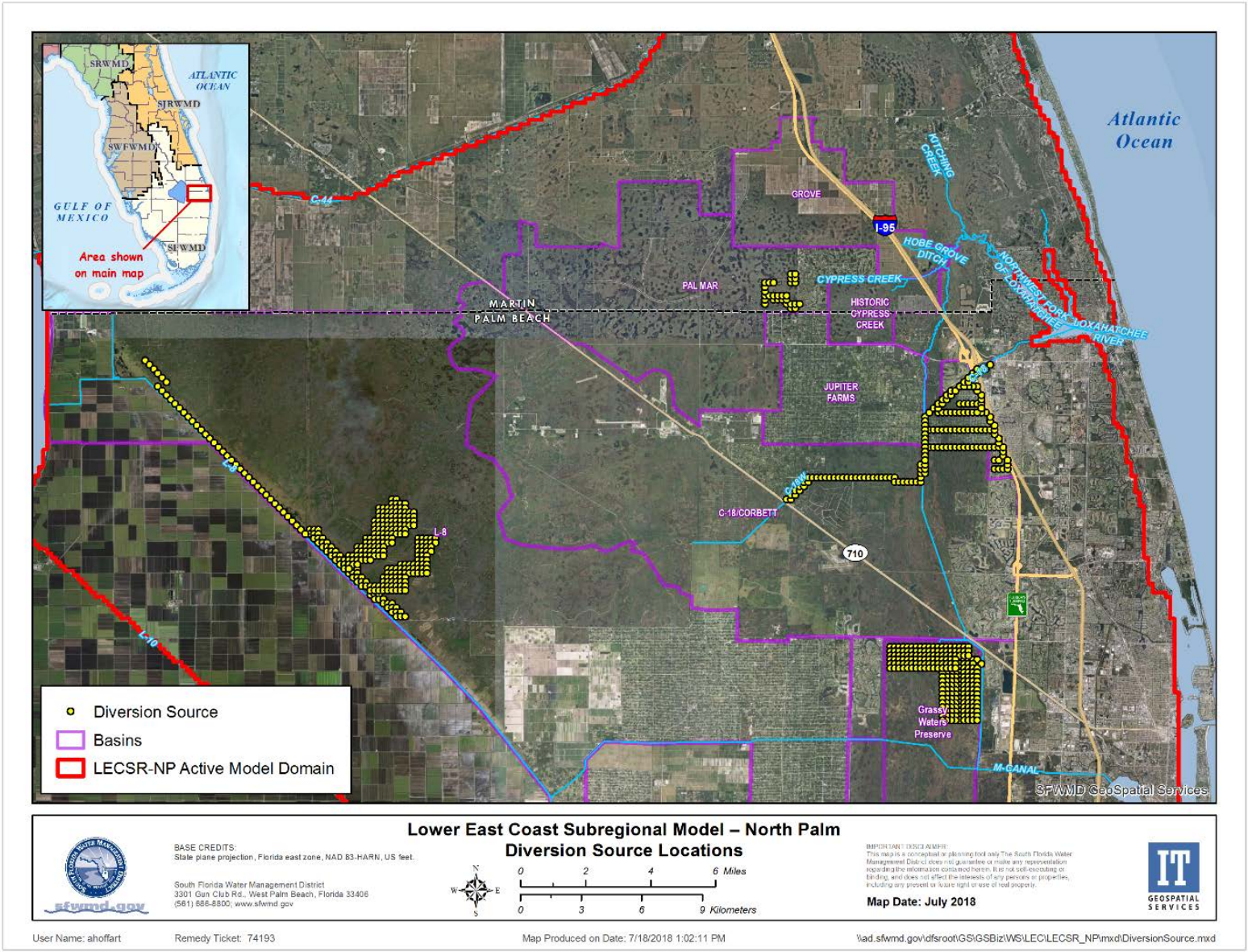

Figure 38. Spatial distribution of Diversion source cells across the LECSR-NP active model area.

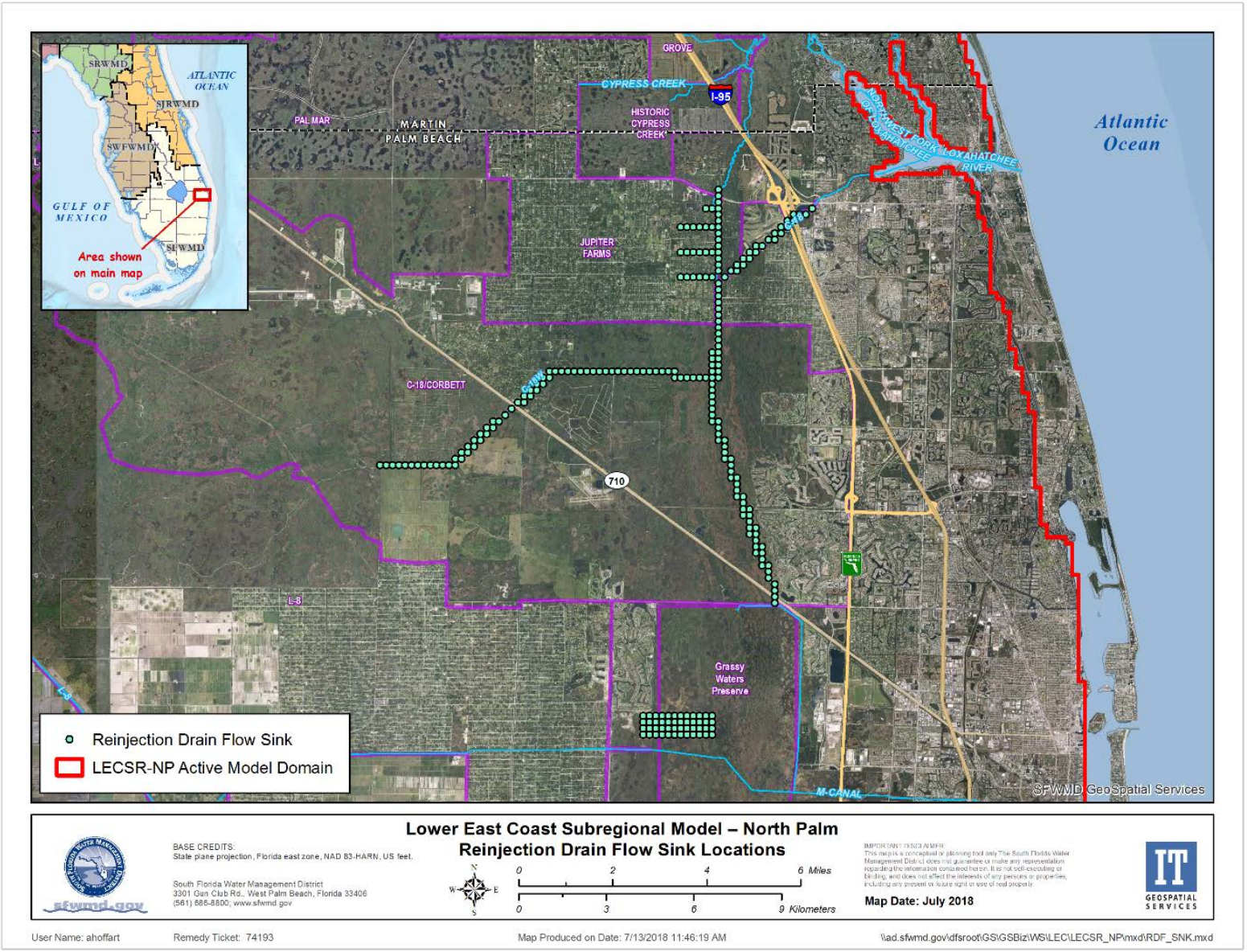

Figure 39. Spatial distribution of Reinjection Drain Flow sink locations across the LECSR-NP active model area.

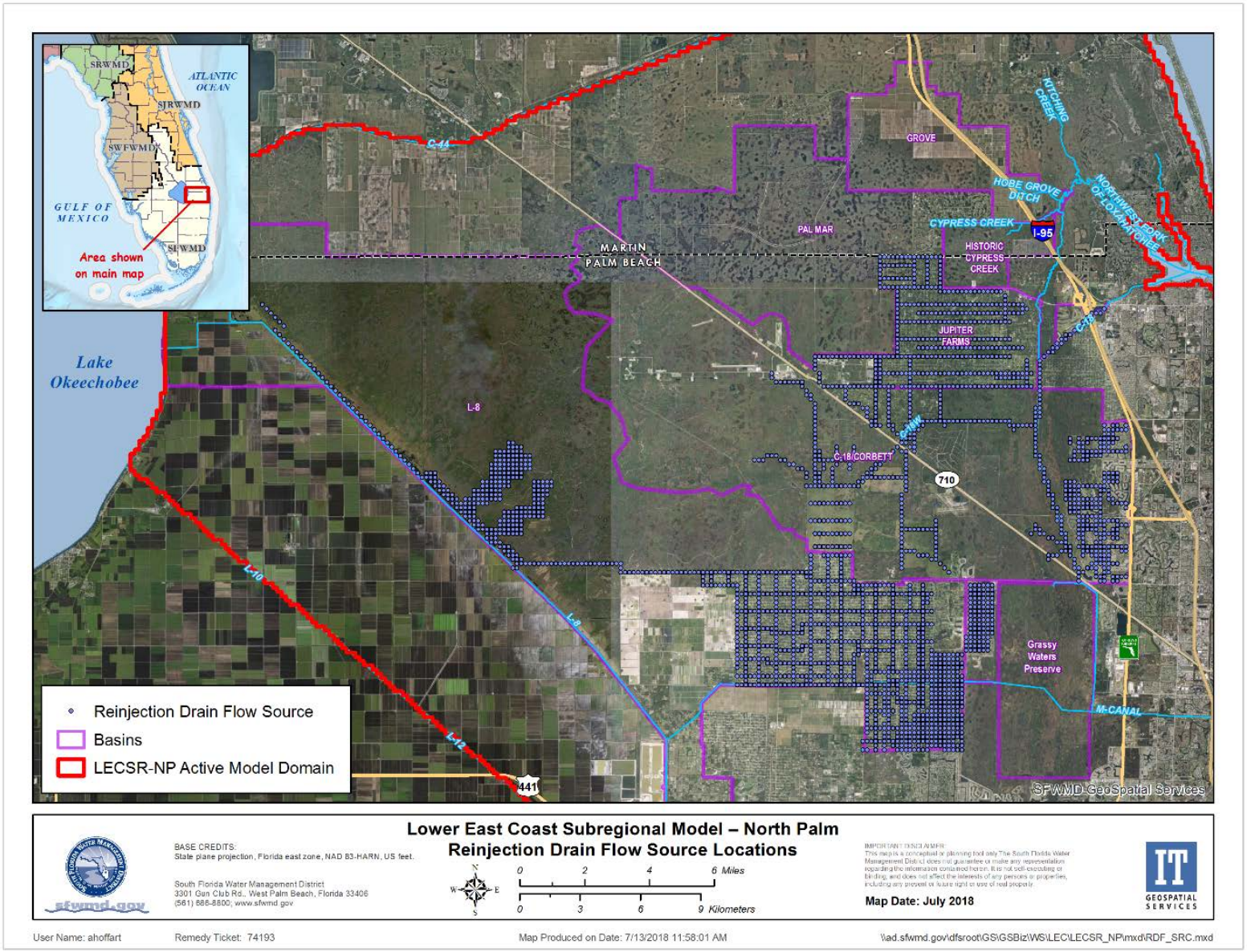

Figure 40. Spatial distribution of Reinjection Drain Flow source cells across the LECSR-NP active model area.

L-8 Basin

The L-8 Basin was simulated with a combination of rivers, drains, diversions, and RDFs. Additionally, because the western border of the L-8 Basin coincides with the boundary of the active model domain, GHB cells are located along the Lake Okeechobee boundary. Rivers were used to simulate the L-8 Canal, with historical data used to simulate canal stages. Drains were used to simulate an existing drainage canal within the Dupuis Management Area and the existing drainage canal network with the agricultural portions of the L-8 Basin. Diversions were used to incorporate the routed runoff from the ET-Recharge program into the Indian Trail Improvement District. The Diversion package was used to simulate the M-O Canal, which is on the south side of Corbett Wildlife Management Area. Runoff from western Corbett and Dupuis management areas and the ditch adjacent to the L-8 Canal were simulated using the RDF package. RDFs were used to keep track of L-8 Basin runoff that would be available for use in alternative simulations for the LRWRP. For the calibration, the water removed from the RDFs was placed in an inactive portion of the model domain.

C-18 Basin

The C-18, Corbett, and Jupiter Farms basins are combined into Flow-way 1 in the LRWRP and simulated with a combination of drains, rivers, diversions, and RDFs. This area of the model contains the C-18 West Canal, C-18 weir, southern leg of the C-18 Canal, G-161, G-160, G-92, S-46, and Lainhart Dam.

The C-18 West Canal was modeled using a combination of drains, diversions, and RDFs. The portion of the canal located west of the C-18 weir was modeled using diversions to simulate the runoff occurring in urban areas. RDFs were used along the C-18 West Canal as well as within Pratt, East Corbett, and Avenir, and were used to simulate the movement of water over the C-18 weir. The portion of the canal east of the C-18 weir was modeled using a combination of drains, diversions, and RDFs. The diversions and RDFs were used to simulate the movement of water from the C-18 West Canal to the C-18 Canal. Drains were used to represent the water that would be sent to the ocean via S-46 when stages in the C-18 West Canal are too high.

The southern leg of the C-18 Canal was simulated primarily with diversions and RDFs. Diversions bring water from the northern portion of GWP through G-161 and into the southern leg of the C-18 Canal. RDFs were used to move runoff from urban areas such as Mirasol and PGA into the southern leg of the C-18 Canal. RDFs were used to move water through G-160, which is to be effectively operated so that during rainfall events, when stages upstream of the structure rise to an elevation of 16.8 feet NGVD29, the structure can be opened to allow stages to recede and closed once stages reach an elevation of 16.2 feet NGVD29. However, for the LECSR-NP calibration, operations for G-160 were determined based on historical data, as documented in the annual South Florida Environmental Reports. Further analysis of G-160 showed operations varied before and after 2009. Therefore, two sets of operation schedules were used during calibration.

Prior to June 2009:

- During the dry season: environmental releases occur when the stage is higher than 12.0 feet NGVD29, with discharge of 40 cfs.
- During the wet season: flood control releases occur when the stage is higher than 14.5 feet NGVD29, with discharge of 150 cfs. Additionally, flood control releases can occur when the stage is higher than 15.0 feet NGVD29.

Figures 41 and **42** show historical releases for the dry and wet seasons prior to June 2009, respectively.

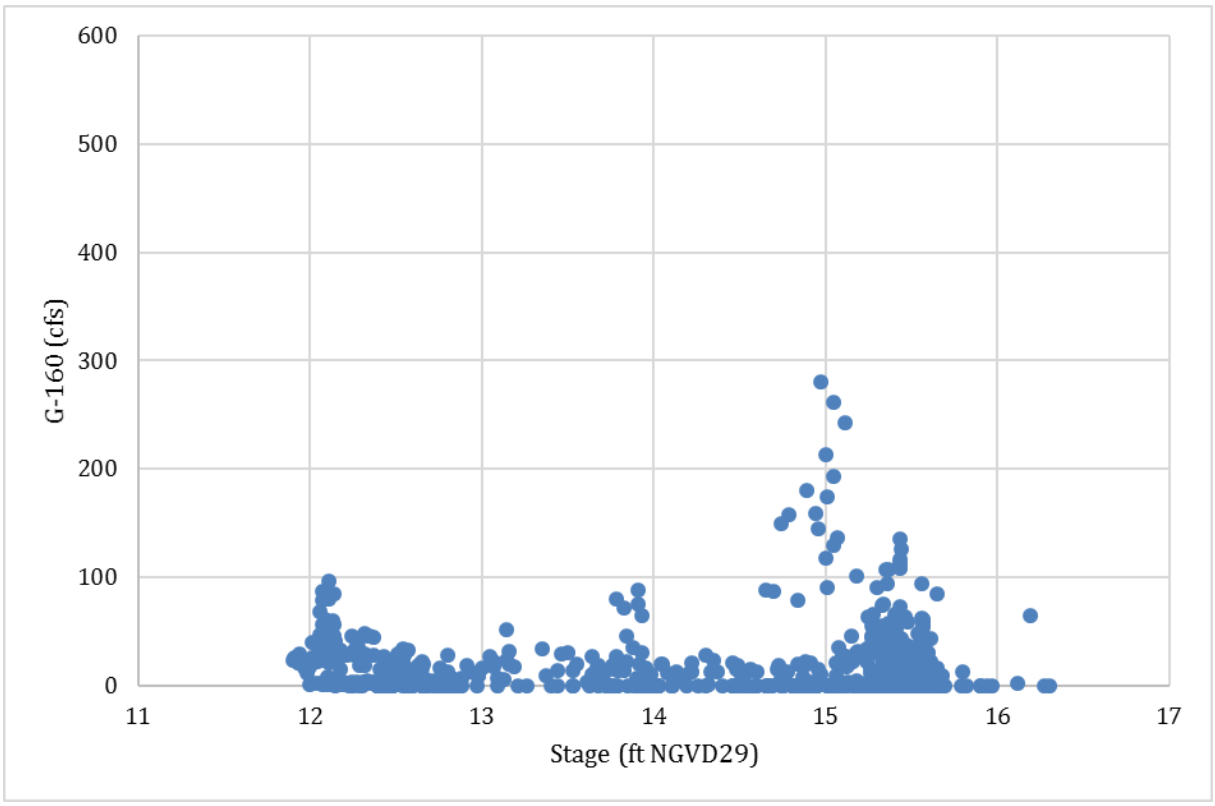

Figure 41. Historical releases before June 2009 at G-160 during the dry season.

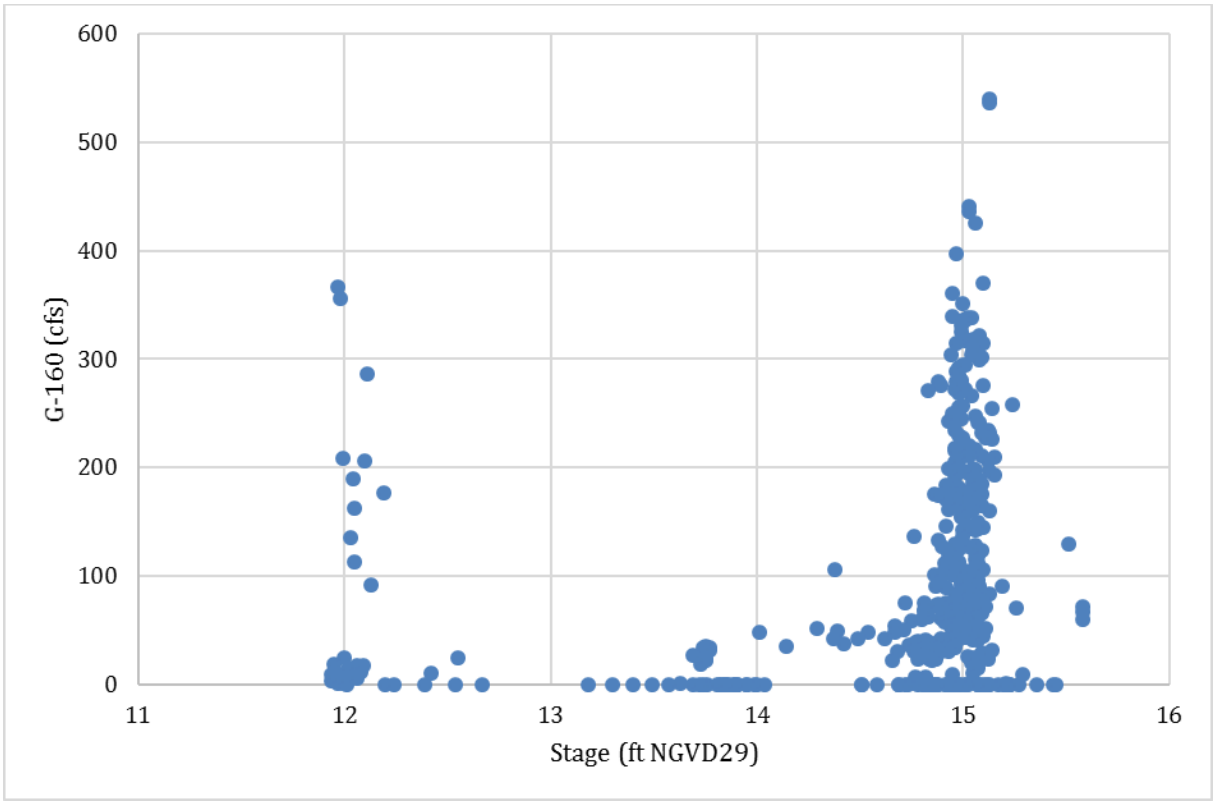

Figure 42. Historical releases before June 2009 at G-160 during the wet season.

After June 2009:

- During the dry season: environmental releases when the stage is higher than 12.0 feet NGVD29, with discharge of 40 cfs.
- During the wet season: flood control releases when the stage is higher than 15.5 feet NGVD29, with discharge of 150 cfs. Additionally, flood control releases can occur when the stage is higher than 16.5 feet NGVD29.

Figures 43 and **44** show historical releases for the dry and wet seasons after June 2009, respectively.

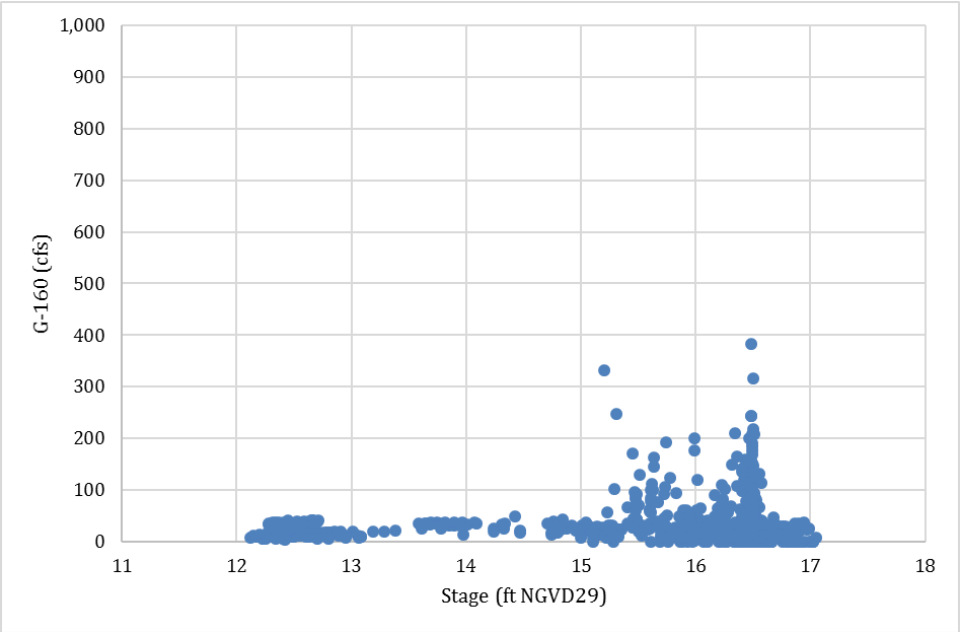

Figure 43. Historical releases after June 2009 at G-160 during the dry season.

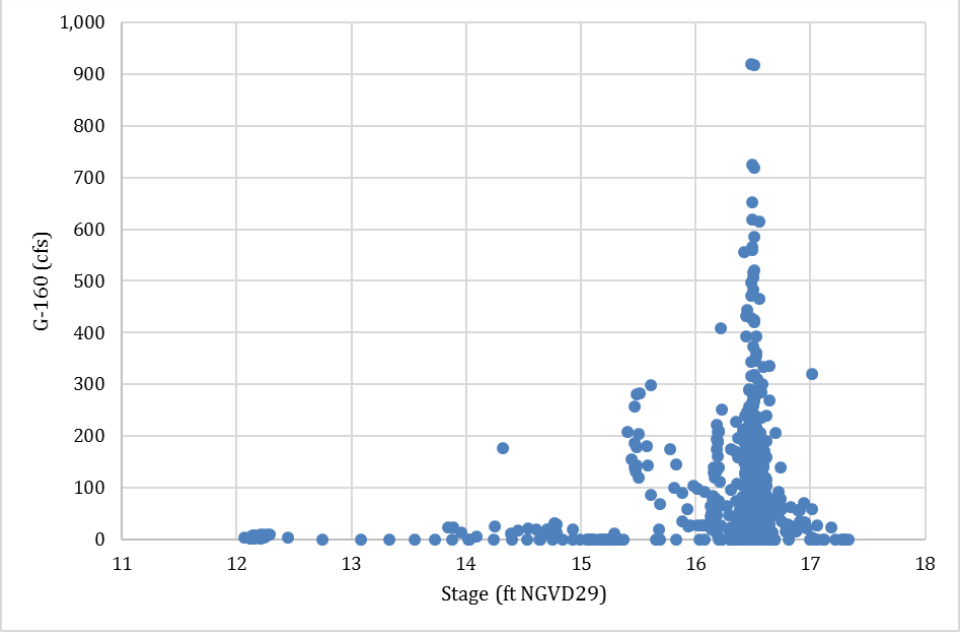

Figure 44. Historical releases after June 2009 at G-160 during the wet season.

The RDF package was used to simulate water as it moves along the C-18 Canal through G-92. The canal reach between G-160 and G-92 also receives water from the South Indian River Control District, which has property on the east and west sides of the C-18 Canal. The South Indian River Control District was simulated as distinct basins in the RDF package, with a control elevation at varying stages consistent with current South Indian River Control District operations. The C-14 Canal and feeder canals receive runoff and base flows from the other basins and discharge over Lainhart Dam using the Drain package at the historical control elevation. The basin is east of the C-18 Canal and discharges downstream of S-46 using the Drain package with the historical control elevation. Runoff from the basin, using the ET-Recharge program, was directly put into the basin at the RDF cells using the Diversion package.

Grassy Waters Preserve Basin

Grassy Waters Preserve (GWP) is an 11,100-acre wetland area owned by the City of West Palm Beach and managed for PWS and as a nature preserve. GWP is simulated in the LECSR-NP using several MODFLOW packages, including Wetland, Diversion, and Wells. Historical flows from the regional system brought into the City's water system via the Control 2 pump station were simulated using the Diversion package. The Diversion cells are located within GWP adjacent to the M-Canal. It should be noted that the City backup wellfield was operational for part of the calibration period and this water was added to the M-Canal Diversion cells. Additional inflow into GWP occurs at the Ibis outfall area and was simulated using the Diversion package. Runoff from Ibis was estimated using the revised ET-Recharge-Runoff program.

Outflow from GWP occurs at three locations. At the north end, water moves out of GWP over the Northlake Blvd. weir into the GWP triangle area, which connects with the southern portion of Loxahatchee Slough, when water levels at the north end rise above 19.2 feet NGVD29 at volumes not to exceed 100 cfs. Additional water leaving out of the north end of GWP can occur through the G-161 structure. This also is simulated using the Diversion package, with the water discharging into the C-18 Canal upstream of the G-160 structure. During the calibration period, there were no set operational criteria for moving water through G-161, so the simulated water released was set equal to the observed flow in the Diversion package. The final major discharge out of GWP occurs to meet the City of West Palm Beach's PWS needs. Because the model does not directly simulate surface water withdrawals by the City of West Palm Beach out of Clear Lake (where the water treatment plant's intake pumps are located), a simplified approach was used. The City's demands were withdrawn from the same stretch of the M-Canal as the Diversion cells, representing the Control 2 inflows using the well package to simulate the PWS demands.

The M-Canal reach to the east and west of GWP was simulated as a river using the River package to quantify any seepage losses or gains between the Control 2 and Control 3 pump stations. A test run of the LECSR-NP showed substantial seepage loss along the M-Canal between the two pump stations (approximately 13 cfs on average). **Figure 45** shows monthly averaged seepage losses between the two pump stations derived from model output associated with the River package. Positive values indicate the M-Canal is recharging the aquifer while negative values indicate the aquifer is recharging the M-Canal. **Figure 45** shows only positive values, indicating the M-Canal always recharges the aquifer. **Table 13** provides the monthly calculated percent loss due to seepage between Control 2 and Control 3 of the M-Canal. In the LECSR-NP, inflow into GWP is historical flows through Control 2 minus seepage losses from Control 2 to Control 3. Historical stages within GWP were compared to modeled stages to ensure the model was capturing this interaction.

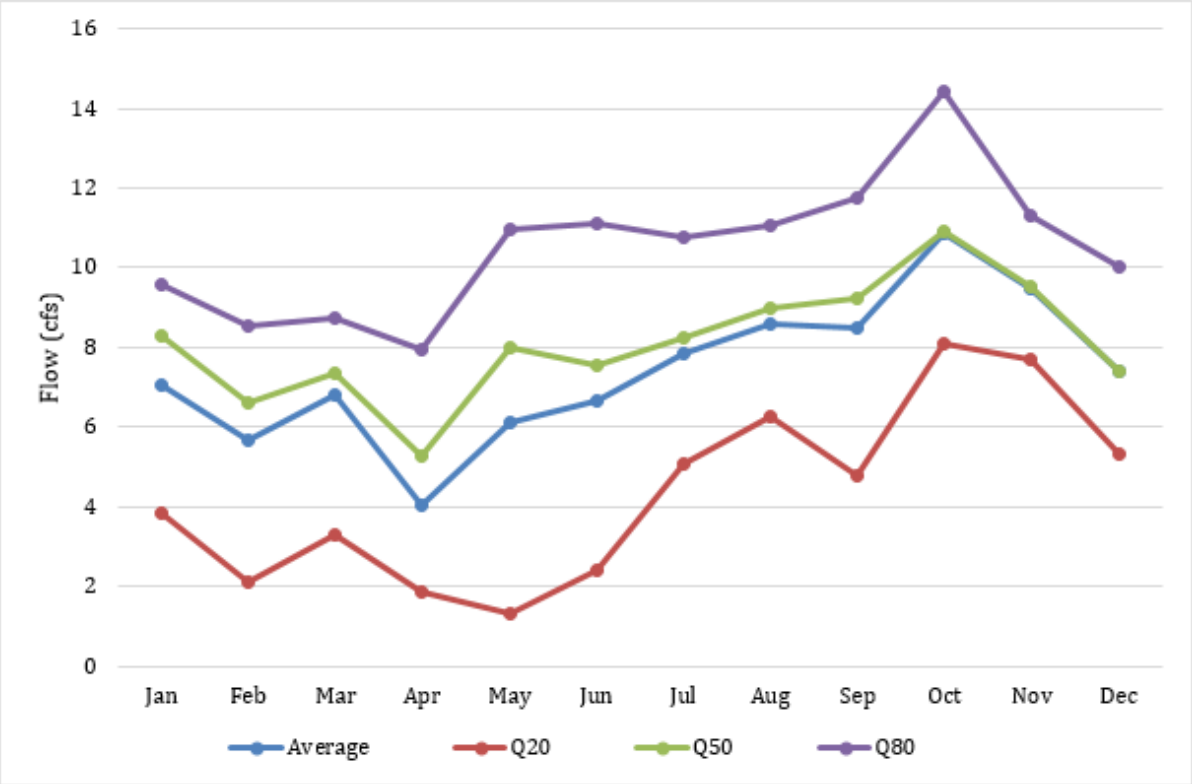

Figure 45. Monthly averaged seepage losses between the Control 2 and Control 3 pump stations from 2006 to 2014 (Q20 = 20th percentile flow; Q50 = 50th percentile flow; Q80 = 80th percentile flow).

Table 13. Monthly averaged percent seepage losses between the Control 2 and Control 3 pump stations.

Month	Percent Seepage Loss
January	7
February	7
March	7
April	5
May	8
June	13
July	27
August	23
September	23
October	17
November	8
December	8

Flow-way 3 Basin

The Flow-way 3 basin is a combination of Pal Mar, Hobe Grove Ditch, and the historical Cypress Creek basins and surrounding areas, including Kitching Creek and the tidal reach of the Northwest Fork of the Loxahatchee River. This area is known as Flow-way 3 in the LRWRP and was simulated using a combination of diversions and drains. The Diversion package was used to simulate the Culpepper outfall

structures, Cypress Creek Canal, Hobe Grove Ditch, and the east-west portion of the Nine Gems drainage system as well as the Nine Gems bypass canal, which feeds into Cypress Creek. Drains were used to represent existing drainage canals within Hobe St. Lucie Unit 2, Nine Gems, Thomas Pepper Farm, Shiloh Farms, and Gulfstream. Drains also were used in the urban areas adjacent to the Cypress Creek Canal. Drain elevations were set based on existing operations of the drainage canals in the area or based on surface water management permits issued by the SFWMD.

Kitching Creek feeds into the Northwest Fork of the Loxahatchee River. The northern portion of Kitching Creek was simulated using source cells for the Diversion package, which introduced the routed runoff as calculated by the ET-Recharge package. This area of Kitching Creek down to the flow gauge was simulated using the Drain package. The southern portion of Kitching Creek was simulated using the River package. The tidal portion of the Northwest Fork of the Loxahatchee River, which begins east of where Hobe Grove Ditch feeds into the river and continues to the intracoastal waterway, was modeled with the River package.

Everglades Agricultural Area Drainage Basin

The eastern portion of the Everglades Agricultural Area is located at the western side of the study area and includes a portion of the S-5A and L-8 drainage basins. The portion of the S-5A drainage basin within the model domain is the area from the L-8 Canal west to the L-10/L-12 borrow canals and Lake Okeechobee. The primary purpose of the project canals and structures is to move excess water from the basin or Lake Okeechobee regulatory releases into Water Conservation Area 1 and the stormwater treatment areas. This will prevent over-drainage of the basin and minimize soil subsidence, provide water supply to the Everglades Agricultural Area users, or convey water east to coastal users. The primary canal(s) for moving water into and out of the basin is the West Palm Beach Canal (L-10/L-12 borrow canals).

Other Basins

Several other basins exist within the study area but are not directly related to the restoration of the Loxahatchee River or watershed wetland systems. These include the C-44, Tidal St. Lucie, Basin 2, and South Coastal drainage basins in Martin County. Local basin runoff in the C-44 Basin or Lake Okeechobee regulatory releases move east towards the S-80 structure in the Tidal St. Lucie basin where it discharges to the ocean. South Coastal and Basin 2 are located along the coast in southern Martin County and ultimately can discharge to the ocean as well. In Palm Beach County, urban basins not previously discussed include the C-51 East, C-51 West, C-17, and Intracoastal basins. These basins are heavily developed and discharge into the C-51 or C-17 canals, which discharge into Lake Worth Lagoon through the S-155 or S-44 structure. The Intracoastal Basin along the coast can directly discharge into the tidal reaches by locally controlled means. These basins are east and south of the study area.

Perimeter Boundary Conditions

In addition to simulating canals and other features in the surface water basins, additional stages need to be imposed in the LECSR-NP along the active edge of the model domain through the use of the GHB package (**Figure 46**). These general heads include Lake Okeechobee, the C-51 and C-44 canals, and the tidal conditions along the coast. Daily historical stages were obtained from the SFWMD's corporate environmental database, DBHYDRO, for Lake Okeechobee and the structures along the C-51 and C-44 canals for the calibration and verification periods. Tidal conditions vary along the eastern edge of the model depending on proximity to an ocean inlet, distance inland, and influence of coastal water control structures. Historical data from surface water gauges seaward of the water control structures and in the downstream reaches of the Loxahatchee River were used for those areas of the coastal boundary conditions. Along the intracoastal waterway, calculated values of the daily mean tide were used.

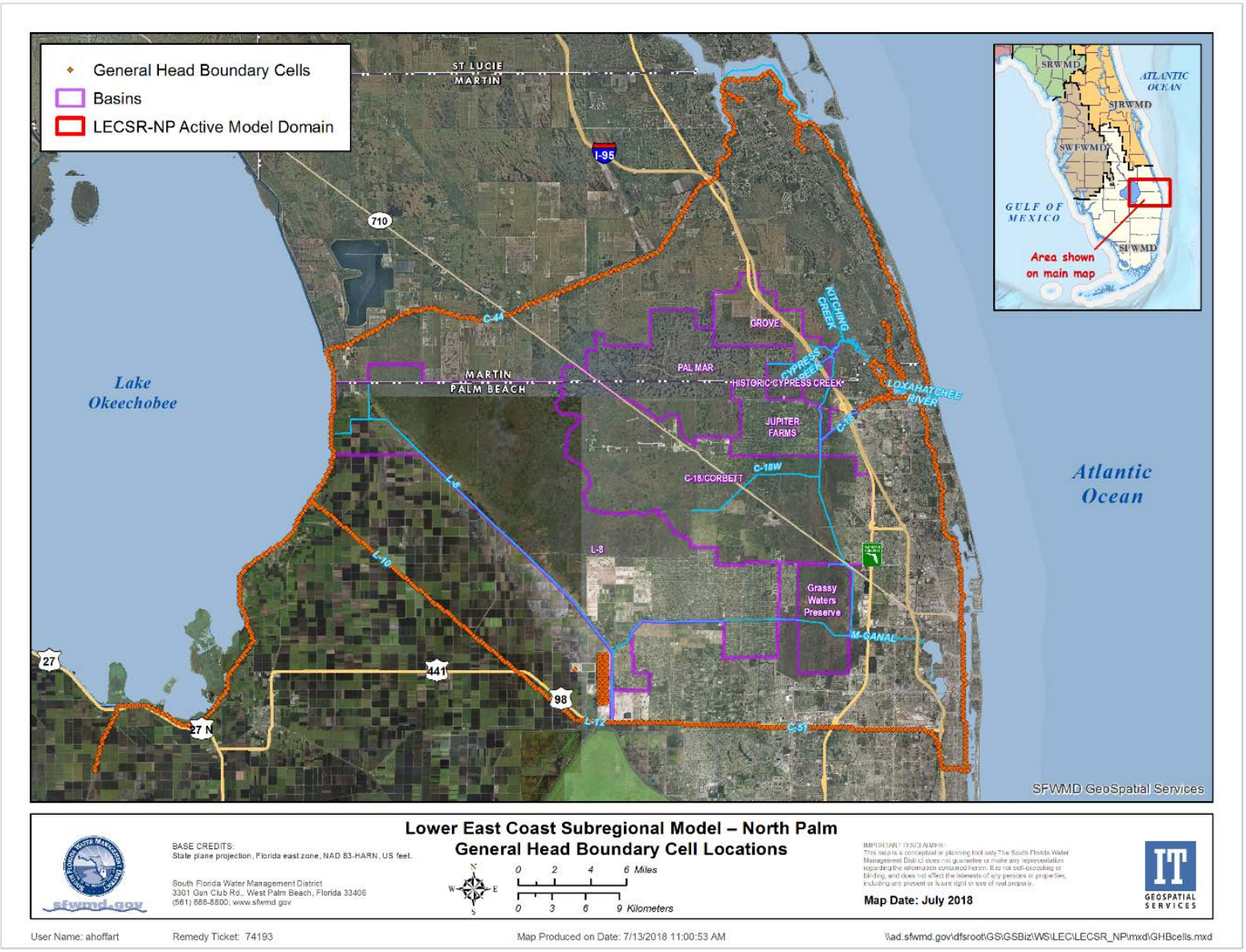

Figure 46. Spatial distribution of General Head Boundary cells across the LECSR-NP active model area.

3.4 Water Use

Information for MODFLOW's Well package was extracted from individual water use permits issued by the SFWMD. Individual permits were screened so only those with a permitted allocation greater than 1 mgd and located within the active model domain were used. Individual permits were divided into two categories: PWS and non-PWS. Water use for PWS permits was aggregated from actual data reported to the SFWMD or Florida Department of Environmental Protection and compiled by the SFWMD or USGS. Water use for non-PWS permits was estimated using AFSIRS.

3.4.1 Public Water Supply

PWS demands were obtained from monthly operating reports supplied by utilities to the SFWMD and Florida Department of Environmental Protection. Individual well withdrawals for each permit were estimated by creating a spatial wellfield distribution percentage and a monthly seasonal component.

Individual well locations within a permit do not change year-by-year during the simulation period. In addition, there was no change in the distribution of the annual demands for each well within a permit in the active model area. Several utilities have restrictions on withdrawals in specific wellfields that limit the amount the wellfield can withdraw; these limitations were included in the LECSR-NP. For example, the Town of Jupiter, the Village of Tequesta, and Seacoast Utility Authority have specific wellfield restrictions to minimize the threat of saltwater intrusion. The LECSR-NP includes all utilities in northern Palm Beach County as well as southern and northeastern Martin County.

A monthly seasonal component was developed using historical pumpage. These values represent the fraction of pumpage distributed throughout the year (monthly seasonality). The fractions add up to 100 percent of the annual withdrawal. Seasonal variability in utility demand reflects the seasonal population and the irrigation of landscape during the dry season. Monthly pumpages were converted to daily values by dividing by the number of days in each month. The daily pumping rate was held constant for each month.

3.4.2 Non-Public Water Supply

Non-PWS use classifications include agriculture, industrial, golf course, nursery, and landscape/recreation areas. **Figure 18** shows the distribution by water use type; **Figure 47** shows water use by type for only non-PWS wells. There are 104 non-PWS permits in the LECSR-NP and 614 non-PWS wells. Due to the lack of historical pumpage data, irrigation demands were estimated using AFSIRS, which calculates irrigation demand based on climate-driven need (Smajstrla et al., 1990). Non-irrigation permit demands for industrial use were calculated from the average annual allocation divided by the number of days in a year. Similar to the PWS wells, demand was distributed evenly among the facilities.

A few permits stipulate an allocation for both groundwater and surface water sources, sometimes based on crop type. When the permits did not specify the allocation between groundwater and surface water sources, the allocation was divided based on the capacity of the facilities. Each facility in a permit was assigned a percentage of the allocation based on the percentage of the facility capacity/total capacity of all the facilities in the permit. Once the distributions were determined, the surface water sources were excluded if water was brought in from outside the basin (e.g., from Lake Okeechobee) to meet the need. All the non-PWS wells were assigned to Layer 2 of the LECSR-NP Model, which is the main production zone within the SAS.

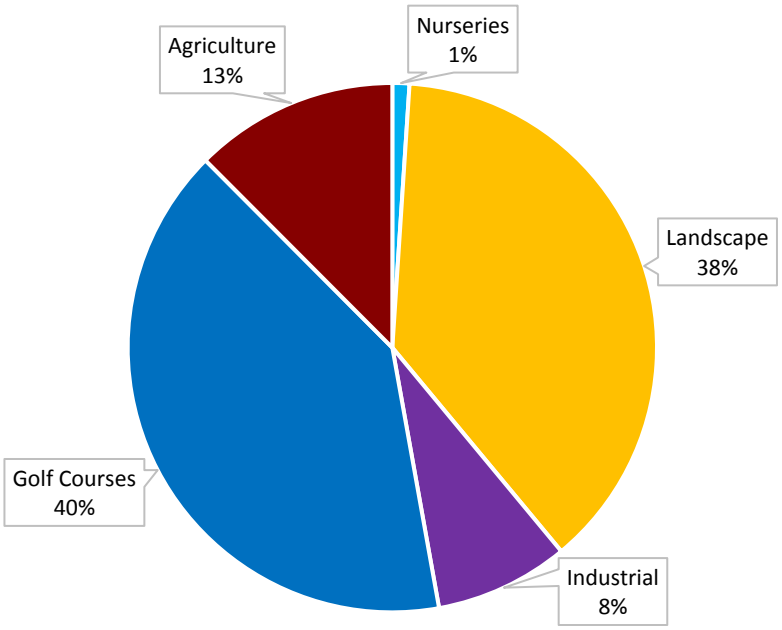

Figure 47. Water use distribution for non-public water supply permits.

4. MODEL CALIBRATION AND VERIFICATION

The goal of model calibration and verification is to achieve the capability of simulating results similar to field measurements within specified tolerances, produce general groundwater flow patterns, and match trends in groundwater heads (levels) and flows. The goal of the calibration process is to change input parameters within a predetermined range in an attempt to produce simulated heads and flows that match historical values. The goal of the verification process is to use the calibrated model with limited change to input data to produce simulated heads and flows that match historical values outside the model calibration period.

4.1 Methodology

Model calibration is the procedure by which input parameters are adjusted within acceptable ranges until a reasonable representation of the physical system is achieved. Model calibration is considered complete when the model is capable of simulating a set of field measurements within specified tolerances. The model was calibrated to transient conditions using a manual trial-and-error process. The historical surface water and groundwater monitoring networked used in the calibration process was obtained from the SFWMD, the USGS, and Palm Beach County. The model simulated daily stages and flows, which were compared to historical values to determine the degree of calibration. Qualitative and quantitative techniques were applied to evaluate the calibration and verification results. The calibration period for the current version of the LECSR-NP is from January 1, 2006 to December 31, 2014, which includes average 12-month SPI values of -1.725 and 1.065, indicating there are extreme wet and dry periods within the calibration period.

The first step in the calibration process was to vary model parameters within acceptable ranges. Model parameters generally were varied one at a time unless data suggested multiple changes could be implemented simultaneously. After completion of the model run, statistics were generated and compared to a base case model to determine any improvements or degradation in model performance. When sufficient improvements were achieved, the base case model was replaced with the revised model and the process continued. This process was repeated multiple times until continued variations of all sensitive parameters resulted in negligible additional improvement. The main parameters varied for the calibration process, as determined by an earlier sensitivity analysis, are as follows:

- Runoff parameters, including curve numbers, land use classifications, and lag time;
- Wetland parameters, including Kadlec values, locations of wetland surfaces, and specific yields for overland flow;
- River, Drain, RDF, and Diversion flow constraints; and
- Hydraulic conductivity, primarily for Layers 1 and 2.

4.2 Calibration Criteria

4.2.1 Flow Discharges

Eight discharge locations, the surface water structures that historically existed within the model domain, were used for model calibration (**Figure 48**). Statistics for each discharge location were used as quantitative calibration criteria for overall model performance. Although the model outputs daily flow data, cumulative monthly flow was used for calibration purposes. This is due to the high variability in day-to-day operations of the flow structures. The statistics chosen include the following:

- Deviation of volume (DV): quantifies the difference in observed and predicted water volumes. Positive DV indicates under-predicted flows while negative DV indicates over-predicted flows.
- Nash-Sutcliffe coefficient (NS): indicates how well a model can predict flow. A value equal to 1 indicates a perfect fit; a value less than 0 indicates a prediction no better than using the average of the historical values.
- Coefficient of determination (R^2): indicates how well the model fits the historical trends in flow. A value equal to 1 indicates the model explains all variability in historical values; a value of 0 indicates the model explains none of the variability in historical flow.

For this project, the DV target was $\leq$15 percent. The targets for NS and R^2 were values $\geq$0.4. These target values have been used for other subregional models in the area and are considered appropriate based on previous work conducted in the Loxahatchee River watershed (SFWMD, 2006).

The following qualitative techniques for flow criteria were chosen:

- Flow hydrographs: show the differences between historical and modeled flow, including low and high flow regimes.
- Cumulative flow curves: show the differences between historical and simulated cumulative flow.

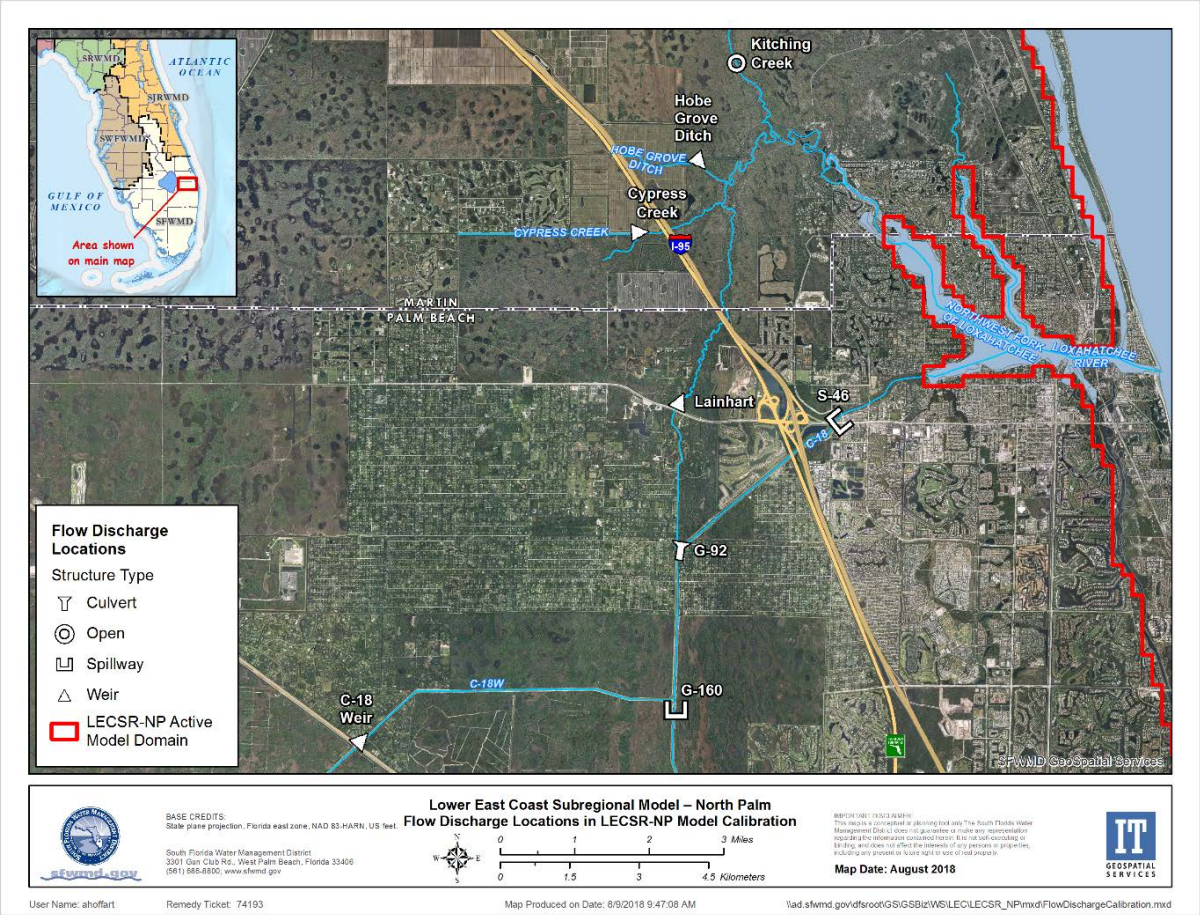

Figure 48. Flow discharge locations used in LECSR-NP calibration.

4.2.2 Water Level Elevations

A total of 76 groundwater monitoring wells and 67 wetland gauges with at least some data within the calibration period were identified. After a joint USACE and SFWMD analysis of the locations, 58 groundwater monitoring wells and 61 wetland stage monitoring gauges were selected for overall model calibration and performance (**Figures 49** and **50**, respectively). Locations were selected based on availability of data that have undergone a quality assurance/quality control process and were within the model domain. Although there were several additional locations with water level data, they were screened out due to their location coinciding with a stage- controlled model cell (such as a river or GHB) or due to the data only being available for a very short period of time during the calibration period. Statistics for each location were used as quantitative calibration criteria for overall performance. The statistics and targets for the groundwater monitoring wells and wetland gauges were chosen based on the LECSR peer review (Andersen et al., 2006) and include the following:

- ±Range error target: percent of time the simulated head is within a plus or minus range error target in feet of the observed head.
- Mean error (feet): the mean difference between measured and simulated heads.
- Mean absolute error (MAE; feet): the mean of the absolute value of the difference between measured and simulated heads.
- Root mean squared error (feet): the average of the root of the squared differences between measured and simulated heads.

Based on the peer review panel's recommendation, each well had its own target based on 20 percent of the absolute difference in minimum and maximum observed values during the calibration period. This computed range was used as a target for the percent of time the simulated head is within the observed head, mean error, MAE, and root mean squared error. For the range error target, the simulated head should be within the observed head range at least 75 percent of the time. The groundwater monitoring wells and wetland gauges were considered calibrated if three out of four calibration criteria are met. Historically, the SFWMD used a target of ±1 foot for the mean error, MAE, and root mean squared error. The peer review panel's recommended calibration criteria and the historical SFWMD calibration criteria were applied to test the validity of the calibration.

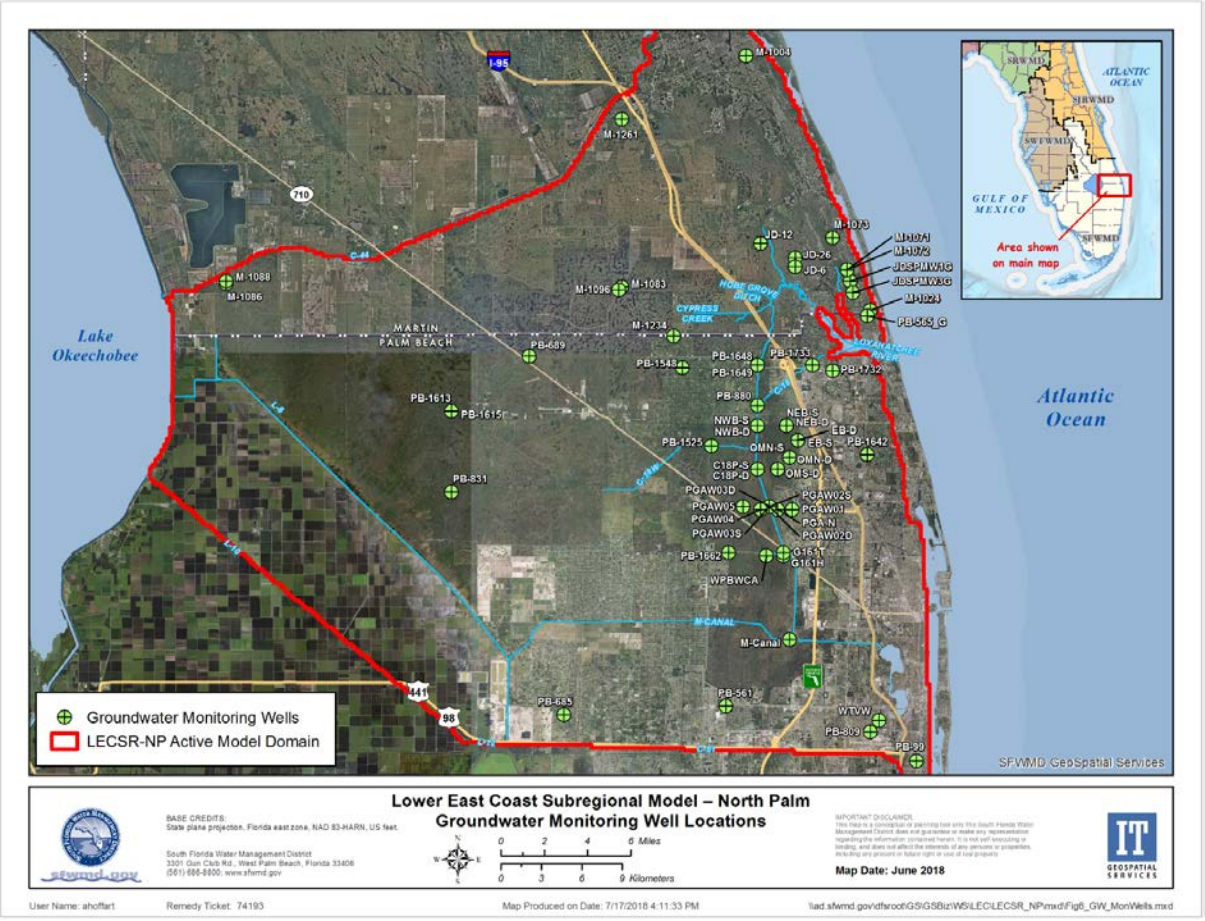

Figure 49. Groundwater monitoring well locations used in LECSR-NP model calibration.

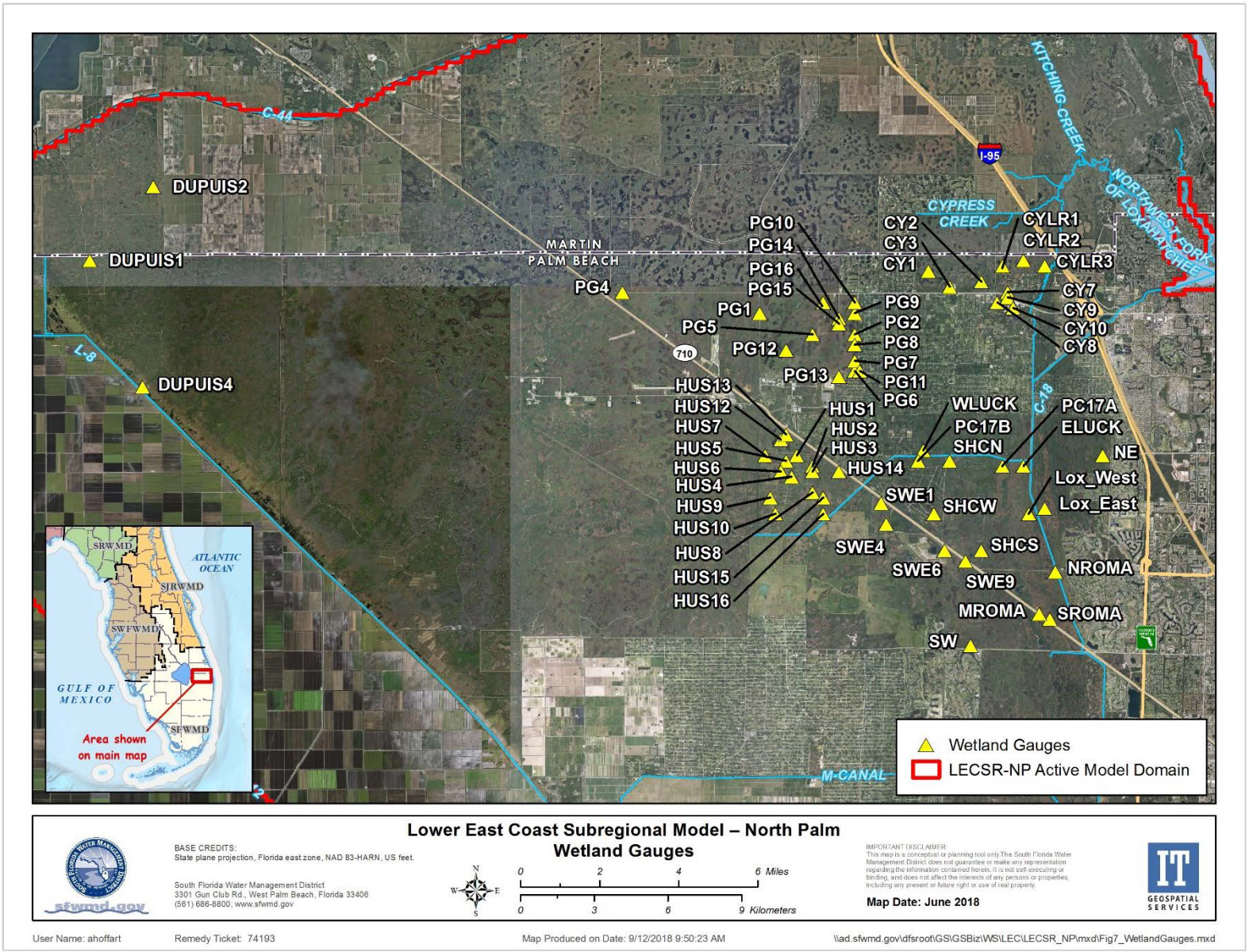

Figure 50. Wetland gauge locations used in LECSR-NP model calibration.

4.2.3 Qualitative Analysis

4.2.3.1 Wetland Rapid Assessment Procedure (WRAP) Cells

The Ecological Subteam of the Project Delivery Team have a list of 56 locations, known as Wetland Rapid Assessment Procedure (WRAP) cells, where historical field conditions have been evaluated (**Figure 51**). Hydrographs and duration curves for the calibration period were plotted and evaluated by a select group of participants from the Ecological Subteam. Hydrographs and duration curves were evaluated to review the duration of inundation and the range of water levels compared to field notes and knowledge. A target was not established for the hydrographs or duration curves as they were used for qualitative analysis of calibration performance.

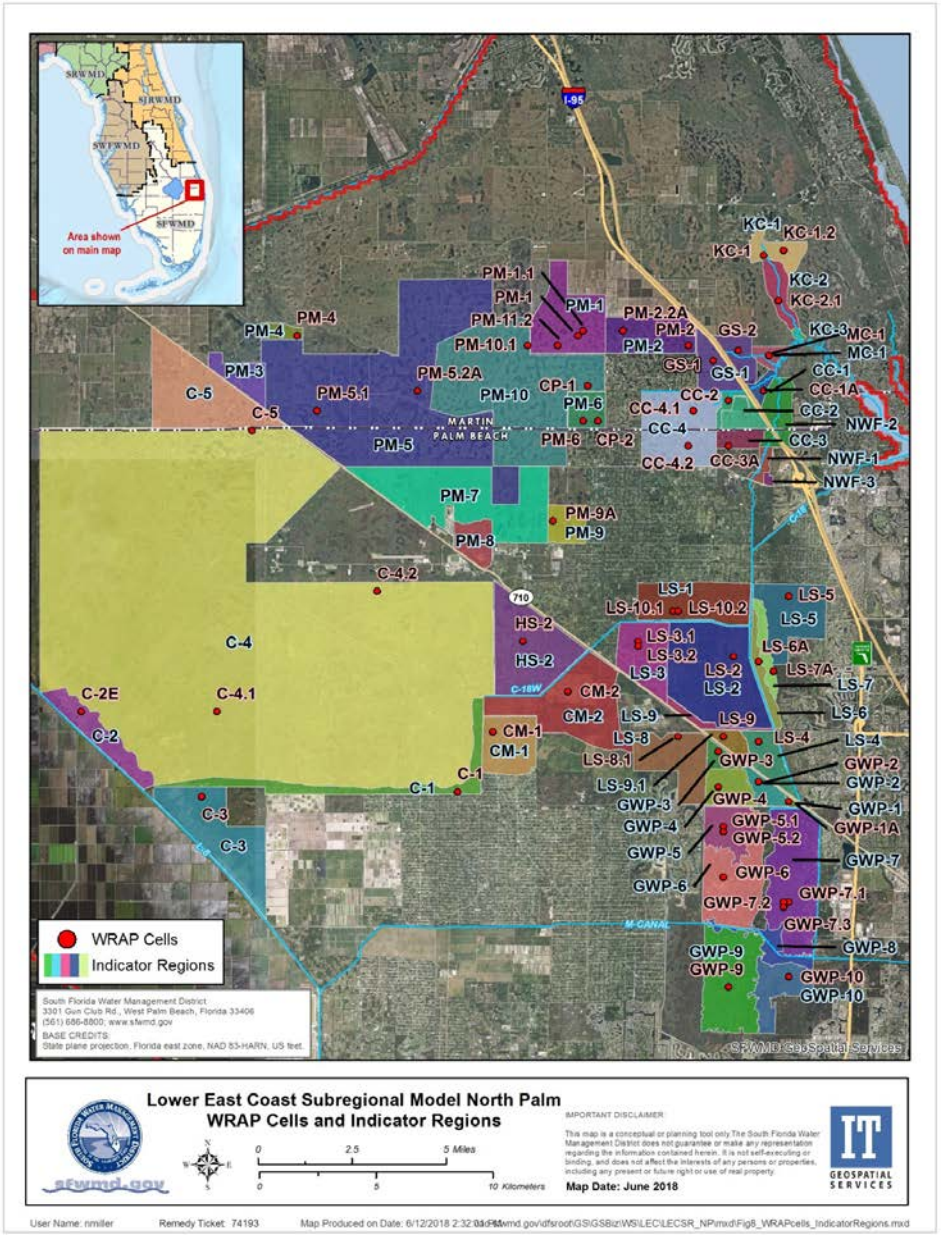

Figure 51. Wetland Rapid Assessment Procedure (WRAP) cells and indicator regions used for LECSR-NP model calibration.

4.2.3.2 Water Budgets

Annual and seasonal water budgets for the C-18 (combination of C-18/Corbett and Jupiter Farms basins), L-8, Flow-way 3 (combination of Pal Mar, Grove, and historical Cypress Creek basins), and GWP basins were used as an overall indicator of bias in the calibration process (**Figure 52**). This criterion is a qualitative technique to evaluate any bias or seasonal trends that may be present. A target was not established for this criterion.

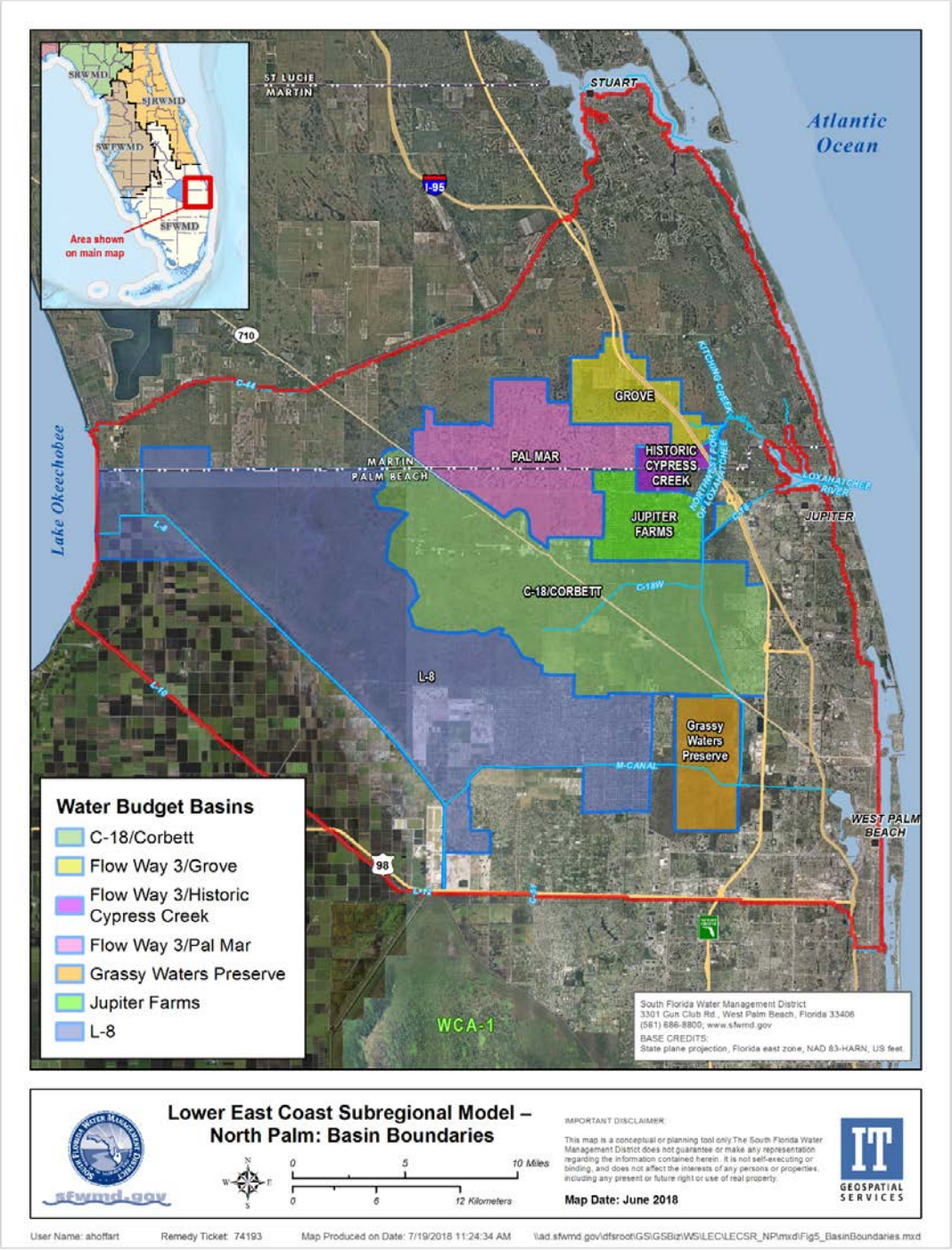

Figure 52. Water budget basin boundaries for the LECSR-NP.

4.3 Calibration Results

4.3.1 Flow Discharges

Table 14 shows the calibration statistics for the flow discharge locations. These statistics were used as quantitative calibration criteria to evaluate overall model performance. Daily flow was aggregated to monthly cumulative flow for simulated and historical conditions. Months with missing data were excluded; therefore, different water control structures have different numbers of months for the period of record.

Table 14. Flow discharge statistics for the calibration period (2006 – 2014).

Monitoring Station	R^2	DV (%)	NS
C-18 Weir	0.57	-1	0.57
Lainhart Dam	0.82	-9	0.80
S-46	0.85	-5	0.82
G-92	0.74	2	0.74
G-160	0.76	-5	0.75
Cypress Creek and Hobe Grove Ditch	0.73	-4	0.70
Kitching Creek	0.79	-6	0.78

DV = deviation of volume; NS = Nash-Sutcliffe coefficient; R2 = coefficient of determination.

The LECSR-NP more than adequately simulated flow for the calibration period. All discharge locations met the NS coefficient and R^2 target of 0.4 for the calibration period. The DV target of less than 15 percent was met at all discharge locations. Due to the complexity in characterizing drainage patterns between the Hobe Grove and historical Cypress Creek basins, the two basins were evaluated together with a combination of flows from Cypress Creek and Hobe Grove Ditch. As discussed previously, G-161 is not included because the flows were based on historical data.

4.3.1.1 C-18 Weir

Figure 53 shows the monthly flow hydrograph for the calibration period at the C-18 weir. The simulated monthly flows were underestimated in the beginning of the calibration period and during peak events. The discrepancy between historical and simulated monthly flows in the beginning of the calibration period may be related to restoration work undertaken by Palm Beach County in the Hungryland Slough area, which contributes flow to the C-18 West Canal and C-18 weir. **Figure 54** illustrates the cumulative monthly flow curve. Based on the curve, the model underestimates historical flows through the C-18 weir between 2007 and 2014. The simulated cumulative flow appears to match historical cumulative flow towards the end of the calibration period.

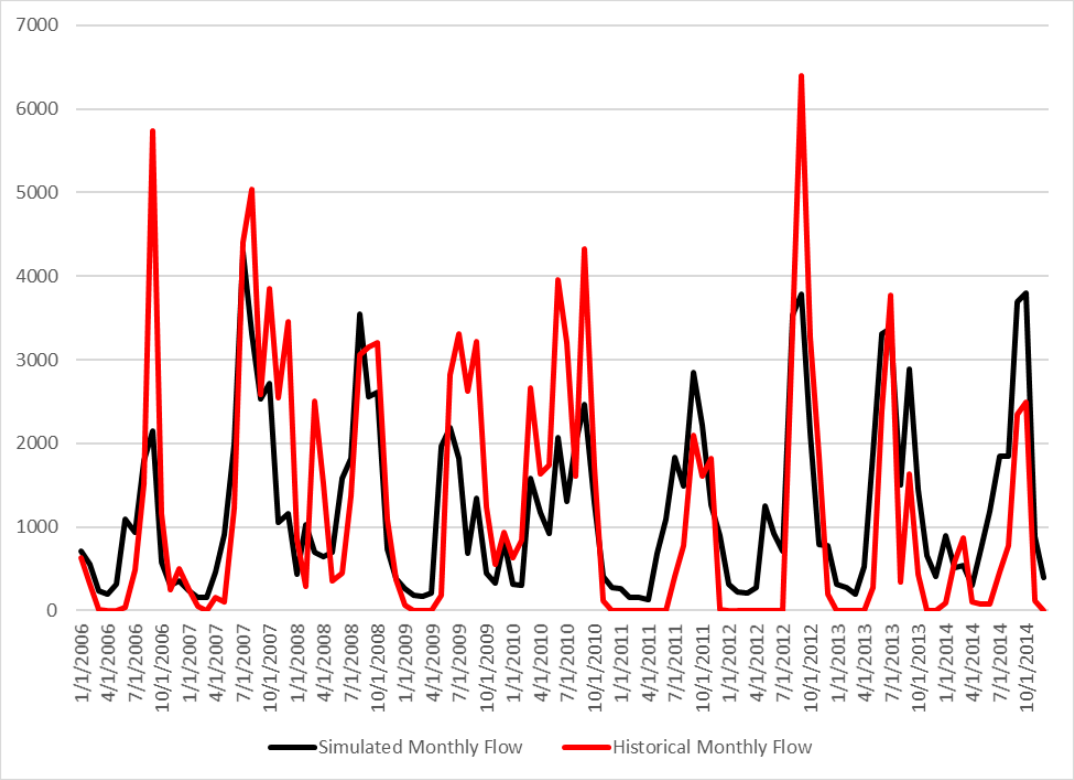

Figure 53. Simulated and historical monthly flow hydrograph for the C-18 weir from 2006 to 2014.

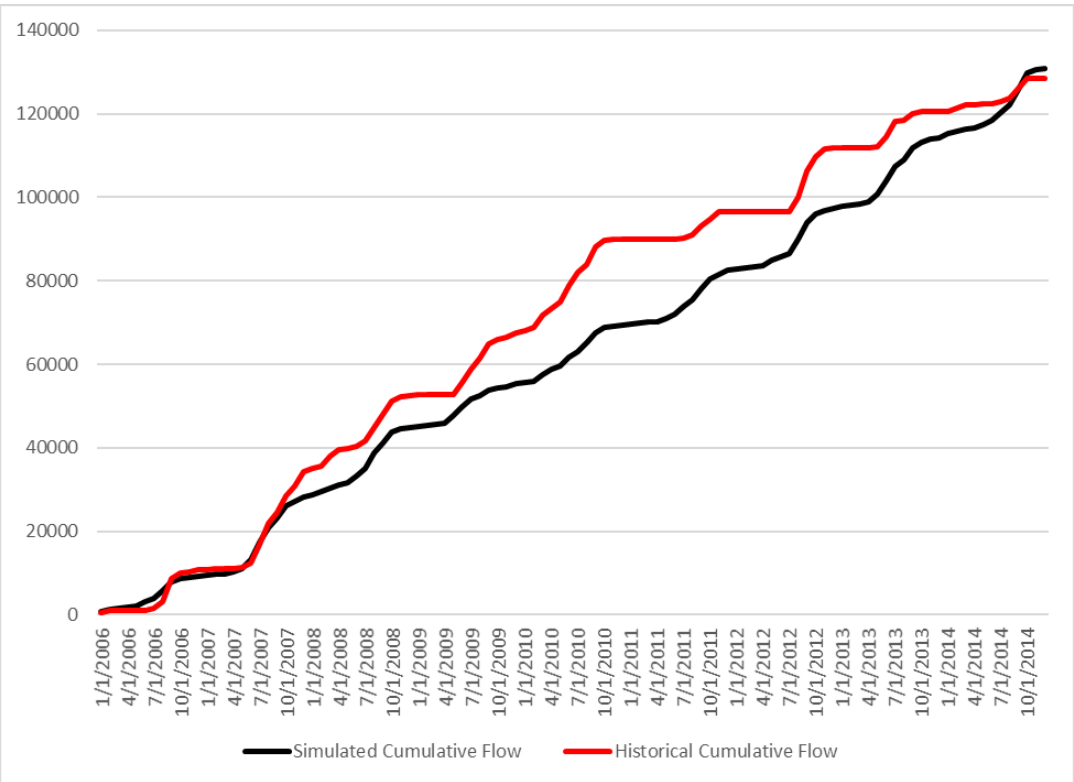

Figure 54. Simulated and historical cumulative monthly flow curve for the C-18 weir from 2006 to 2014.

4.3.1.2 Lainhart Dam

Figure 55 shows the monthly flow hydrograph for the calibration period at Lainhart Dam. The model appears able to simulate high- and low-flow conditions when compared to historical flow. **Figure 56** illustrates the cumulative monthly flow curve. Based on the curve, the simulated and historical cumulative flow match from 2006 through 2010. There is a slight deviation in the simulated and historical cumulative flow curves, with the model slightly over-predicting historical conditions.

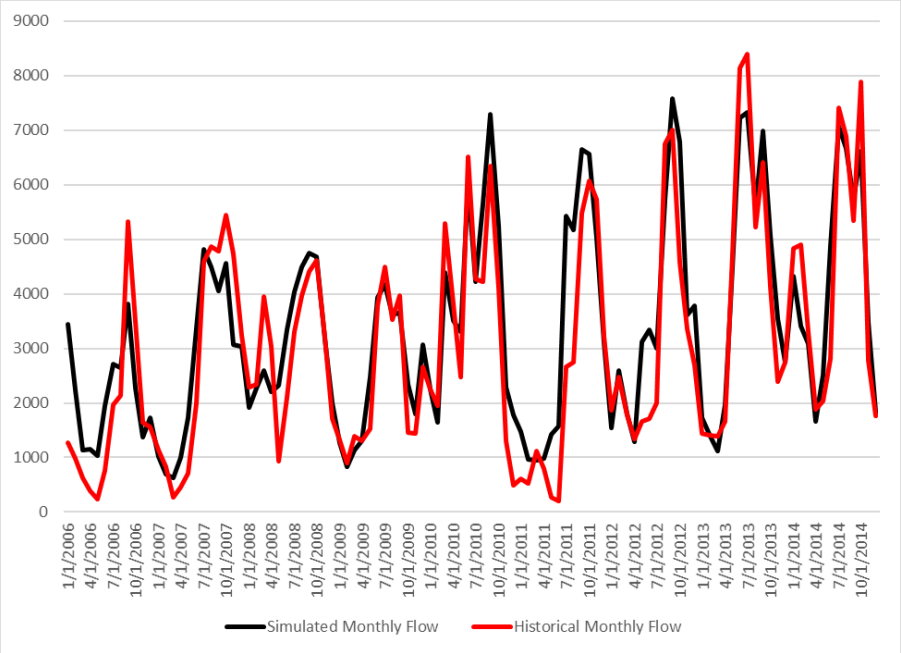

Figure 55. Simulated and historical monthly flow hydrograph for Lainhart Dam from 2006 to 2014.

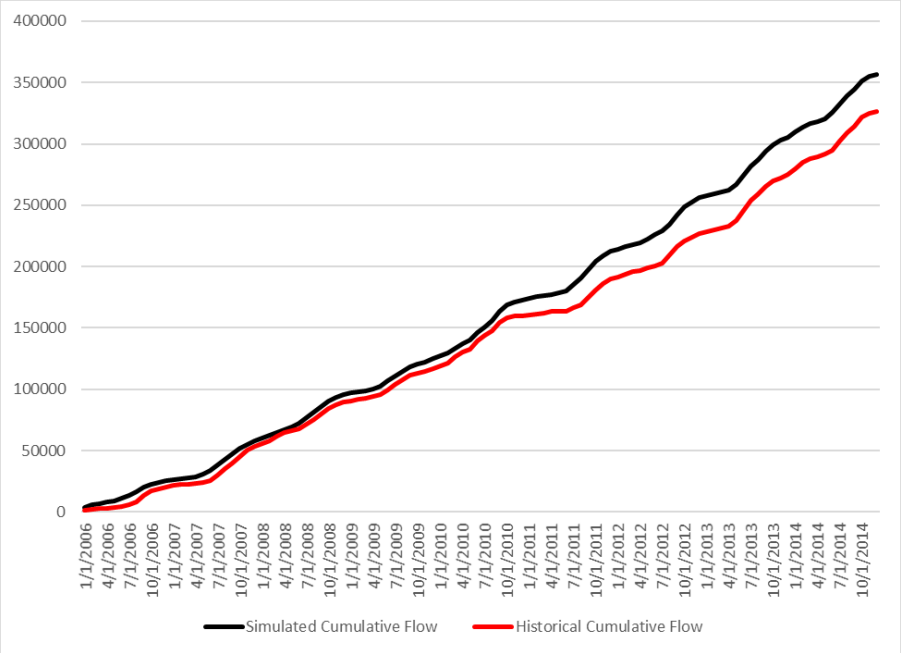

Figure 56. Simulated and historical cumulative monthly flow curve for Lainhart Dam from 2006 to 2014.

4.3.1.3 S-46

Figure 57 shows the monthly flow hydrograph for the calibration period at S-46. The simulated and historical monthly flows generally match, except for high peak events such as in August 2012 during Tropical Storm Isaac. **Figure 58** illustrates the cumulative monthly flow curve. Based on the curve, the model overestimates historical flows through S-46 from 2009 through the end of the calibration period. Deviations between simulated and historical cumulative flow appear to decrease from 2013 onward.

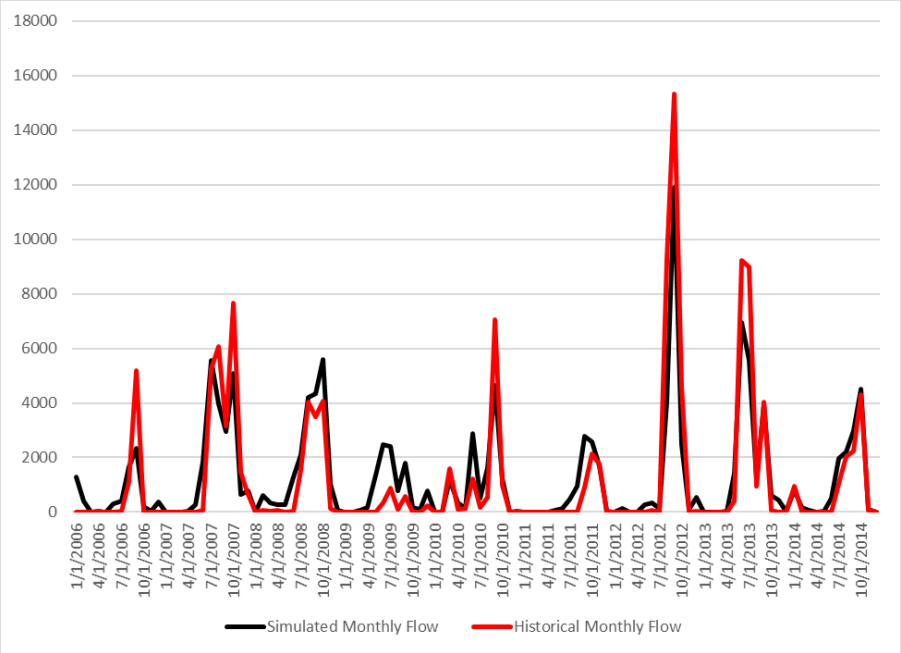

Figure 57. Simulated and historical monthly flow hydrograph for S-46 from 2006 to 2014.

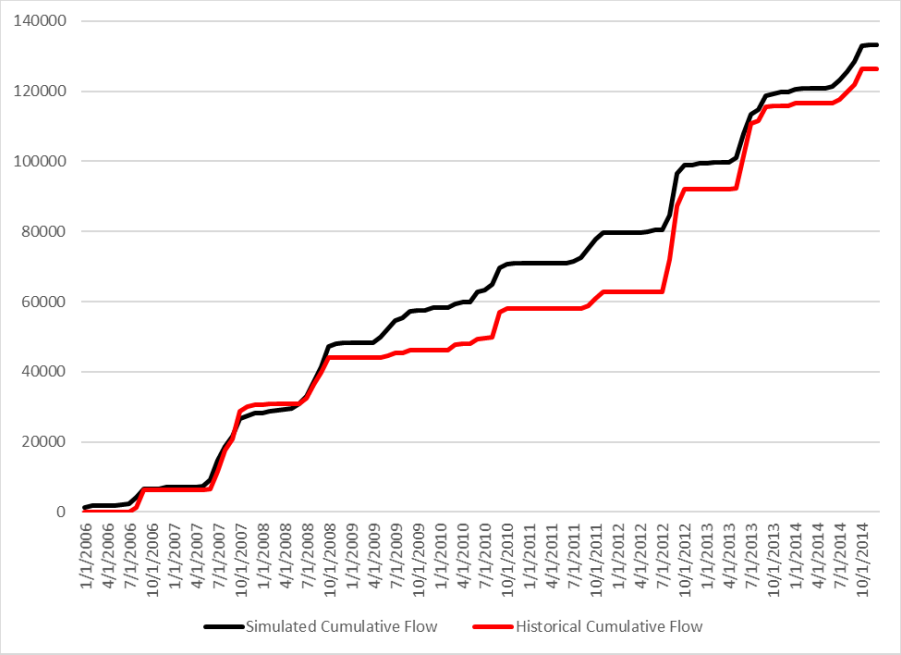

Figure 58. Simulated and historical cumulative monthly flow curve for S-46 from 2006 to 2014.

4.3.1.4 G-92

Figure 59 shows the monthly flow hydrograph for the calibration period at G-92. There does not appear to be any specific trend of under- or overestimation of the monthly flows. The model occasionally simulates higher monthly flow than historical conditions, but sometimes the model simulates lower monthly flow than the historical conditions. The model did not simulate the reverse flow capabilities of G-92 and thus will over-predict during months when reverse flow occurred. **Figure 60** illustrates the cumulative monthly flow curve. Based on the curve, the simulated and historical cumulative flows appear to match very well, with only very slight deviations and no consistent over- or under-prediction trends throughout the calibration period.

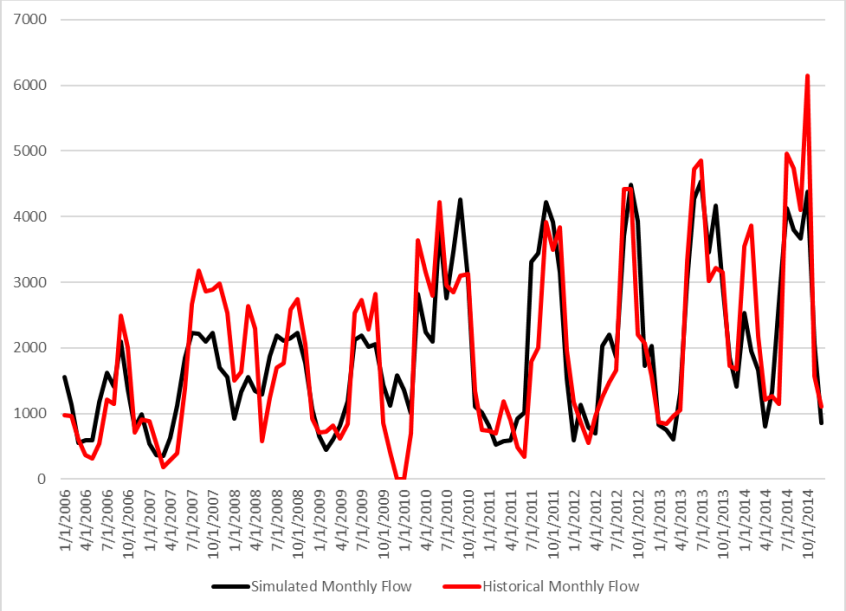

Figure 59. Simulated and historical monthly flow hydrograph for G-92 from 2006 to 2014.

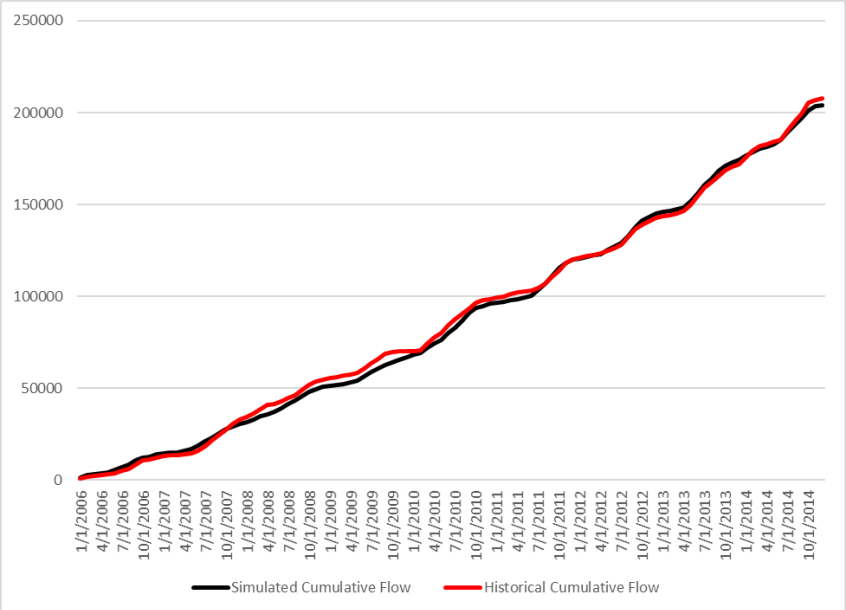

Figure 60. Simulated and historical cumulative monthly flow curve for G-92 from 2006 to 2014.

4.3.1.5 G-160

Figure 61 shows the monthly flow hydrograph for the calibration period at G-160. There does not appear to be any specific trend of under- or overestimation of the monthly flows. The model occasionally simulates higher monthly flow than historical conditions, but sometimes the model simulates lower monthly flow than historical conditions. Between 2007 and 2009, when flow through G-160 did not follow a specific operational protocol, the model could not match the monthly flows. **Figure 62** illustrates the cumulative monthly flow curve. Based on the curve, the model slightly overestimates flows from 2010 through the end of the calibration period.

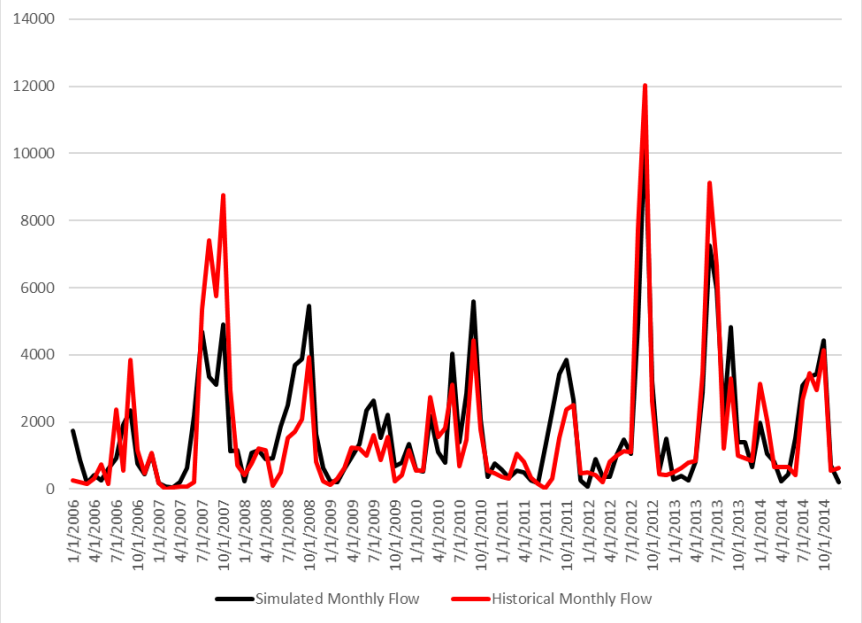

Figure 61. Simulated and historical monthly flow hydrograph for G-160 from 2006 to 2014.

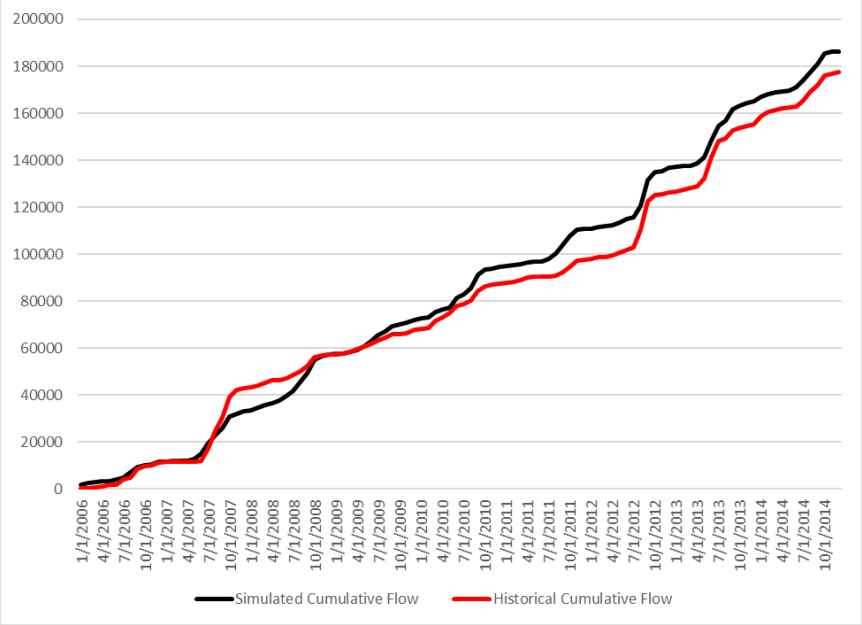

Figure 62. Simulated and historical cumulative monthly flow curve for G-160 from 2006 to 2014.

4.3.1.6 Cypress Creek and Hobe Grove Ditch

Figure 63 shows the monthly flow hydrograph for the calibration period for Cypress Creek and Hobe Grove Ditch. Due to the complexity of differentiating contributing areas, the two structures were assessed together. Additionally, historical data were only available through 2009. There does not appear to be any specific trend of under- or overestimation of the monthly flows. The model occasionally simulates higher monthly flow than historical conditions, but sometimes the model simulates lower monthly flow than historical conditions. **Figure 64** illustrates the cumulative monthly flow curve through 2009 when historical data were available. Based on the curve, the simulated and historical cumulative flows appear to match very well, with only very slight deviations and no consistent over- or under-prediction trends.

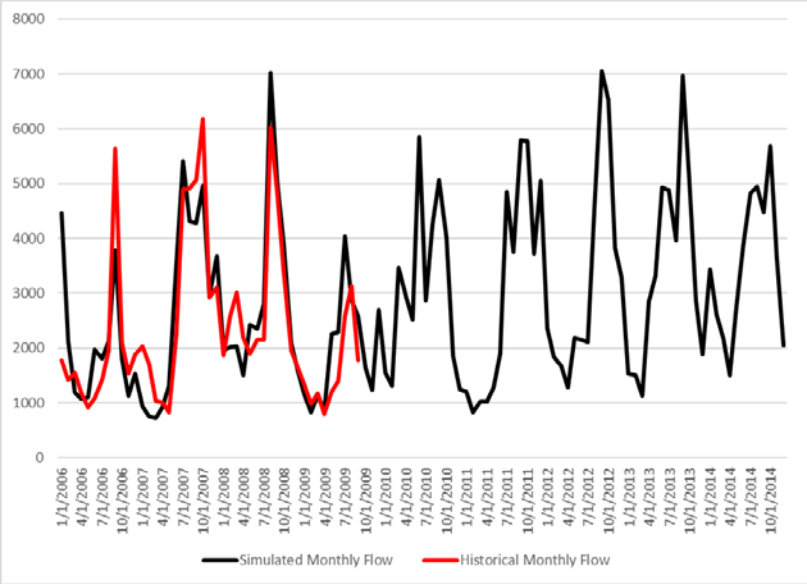

Figure 63. Simulated and historical monthly flow hydrograph for Cypress Creek and Hobe Grove Ditch from 2006 to 2014.

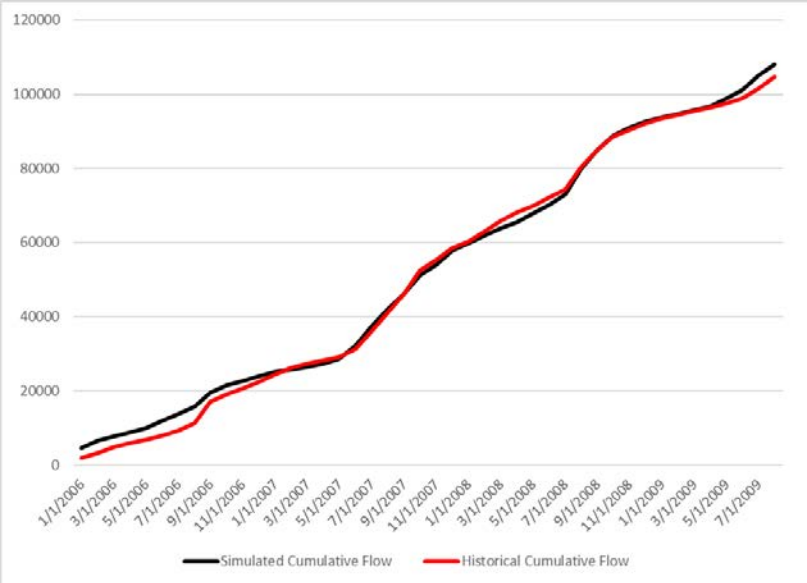

Figure 64. Simulated and historical cumulative monthly flow curve for Cypress Creek and Hobe Grove Ditch from 2006 to 2009.

4.3.1.7 Kitching Creek

Figure 65 shows the monthly flow hydrograph for the calibration period for Kitching Creek. There does not appear to be any specific trend of under- or overestimation of the monthly flows. The model occasionally simulates higher monthly flow than historical conditions, but sometimes the model simulates lower monthly flow than historical conditions. **Figure 66** illustrates the cumulative monthly flow curve through 2009 when historical data were available. Based on the curve, the simulated cumulative flow appears to have some deviations from the historical cumulative flow. However, there does not appear to be a consistent prediction bias as the cumulative flow can be under- or over-predicted by the model.

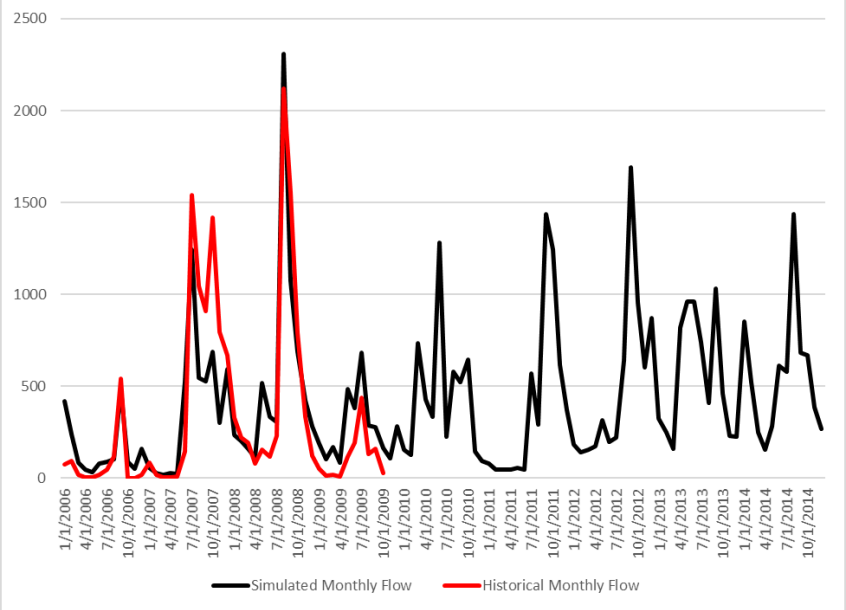

Figure 65. Simulated and historical monthly flow hydrograph for Kitching Creek from 2006 to 2014.

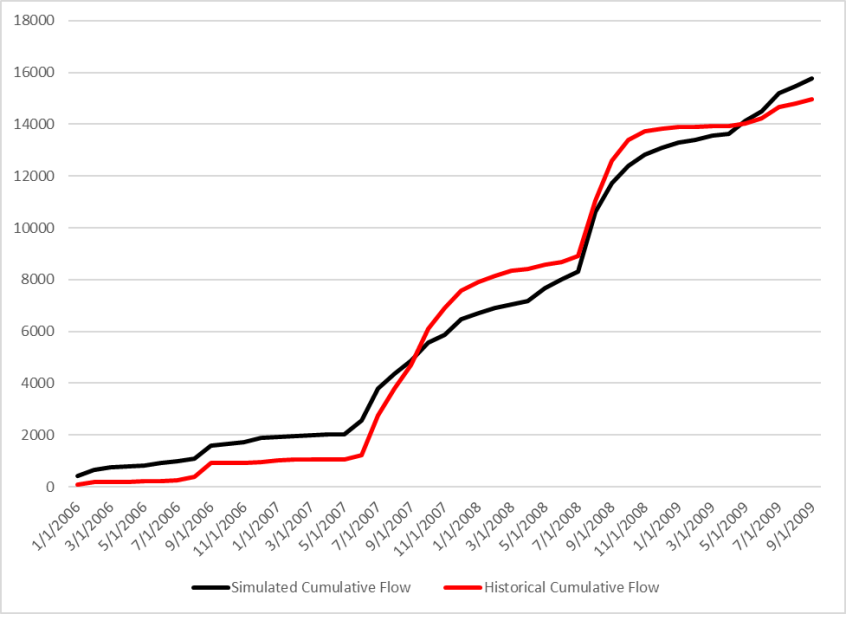

Figure 66. Simulated and historical cumulative monthly flow curve for Kitching Creek from 2006 to 2009.

4.3.2 Water Level Elevations

Table 15 shows the statistics for the groundwater monitoring wells; 54 of the 58 groundwater monitor wells are calibrated. The overall MAE for the groundwater wells was 0.56 feet. **Appendix A** presents hydrographs of historical and simulated water levels for the 58 monitor wells. **Table 16** shows the calibration statistics for the wetland gauges; 47 of the 61 wetland gauges are calibrated. It is critical to note that of the 14 wetland gauges that are not calibrated, 7 have very small ranges (close to 0.5 feet or less). It is very difficult to calibrate a regional groundwater model to such a small range, which is why SFWMD groundwater models historically are calibrated to the ±1-foot threshold. Using the historical criteria, 50 of the 61 wetland gauges met the calibration criteria. The overall MAE for the wetland gauges is 0.68 feet. **Appendix B** presents hydrographs of the historical and simulated water levels for the 61 wetland gauges. **Table 17** shows the statistics for the calibration locations that were sequestered due to a lack of historical data or based on proximity to river and GHB cells.

Table 15. Groundwater monitoring well statistics for the calibration period (2006 – 2014).

Monitor Well	Layer	Mean Error (feet)	Mean Absolute Error (feet)	Root Mean Square Error (feet)	Water Level Stage Range	Percent of Time Within 20% of the Range	Calibration Met (Individual Stage Criterion)	Calibration Met (±1 foot Criterion)
PB-565_G	1	-0.04	0.44	0.56	1.32	96.87	Y	Y
PB-809	1	0.26	0.46	0.59	1.30	96.09	Y	Y
M-1004	1	-0.26	0.57	0.71	1.76	91.83	Y	Y
M-1024	2	0.03	0.27	0.35	0.98	98.04	Y	Y
PB-1733	3	-0.23	0.58	0.69	0.84	75.68	Y	Y
PB-1732	3	-0.21	0.35	0.44	0.58	82.43	Y	Y
PB-1642	1	-0.09	0.39	0.51	0.87	94.01	Y	Y
M-1261	1	-0.13	0.87	1.04	1.76	91.83	Y	Y
M-1071	2	0.04	0.51	0.64	1.12	94.23	Y	Y
M-1072	2	0.03	0.51	0.65	1.10	93.35	Y	Y
M-1073	2	-0.03	0.40	0.59	1.17	90.96	Y	Y
M-1083	1	-0.33	0.59	0.74	0.88	75.91	Y	Y
M-1086	2	-0.21	0.93	1.21	1.51	81.62	Y	Y
M-1088	3	-0.15	0.95	1.24	1.45	78.92	Y	Y
M-1096	3	0.43	0.54	0.64	0.89	80.45	Y	Y
M-1234	1	-0.02	0.31	0.45	1.36	98.54	Y	Y
PB-1525	1	0.40	0.76	1.02	0.97	71.49	N	N
PB-1548	2	-0.42	0.70	0.56	1.22	82.50	Y	Y
PB-1613	3	0.17	0.36	0.45	0.98	95.59	Y	Y
PB-1615	1	0.28	0.44	0.53	1.01	94.83	Y	Y
PB-1648	1	0.35	0.63	0.85	1.26	87.64	Y	Y
PB-1649	3	-0.22	0.54	0.67	1.17	93.62	Y	Y
PB-1662	1	0.68	0.68	0.79	0.92	73.91	Y	Y
PB-561	1	0.07	0.40	0.49	0.62	81.82	Y	Y
PB-685	1	-0.43	0.73	0.96	1.32	83.93	Y	Y
PB-689	1	0.45	0.47	0.52	0.90	97.34	Y	Y
WTVW	1	0.56	0.56	0.62	0.65	64.83	Y	Y
PB-831	1	0.35	0.55	0.73	0.96	79.98	Y	Y

Monitor Well	Layer	Mean Error (feet)	Mean Absolute Error (feet)	Root Mean Square Error (feet)	Water Level Stage Range	Percent of Time Within 20% of the Range	Calibration Met (Individual Stage Criterion)	Calibration Met (±1 foot Criterion)
PB-880	2	0.80	0.82	0.99	0.87	57.97	N	Y
PB-99	1	-0.27	0.46	0.59	1.10	95.23	Y	Y
JD-12	1	0.37	0.87	1.04	1.10	66.90	Y	N
JD-26	1	0.14	0.76	0.92	1.12	77.41	Y	Y
JD-6	1	0.09	0.71	0.87	1.11	78.48	Y	Y
JDSPMW1G	2	0.36	0.63	0.78	1.22	89.81	Y	Y
JDSPMW3G	2	-0.02	0.55	0.66	1.31	95.80	Y	Y
C18P-D	2	0.66	0.69	0.96	1.02	75.79	Y	Y
C18P-S	1	0.76	0.81	1.11	1.04	71.42	N	N
EB-D	2	0.02	0.38	0.49	1.08	96.28	Y	Y
EB-S	1	0.41	0.53	0.69	1.11	94.04	Y	Y
NEB-D	2	-0.10	0.35	0.44	1.10	99.16	Y	Y
NEB-S	1	0.13	0.31	0.39	1.07	99.35	Y	Y
NWB-D	2	0.40	0.51	0.70	0.78	75.33	Y	Y
NWB-S	1	0.27	0.53	0.72	0.79	77.93	Y	Y
OMN-D	2	0.38	0.57	0.74	1.08	84.45	Y	Y
OMN-S	1	-0.02	0.40	0.51	0.96	95.07	Y	Y
OMS-D	2	0.62	0.64	0.90	1.05	78.31	Y	Y
PGA-N	2	0.56	0.56	0.68	0.81	82.50	Y	Y
PGAW01	1	-0.22	0.43	0.60	1.57	97.89	Y	Y
PGAW02D	3	0.32	0.60	0.79	1.07	83.38	Y	Y
PGAW02S	1	0.70	0.85	1.10	1.04	70.76	N	N
PGAW03D	2	0.17	0.55	0.74	1.11	85.32	Y	Y
PGAW03S	1	0.25	0.60	0.80	1.08	80.23	Y	Y
PGAW04	1	0.20	0.42	0.57	1.19	95.76	Y	Y
PGAW05	1	0.40	0.45	0.67	1.18	91.08	Y	Y
WPBWCA	1	-0.27	0.55	0.69	0.90	79.30	Y	Y
M-Canal	1	-0.01	0.37	0.49	1.18	95.00	Y	Y
G161H	1	-0.12	0.47	0.60	0.95	88.97	Y	Y
G161T	1	0.13	0.61	0.83	0.96	77.22	Y	Y
Overall		**0.15**	**0.56**	**0.71**	**1.09**	**85.68**	**93.10%**	**93.10%**

Table 16. Wetland gauge statistics for the calibration period (2006 – 2014).

Region	Wetland Gauge	Mean Error (feet)	Mean Absolute Error (feet)	Root Mean Square Error (feet)	Water Level Stage Range	Percent of Time Within 20% of the Range	Calibration Met (Individual Stage Criterion)	Calibration Met (±1 foot Criterion)
Dupuis	DUPUIS1	0.09	0.65	0.82	0.85	67.95	Y	Y
	DUPUIS2	-0.54	0.72	0.83	0.85	61.85	Y	Y
	DUPUIS4	0.36	1.06	1.35	1.40	75.58	Y	N
Pine Glades	PG1	-0.05	0.30	0.39	0.95	98.04	Y	Y
	PG2	-0.01	0.69	0.98	1.22	78.43	Y	Y
	PG4	0.45	0.47	0.53	0.92	98.06	Y	Y
	PG5	1.02	1.02	1.11	1.01	49.51	N	N
	PG6	-0.43	0.92	1.23	1.38	80.39	Y	Y
	PG7	0.37	0.77	0.95	1.38	87.38	Y	Y
	PG8	0.13	0.69	0.89	1.42	84.47	Y	Y
	PG9	-0.30	0.86	1.18	1.46	84.47	Y	Y
	PG10	-1.12	1.24	1.51	1.51	62.38	Y	N
	PG11	0.52	0.56	0.70	0.40	41.58	N	Y
	PG12	0.61	0.62	0.78	0.80	76.77	Y	Y
	PG13	0.65	1.01	1.34	1.14	63.93	N	N
	PG14	-0.26	0.54	0.66	1.14	95.45	Y	Y
	PG15	-0.28	0.59	0.71	1.00	83.33	Y	Y
	PG16	0.26	0.47	0.59	0.95	84.85	Y	Y
Loxahatchee Slough	SROMA	0.10	0.47	0.62	0.97	87.74	Y	Y
	MROMA	0.47	0.56	0.72	0.94	76.42	Y	Y
	NROMA	0.76	0.76	1.04	1.20	75.47	Y	Y
	SHCW	0.26	0.44	0.68	0.99	89.62	Y	Y
	WLUCK	0.72	1.29	1.55	1.27	48.11	N	N
	ELUCK	0.24	0.76	0.97	1.13	77.36	Y	Y
	NE	-1.20	1.26	1.50	1.04	43.40	N	N
	SW	0.66	0.83	1.00	0.79	52.83	N	N
	SHCS	1.12	1.14	1.30	0.47	13.04	N	N
	SHCN	0.01	0.57	0.80	0.47	48.84	N	Y
	PC17A	0.09	0.74	0.94	0.86	68.18	N	Y
	PC17B	-0.19	0.70	0.87	0.72	58.14	N	Y
Hungryland Slough	HUS1	0.04	0.47	0.53	0.92	98.06	Y	Y
	HUS2	1.02	1.02	0.81	1.02	79.00	Y	N
	HUS3	0.14	0.57	0.79	1.03	84.00	Y	Y
	HUS4	-0.27	0.65	0.80	0.95	78.00	Y	Y
	HUS5	-0.63	0.70	0.81	0.85	68.00	Y	Y
	HUS6	-0.38	0.63	0.82	1.05	80.00	Y	Y
	HUS7	-0.07	0.67	0.83	0.90	68.00	Y	Y
	HUS8	-0.28	0.60	0.73	0.79	86.00	Y	Y
	HUS9	-0.18	0.41	0.62	0.81	93.00	Y	Y
	HUS10	-0.06	0.54	0.70	0.97	84.00	Y	Y
	HUS12	-0.37	0.77	0.95	1.27	89.00	Y	Y

Region	Wetland Gauge	Mean Error (feet)	Mean Absolute Error (feet)	Root Mean Square Error (feet)	Water Level Stage Range	Percent of Time Within 20% of the Range	Calibration Met (Individual Stage Criterion)	Calibration Met (±1 foot Criterion)
	HUS13	0.50	0.71	1.06	1.24	86.00	Y	Y
	HUS14	0.04	0.61	0.85	1.21	86.00	Y	Y
	HUS15	-0.30	0.69	0.83	0.98	74.00	Y	Y
	HUS16	-0.51	0.71	0.91	1.02	76.00	Y	Y
Cypress Creek	CY1	-0.27	0.59	0.69	0.72	69.66	Y	Y
	CY2	-0.19	0.42	0.52	0.54	69.88	Y	Y
	CY3	0.15	0.37	0.45	0.36	54.41	N	Y
	CY7	0.07	0.58	0.72	0.54	58.00	N	Y
	CY8	-0.05	0.38	0.49	0.38	56.76	N	Y
	CY9	0.71	0.75	0.85	0.53	36.11	N	Y
	CY10	0.20	0.38	0.47	0.57	75.00	Y	Y
	CYLR1	-0.15	0.61	0.79	1.21	90.29	Y	Y
	CYLR2	-0.13	0.93	1.13	1.40	69.61	Y	N
	CYLR3	-0.34	1.02	1.18	1.32	73.68	Y	N
Loxahatchee Slough	Lox_East	-0.06	0.39	0.54	0.81	87.97	Y	Y
	Lox_West	-0.46	0.56	0.68	0.84	80.47	Y	Y
	SWE1	0.52	0.61	0.80	0.96	77.36	Y	Y
	SWE4	-0.04	0.39	0.54	0.99	90.38	Y	Y
	SWE6	-0.56	0.64	0.72	0.93	75.96	Y	Y
	SWE9	-0.26	0.40	0.55	1.20	96.23	Y	Y
Overall		**0.04**	**0.68**	**0.85**	**0.97**	**73.84**	**77.05%**	**81.97%**

Table 17. Statistics for sequestered locations for the calibration period (2006 – 2014).

Name	Calibration Type	Layer	Mean Error (feet)	Mean Absolute Error (feet)	Root Mean Square Error (feet)	Water Level Stage Range	Percent of Time Within 20% of the Range	Calibration Met (Individual Stage Criterion)	Calibration Met (±1 foot Criterion)
PMW-103L	Groundwater Well	2	0.01	0.34	0.43	0.48	75.53	Y	Y
PMW-103U	Groundwater Well	1	0.05	0.30	0.36	0.38	64.08	Y	Y
PMW-106L	Groundwater Well	2	2.04	2.06	2.62	1.27	57.95	N	N
PMW-1L	Groundwater Well	2	-0.02	0.46	0.61	0.65	70.61	Y	Y
PMW-1U	Groundwater Well	1	0.06	0.43	0.56	0.61	76.33	Y	Y
PZ5B	Groundwater Well	1	-1.31	2.32	3.09	1.81	61.93	N	N
PZ5C	Groundwater Well	2	1.02	1.11	1.22	0.56	17.42	N	N
PZ5D	Groundwater Well	3	0.08	1.10	1.40	1.47	78.85	Y	N
PZ8A	Groundwater Well	1	-1.11	1.20	1.69	0.77	53.64	N	N
PZ8B	Groundwater Well	2	2.61	2.61	2.73	0.57	0.00	N	N
PB-1817S	Groundwater Well	2	0.26	0.40	0.47	0.51	66.67	Y	Y
PB-1815S	Groundwater Well	2	0.15	0.44	0.56	0.56	55.00	Y	Y
OMS-S	Groundwater Well	1	0.22	0.28	0.35	0.35	67.61	Y	Y
PGA-S	Groundwater Well	1	0.26	0.31	0.44	0.51	68.89	Y	Y
PB-1734	Groundwater Well	2	0.05	0.19	0.27	0.39	82.86	Y	Y
PB-1727	Groundwater Well	3	0.31	0.63	0.80	1.13	80.00	Y	Y
PB-1726	Groundwater Well	3	0.12	0.49	0.60	1.04	91.43	Y	Y
ENR001W1	Groundwater Well	1	-0.16	0.24	0.31	0.38	81.63	Y	Y
SWE2	Wetland Gauge	1	-0.09	0.11	0.15	0.29	93.33	Y	Y
SWE3	Wetland Gauge	1	-0.12	0.17	0.22	0.19	66.67	N	Y
PG17	Wetland Gauge	1	0.07	0.52	0.69	0.70	75.00	Y	Y
HUS11	Wetland Gauge	1	-1.01	1.27	1.52	1.18	50.00	N	N
HUS17	Wetland Gauge	1	1.18	1.33	1.58	1.26	53.00	N	N
HUS18	Wetland Gauge	1	0.52	0.86	1.15	1.23	73.00	Y	N

Figures 67 and **68** show the spatial distribution of the groundwater monitoring wells and wetland gauges, respectively, with the calibration status based on the individual water level criteria. Points are represented in green if calibration targets were met and in red if calibration targets were not met. The size of the points is proportional to the MAE for each calibration location. The larger the point, the larger the MAE for the calibration location. Based on **Figure 67**, there does not appear to be any spatial clustering of bias in groundwater monitoring wells across the model domain. The four monitor wells that did not meet calibration criteria are located along canals. If a choice had to be made, the modelers favored better canal flow calibration over groundwater level calibration due the importance of quantifying flows to meet project objectives per the Project Delivery Team. Based on **Figure 68**, there appears to be slight clustering of bias in wetland gauges within Loxahatchee Slough. This bias may be attributed to the restoration efforts undertaken by Palm Beach County throughout the calibration period. Loxahatchee Slough South was restored between 2003 and 2007, with western portions restored between 2005 and 2015. The model simulated the restored conditions within Loxahatchee Slough, and thus would not be able to adequately simulate the conditions that existed prior to restoration. Other than the wetland gauges in Loxahatchee Slough, there does not appear to be any other clustering of bias in wetland gauges across the model domain.

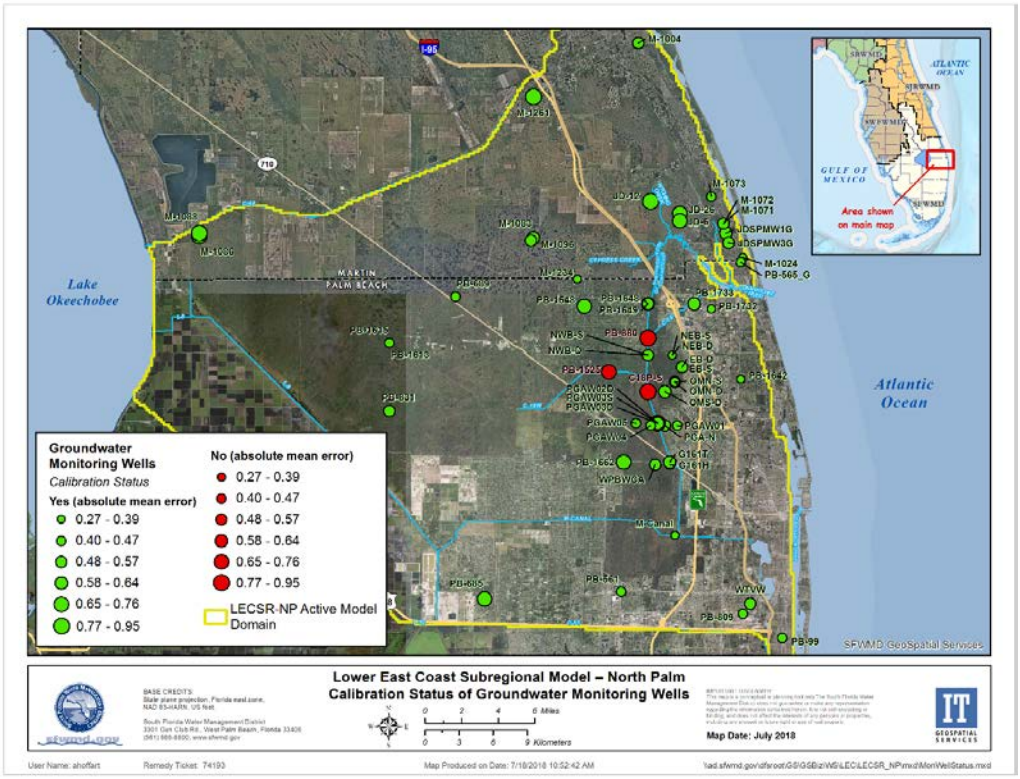

Figure 67. Calibration status and mean absolute error for groundwater monitoring wells used in LECSR-NP calibration.

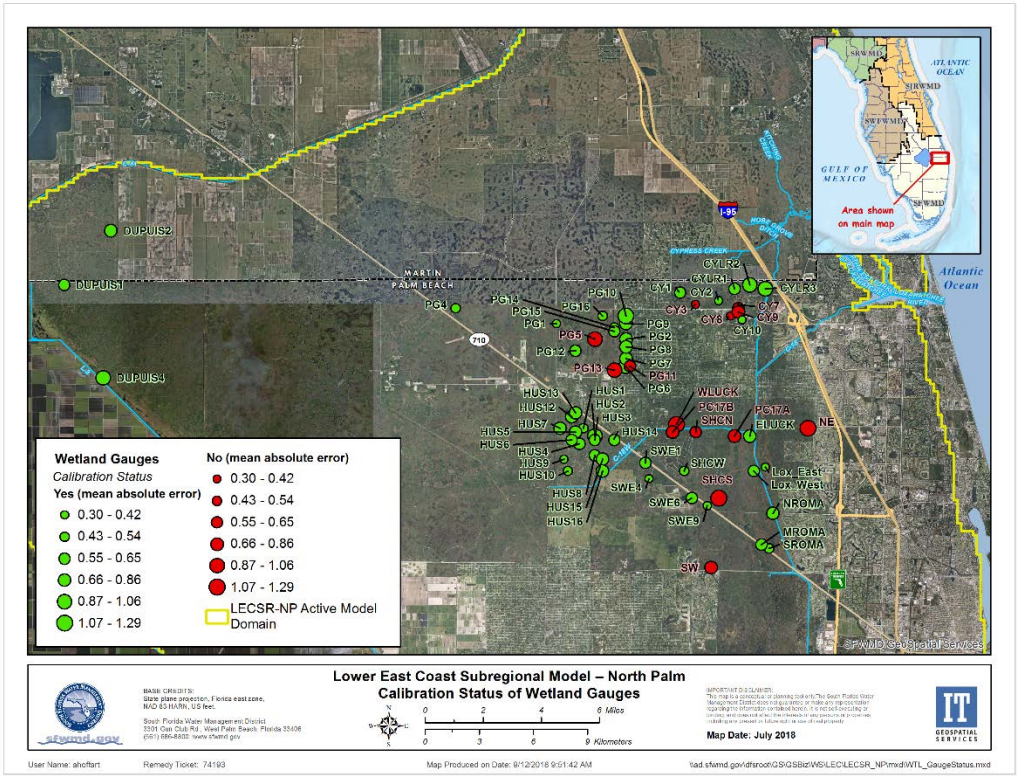

Figure 68. Calibration status and mean absolute error of wetland gauges used in LECSR-NP calibration.

4.3.3 Wetland Rapid Assessment Procedure (WRAP) Cells

Select members of the Ecological Subteam of the Project Delivery Team reviewed the hydrographs and stage duration curves for the WRAP cells (**Appendix C**). Hydrographs and stage duration curves were plotted against model cell topography to determine the percent inundated and to calculate the number of days during the calibration period that the wetland would be inundated. The model cell topography was averaged across the 704-foot cells and therefore does not capture the variability in various wetland and upland areas that may occur in a single cell. To determine if the model cell topography used in the graphics was appropriate, a combination of field data, best professional judgement, and the SFWMD's 5-foot LiDAR data was used. **Appendix C** shows the 5-foot digital elevation model for each model cell containing a WRAP cell and shows the variability in ground elevations across each model cell.

Simulated water levels and inundation duration were compared to field assessments for WRAP indicator regions. Field assessments included a field hydrology score, between 0 and 3, which was converted to an index score and multiplied by the total number of days during the period of record to determine the number of days inundated. Field assessment and procedure are discussed in the final report by Ecology and Environment, Inc. (2004b). **Table 18** shows the number of days of inundation for the calibration period compared to the number of days of inundation predicted by the field hydrology score. Methodology for determining the number of days from the field hydrology score also is discussed in the report by Ecology and Environment, Inc. (2004b). Although the WRAP cells did not have a specified calibration criterion, a 20 percent threshold was applied to quantitatively look at the comparison of simulated and field observed inundation percentages. The Cypress Creek area appears to be simulating drier conditions than the field observed estimates. Additionally, the Loxahatchee Slough area appears to have some inconsistencies in performance between simulated and estimated inundation. This could be due to the extensive restoration conducted by Palm Beach County throughout the calibration period, but after the field measurements were taken in 2004. Finally, GWP triangle area appears to be simulated as wetter than estimated. This is due to the construction of the Northlake weir, which is designed to send up to 100 cfs from GWP into the triangle area whenever the stage in the northern portion of GWP is higher than +19.2 feet NGVD29. The Northlake weir was constructed in 2006 and not in place when the field estimates were taken. The Ecological Subteam concluded the WRAP cells performed as expected during the calibration period with the exceptions noted above.

Table 18. Field estimated and simulated inundation for Wetland Rapid Assessment Procedure cells.

Region	Indicator Region	WRAP Cell	Number of Days Inundated	Percent Inundated	Field Estimated Number of Days Inundated	Field Estimated Percent Inundated	Simulated Within 20% of Field Estimated
Corbett	C-1	C-1	1,542	47%	1,440	44%	Y
	C-2	C-2E	2,453	75%	2,879	88%	Y
	C-3	C-3	140	4%	765	23%	Y
	C-4	C-4.2	528	16%	1,800	55%	N
	C-4	C-4.1	1,312	40%	1,800	55%	Y
	C-5	C-5	570	17%	1,800	55%	N
Cypress Creek	CC-1	CC-1A	3	0%	540	16%	Y
	CC-2	CC-2	0	0%	270	8%	Y
	CC-3	CC-3A	89	3%	900	27%	N
	CC-4	CC-4.1	0	0%	1,080	33%	N
Mecca	CM-1	CM-1	832	25%	360	11%	Y
	CM-2	CM-2	2,302	70%	360	11%	N

Region	Indicator Region	WRAP Cell	Number of Days Inundated	Percent Inundated	Field Estimated Number of Days Inundated	Field Estimated Percent Inundated	Simulated Within 20% of Field Estimated
Gulfstream	GS-1	GS-1	0	0%	360	11%	Y
	GS-2	GS-2	0	0%	360	11%	Y
Grassy Waters Triangle	GWP-1	GWP-1A	2,824	86%	1,148	35%	N
	GWP-2	GWP-2	2,733	83%	1,530	47%	N
	GWP-3	GWP-3	2,720	83%	1,530	47%	N
	GWP-4	GWP-4	2,169	66%	2,295	70%	Y
Grassy Waters Preserve	GWP-5	GWP-5.1	1,790	54%	1,913	58%	Y
	GWP-5	GWP-5.2	1,614	49%	1,913	58%	Y
	GWP-6	GWP-6	3,035	92%	2,295	70%	N
	GWP-7	GWP-7.1	2,875	87%	2,295	70%	Y
	GWP-7	GWP-7.2	2,916	89%	2,295	70%	Y
	GWP-7	GWP-7.3	2,500	76%	2,295	70%	Y
	GWP-9	GWP-9	2,714	83%	2,295	70%	Y
	GWP-10	GWP-10	3,126	95%	2,295	70%	N
Hungryland Slough	HS-2	HS-2	2,063	63%	1,800	55%	Y
Kitching Creek	KC-1	KC-1	657	20%	810	25%	Y
	KC-1	KC-1.2	609	19%	810	25%	Y
	KC-2	KC-2.1	46	1%	1,080	33%	N
Loxahatchee Slough	LS-10	LS-10.1	1,340	41%	2,190	67%	N
	LS-10	LS-10.2	1,762	54%	2,190	67%	Y
	LS-2	LS-2	2,436	74%	1,440	44%	N
	LS-3.1	LS-3.1	948	29%	1,080	33%	Y
	LS-3.1	LS-3.2	1,215	37%	1,080	33%	Y
	LS-4	LS-4	2,678	81%	1,080	33%	N
	LS-5	LS-5	1,350	41%	1,080	33%	Y
	LS-6	LS-6A	2,345	71%	1,440	44%	N
	LS-7	LS-7A	2,239	68%	1,530	47%	N
	LS-8	LS-8.1	1,724	52%	1,440	44%	Y
	LS-9	LS-9	2,427	74%	1,440	44%	N
Moonshine Creek	MC-1	MC-1	0	0%	270	8%	Y
Nine Gems	PM-1	PM-1	20	1%	1,080	33%	N
	PM-1	PM-1.1	112	3%	1,080	33%	N
	PM-10	PM-10.1	1,185	36%	1,800	55%	Y
	PM-1	PM-11.2	0	0%	1,080	33%	N
	PM-2	PM-2	1,350	41%	720	22%	Y
	PM-2	PM-2.2A	271	8%	720	22%	Y
	PM-4	PM-4	1,426	43%	1,800	55%	Y
	PM-5	PM-5.1	16	0%	1,800	55%	N
	PM-5	PM-5.2A	1,172	36%	1,800	55%	Y
Culpepper	PM-6	PM-6	98	3%	1,440	44%	N
Pine Glades	PM-9	PM-9A	3,117	95%	1,440	44%	N

4.3.4 Water Budgets

Annual water budgets for selected areas were used as an overall indicator of bias in the calibration process. Water budgets were prepared for the four main portions of the study area: GWP, L-8 Basin, C-18 Basin (C-18/Corbett and Wild and Scenic/Jupiter Farms basins combined), and Flow-way 3 (Pal Mar, Hobe Grove Ditch, and historical Cypress Creek basins). Water budget values were calculated using the MultiBud (MBUD) package in MODFLOW (Ecology and Environment, Inc., 2004a). The MultiBud package calculates the sums of the net flow (as well as inflow and outflow) for all boundary cell faces in a defined area by stress period in separate reports. The water budget basin boundaries, as defined for MultiBud, are shown in **Figure 52**. Annual water budget schematics are provided in **Appendix D**. Water budget schematics were created using MODFLOW groundwater terminology to look at inflows and outflows into each basin. Change in storage also is provided, along with the calculated residual or error term. **Table 19** brief describes each of the terms in the water budget schematics. Inflow and outflow terms vary by basin depending on how various features were simulated. Inflow values are shown in blue, and outflow values are shown in green. The change in storage is shown in red, and the residual value is highlighted in pink. Structure flows, contained in yellow boxes, show the simulated average annual structure flow but are not a part of the water budget equation. All terms are given in units of thousands of acre-feet.

Table 19. Description of MODFLOW terminology used in water budget schematics.

Term	Description
ΔS	Change in storage.
GW	Sum of groundwater flow in or out of the basin from each of the faces (North, South East, and West).
Diversions	Movement of water due to diversions. Runoff from ET-Recharge package is added into the diversions.
Rivers	Inflow or outflow representing baseflow from rivers.
Recharge	Gross groundwater recharge.
ET	ET from saturated zone.
Drains	Movement of water out of the basin due to drains.
Boundary	Movement of water due to head-dependent boundary conditions.
Wells	Water removed from the basin for irrigation or public water supply uses.
RDF	Movement of water due to reinjection drain flow.
Residual	Term used to quantify the error or closure to achieve mass balance within the basin.

ET = evapotranspiration; GW = groundwater; RDF = reinjection drain flow; S = storage.

The C-18 Basin is modeled with a combination of rivers, drains, and diversions. Because RDFs are not used within the basin, this term does not appear in the water budget. The largest inflow into the basin is groundwater baseflow from the West face, and the second largest inflow into the basin is gross groundwater recharge. The largest outflow from the basin is the groundwater base flow from the East face, and the second largest outflow from the basin is the saturated zone ET. The groundwater baseflows from the East and West faces are almost equal, with the East face groundwater baseflow out of the basin slightly greater than the inflow from the West face flow. As expected, there is more groundwater baseflow during the wet season than the dry season. Recharge also is higher during the wet season due to increased rainfall during these months. Saturated zone ET is about the same during the wet and dry seasons across the C-18 Basin. During the wet season, the amount of water moved via drains and diversions is larger than during the dry season. The overall residual for the C-18 Basin is 0.08, which is several orders of magnitude smaller than the largest inflow and outflow terms.

The GWP Basin is modeled with a combination of diversions and RDFs. Drains and rivers are not used within the basin and, therefore, do not appear in the water budget. The largest inflow into the basin is from gross groundwater recharge, and the second largest inflow is from diversions. Although diversions are used to move water into and out of the basin, the net diversion is inflow. This is due to the large amount of water brought into the GWP Basin from the Control 2 pump station along the M-Canal to meet the City of West Palm Beach's PWS demands while maintaining the M-Canal within the GWP Basin at +18.9 feet NGVD29. The largest outflow from the basin is saturated zone ET, and the second largest outflow from the basin is from wells, which are used to simulate PWS demand. As expected, during the wet season, gross groundwater recharge is higher than during the dry season. During the dry season, the PWS demand is slightly higher than during the wet season; therefore, the inflow from diversions also is higher during the dry season. The overall residual for the GWP Basin is 0.11, which is several orders of magnitude smaller than the largest inflow and outflow terms.

The Flow-way 3 Basin is modeled with a combination of rivers, drains, and diversions. Because RDFs are not used within the basin, this term does not appear in the water budget. The largest inflow into the basin is the groundwater baseflow from the West face, and the second largest inflow is the gross groundwater recharge. The largest outflow from the basin is the groundwater baseflow from the East face, and the second largest outflow from the basin is the drains. The groundwater baseflows from the East and West faces are almost equal, with the East face groundwater baseflow out of the basin slightly greater than the inflow from the West face flow. As expected, during the wet season, the gross groundwater recharge and the groundwater baseflows from the East and West faces are almost double the dry season values. The overall residual for the Flow-way 3 Basin is 0.07, which is several orders of magnitude smaller than the largest inflow and outflow terms.

The L-8 Basin is modeled with a combination of rivers, drains, diversions, and RDFs. The largest inflow is the groundwater baseflow from the West face, and the second largest inflow is from the gross groundwater recharge. The largest outflow from the basin is the groundwater baseflow from the East face, and the second largest outflow is from the saturated zone ET. The groundwater baseflows from the East and West faces are almost equal, with the West face groundwater baseflow out of the basin slightly greater than the inflow from the East face flow. As expected, during the wet season, the gross groundwater recharge, the groundwater baseflows from the East and West faces, and the movement of water from the diversions and RDFs are almost double the dry season values. The overall residual for the L-8 Basin is 0.05, which is several orders of magnitude smaller than the largest inflow and outflow terms.

Analysis of the water budgets and the residual terms indicates that within the C-18, GWP, Flow-way 3, and L-8 basins, there is no inherent model bias. The residual values in each basin are several orders of magnitude smaller than the largest inflow and outflow terms, which indicates the model is performing reasonably well, especially within these basins.

4.4 Model Verification

Model verification demonstrates that the calibrated model matches a set of field data independent of the data used to calibrate the model. In general, model verification is used as a post-audit analysis to check the model's performance. In this case, the verification process was conducted to understand the model's overall response to a new set of variables without notably altering the primary groundwater model data sets. The verification period chosen is from January 1, 2000 to December 31, 2005. This period includes average 12-month SPI values of -1.325 and 1.265, indicating there are extreme drought events as well as extreme rainfall conditions. One of the primary objectives of model verification is to understand the behavior of the model when two major water control structures (G-160 and G-161) are removed. Understanding model performance when G-160 and G-161 are removed is critical because the water control structures are not included in the LRWRP 2014 Existing Base Condition nor the 2070 Future Without Project Condition. Primary changes made to the model for the verification period also include 1) adjusting groundwater withdrawals to reflect observed withdrawals experienced during that time frame, and 2) incorporating daily rainfall and ET observed for the verification period.

In addition to the removal of G-160 and G-161 and other primary changes, changes to land use were incorporated to account for the restoration undertaken by Palm Beach County, which had not occurred before 2005. Additionally, large parcels of State-owned lands in the project area had not been acquired; thus, these parcels were converted to the historical land use.

Calibration criteria remained the same for the flow discharges and water level elevations. The only deviation in criteria is related to the calculated range for the water level elevations. The maximum and minimum values used to calculate the range used a combination of the verification and calibration period of records, from January 1, 2000 through December 31, 2014.

4.4.1 Flow Discharges

There are six flow discharge locations with available data during the verification period. Based on the verification results (**Table 20**), all flow discharge structures meet the calibration criteria, as previously defined. **Figures 69** to **80** show the monthly flow hydrographs and the cumulative flow curves for each discharge location.

Table 20. Flow structure statistics for the verification period (2000 – 2005).

Monitoring Station	R^2	DV (%)	NS
C-18 Weir	0.71	3	0.71
Lainhart Dam	0.80	-6	0.71
S-46	0.85	6	0.82
G-92	0.60	2	0.56
Cypress Creek and Hobe Grove Ditch	0.88	7	0.87
Kitching Creek	0.83	3	0.81

DV = deviation of volume; NS = Nash-Sutcliffe coefficient; R2 = coefficient of determination.

4.4.1.1 C-18 Weir

Figure 69 shows the monthly flow hydrograph for the verification period at the C-18 weir. The simulated monthly flows occasionally over- or underestimate the peak flows, but consistently overestimate the low flows slightly. Based on the cumulative monthly flow curve (**Figure 70**), the simulated cumulative flow appears to overestimate historical cumulative flow over the course of the verification period.

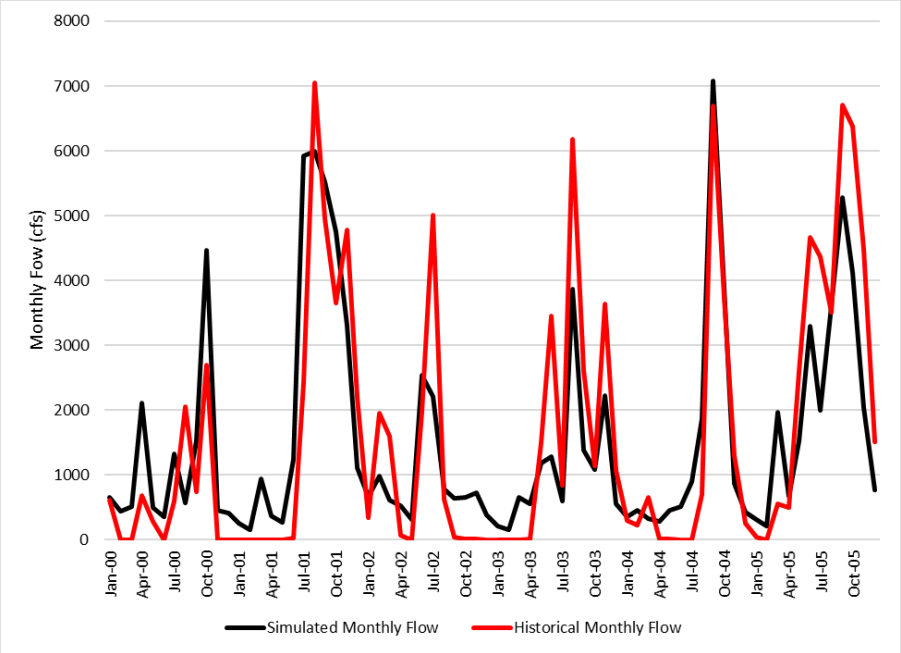

Figure 69. Simulated and historical monthly flow hydrograph for the C-18 weir from 2000 to 2005.

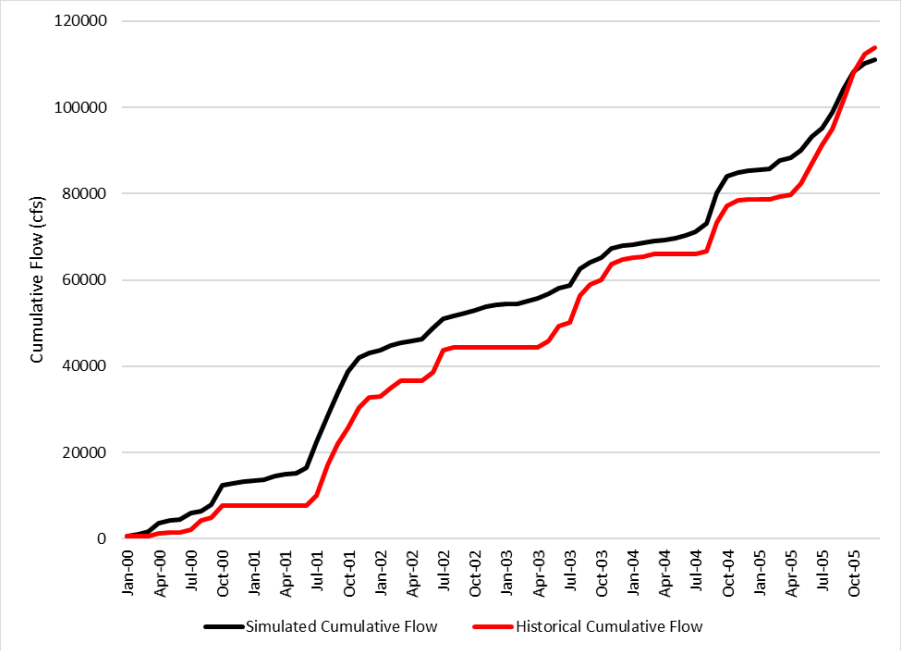

Figure 70. Simulated and historical cumulative monthly flow curve for the C-18 weir from 2000 to 2005.

4.4.1.2 Lainhart Dam

Figure 71 shows the monthly flow hydrograph for the verification period at Lainhart Dam. The model appears to underestimate peak historical monthly flows. Based on the cumulative monthly flow curve (**Figure 72**), the model overestimates the historical cumulative flow. This indicates that during the verification period, although the model appears to under-predict the high peak flows, overall the model slightly over-predicts flows over Lainhart Dam.

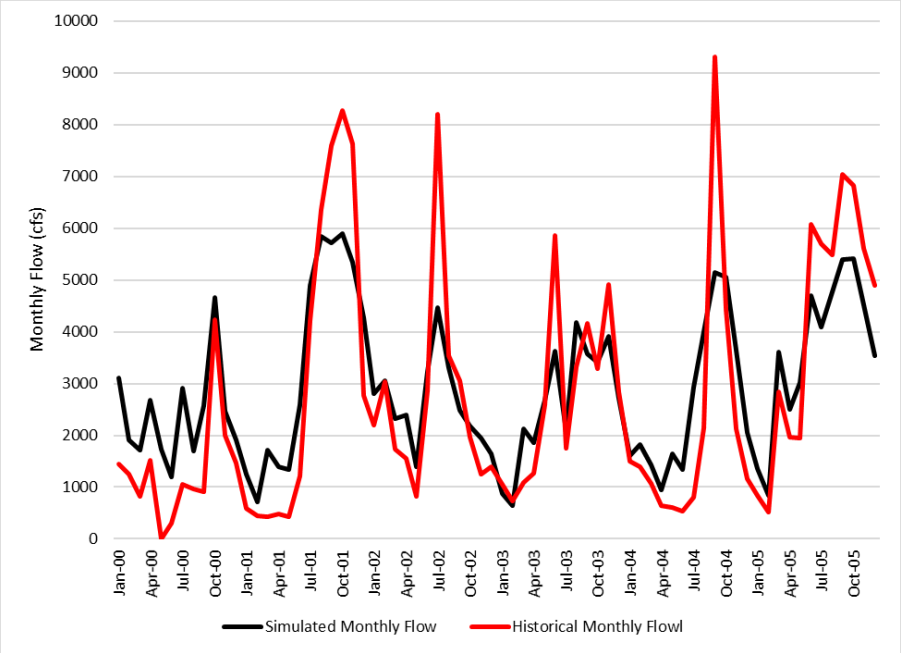

Figure 71. Simulated and historical monthly flow hydrograph for Lainhart Dam from 2000 to 2005.

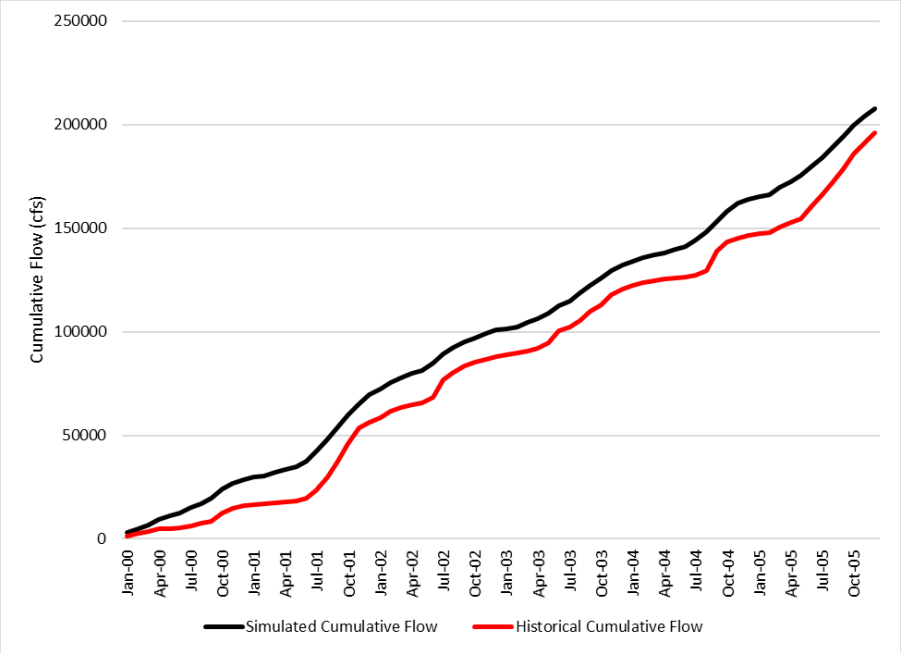

Figure 72. Simulated and historical cumulative monthly flow curve for Lainhart Dam from 2000 to 2005.

4.4.1.3 S-46

Figure 73 shows the monthly flow hydrograph for the verification period at S-46. The simulated and historical monthly flows generally match, except for high peak events. Based on the cumulative monthly flow curve (**Figure 74**), the model occasionally overestimates historical flows at S-46 through early 2004. Deviations between simulated and historical cumulative flow appear to decrease from mid-2004 through the end of the verification period.

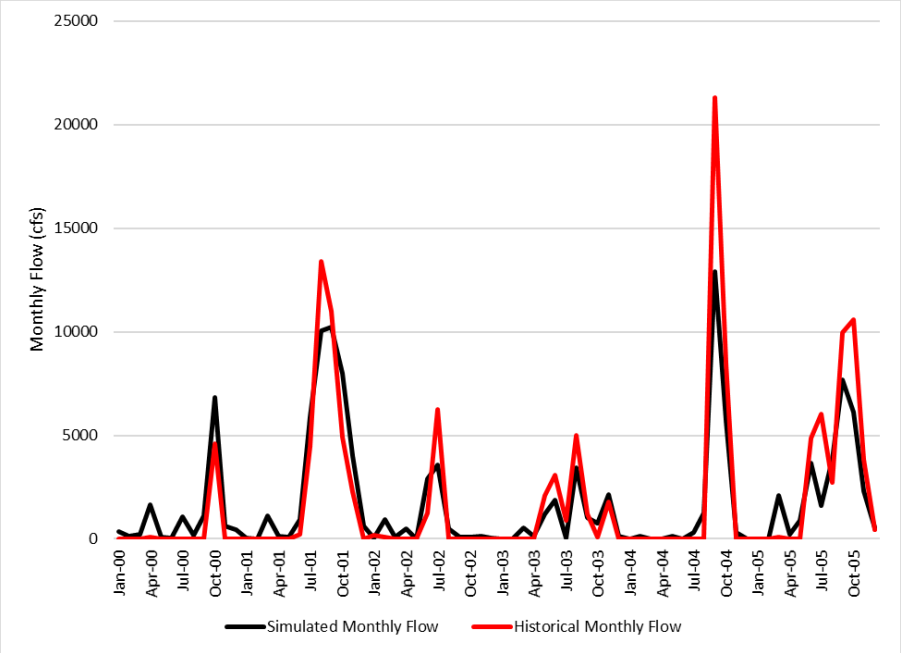

Figure 73. Simulated and historical monthly flow hydrograph for S-46 from 2000 to 2005.

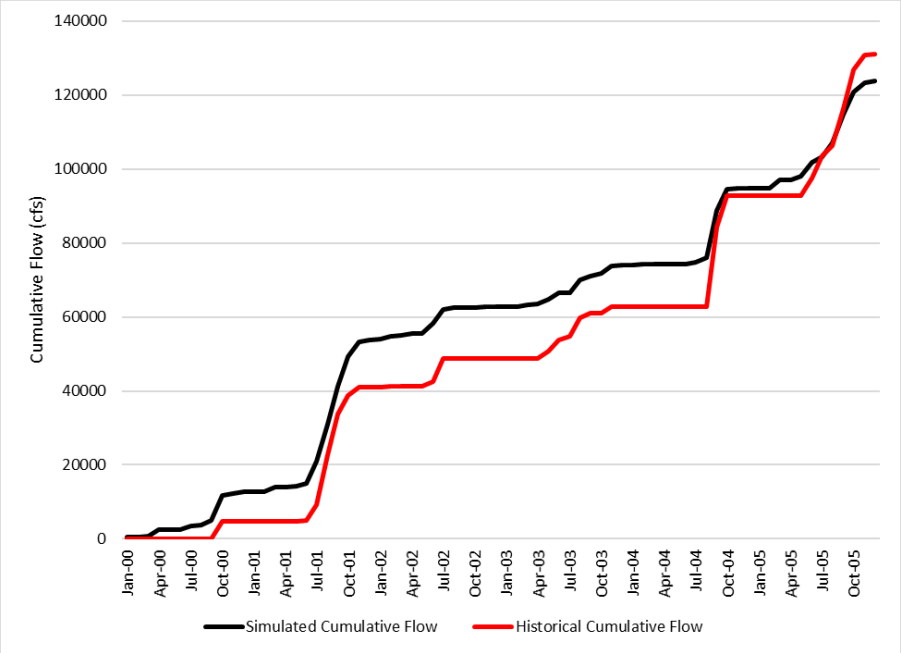

Figure 74. Simulated and historical cumulative monthly flow curve for S-46 from 2000 to 2005.

4.4.1.4 G-92

Figure 75 shows the monthly flow hydrograph for the verification period at G-92. There does not appear to be any specific trend of under- or overestimation of the monthly flows. The model occasionally simulates higher monthly flow than historical conditions, but sometimes the model simulates lower monthly flow than historical conditions. Additionally, the model did not simulate the reverse flow capabilities of G-92, and thus will over-predict during months where reverse flow occurred. Based on the cumulative monthly flow curve (**Figure 76**), the simulated and historical cumulative flow appear to match very well, with only very slight deviations and no consistent over- or under-prediction trends throughout the verification period.

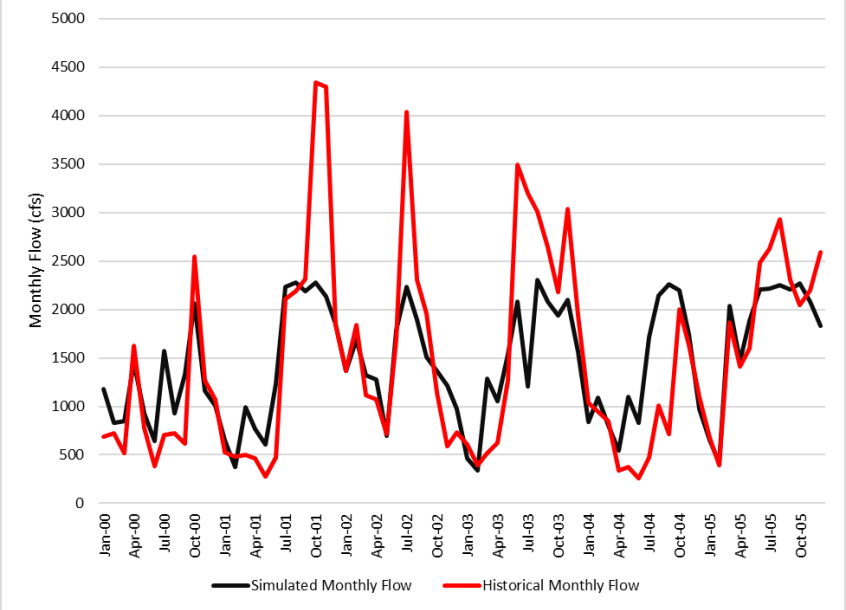

Figure 75. Simulated and historical monthly flow hydrograph for G-92 from 2000 to 2005.

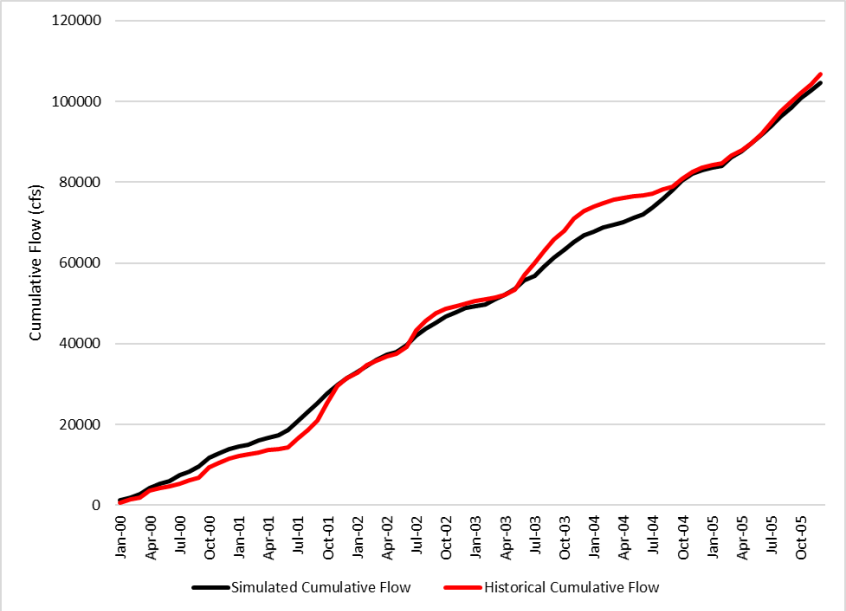

Figure 76. Simulated and historical cumulative monthly flow curve for G-92 from 2000 to 2005.

4.4.1.5 Cypress Creek and Hobe Grove Ditch

Figure 77 shows the monthly flow hydrograph for the verification period for Cypress Creek and Hobe Grove Ditch. Due to the complexity of differentiating contributing areas, the two structures were assessed together. Additionally, historical data were only available after 2002. There does not appear to be any specific trend of under- or over-estimation of the monthly flows. The model occasionally simulates higher monthly flow than historical conditions, but sometimes the model simulates lower monthly flow than historical conditions. **Figure 78** illustrates the cumulative monthly flow curve from 2002 through the end of the verification period, when historical data are available. Based on the curve, the simulated and historical cumulative flows appear to match very well, with only very slight deviations and no consistent over- or under-prediction trends.

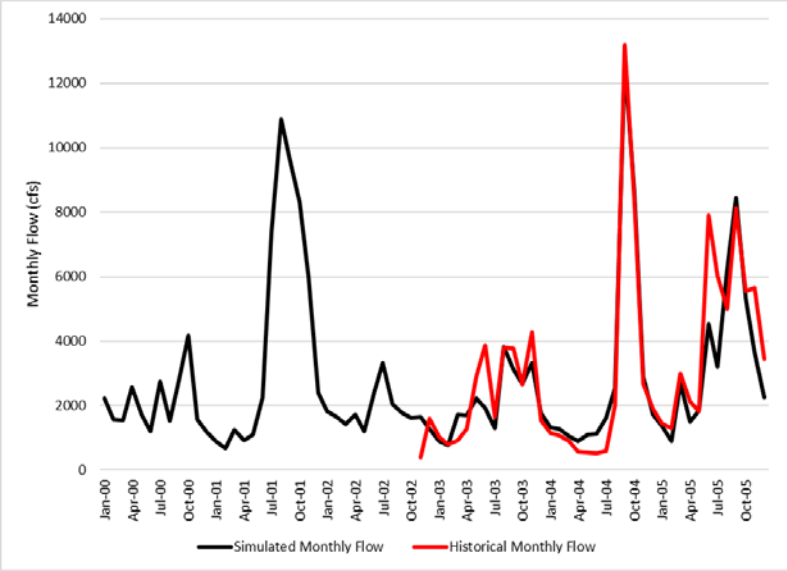

Figure 77. Simulated and historical monthly flow hydrograph for Cypress Creek and Hobe Grove Ditch from 2000 to 2005.

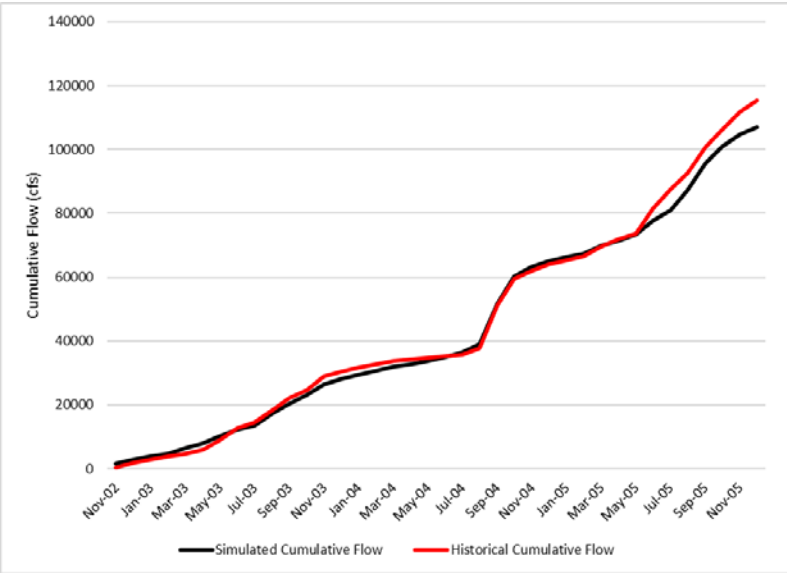

Figure 78. Simulated and historical cumulative monthly flow curve for Cypress Creek and Hobe Grove Ditch from 2002 to 2005.

4.4.1.6 Kitching Creek

Figure 79 shows the monthly flow hydrograph for the verification period for Kitching Creek. There does not appear to be any specific trend of under- or overestimation of the monthly flows. The model occasionally simulates higher monthly flow than historical conditions, but sometimes the model simulates lower monthly flow than the historical conditions. Based on the cumulative monthly flow curve (**Figure 80**), the simulated cumulative flow appears to have some deviations from the historical cumulative flow. However, there does not appear to be a consistent prediction bias because the cumulative flow can be under- or over-predicted by the model.

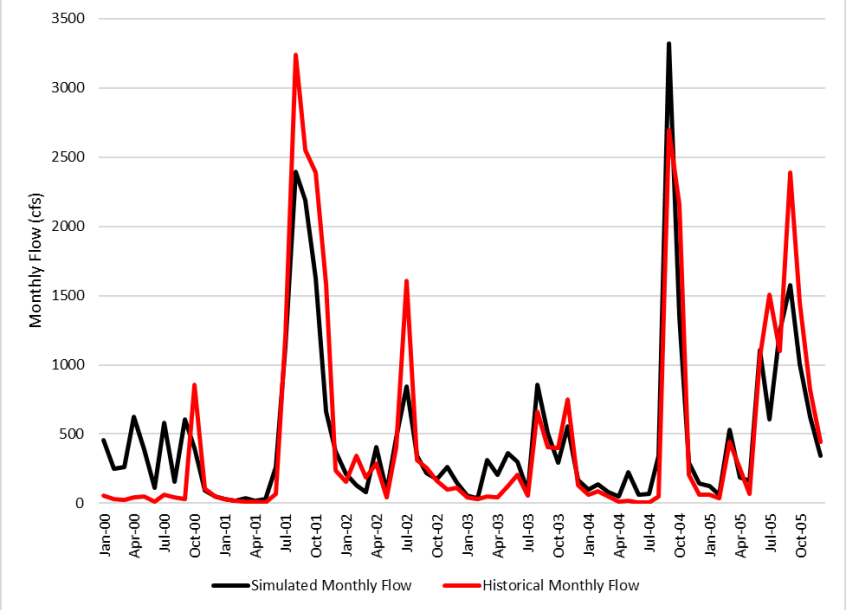

Figure 79. Simulated and historical monthly flow hydrograph for Kitching Creek from 2000 to 2005.

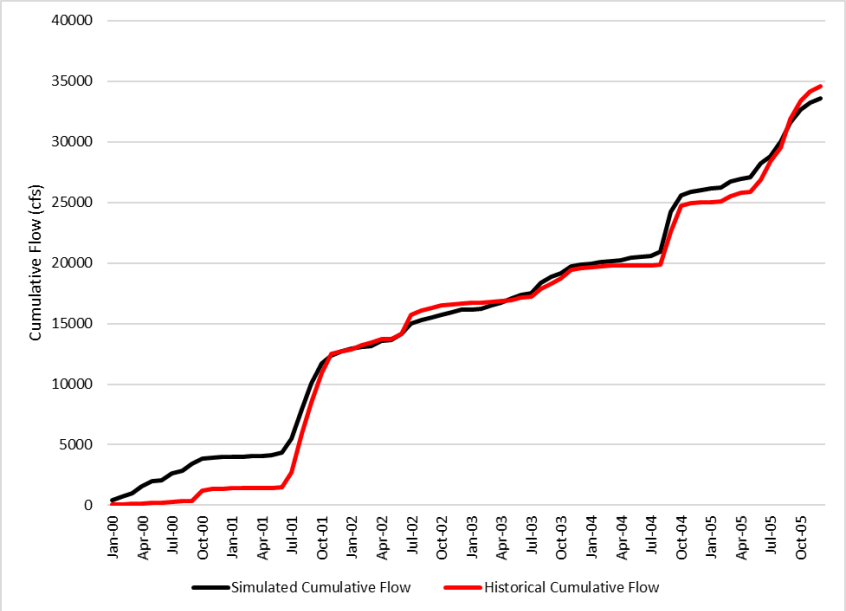

Figure 80. Simulated and historical cumulative monthly flow curve for Kitching Creek from 2000 to 2005.

4.4.2 Water Level Elevations

For model verification, 44 groundwater monitoring wells were used as indicators of model performance (**Figure 81)**. Based on the statistics in **Table 21**, 42 of the 44 wells met the individual well criteria. For model verification, 26 wetland gauges were used as indicators of model performance (**Figure 82**). Based on the statistics in **Table 22**, 23 of the 26 gauges met the individual gauge criteria. **Figures 83** and **84** show the spatial distribution of the groundwater monitoring wells and wetland gauges used during model verification. Locations that met criteria are shown in green, while locations that did not meet criteria are shown in red. There does not appear to be any spatial bias in overall model performance. Hydrographs for the simulated and historical water levels for the groundwater monitoring wells and wetland gauges are provided in **Appendix E**.

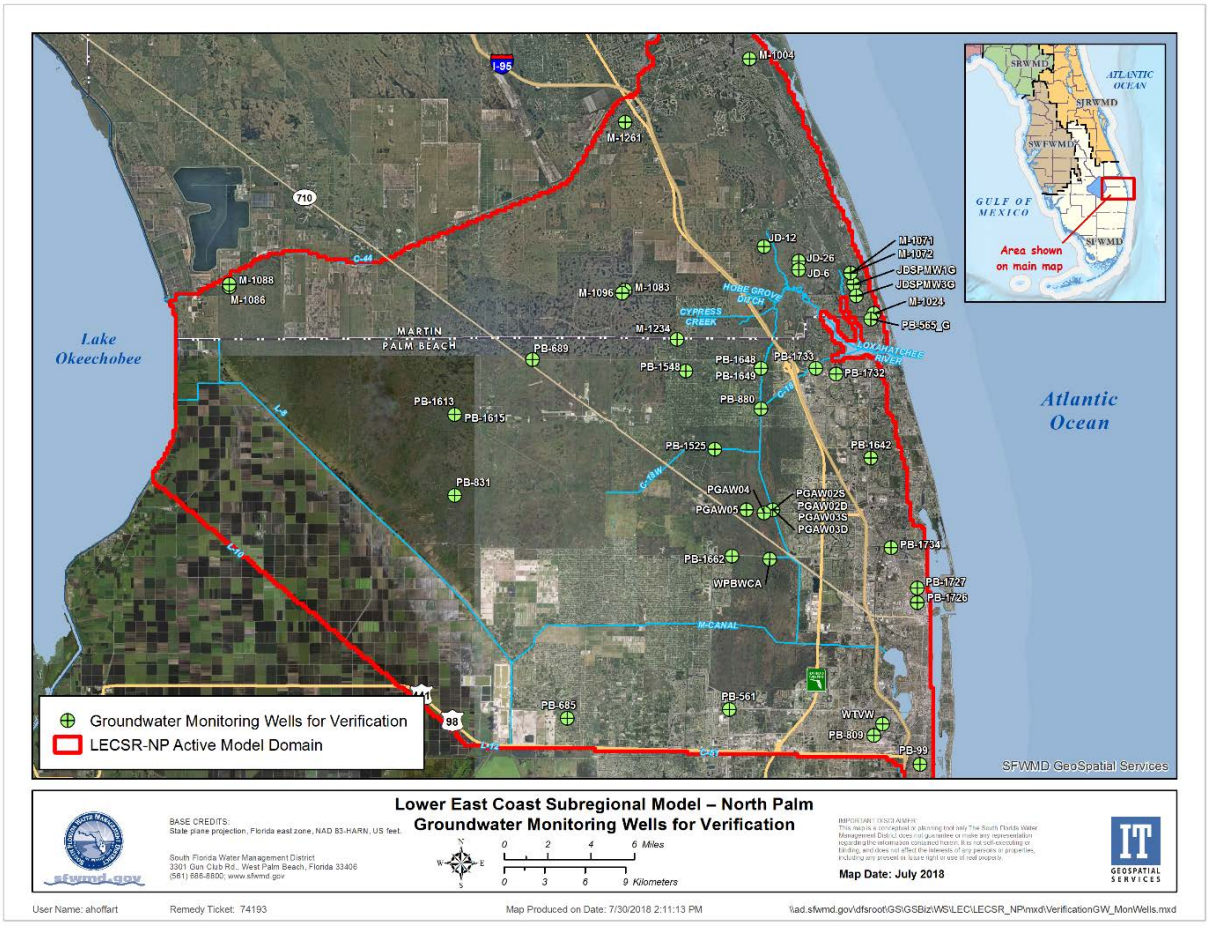

Figure 81. Groundwater monitoring wells used in LECSR-NP verification.

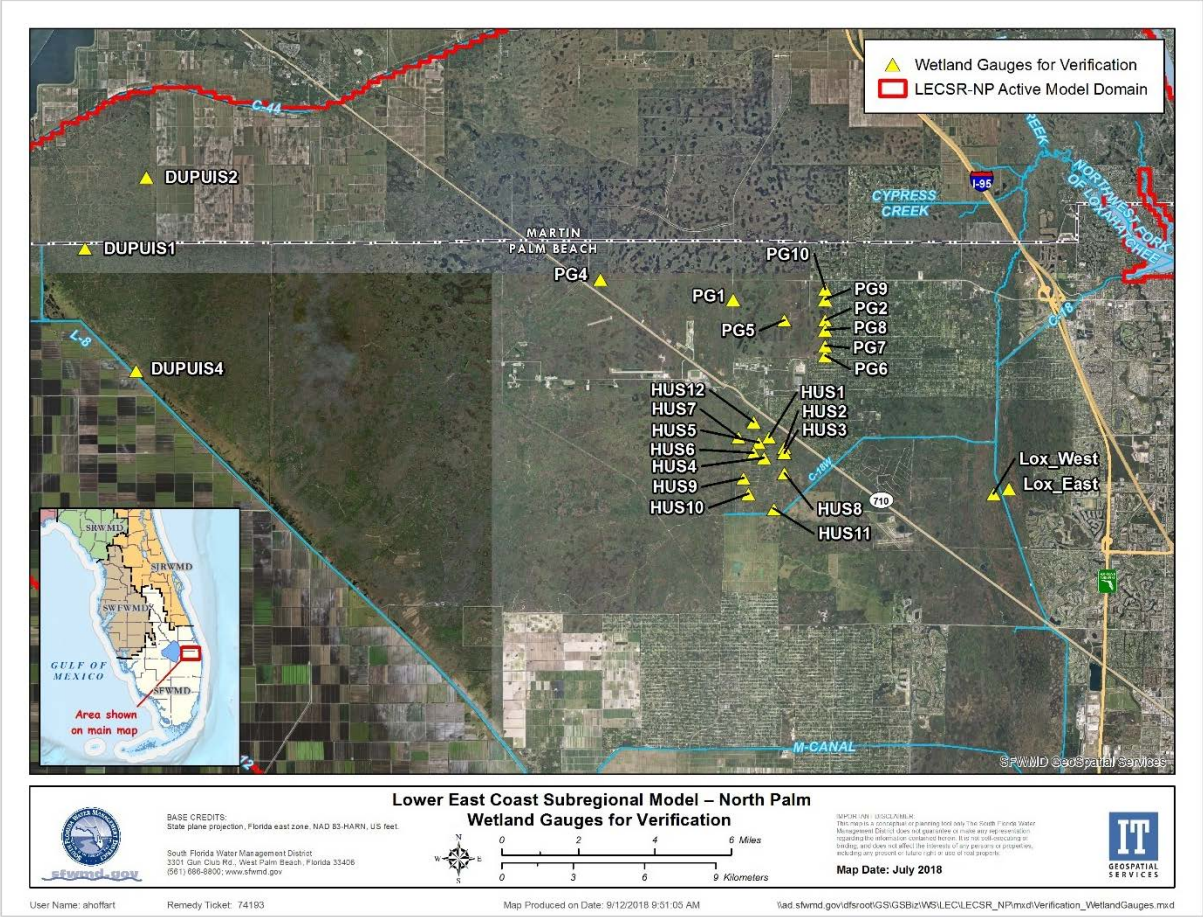

Figure 82. Wetland gauges used in LECSR-NP verification.

Table 21. Groundwater monitoring well statistics for the verification period (2000 – 2005).

Monitor Well	Mean Difference (feet)	Mean Absolute Difference (feet)	Root Mean Square Error (feet)	Water Level Stage Range	Percent of Time Within 20% of the Range	Calibration Met (Individual Stage Criterion)	Calibration Met (±1 foot Criterion)
PB-565_G	-0.18	0.73	1.02	1.83	92.62	Y	Y
PB-809	-0.27	0.50	0.59	1.37	98.66	Y	Y
M-1004	-0.45	0.58	0.68	1.27	97.06	Y	Y
M-1024	-0.10	0.44	0.60	1.32	93.88	Y	Y
PB-1733	0.55	0.80	0.96	0.85	78.69	Y	Y
PB-1732	0.04	0.38	0.54	0.72	95.16	Y	Y
PB-1642	-0.13	0.47	0.70	1.53	95.24	Y	Y
PB-1734	0.11	0.34	0.45	0.51	98.39	Y	Y
PB-1727	-0.09	0.57	0.70	1.28	96.77	Y	Y
PB-1726	-0.44	0.72	0.86	1.08	88.71	Y	Y
PB-1649	-0.20	0.32	0.40	1.17	100.00	Y	Y
M-1261	-0.25	1.12	1.38	1.80	79.52	Y	N
M-1071	0.11	0.50	0.62	1.12	91.44	Y	Y
M-1072	0.14	0.50	0.63	1.10	89.63	Y	Y
M-1083	-0.17	0.39	0.51	0.88	97.06	Y	Y
M-1086	-0.64	0.79	1.01	1.51	83.46	Y	Y
M-1088	-0.55	0.74	0.92	1.49	89.37	Y	Y
M-1096	0.45	0.52	0.63	0.89	81.62	Y	Y
M-1234	-0.02	0.39	0.58	1.45	96.82	Y	Y
PB-1525	0.23	0.33	0.74	0.97	92.12	Y	Y
PB-1548	-0.63	0.81	1.00	1.32	81.10	Y	Y
PB-1613	-0.13	0.23	0.29	1.06	100.00	Y	Y
PB-1615	-0.04	0.19	0.26	1.06	99.90	Y	Y
PB-1648	0.68	0.74	0.87	1.26	85.43	Y	Y
PB-1662	1.08	1.08	1.16	0.92	37.32	N	N
PB-561	0.32	0.57	0.68	1.16	92.51	Y	Y
PB-685	-0.24	0.81	1.03	1.33	84.31	Y	Y
PB-689	0.59	0.59	0.68	0.90	83.60	Y	Y
WTVW	0.18	0.32	0.41	0.84	94.84	Y	Y
PB-831	0.39	0.55	0.75	0.97	81.49	Y	Y
PB-880	0.30	0.33	0.41	0.83	93.94	Y	Y
PB-99	-0.65	0.71	0.84	1.25	87.83	Y	Y
JD-12	-0.45	0.70	0.89	1.14	80.29	Y	Y
JD-26	-0.64	0.99	1.16	1.14	99.77	Y	Y
JD-6	-0.75	1.09	1.25	1.17	60.68	N	N
JDSPMW1G	0.23	0.59	0.75	1.20	86.96	Y	Y
JDSPMW3G	0.06	0.56	0.69	1.31	96.62	Y	Y
PGAW02D	-0.47	0.47	0.47	1.07	100.00	Y	Y
PGAW02S	-0.05	0.05	0.06	1.04	100.00	Y	Y
PGAW03D	-0.62	0.62	0.62	1.11	100.00	Y	Y
PGAW03S	-0.64	0.64	0.65	1.08	100.00	Y	Y
PGAW04	-0.56	0.56	0.57	1.19	100.00	Y	Y
PGAW05	-0.16	0.16	0.20	1.18	100.00	Y	Y
WPBWCA	-0.05	0.44	0.56	0.73	82.72	Y	Y
Overall	**-0.09**	**0.57**	**0.70**	**1.15**	**90.13**	**95.45%**	**93.18%**

Table 22. Wetland gauge statistics for the verification period (2000 – 2005).

Wetland Gauge	Mean Error (feet)	Mean Absolute Error (feet)	Root Mean Square Error (feet)	Water Level Stage Range	Percent of Time Within 20% of the Range	Calibration Met (Individual Stage Criterion)	Calibration Met (±1 foot Criterion)
DUPUIS1	-0.25	0.56	0.68	0.86	73.08	Y	Y
DUPUIS2	-0.54	0.72	0.86	0.88	59.40	Y	Y
DUPUIS4	0.22	1.26	1.49	1.47	69.11	N	N
Lox East	-0.54	0.55	0.62	0.81	81.87	Y	Y
Lox West	-1.28	1.28	1.29	0.84	0.00	N	N
PG1	0.03	0.29	0.32	0.95	100.00	Y	Y
PG2	-0.10	0.43	0.56	1.22	100.00	Y	Y
PG4	0.31	0.31	0.34	0.92	100.00	Y	Y
PG5	0.73	0.79	0.83	1.01	87.50	Y	Y
PG6	-0.32	0.52	0.65	1.38	100.00	Y	Y
PG7	-0.49	0.69	0.77	1.38	100.00	Y	Y
PG8	-0.48	0.68	0.77	1.42	100.00	Y	Y
PG9	-0.61	0.71	0.98	1.46	85.71	Y	Y
PG10	-1.52	1.58	1.95	1.51	57.14	N	N
HUS1	0.04	0.46	0.67	1.02	81.82	Y	Y
HUS2	0.06	0.40	0.58	1.02	90.91	Y	Y
HUS3	-0.15	0.31	0.38	1.03	100.00	Y	Y
HUS4	-0.09	0.56	0.71	0.95	81.82	Y	Y
HUS5	-0.38	0.45	0.53	0.85	90.91	Y	Y
HUS6	-0.28	0.55	0.59	1.05	100.00	Y	Y
HUS7	0.07	0.54	0.74	0.90	81.82	Y	Y
HUS8	-0.27	0.43	0.53	0.84	90.91	Y	Y
HUS9	-0.03	0.52	0.61	0.81	81.82	Y	Y
HUS10	0.49	0.69	0.79	0.97	72.73	Y	Y
HUS11	-1.01	1.01	1.11	1.18	72.73	Y	N
HUS12	-0.26	0.61	0.78	1.27	90.91	Y	Y
Overall	**-0.26**	**0.65**	**0.77**	**1.08**	**82.70**	**88.46%**	**84.62%**

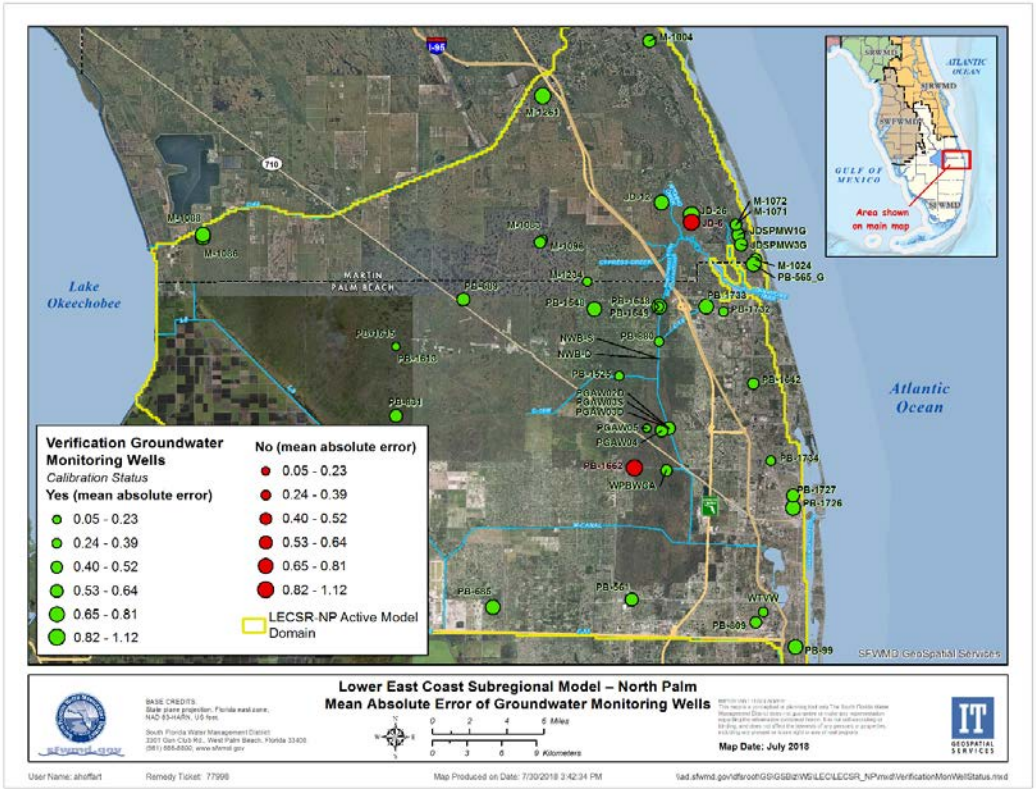

Figure 83. Status and mean absolute error for groundwater monitoring wells used in LECSR-NP verification.

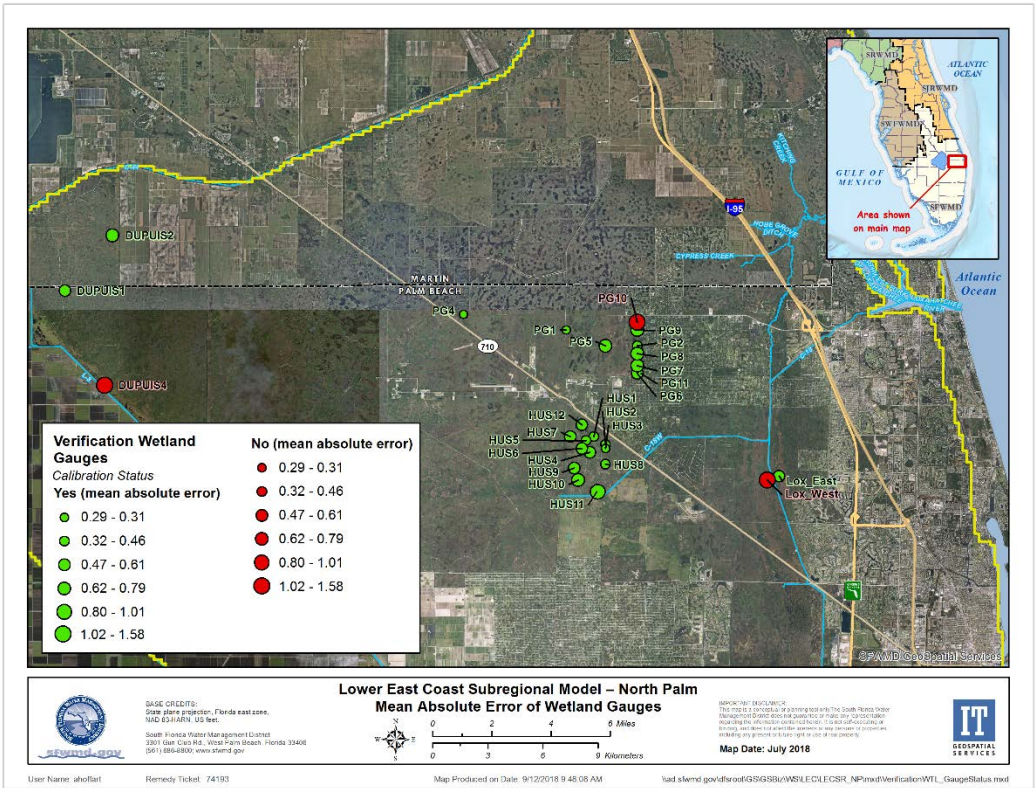

Figure 84. Status and mean absolute error for wetland gauges used in LECSR-NP verification.

4.5 Sensitivity Analysis

Sensitivity analysis is a part of model calibration used to evaluate model input parameters to determine how they impact model outputs such as heads and flows. Sensitivity analysis is essential to understanding the simulated system, and results from the sensitivity analysis determine which model input parameters will be most important to making the simulated heads and flows match observed values (Reilly and Harbaugh, 2004).

4.5.1 Parameters and Methodology

Manual sensitivity analysis was used to determine which model input parameters were most sensitive within the model domain. During the sensitivity analysis, one parameter was changed at a time so the effect of its variations on the model could be individually assessed. Parameter ranges were varied within acceptable ranges based on the data range for each parameter.

The sensitivity analysis for the LECSR-NP was used to determine which parameters were most sensitive to the simulated heads at the groundwater monitoring well and wetland gauge calibration locations. The sensitivity analysis also was used to determine which parameters were most sensitive to the simulated flows at the flow discharge locations. **Table 23** shows the model input parameters used in the sensitivity analysis and the different multipliers that were tested for each parameter. The tested parameters include vertical hydraulic conductivity in Layers 1 and 2; horizontal hydraulic conductivity in Layers 1, 2, and 3; conductance values for drains, rivers, and GHB cells; specific yield; groundwater recharge; and saturated zone ET. For each parameter, several model runs were completed using various multipliers (**Table 23**). The simulation period for the sensitivity analysis is from January 1, 2006 to December 31, 2014, which is the same as the calibration period for the LECSR-NP.

Table 23. Parameters and multipliers of sensitivity analysis for the LECSR-NP.

Parameters	Multipliers					
Vertical Hydraulic Conductivity Layer 1	0.1	0.2	0.5	2	5	10
Vertical Hydraulic Conductivity Layer 2	0.1	0.2	0.5	2	5	10
Horizontal Hydraulic Conductivity Layer 1	0.1	0.2	0.5	2	5	10
Horizontal Hydraulic Conductivity Layer 2	0.1	0.2	0.5	2	5	10
Horizontal Hydraulic Conductivity Layer 3	0.1	0.2	0.5	2	5	10
Drain Conductance	0.01	0.1	10	100		
River Conductance	0.01	0.1	10	100		
General Head Boundary Conductance	0.01	0.1	10	100		
Saturated Zone Evapotranspiration	0.8	0.9	1.1	1.2		
Recharge	0.8	0.9	1.1	1.2		
Specific Yield	0.5	0.75	1.25	1.5		

Note: Blank cells are present for parameters that only had four test runs.

4.5.2 Sensitivity Results

After each sensitivity run, simulated heads were compared to observed heads for the simulation period at 58 groundwater monitoring wells and 61 wetland gauges (119 monitoring locations total). The MAE was calculated for each site, while the average MAE was calculated for the groundwater monitoring wells and wetland gauges separately as well as for the overall model. The average MAE at a multiplier of 1 shows the value for the calibrated model, which is used to compare the sensitivity run performance to the model calibration. **Table 24** shows the average MAE for the groundwater monitoring wells and the wetland gauges

as well as the overall MAE for each sensitivity run and the model calibration. **Table 24** also shows the frequency distribution for the 119 monitoring locations. Additionally, the simulated flows were compared to the observed flows for the simulation period at 7 discharge locations. The R^2 was calculated for each location. The R^2 value at a multiplier of 1 shows the value for the calibrated model, which is used to compare the sensitivity run performance to the model calibration. **Table 25** shows the R^2 values for each sensitivity run.

Horizontal hydraulic conductivity values for Layers 1, 2, and 3 were varied between 0.1 and 10 times the calibrated values. Changes in model performance can be seen in **Tables 24** and **25**. **Figure 85** shows the sensitivity of the performance of groundwater monitoring wells to changes in the horizontal hydraulic conductivity values for the three layers of the LECSR-NP. Overall, increases and decreases to the horizontal hydraulic conductivity in Layer 2 resulted in substantial increases in the MAE for both the groundwater wells and the wetland gauges, up to 0.72 and 0.48 feet, respectively. More extreme changes in the horizontal hydraulic conductivity of Layer 2 caused decreases in the R^2 value at Cypress Creek and Hobe Grove Ditch (change of 0.07) and at Kitching Creek (change of 0.18). The model appears to be sensitive in the groundwater monitoring wells, wetland gauges, and flows at Cypress Creek, Hobe Grove Ditch, and Kitching Creek to changes in the horizontal hydraulic conductivity of Layer 3 for more extreme values as well; however, the change in MAE is not as drastic as the changes shown in Layer 2 (change of 0.25 feet in MAE for groundwater monitoring wells, change of 0.18 feet in MAE for wetland gauges, change of 0.06 in R^2 for Cypress Creek and Hobe Grove Ditch and change of 0.05 in R^2 for Kitching Creek). Both increases and decreases to hydraulic conductivity values in Layer 1 appear to have minimal impact on overall model performance in simulated heads and flows.

Drain conductance values across the entire model domain were varied between 0.01 and 100 times the calibrated conductance values. Changes in model performance can be seen in **Tables 24** and **25**. **Figure 86** shows the sensitivity of the performance for the wetland gauges to changes in the drain conductance values across the model domain. Overall, increases and decreases to the drain conductance resulted in substantial increases in the MAE (more than 0.5-foot change for each sensitivity run in the MAE for groundwater monitoring wells and 0.19-foot change for the wetland gauges). Changes to the drain conductance value also caused a decrease in the R^2 values for Cypress Creek, Hobe Grove Ditch, and Kitching Creek. For these locations, the R^2value changed by a maximum of 0.54 for Cypress Creek and Hobe Grove Ditch and 0.2 for Kitching Creek. Decreases to the drain conductance also caused a maximum decrease in the R^2value of 0.28 for Lainhart Dam.

GHB conductance values across the entire model domain were varied between 0.01 and 100 times the calibrated conductance values. Changes in model performance can be seen in **Tables 24** and **25**. **Figure 87** shows the sensitivity of the performance for the groundwater monitoring wells to changes in the GHB conductance values across the model domain. Increases and decreases to the GHB conductance term typically caused an increase in the overall MAE of the groundwater monitoring wells. When the conductance was multiplied by 0.01, the MAE decreased 0.14 feet; however, this appears to be an anomaly. The MAE of the wetland gauges did not change due to changes in GHB conductance. Changes in GHB conductance did not impact any of the flow discharge locations. This may be attributed to the wetland gauge and flow discharge locations being farther away from the GHB cells compared to the groundwater monitoring well locations.

Table 24. Frequency distribution of mean head residuals based on 58 groundwater monitoring wells and 61 wetland gauges.

Sensitivity Run	Multiplier	Mean Absolute Error (feet)			Class Observation Frequency						
		Monitoring Wells	Wetland Gauges	Overall	<0.25	0.25-0.5	0.5-0.75	0.75-1.00	1.00-1.25	1.25-1.50	>1.5
Calibration	×1	0.56	0.68	0.62	0	35	58	17	7	2	0
Drain Conductance	×10	1.25	0.82	1.04	0	30	48	17	7	3	14
	×100	1.29	0.84	1.06	0	29	47	18	7	3	15
	×0.1	16.03	0.74	8.39	0	27	52	16	11	2	11
	×0.01	1.01	0.87	0.94	0	27	46	18	11	5	12
General Head Boundary Conductance	×10	0.66	0.68	0.67	0	34	57	15	8	2	3
	×100	0.73	0.68	0.71	0	35	55	16	7	2	4
	×0.1	0.60	0.68	0.64	0	35	55	17	8	3	1
	×0.01	0.80	0.68	0.74	0	30	51	21	10	5	2
River Conductance	×10	0.57	0.68	0.62	1	34	56	19	8	1	0
	×100	0.58	0.68	0.63	1	33	57	18	8	2	0
	×0.1	0.61	0.69	0.65	0	33	56	18	8	2	2
	×0.01	0.69	0.70	0.70	0	33	56	16	6	2	6
Horizontal Hydraulic Conductivity – Layer 1	×2	0.56	0.68	0.62	0	36	56	19	5	3	0
	×0.5	0.56	0.68	0.62	0	36	56	18	8	1	0
	×5	0.58	0.70	0.64	0	35	56	19	5	4	0
	×0.2	0.56	0.68	0.62	0	37	55	18	8	1	0
	×10	0.62	0.71	0.66	0	31	58	17	7	4	2
	×0.1	0.56	0.68	0.62	0	37	55	18	8	1	0
Horizontal Hydraulic Conductivity – Layer 2	×2	0.64	0.73	0.69	0	32	54	21	8	2	2
	×0.5	0.72	0.68	0.70	0	31	52	22	9	1	4
	×5	0.92	0.92	0.92	0	25	36	24	8	14	12
	×0.2	1.05	0.69	0.87	0	27	49	18	12	5	8
	×10	1.20	1.16	1.18	0	18	35	15	12	7	32
	×0.1	1.28	0.71	0.99	0	25	48	19	13	3	11

Sensitivity Run	Multiplier	Mean Absolute Error (feet)			Class Observation Frequency						
		Monitoring Wells	Wetland Gauges	Overall	<0.25	0.25-0.5	0.5-0.75	0.75-1.00	1.00-1.25	1.25-1.50	>1.5
Horizontal Hydraulic Conductivity – Layer 3	×2	0.57	0.69	0.63	0	36	56	19	5	3	0
	×0.5	0.58	0.68	0.63	0	33	56	19	10	1	0
	×5	0.66	0.76	0.71	0	27	54	21	9	4	4
	×0.2	0.63	0.69	0.66	0	35	51	20	8	4	1
	×10	0.81	0.86	0.83	1	21	47	24	10	5	11
	×0.1	0.65	0.69	0.67	0	36	48	21	8	4	2
Vertical Hydraulic Conductivity – Layer 1	×2	0.57	0.68	0.62	0	36	57	17	6	3	0
	×0.5	0.56	0.68	0.62	0	36	56	18	7	2	0
	×5	0.57	0.69	0.63	0	33	58	19	6	3	0
	×0.2	0.57	0.68	0.63	0	36	55	17	9	2	0
	×10	0.58	0.69	0.63	0	33	58	19	6	3	0
	×0.1	0.60	0.69	0.64	1	34	54	17	10	2	1
Vertical Hydraulic Conductivity – Layer 2	×2	0.56	0.68	0.62	0	35	58	18	5	3	0
	×0.5	0.56	0.68	0.62	0	35	57	18	7	2	0
	×5	0.57	0.68	0.62	0	34	58	19	5	3	0
	×0.2	0.56	0.68	0.62	0	38	54	18	7	2	0
	×10	0.57	0.68	0.63	0	34	58	19	5	3	0
	×0.1	0.57	0.68	0.62	0	36	55	18	8	2	0
Recharge	×1.1	0.61	0.71	0.66	0	27	56	28	6	2	0
	×1.2	0.7	0.77	0.74	0	23	46	29	14	6	1
	×0.9	0.58	0.72	0.65	0	36	48	23	9	1	2
	×0.8	0.68	0.84	0.76	0	26	44	25	16	3	5
Saturated Zone Evapotranspiration	×1.1	0.55	0.69	0.62	0	37	55	20	4	2	1
	×1.2	0.56	0.72	0.64	0	38	48	25	4	3	1
	×0.9	0.59	0.7	0.65	0	29	60	20	9	1	0
	×0.8	0.63	0.75	0.69	0	28	53	23	9	5	1
Specific Yield	×0.1	0.57	0.69	0.63	1	29	63	18	5	3	0
	×0.15	0.56	0.68	0.62	0	32	61	17	6	3	0
	×0.25	0.57	0.68	0.63	0	35	57	18	7	2	0
	×0.3	0.58	0.68	0.63	0	32	46	24	10	2	5

Table 25. Coefficient of determination (R^2) values for sensitivity runs at seven discharge locations.

Sensitivity Run	Multiplier	C-18 Weir	G-160	S-46	G-92	Lainhart Dam	Cypress Creek and Hobe Grove Ditch	Kitching Creek
Calibration	×1	0.57	0.76	0.85	0.74	0.82	0.73	0.79
Drain Conductance	×10	0.56	0.75	0.84	0.74	0.83	0.34	0.66
	×100	0.56	0.74	0.83	0.74	0.83	0.3	0.61
	×0.1	0.57	0.75	0.82	0.02	0.54	0.19	0.72
	×0.01	0.57	0.74	0.82	0.74	0.72	0.69	0.59
General Head Boundary Conductance	×10	0.57	0.76	0.85	0.74	0.82	0.73	0.79
	×100	0.57	0.76	0.85	0.74	0.82	0.73	0.79
	×0.1	0.57	0.76	0.85	0.74	0.82	0.73	0.79
	×0.01	0.57	0.76	0.85	0.74	0.82	0.73	0.79
River Conductance	×10	0.57	0.76	0.85	0.74	0.82	0.73	0.79
	×100	0.57	0.76	0.85	0.74	0.82	0.73	0.79
	×0.1	0.57	0.76	0.85	0.74	0.82	0.73	0.79
	×0.01	0.57	0.76	0.86	0.74	0.82	0.73	0.79
Horizontal Hydraulic Conductivity – Layer 1	×2	0.57	0.76	0.85	0.74	0.82	0.73	0.79
	×0.5	0.57	0.76	0.85	0.74	0.82	0.73	0.79
	×5	0.57	0.76	0.86	0.74	0.82	0.72	0.79
	×0.2	0.57	0.76	0.85	0.74	0.82	0.73	0.79
	×10	0.57	0.76	0.86	0.74	0.82	0.71	0.79
	×0.1	0.57	0.76	0.85	0.74	0.82	0.73	0.79
Horizontal Hydraulic Conductivity – Layer 2	×2	0.57	0.76	0.86	0.74	0.82	0.71	0.78
	×0.5	0.57	0.75	0.85	0.74	0.82	0.74	0.78
	×5	0.57	0.78	0.87	0.74	0.82	0.68	0.73
	×0.2	0.57	0.75	0.85	0.74	0.82	0.74	0.77
	×10	0.57	0.79	0.86	0.73	0.82	0.66	0.61
	×0.1	0.57	0.75	0.84	0.73	0.82	0.74	0.77
Horizontal Hydraulic Conductivity – Layer 3	×2	0.57	0.76	0.85	0.74	0.82	0.71	0.78
	×0.5	0.57	0.76	0.85	0.74	0.82	0.74	0.79
	×5	0.56	0.76	0.85	0.74	0.82	0.69	0.77
	×0.2	0.56	0.76	0.85	0.74	0.82	0.74	0.79
	×10	0.56	0.77	0.85	0.74	0.82	0.67	0.74
	×0.1	0.56	0.76	0.85	0.74	0.82	0.74	0.79
Vertical Hydraulic Conductivity – Layer 1	×2	0.57	0.76	0.85	0.74	0.82	0.72	0.79
	×0.5	0.57	0.76	0.85	0.74	0.82	0.73	0.79
	×5	0.57	0.76	0.85	0.74	0.82	0.72	0.79
	×0.2	0.56	0.76	0.85	0.74	0.82	0.74	0.79
	×10	0.57	0.76	0.86	0.74	0.82	0.72	0.79
	×0.1	0.56	0.76	0.85	0.74	0.82	0.74	0.79
Vertical Hydraulic Conductivity – Layer 2	×2	0.57	0.76	0.85	0.74	0.82	0.73	0.79
	×0.5	0.57	0.76	0.85	0.74	0.82	0.73	0.79
	×5	0.57	0.76	0.85	0.74	0.82	0.73	0.79
	×0.2	0.57	0.76	0.85	0.74	0.82	0.73	0.79
	×10	0.57	0.76	0.85	0.74	0.82	0.73	0.79
	×0.1	0.56	0.76	0.85	0.74	0.82	0.73	0.79

Sensitivity Run	Multiplier	C-18 Weir	G-160	S-46	G-92	Lainhart Dam	Cypress Creek and Hobe Grove Ditch	Kitching Creek
Recharge	×1.1	0.6	0.74	0.83	0.73	0.82	0.78	0.8
	×1.2	0.62	0.69	0.79	0.72	0.81	0.81	0.81
	×0.9	0.53	0.76	0.85	0.74	0.82	0.64	0.76
	×0.8	0.48	0.75	0.82	0.72	0.8	0.58	0.73
Saturated Zone Evapotranspiration	×1.1	0.55	0.76	0.86	0.74	0.82	0.69	0.78
	×1.2	0.53	0.76	0.85	0.73	0.82	0.66	0.78
	×0.9	0.59	0.75	0.85	0.74	0.82	0.76	0.79
	×0.8	0.6	0.74	0.83	0.73	0.81	0.79	0.79
Specific Yield	×0.1	0.57	0.76	0.85	0.74	0.81	0.75	0.79
	×0.15	0.57	0.76	0.85	0.74	0.82	0.74	0.79
	×0.25	0.57	0.76	0.85	0.74	0.82	0.71	0.79
	×0.3	0.57	0.76	0.85	0.74	0.82	0.69	0.79

Groundwater recharge and saturated zone ET values across the entire model domain were varied between 0.8 and 1.2 times the calibrated values. Changes in groundwater recharge caused slight increases in the MAE of the groundwater monitor wells and wetland gauges (maximum change of 0.14 feet for groundwater monitoring wells and 0.16 feet for wetland gauges). Changes in groundwater recharge also caused changes in R^2 values at the C-18 weir, Cypress Creek, Hobe Grove Ditch, and Kitching Creek. Increases in groundwater recharge caused increases in R^2 values for the C-18 weir, and Cypress Creek by a maximum of 0.05 and caused decreases in R^2 for G-160 and S-46 by 0.05. Decreases in groundwater recharge caused decreases in R^2 values for the C-18 weir, Cypress Creek and Hobe Grove Ditch, and Kitching Creek by approximately 0.06. Changes in saturated zone ET caused slight increases in the MAE of monitoring wells and wetland gauges. The maximum change in the groundwater monitoring wells is 0.07 feet and the maximum change in the wetland gauges is 0.07 feet. Increases in saturated zone ET caused a decrease in the R^2 value at the C-18 weir and at Cypress Creek and Hobe Grove Ditch by 0.04 and 0.07, respectively. Decreases in saturated zone ET caused increases in the R^2 value at the C-18 weir and at Cypress Creek and Hobe Grove Ditch by 0.03 and 0.06, respectively.

Overall, based on the results of the sensitivity analysis, the model is most sensitive to hydraulic conductivity in Layers 2 and 3, drain conductance, GHB conductance, groundwater recharge, and saturated zone ET. The LECSR-NP does not appear to be sensitive to specific yield, river conductance, or vertical hydraulic conductivity. Additionally, comparing the overall MAE for the calibration and sensitivity runs, the minimum MAE is 0.62 feet, which occurs for the calibration and sensitivity runs on model parameters that do not impact calibration statistics. While there may be instances when a sensitivity run might appear superior to the calibration run for one or more parameters, the chosen calibration run was superior when considering the MAE and R^2 for all parameters. During the calibration process, horizontal hydraulic conductivity and conductance values typically were varied to attain the best model performance. Low confidence in the conductance values due to a lack of field data justified using a range of values to achieve the best calibration performance. Due to the high confidence in rainfall and reference ET data and in AFSIRS and the ET-Recharge-Runoff Program, groundwater recharge and saturated zone ET inputs were not altered. Localized changes that impact groundwater recharge and saturated zone ET occurred during creation of the ET and recharge inputs by varying curve numbers for a given land use.

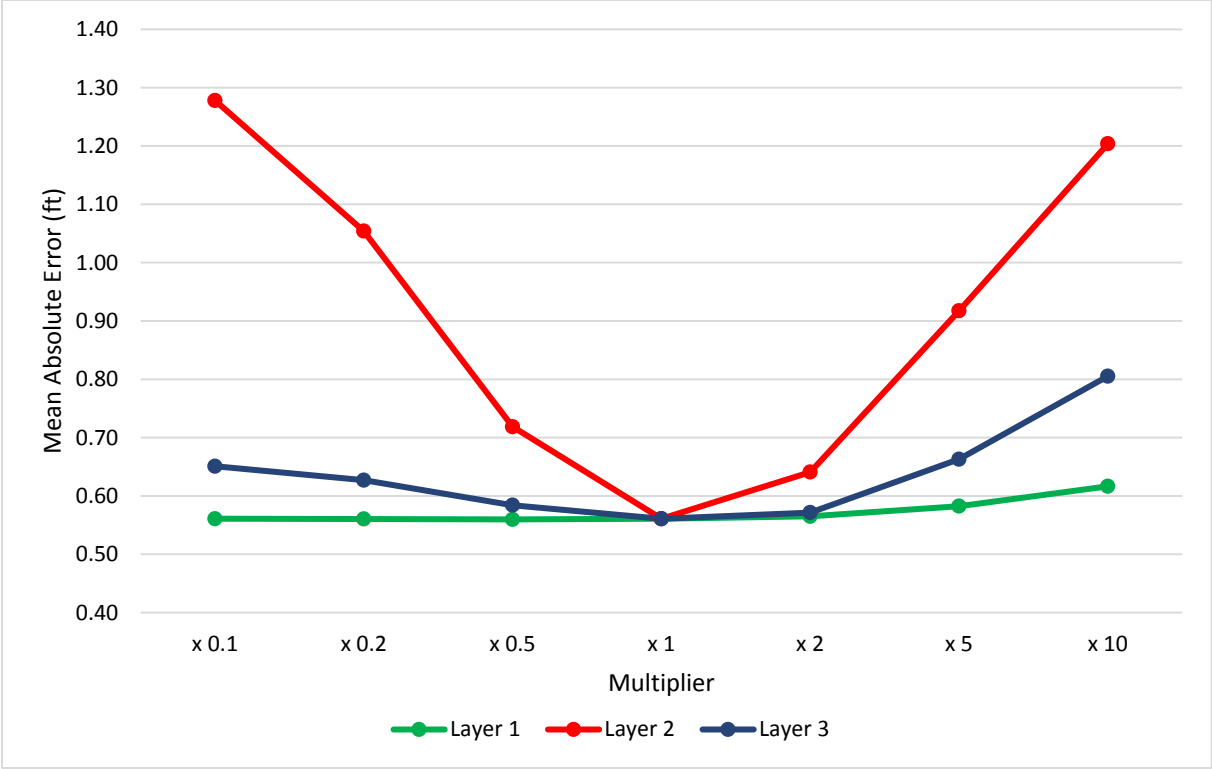

Figure 85. Sensitivity of simulated heads to changes in horizontal hydraulic conductivity in groundwater monitoring wells.

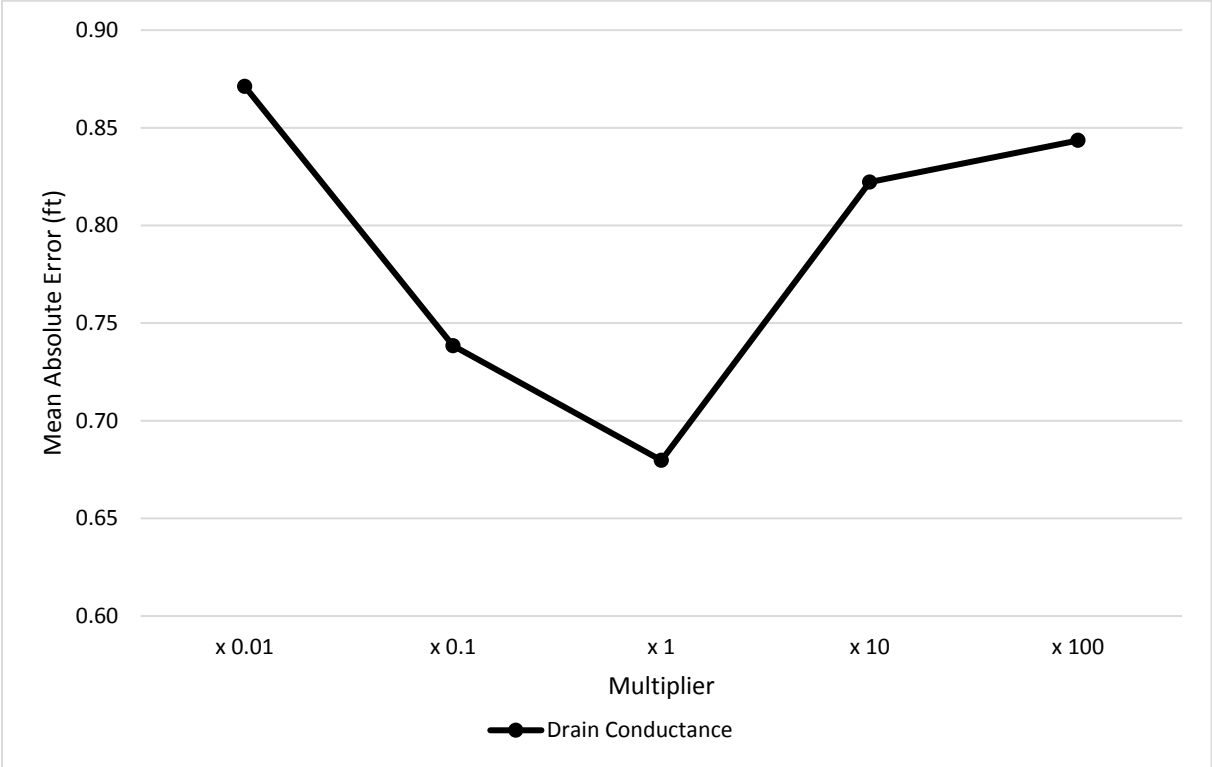

Figure 86. Sensitivity of simulated heads to global changes in drain conductance in wetland gauges.

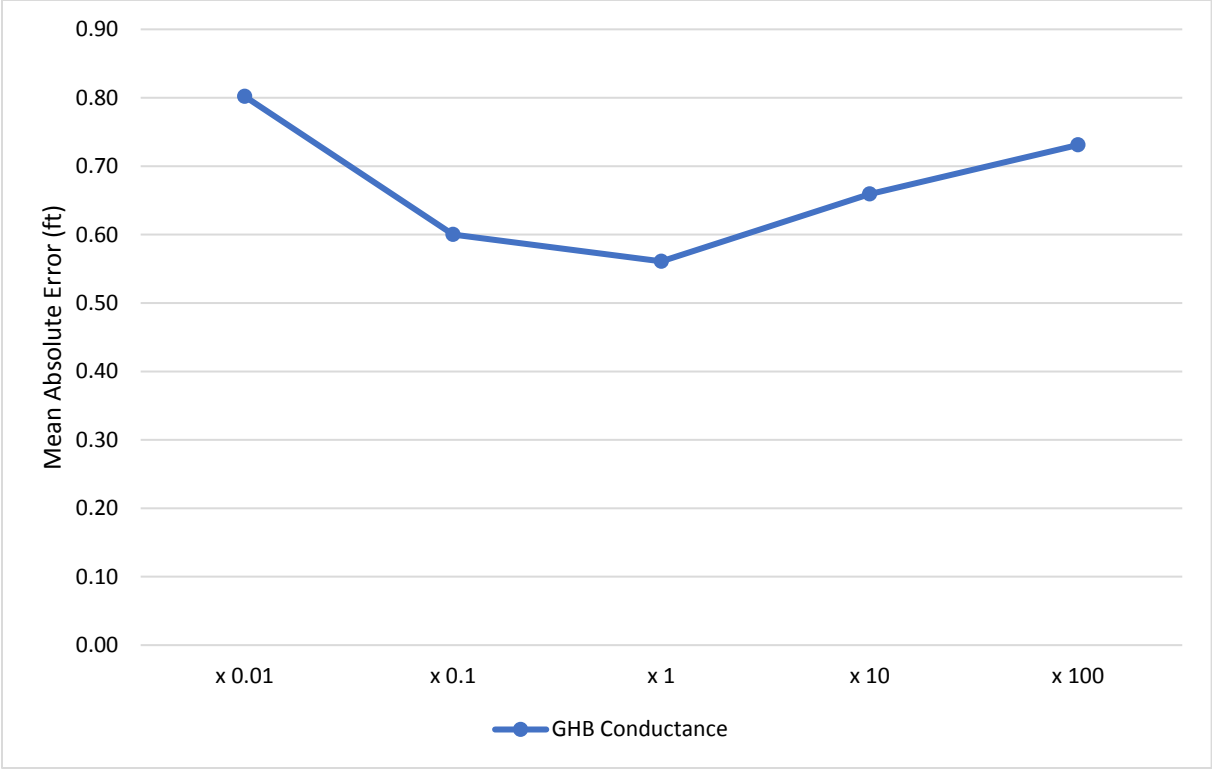

Figure 87. Sensitivity of simulated heads to global changes in general head boundary conductance in groundwater monitoring wells.

5. CONCLUSIONS

The LECSR-NP is a well calibrated subregional hydrologic model based on MODFLOW (McDonald and Harbaugh, 1988; Harbaugh and McDonald, 1996) that will be used to support a detailed planning-level analysis of system responses for formulation and evaluation for the LRWRP of the Comprehensive Everglades Restoration Plan (CERP). This report serves as documentation of the model development and calibration process. The model itself should be used within the boundaries of this project in regards to project assumptions, goals, and objectives. Application of the model to other projects will depend on several factors, including a project's modeling objectives, and should be reviewed on a case-by-case-basis for each modeling request.

The LECSR-NP more than adequately met the calibration targets selected for this project's goals. The model shall not be applied for more detailed engineering analyses, such as flood events or canal and pump sizing. Model results are to be evaluated comparatively (i.e., evaluating the relative difference between two simulations) for predictions; results from a particular simulation should not be taken as absolutes.

5.1 Limitations

The LECSR-NP assumes constant fluid density, no transport, and no hydraulic routing. The model lacks canal-sizing capabilities and assumes canals have the capacity to route flows.

For the LRWRP area, improvements were made for lumped hydrologic routing in order to route basin runoff (with the Muskingum hydrologic routing procedure) to canals. The hydrologic routing for runoff is not coupled to MODFLOW, which is a limitation. However, an iterative process was used to account for the total runoff and canal baseflow during calibration and application.

The Wetland package was used to route water along canals, making use of preferential flow paths. The Wetland package was developed for routing overland flows using the Kadlec equation but was not designed to route open-channel flows.

Land use in northern Palm Beach County has been substantially altered during the past decade due to urbanization and ongoing restoration projects. Currently, the LECSR-NP uses a single land use year (2013) for the entire calibration period. Therefore, accurately simulating overland flow processes, including estimating runoff and recharge in areas where land use has changed, is challenging.

The LECSR-NP does not simulate the regional water management system. Historical data were used to simulate boundary conditions to reflect the response of the regional system. However, internal project features such as the L-8 Reservoir, C-18 Basin, and GWP do not use internal boundary conditions.

Moreover, executing the true operational intent of the project is limited by factors such as model source code flexibility and scale. Simplified assumptions were made to mimic complex system interactions while preserving operational intent.

6. LITERATURE CITED

Arcadis. 2015. Mecca Flow Equalization Basin Design Documentation Report. West Palm Beach, FL.

Anderson, M.P. and W.M. Woessner. 1992. Applied Groundwater Modeling: Simulation of Flow and Advective Transport. Academic Press, San Diego, CA.

Andersen, P.F., R. Peralta, and J.M. Shafer. 2006. Peer Review Report of the Lower East Coast Subregional Groundwater Flow Model and Draft Model Documentation. Prepared for the Resource Evaluation and Subregional Modeling Division, Water Supply Bureau, South Florida Water Management District, West Palm Beach, FL. 201 pages.

Bandara, U. 2018. Development and Verification of a Numerical Model to Simulate Evapotranspiration and Recharge for Regional Scale Groundwater Models. Florida Water Resource Conference. April 2018. Daytona Beach, FL.

Brown, C. 2013. Reference Evapotranspiration (1948-2013) using 51-year Hydrological Reanalysis and North American Regional Reanalysis, South Florida Water Management District, West Palm Beach, FL.

Brown, C. 2014. QA/QC of NEXRAD Rainfall (2001-2012), South Florida Water Management District, West Palm Beach, FL.

Chow, V.T., D.R. Maidment, and L.W. Mays. 1988. Applied Hydrology. McGraw-Hill. New York.

Collins, B., B. Kacvinsky, E. Geddes, A. Dodd, and L. Lindstrom. 2016. G-160 and Loxahatchee Slough Groundwater – Surface Water Interaction Study Technical Report. SFWMD Technical Publication WS-40. South Florida Water Management District, West Palm Beach, FL.

Cooper, Jr., H.H. and C.E. Jacob. 1946. A Generalized Graphical Method for Evaluating Formation Constants and Summarizing Well-Field History. American Geophysical Union Transactions 27(4):526-534.

Cunge, J.A. 1969. On the Subject of a Flood Propagation Computation Method (Muskingum Method). Journal of Hydraulic Research 7(2):205-230.

Dunkelberger Engineering and Testing, Inc. 2009. Test Well Installation and Chloride Content Determination, Palm Beach Aggregates Western Rock Expansion. Palm Beach County, Florida. Prepared for Palm Beach Aggregates, Loxahatchee, FL.

Ecology and Environment, Inc. 2004a. Multibud Utility for MODFLOW-96. [computer software] Prepared for the South Florida Water Management District, West Palm Beach, FL.

Ecology and Environment, Inc. 2004b. Final Report: Procedural Approach for Ecological Benefit and Impact Analyses of Alternative Plans: North Palm Beach County – Part 1 Watershed Wetlands. Prepared for South Florida Water Management District and the U.S. Army Corps of Engineers, Jacksonville District.

Florida Department of Environmental Protection and SFWMD. 2010. Loxahatchee River National Wild and Scenic River Management Plan. Plan Update 2010.

Food and Agriculture Organization of the United Nations. 1990. Expert Consultation on Revision of FAO Methodologies for Crop Water Requirements.

Gannett Fleming. 2015. Palm Beach County Groundwater Modeling for L-8 FEB Phase V. Supplemental Data Acquisition at the East Side of the Project Domain. West Palm Beach, FL.

Gannett Fleming. 2016. J.W. Corbett Wildlife Management Area Final Geotechnical Data Report. West Palm Beach, FL.

Giddings, J.B., L.L. Kuebler, J.I. Restrepo, K.A. Rodberg, A.M. Montoya, and H.A. Radin. 2006. Draft Lower East Coast Subregional MODFLOW Model Documentation. South Florida Water Management District, West Palm Beach, FL.

Harbaugh, A.W., E.R. Banta, M.C. Hill, and M.G. McDonald. 2000. MODFLOW-2000, The U.S. Geological Survey Modular Ground-water Model – User Guide to Modularization Concepts and the Ground-water Flow Process. Open-File Report 00-92. U.S. Geological Survey, Reston, VA.

Jones, M. 1999. A Reinjection Drainflow Package for MODFLOW. Albuquerque, NM. 33 pp.

Kadlec, R.H. 1990. Overland flow in wetlands: Vegetation resistance. Journal of Hydraulic Engineering 116(5).

Lal, W. 2015. Field Test to Estimate Conveyance Losses in the M-1 Canal. SFWMD Internal Memorandum. South Florida Water Management District, West Palm Beach, FL.

Montoya, A., L. Kuebler, H. Radin, and V. Mullen. 2010. Model Implementation of the Northern Palm Beach County version of the Lower East Coast Subregional Model (LECSR-NP-2010). South Florida Water Management District, West Palm Beach, FL.

Montoya, A. and L. Kuebler. 2016. Water Availability Assessment for the Mecca Impoundment of the Loxahatchee River Watershed Restoration Project. South Florida Water Management District, West Palm Beach, FL.

Randall, D. 1992. User's Documentation for the MODFLOW-96 Trigger Package. Water Resources Management, Inc. 13 pp.

Reese, R.S. and M.A. Wacker. 2007. Hydrostratigraphic Framework and Selection and Correlation of Geophysical Markers in the Surficial Aquifer System, Palm Beach County, Florida. USGS Scientific Investigations Map 2971. U.S. Geological Survey, Reston, VA.

Reese, R.S. and M.A. Wacker. 2009. Hydrogeologic and Hydraulic Characteristics of the Surficial Aquifer System, and Origin of High Salinity Groundwater, Palm Beach County, FL. USGS Scientific Investigative Report 2009-5113. U.S. Geological Survey, Reston, VA. 83 pp.

Reilly, T.E. and A.W. Harbaugh. 2004. Guidelines for Evaluating Ground-Water Flow Models. USGS Paper 5038

Restrepo, J.I. and J.B. Giddings. 1994. Physical Based Methods to Estimate ET and Recharge Rates Using GIS, pp. 65-74. In: American Water Resources Association, Conference Proceedings—Effects of Human-Induced Changes on Hydrologic Systems. Bethesda, Maryland.

Restrepo, J.I., A.M. Montoya, and J. Obeysekera. 1998. A Wetland Simulation Module for the MODFLOW Ground Water Model. Ground Water 36(5):764-770.

Restrepo, J.I., A.M. Montoya, and D. Garces. 2003. The Updated Utility Generation Package (UGEN) for the Groundwater Flow Model, MODFLOW. Developed by the Hydrological Research Center at Florida Atlantic University, Boca Raton, FL, in cooperation with the South Florida Water Management District, West Palm Beach, FL.

Rodberg, K. 1999. Multiple Wells Package for MODFLOW-96. [computer software] South Florida Water Management District, West Palm Beach, FL.

SFWMD. 2002. MFLs for the North West Fork of the Loxahatchee River. South Florida Water Management District, West Palm Beach, FL.

SFWMD. 2006. Restoration Plan for the Northwest Fork of the Loxahatchee River. South Florida Water Management District, West Palm Beach, FL. pp. 6-1 to 6-52.

SFWMD. 2011. Past and Projected Trends in Climate and Sea Level for South Florida. Technical Report. South Florida Water Management District, West Palm Beach, FL.

SFWMD. 2015. Summary of May 2015 Field Measurements of M-Canal Conveyance Losses and Estimated Flows to Offset Structure G-161 Withdrawals from Grassy Waters Preserve. South Florida Water Management District, West Palm Beach, FL. 22 pp.

Smajstrla, A.G. 1990. Agricultural Field-Scale Irrigation Requirements Simulation (AFSIRS) Model, Version 3.8. Agricultural Engineering Department, University of Florida, Gainesville, FL. 247 pp.

Smith, D.L. and K.M. Lord. 1997. Tectonic Evolution and Geophysics of the Florida Basement, pp. 13-26. In: A.F. Randazzo and D.S. Jones, The Geology of Florida. University Press of Florida, Gainesville, FL. 327 pp.

United States Department of Agriculture. 1986. Urban Hydrology for Small Watersheds. Technical Release 55 (TR-55). Natural Resources Conservation Service, Conservation Engineering Division, Washington, D.C.

United States Department of Agriculture. 2007. Chapter 7: Hydrologic Soil Groups. National Engineering Handbook Part 630, Hydrology. United States Department of Agriculture, Natural Resources Conservations Service. May 2007.

USACE and SFWMD. 1999. Central and Southern Florida [Flood Control] Project Comprehensive Review Study Final Integrated Feasibility Report and Programmatic Environmental Impact Statement. USACE, Jacksonville, FL, and SFWMD, West Palm Beach, FL.

Welter, D. 1999. Output Summation Utility for MODFLOW-96. [computer software] South Florida Water Management District, West Palm Beach, FL.

Zahina, J., K. Liudahl, T. Liebermann, K. Saari, J. Krenz, and V. Mullen. 2001. Soil Classification Database: Categorization of County Soil Survey Data within the SFWMD Including Natural Soils Landscape Positions. Technical Publication WS-06. South Florida Water Management District, West Palm Beach, FL.

APPENDIX A: GROUNDWATER WELLS

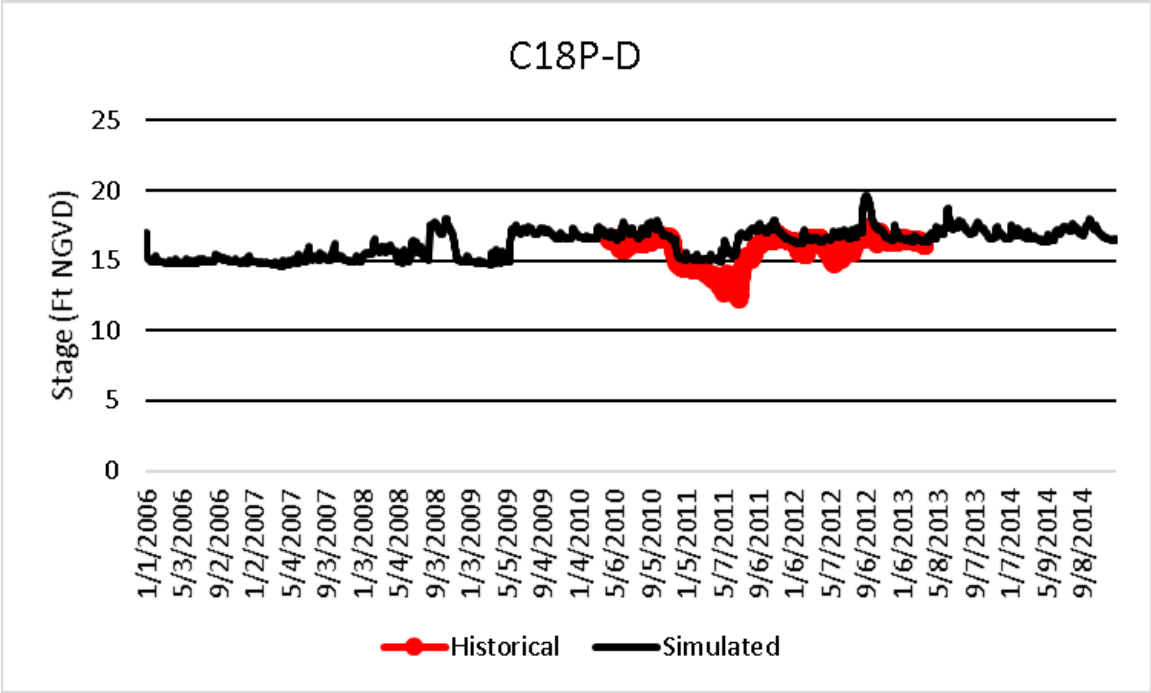

Figure A-1. Historical and simulated groundwater monitoring well stage hydrograph (2006 – 2014) for C18P-D.

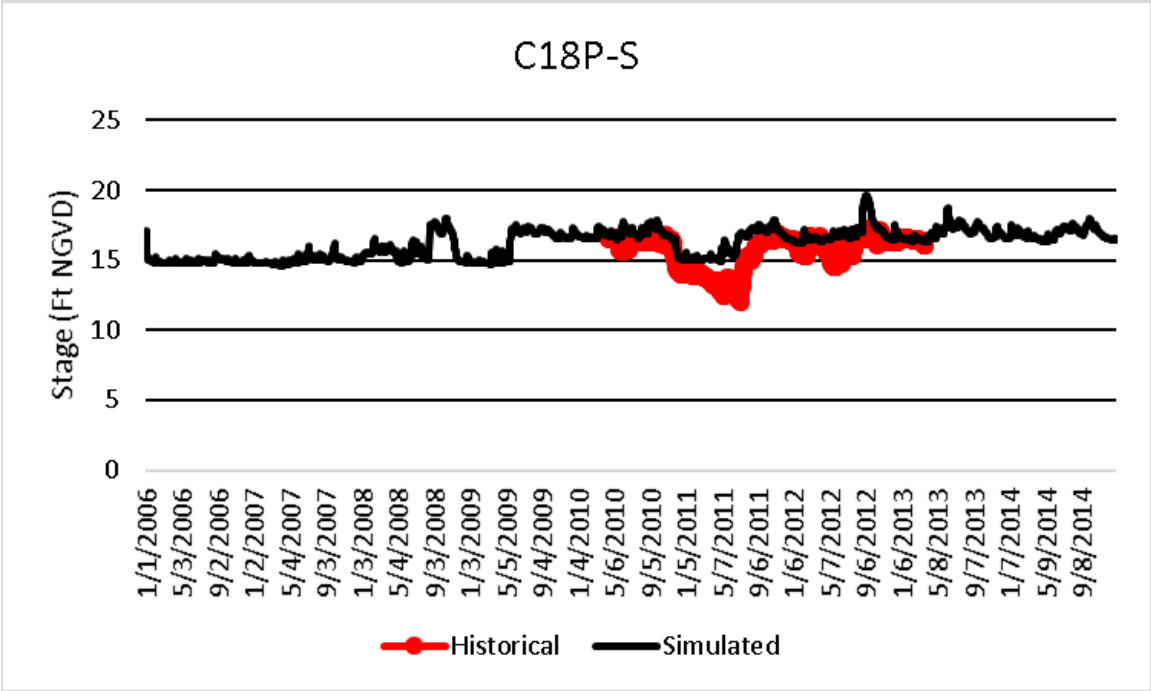

Figure A-2. Historical and simulated groundwater monitoring well stage hydrograph (2006 – 2014) for C18P-S.

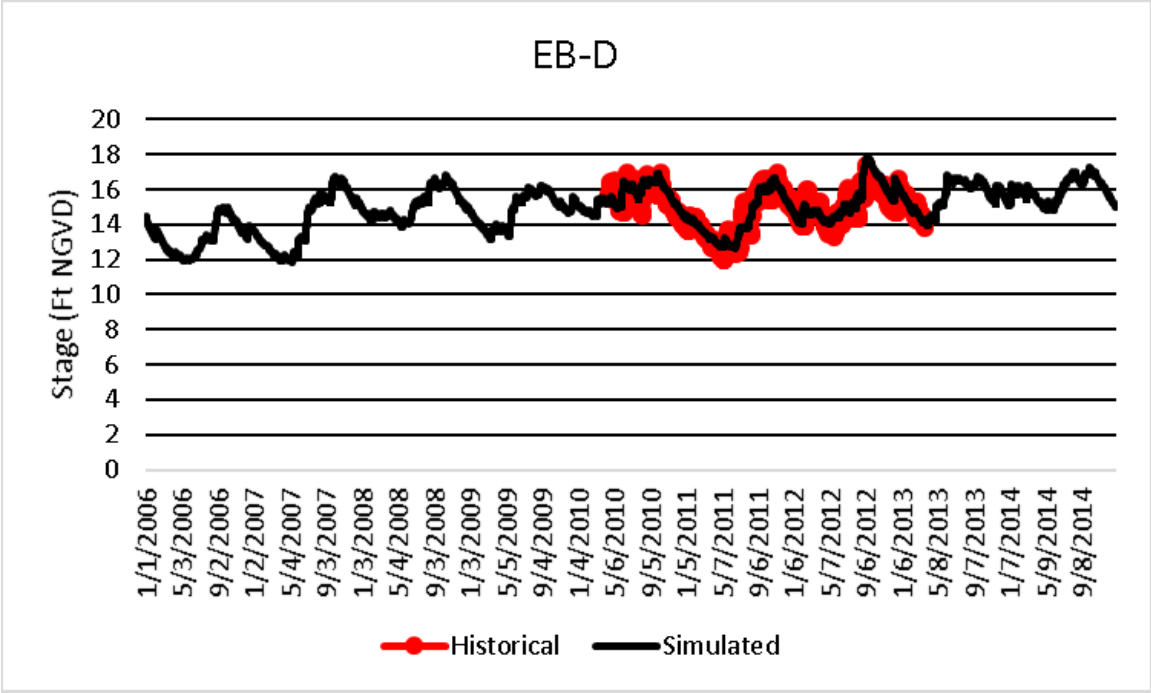

Figure A-3. Historical and simulated groundwater monitoring well stage hydrograph (2006 – 2014) for EB-D.

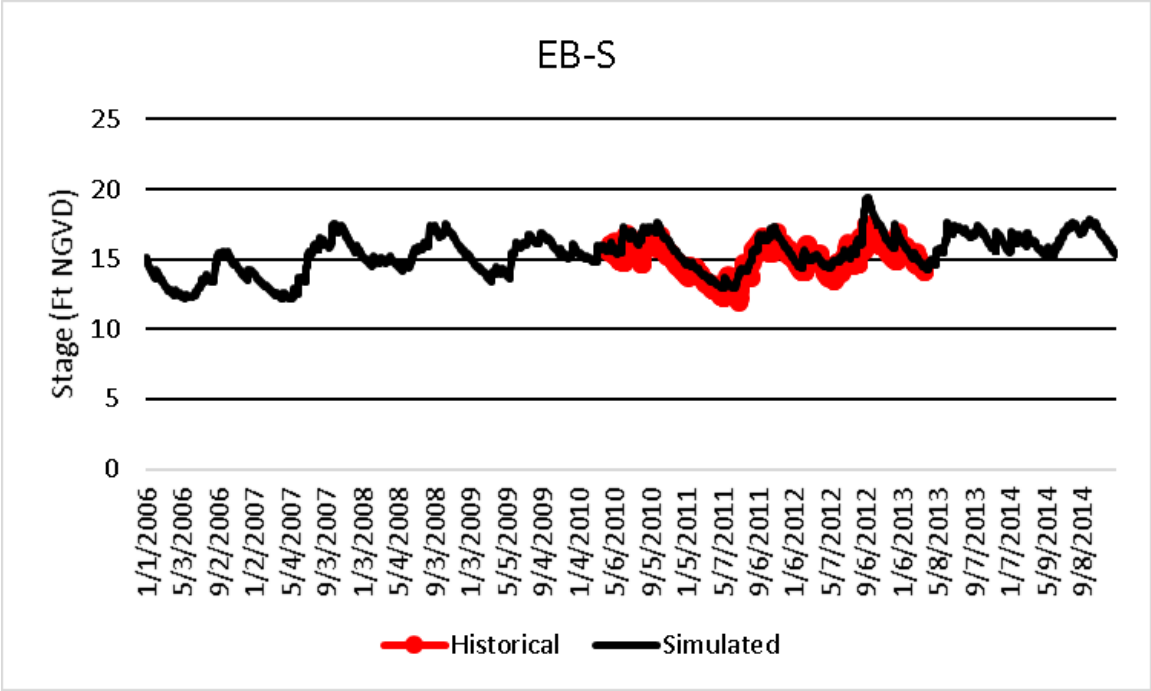

Figure A-4. Historical and simulated groundwater monitoring well stage hydrograph (2006 – 2014) for EB-S.

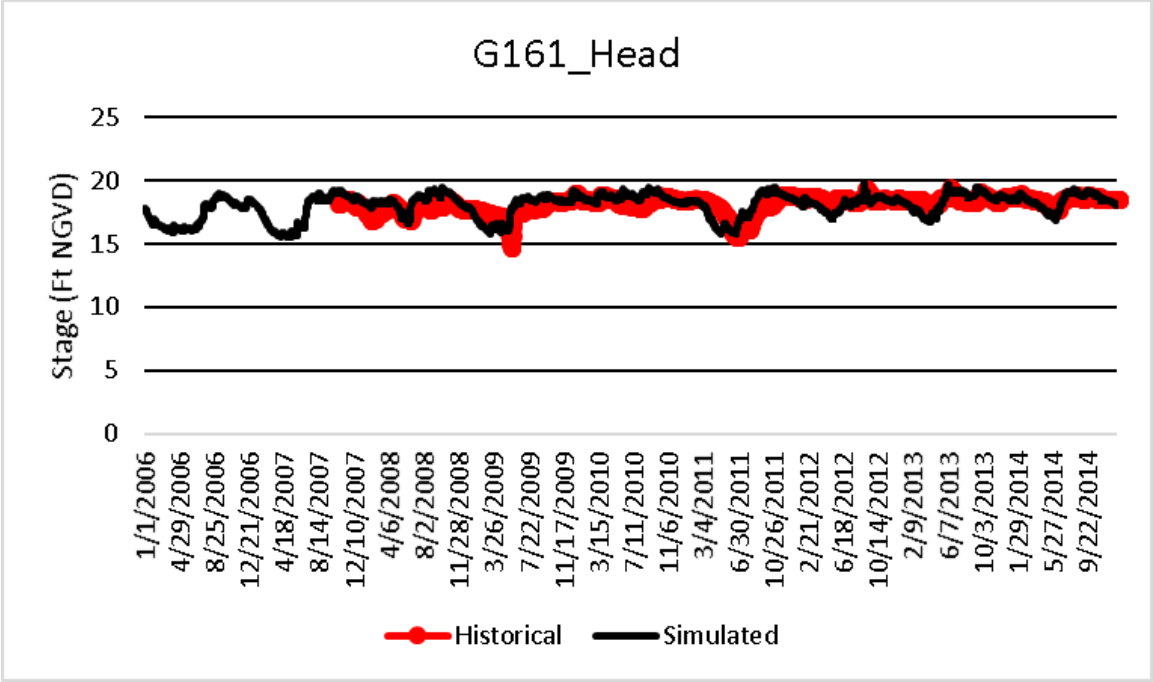

Figure A-5. Historical and simulated groundwater monitoring well stage hydrograph (2006 – 2014) for G161_Head.

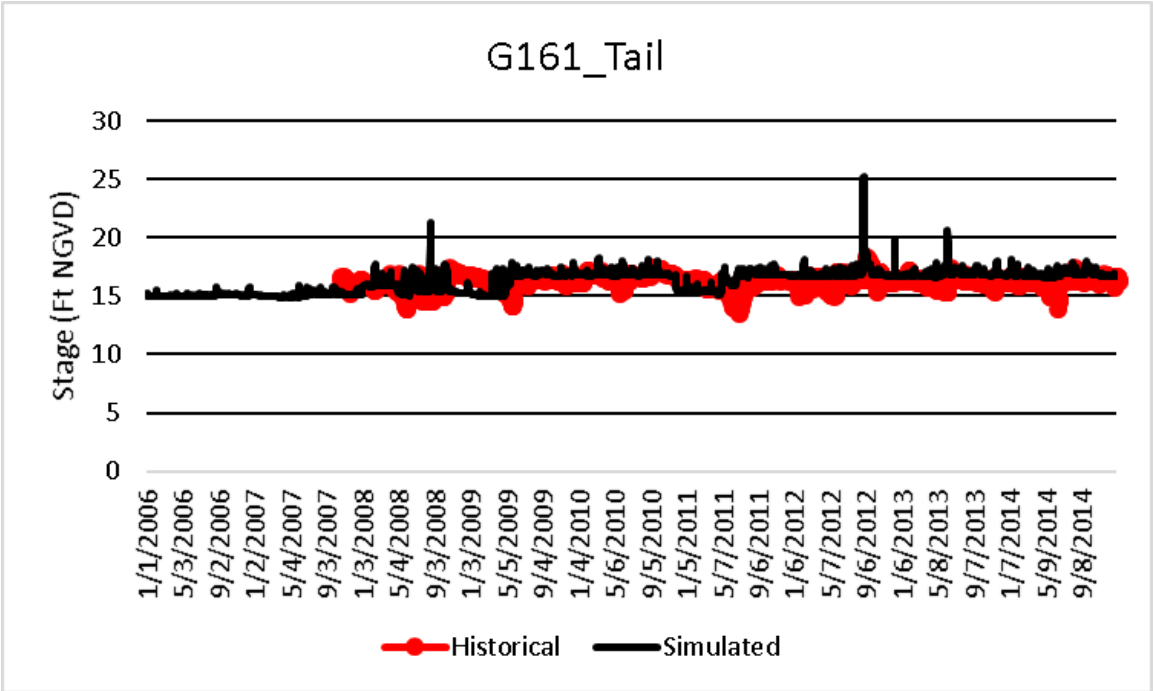

Figure A-6. Historical and simulated groundwater monitoring well stage hydrograph (2006 – 2014) for G161_Tail.

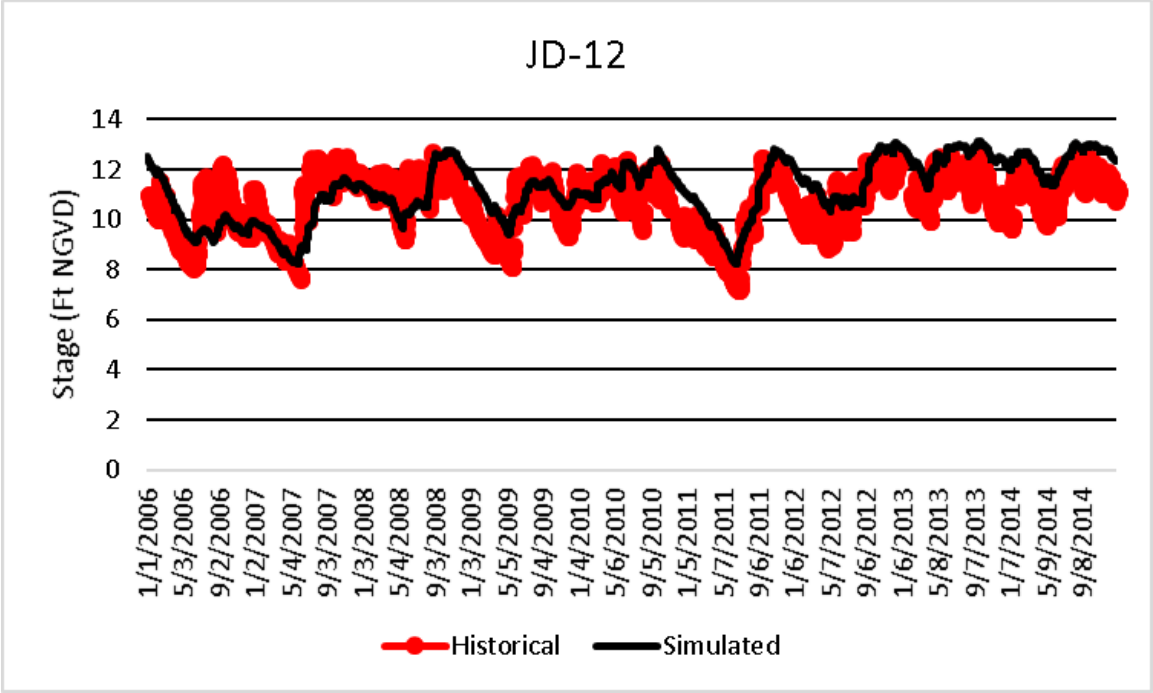

Figure A-7. Historical and simulated groundwater monitoring well stage hydrograph (2006 – 2014) for JD-12.

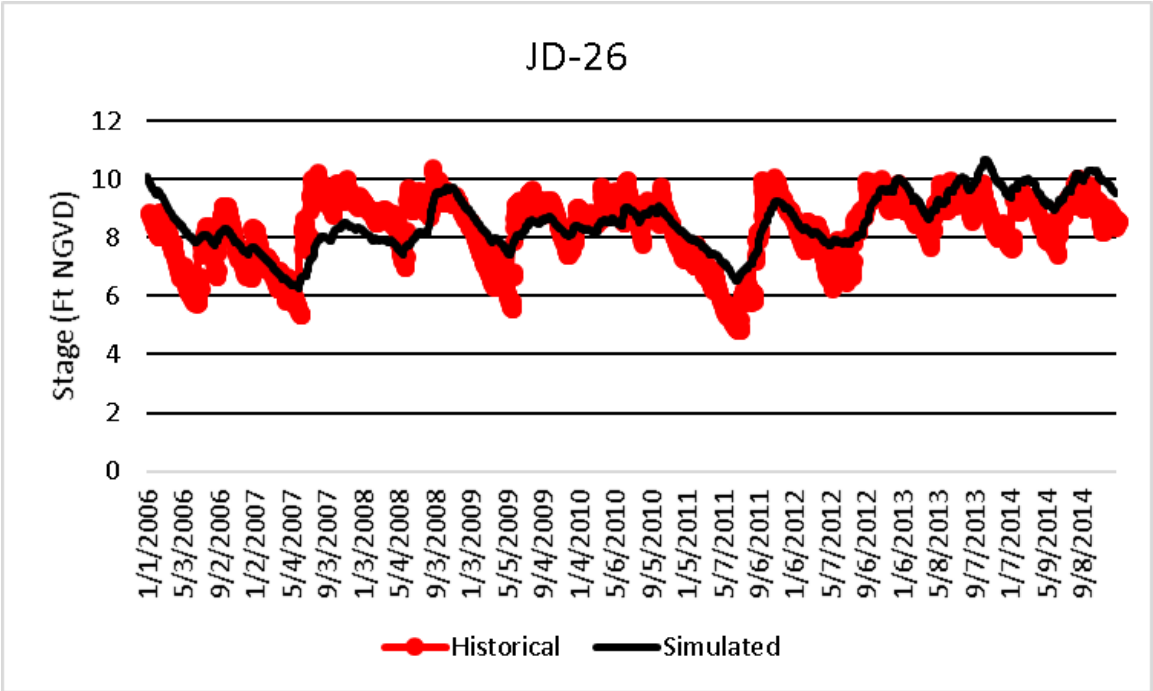

Figure A-8. Historical and simulated groundwater monitoring well stage hydrograph (2006 – 2014) for JD-26.

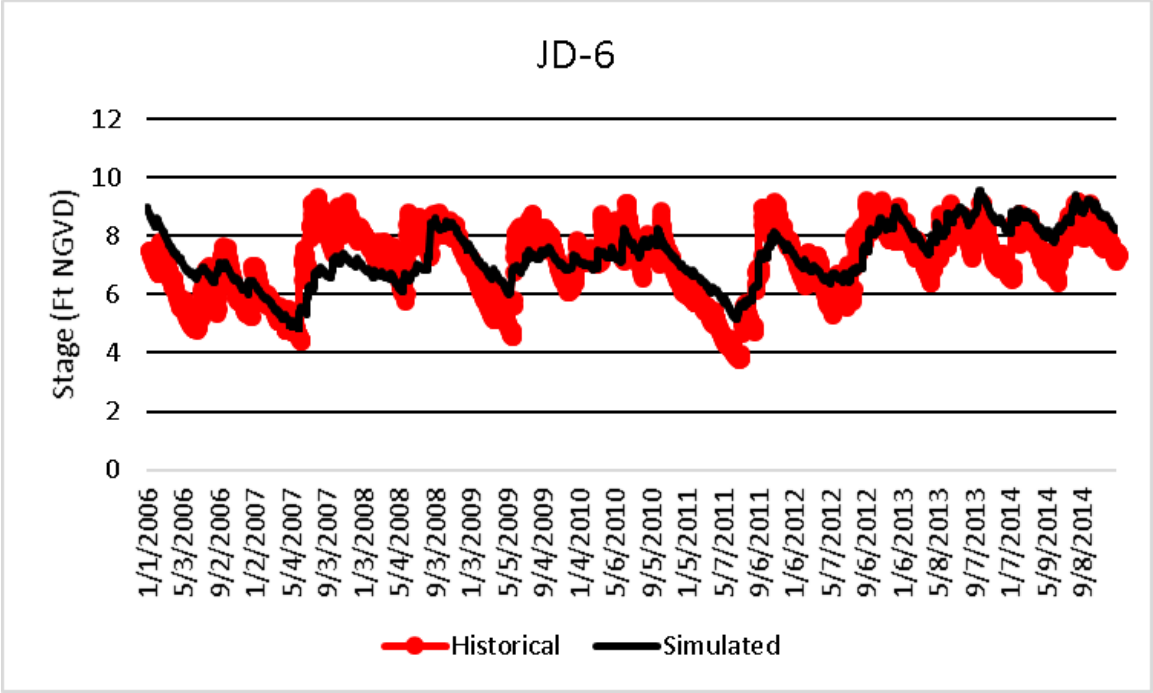

Figure A-9. Historical and simulated groundwater monitoring well stage hydrograph (2006 – 2014) for JD-6.

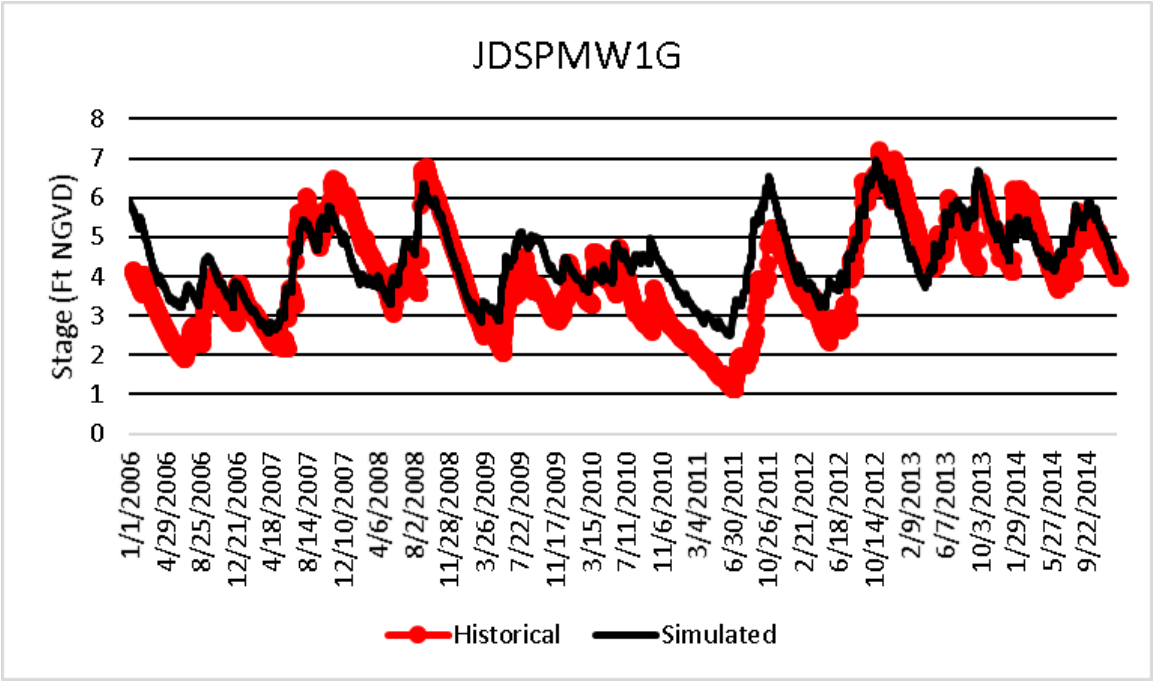

Figure A-10. Historical and simulated groundwater monitoring well stage hydrograph (2006 – 2014) for JDSPMW1G.

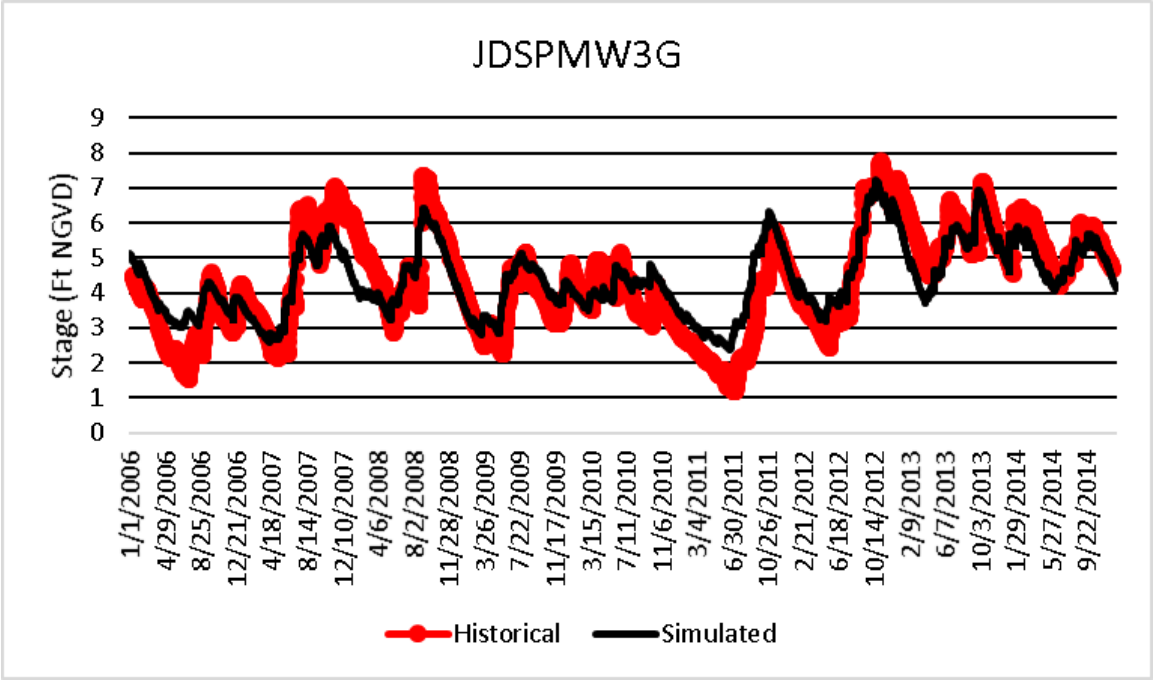

Figure A-11. Historical and simulated groundwater monitoring well stage hydrograph (2006 – 2014) for JDSPMW3G.

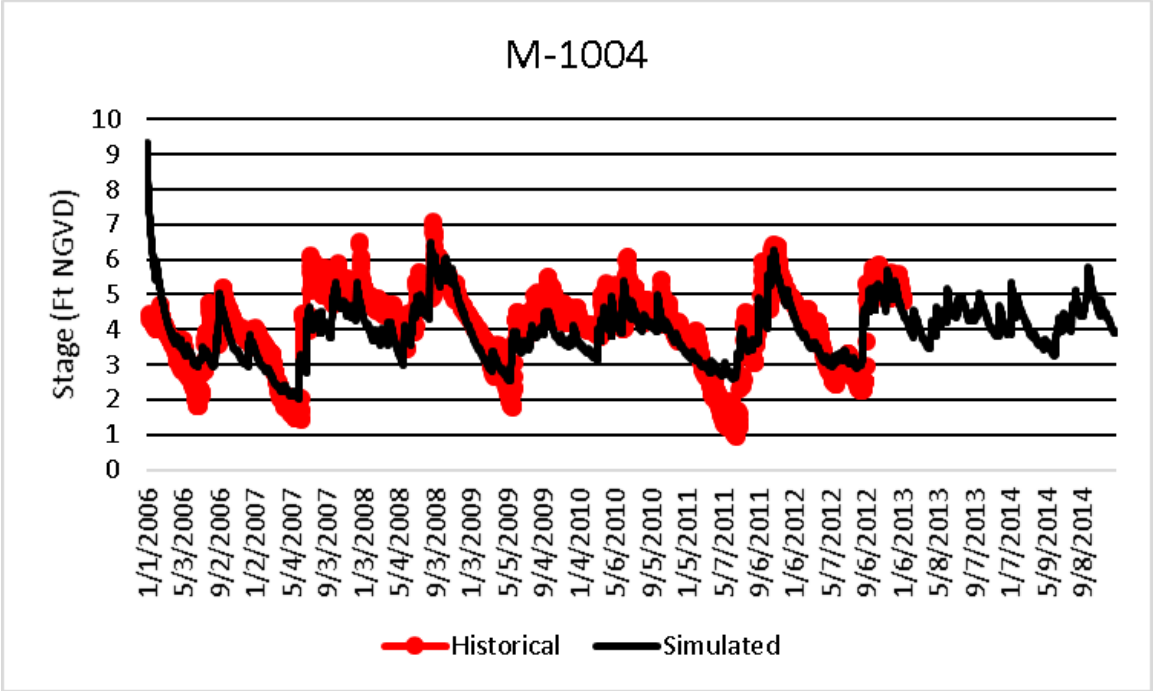

Figure A-12. Historical and simulated groundwater monitoring well stage hydrograph (2006 – 2014) for M-1004.

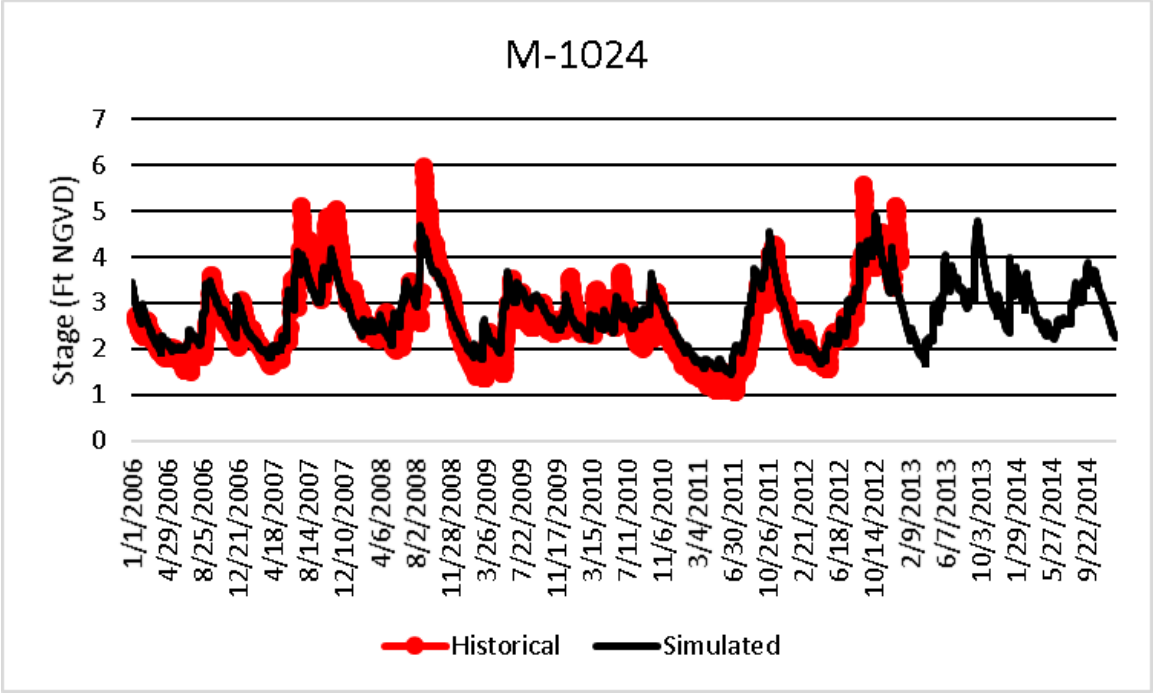

Figure A-13. Historical and simulated groundwater monitoring well stage hydrograph (2006 – 2014) for M-1024.

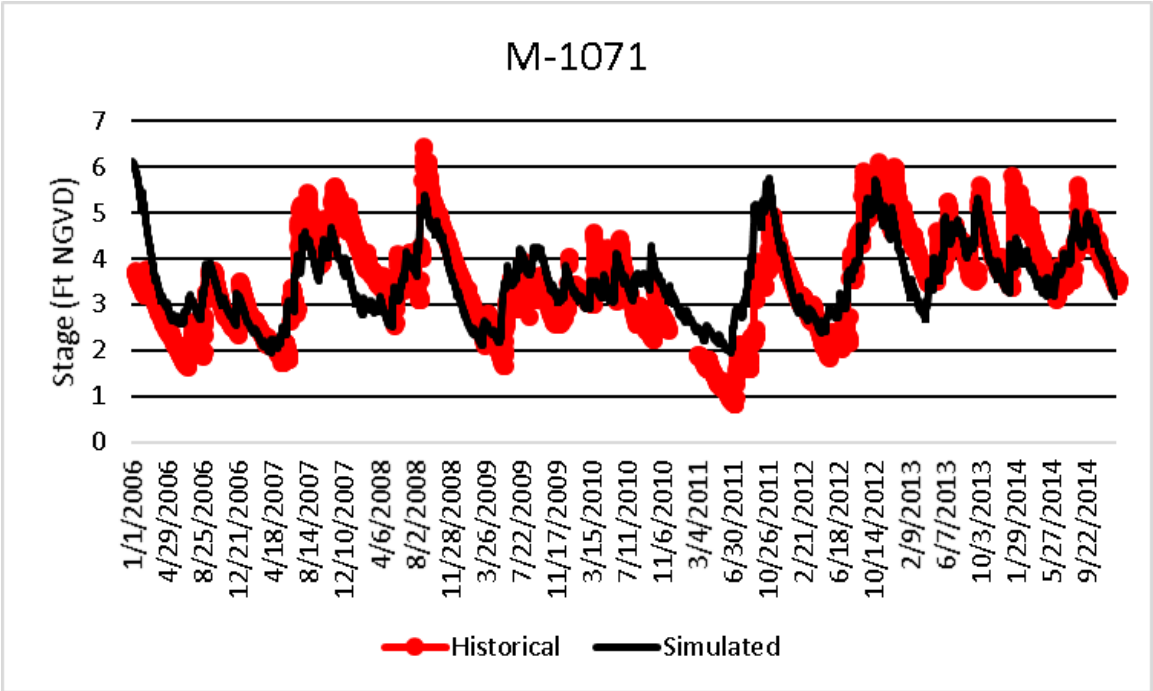

Figure A-14. Historical and simulated groundwater monitoring well stage hydrograph (2006 – 2014) for M-1071.

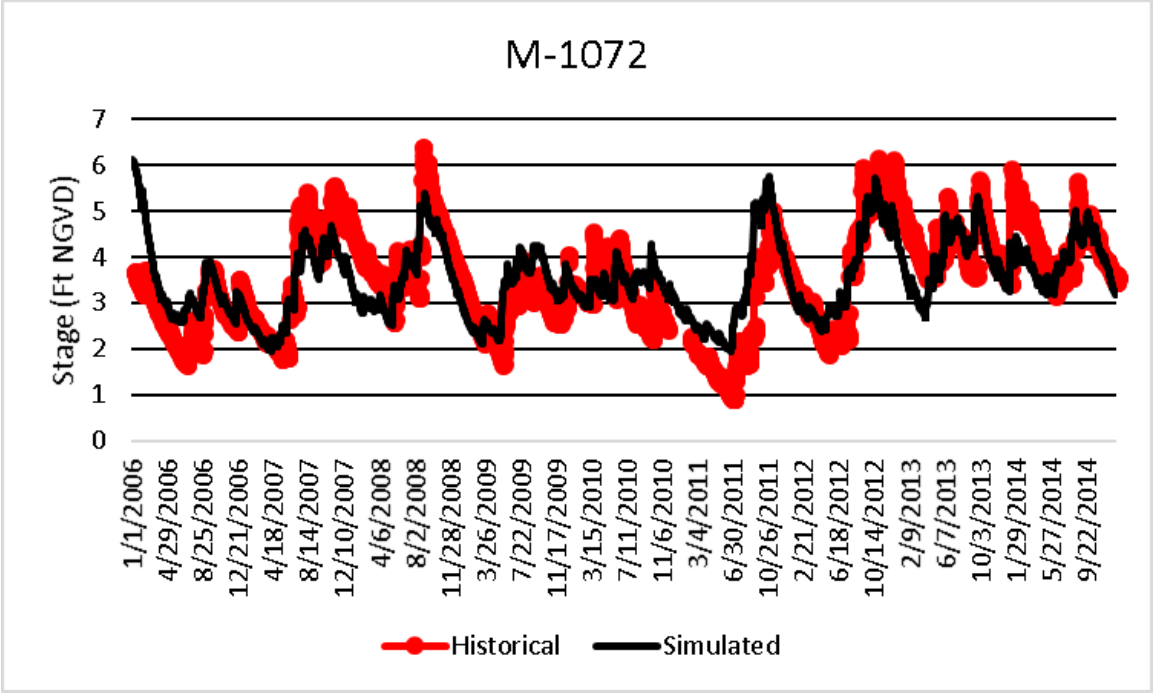

Figure A-15. Historical and simulated groundwater monitoring well stage hydrograph (2006 – 2014) for M-1072.

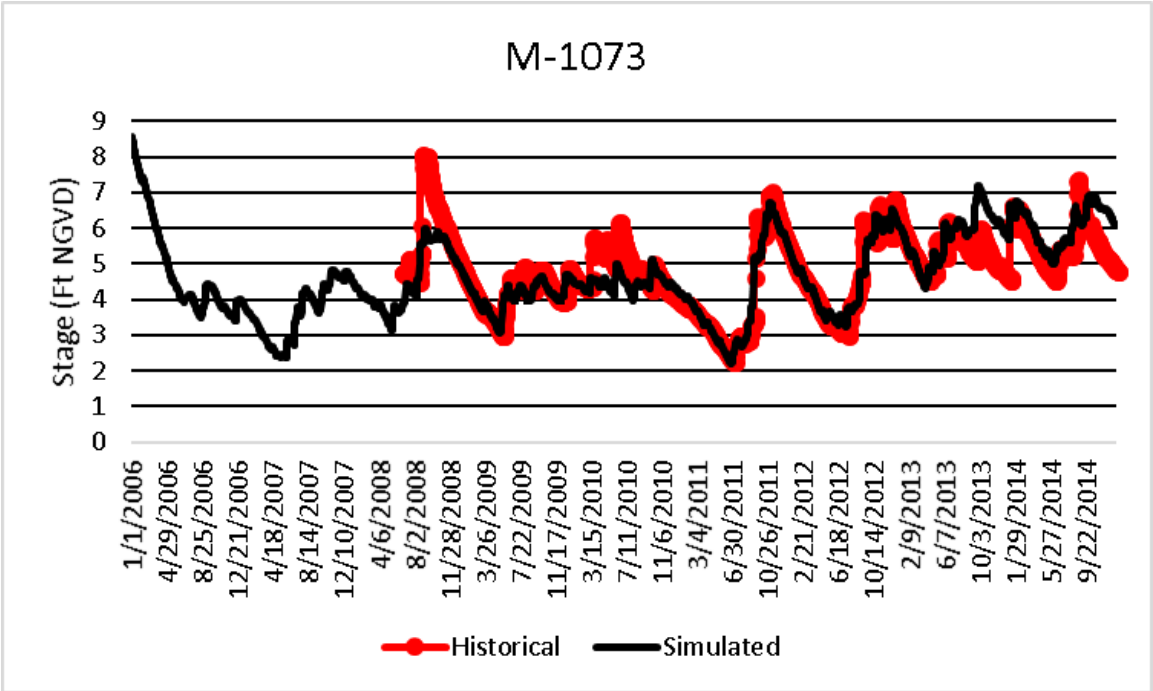

Figure A-16. Historical and simulated groundwater monitoring well stage hydrograph (2006 – 2014) for M-1073.

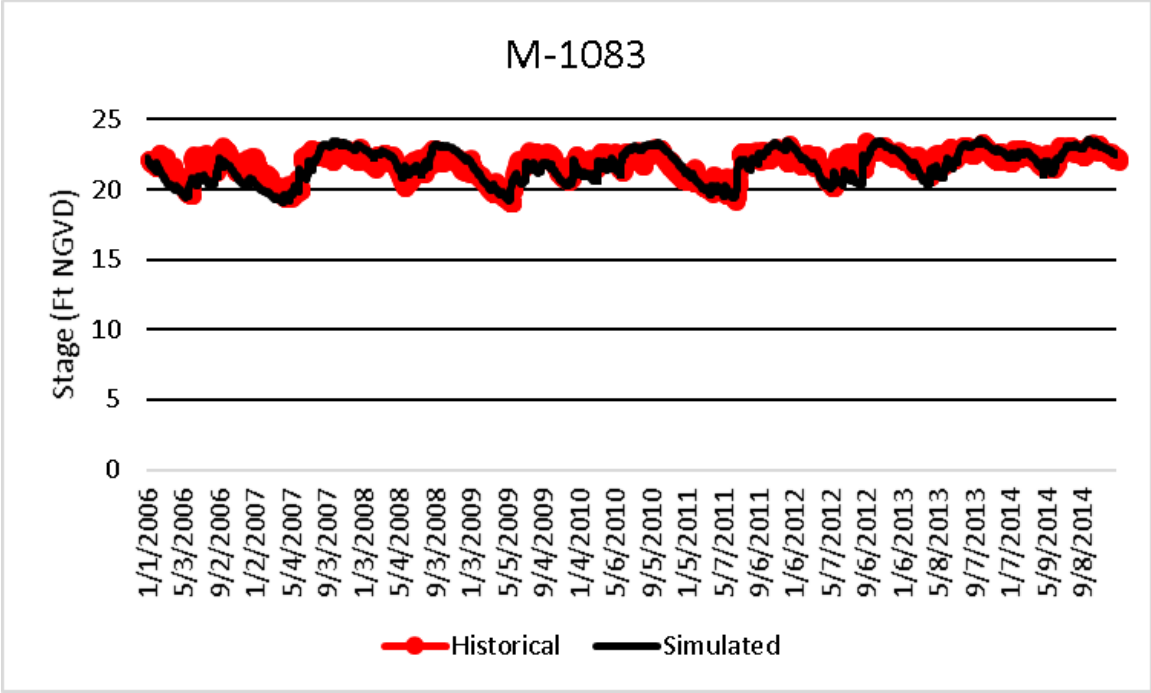

Figure A-17. Historical and simulated groundwater monitoring well stage hydrograph (2006 – 2014) for M-1083.

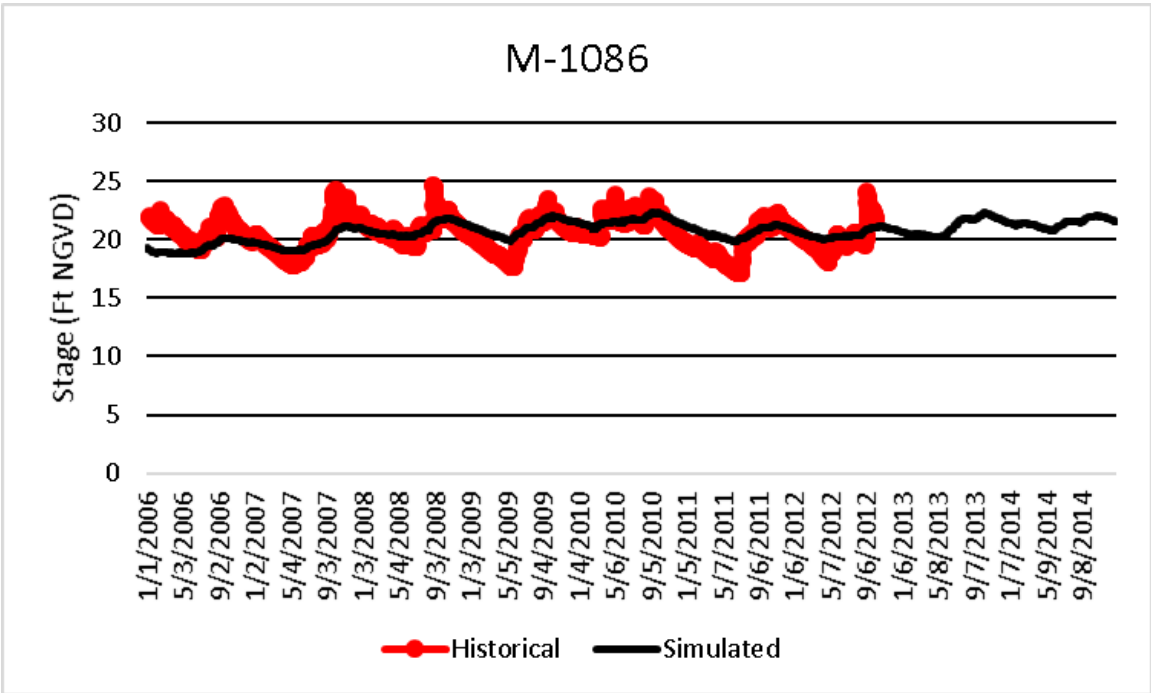

Figure A-18. Historical and simulated groundwater monitoring well stage hydrograph (2006 – 2014) for M-1086.

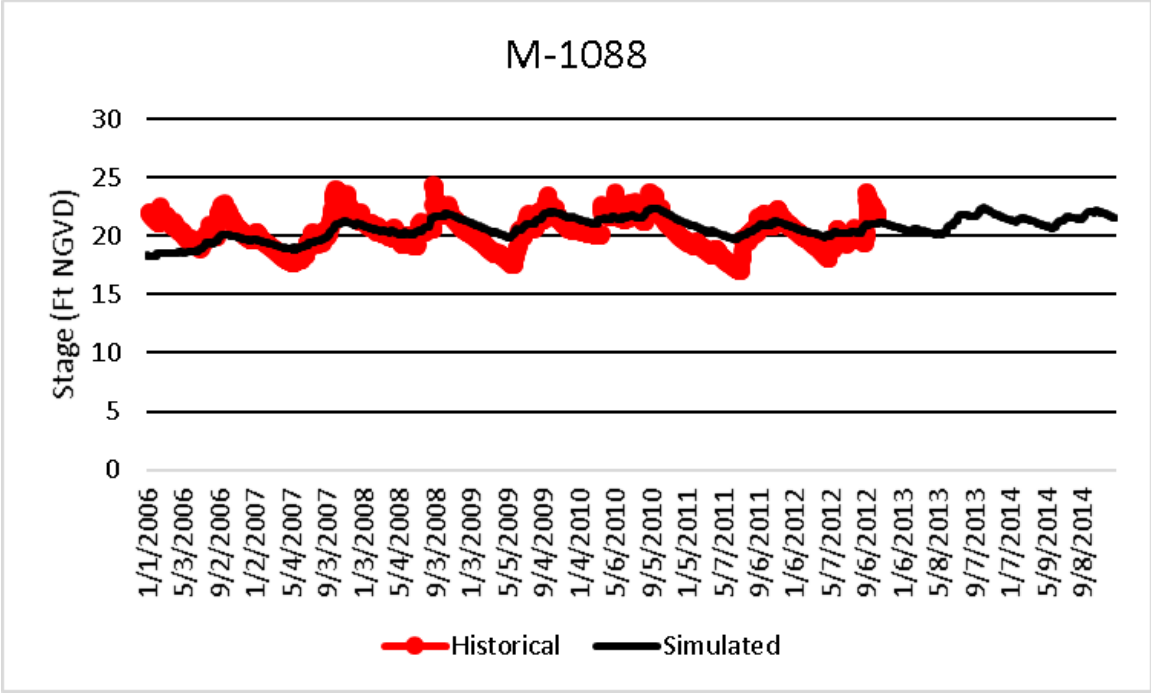

Figure A-19. Historical and simulated groundwater monitoring well stage hydrograph (2006 – 2014) for M-1088.

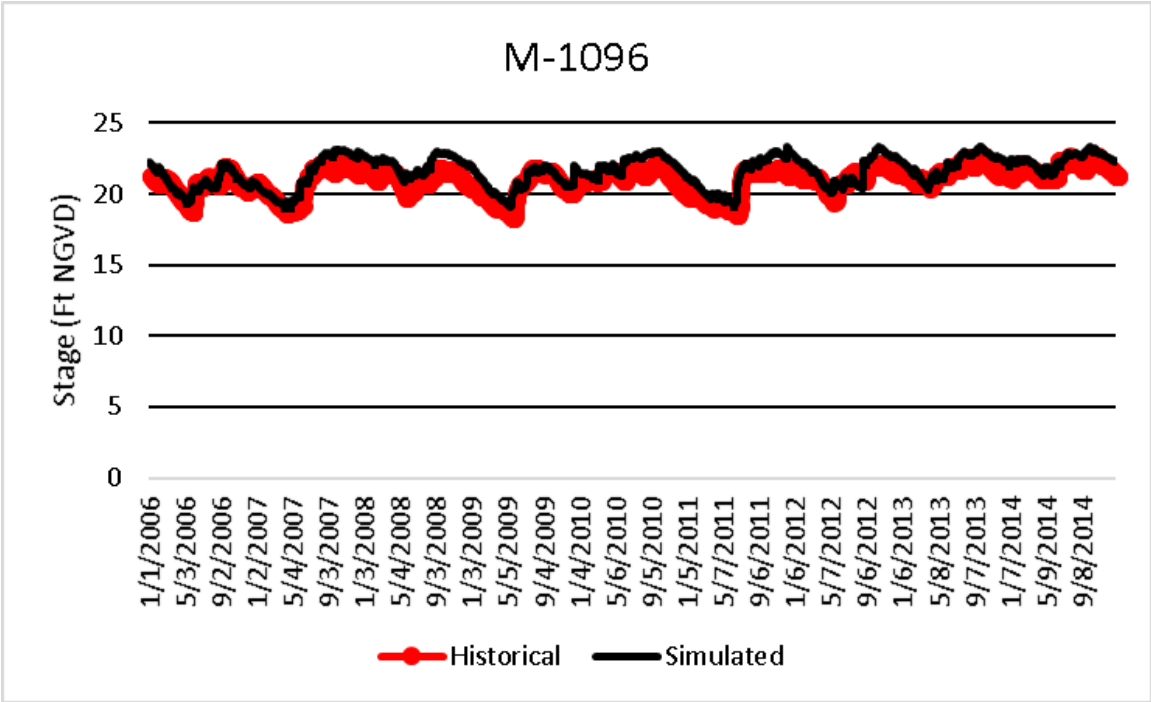

Figure A-20. Historical and simulated groundwater monitoring well stage hydrograph (2006 – 2014) for M-1096.

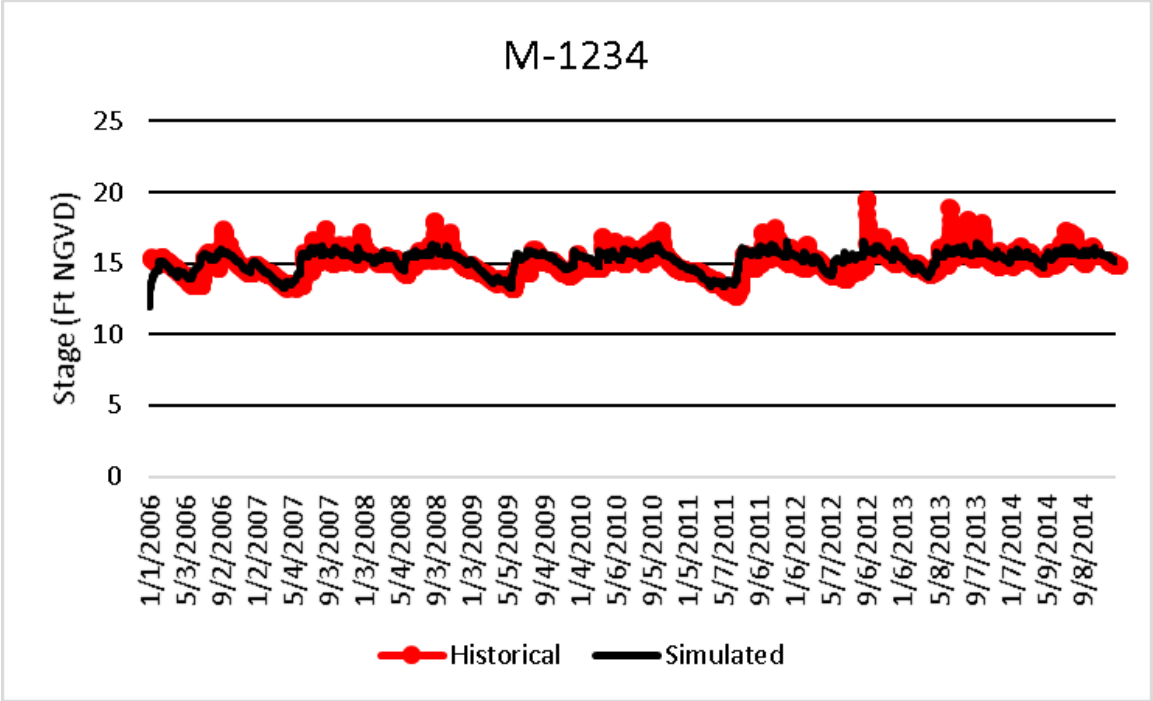

Figure A-21. Historical and simulated groundwater monitoring well stage hydrograph (2006 – 2014) for M-1234.

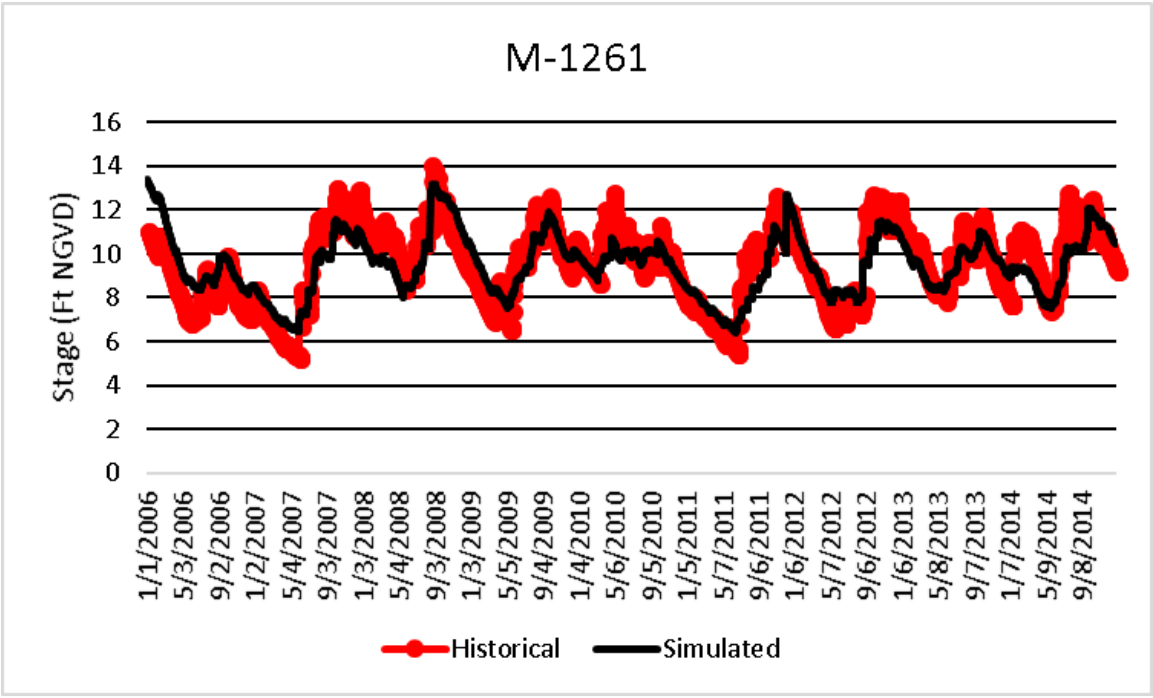

Figure A-22. Historical and simulated groundwater monitoring well stage hydrograph (2006 – 2014) for M-1261.

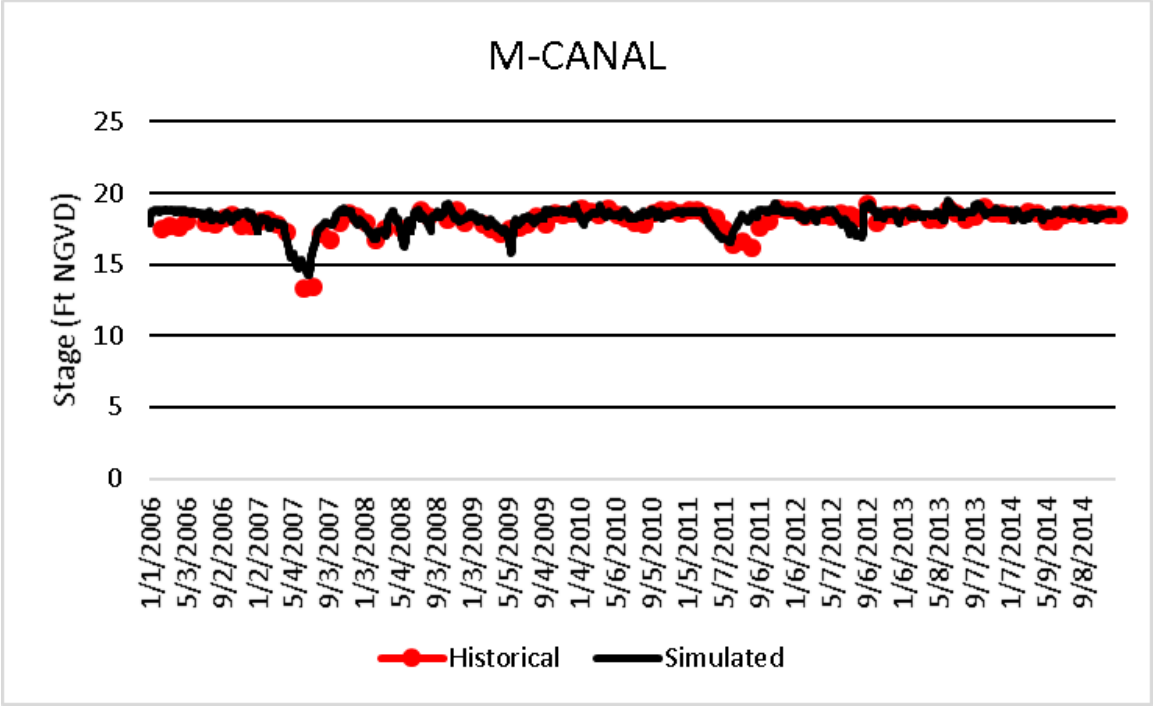

Figure A-23. Historical and simulated groundwater monitoring well stage hydrograph (2006 – 2014) for M-Canal.

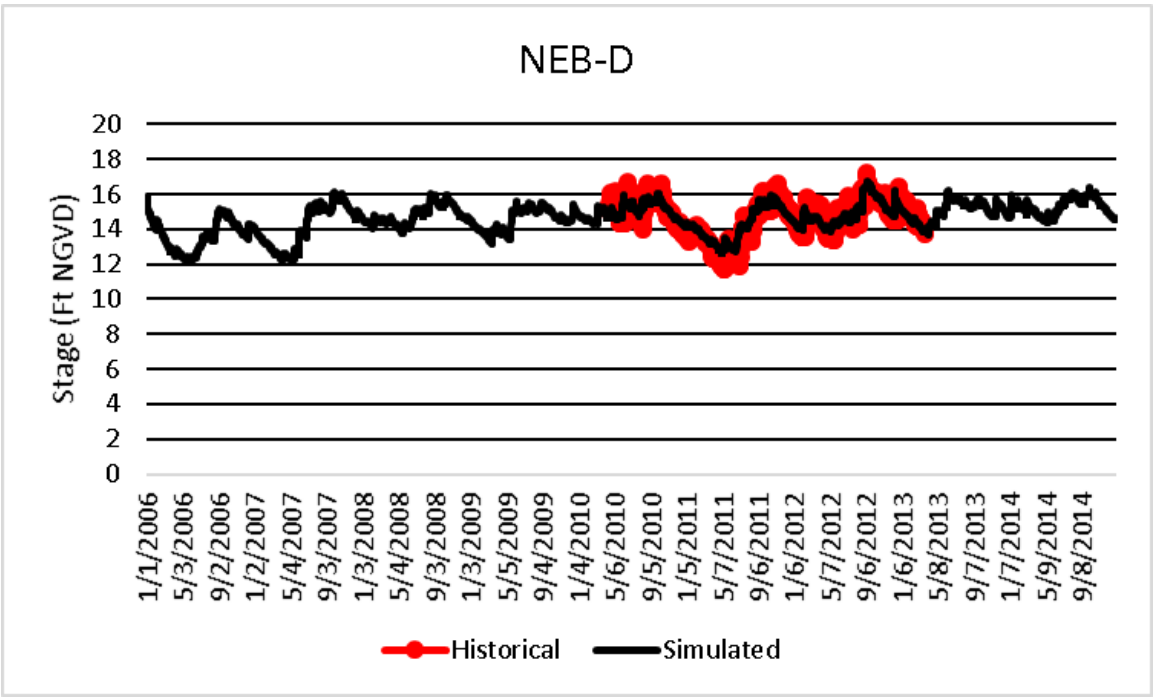

Figure A-24. Historical and simulated groundwater monitoring well stage hydrograph (2006 – 2014) for NEB-D.

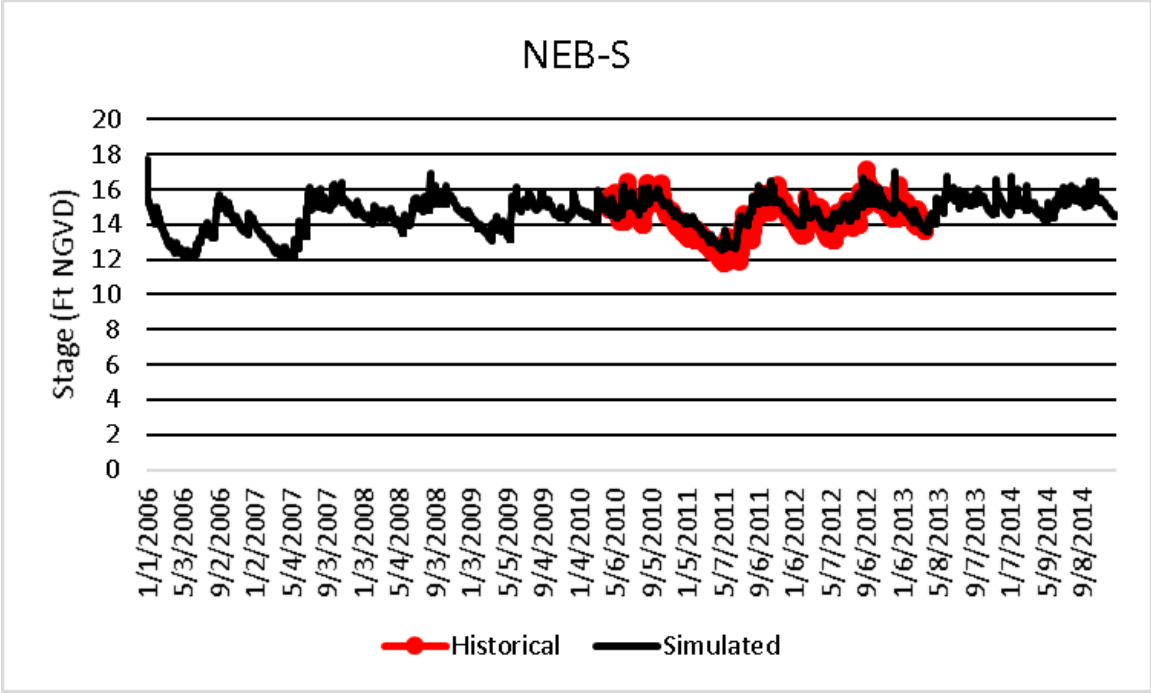

Figure A-25. Historical and simulated groundwater monitoring well stage hydrograph (2006 – 2014) for NEB-S.

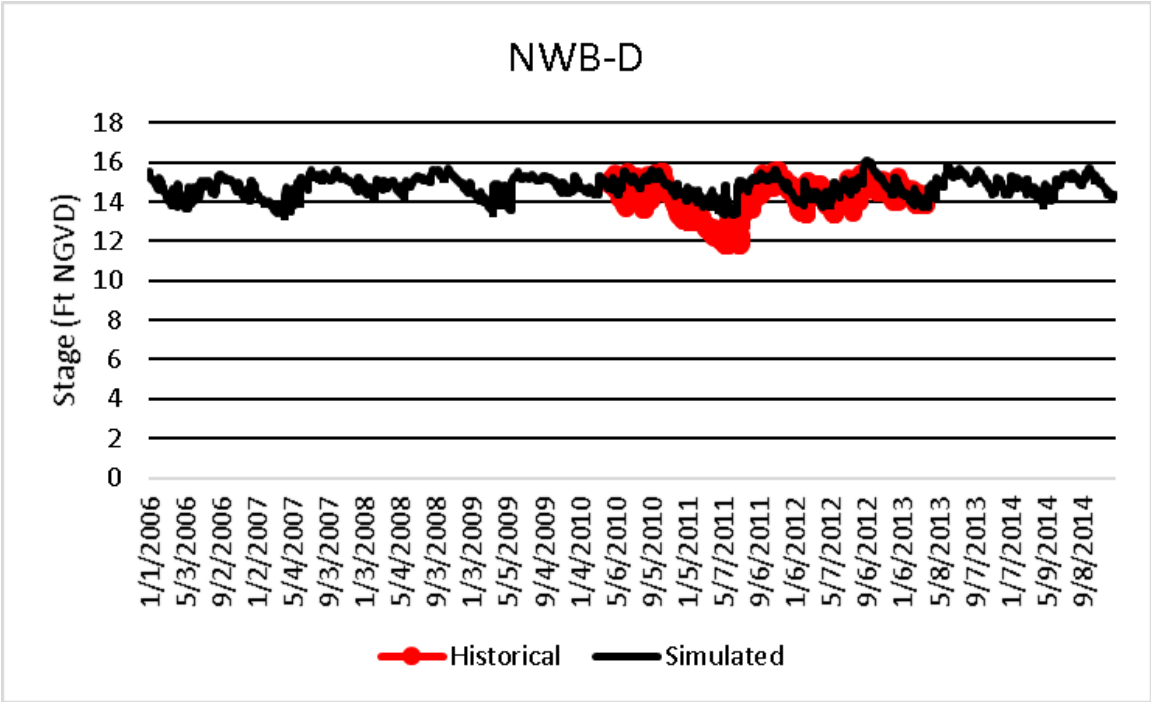

Figure A-26. Historical and simulated groundwater monitoring well stage hydrograph (2006 – 2014) for NWB-D.

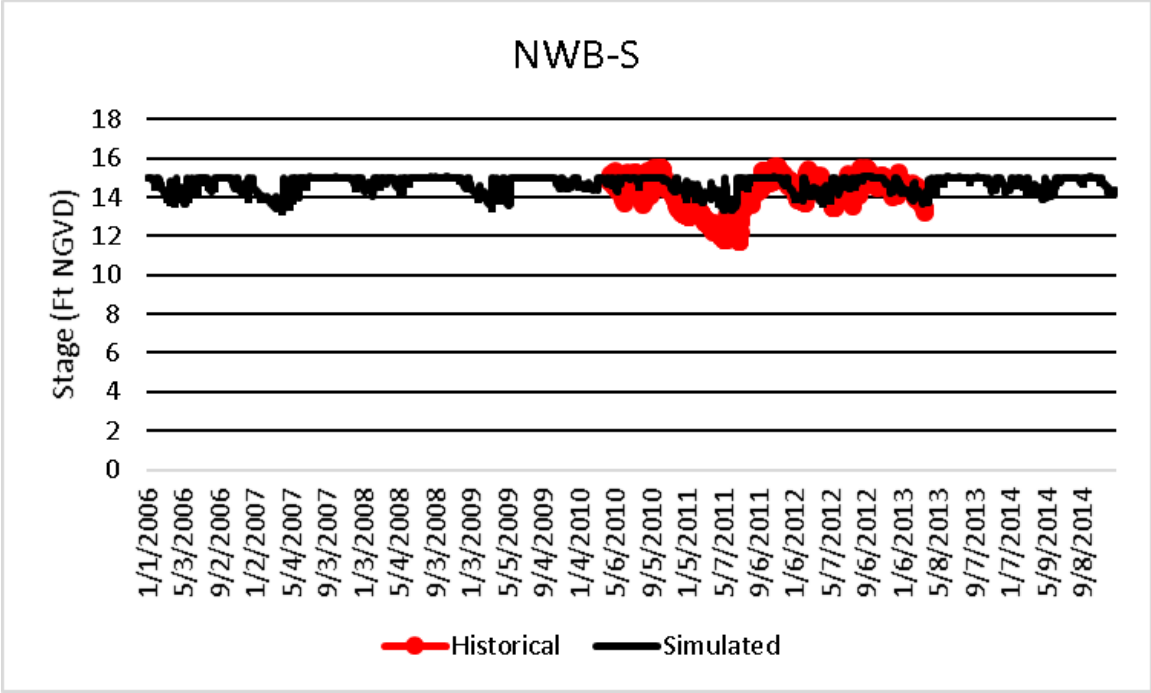

Figure A-27. Historical and simulated groundwater monitoring well stage hydrograph (2006 – 2014) for NWB-S.

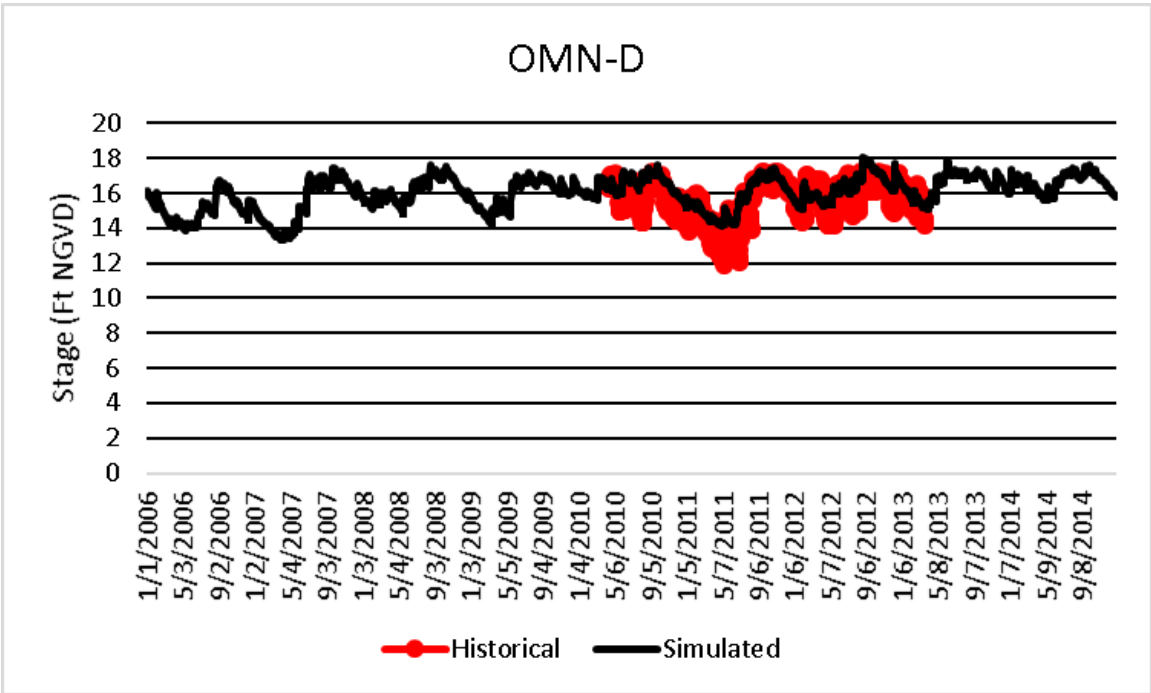

Figure A-28. Historical and simulated groundwater monitoring well stage hydrograph (2006 – 2014) for OMN-D.

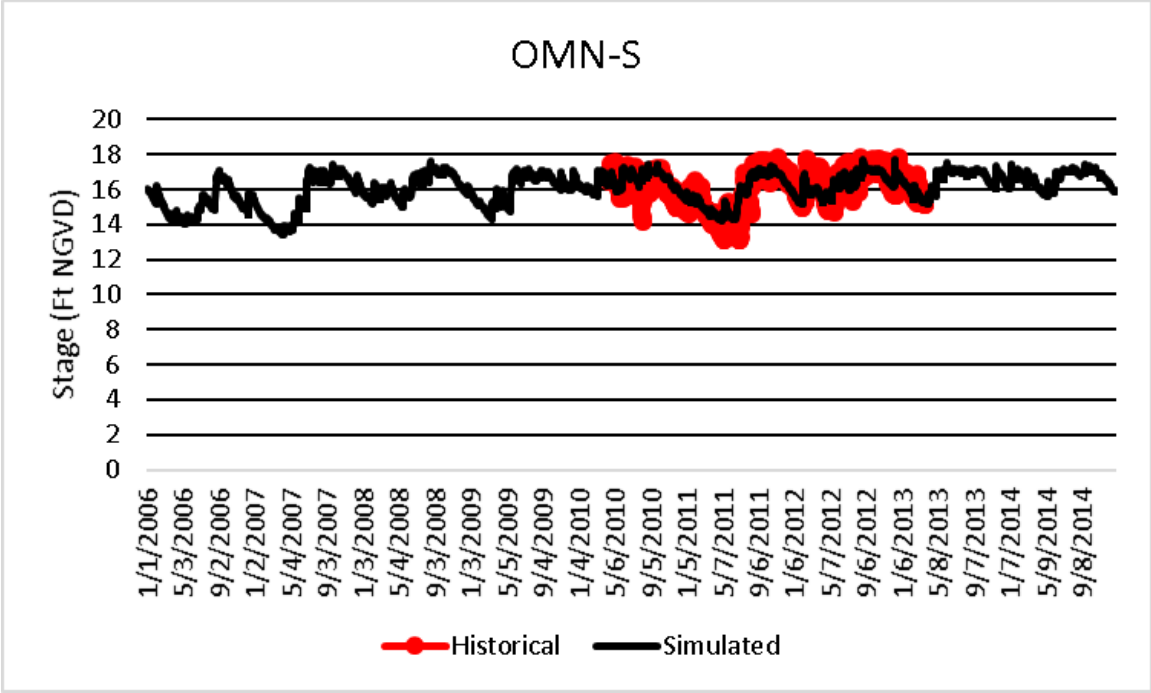

Figure A-29. Historical and simulated groundwater monitoring well stage hydrograph (2006 – 2014) for OMN-S.

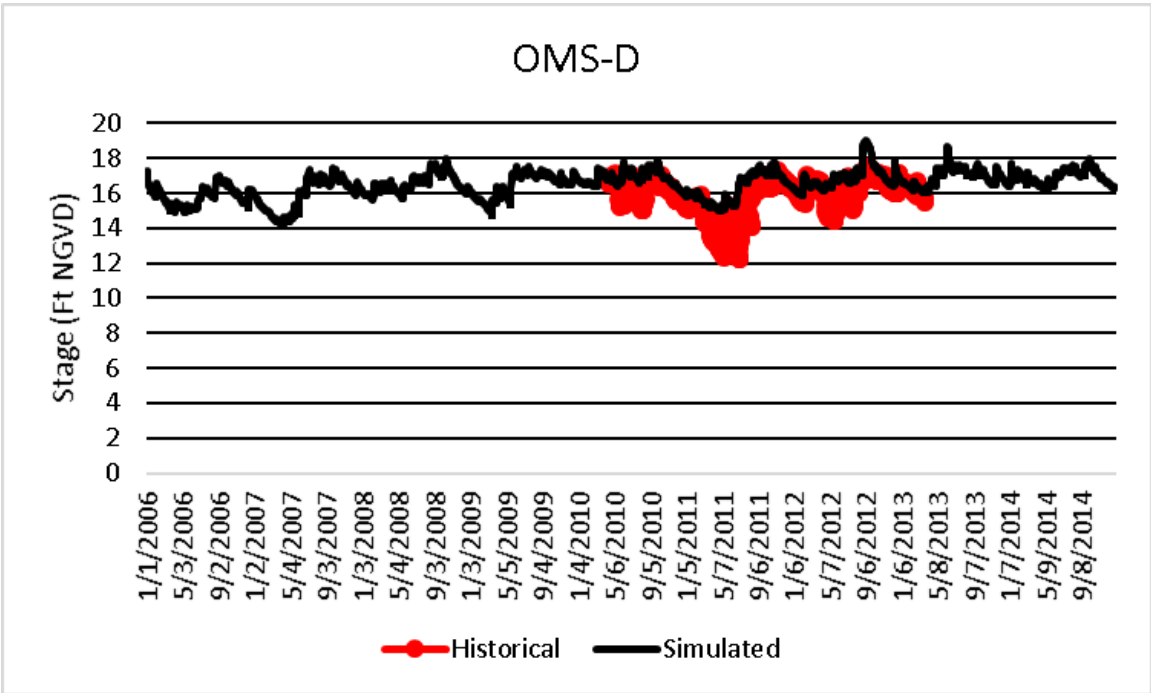

Figure A-30. Historical and simulated groundwater monitoring well stage hydrograph (2006 – 2014) for OMS-D.

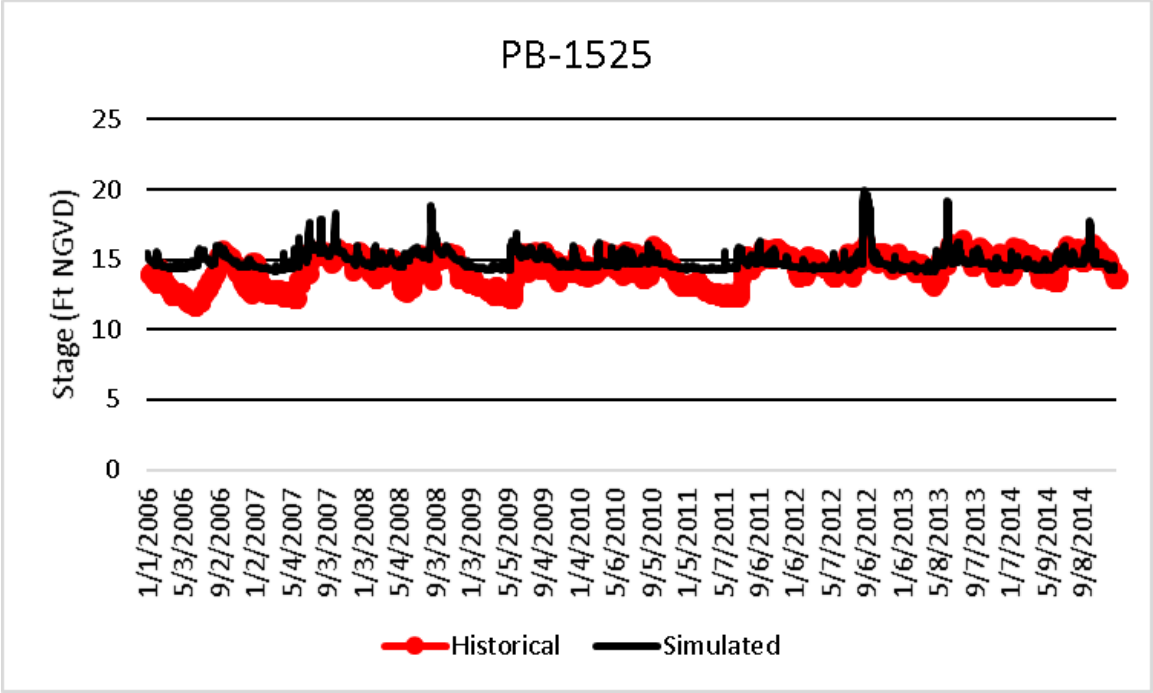

Figure A-31. Historical and simulated groundwater monitoring well stage hydrograph (2006 – 2014) for PB-1525.

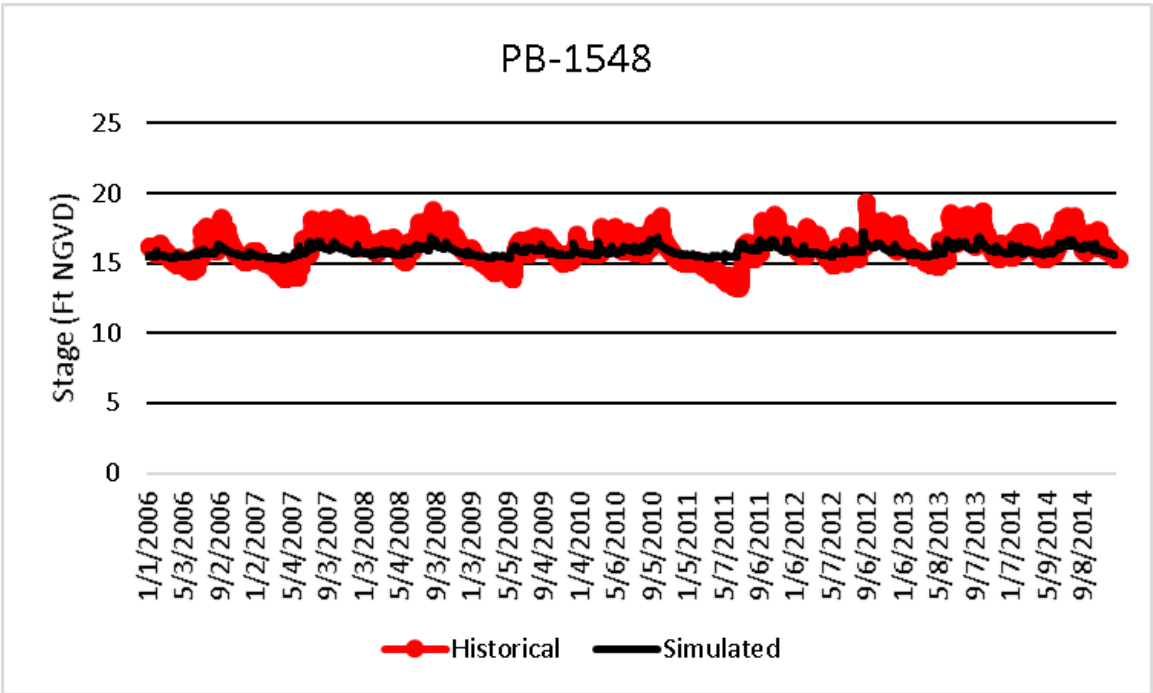

Figure A-32. Historical and simulated groundwater monitoring well stage hydrograph (2006 – 2014) for PB-1548.

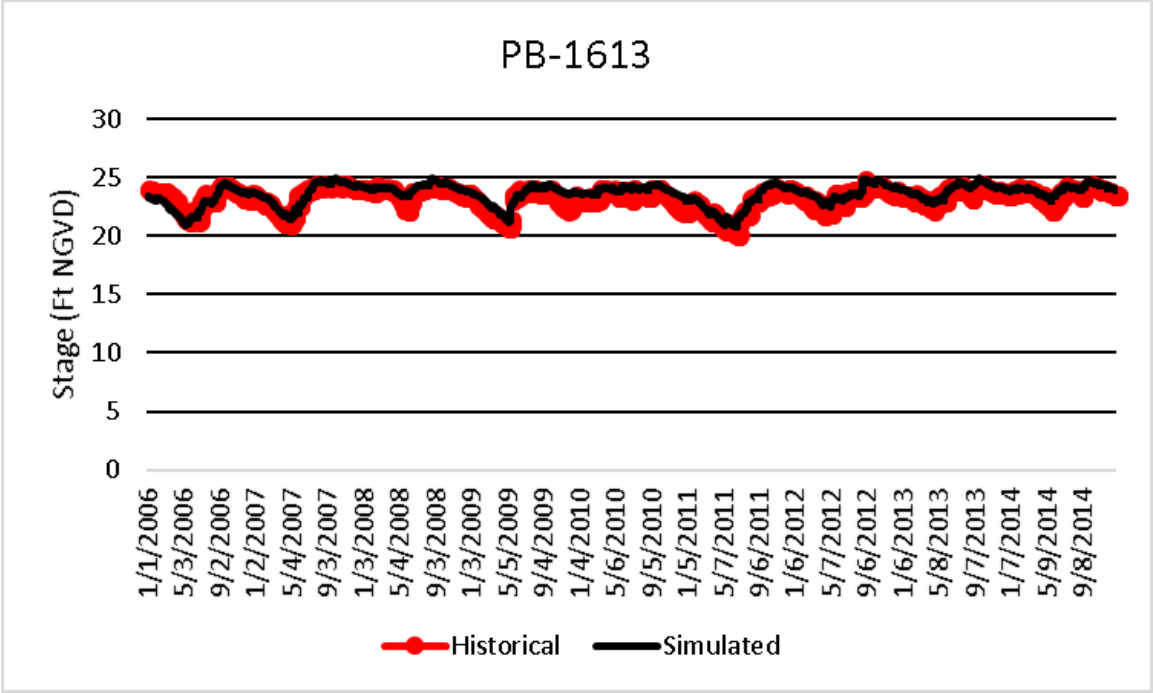

Figure A-33. Historical and simulated groundwater monitoring well stage hydrograph (2006 – 2014) for PB-1613.

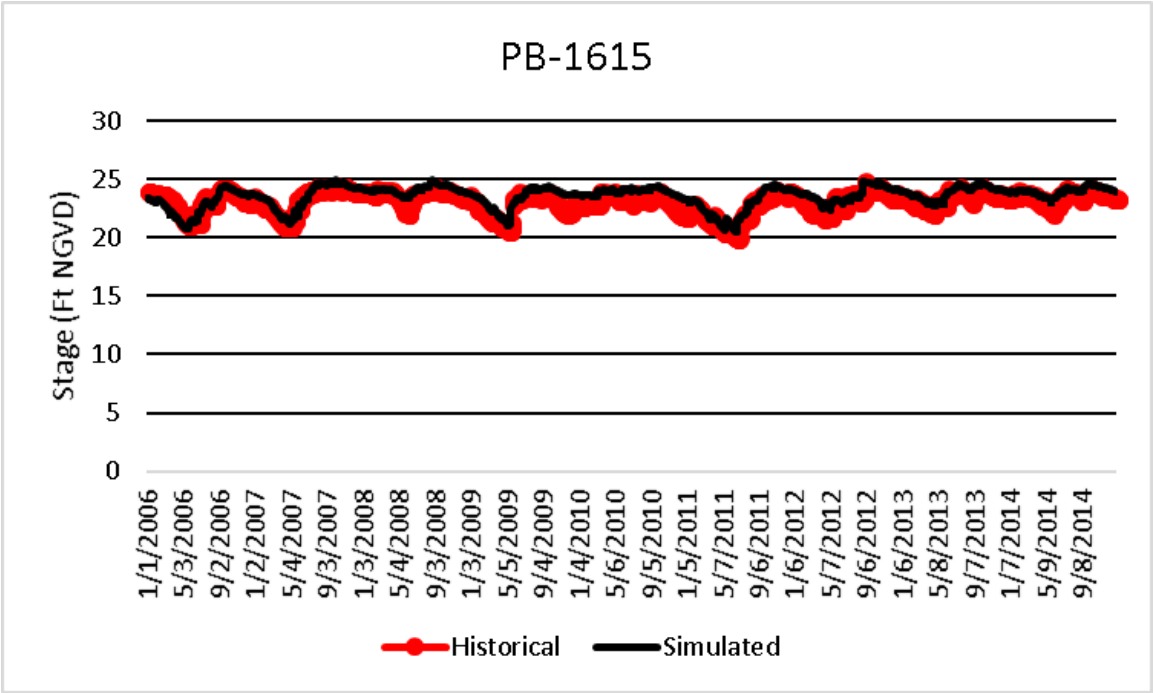

Figure A-34. Historical and simulated groundwater monitoring well stage hydrograph (2006 – 2014) for PB-1615.

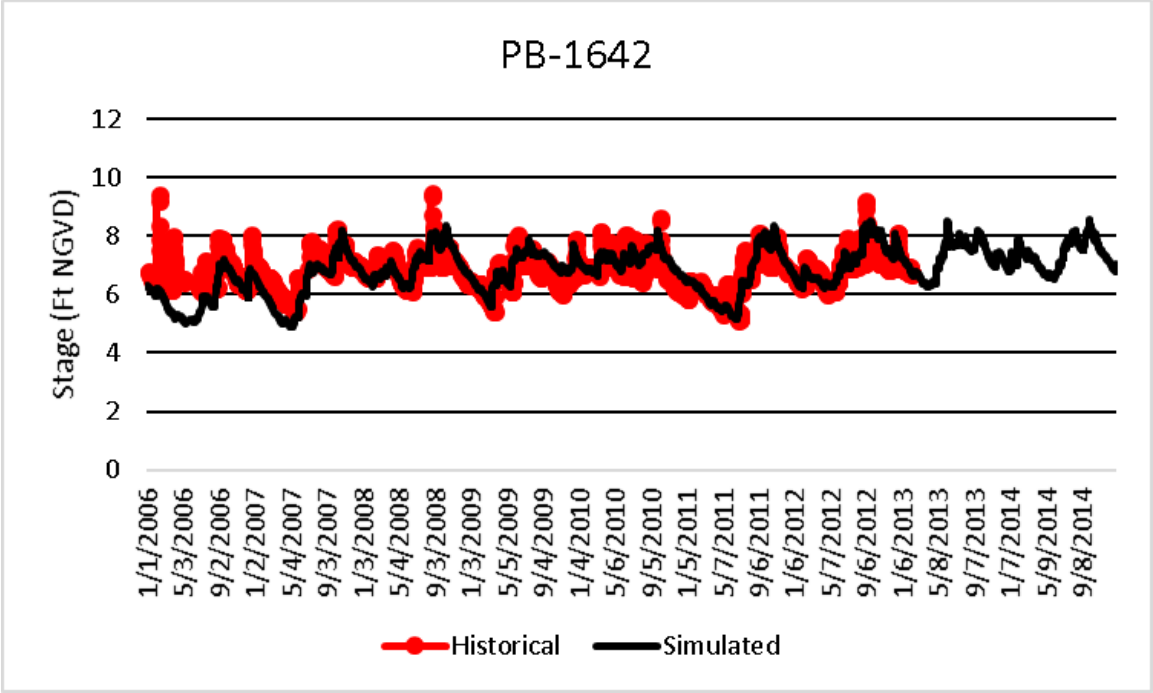

Figure A-35. Historical and simulated groundwater monitoring well stage hydrograph (2006 – 2014) for PB-1642.

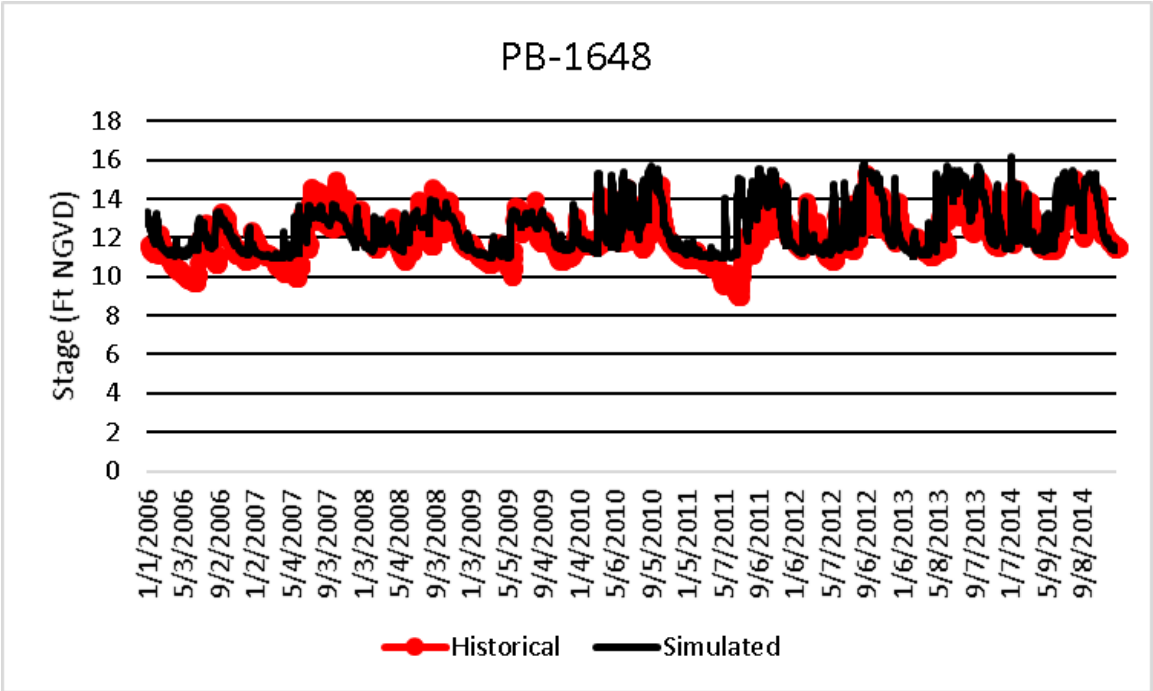

Figure A-36. Historical and simulated groundwater monitoring well stage hydrograph (2006 – 2014) for PB-1648.

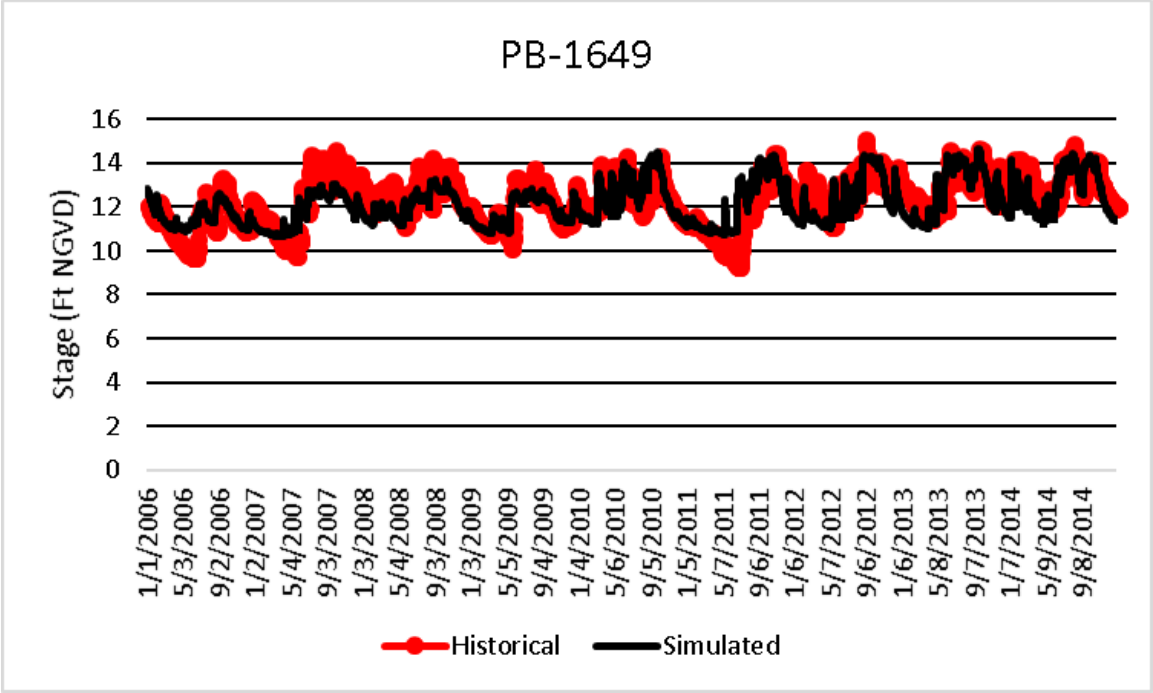

Figure A-37. Historical and simulated groundwater monitoring well stage hydrograph (2006 – 2014) for PB-1649.

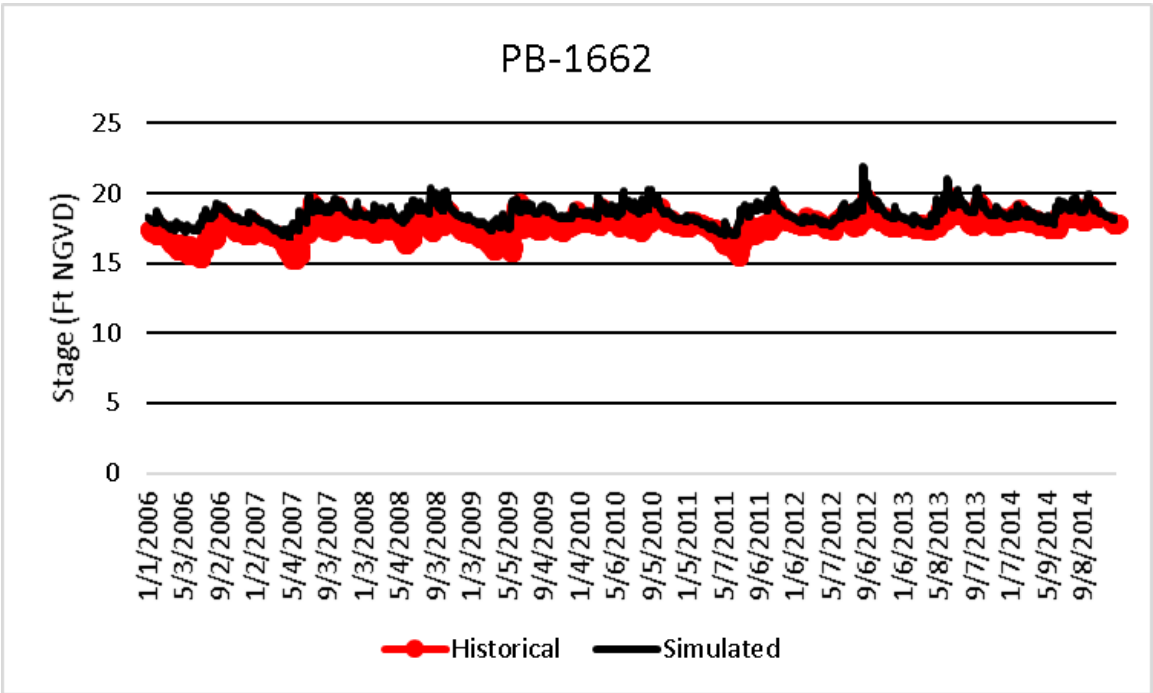

Figure A-38. Historical and simulated groundwater monitoring well stage hydrograph (2006 – 2014) for PB-1662.

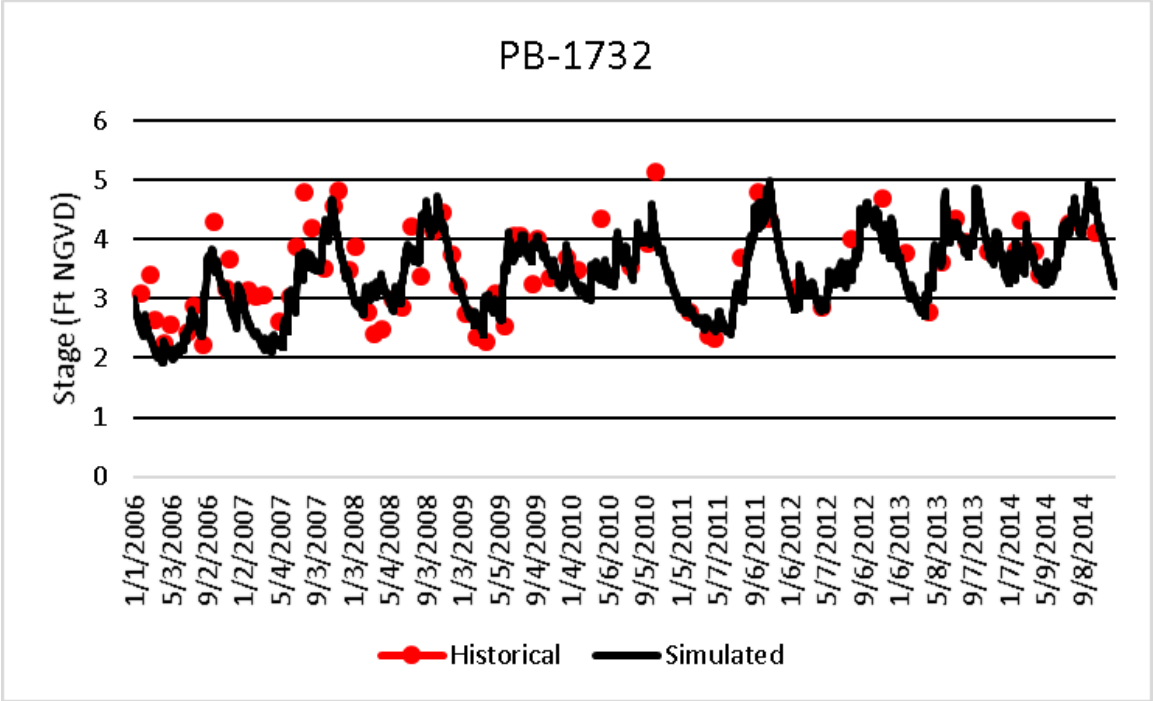

Figure A-39. Historical and simulated groundwater monitoring well stage hydrograph (2006 – 2014) for PB-1732.

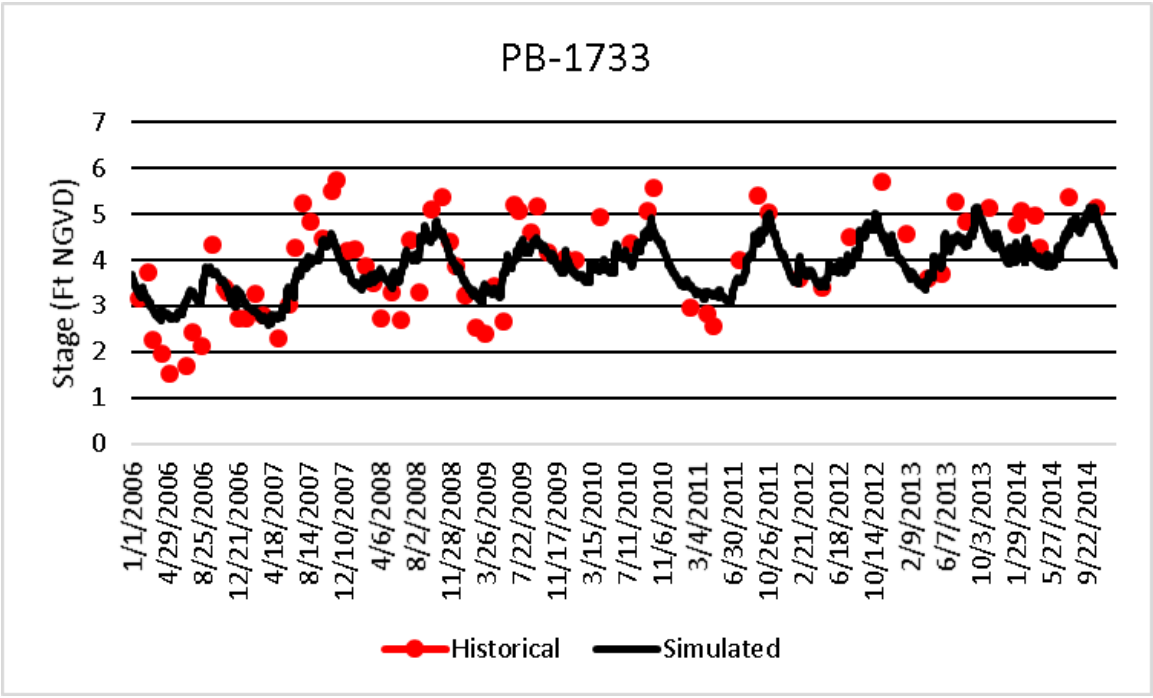

Figure A-40. Historical and simulated groundwater monitoring well stage hydrograph (2006 – 2014) for PB-1733.

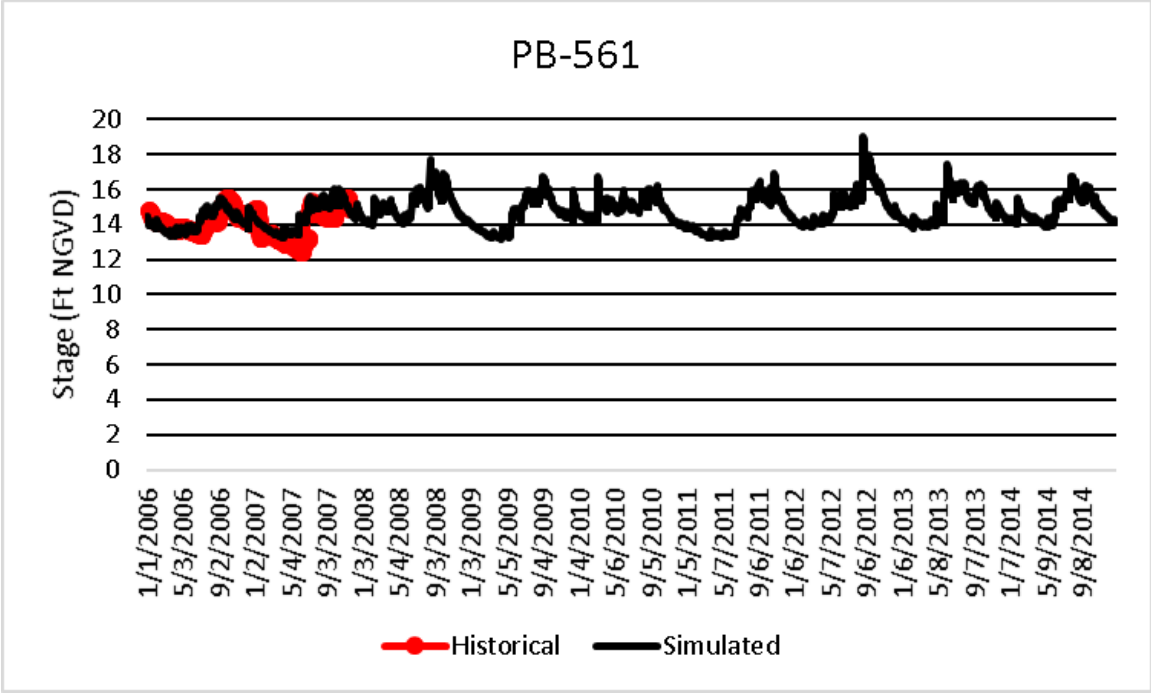

Figure A-41. Historical and simulated groundwater monitoring well stage hydrograph (2006 – 2014) for PB-561.

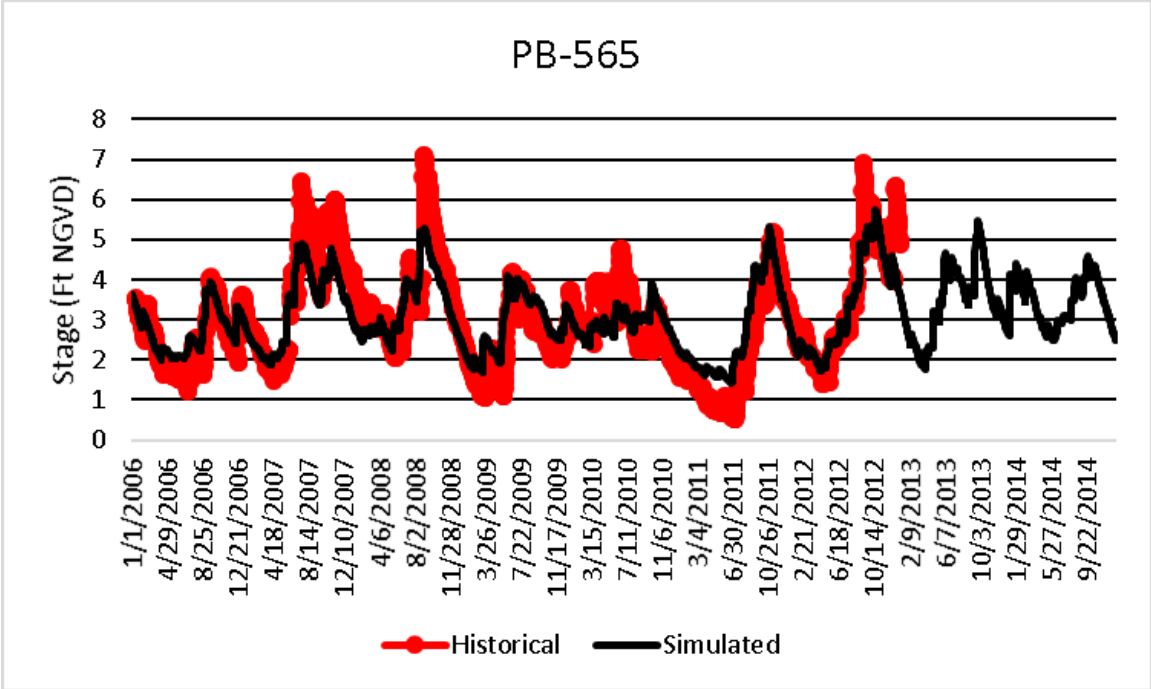

Figure A-42. Historical and simulated groundwater monitoring well stage hydrograph (2006 – 2014) for PB-565.

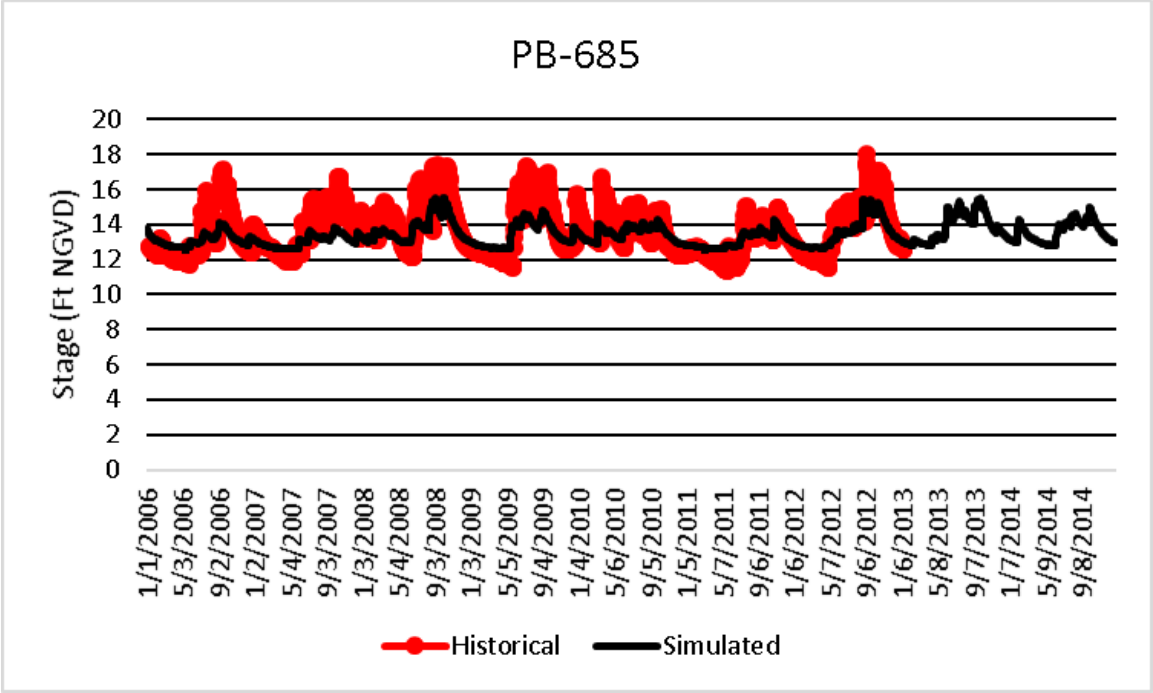

Figure A-43. Historical and simulated groundwater monitoring well stage hydrograph (2006 – 2014) for PB-685.

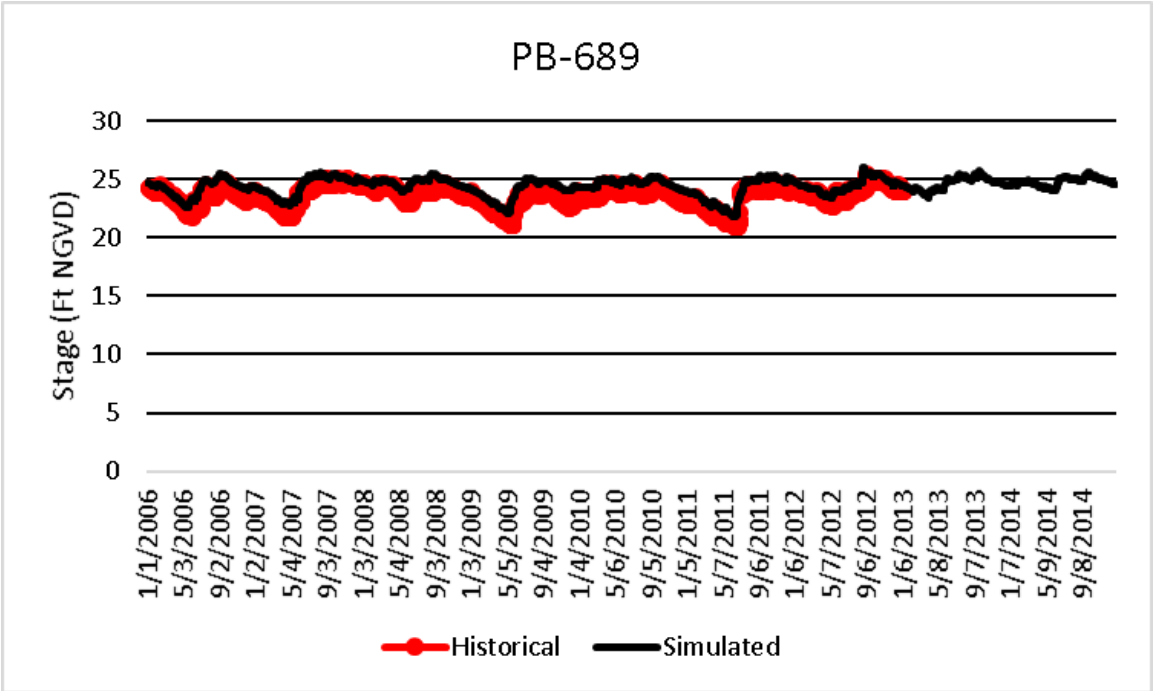

Figure A-44. Historical and simulated groundwater monitoring well stage hydrograph (2006 – 2014) for PB-689.

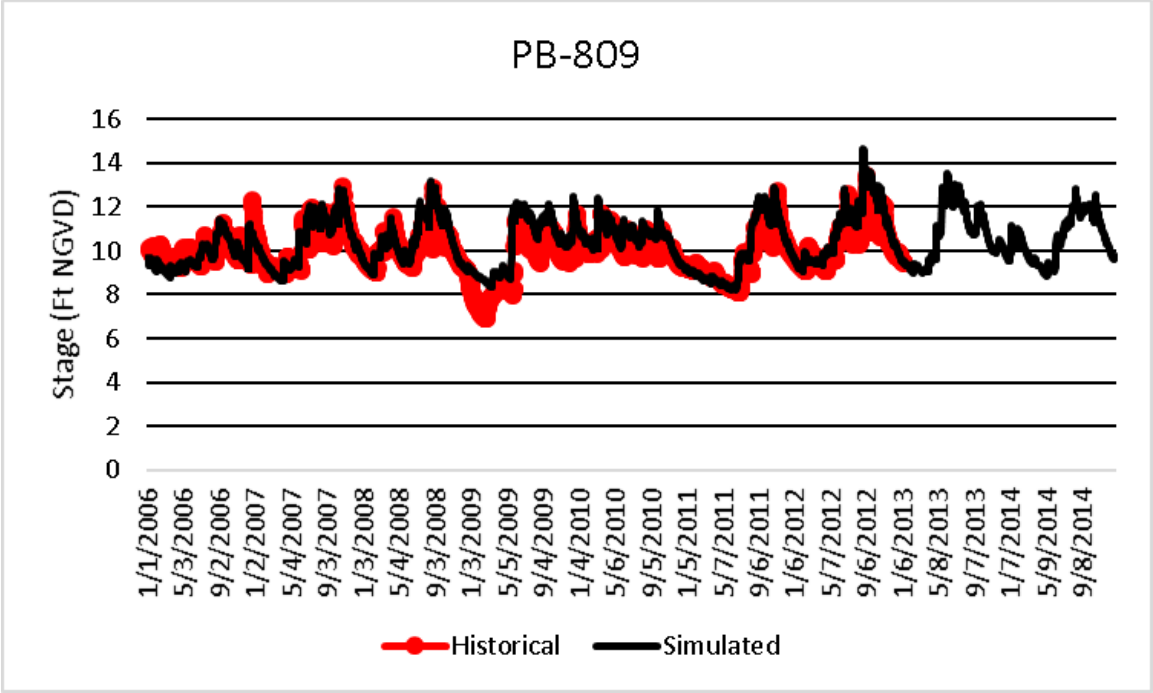

Figure A-45. Historical and simulated groundwater monitoring well stage hydrograph (2006 – 2014) for PB-809.

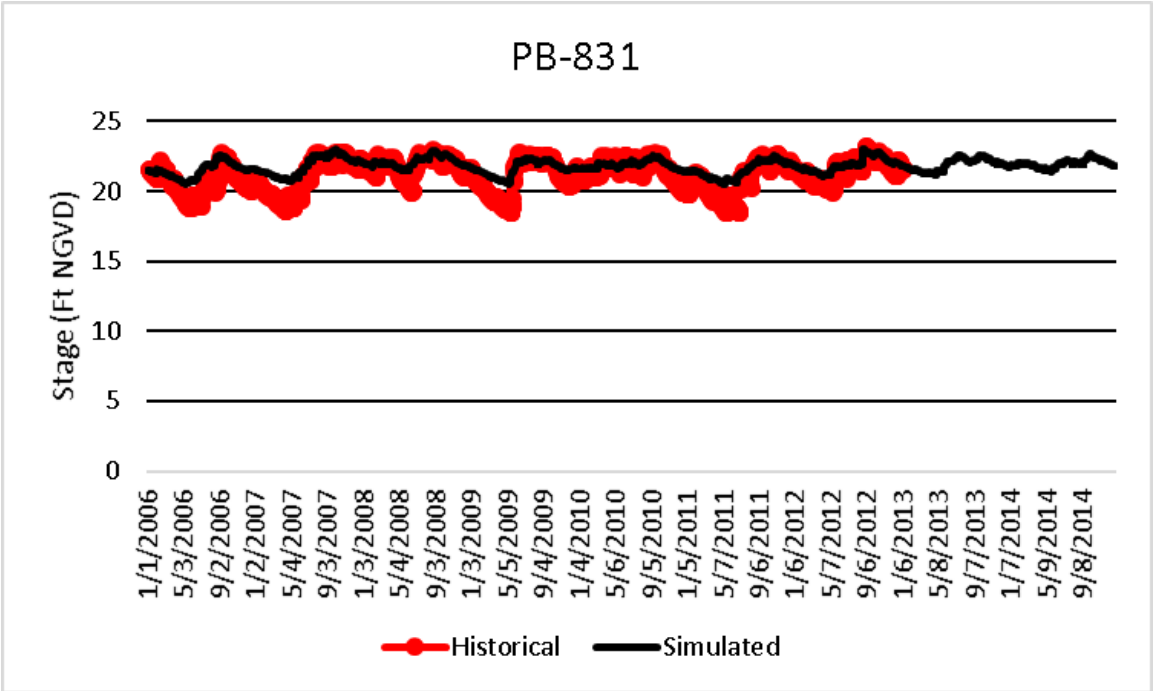

Figure A-46. Historical and simulated groundwater monitoring well stage hydrograph (2006 – 2014) for PB-831.

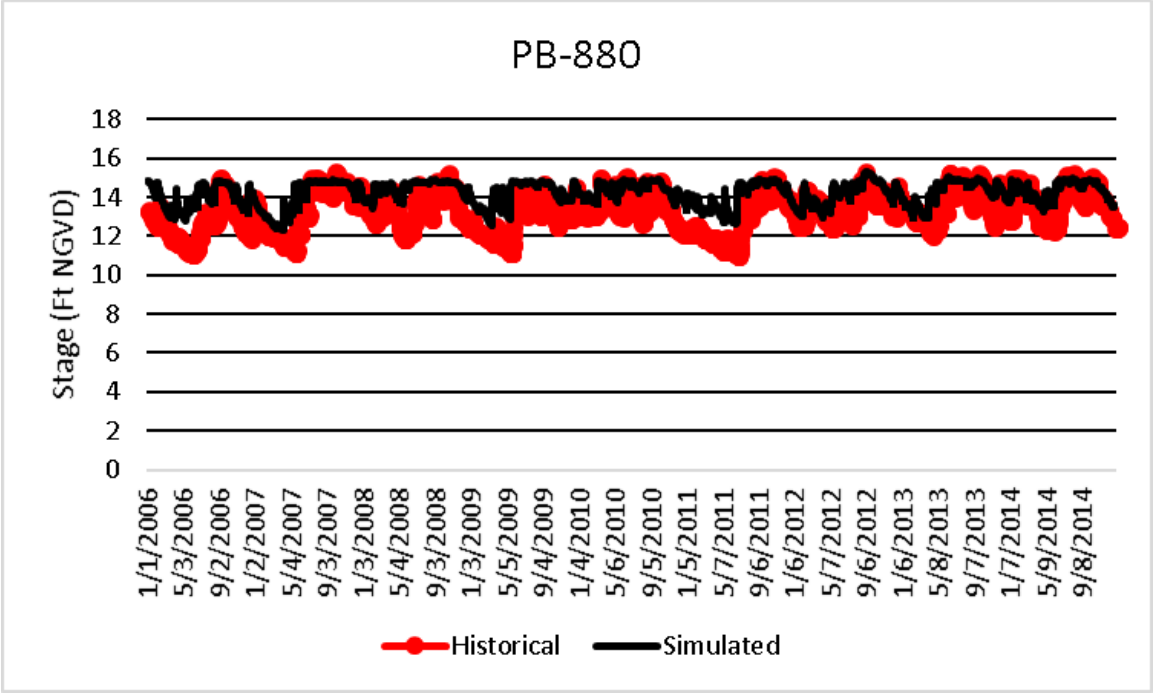

Figure A-47. Historical and simulated groundwater monitoring well stage hydrograph (2006 – 2014) for PB-880.

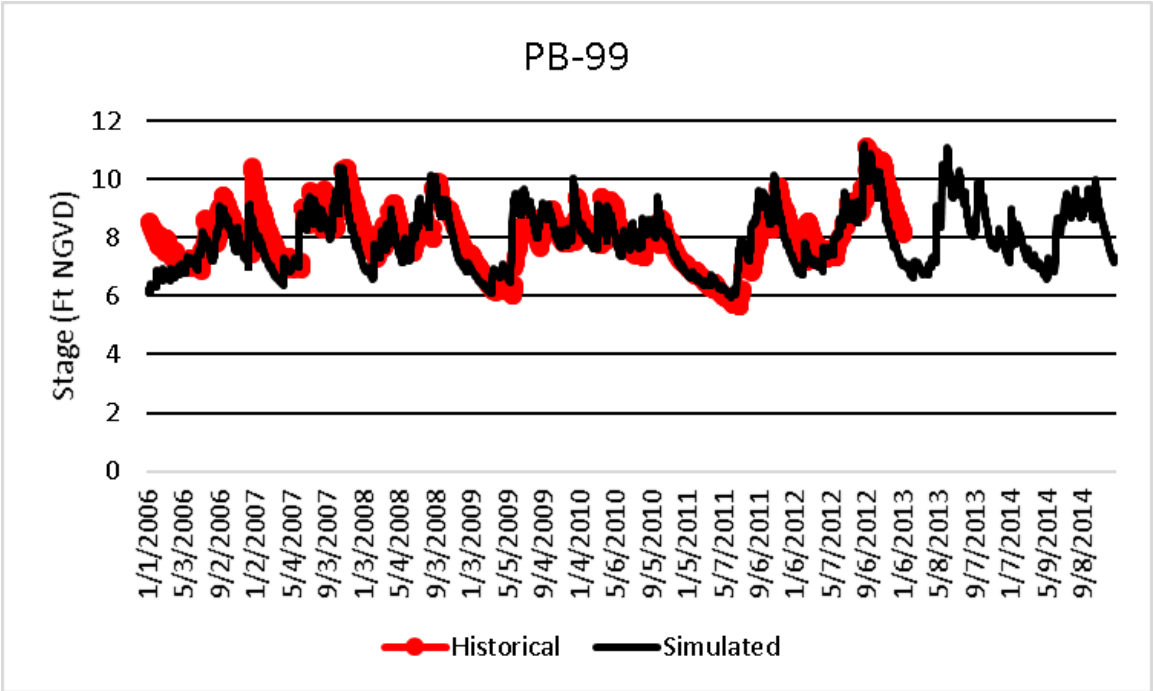

Figure A-48. Historical and simulated groundwater monitoring well stage hydrograph (2006 – 2014) for PB-99.

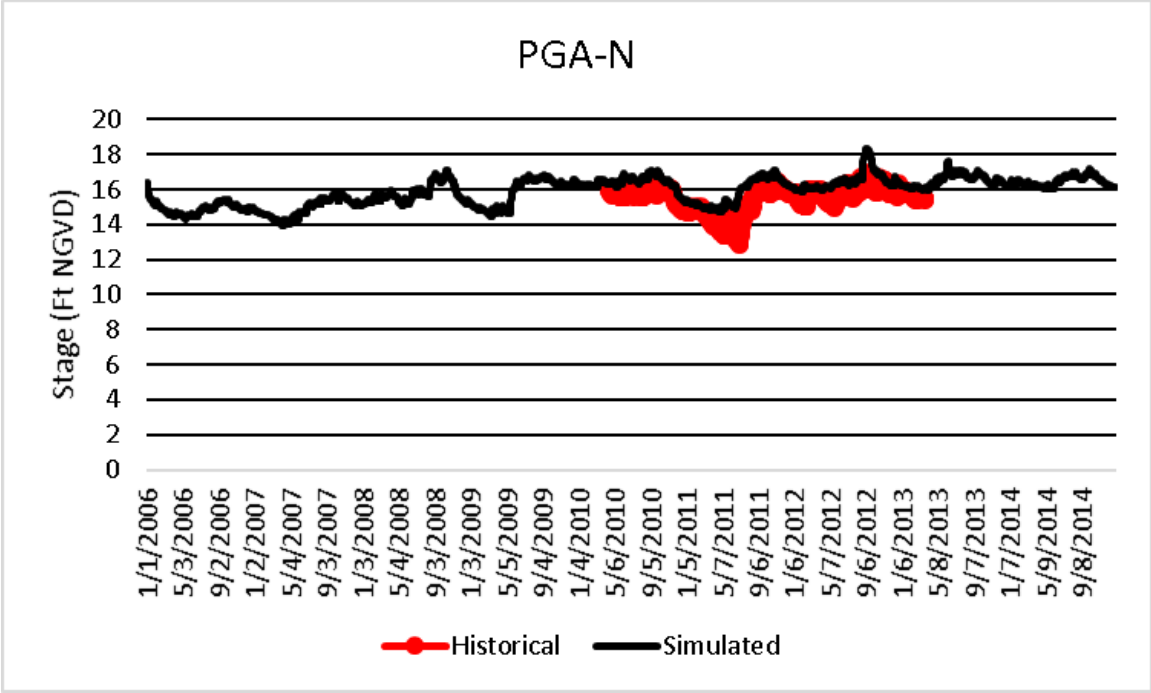

Figure A-49. Historical and simulated groundwater monitoring well stage hydrograph (2006 – 2014) for PGA-N.

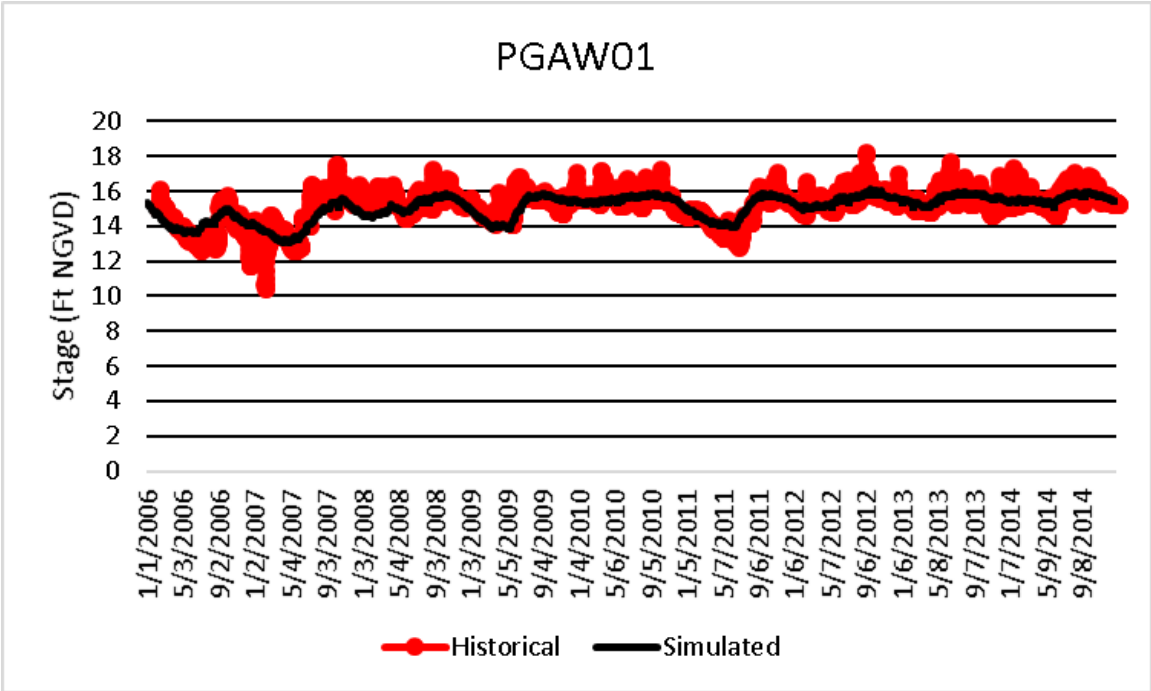

Figure A-50. Historical and simulated groundwater monitoring well stage hydrograph (2006 – 2014) for PGAW01.

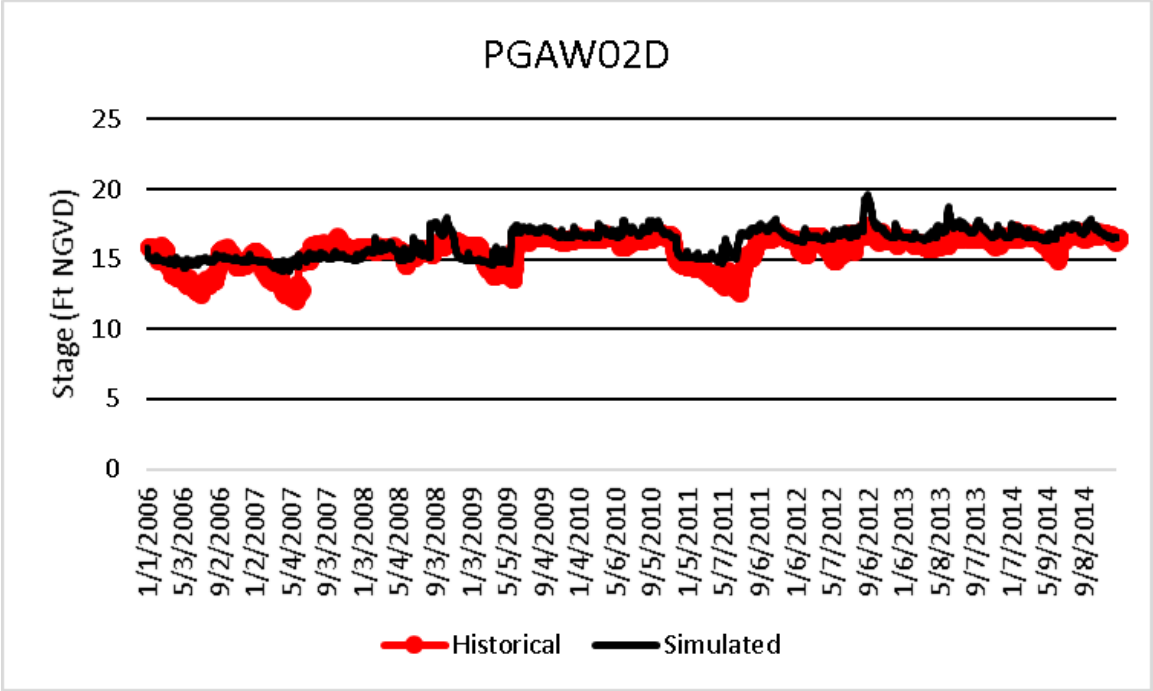

Figure A-51. Historical and simulated groundwater monitoring well stage hydrograph (2006 – 2014) for PGAW02D.

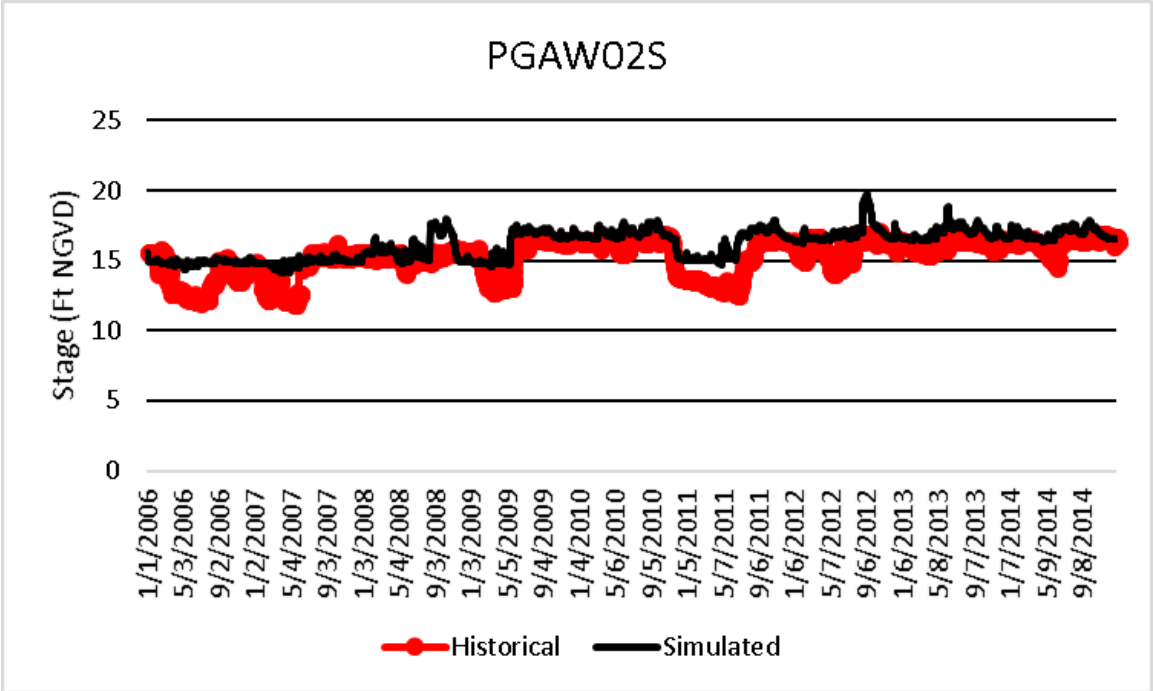

Figure A-52. Historical and simulated groundwater monitoring well stage hydrograph (2006 – 2014) for PGAW02S.

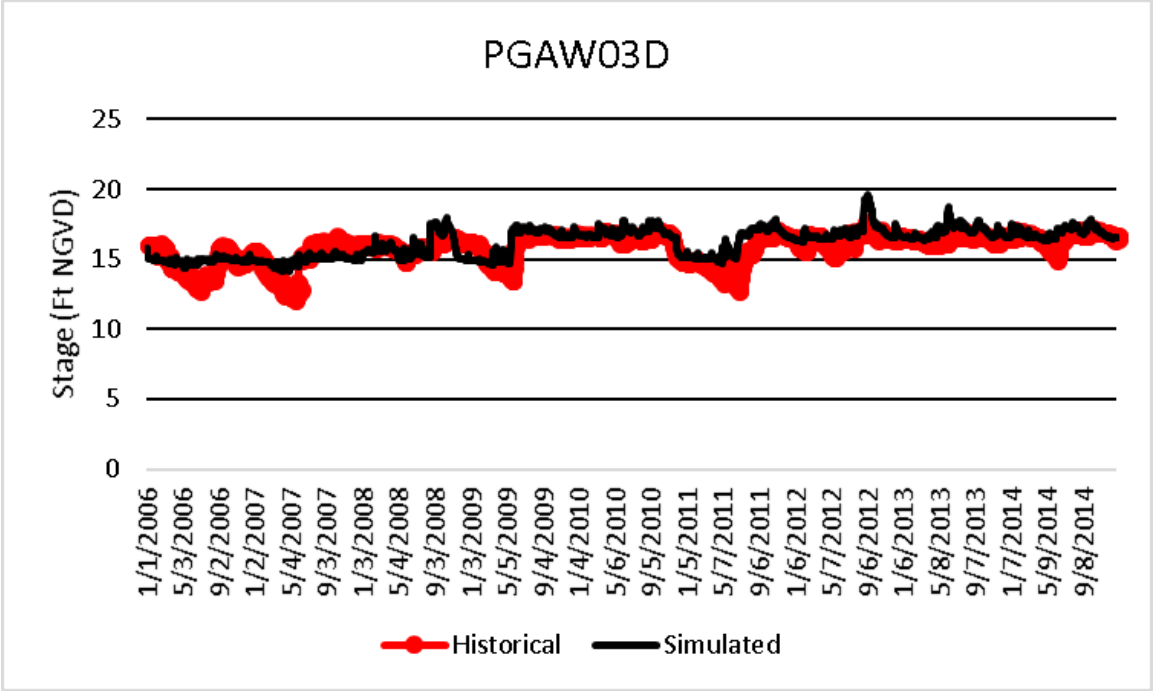

Figure A-53. Historical and simulated groundwater monitoring well stage hydrograph (2006 – 2014) for PGAW03D.

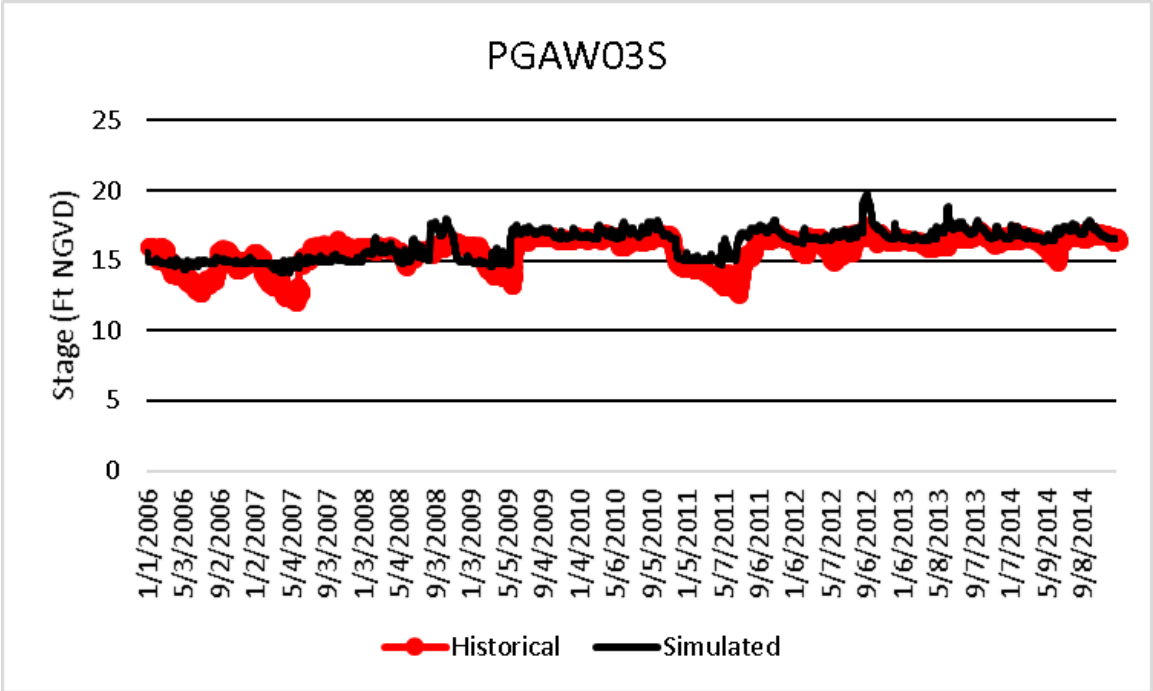

Figure A-54. Historical and simulated groundwater monitoring well stage hydrograph (2006 – 2014) for PGAW03S.

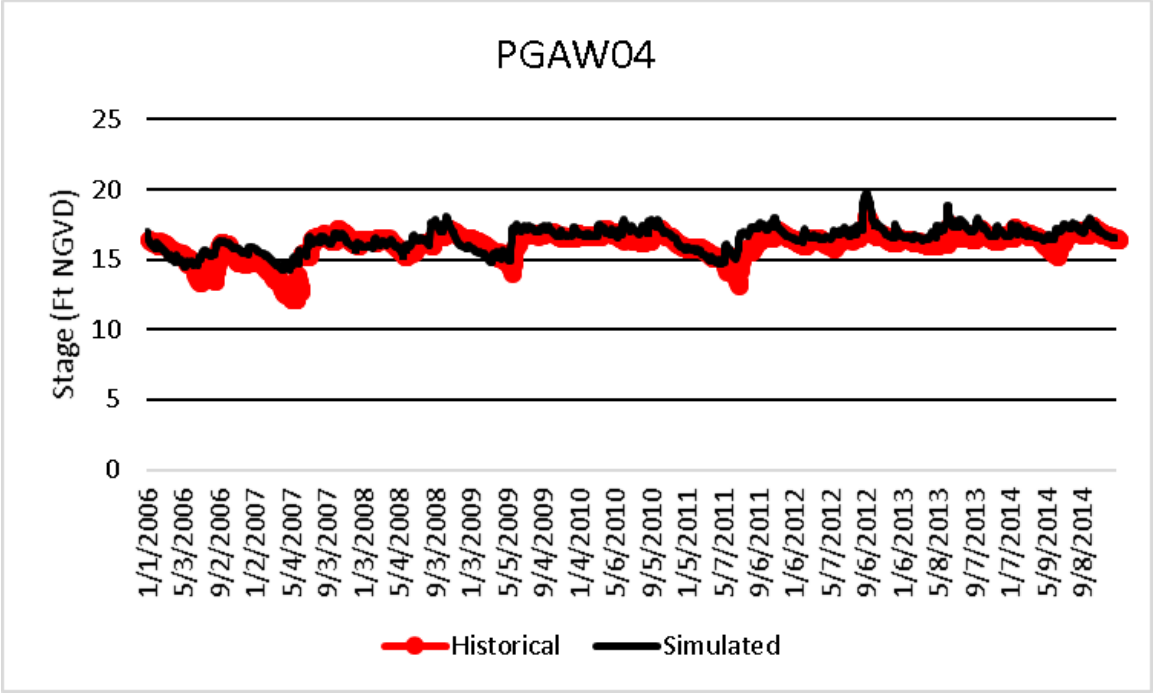

Figure A-55. Historical and simulated groundwater monitoring well stage hydrograph (2006 – 2014) for PGAW04.

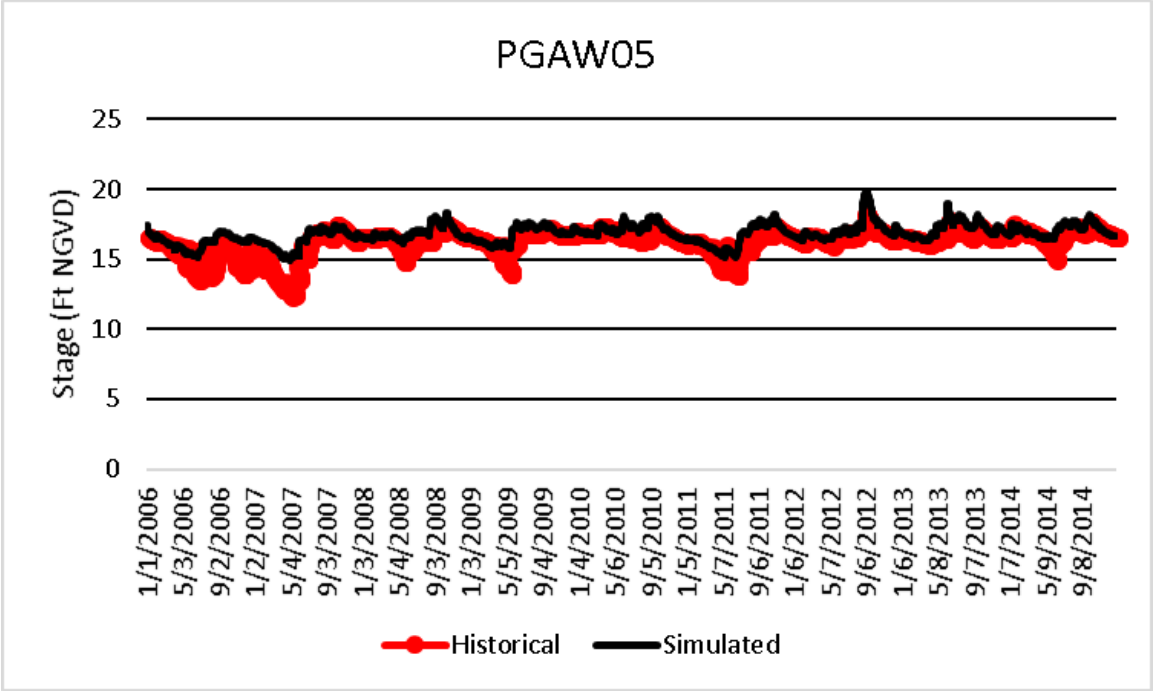

Figure A-56. Historical and simulated groundwater monitoring well stage hydrograph (2006 – 2014) for PGAW05.

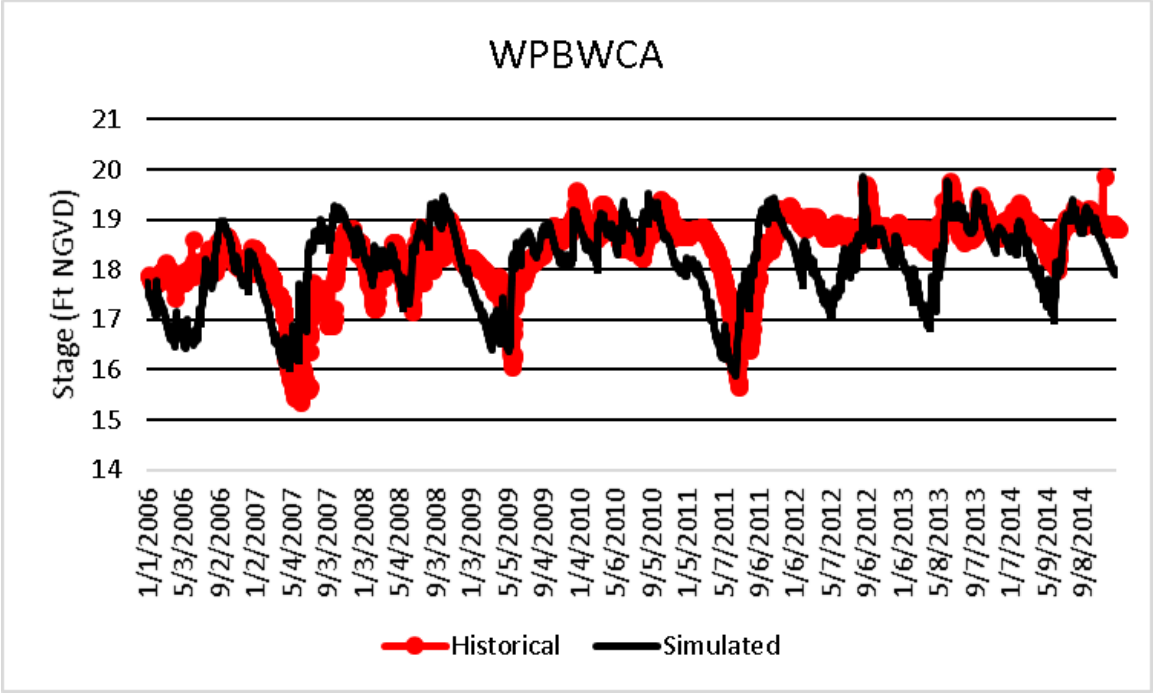

Figure A-57. Historical and simulated groundwater monitoring well stage hydrograph (2006 – 2014) for WPBWCA.

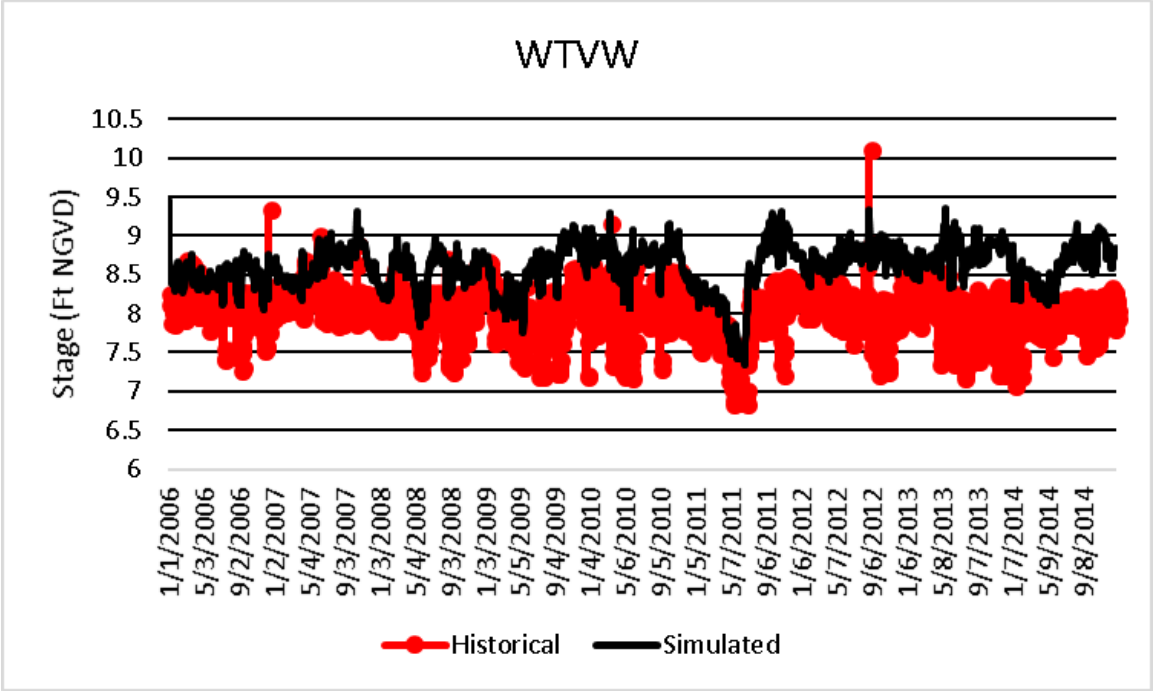

Figure A-58. Historical and simulated groundwater monitoring well stage hydrograph (2006 – 2014) for WTVW.

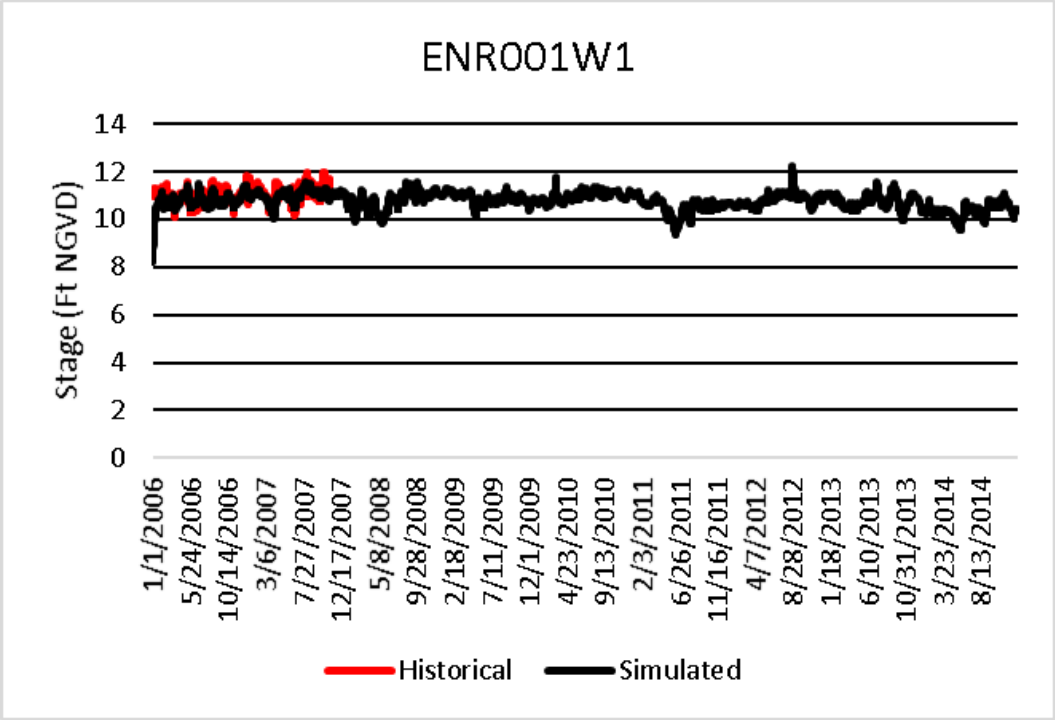

Figure A-59. Historical and simulated groundwater monitoring well stage hydrograph (2006 – 2014) for ENR001W1 (sequestered station).

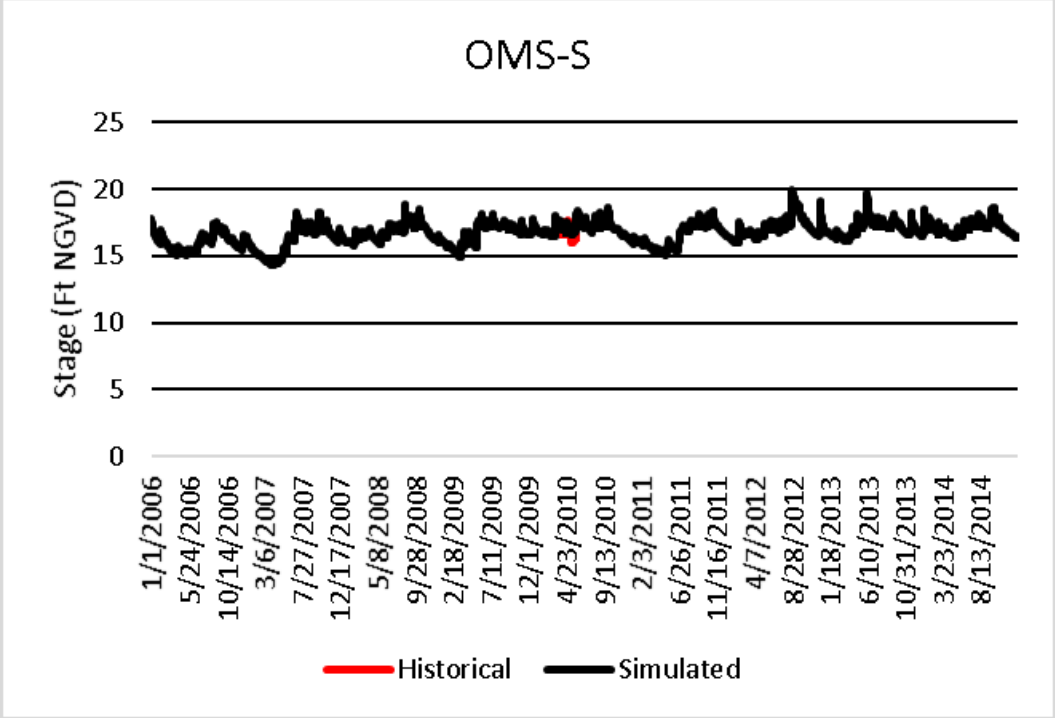

Figure A-60. Historical and simulated groundwater monitoring well stage hydrograph (2006 – 2014) for OMS-S (sequestered station).

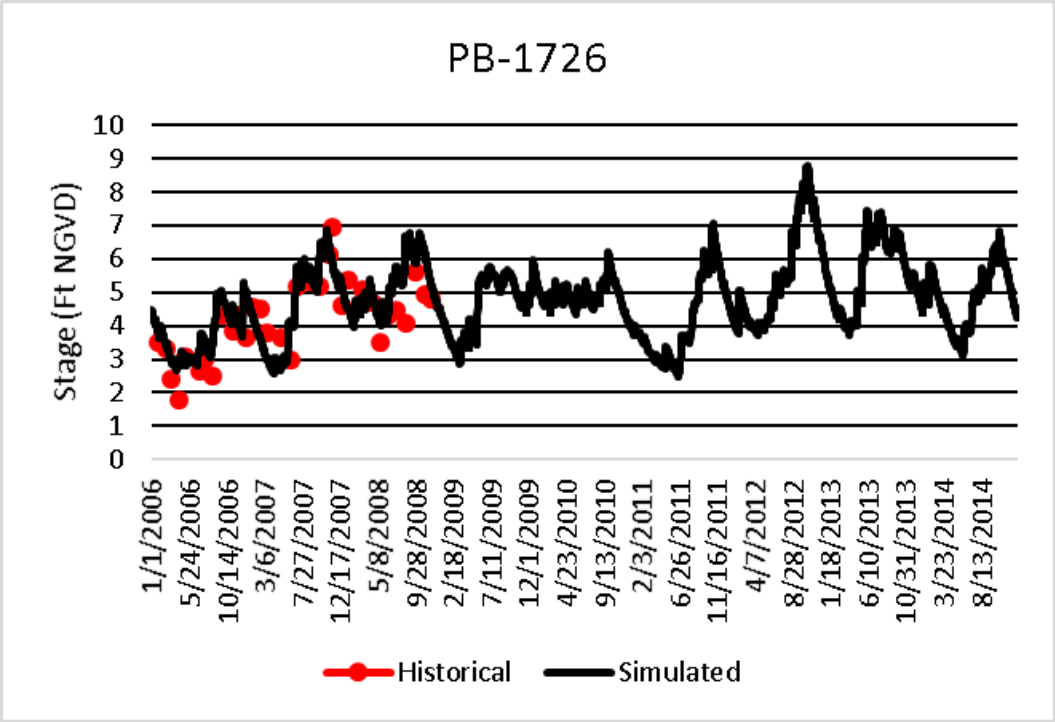

Figure A-61. Historical and simulated groundwater monitoring well stage hydrograph (2006 – 2014) for PB-1726 (sequestered station).

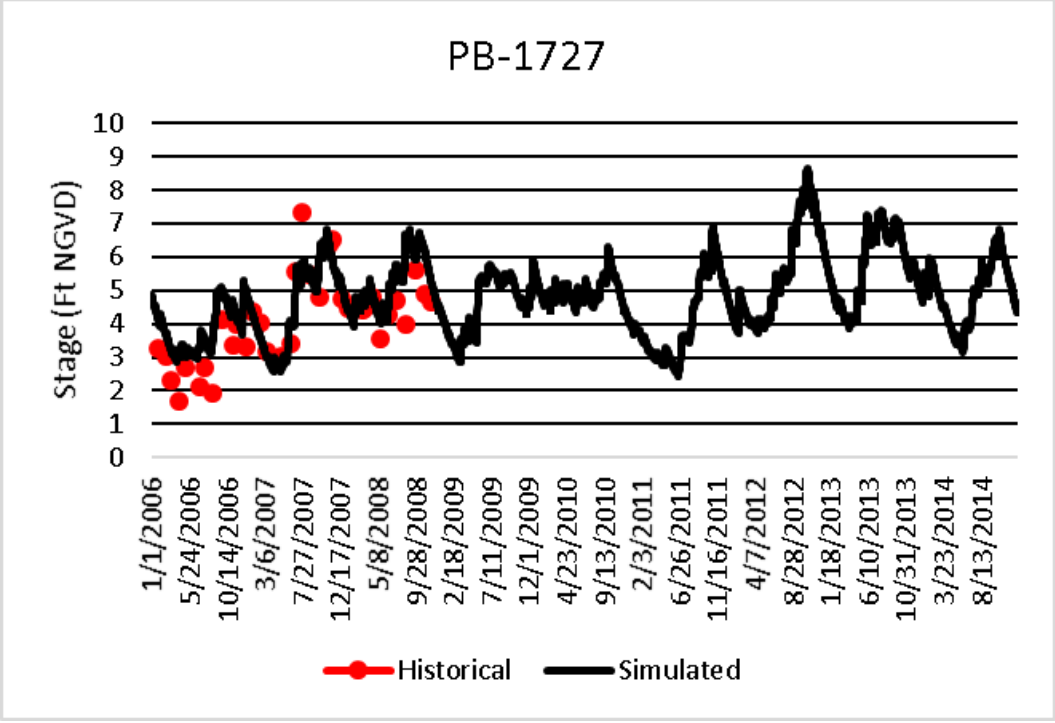

Figure A-62. Historical and simulated groundwater monitoring well stage hydrograph (2006 – 2014) for PB-1727 (sequestered station).

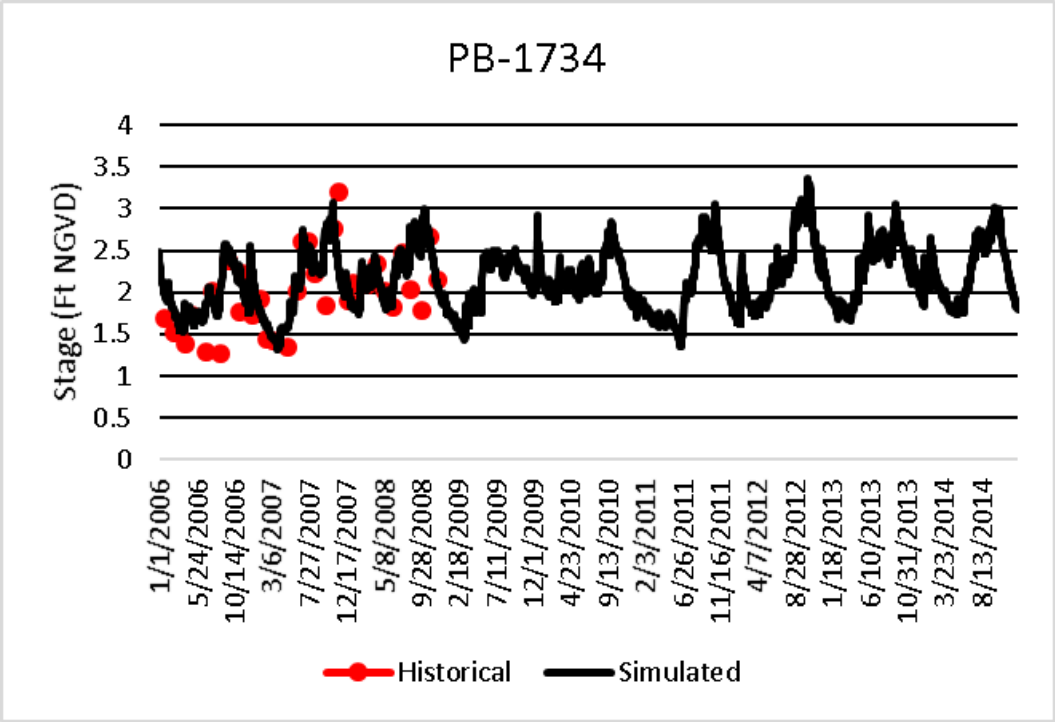

Figure A-63. Historical and simulated groundwater monitoring well stage hydrograph (2006 – 2014) for PB-1734 (sequestered station).

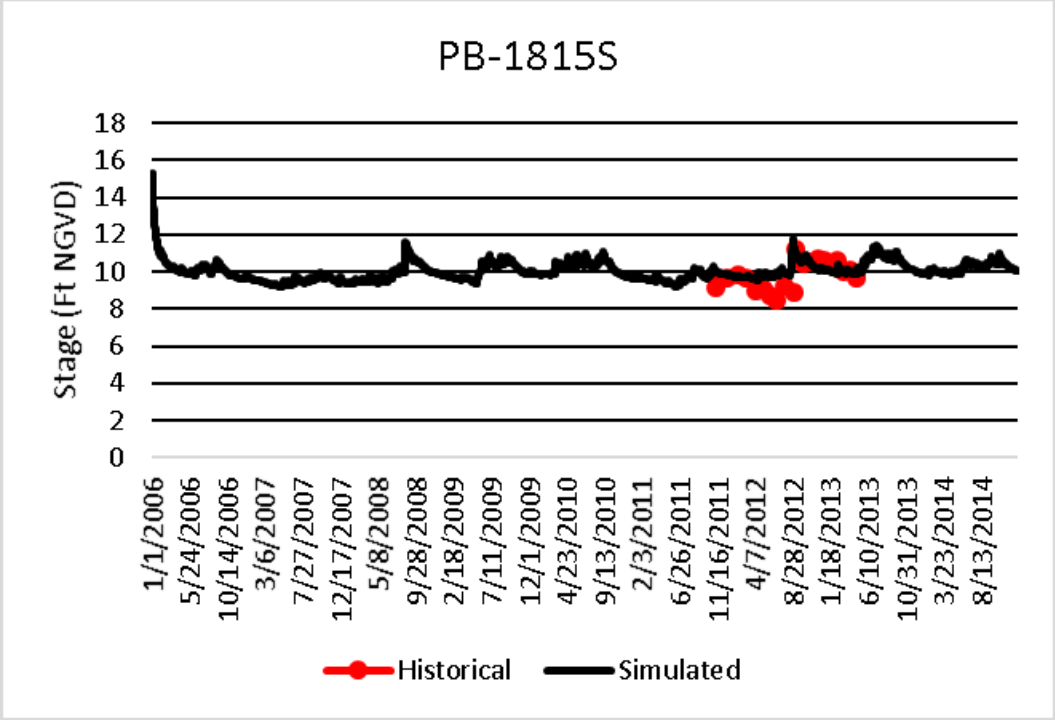

Figure A-64. Historical and simulated groundwater monitoring well stage hydrograph (2006 – 2014) for PB-1815S (sequestered station).

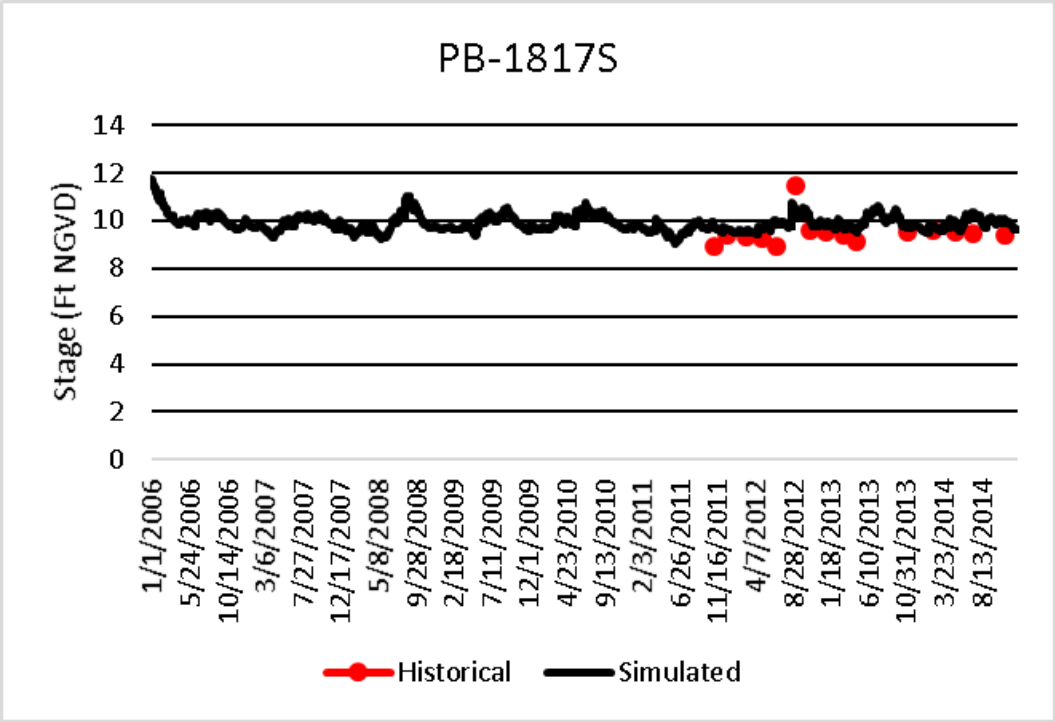

Figure A-65. Historical and simulated groundwater monitoring well stage hydrograph (2006 – 2014) for PB-1817S (sequestered station).

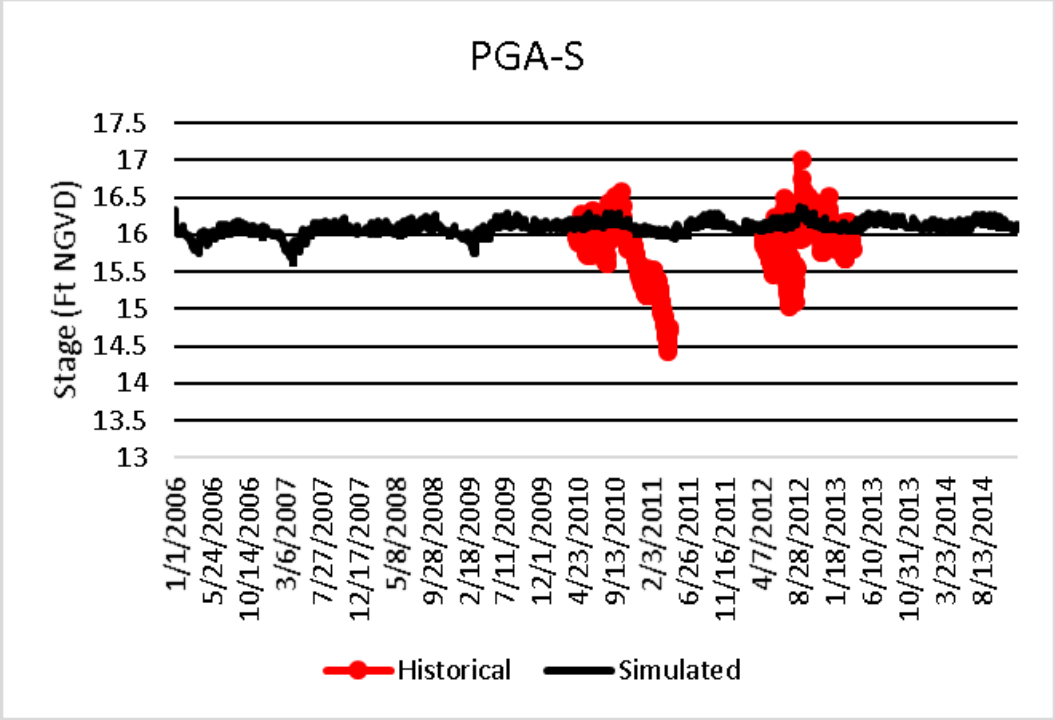

Figure A-66. Historical and simulated groundwater monitoring well stage hydrograph (2006 – 2014) for PGA-S (sequestered station).

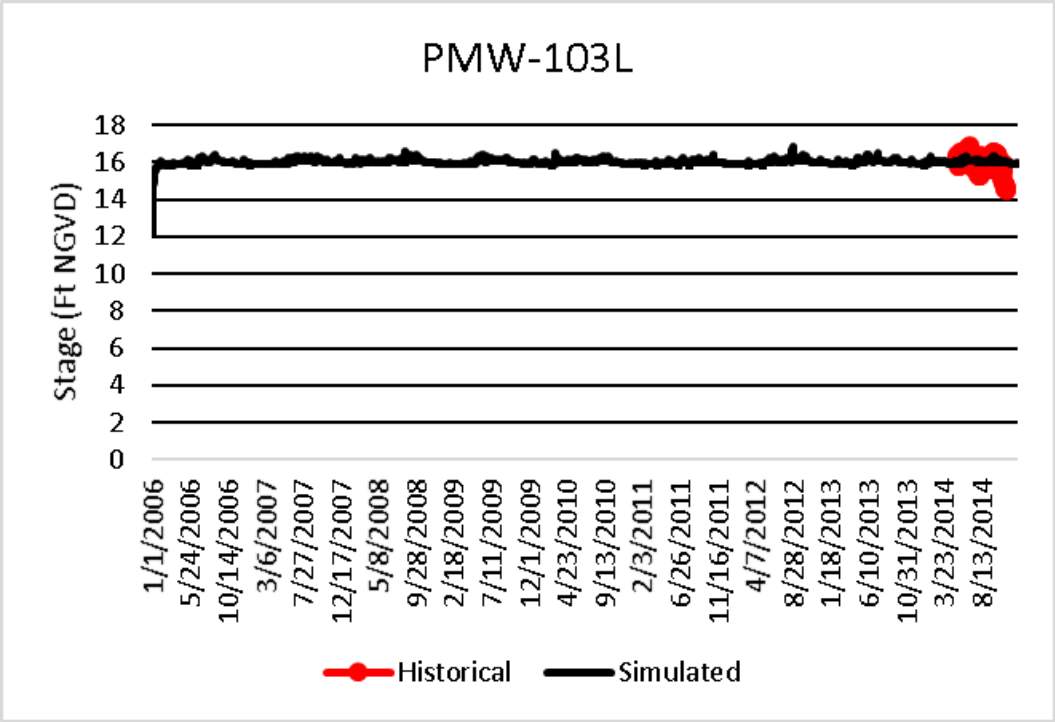

Figure A-67. Historical and simulated groundwater monitoring well stage hydrograph (2006 – 2014) for PMW-103L (sequestered station).

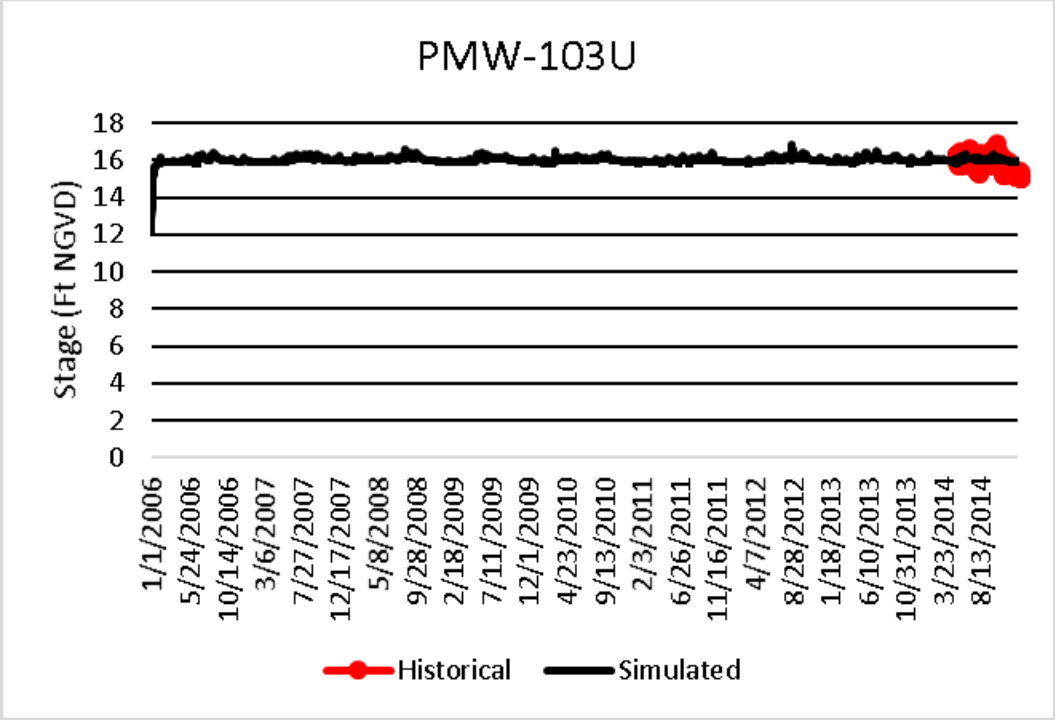

Figure A-68. Historical and simulated groundwater monitoring well stage hydrograph (2006 – 2014) for PMW-103U (sequestered station).

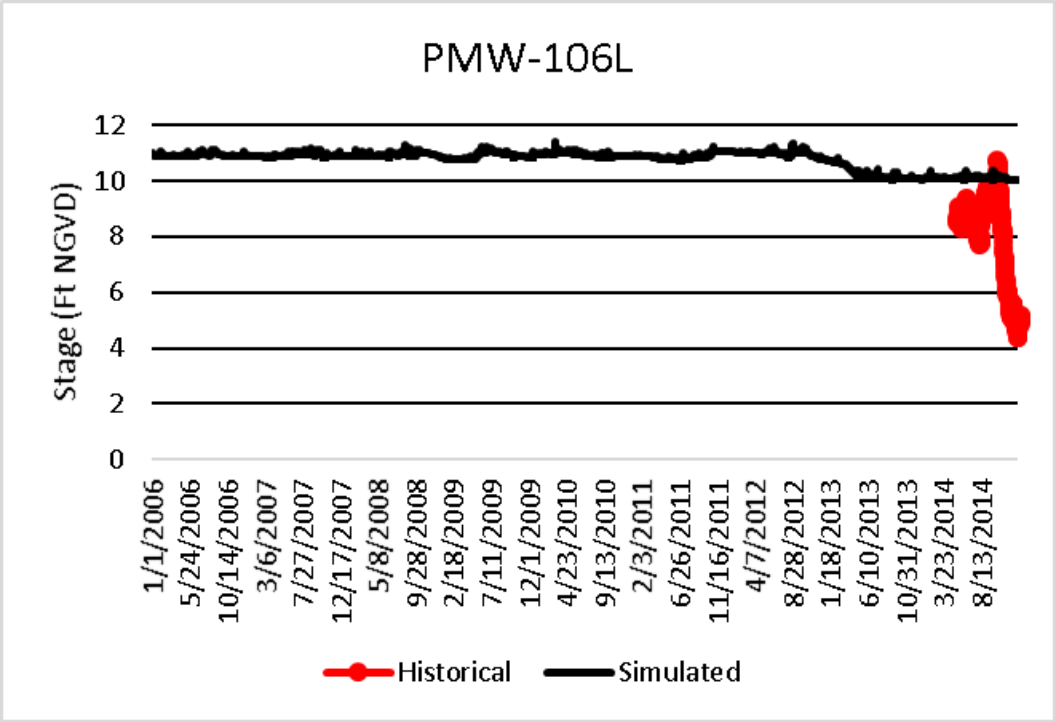

Figure A-69. Historical and simulated groundwater monitoring well stage hydrograph (2006 – 2014) for PMW-106L (sequestered station).

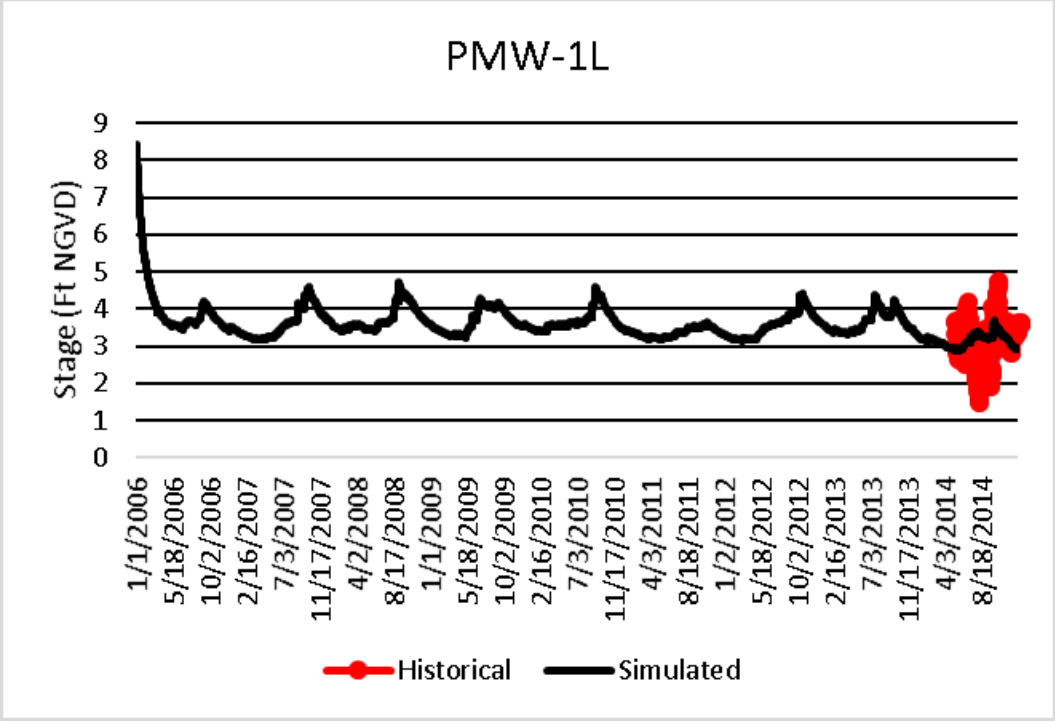

Figure A-70. Historical and simulated groundwater monitoring well stage hydrograph (2006 – 2014) for PMW-1L (sequestered station).

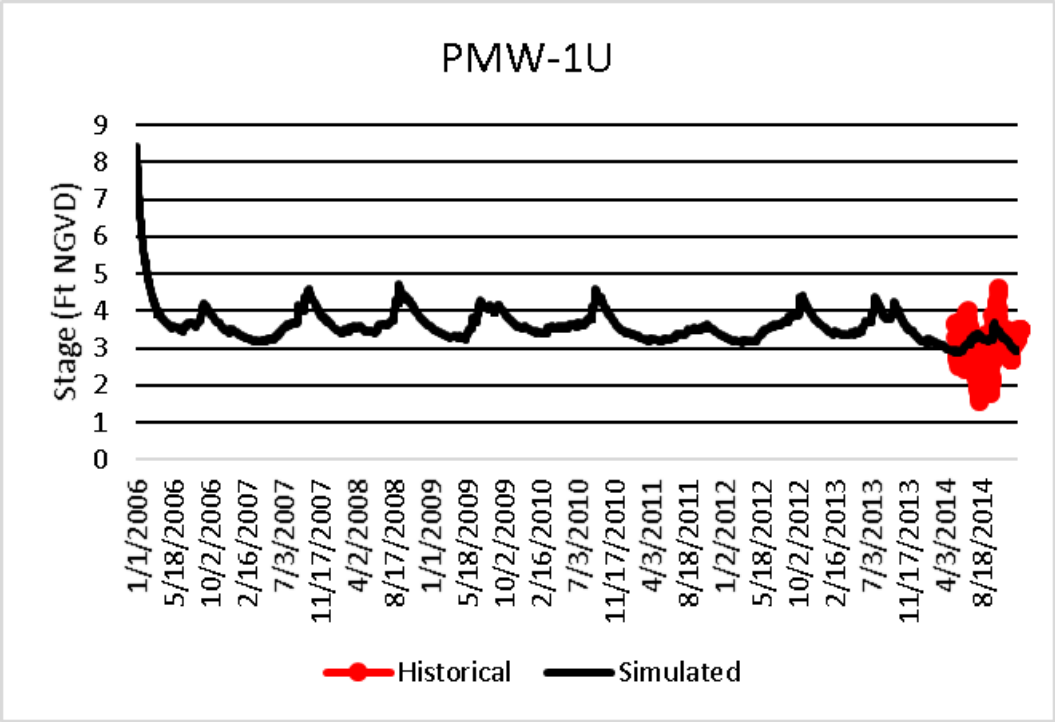

Figure A-71. Historical and simulated groundwater monitoring well stage hydrograph (2006 – 2014) for PMW-1U (sequestered station).

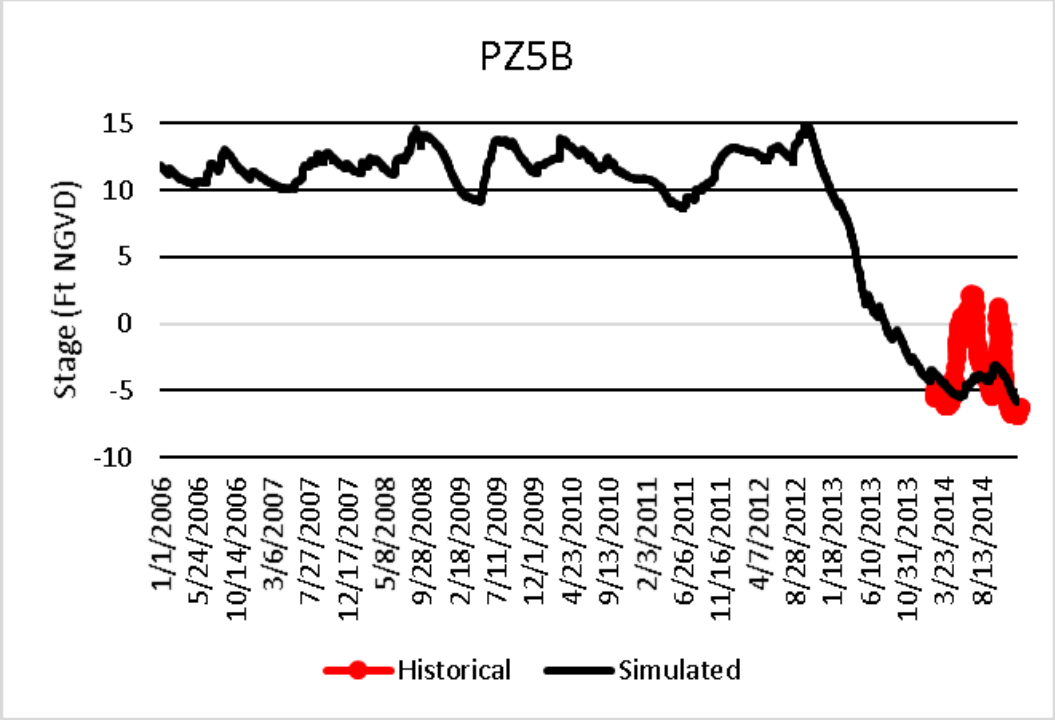

Figure A-72. Historical and simulated groundwater monitoring well stage hydrograph (2006 – 2014) for PZ5B (sequestered station).

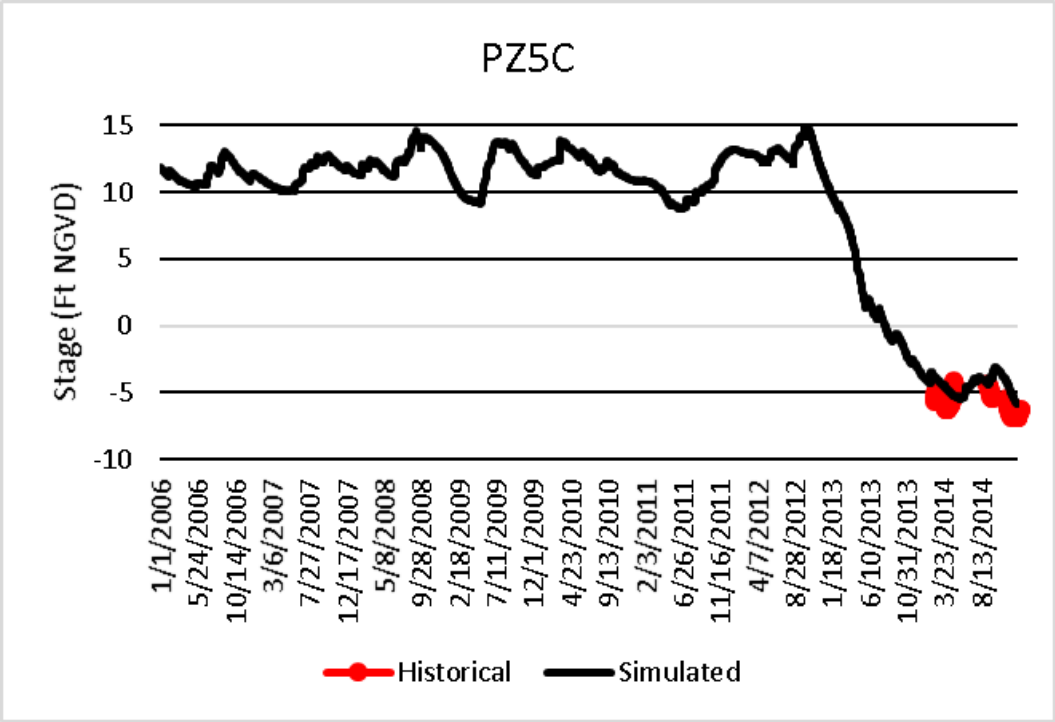

Figure A-73. Historical and simulated groundwater monitoring well stage hydrograph (2006 – 2014) for PZ5C (sequestered station).

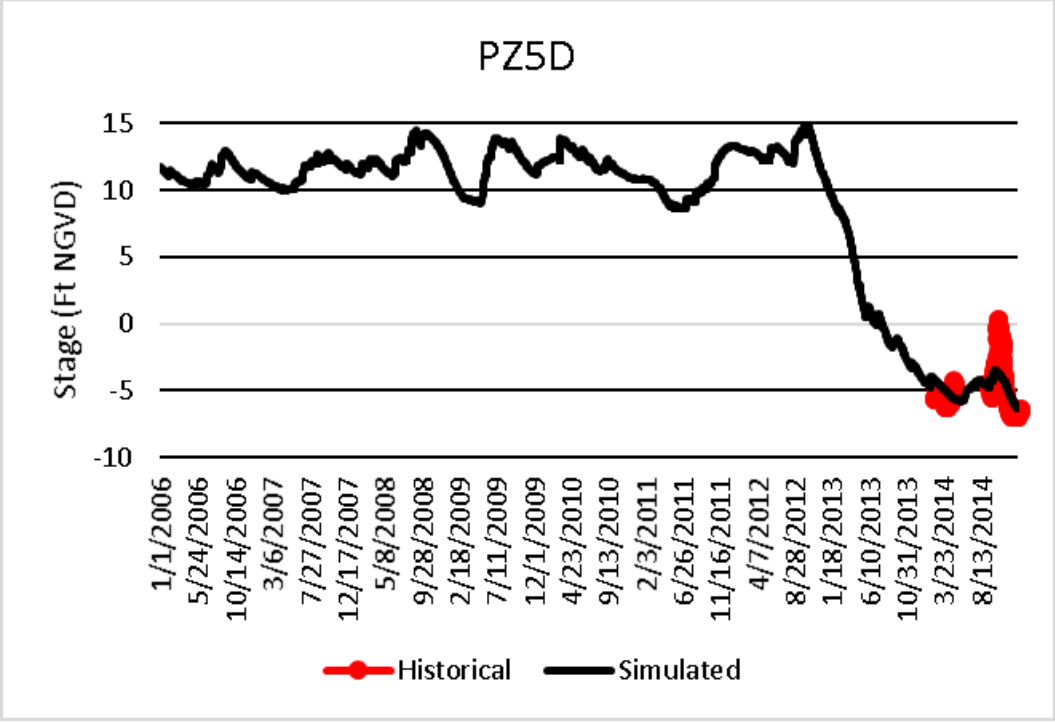

Figure A-74. Historical and simulated groundwater monitoring well stage hydrograph (2006 – 2014) for PZ5D (sequestered station).

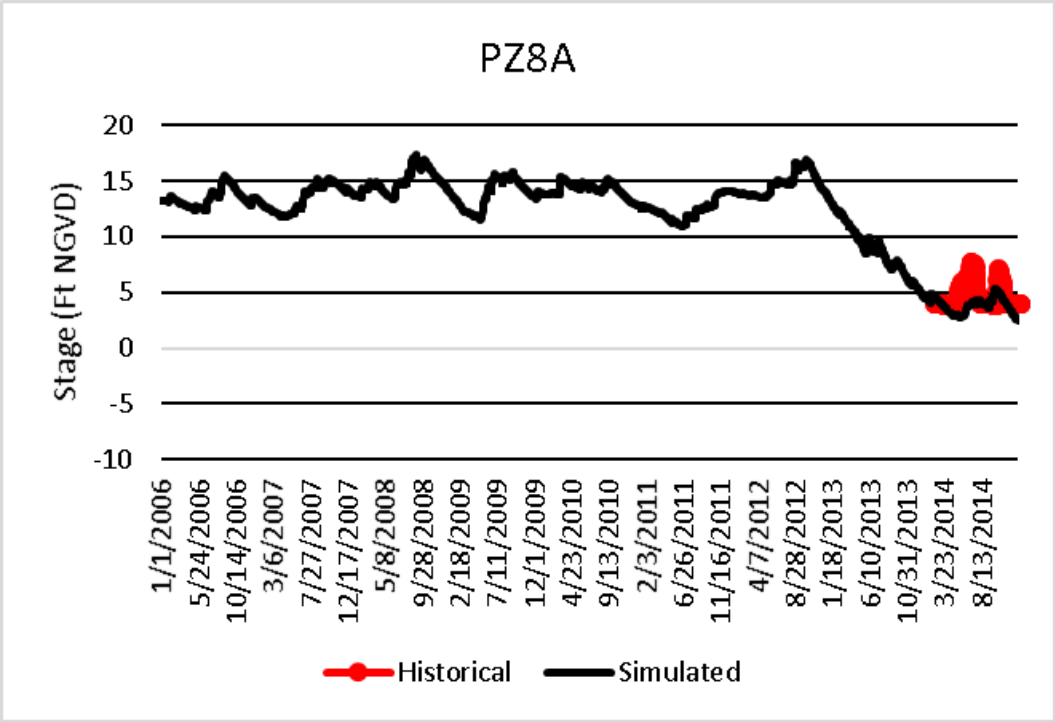

Figure A-75. Historical and simulated groundwater monitoring well stage hydrograph (2006 – 2014) for PZ8A (sequestered station).

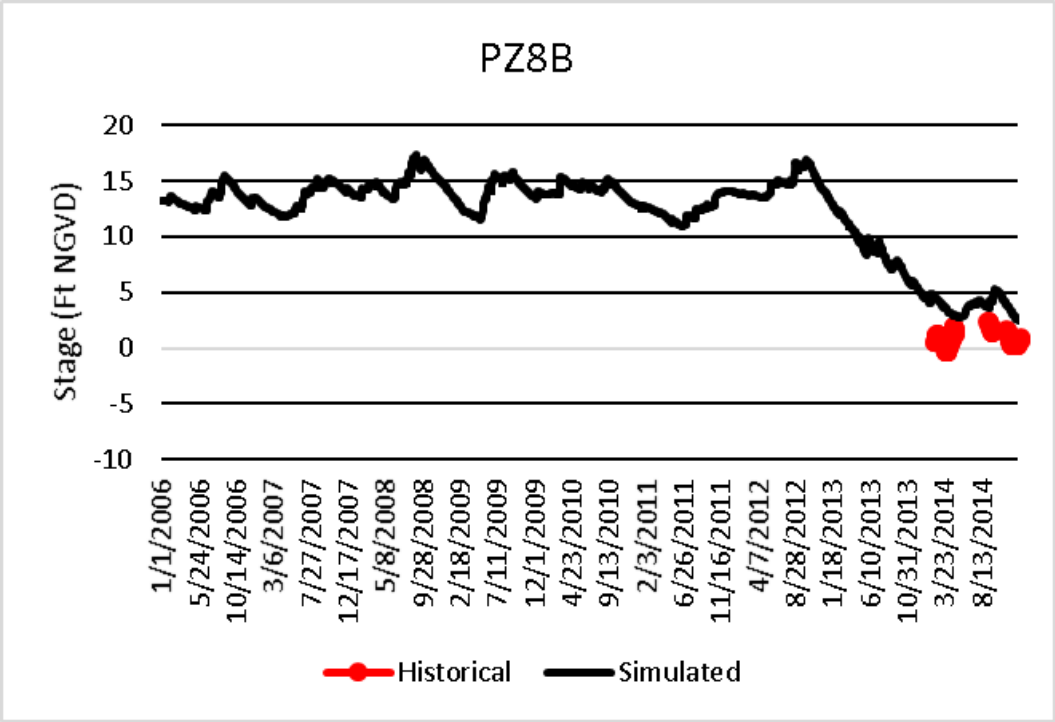

Figure A-76. Historical and simulated groundwater monitoring well stage hydrograph (2006 – 2014) for PZ8B (sequestered station).

APPENDIX B: WETLAND GAUGES

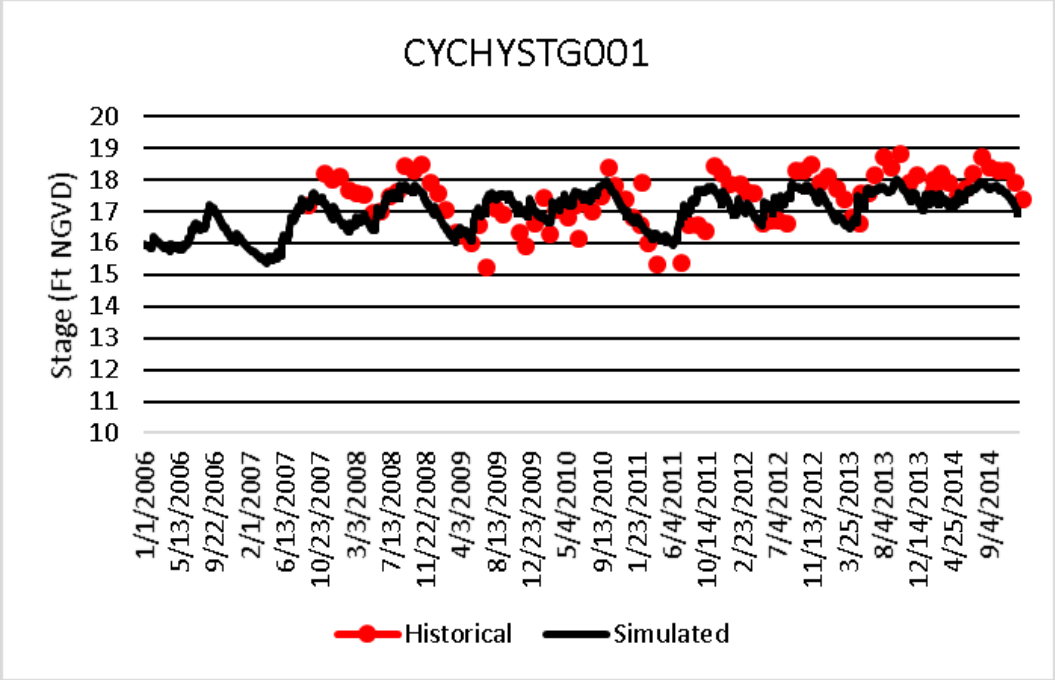

Figure B-1. Historical and simulated wetland gauge stage hydrograph (2006 – 2014) for CYCHYSTG001.

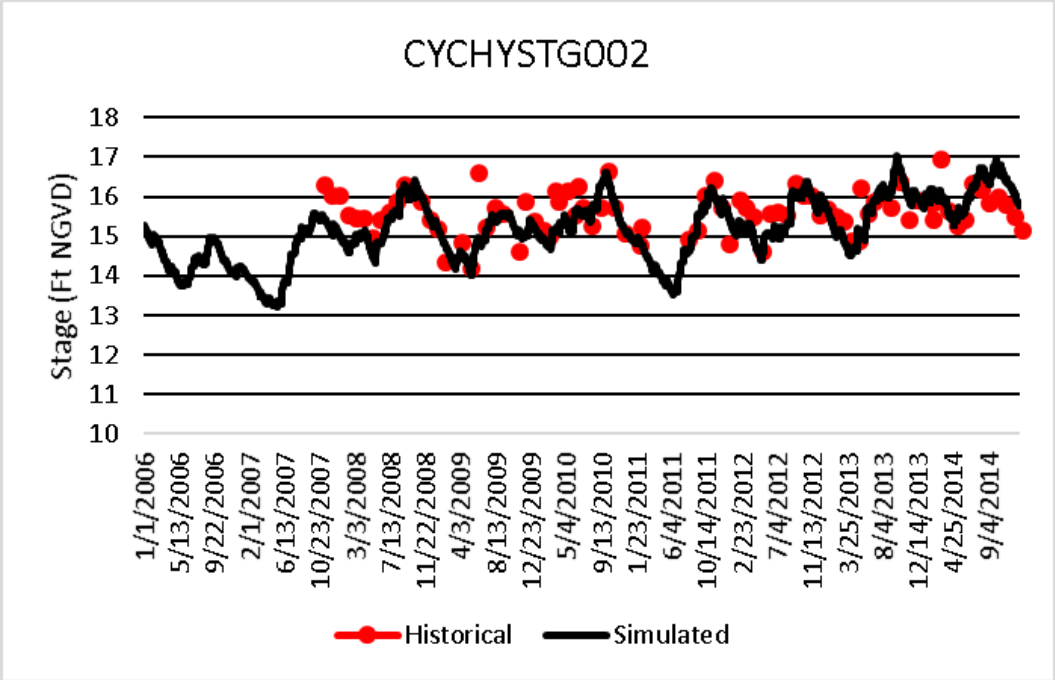

Figure B-2. Historical and simulated wetland gauge stage hydrograph (2006 – 2014) for CYCHYSTG002.

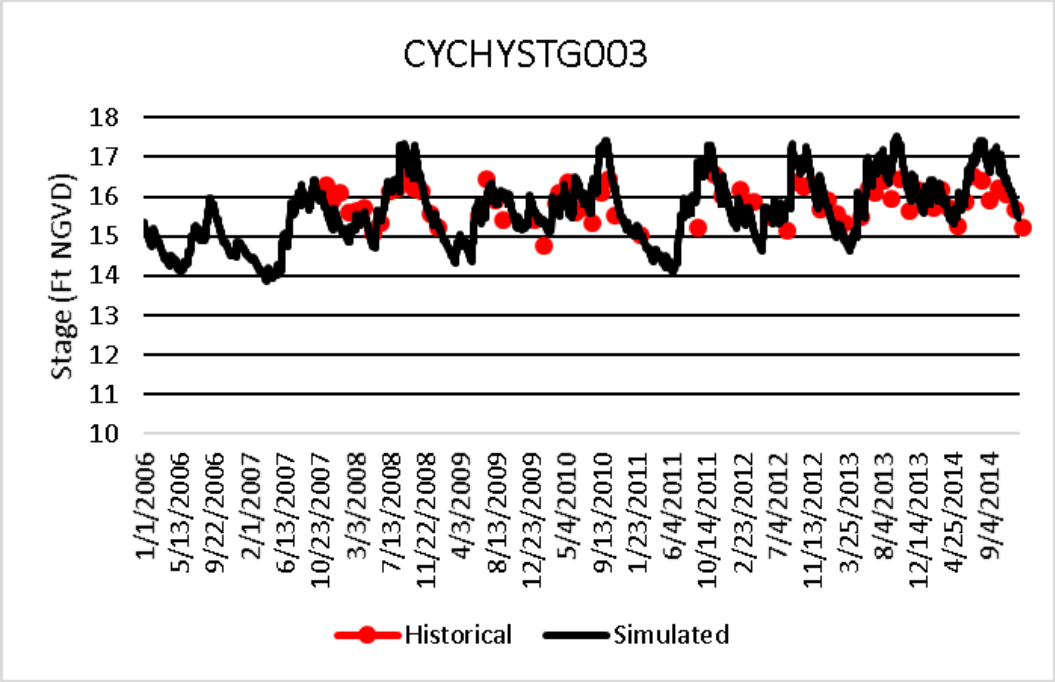

Figure B-3. Historical and simulated wetland gauge stage hydrograph (2006 – 2014) for CYCHYSTG003.

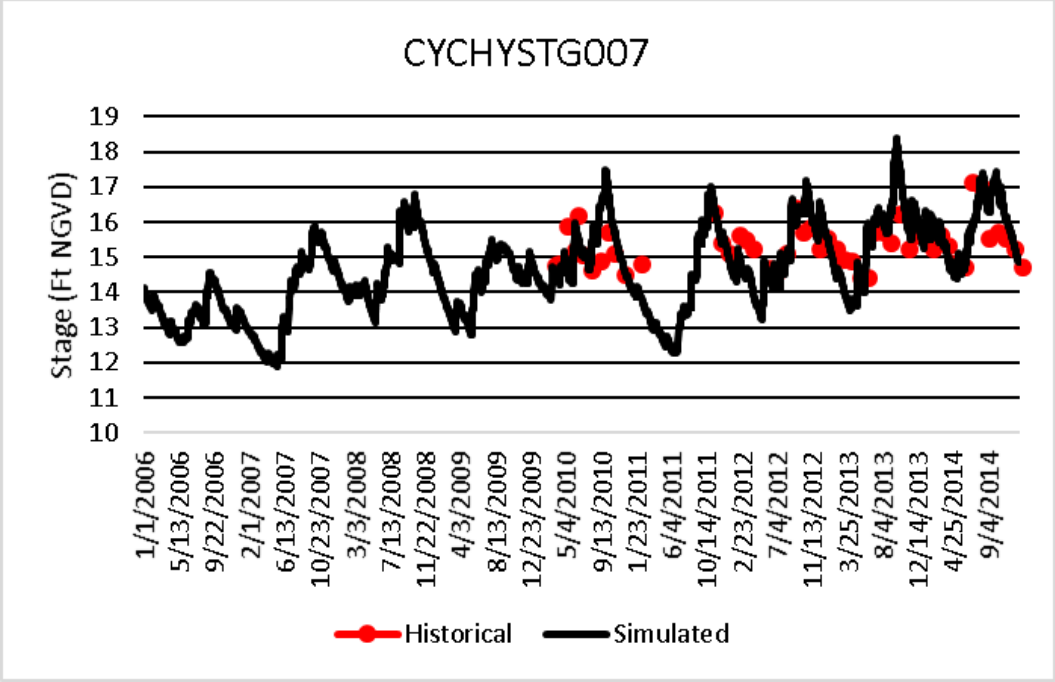

Figure B-4. Historical and simulated wetland gauge stage hydrograph (2006 – 2014) for CYCHYSTG007.

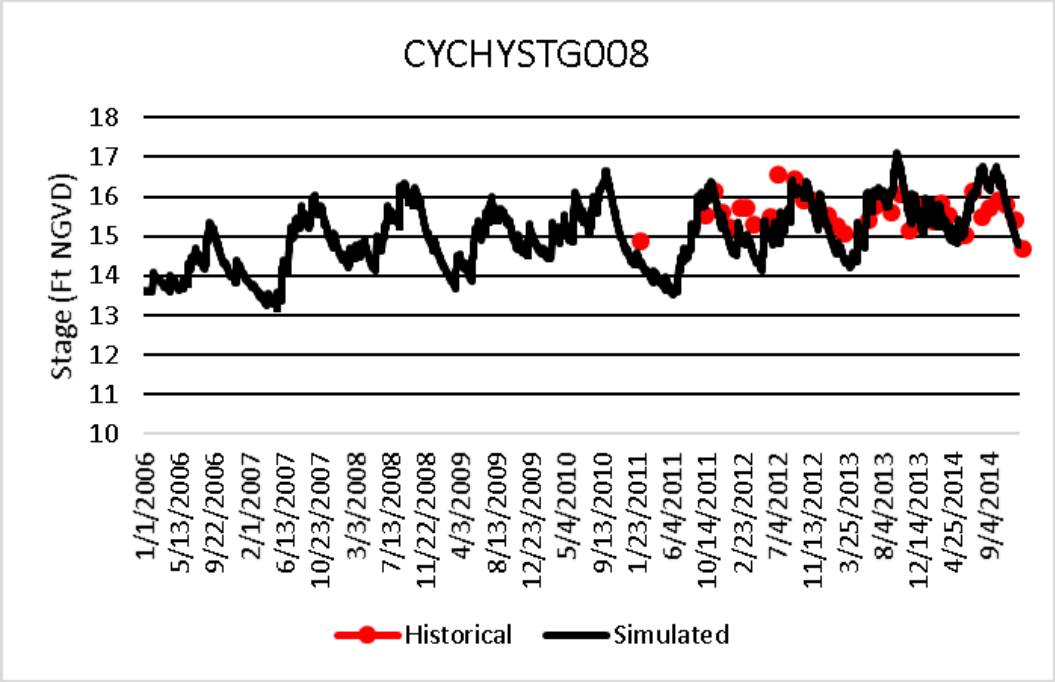

Figure B-5. Historical and simulated wetland gauge stage hydrograph (2006 – 2014) for CYCHYSTG008.

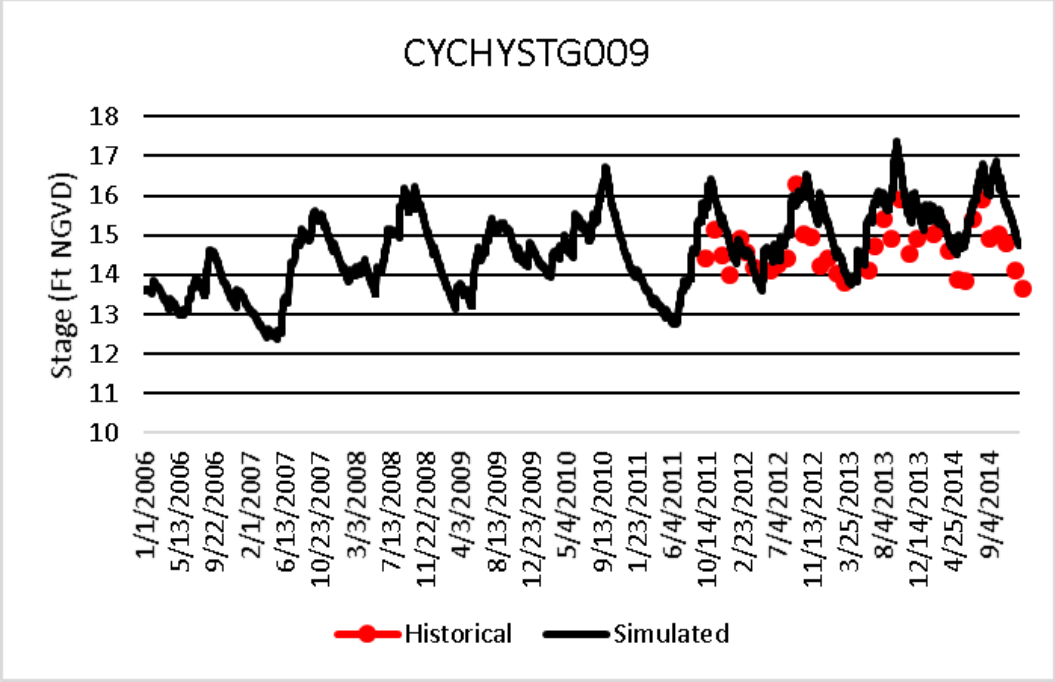

Figure B-6. Historical and simulated wetland gauge stage hydrograph (2006 – 2014) for CYCHYSTG009.

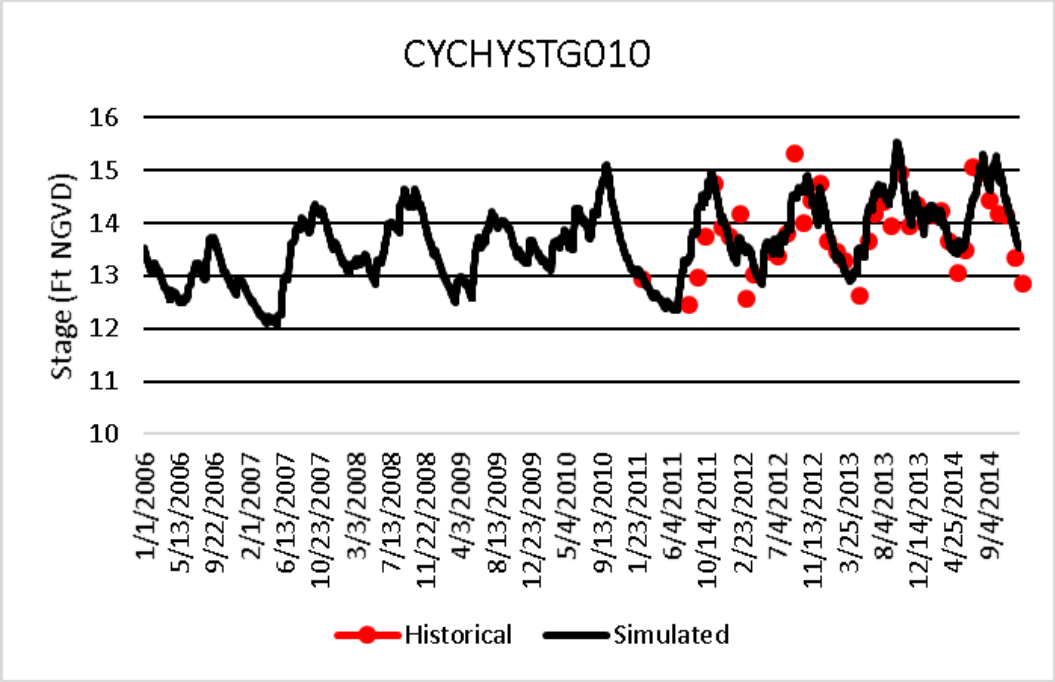

Figure B-7. Historical and simulated wetland gauge stage hydrograph (2006 – 2014) for CYCHYSTG010.

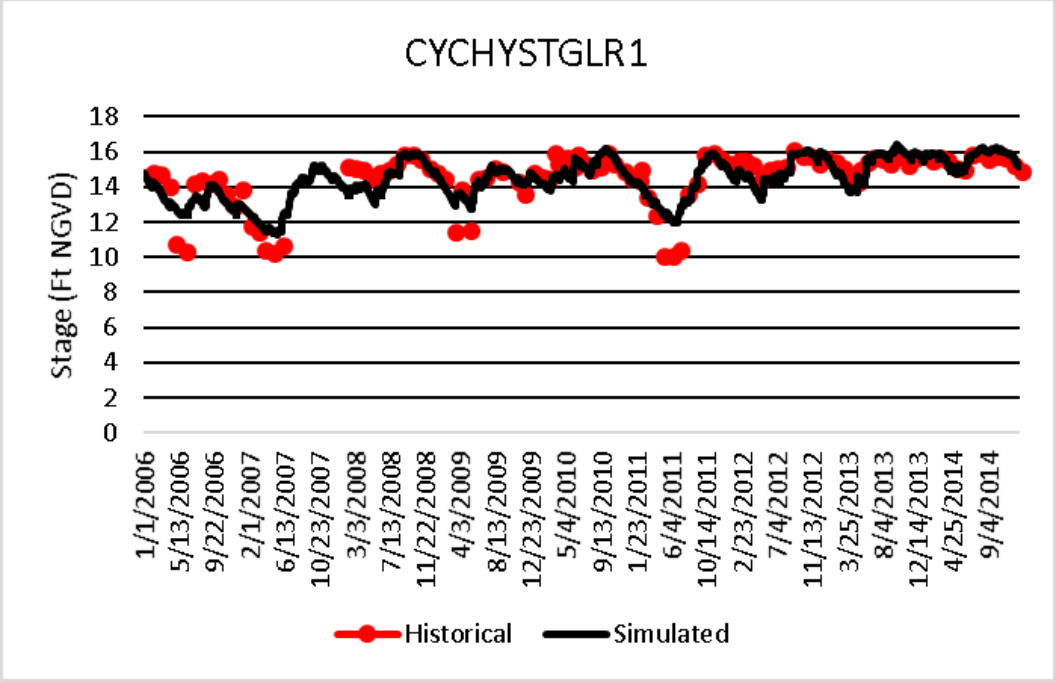

Figure B-8. Historical and simulated wetland gauge stage hydrograph (2006 – 2014) for CYCHYSTGLR1.

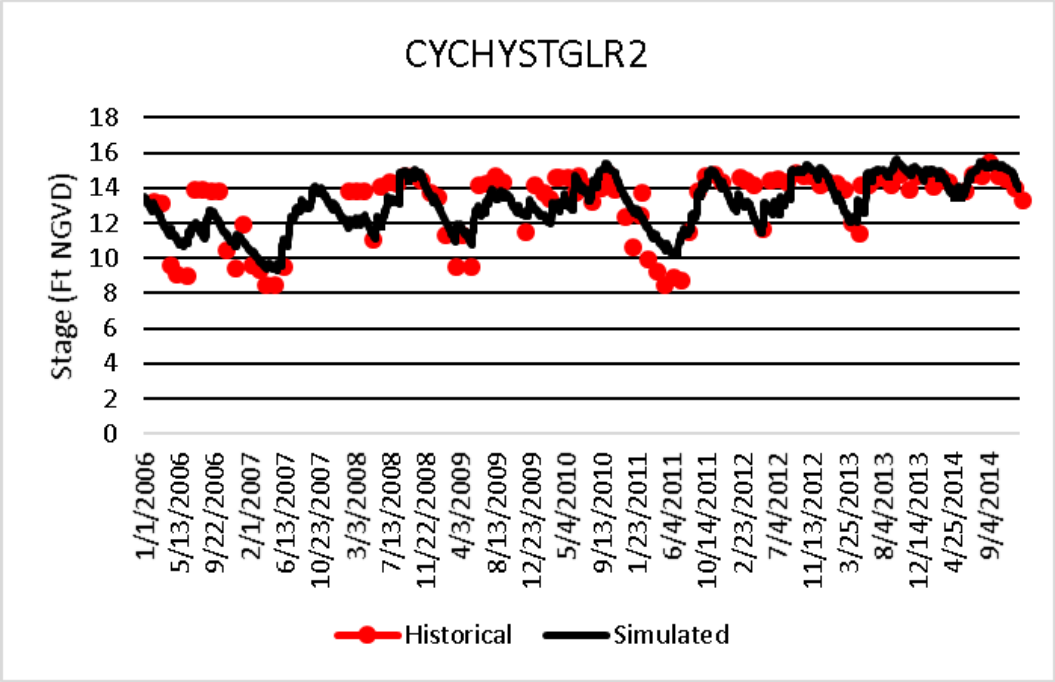

Figure B-9. Historical and simulated wetland gauge stage hydrograph (2006 – 2014) for CYCHYSTGLR2.

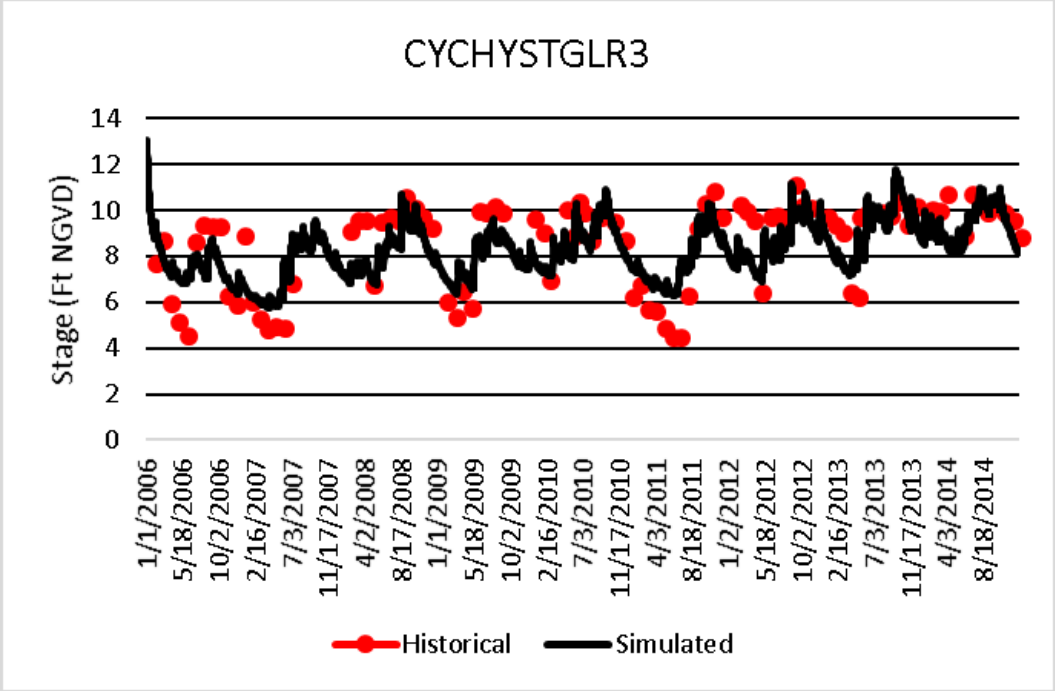

Figure B-10. Historical and simulated wetland gauge stage hydrograph (2006 – 2014) for CYCHYSTGLR3.

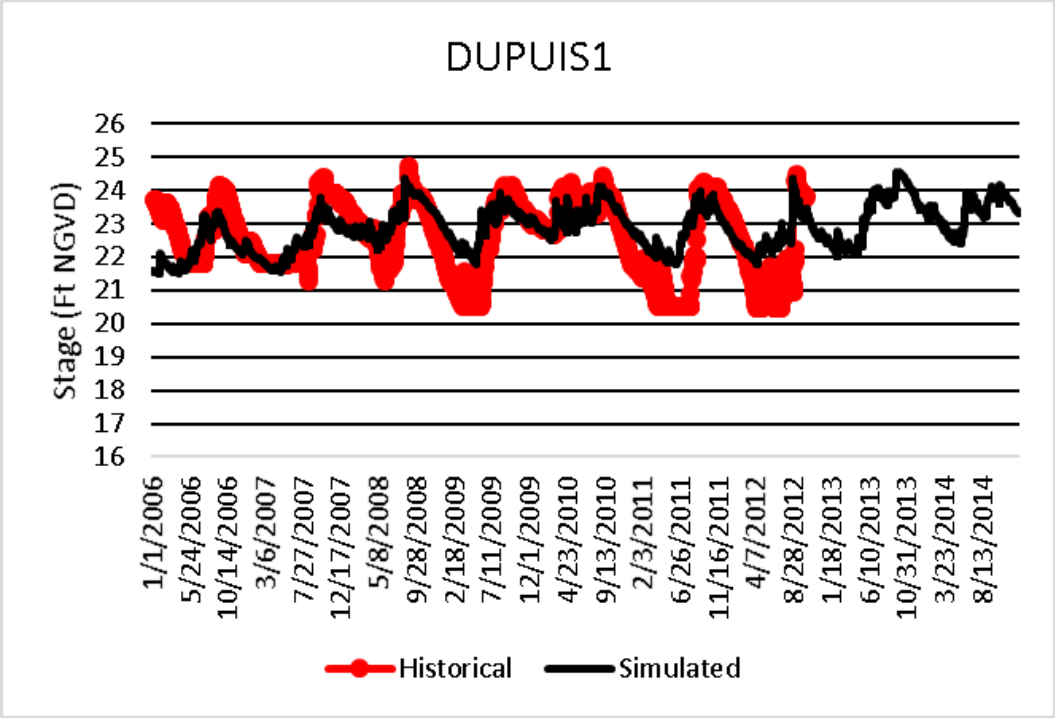

Figure B-11. Historical and simulated wetland gauge stage hydrograph (2006 – 2014) for Dupuis1.

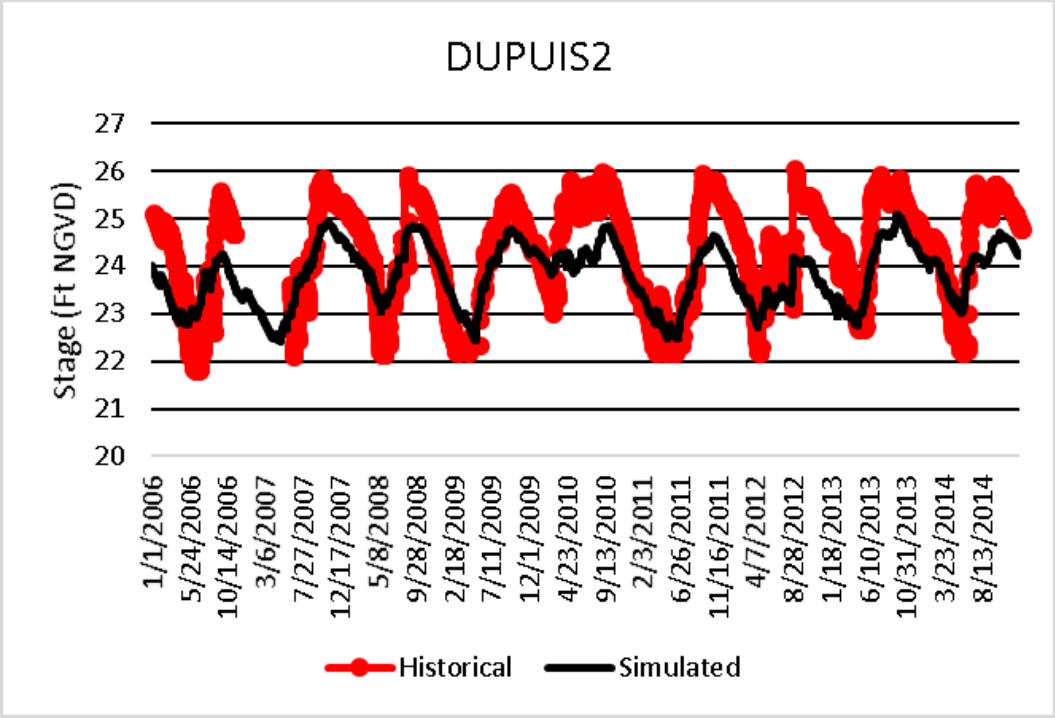

Figure B-12. Historical and simulated wetland gauge stage hydrograph (2006 – 2014) for Dupuis2.

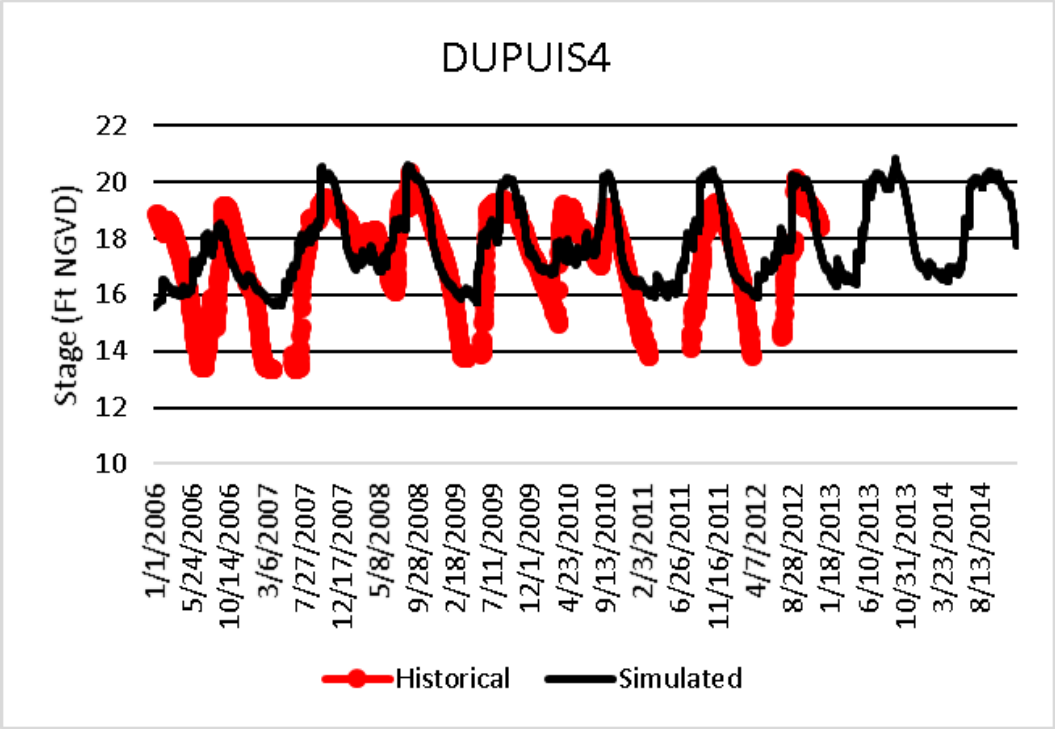

Figure B-13. Historical and simulated wetland gauge stage hydrograph (2006 – 2014) for Dupuis4.

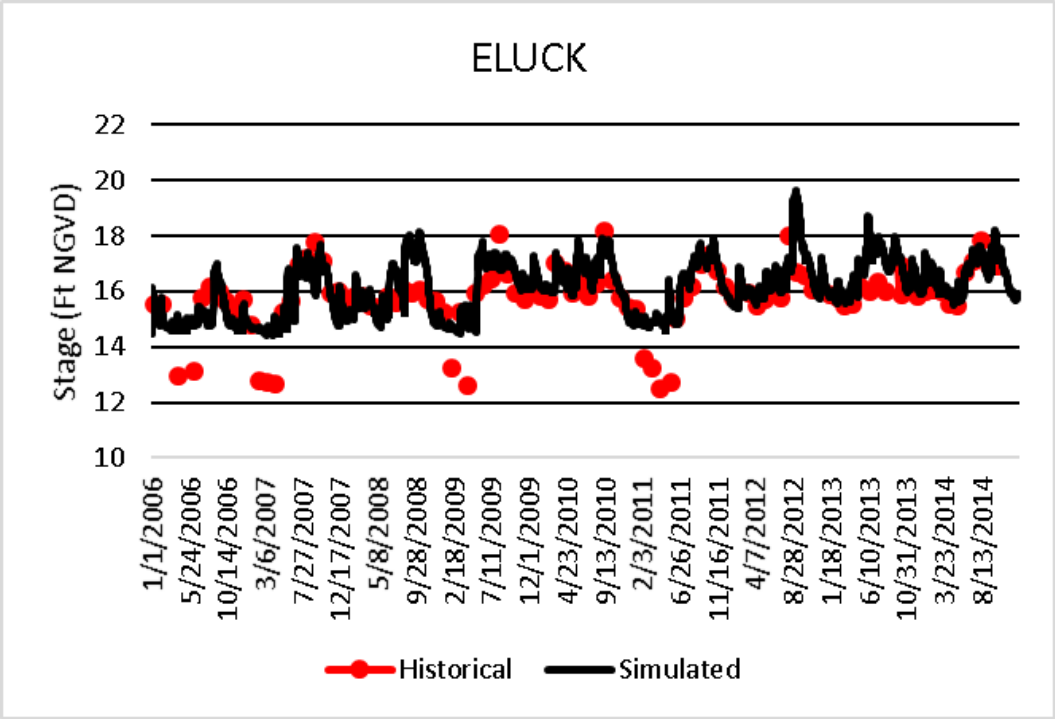

Figure B-14. Historical and simulated wetland gauge stage hydrograph (2006 – 2014) for ELUCK.

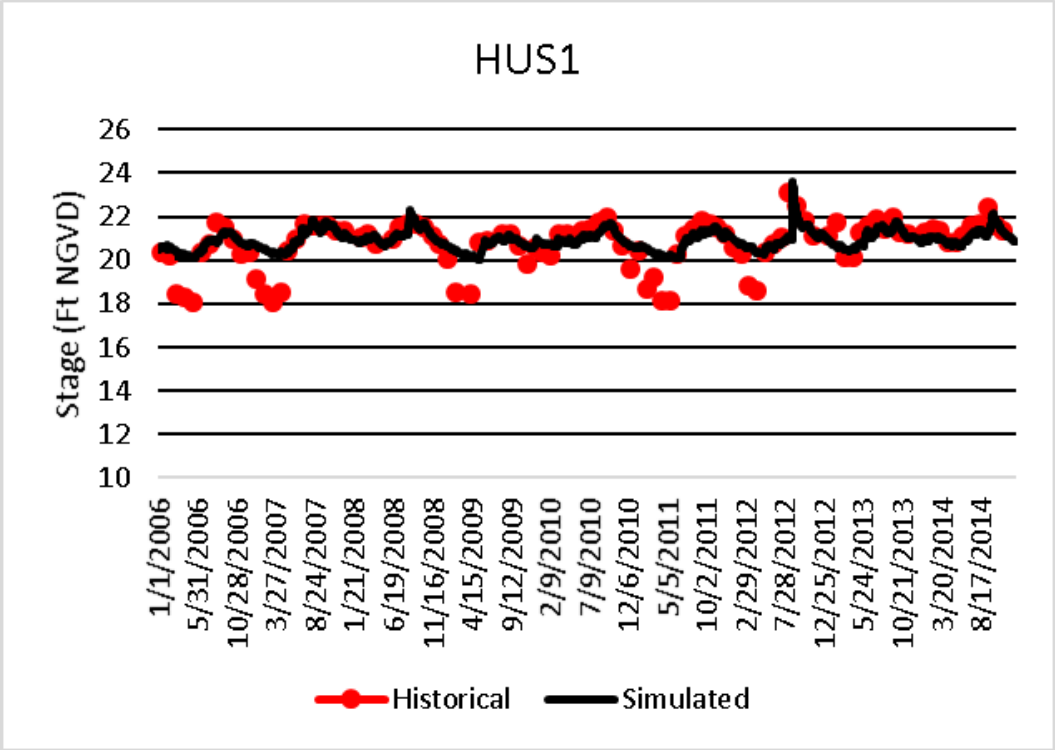

Figure B-15. Historical and simulated wetland gauge stage hydrograph (2006 – 2014) for HUS1.

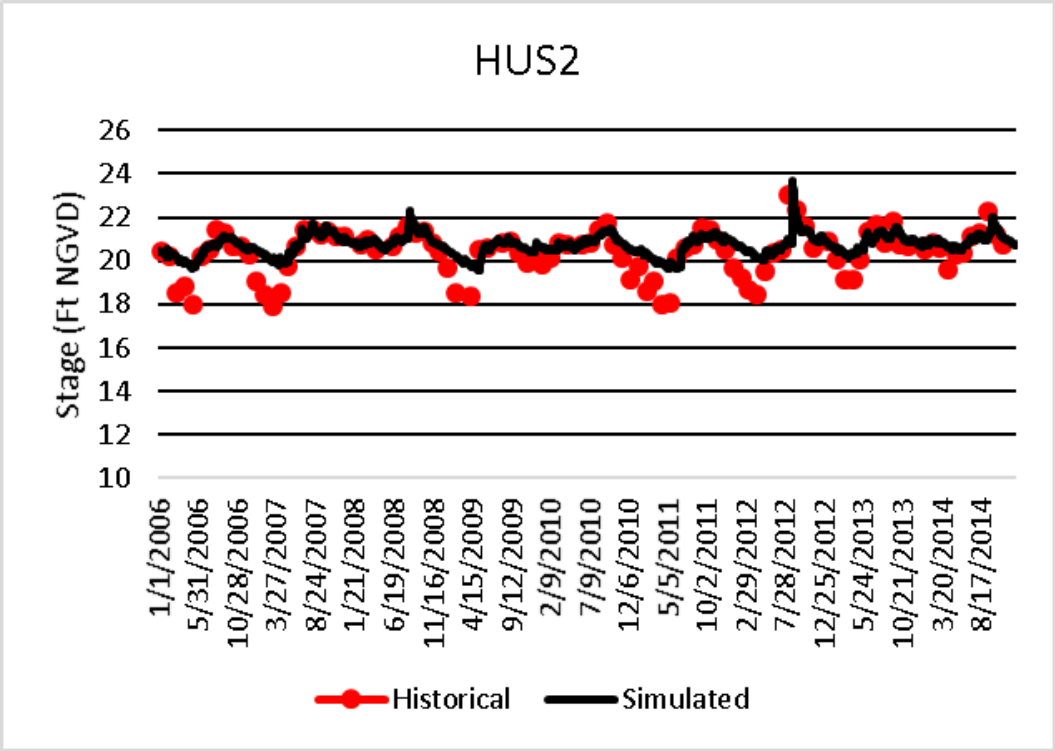

Figure B-16. Historical and simulated wetland gauge stage hydrograph (2006 – 2014) for HUS2.

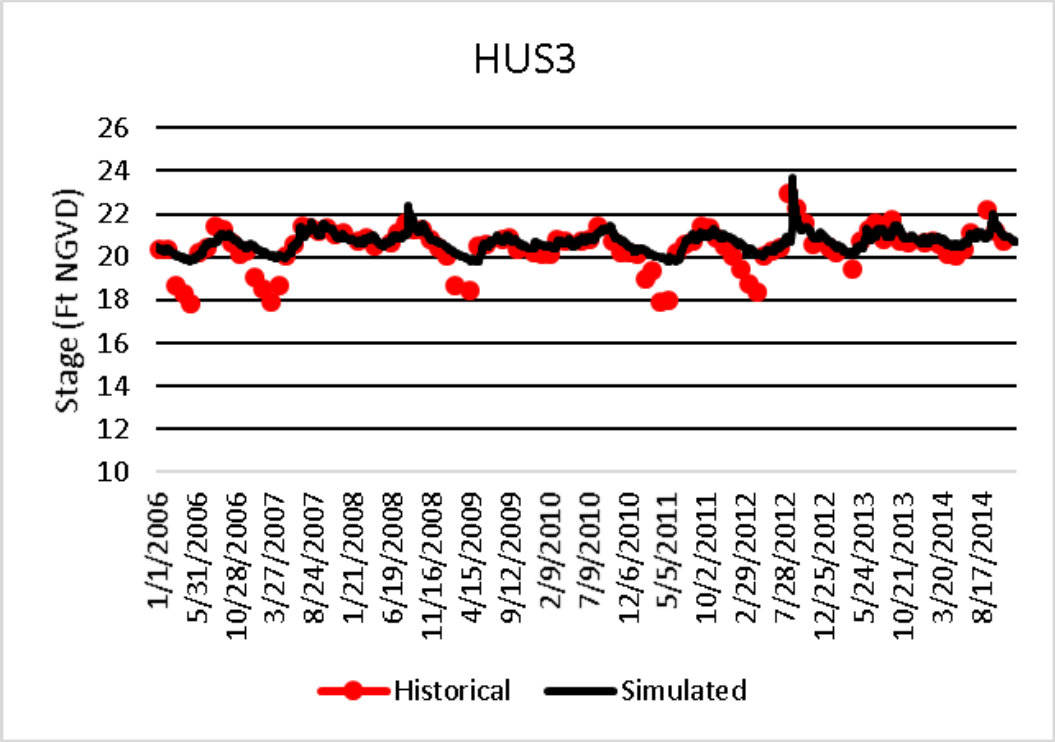

Figure B-17. Historical and simulated wetland gauge stage hydrograph (2006 – 2014) for HUS3.

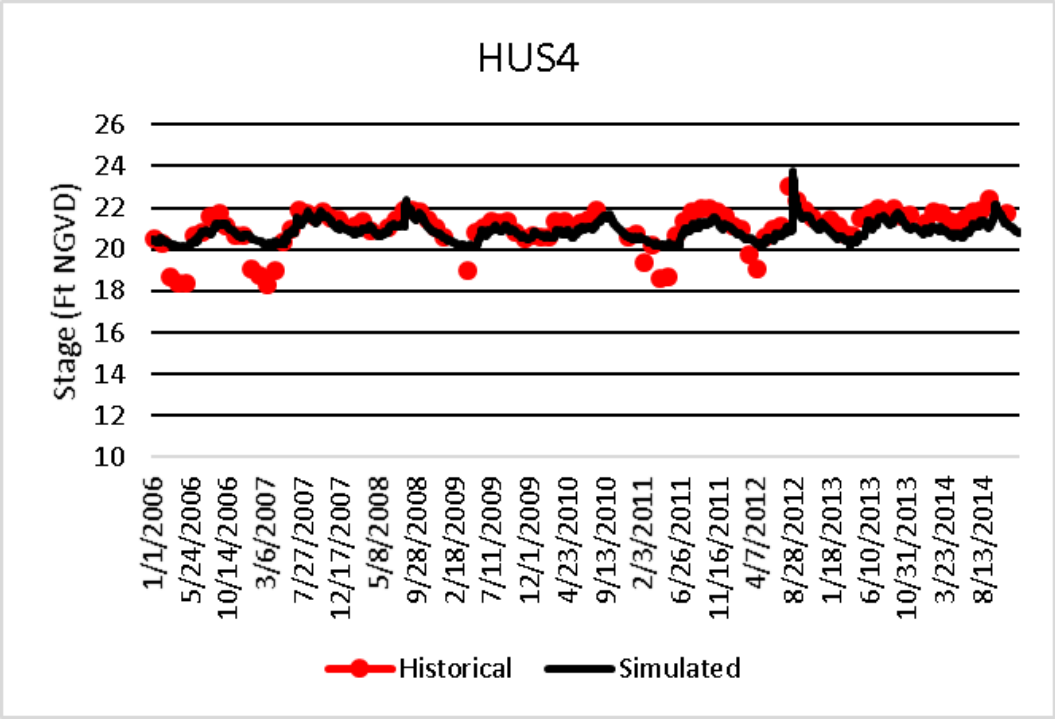

Figure B-18. Historical and simulated wetland gauge stage hydrograph (2006 – 2014) for HUS4.

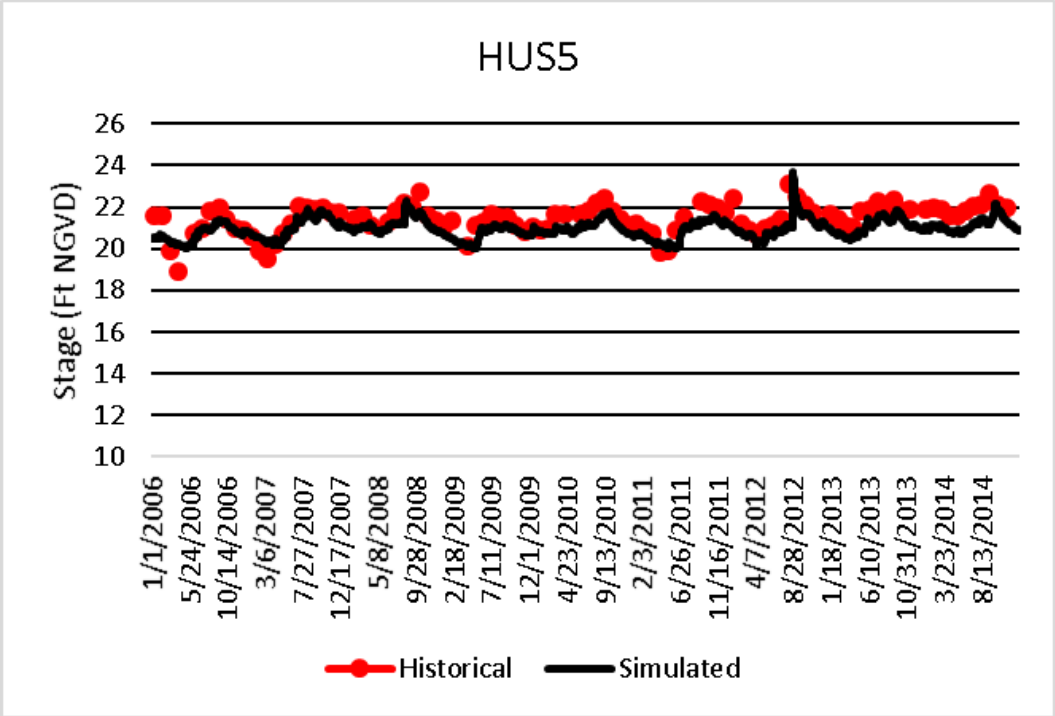

Figure B-19. Historical and simulated wetland gauge stage hydrograph (2006 – 2014) for HUS5.

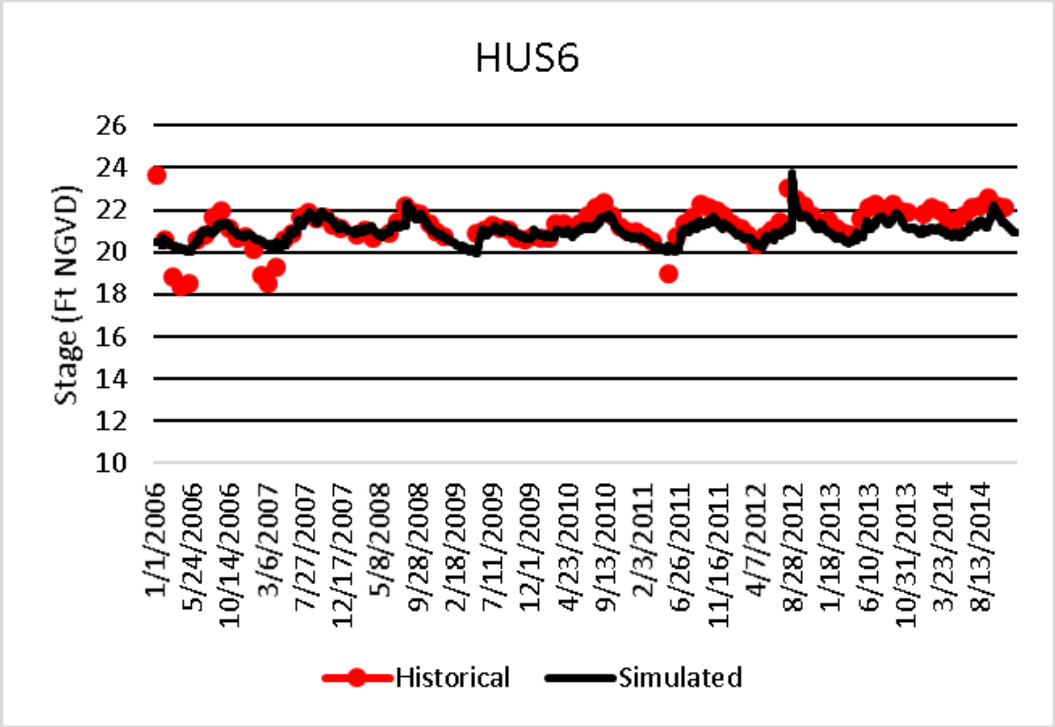

Figure B-20. Historical and simulated wetland gauge stage hydrograph (2006 – 2014) for HUS6.

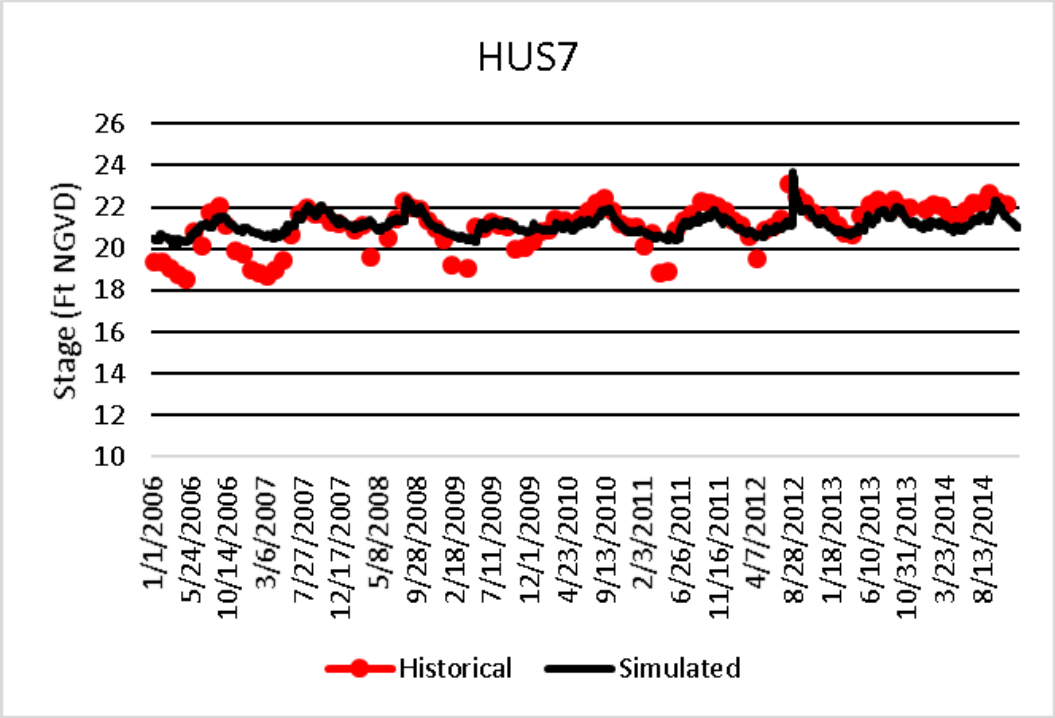

Figure B-21. Historical and simulated wetland gauge stage hydrograph (2006 – 2014) for HUS7.

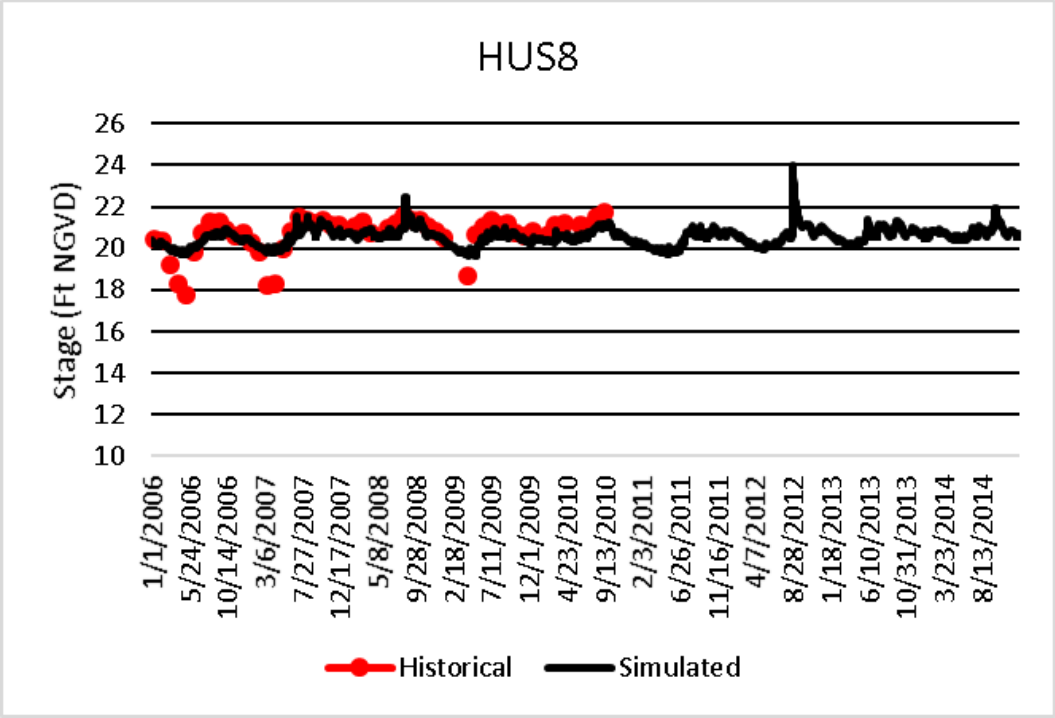

Figure B-22. Historical and simulated wetland gauge stage hydrograph (2006 – 2014) for HUS8.

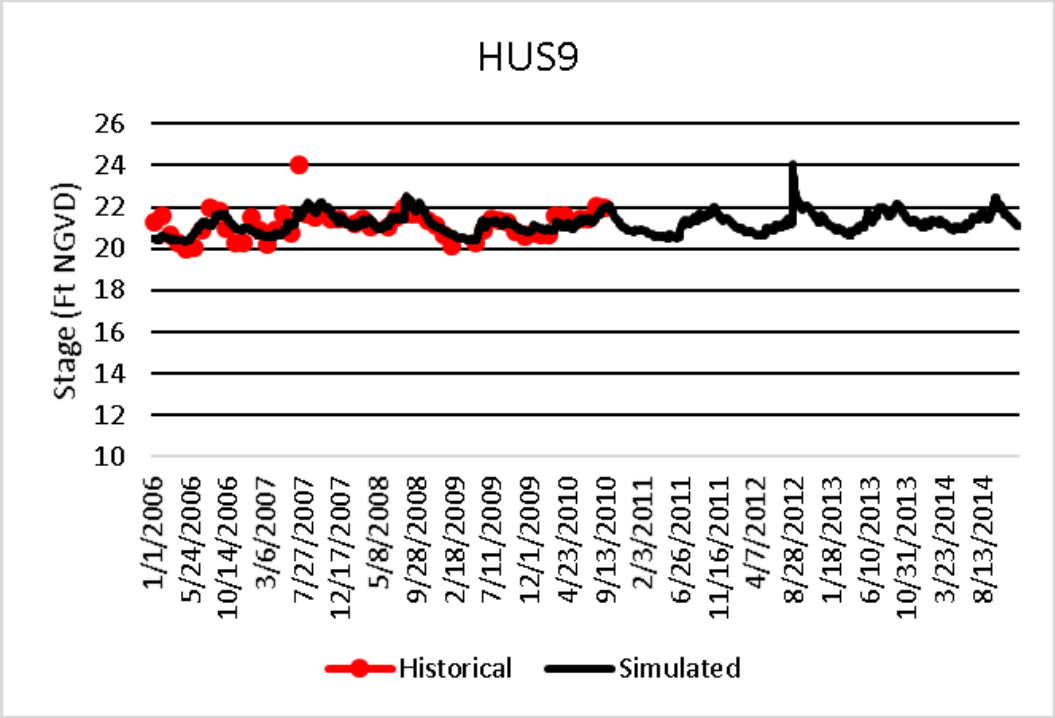

Figure B-23. Historical and simulated wetland gauge stage hydrograph (2006 – 2014) for HUS9.

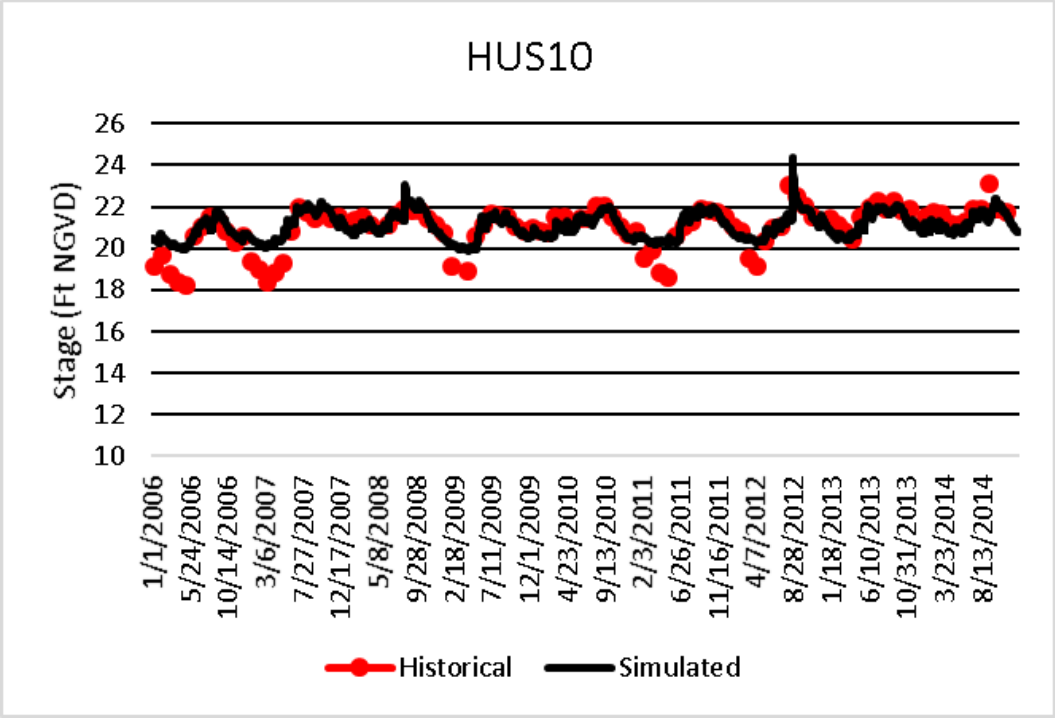

Figure B-24. Historical and simulated wetland gauge stage hydrograph (2006 – 2014) for HUS10.

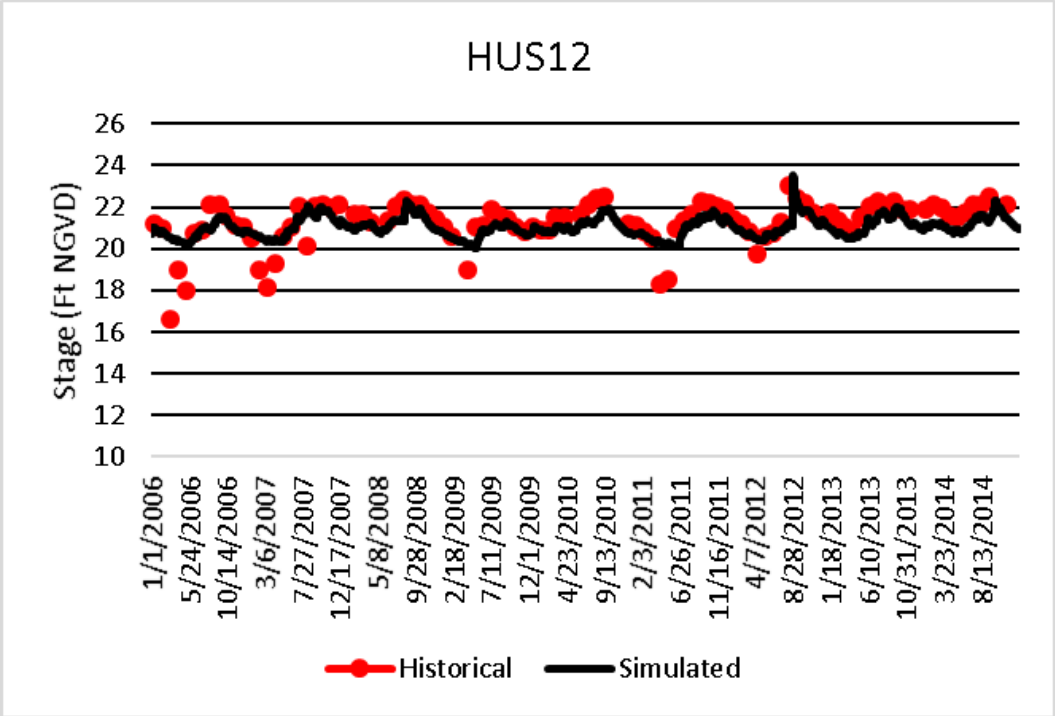

Figure B-25. Historical and simulated wetland gauge stage hydrograph (2006 – 2014) for HUS12.

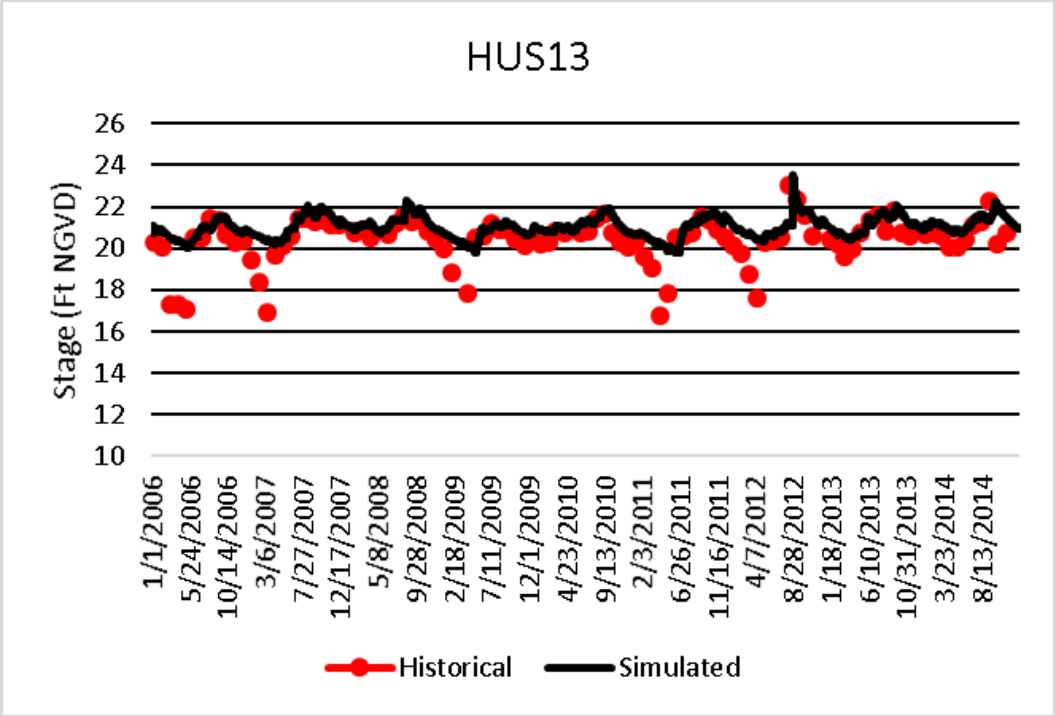

Figure B-26. Historical and simulated wetland gauge stage hydrograph (2006 – 2014) for HUS13.

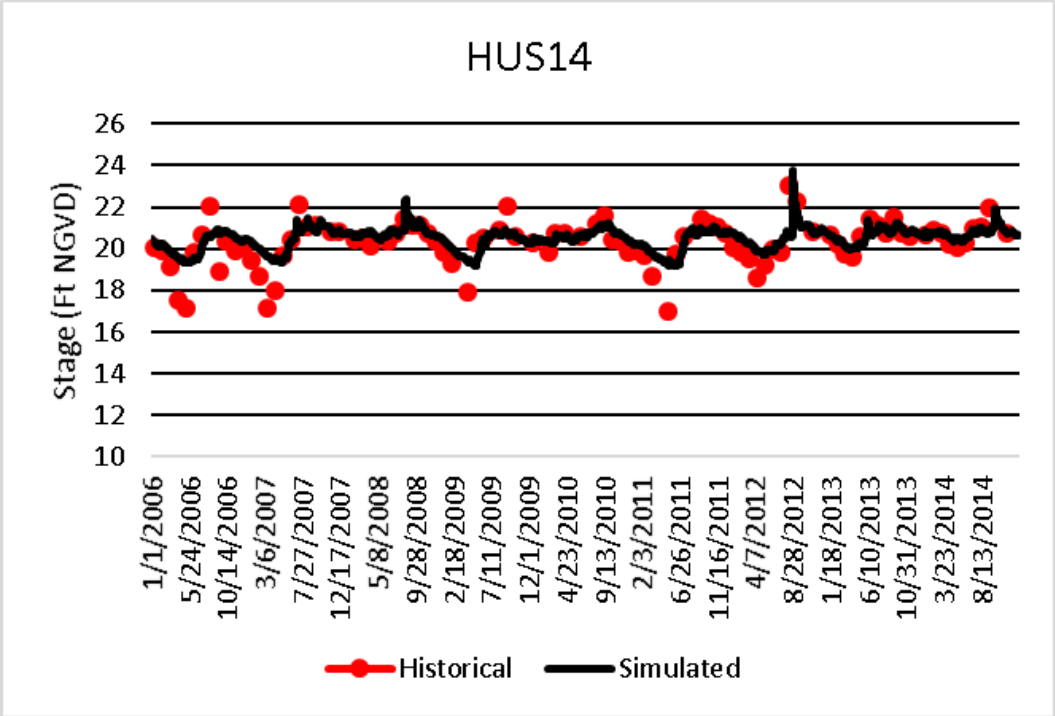

Figure B-27. Historical and simulated wetland gauge stage hydrograph (2006 – 2014) for HUS14.

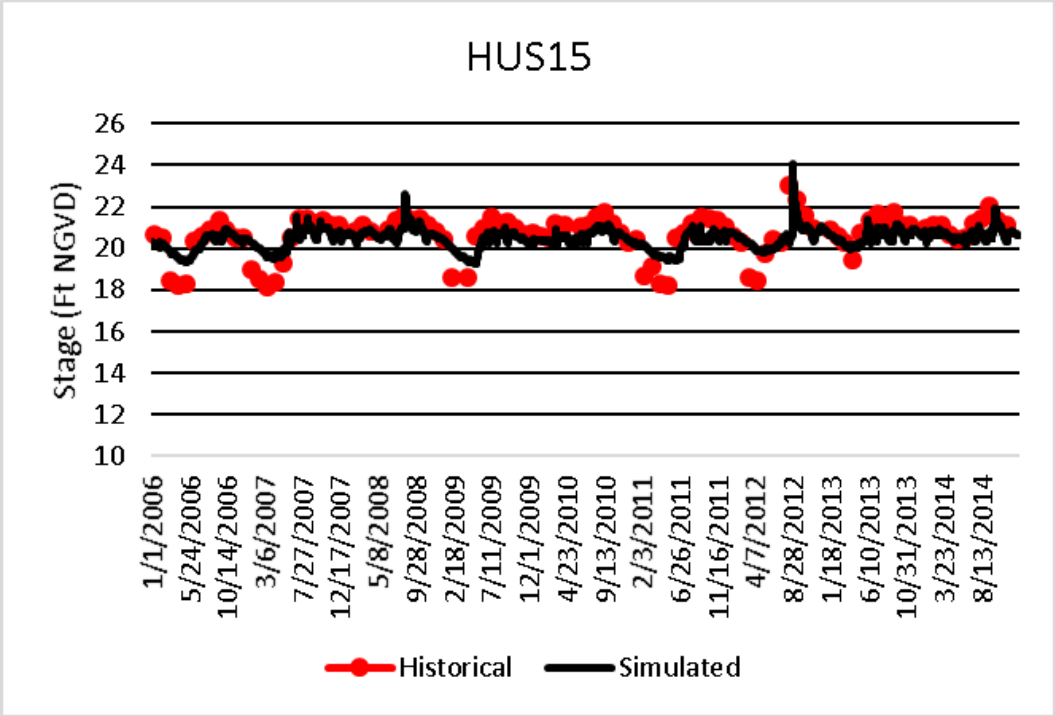

Figure B-28. Historical and simulated wetland gauge stage hydrograph (2006 – 2014) for HUS15.

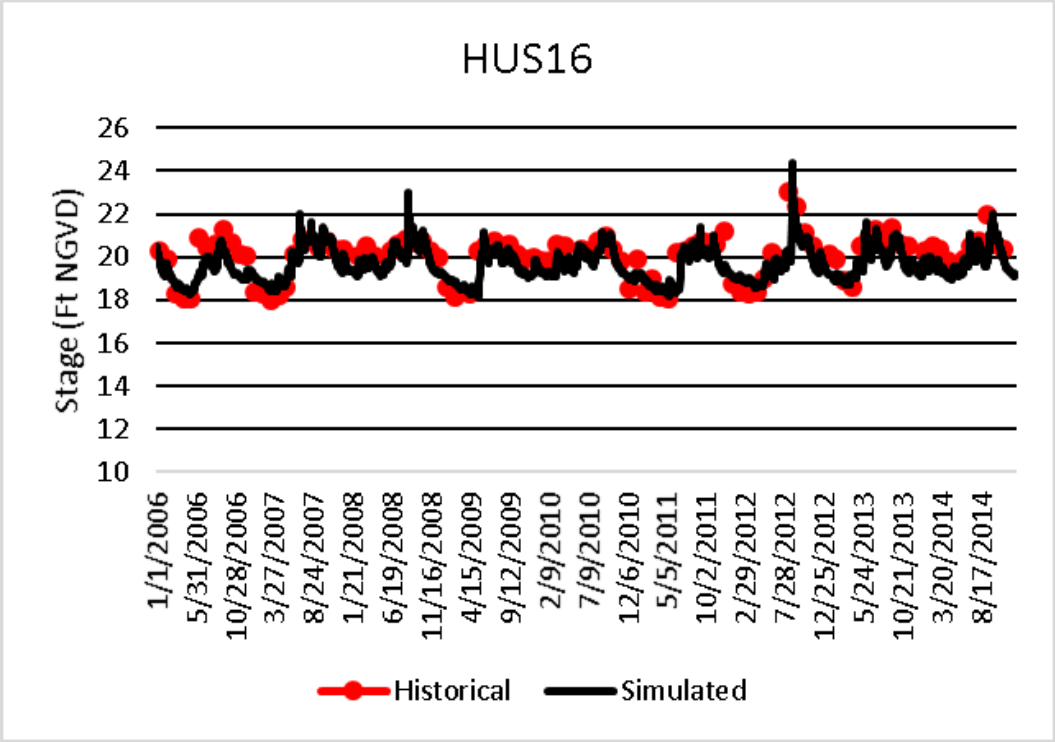

Figure B-29. Historical and simulated wetland gauge stage hydrograph (2006 – 2014) for HUS16.

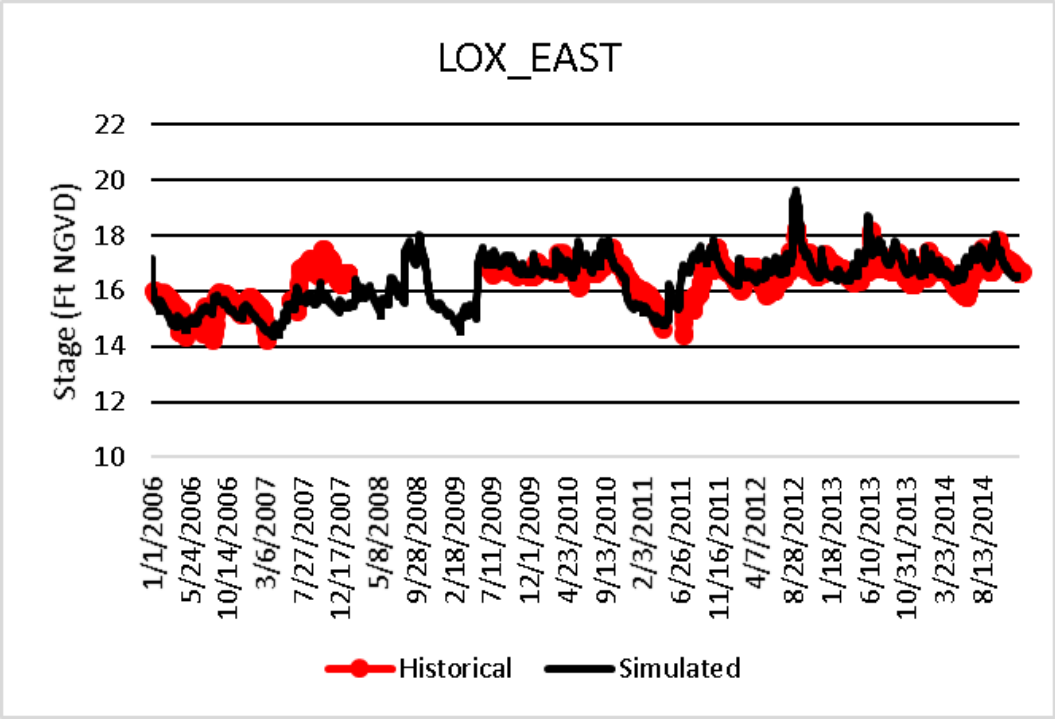

Figure B-30. Historical and simulated wetland gauge stage hydrograph (2006 – 2014) for Lox_East.

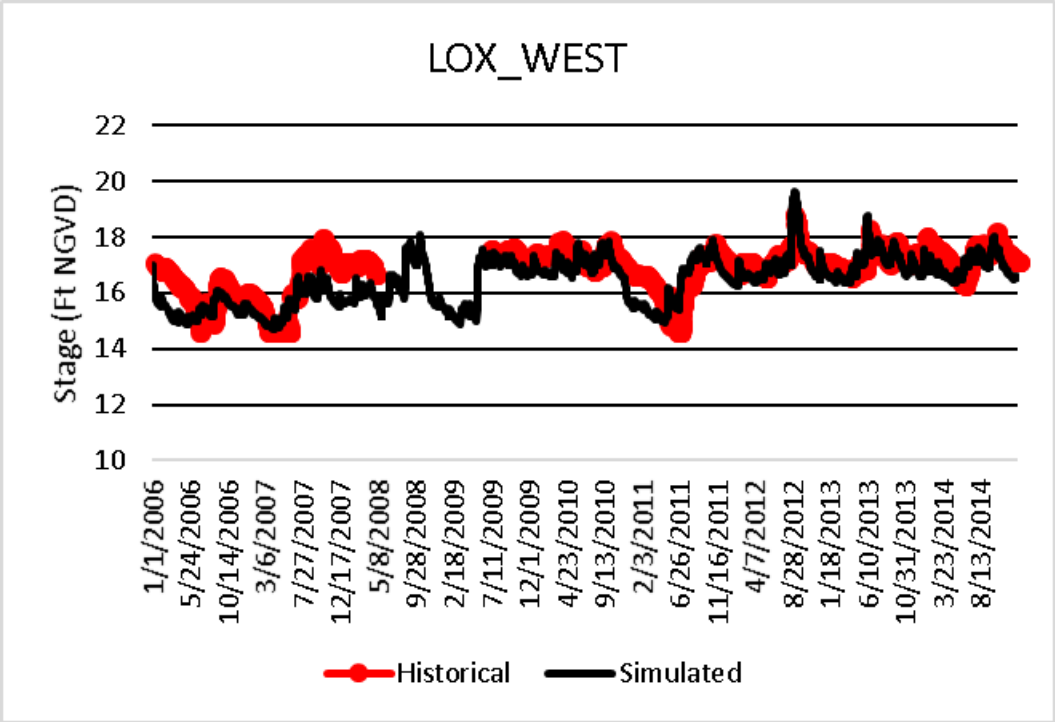

Figure B-31. Historical and simulated wetland gauge stage hydrograph (2006 – 2014) for Lox_West.

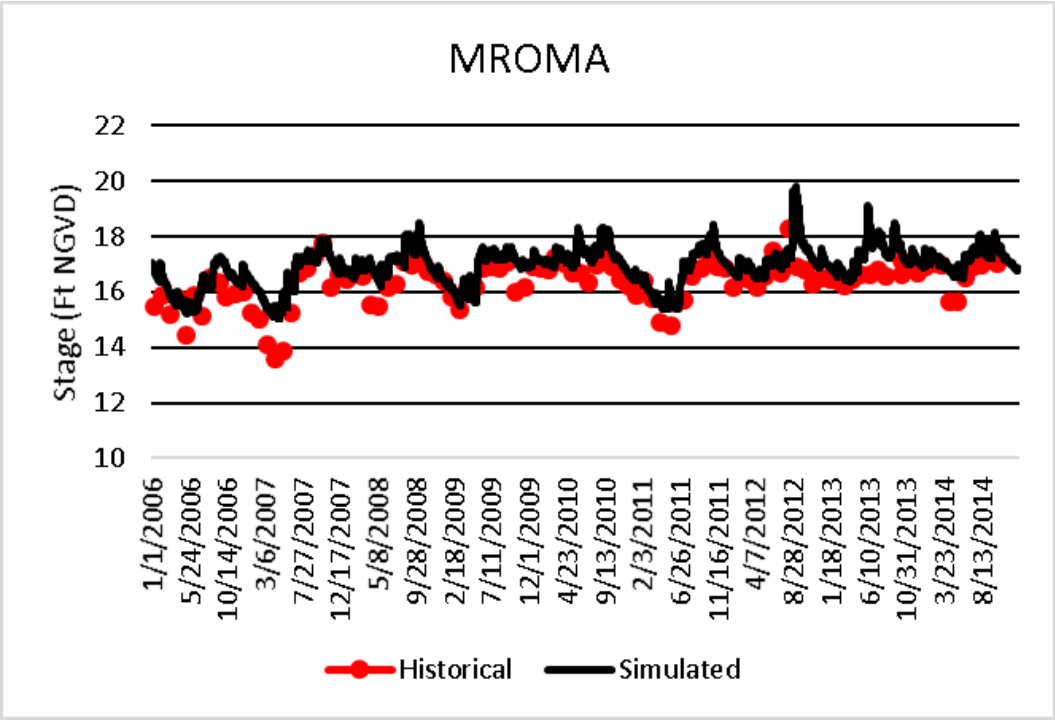

Figure B-32. Historical and simulated wetland gauge stage hydrograph (2006 – 2014) for MROMA.

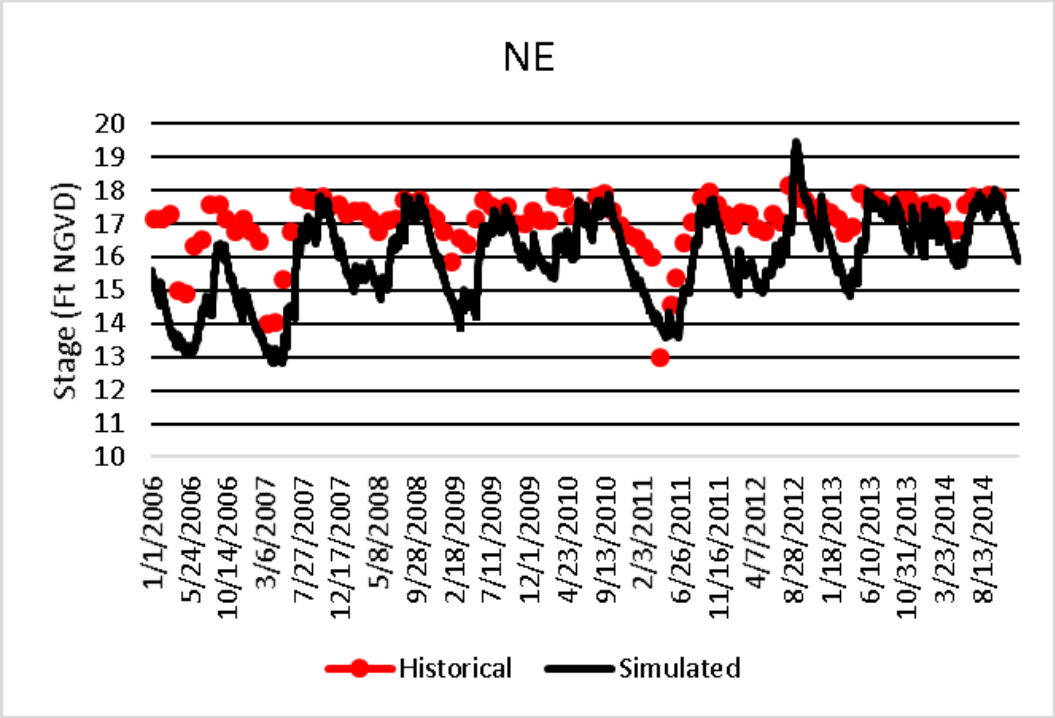

Figure B-33. Historical and simulated wetland gauge stage hydrograph (2006 – 2014) for NE.

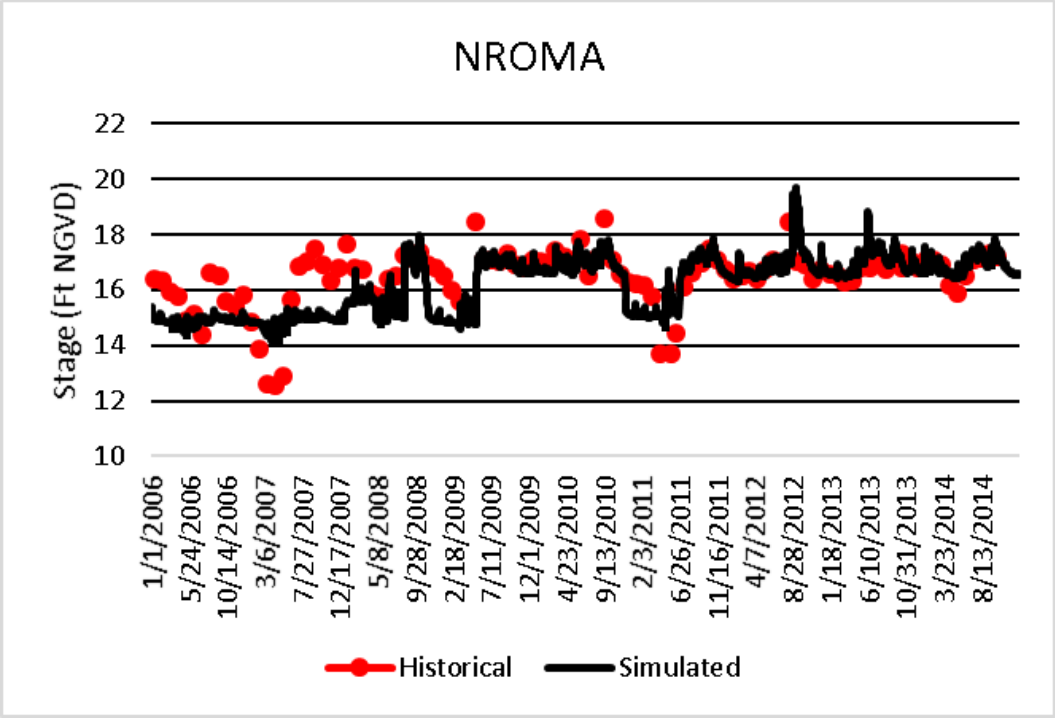

Figure B-34. Historical and simulated wetland gauge stage hydrograph (2006 – 2014) for NROMA.

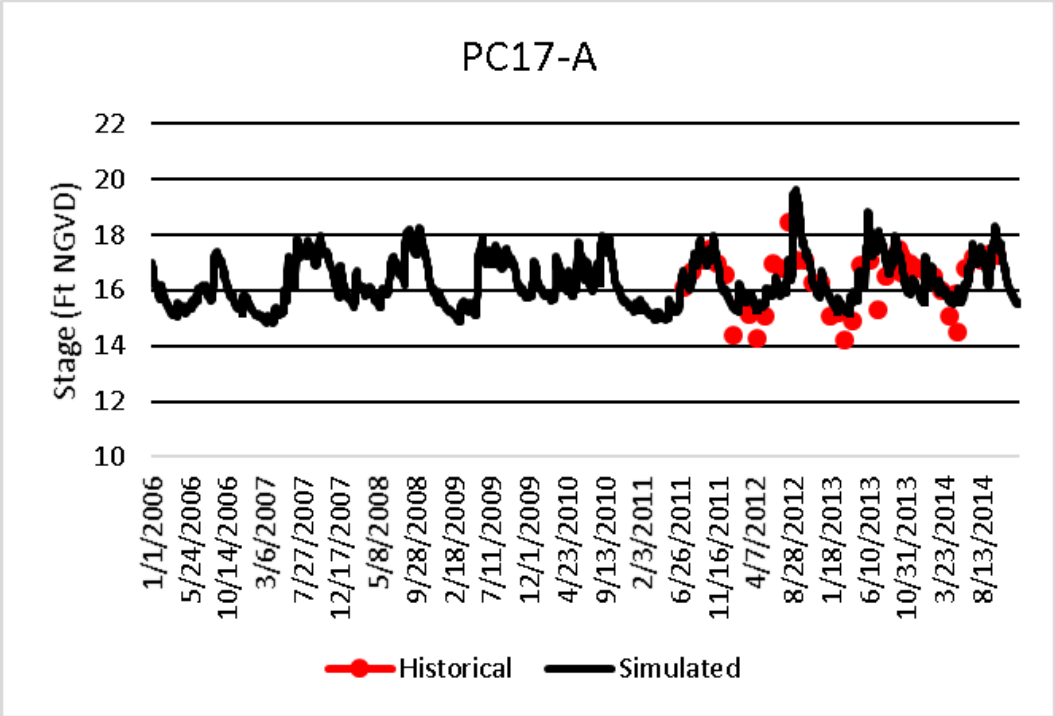

Figure B-35. Historical and simulated wetland gauge stage hydrograph (2006 – 2014) for PC17-A.

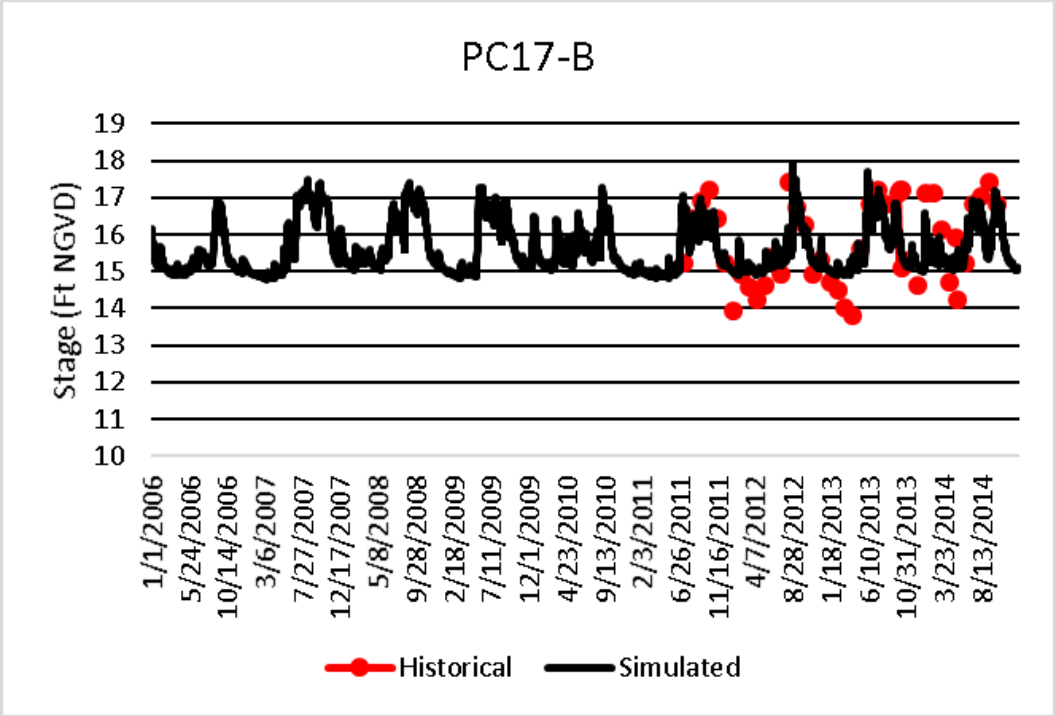

Figure B-36. Historical and simulated wetland gauge stage hydrograph (2006 – 2014) for PC17-B.

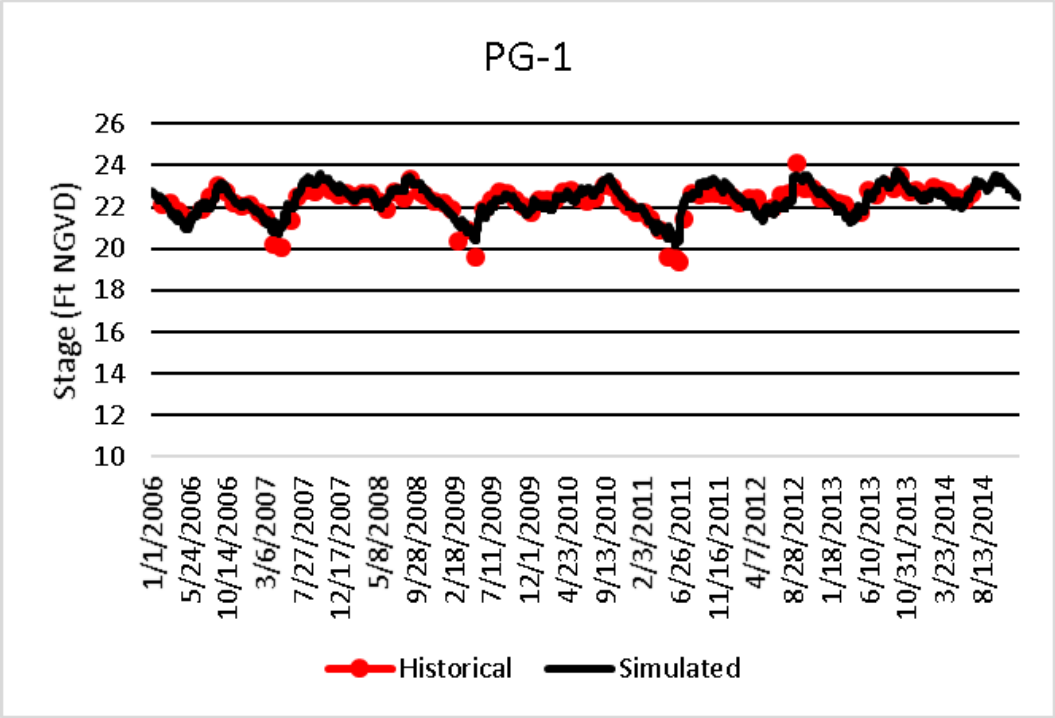

Figure B-37. Historical and simulated wetland gauge stage hydrograph (2006 – 2014) for PG-1.

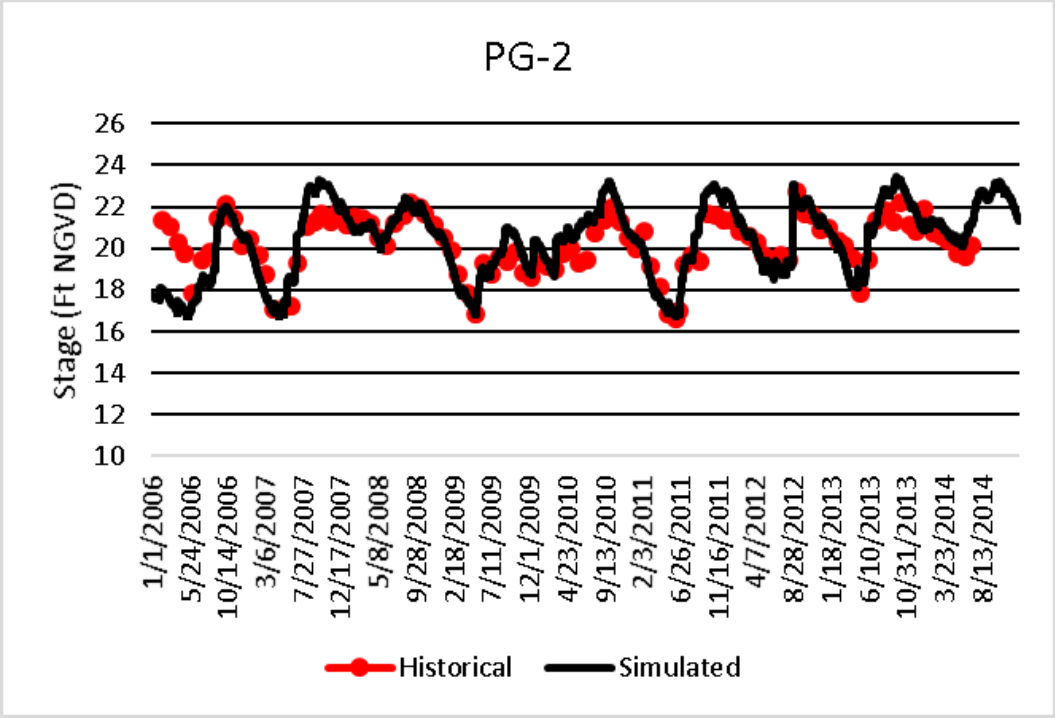

Figure B-38. Historical and simulated wetland gauge stage hydrograph (2006 – 2014) for PG-2.

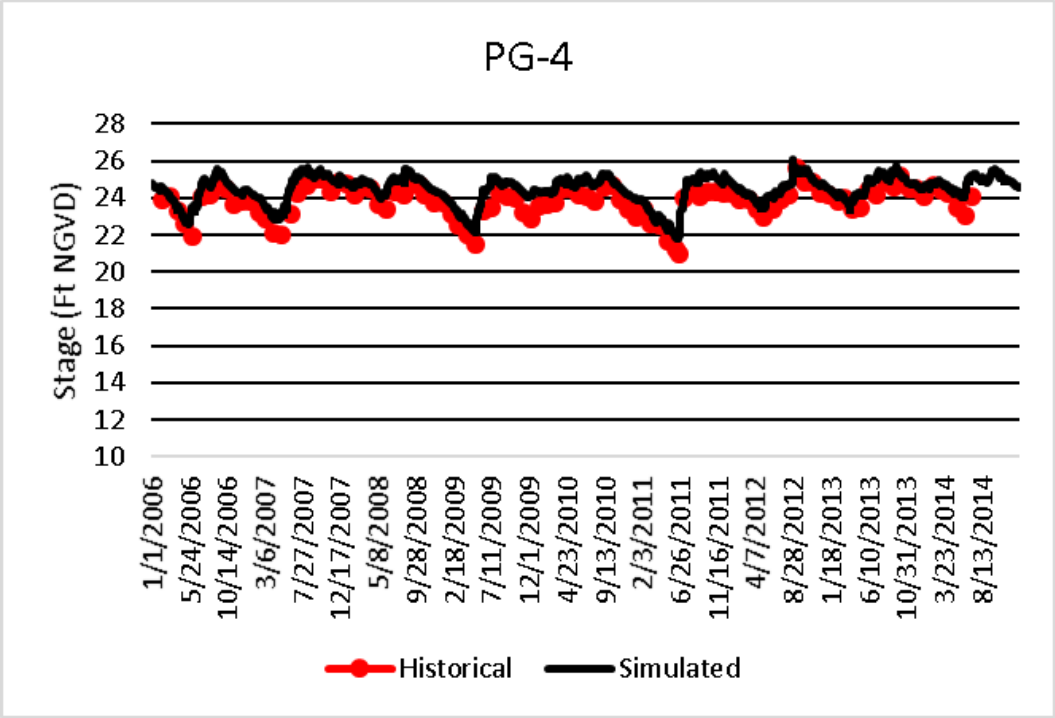

Figure B-39. Historical and simulated wetland gauge stage hydrograph (2006 – 2014) for PG-4.

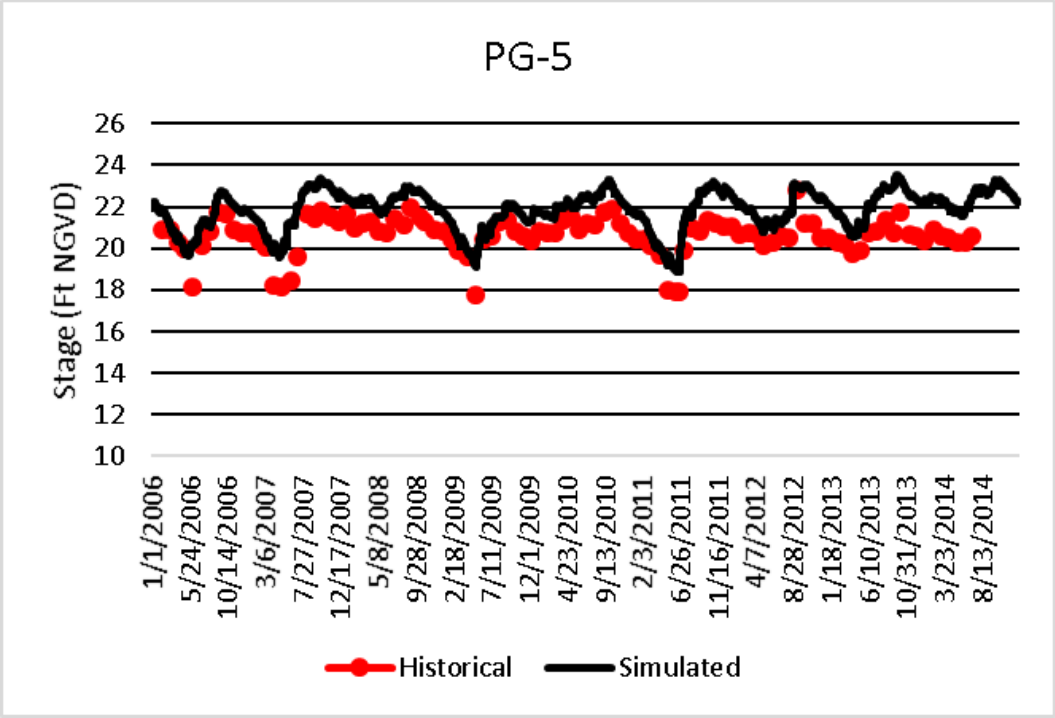

Figure B-40. Historical and simulated wetland gauge stage hydrograph (2006 – 2014) for PG-5.

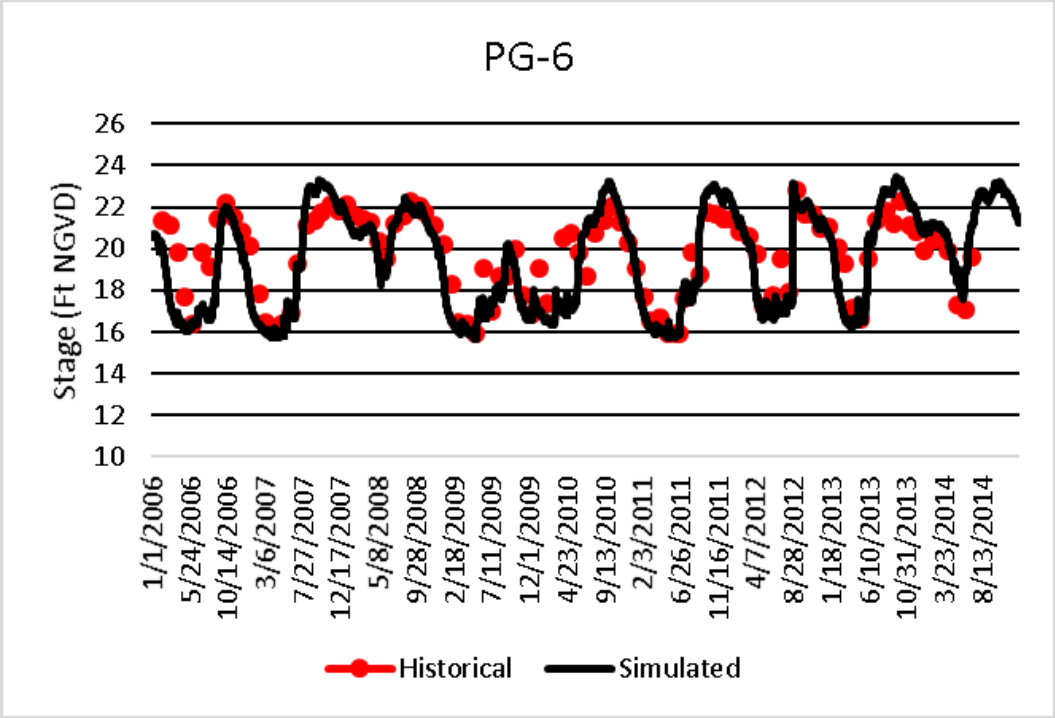

Figure B-41. Historical and simulated wetland gauge stage hydrograph (2006 – 2014) for PG-6.

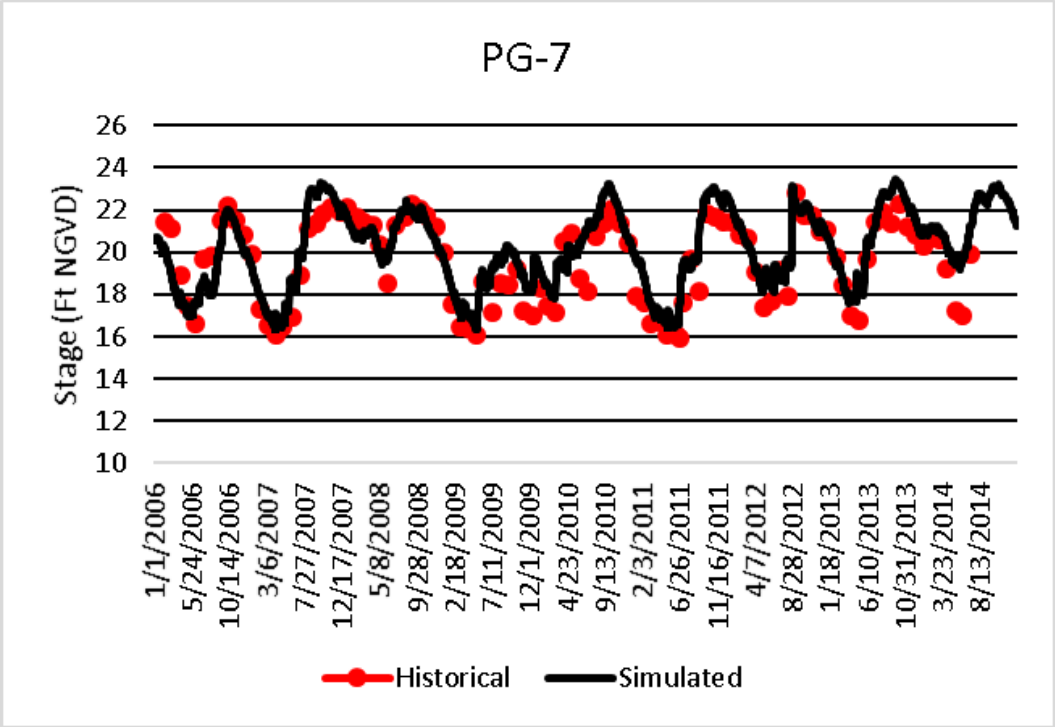

Figure B-42. Historical and simulated wetland gauge stage hydrograph (2006 – 2014) for PG-7.

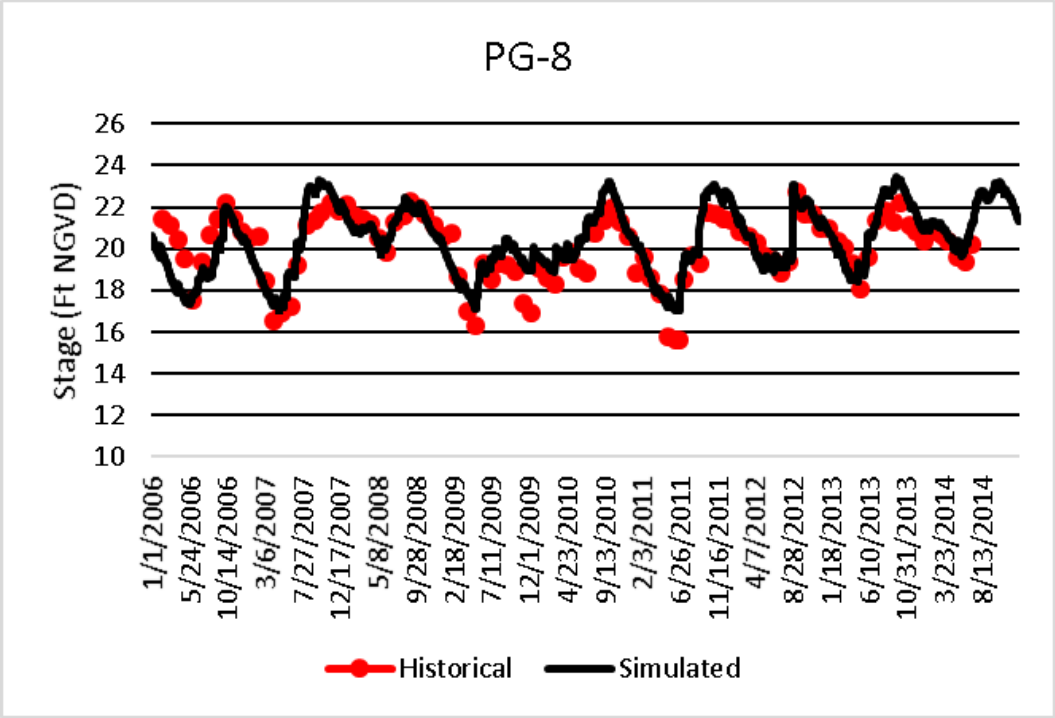

Figure B-43. Historical and simulated wetland gauge stage hydrograph (2006 – 2014) for PG-8.

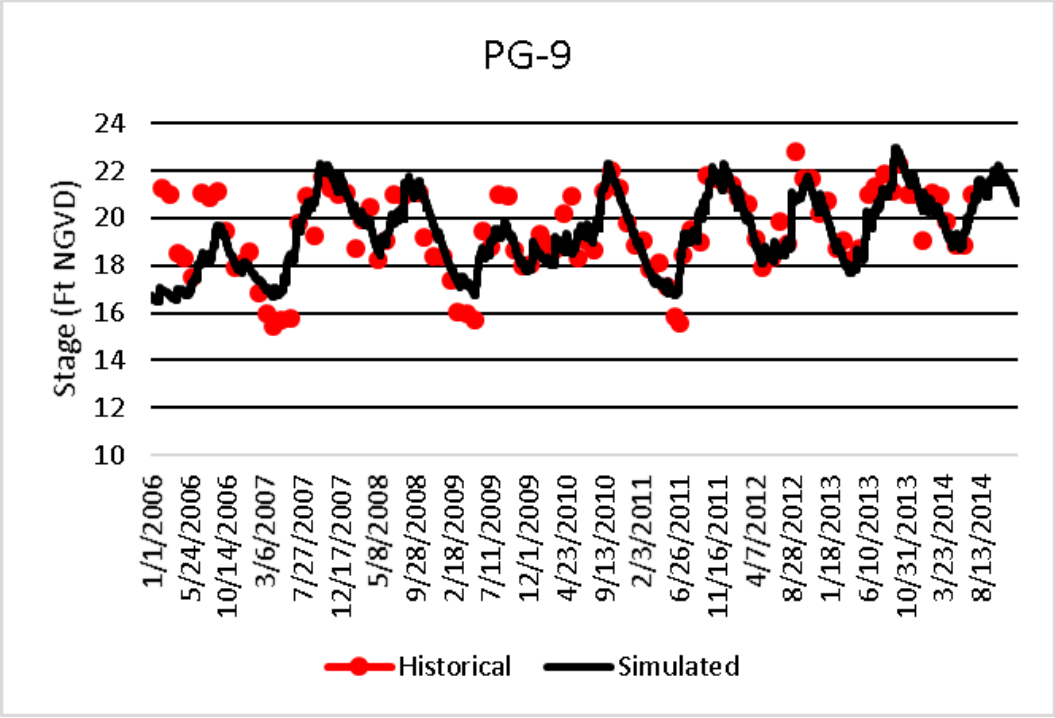

Figure B-44. Historical and simulated wetland gauge stage hydrograph (2006 – 2014) for PG-9.

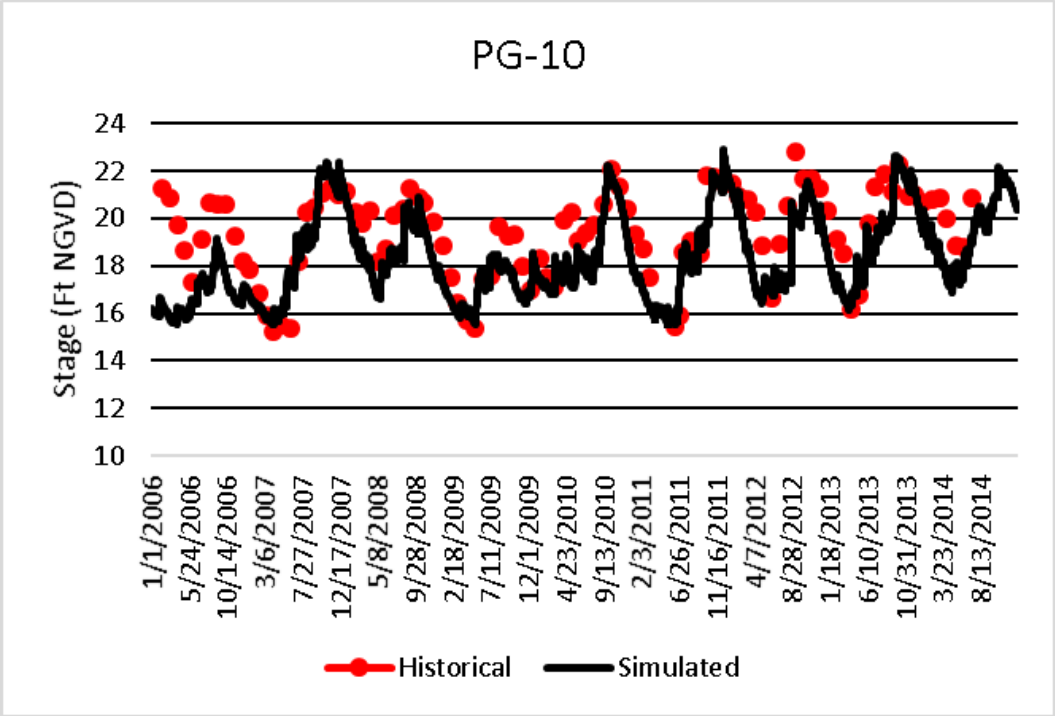

Figure B-45. Historical and simulated wetland gauge stage hydrograph (2006 – 2014) for PG-10.

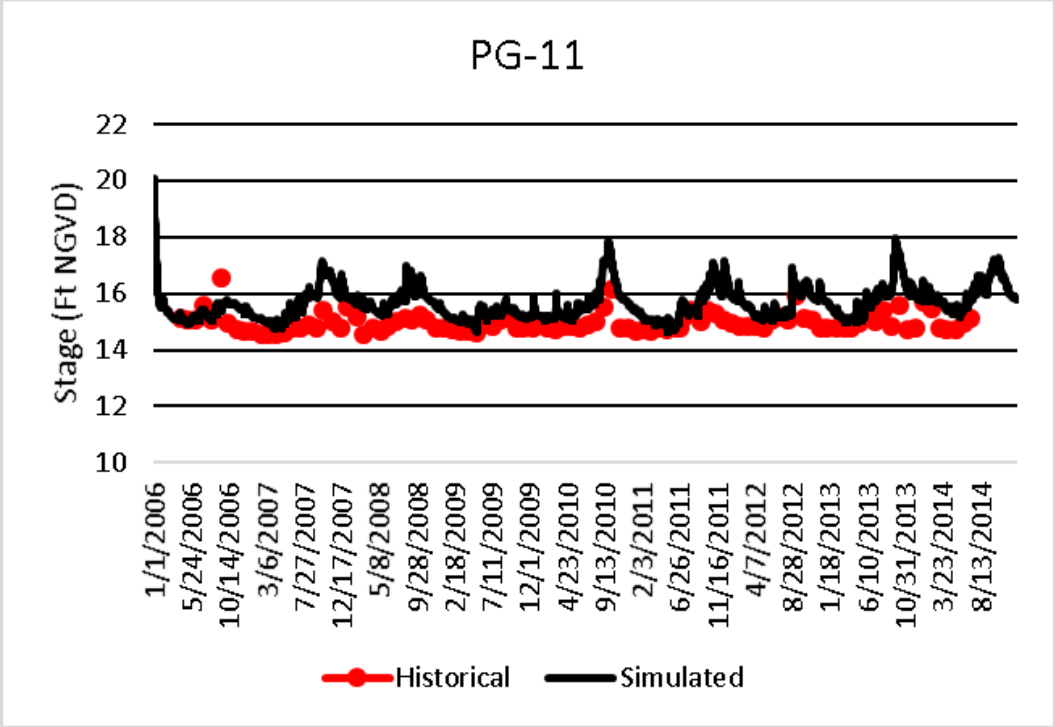

Figure B-46. Historical and simulated wetland gauge stage hydrograph (2006 – 2014) for PG-11.

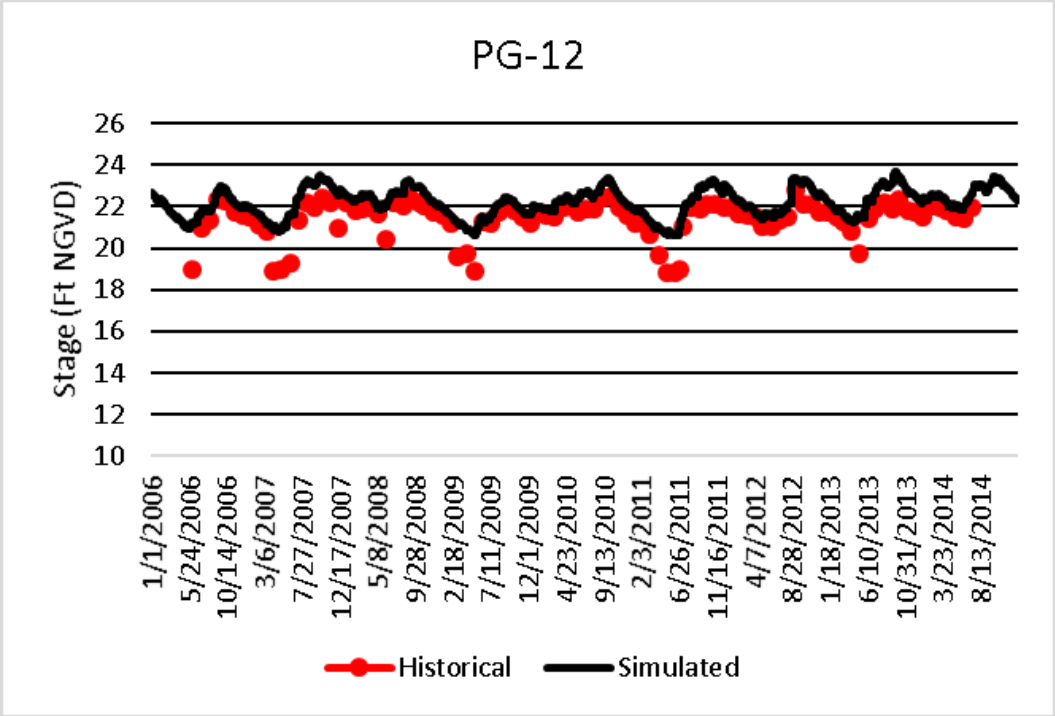

Figure B-47. Historical and simulated wetland gauge stage hydrograph (2006 – 2014) for PG-12.

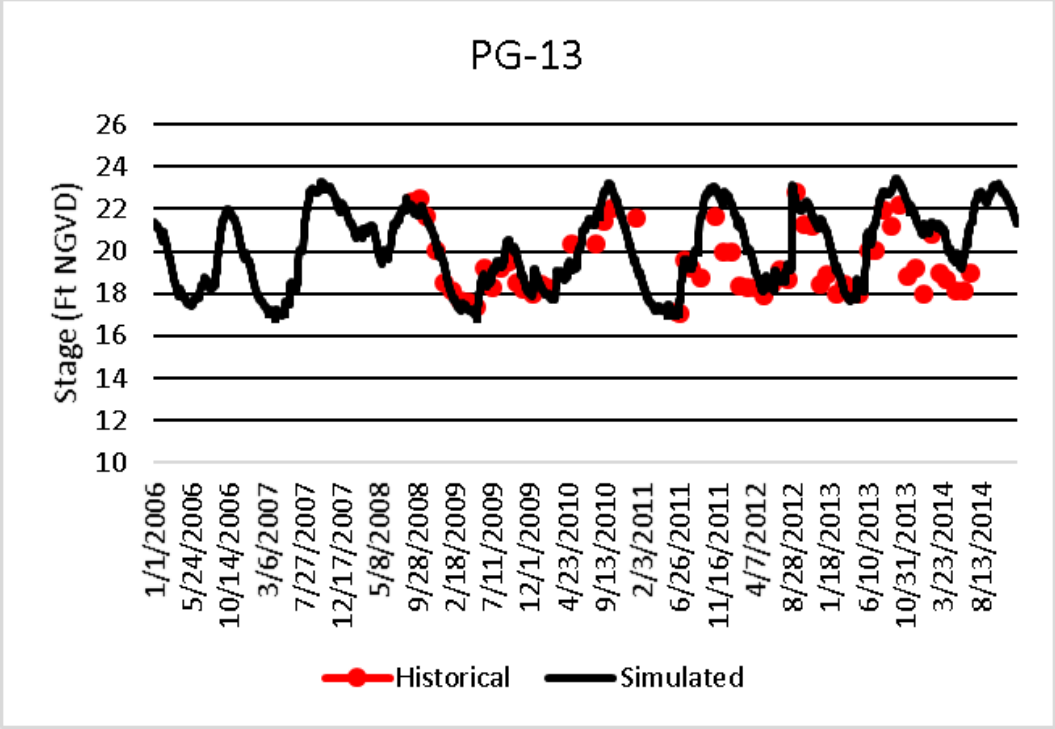

Figure B-48. Historical and simulated wetland gauge stage hydrograph (2006 – 2014) for PG-13.

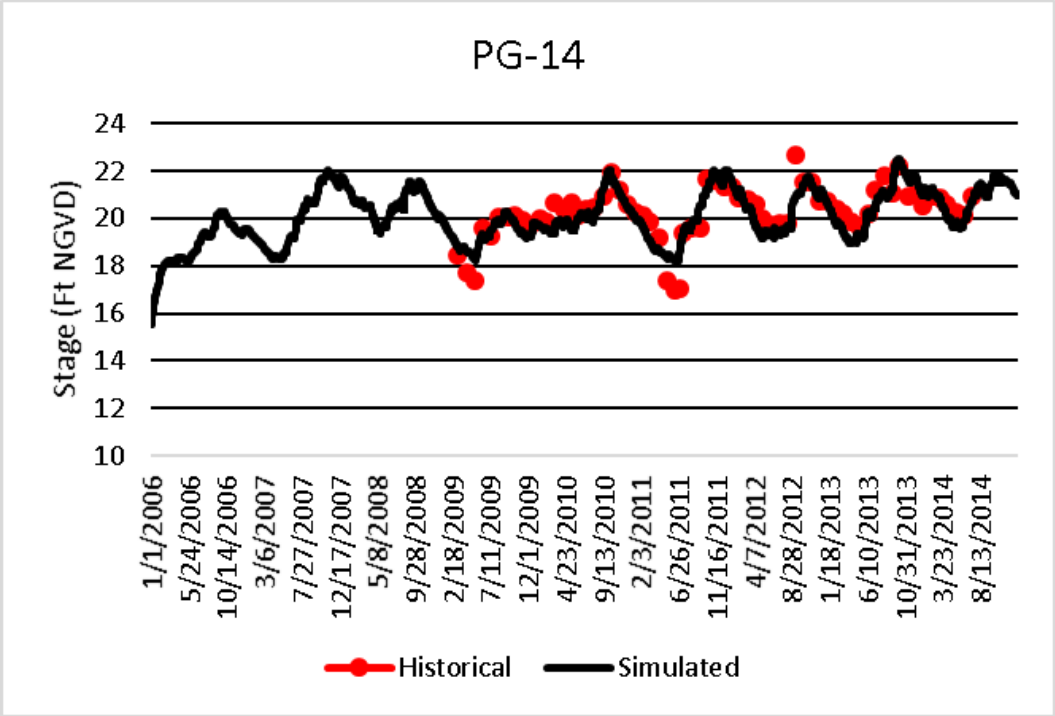

Figure B-49. Historical and simulated wetland gauge stage hydrograph (2006 – 2014) for PG-14.

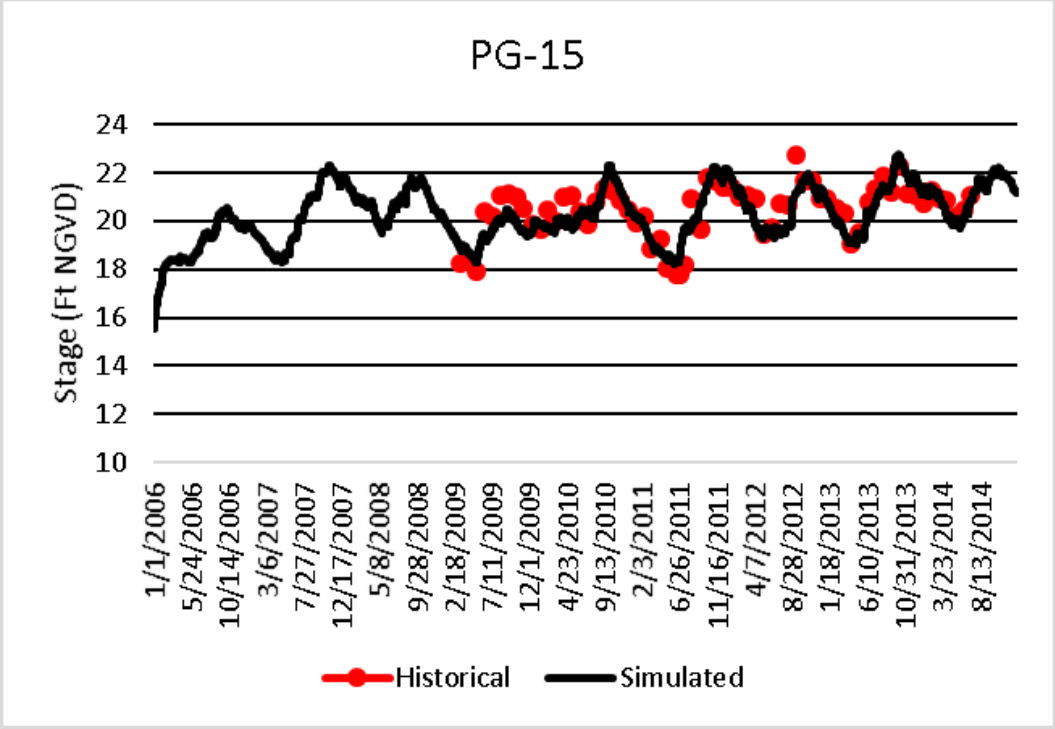

Figure B-50. Historical and simulated wetland gauge stage hydrograph (2006 – 2014) for PG-15.

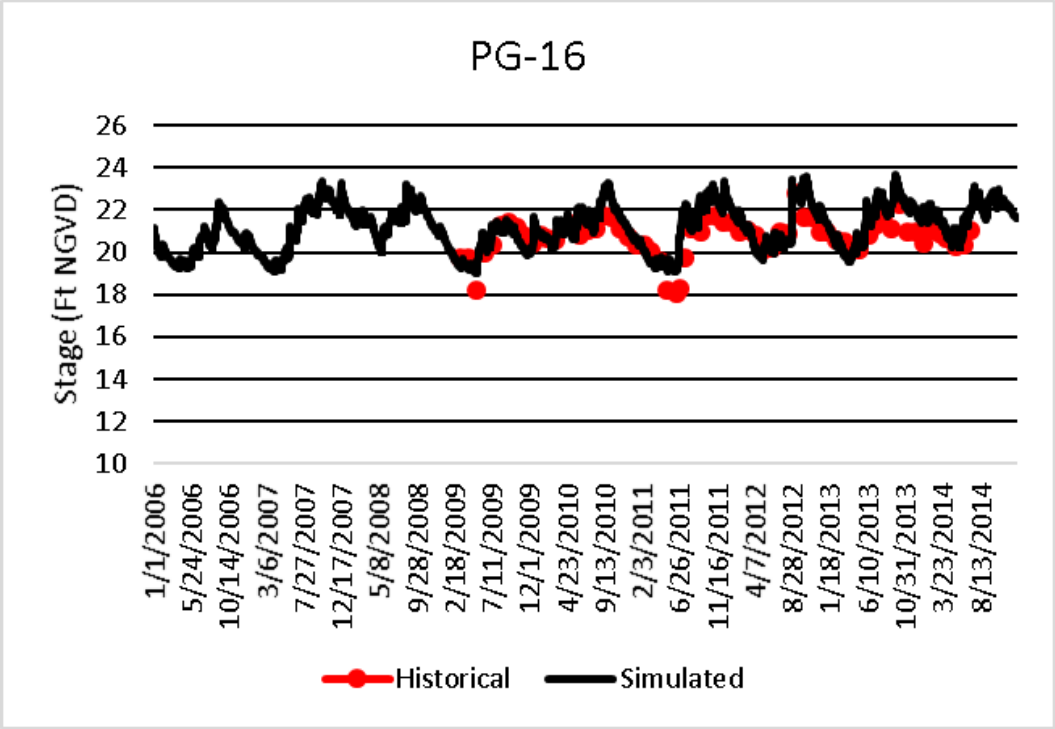

Figure B-51. Historical and simulated wetland gauge stage hydrograph (2006 – 2014) for PG-16.

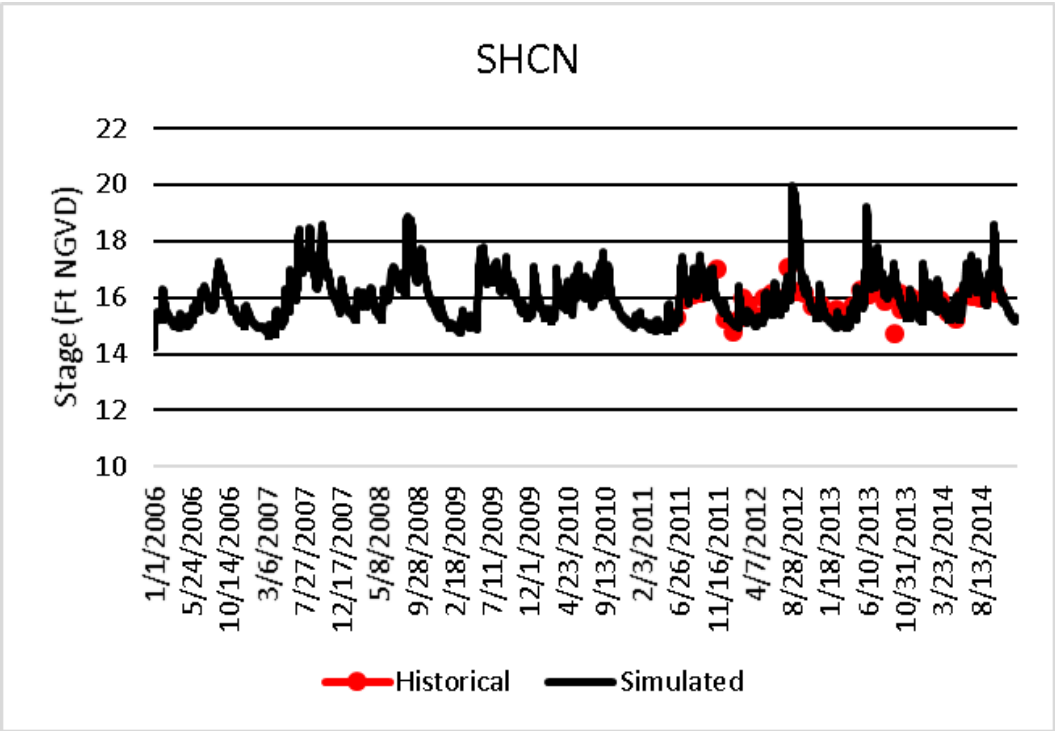

Figure B-52. Historical and simulated wetland gauge stage hydrograph (2006 – 2014) for SHCN.

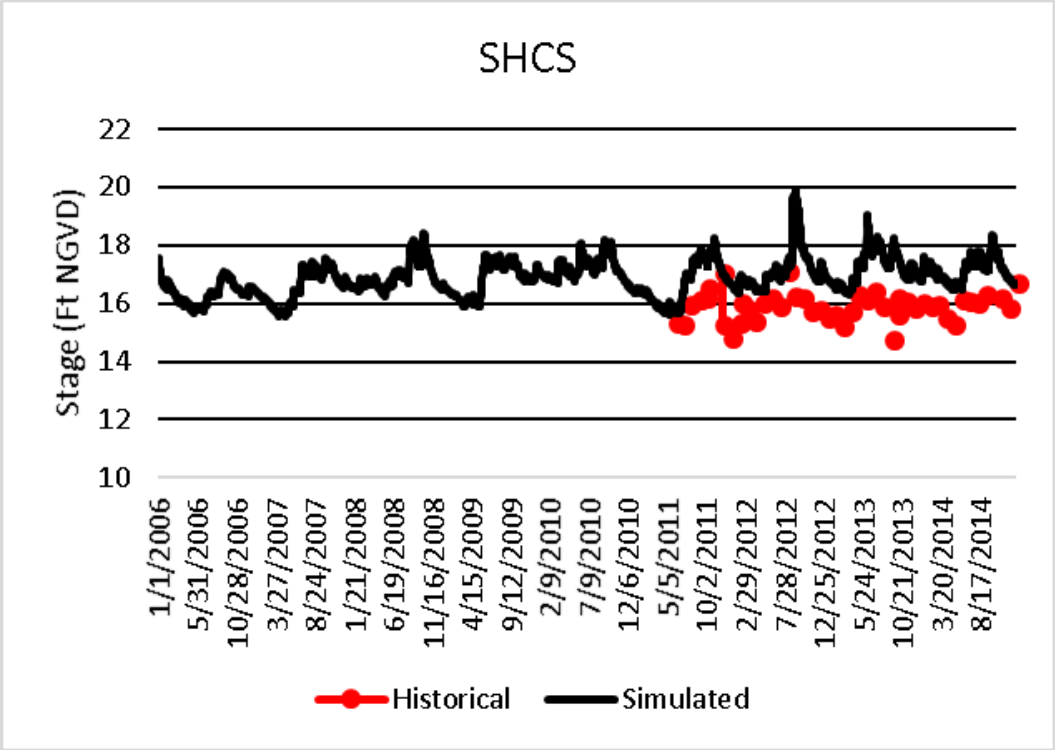

Figure B-53. Historical and simulated wetland gauge stage hydrograph (2006 – 2014) for SHCS.

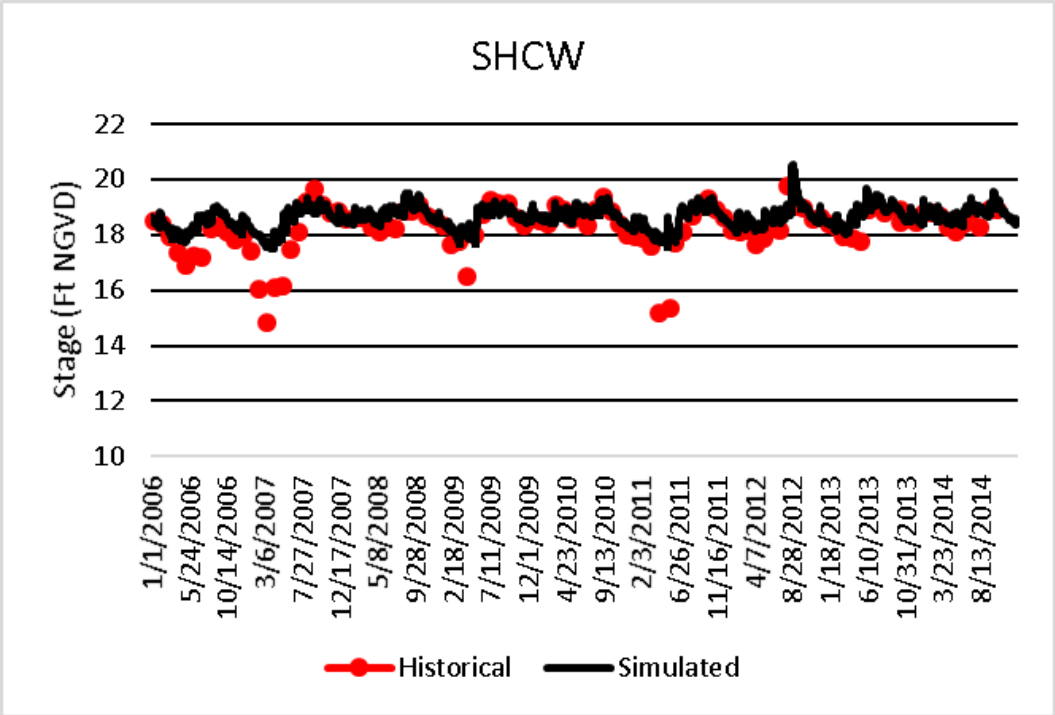

Figure B-54. Historical and simulated wetland gauge stage hydrograph (2006 – 2014) for SHCW.

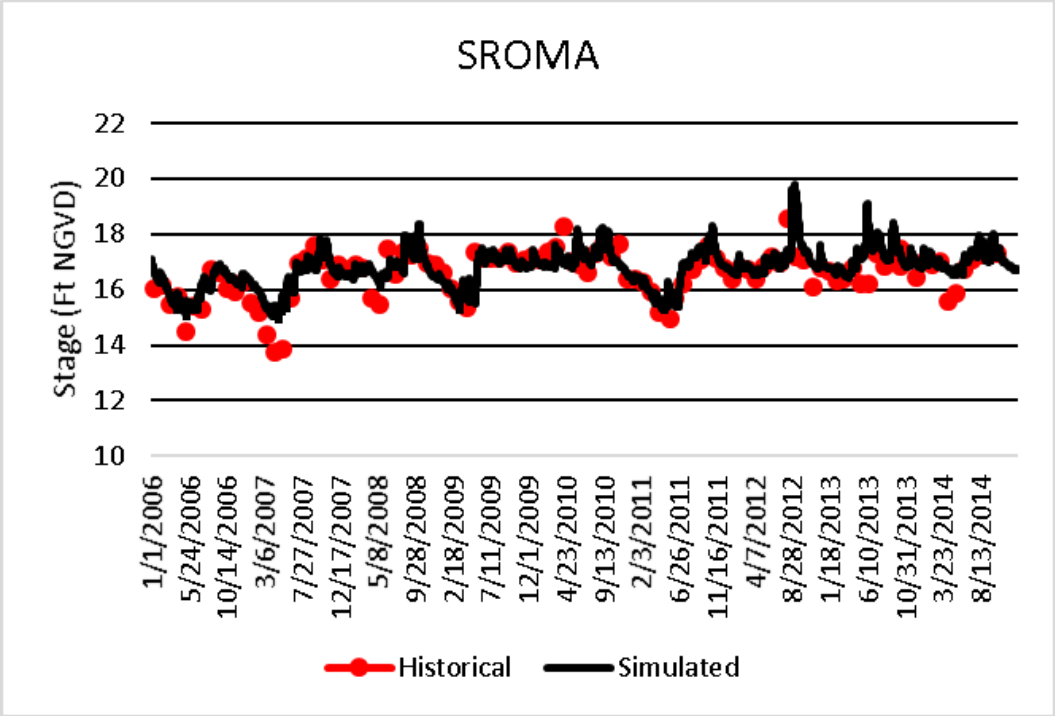

Figure B-55. Historical and simulated wetland gauge stage hydrograph (2006 – 2014) for SROMA.

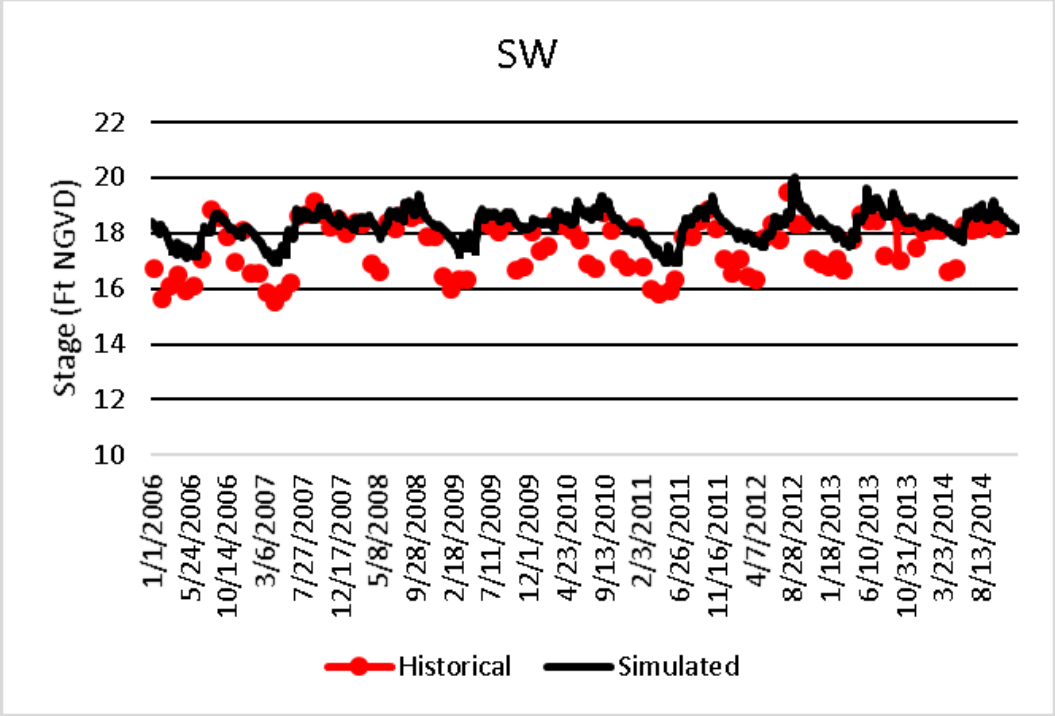

Figure B-56. Historical and simulated wetland gauge stage hydrograph (2006 – 2014) for SW.

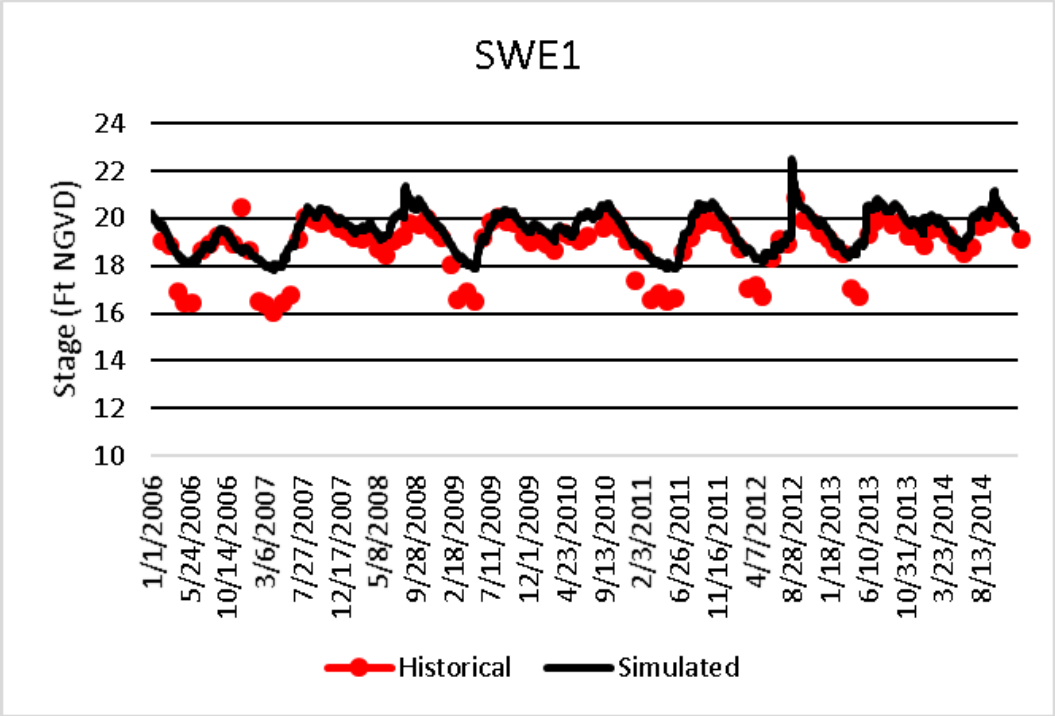

Figure B-57. Historical and simulated wetland gauge stage hydrograph (2006 – 2014) for SWE1.

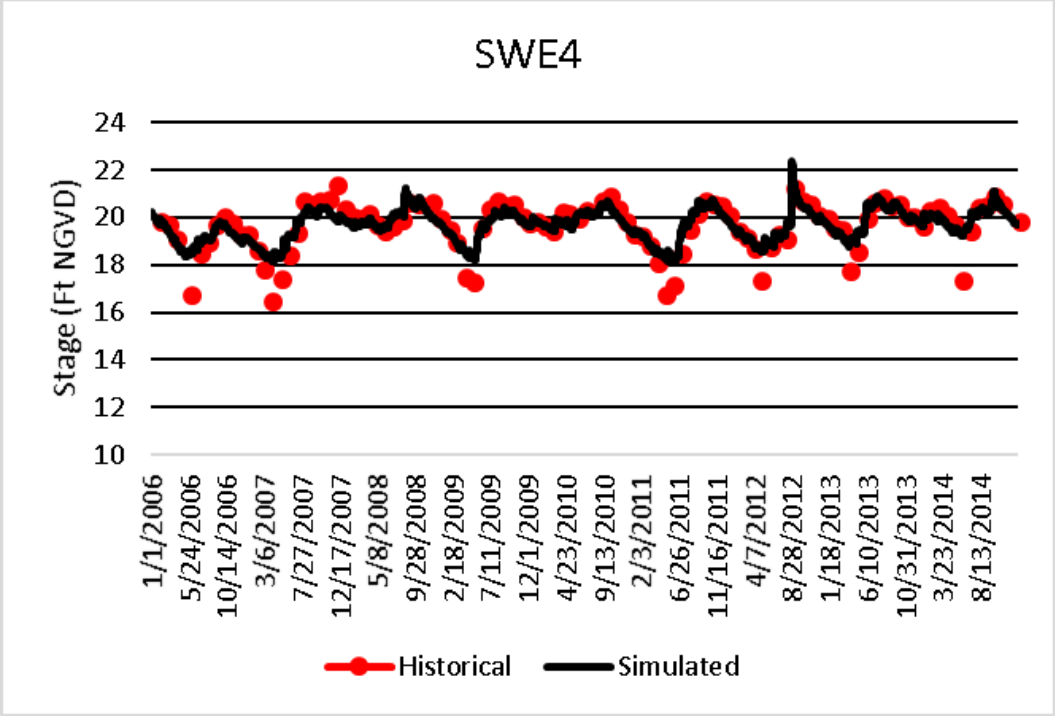

Figure B-58. Historical and simulated wetland gauge stage hydrograph (2006 – 2014) for SWE4.

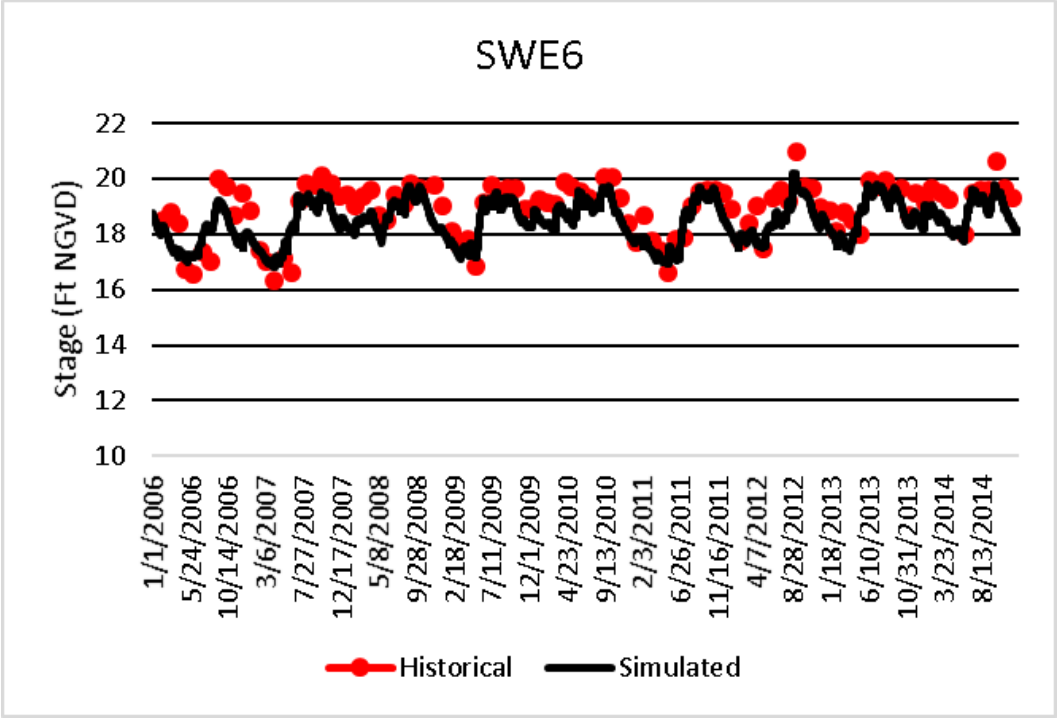

Figure B-59. Historical and simulated wetland gauge stage hydrograph (2006 – 2014) for SWE6.

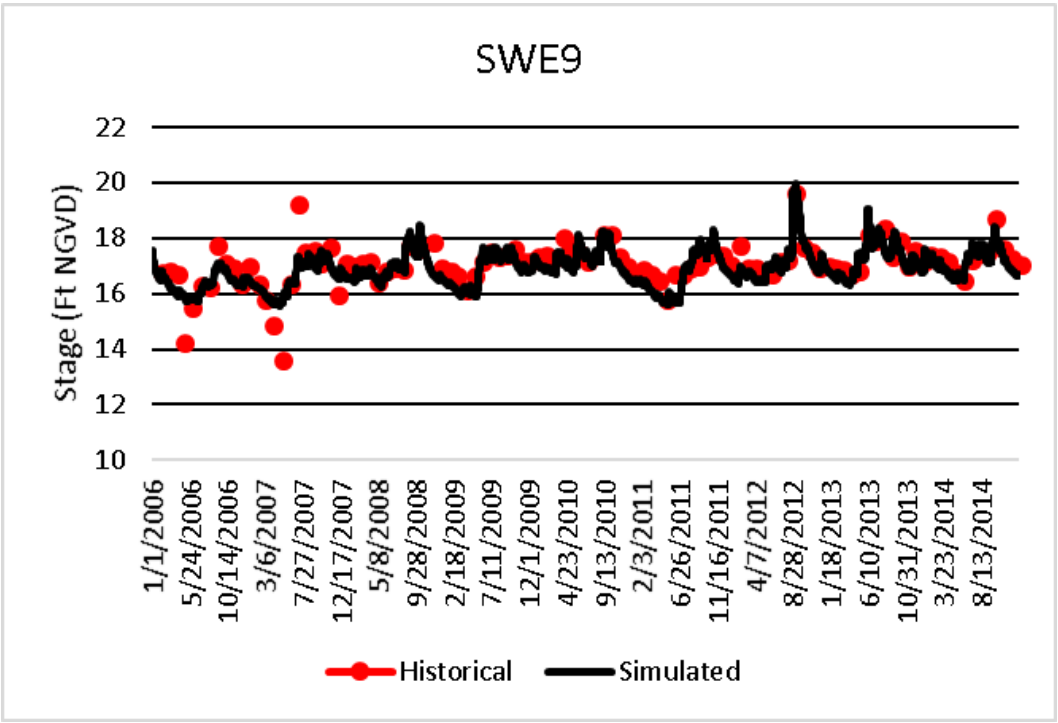

Figure B-60. Historical and simulated wetland gauge stage hydrograph (2006 – 2014) for SWE9.

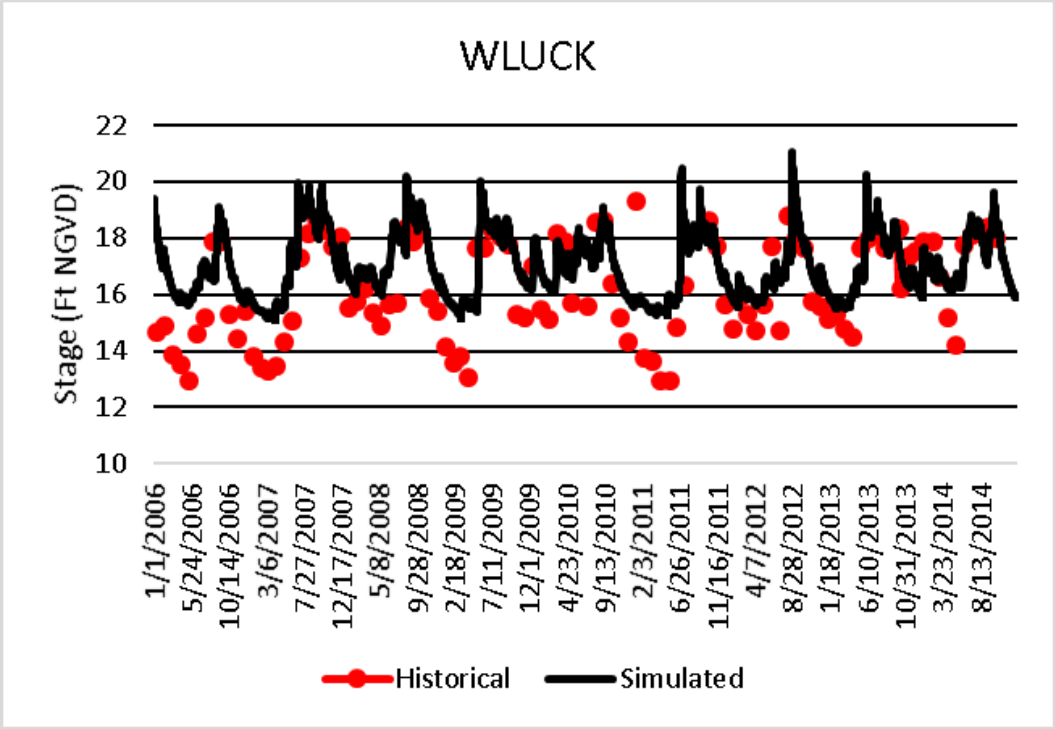

Figure B-61. Historical and simulated wetland gauge stage hydrograph (2006 – 2014) for WLUCK.

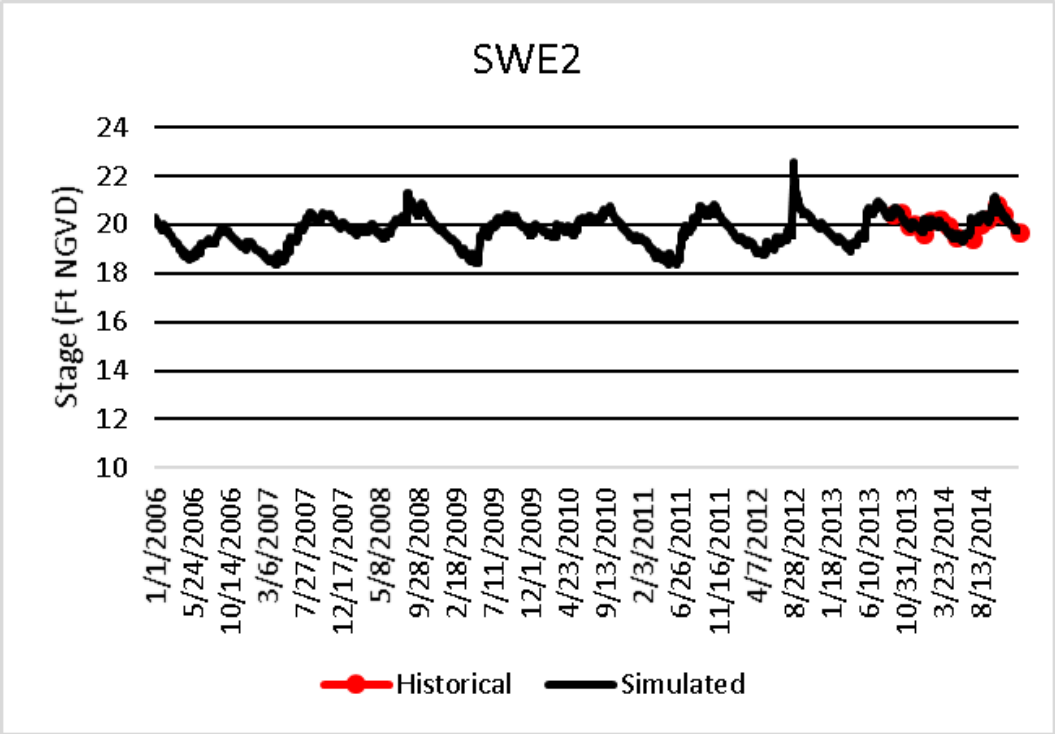

Figure B-62. Historical and simulated wetland gauge stage hydrograph (2006 – 2014) for SWE2 (sequestered location).

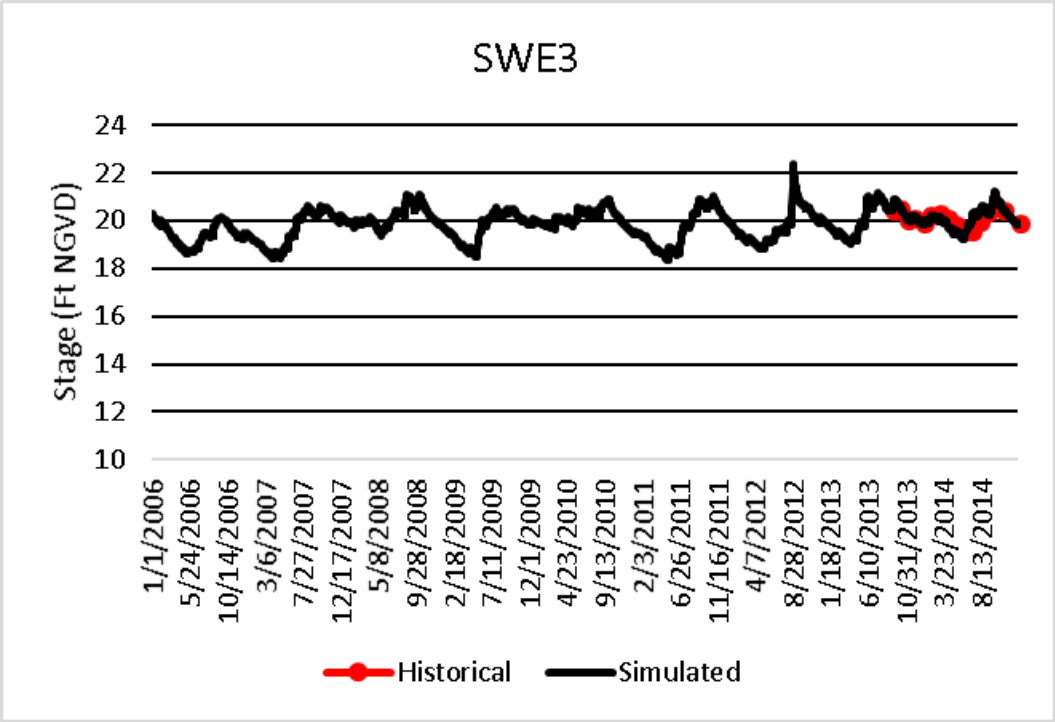

Figure B-63. Historical and simulated wetland gauge stage hydrograph (2006 – 2014) for SWE3 (sequestered location).

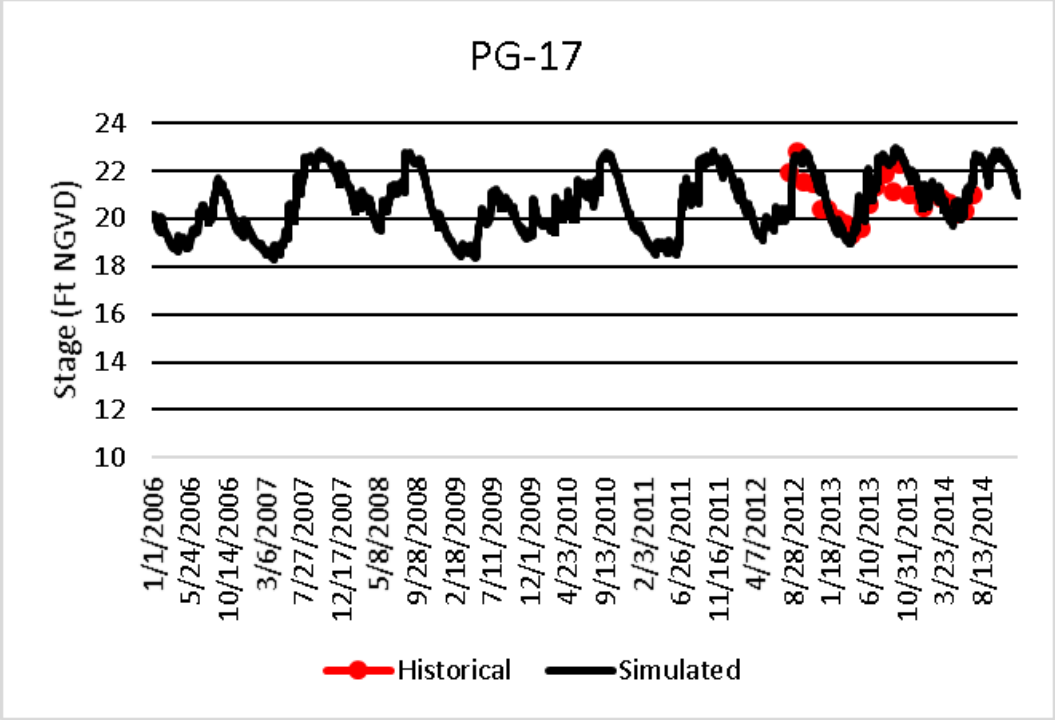

Figure B-64. Historical and simulated wetland gauge stage hydrograph (2006 – 2014) for PG-17 (sequestered location).

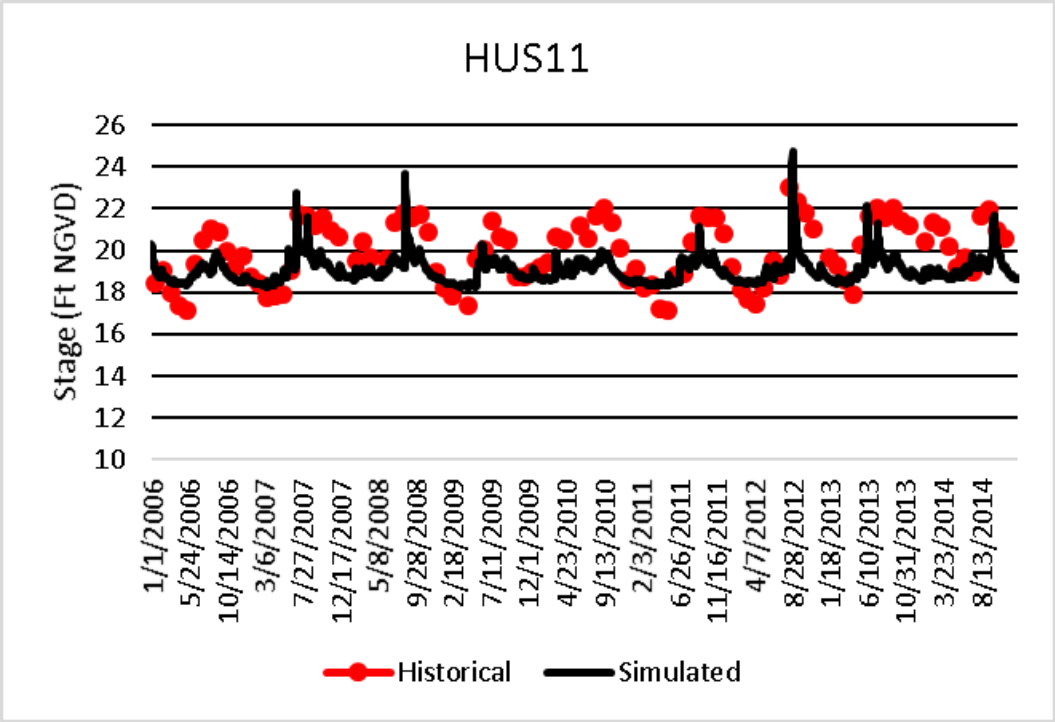

Figure B-65. Historical and simulated wetland gauge stage hydrograph (2006 – 2014) for HUS11 (sequestered location).

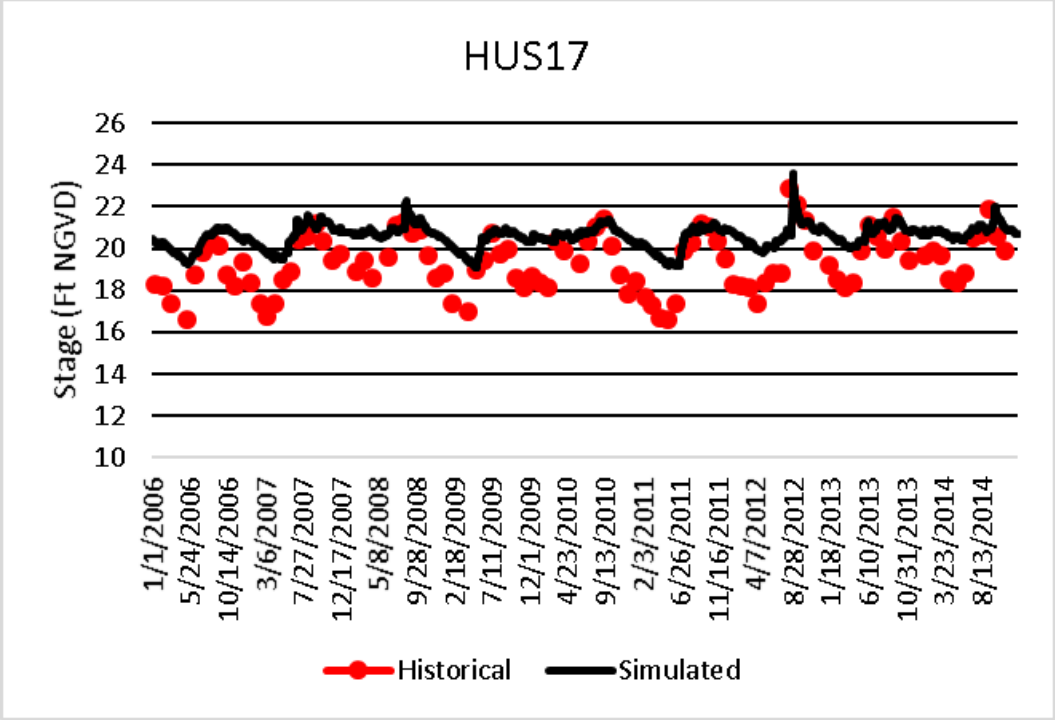

Figure B-66. Historical and simulated wetland gauge stage hydrograph (2006 – 2014) for HUS17 (sequestered location).

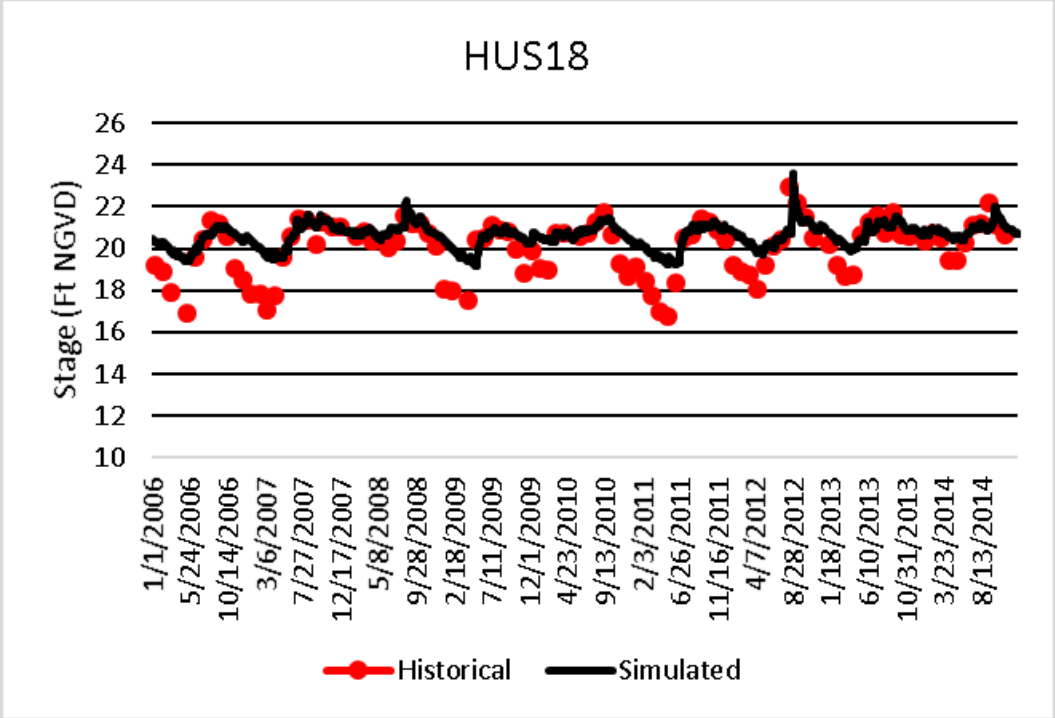

Figure B-67. Historical and simulated wetland gauge stage hydrograph (2006 – 2014) for HUS18 (sequestered location).

APPENDIX C: WRAP CELLS

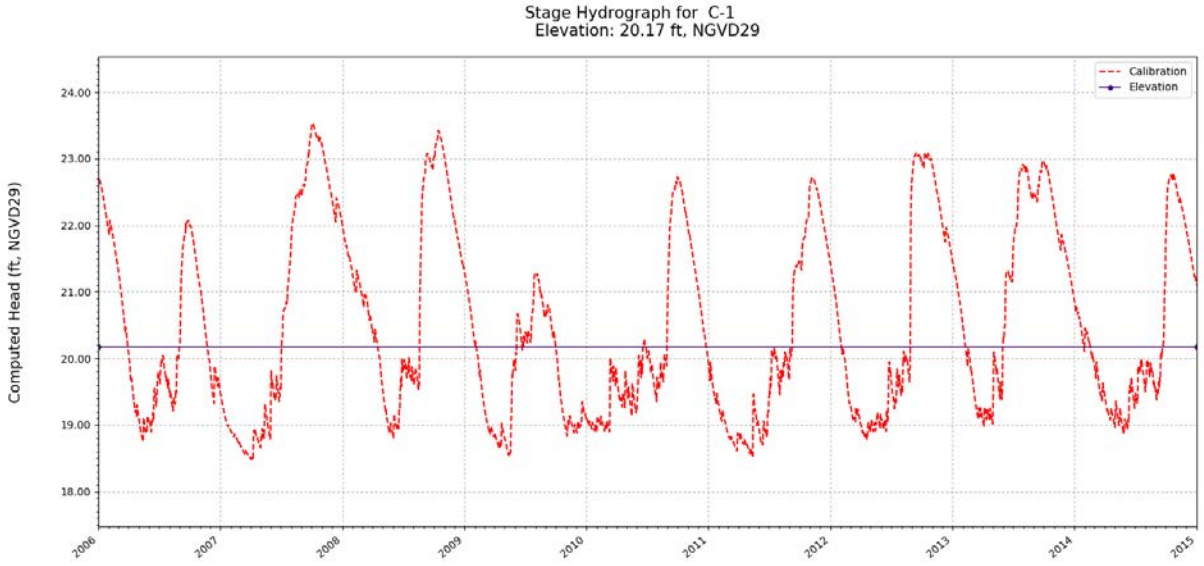

Figure C-1. Simulated stage hydrograph (2006 – 2014) and model cell topography for WRAP cell C-1.

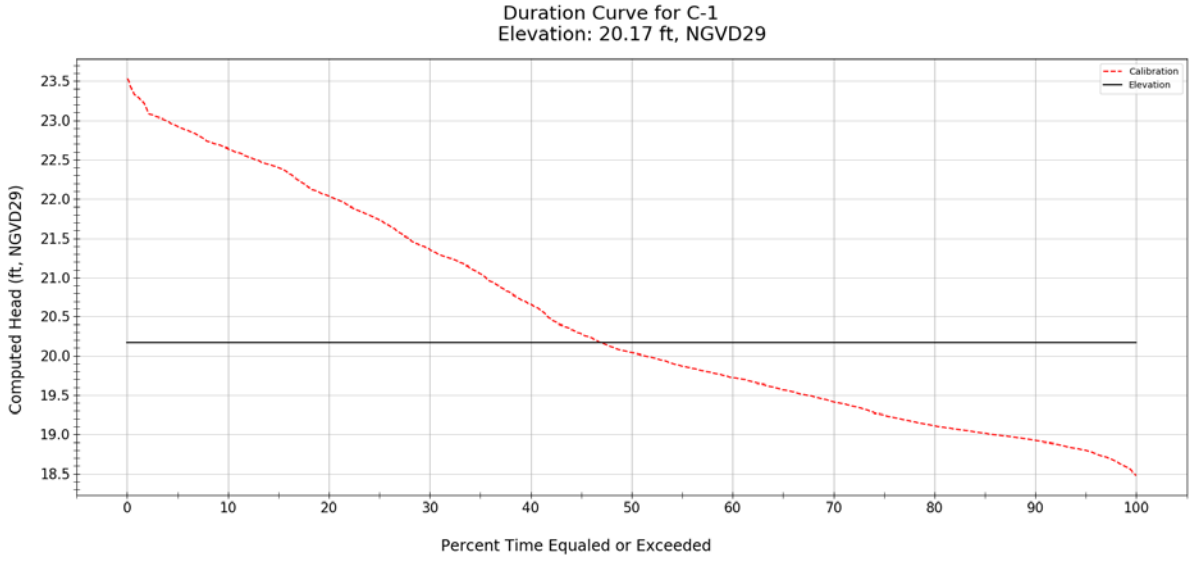

Figure C-2. Simulated stage duration curve (2006 – 2014) and model cell topography for WRAP cell C-1.

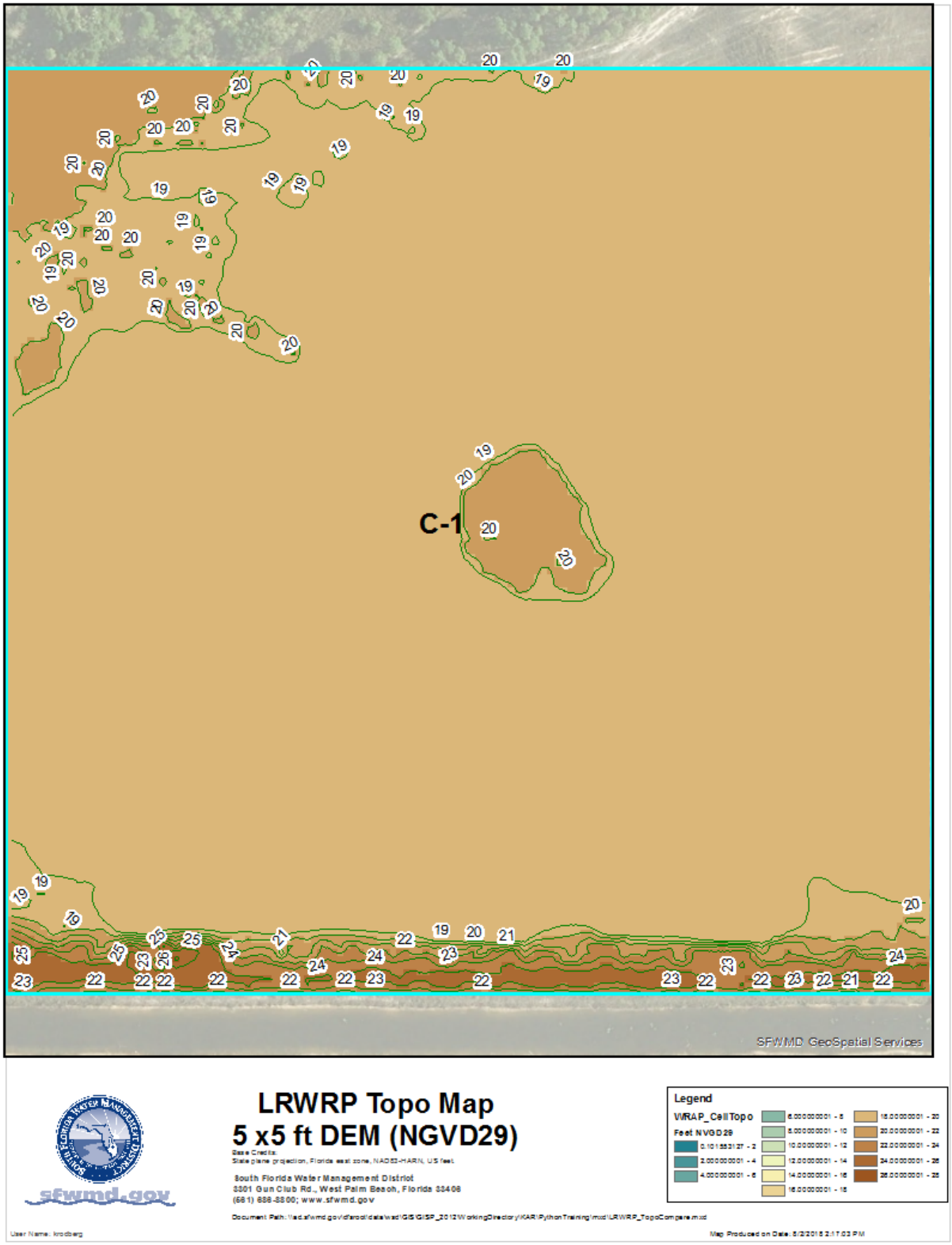

Figure C-3. Variation of model cell topography based on SFWMD's 5 ft LiDAR within WRAP cell C-1.

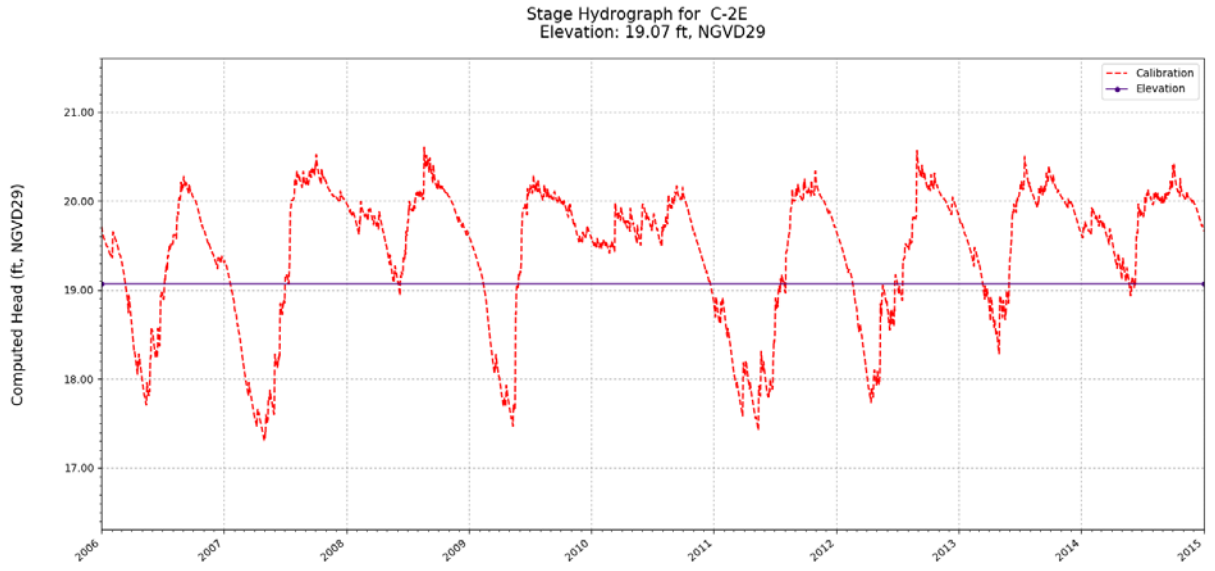

Figure C-4. Simulated stage hydrograph (2006 – 2014) and model cell topography for WRAP cell C-2E.

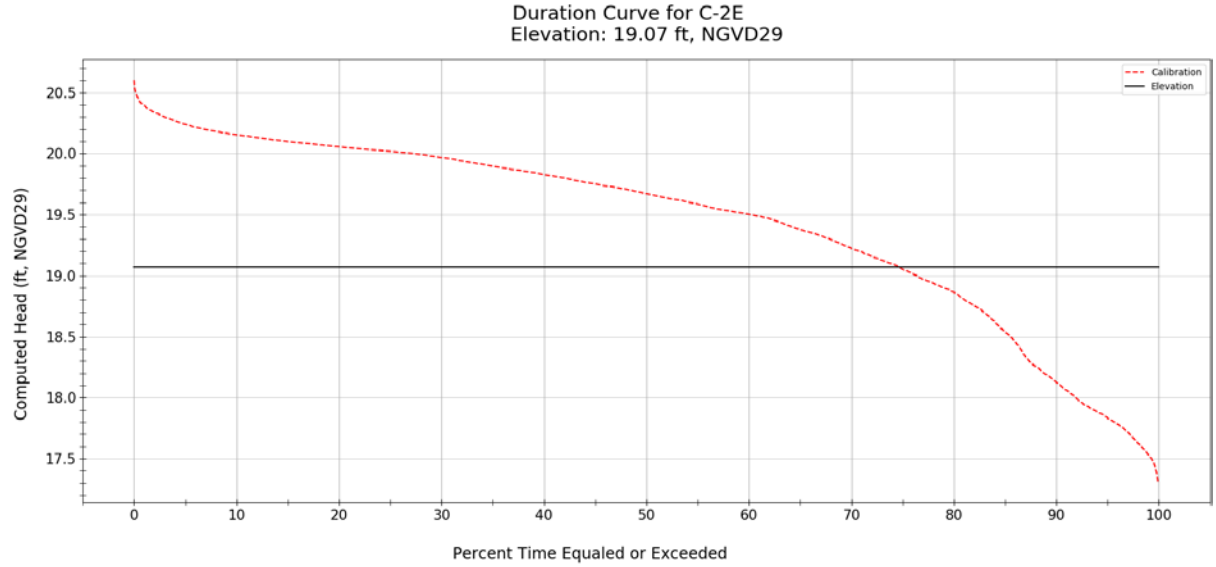

Figure C-5. Simulated stage duration curve (2006 – 2014) and model cell topography for WRAP cell C-2E.

Figure C-6. Variation of model cell topography based on SFWMD's 5 ft LiDAR within WRAP cell C-2E.

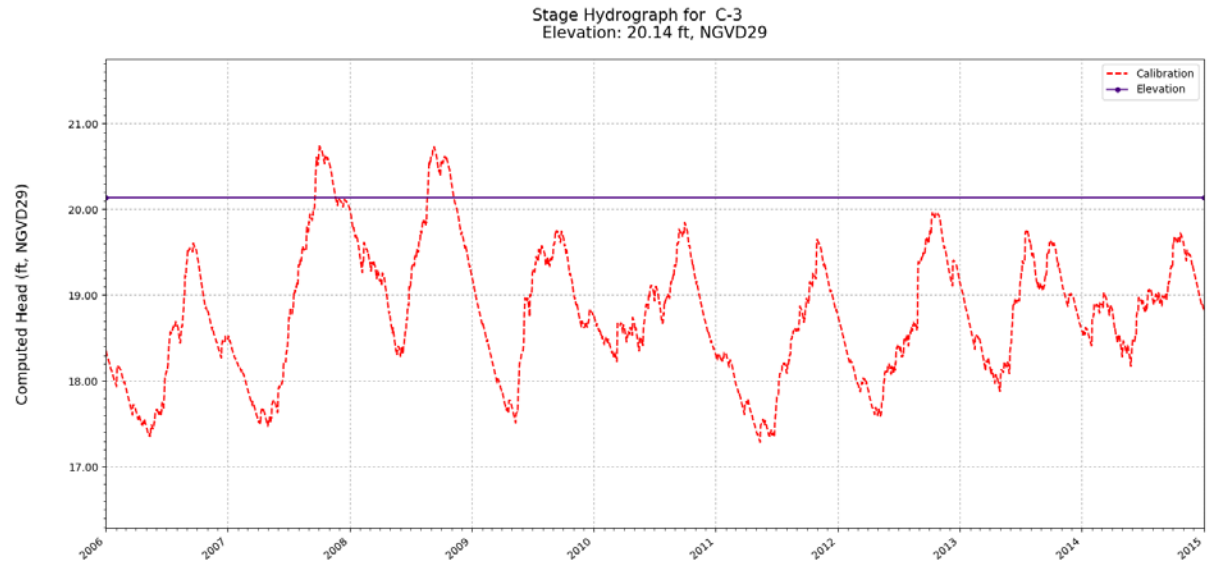

Figure C-7. Simulated stage hydrograph (2006 – 2014) and model cell topography for WRAP cell C-3.

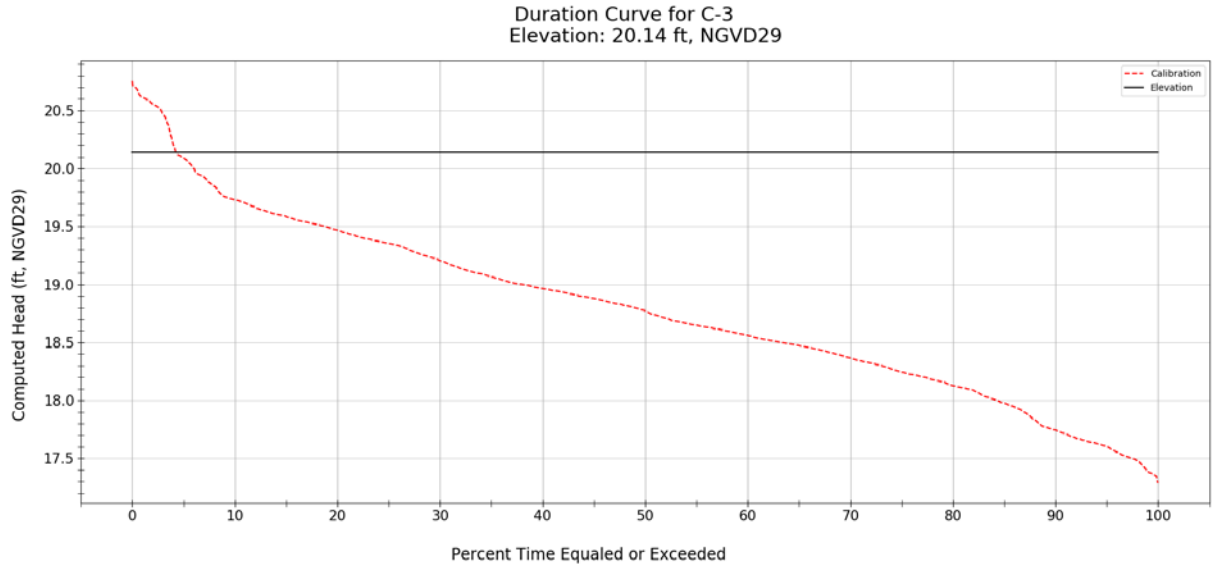

Figure C-8. Simulated stage duration curve (2006 – 2014) and model cell topography for WRAP cell C-3.

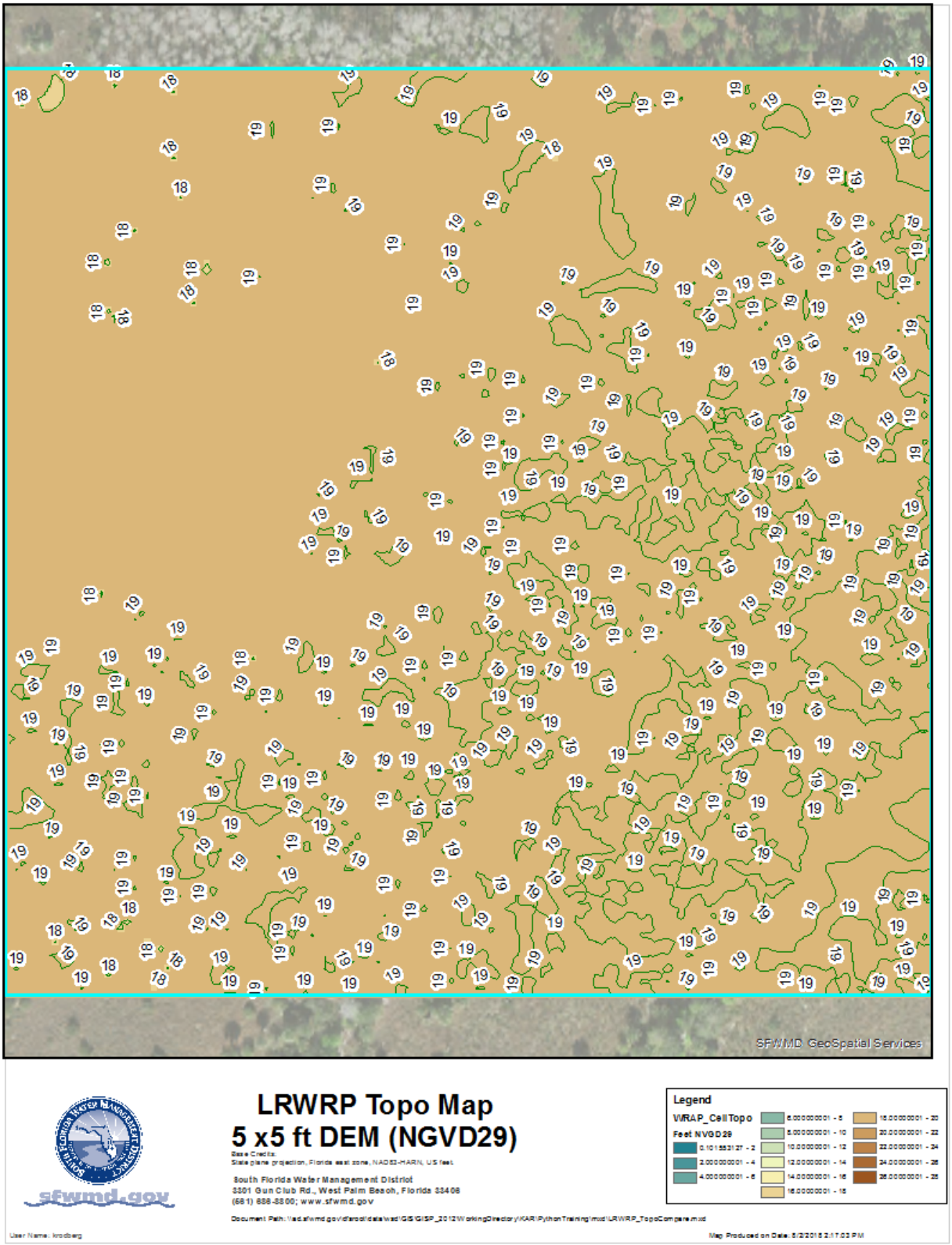

Figure C-9. Variation of model cell topography based on SFWMD's 5 ft LiDAR within WRAP cell C-3.

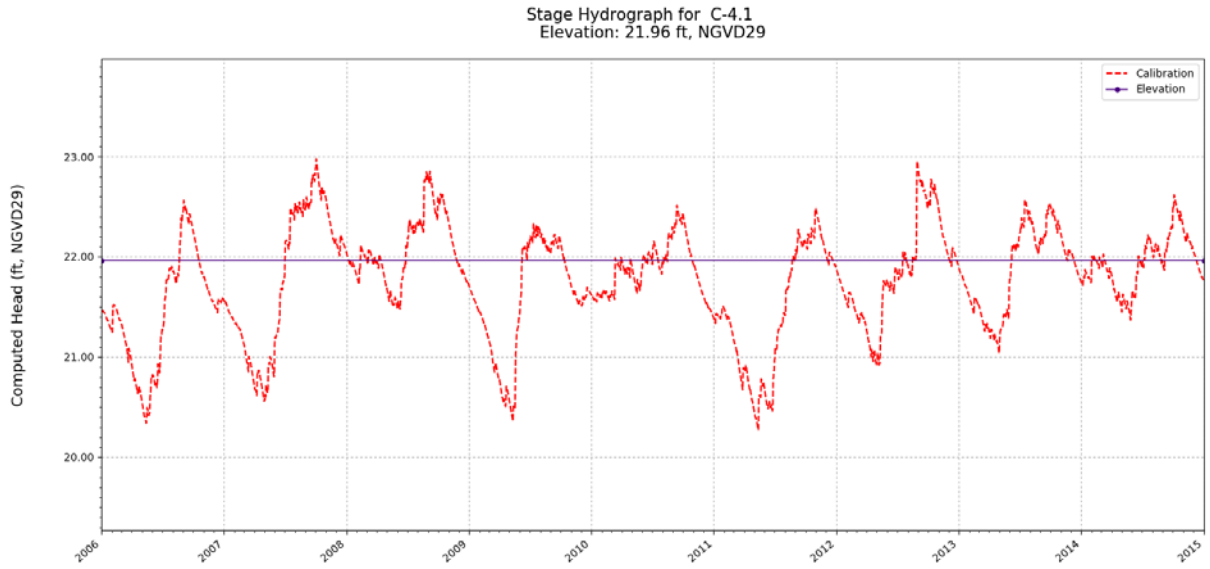

Figure C-10. Simulated stage hydrograph (2006 – 2014) and model cell topography for WRAP cell C-4.1.

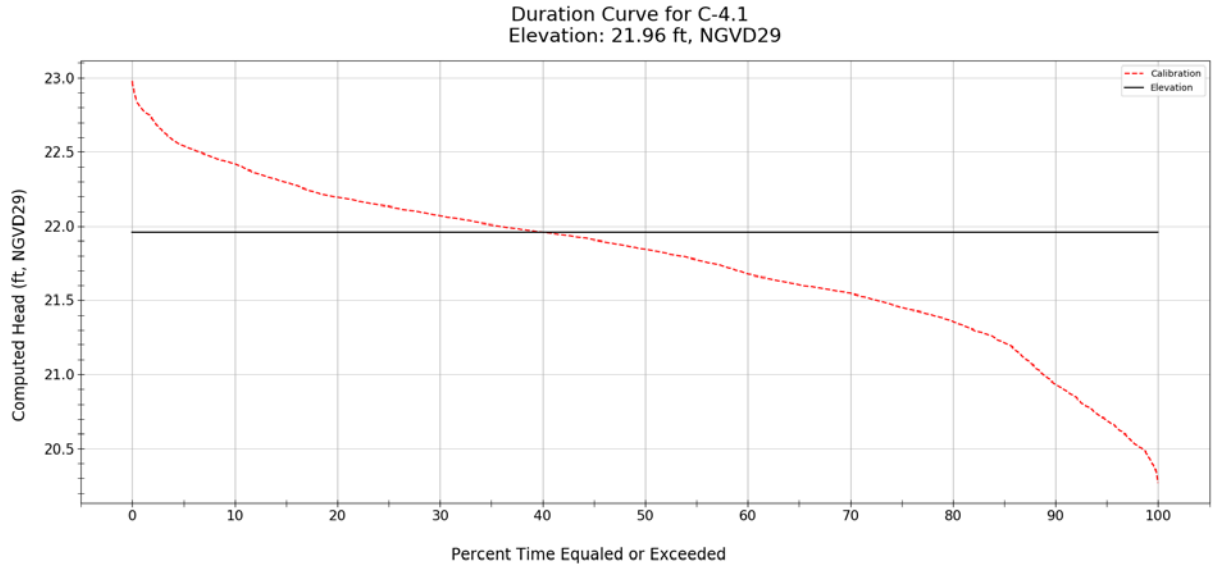

Figure C-11. Simulated stage duration curve (2006 – 2014) and model cell topography for WRAP cell C-4.1.

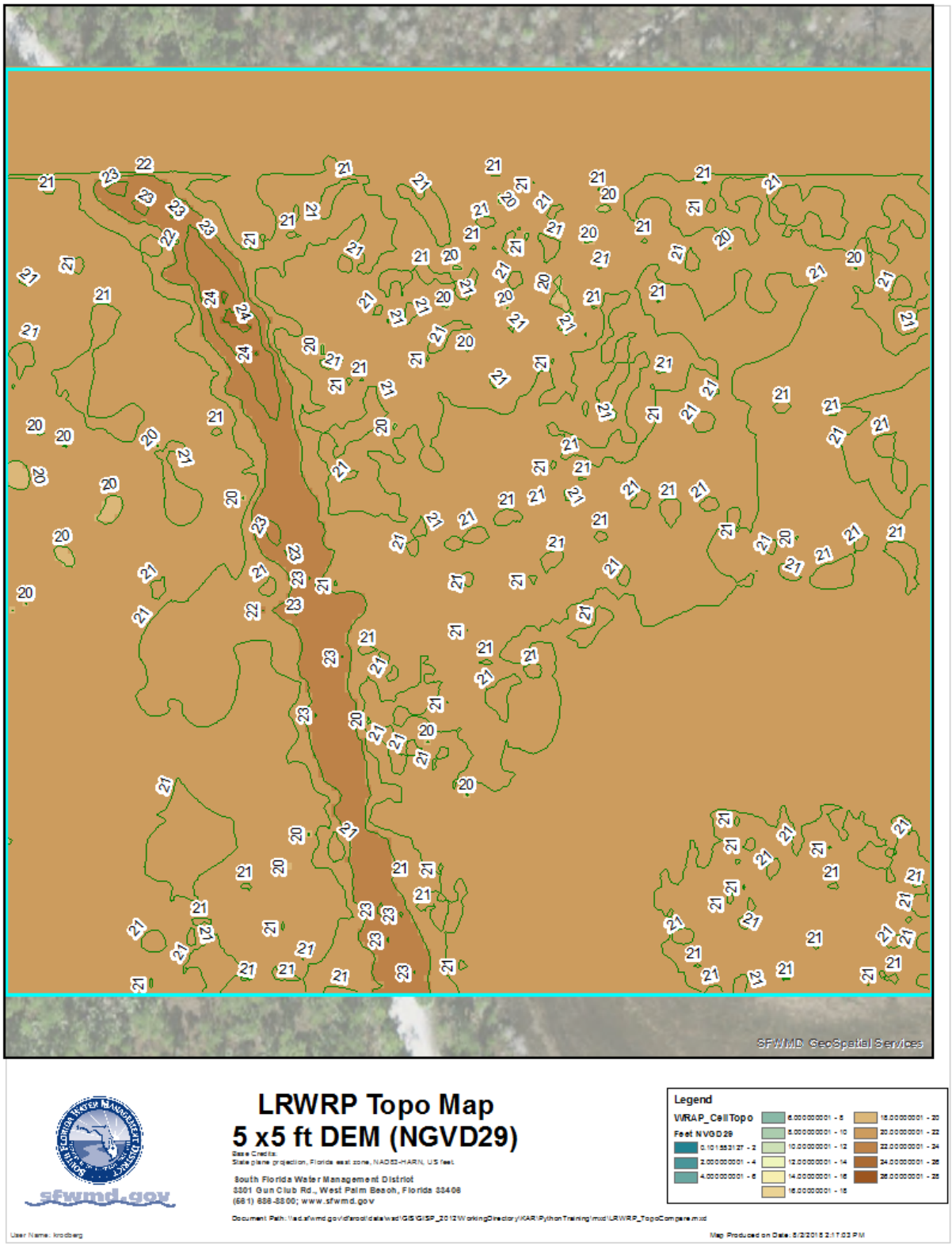

Figure C-12. Variation of model cell topography based on SFWMD's 5 ft LiDAR within WRAP cell C-4.1.

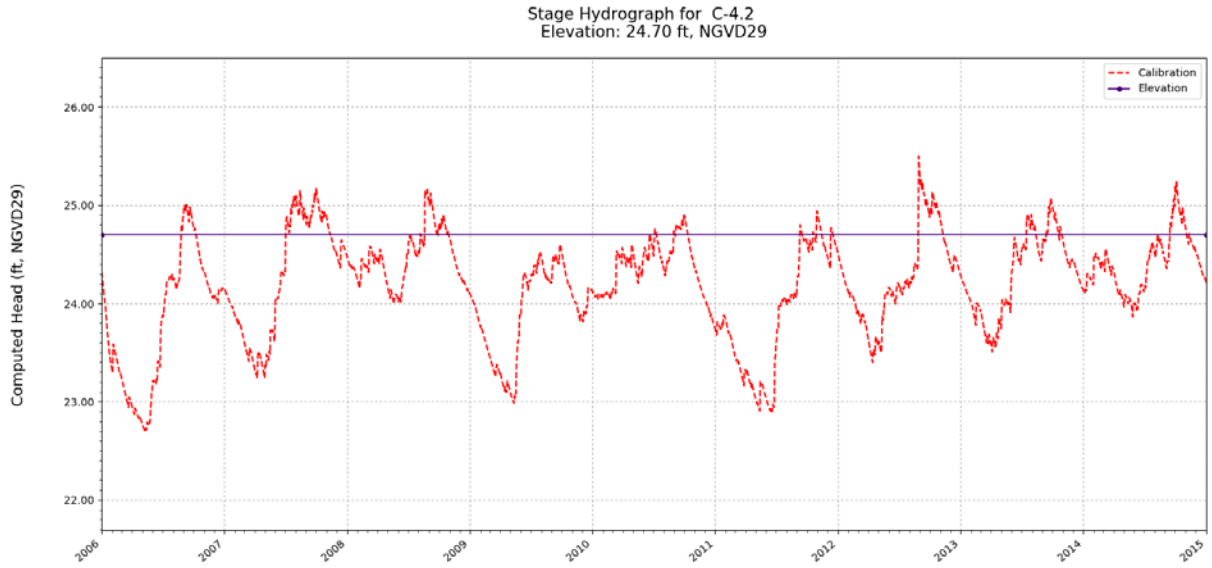

Figure C-13. Simulated stage hydrograph (2006 – 2014) and model cell topography for WRAP cell C-4.2.

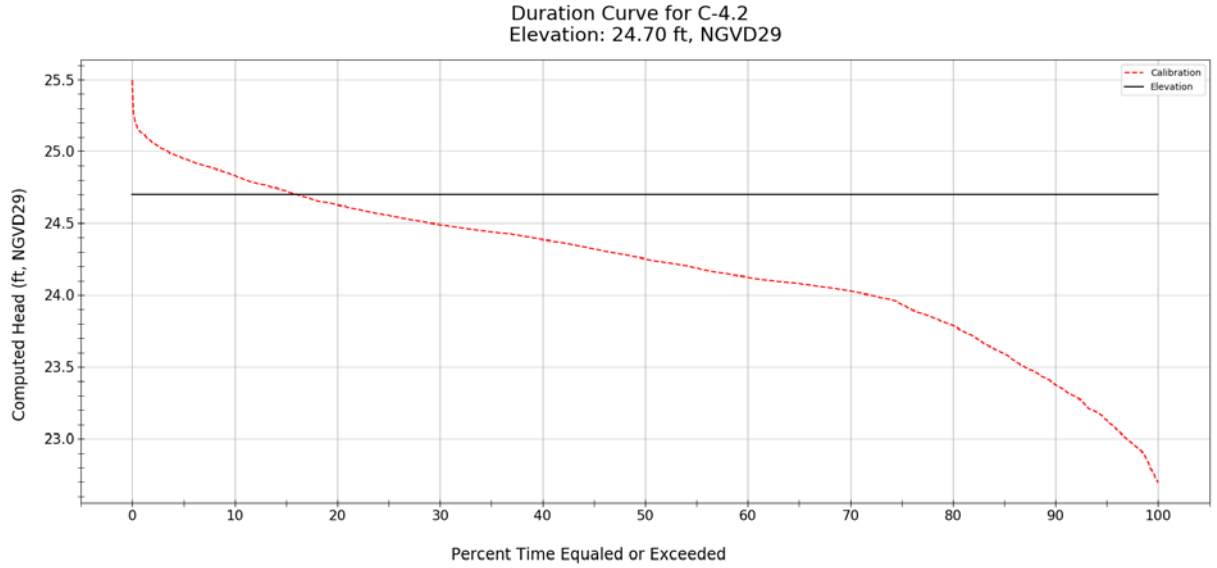

Figure C-14. Simulated stage duration curve (2006 – 2014) and model cell topography for WRAP cell C-4.2.

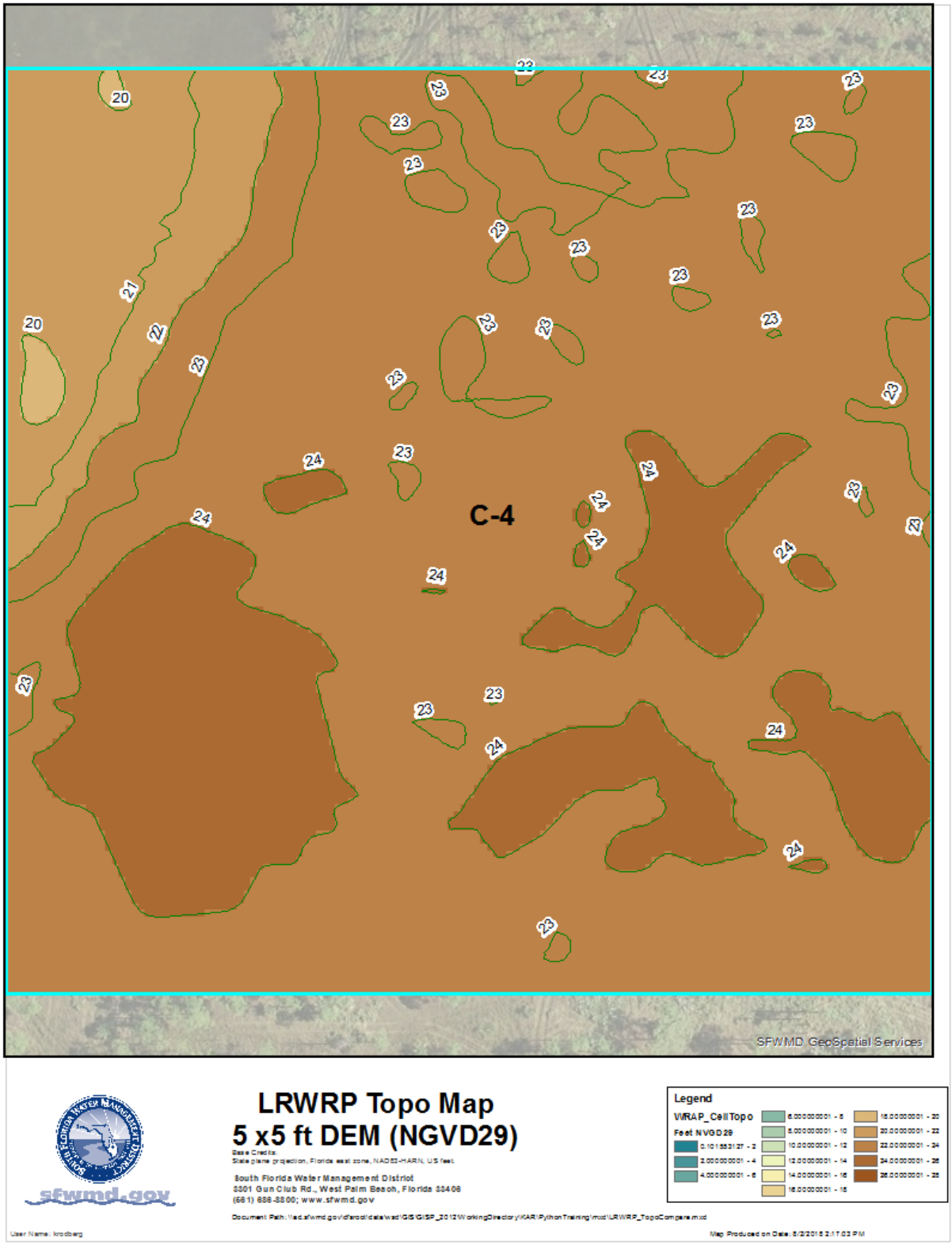

Figure C-15. Variation of model cell topography based on SFWMD's 5 ft LiDAR within WRAP cell C-4.2.

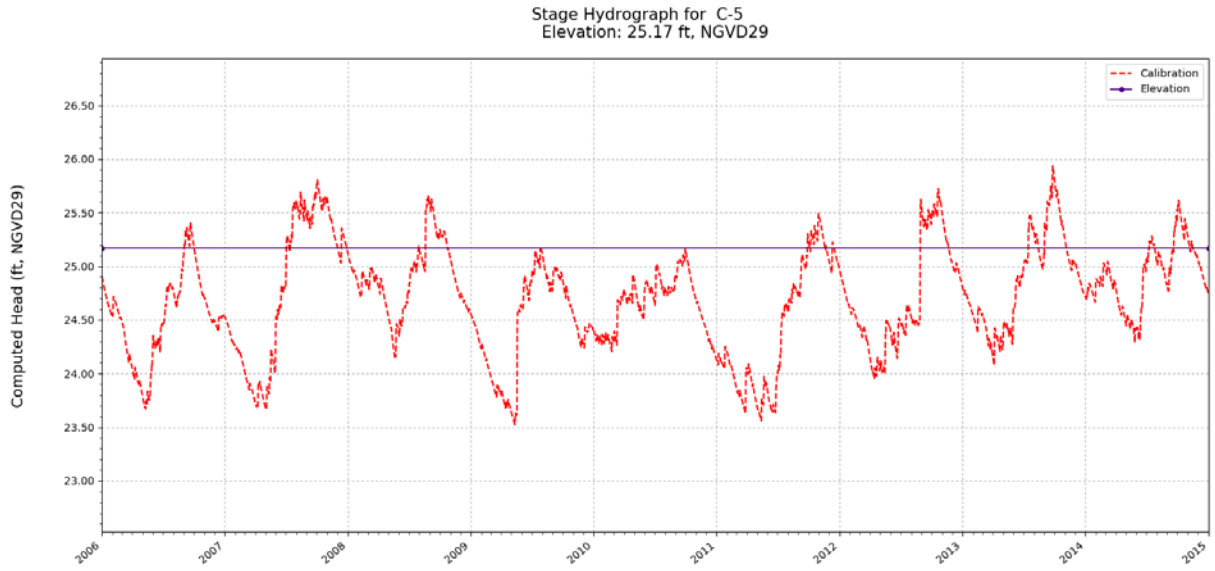

Figure C-16. Simulated stage hydrograph (2006 – 2014) and model cell topography for WRAP cell C-5.

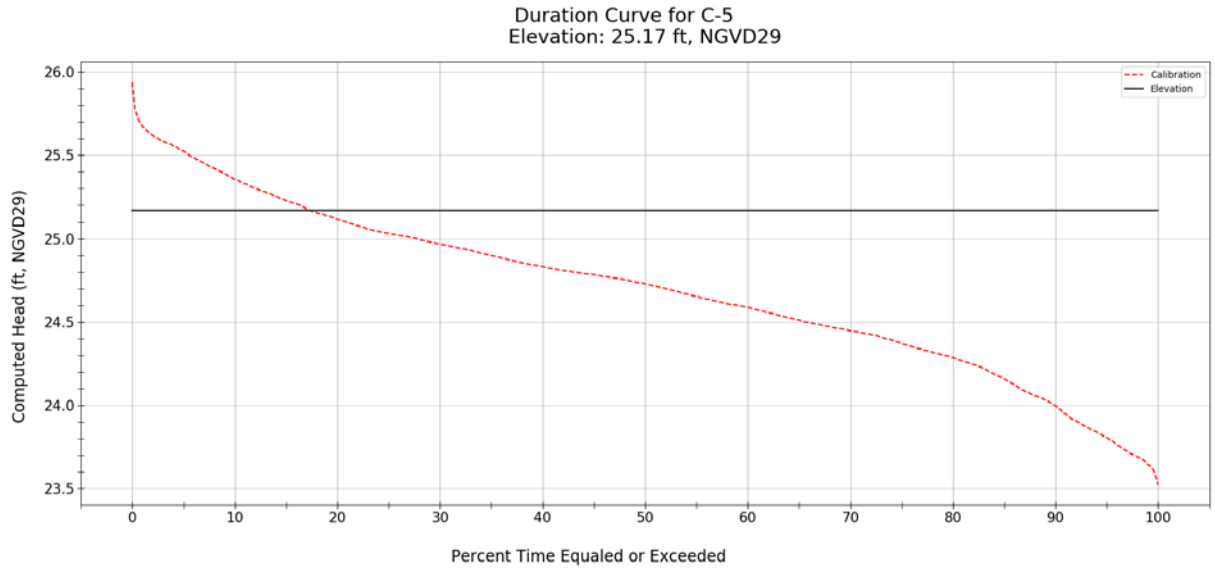

Figure C-17. Simulated stage duration curve (2006 – 2014) and model cell topography for WRAP cell C-5.

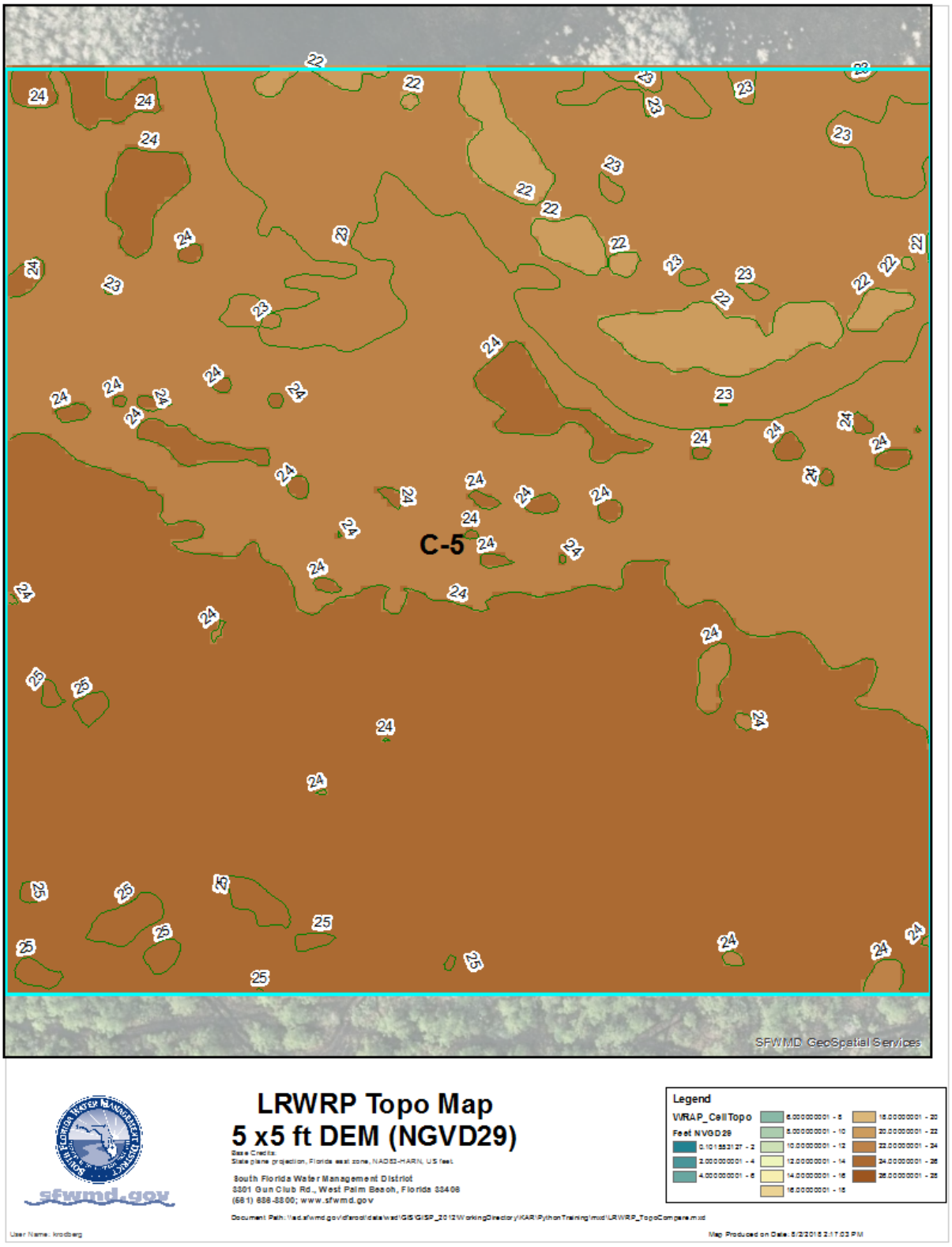

Figure C-18. Variation of model cell topography based on SFWMD's 5 ft LiDAR within WRAP cell C-5.

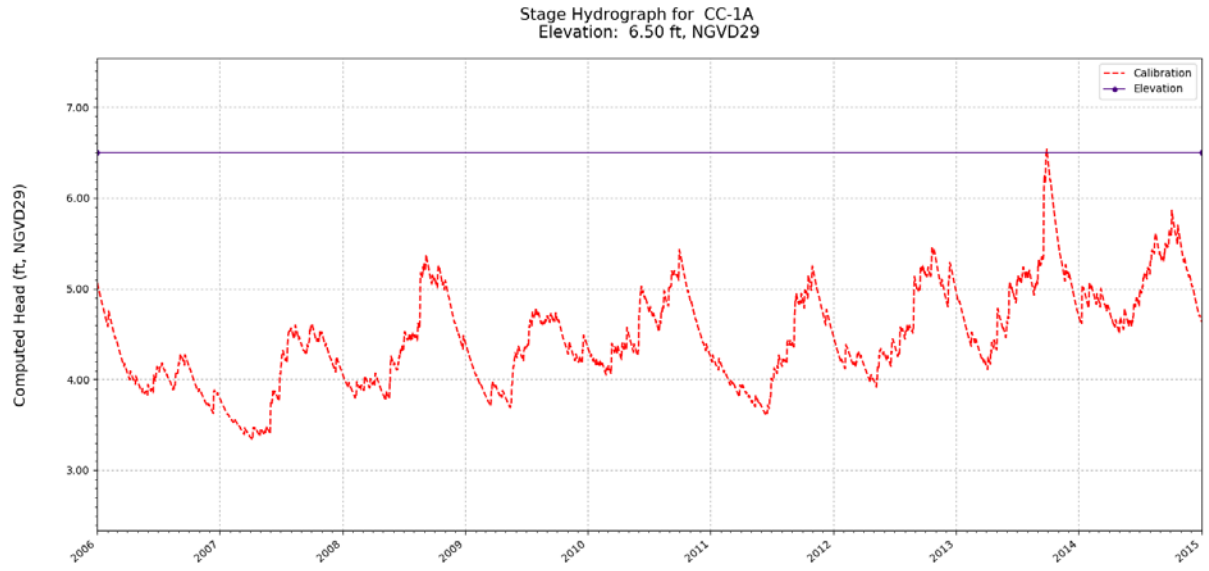

Figure C-19. Simulated stage hydrograph (2006 – 2014) and model cell topography for WRAP cell CC-1A.

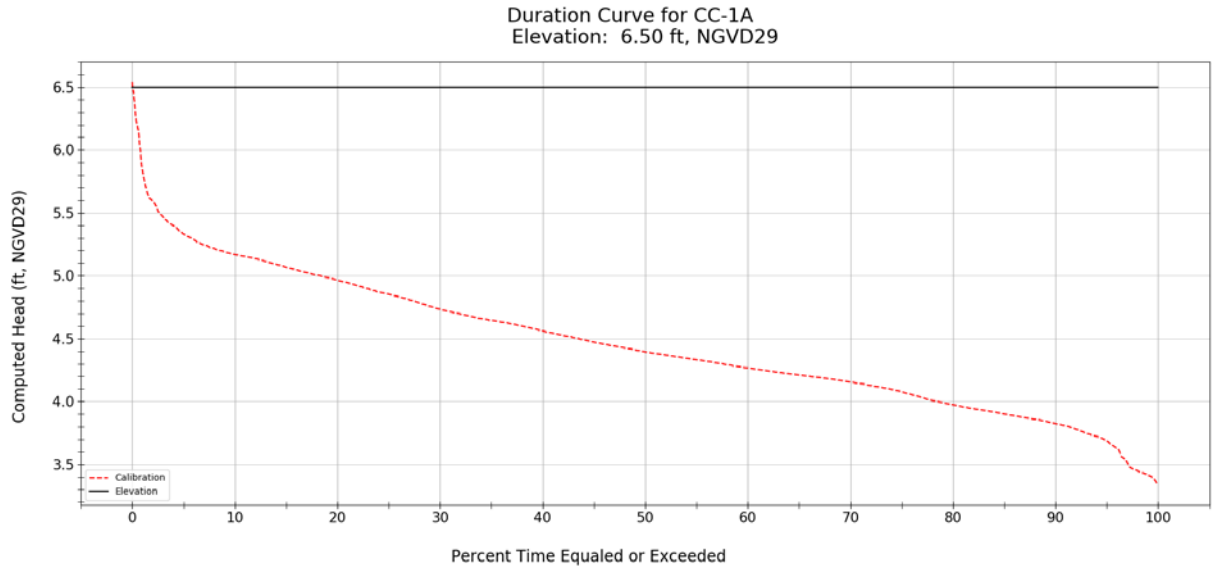

Figure C-20. Simulated stage duration curve (2006 – 2014) and model cell topography for WRAP cell CC-1A.

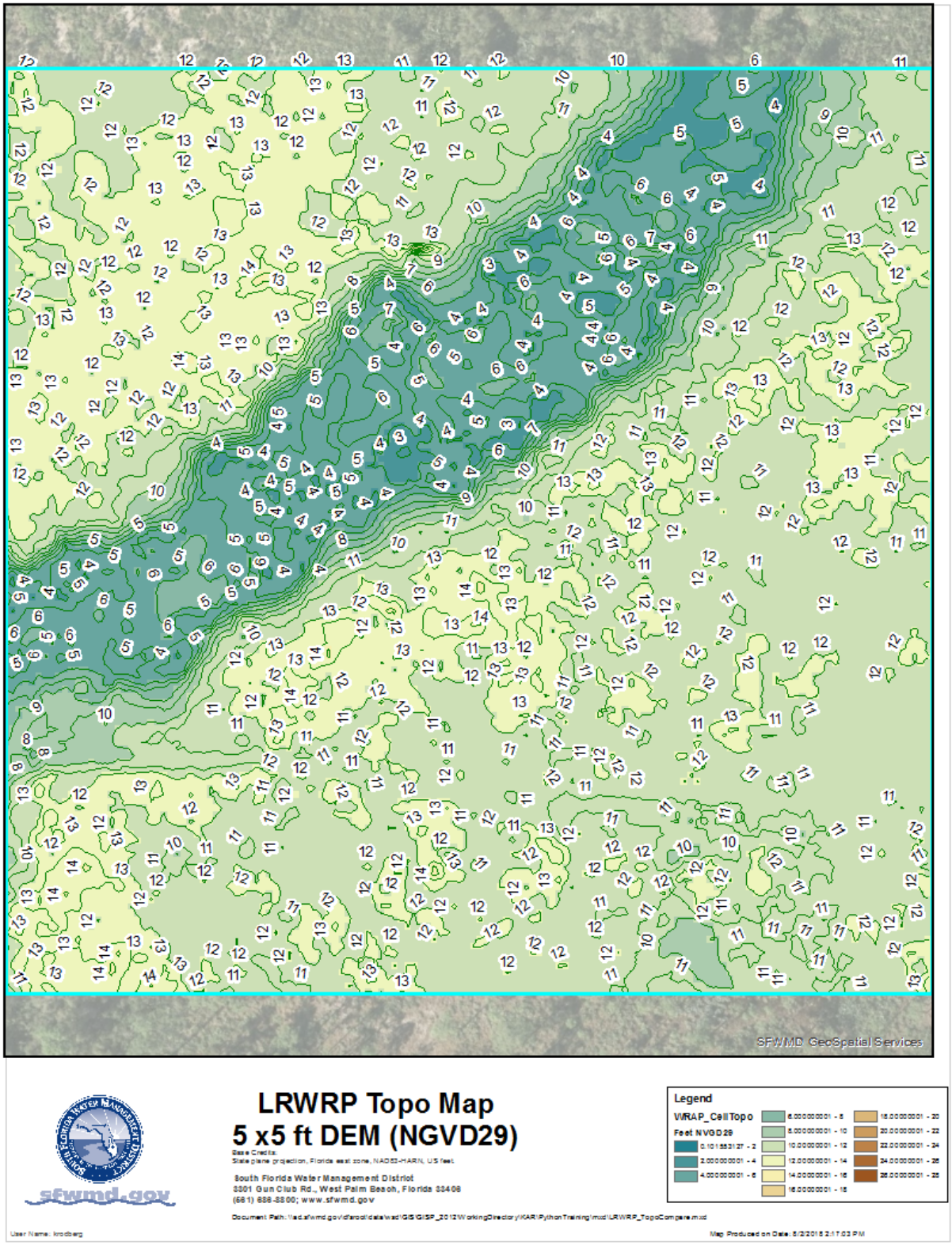

Figure C-21. Variation of model cell topography based on SFWMD's 5 ft LiDAR within WRAP cell CC-1A.

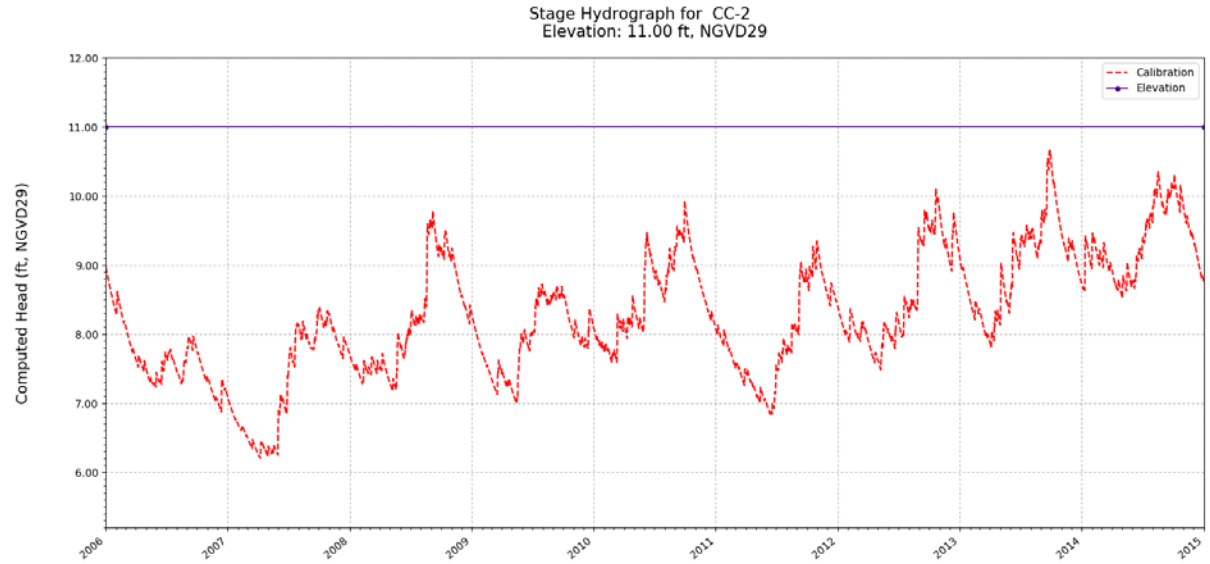

Figure C-22. Simulated stage hydrograph (2006 – 2014) and model cell topography for WRAP cell CC-2.

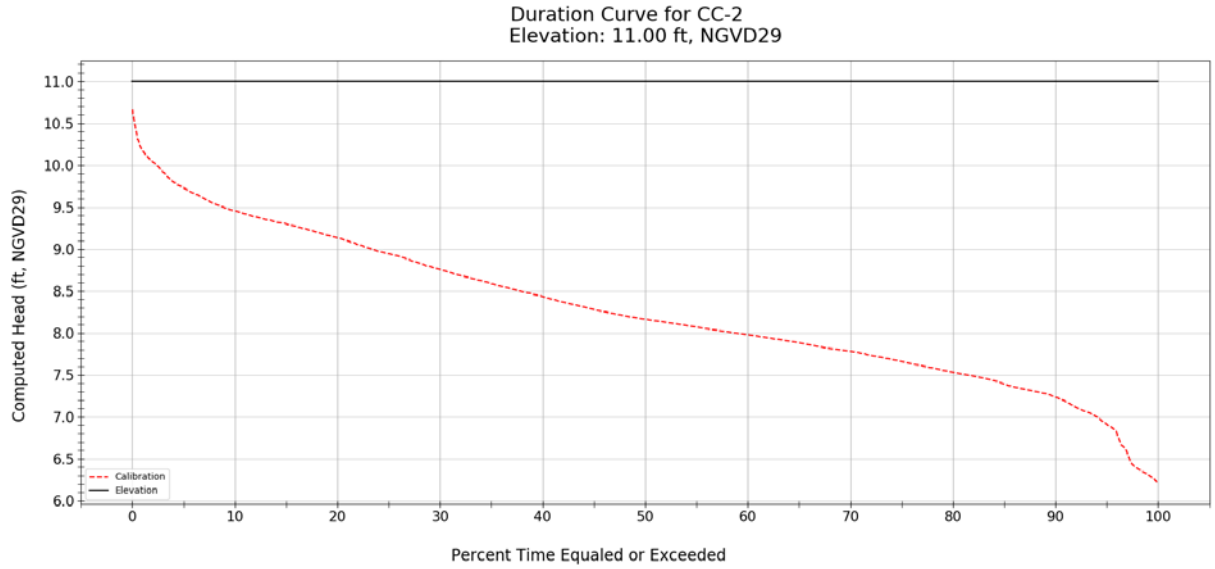

Figure C-23. Simulated stage duration curve (2006 – 2014) and model cell topography for WRAP cell CC-2.

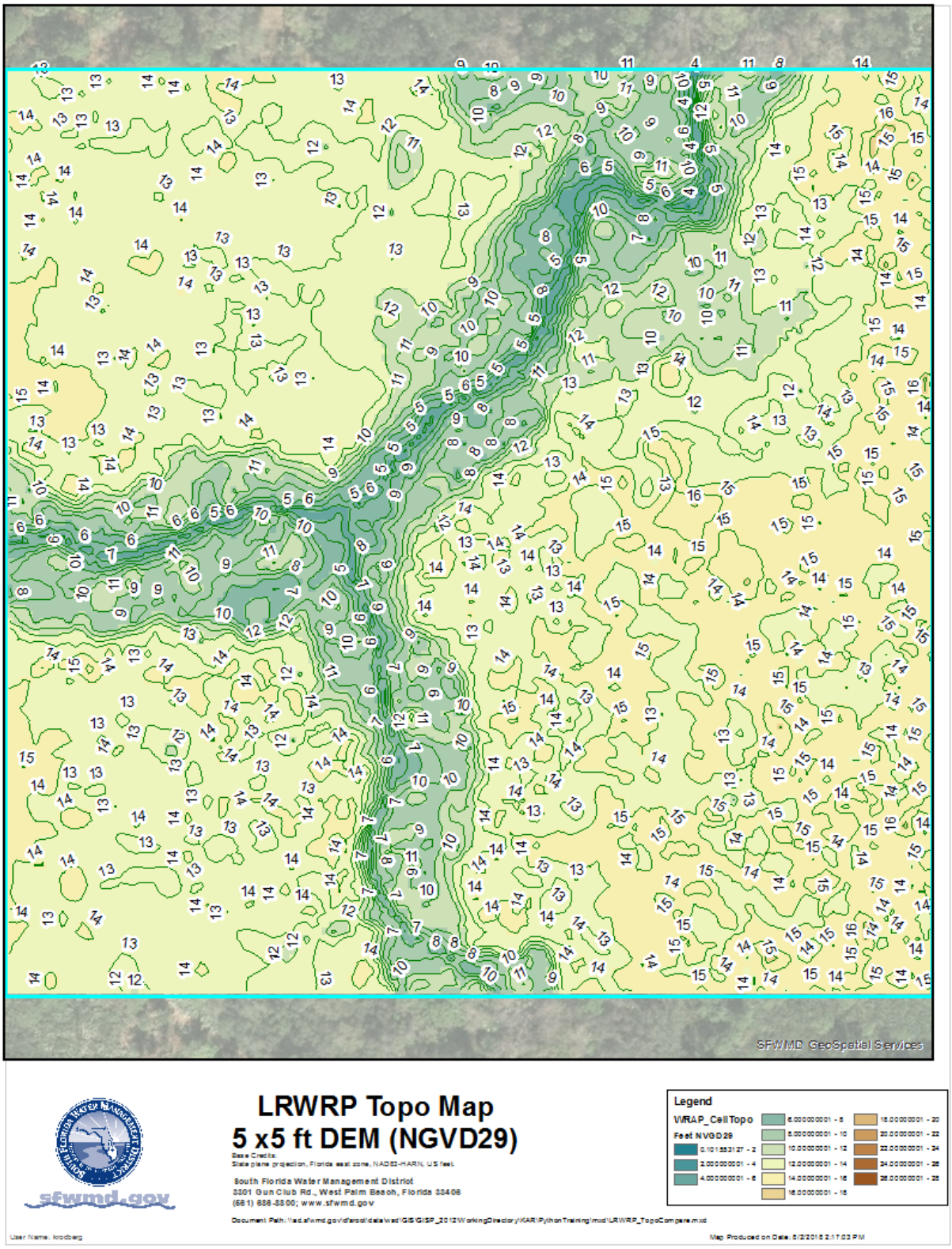

Figure C-24. Variation of model cell topography based on SFWMD's 5 ft LiDAR within WRAP cell CC-2.

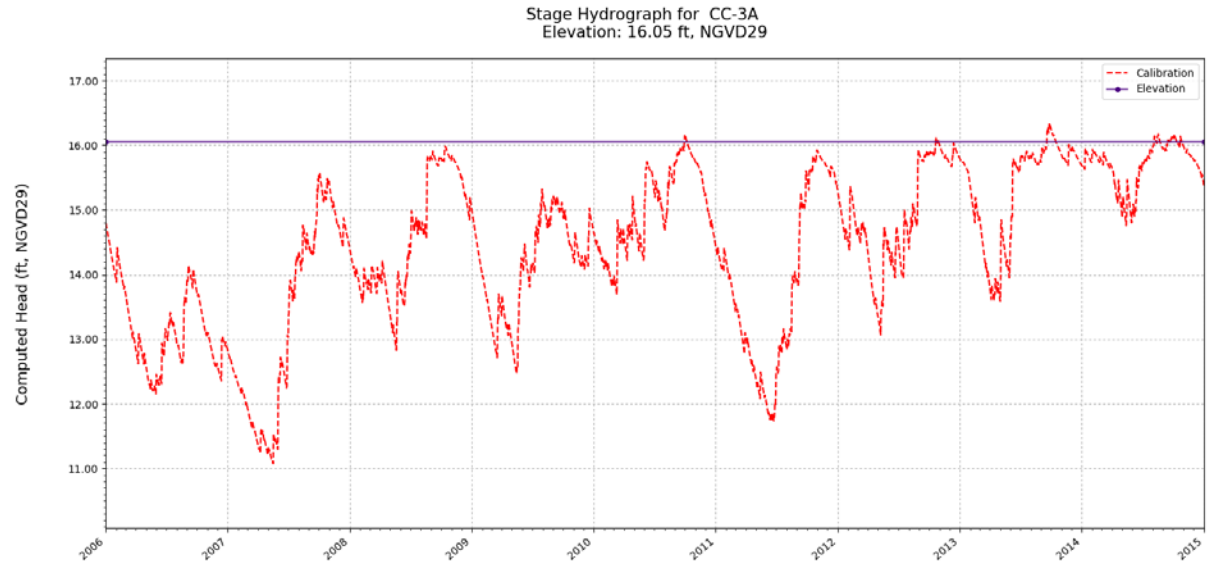

Figure C-25. Simulated stage hydrograph (2006 – 2014) and model cell topography for WRAP cell CC-3A.

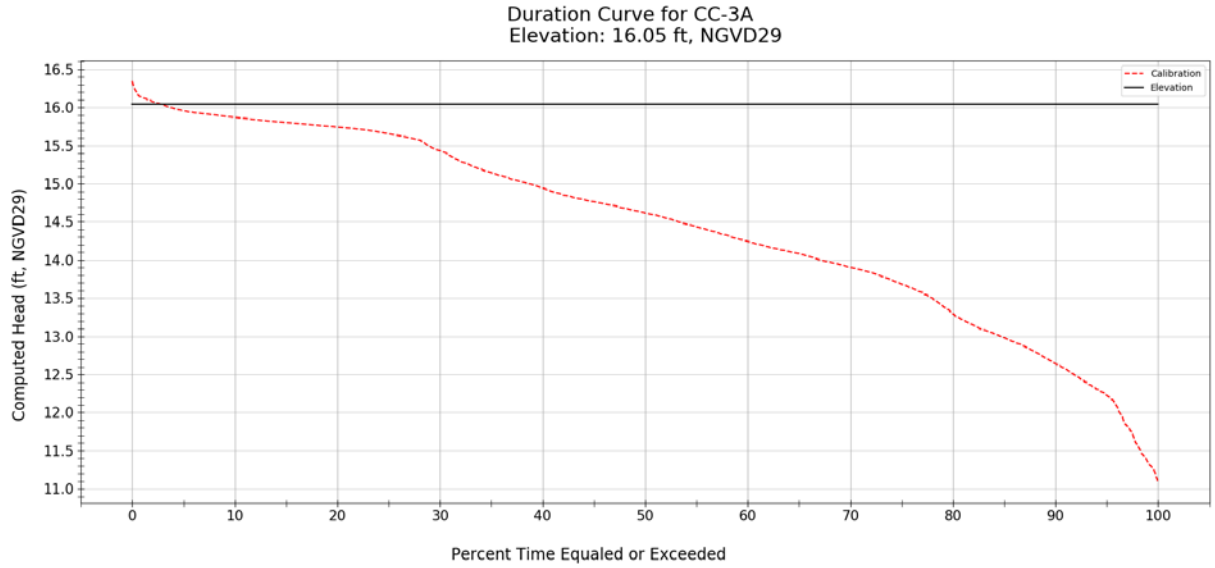

Figure C-26. Simulated stage duration curve (2006 – 2014) and model cell topography for WRAP cell CC-3A.

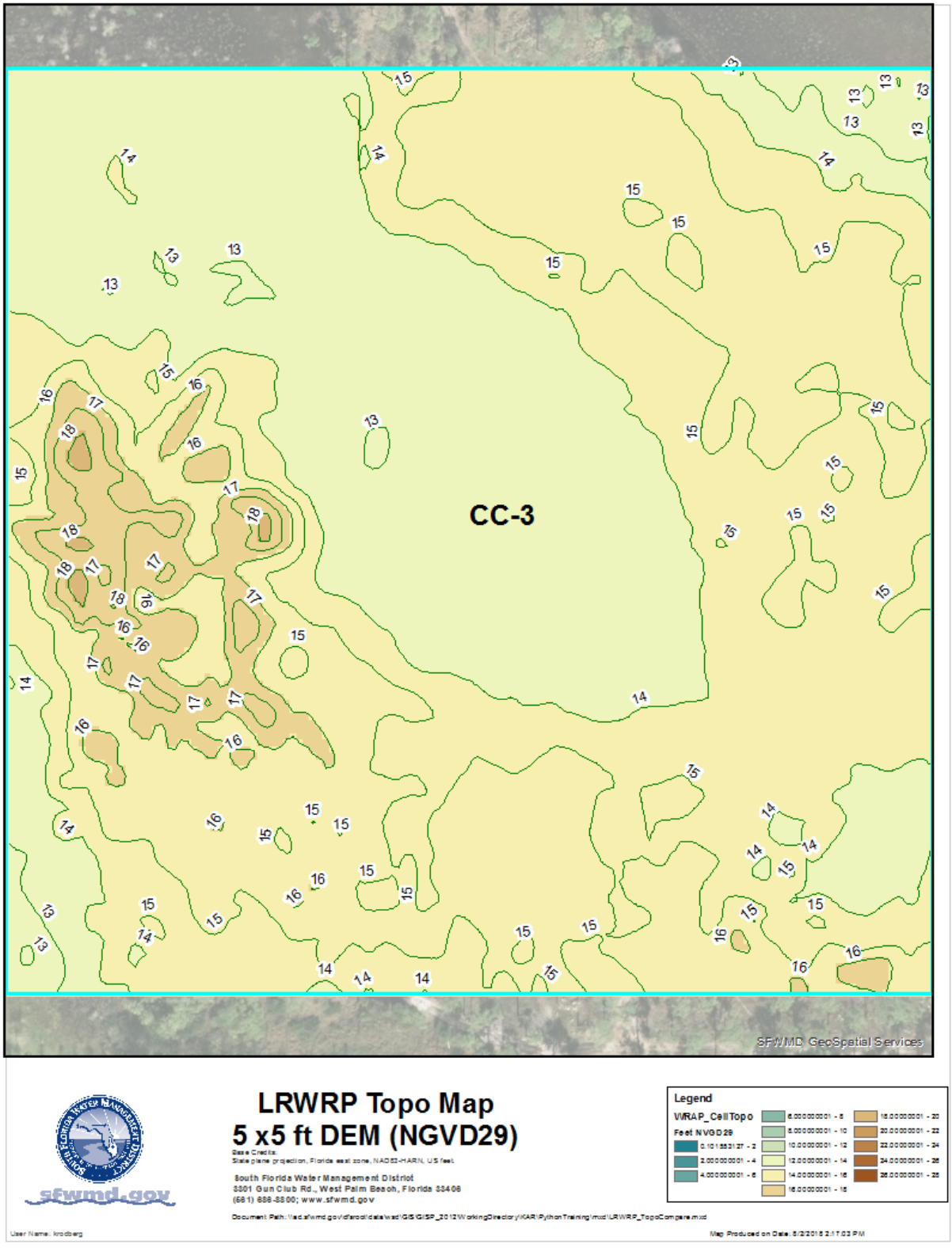

Figure C-27. Variation of model cell topography based on SFWMD's 5 ft LiDAR within WRAP cell CC-3A.

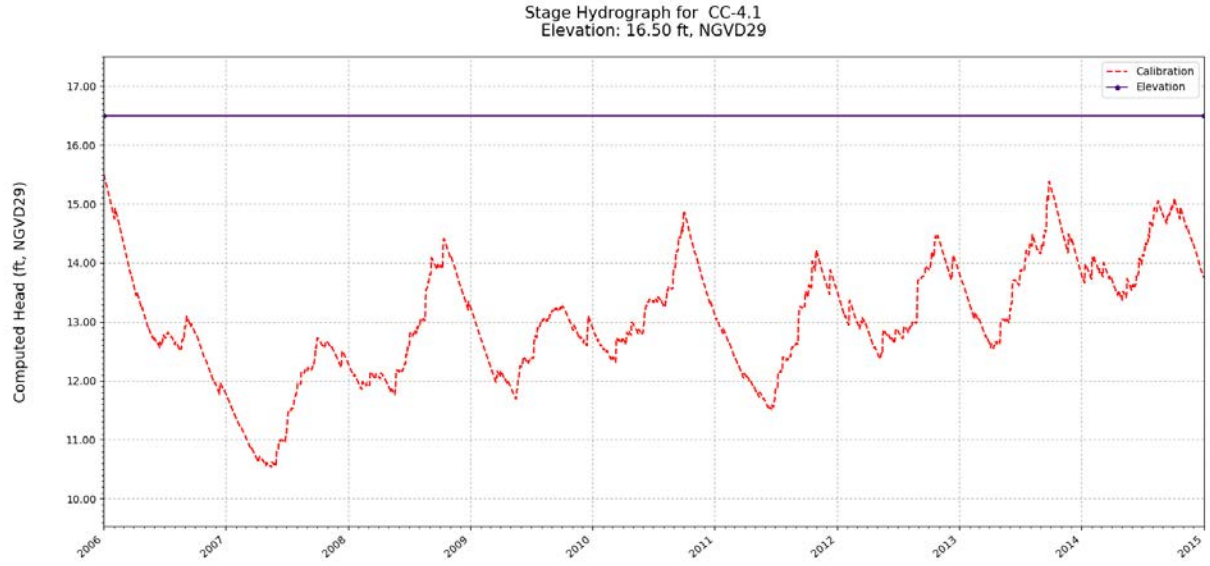

Figure C-28. Simulated stage hydrograph (2006 – 2014) and model cell topography for WRAP cell CC-4.1.

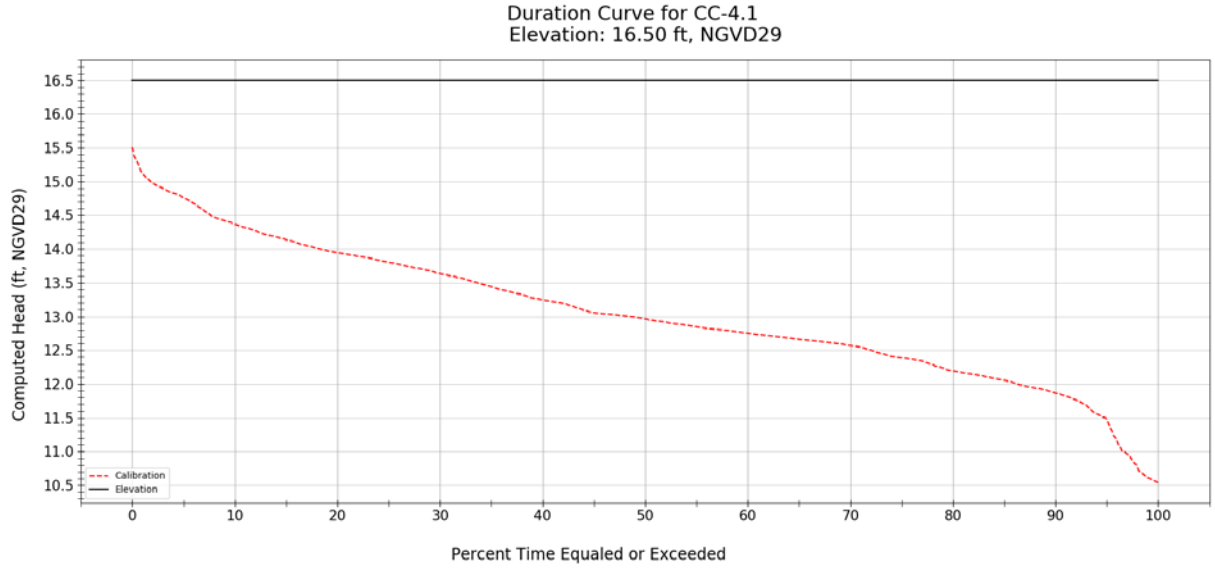

Figure C-29. Simulated stage duration curve (2006 – 2014) and model cell topography for WRAP cell CC-4.1.

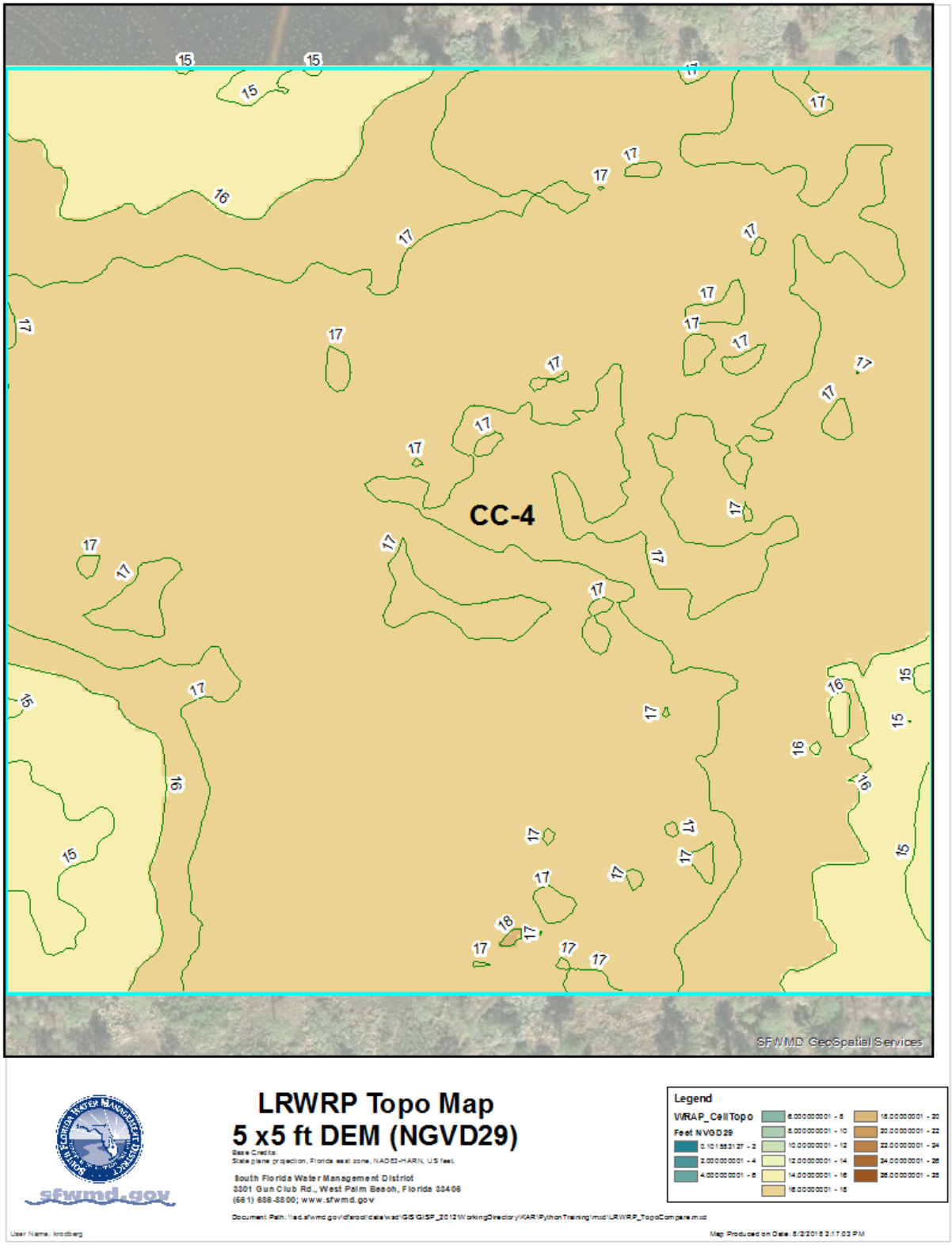

Figure C-30. Variation of model cell topography based on SFWMD's 5 ft LiDAR within WRAP cell CC-4.1.

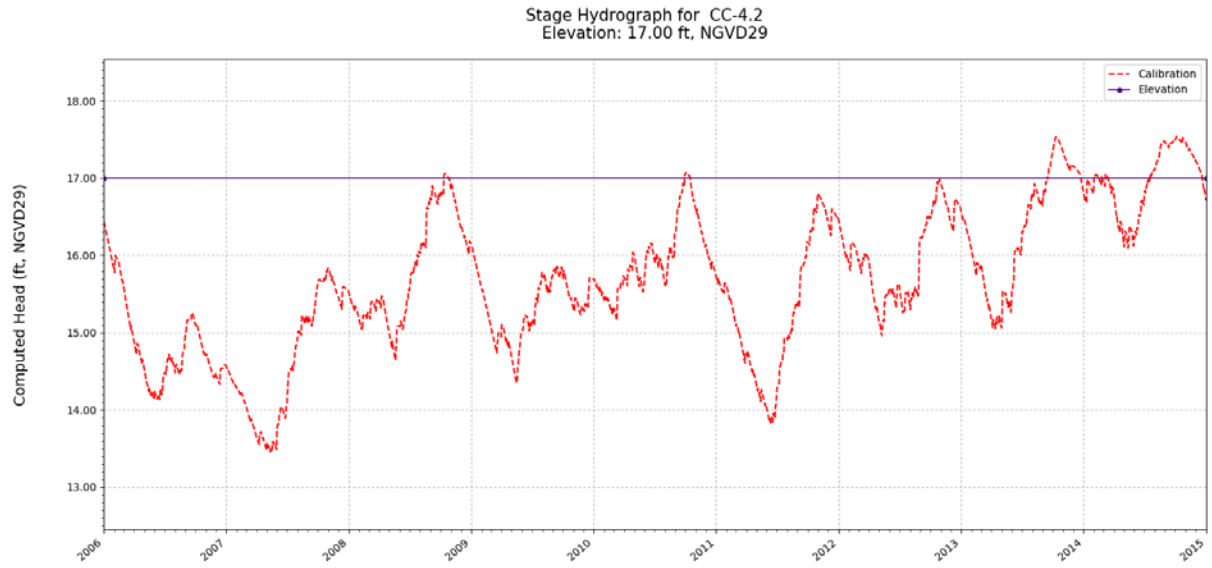

Figure C-31. Simulated stage hydrograph (2006 – 2014) and model cell topography for WRAP cell CC-4.2.

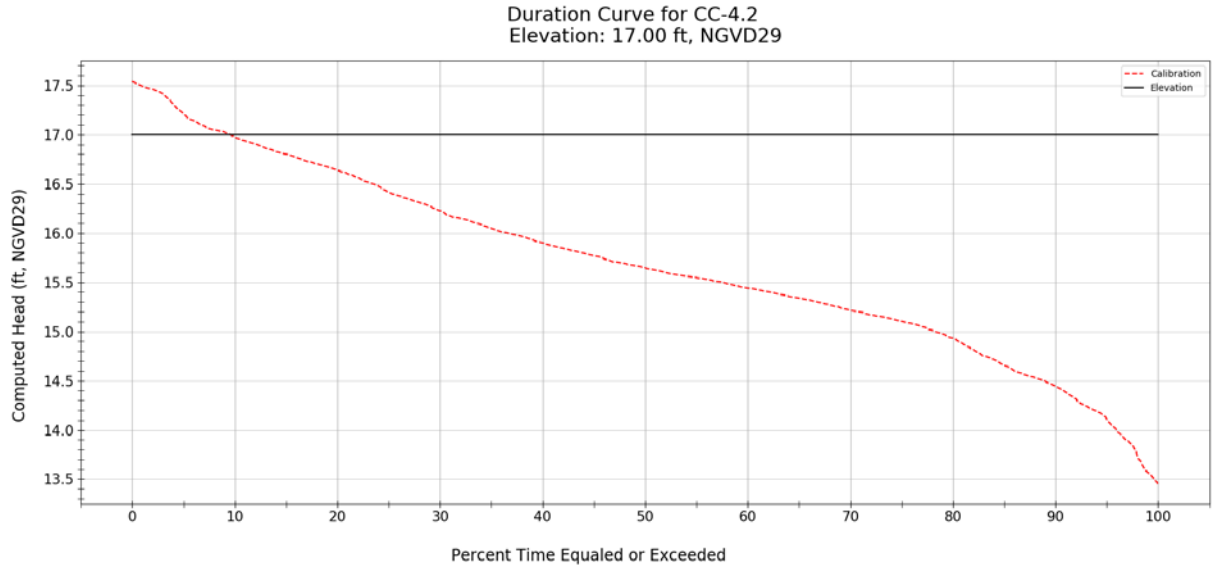

Figure C-32. Simulated stage duration curve (2006 – 2014) and model cell topography for WRAP cell CC-4.2.

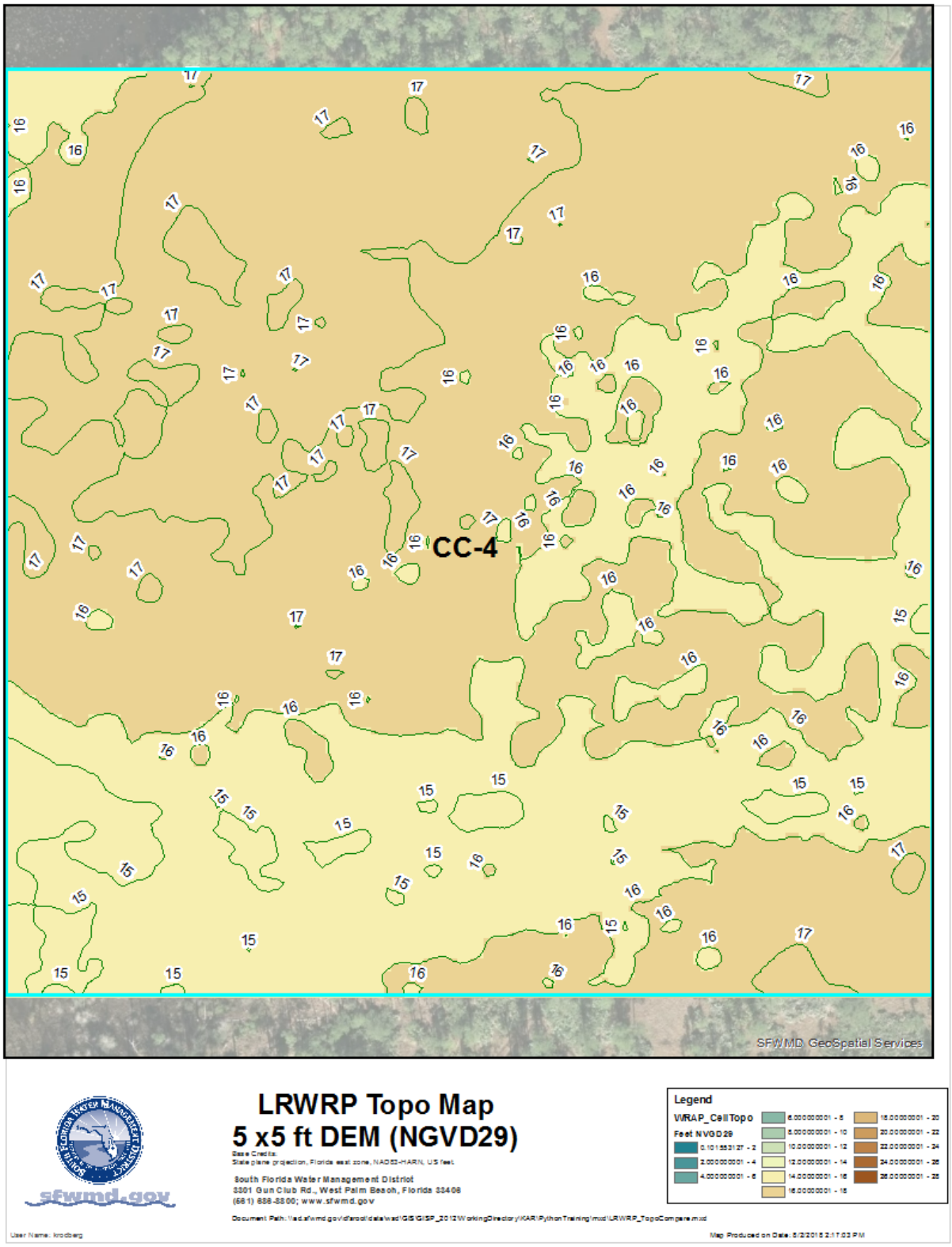

Figure C-33. Variation of model cell topography based on SFWMD's 5 ft LiDAR within WRAP cell CC-4.2.

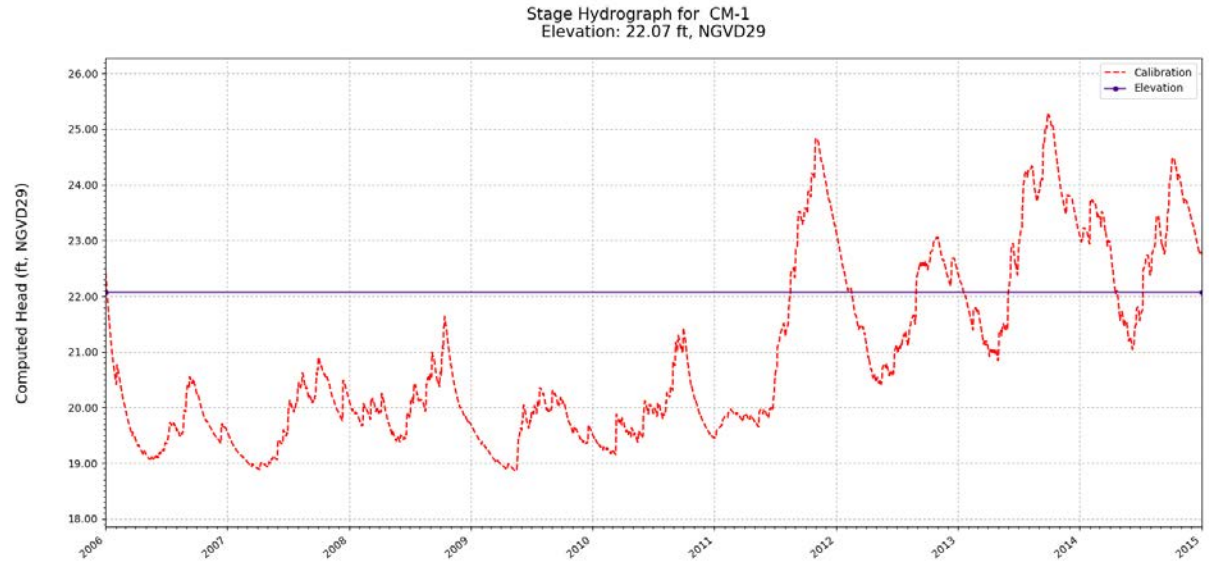

Figure C-34. Simulated stage hydrograph (2006 – 2014) and model cell topography for WRAP cell CM-1.

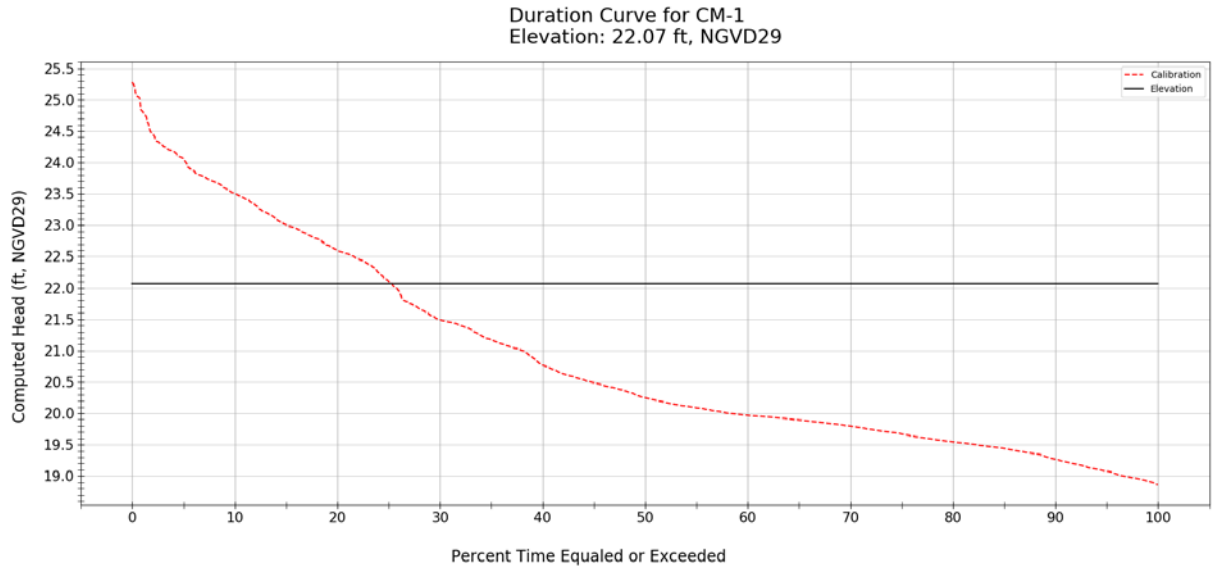

Figure C-35. Simulated stage duration curve (2006 – 2014) and model cell topography for WRAP cell CM-1.

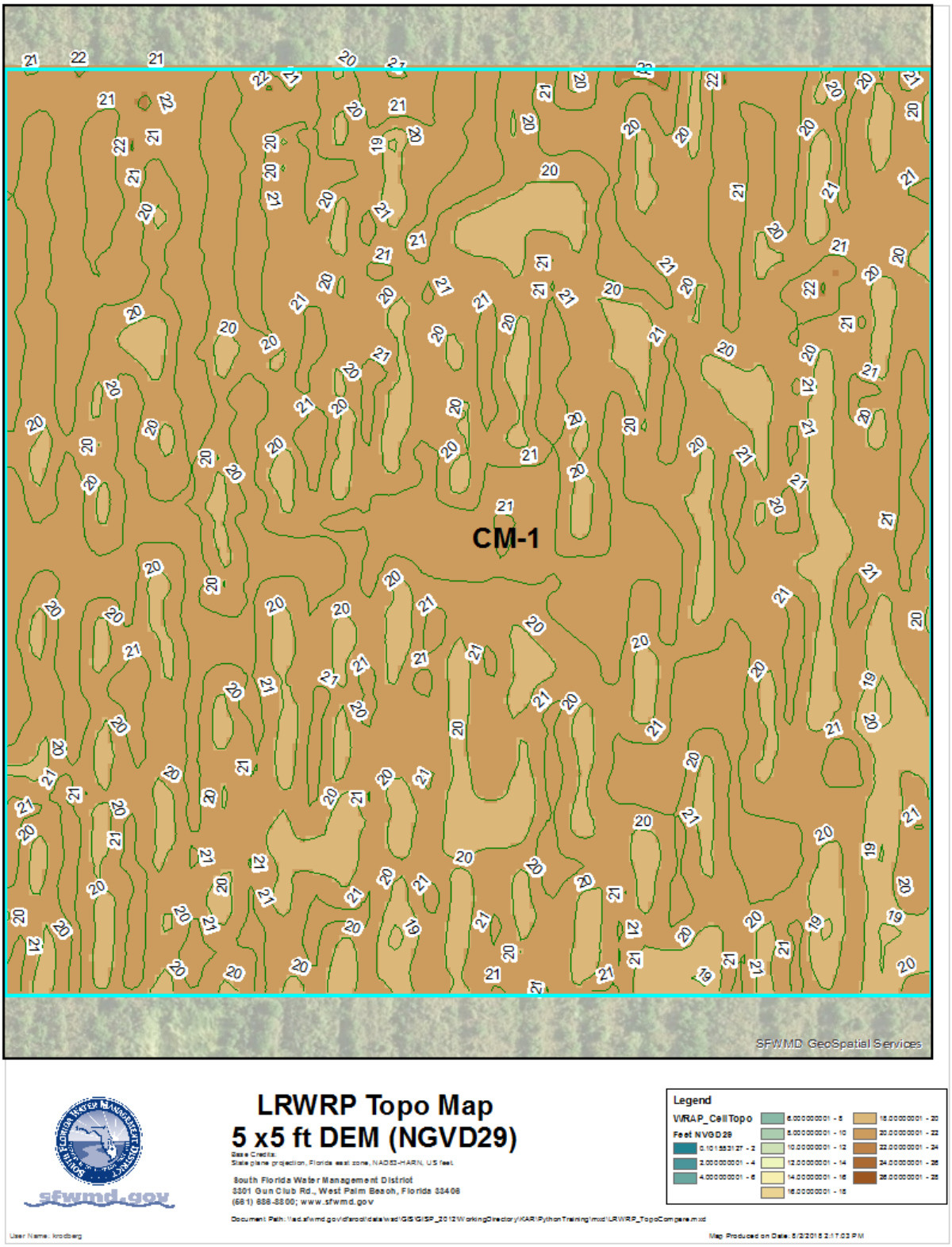

Figure C-36. Variation of model cell topography based on SFWMD's 5 ft LiDAR within WRAP cell CM-1.

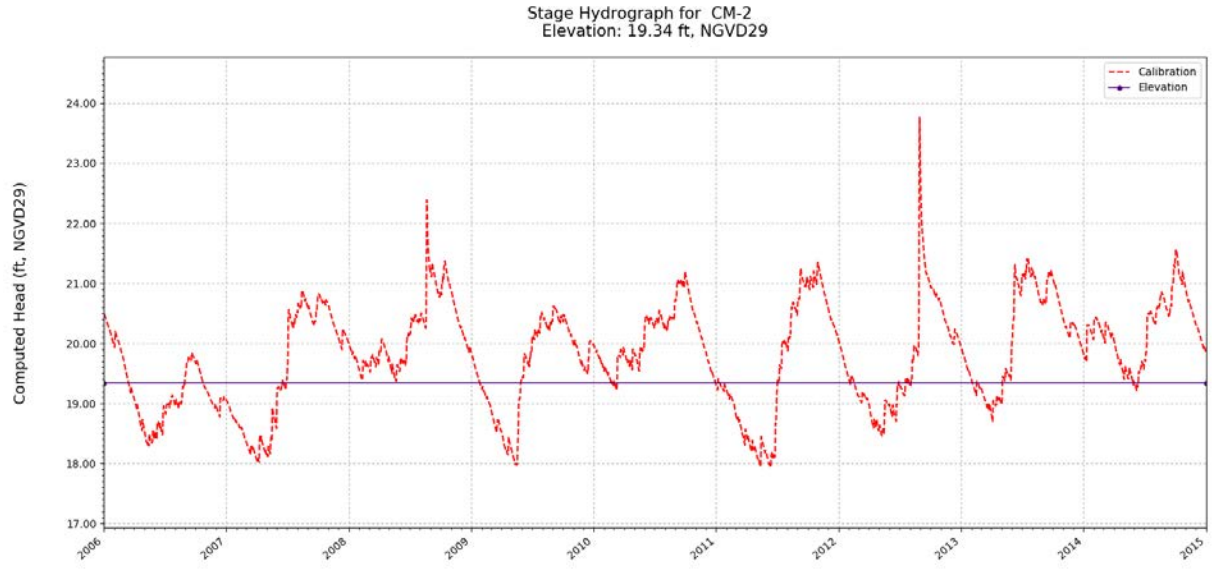

Figure C-37. Simulated stage hydrograph (2006 – 2014) and model cell topography for WRAP cell CM-2.

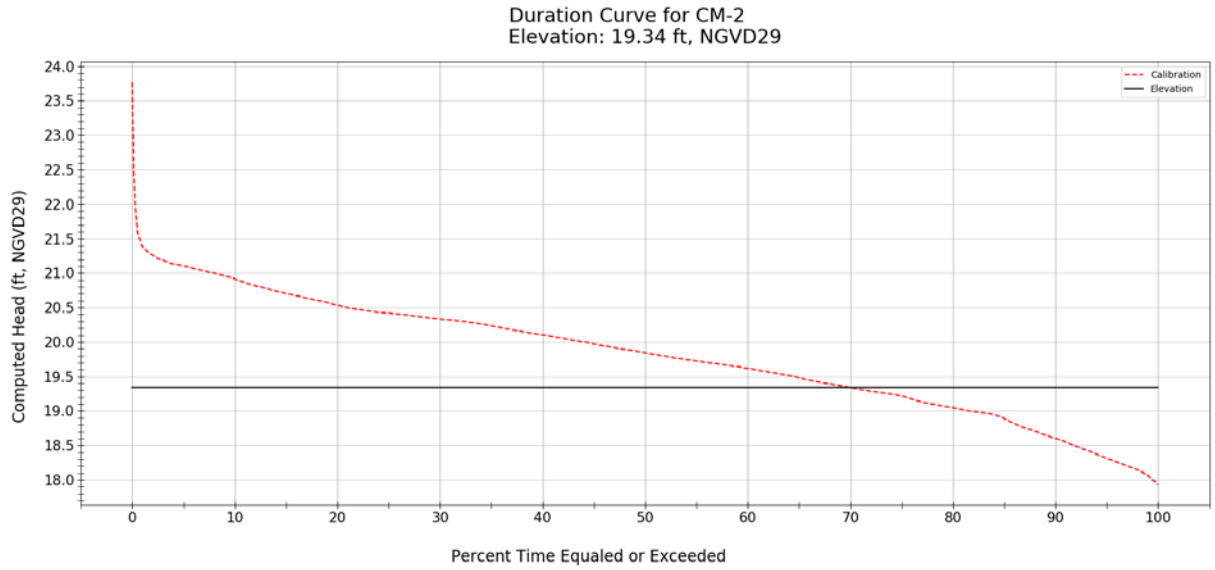

Figure C-38. Simulated stage duration curve (2006 – 2014) and model cell topography for WRAP cell CM-2.

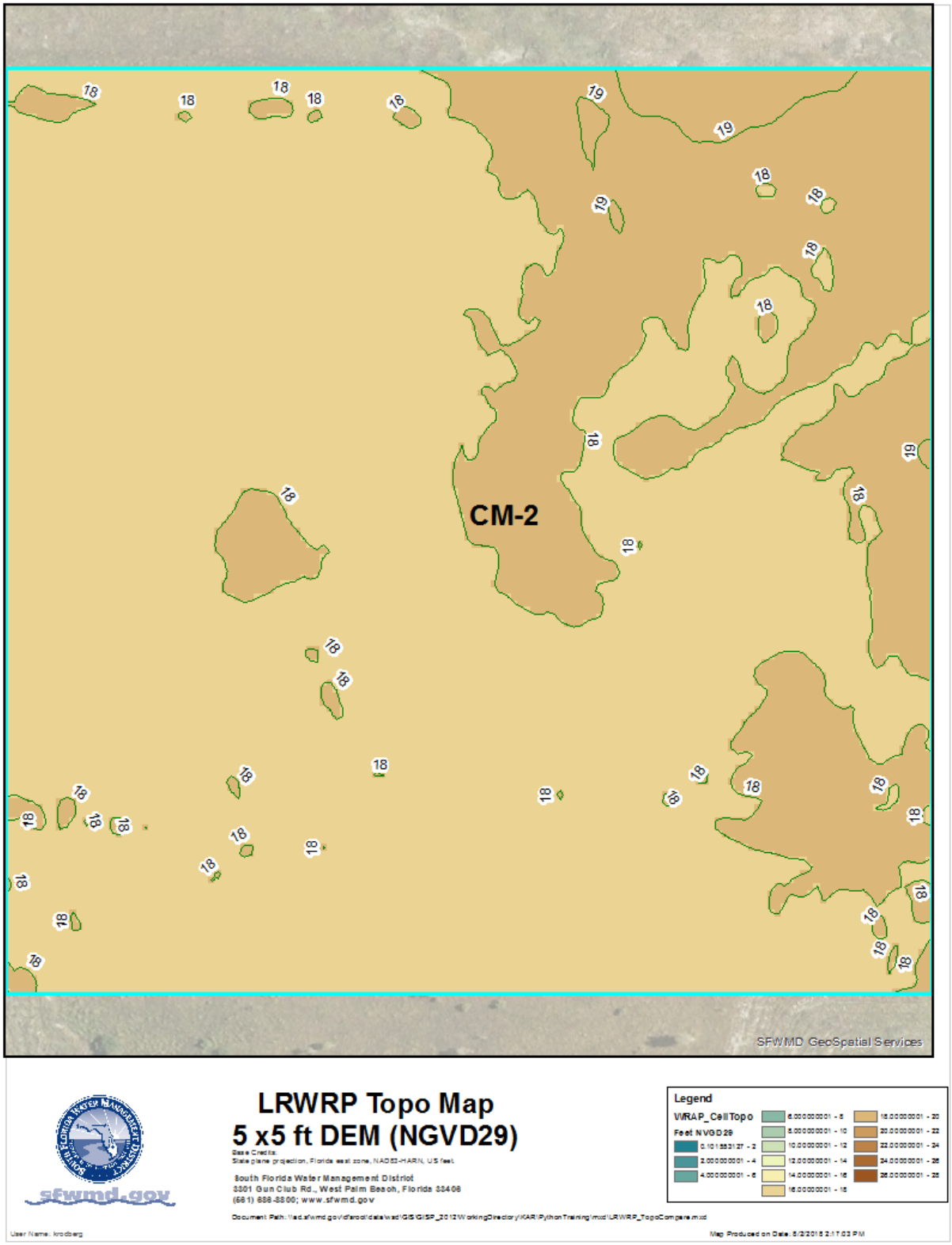

Figure C-39. Variation of model cell topography based on SFWMD's 5 ft LiDAR within WRAP cell CM-2.

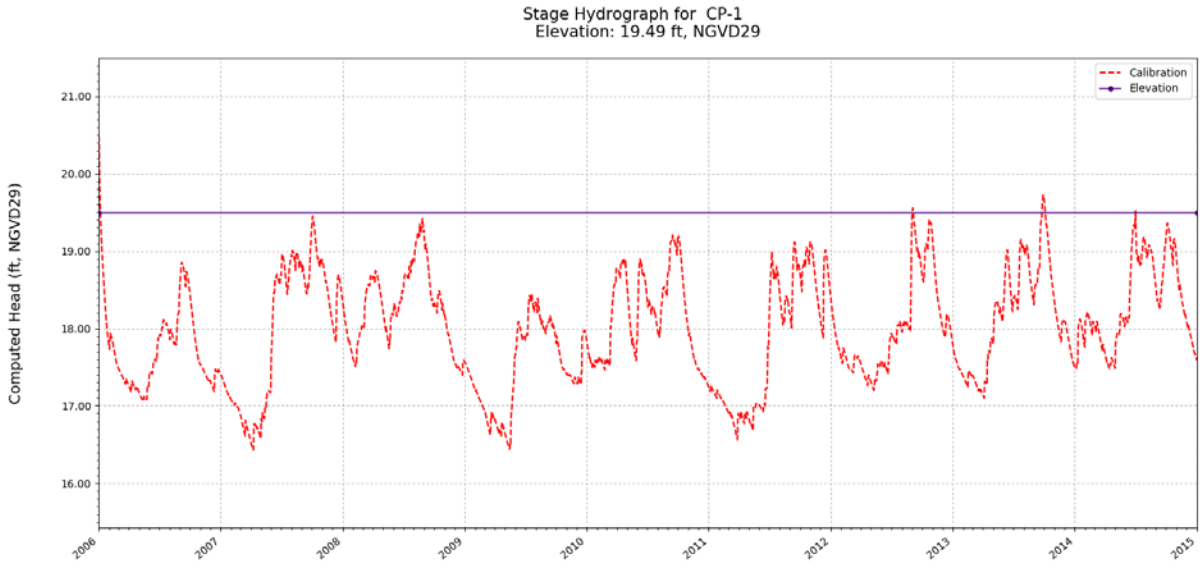

Figure C-40. Simulated stage hydrograph (2006 – 2014) and model cell topography for WRAP cell CP-1.

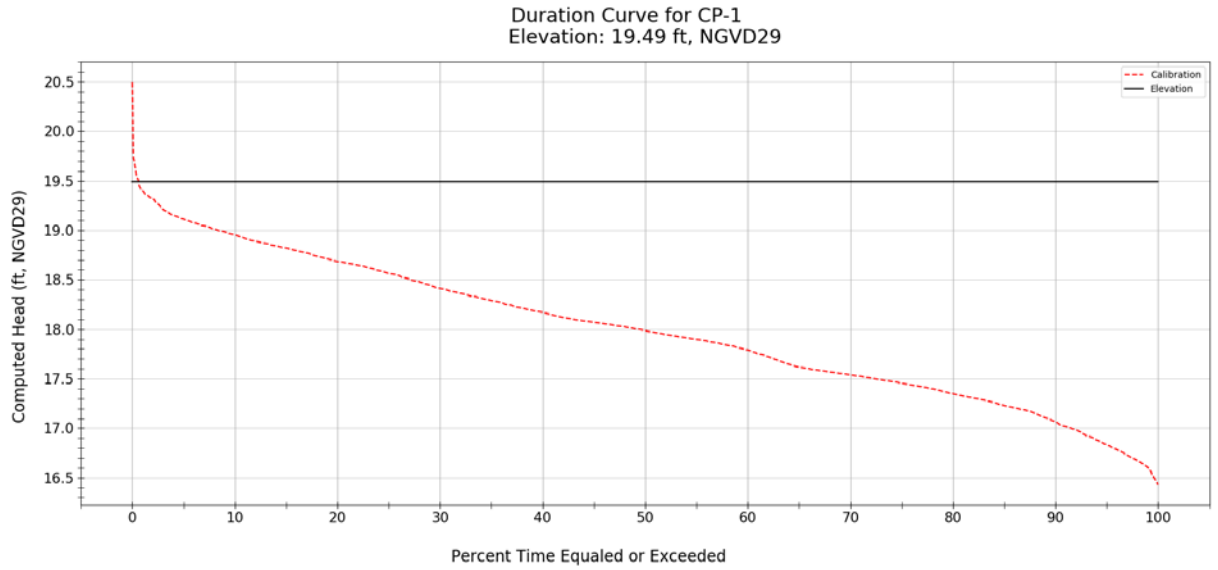

Figure C-41. Simulated stage duration curve (2006 – 2014) and model cell topography for WRAP cell CP-1.

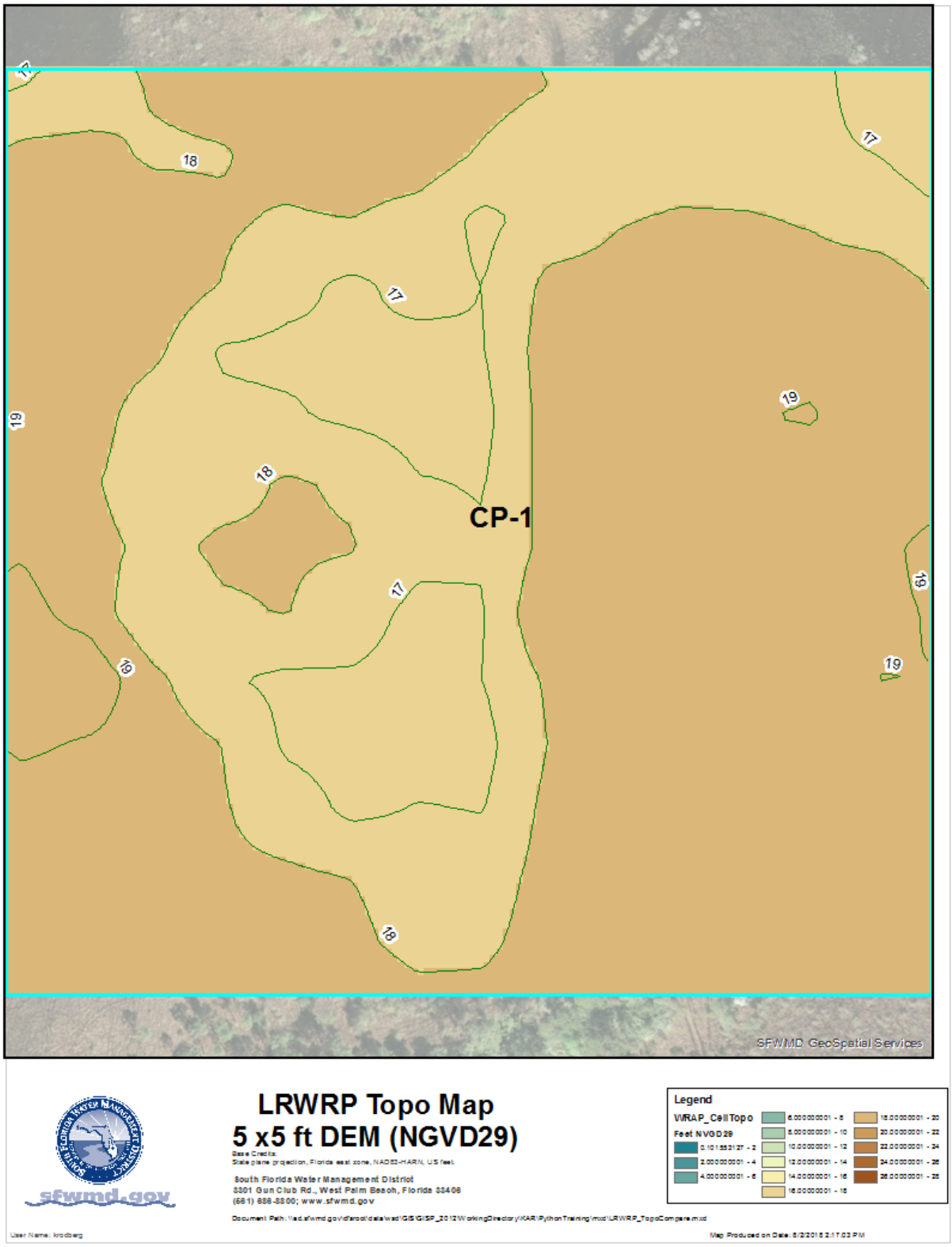

Figure C-42. Variation of model cell topography based on SFWMD's 5 ft LiDAR within WRAP cell CP-1.

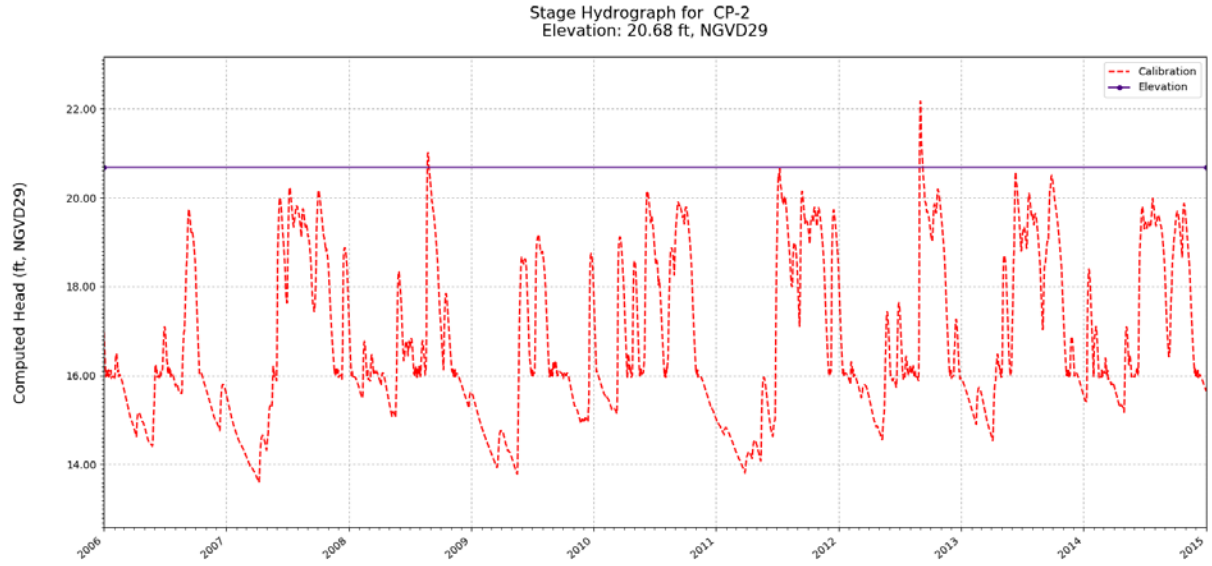

Figure C-43. Simulated stage hydrograph (2006 – 2014) and model cell topography for WRAP cell CP-2.

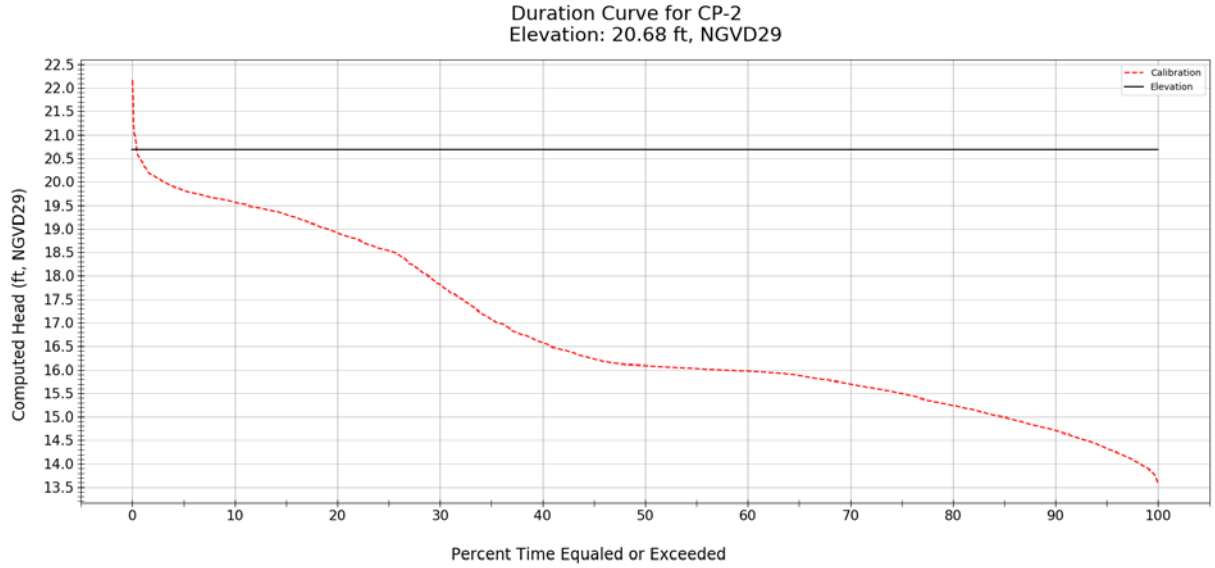

Figure C-44. Simulated stage duration curve (2006 – 2014) and model cell topography for WRAP cell CP-2.

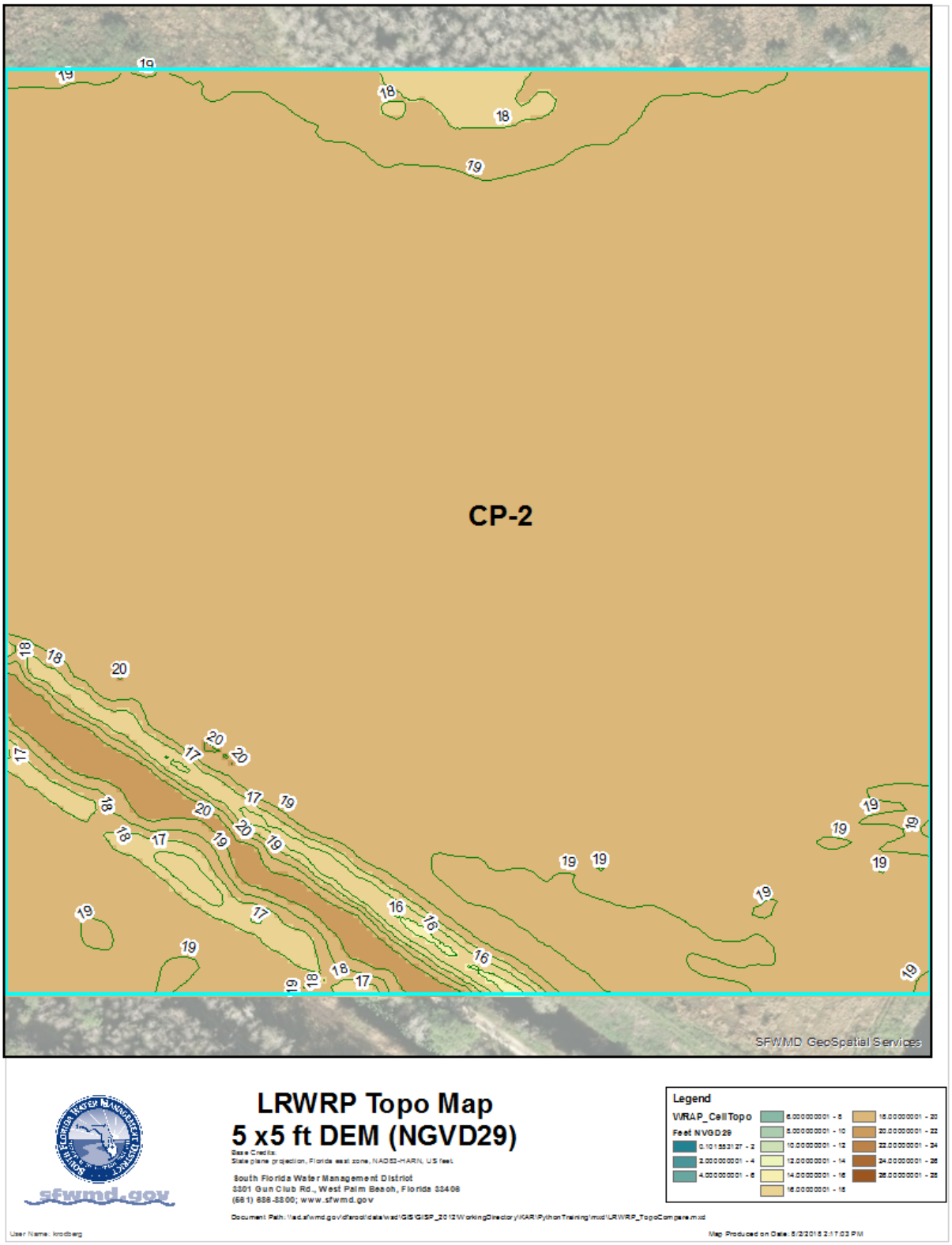

Figure C-45. Variation of model cell topography based on SFWMD's 5 ft LiDAR within WRAP cell CP-2.

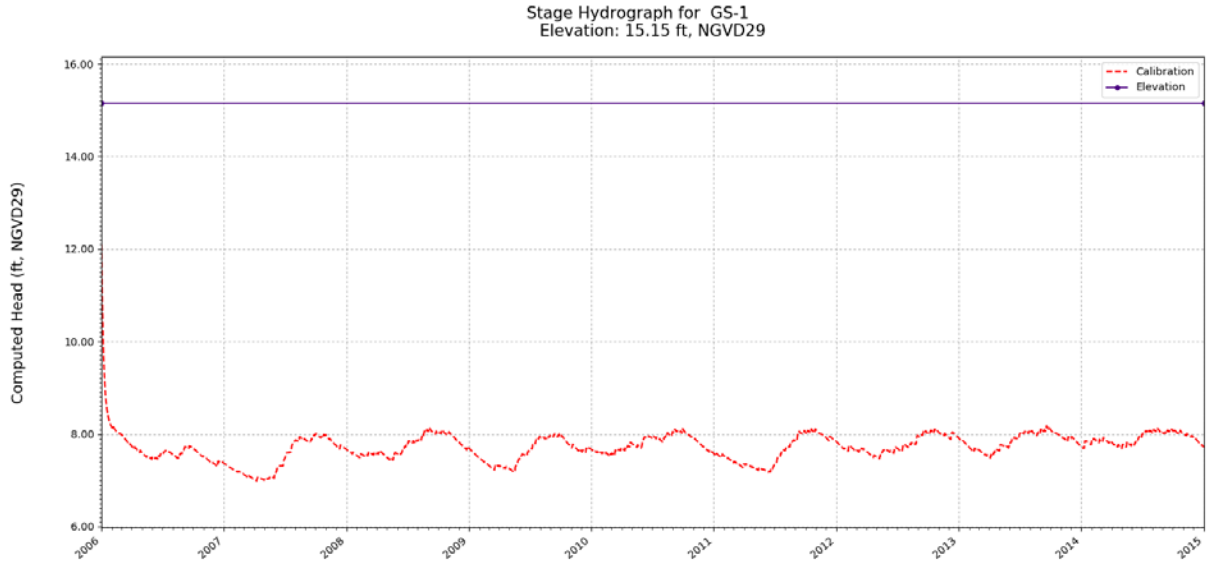

Figure C-46. Simulated stage hydrograph (2006 – 2014) and model cell topography for WRAP cell GS-1.

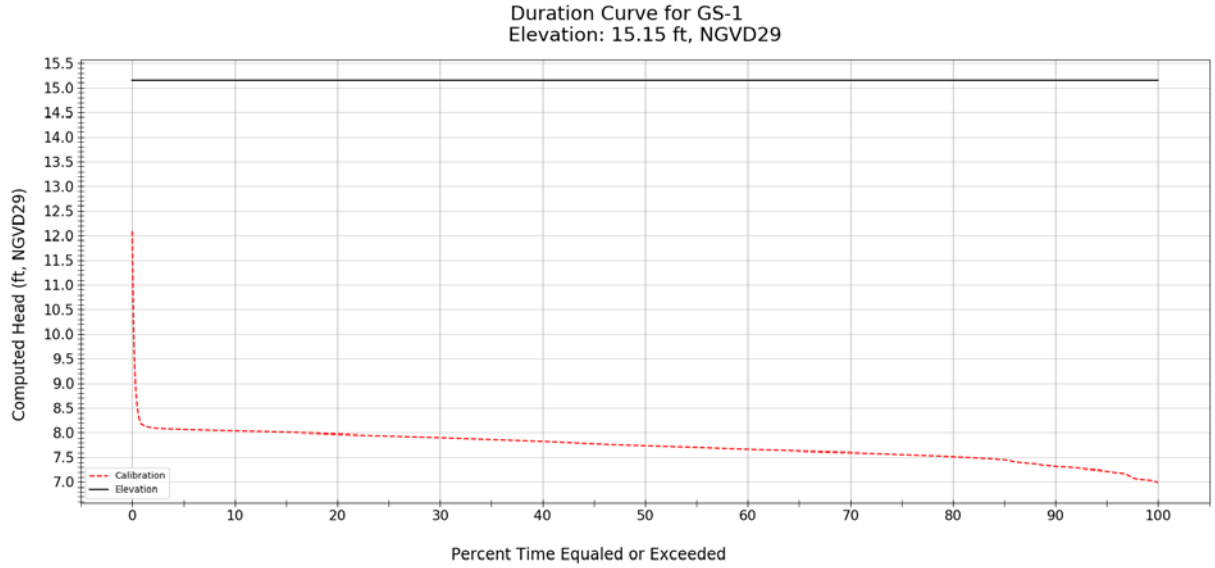

Figure C-47. Simulated stage duration curve (2006 – 2014) and model cell topography for WRAP cell GS-1.

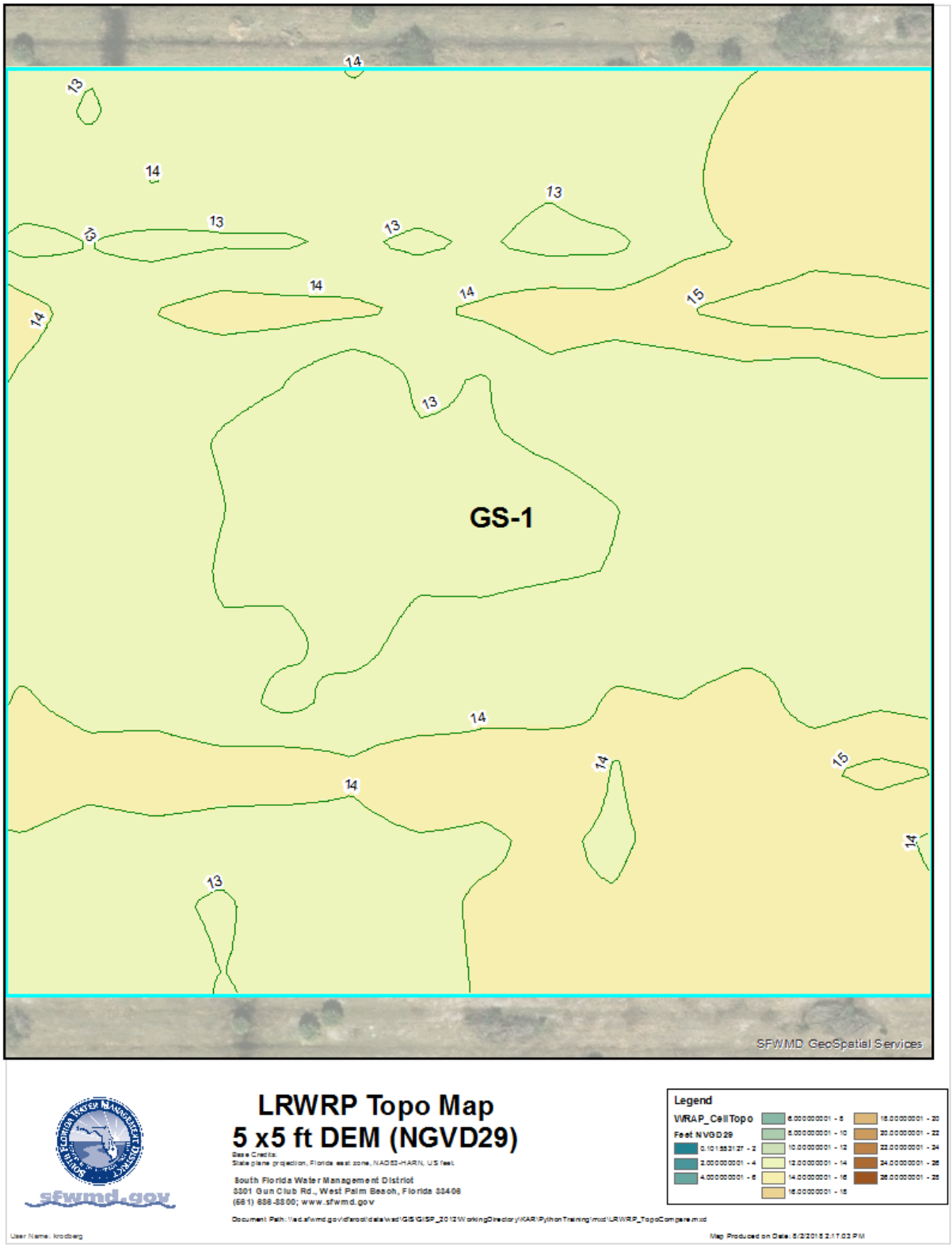

Figure C-48. Variation of model cell topography based on SFWMD's 5 ft LiDAR within WRAP cell GS-1.

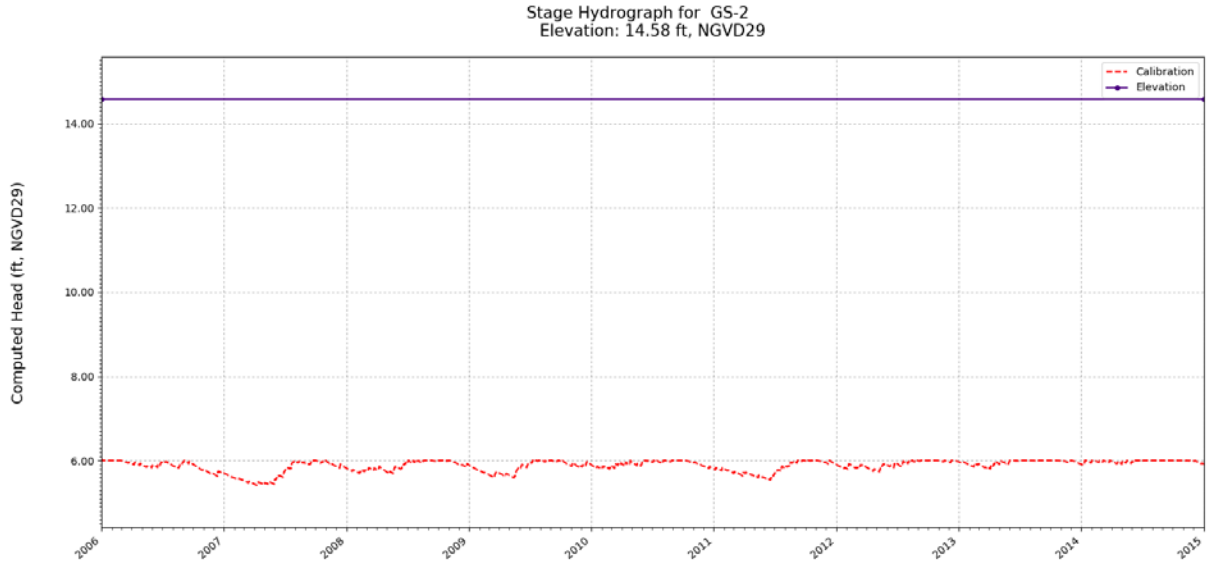

Figure C-49. Simulated stage hydrograph (2006 – 2014) and model cell topography for WRAP cell GS-2.

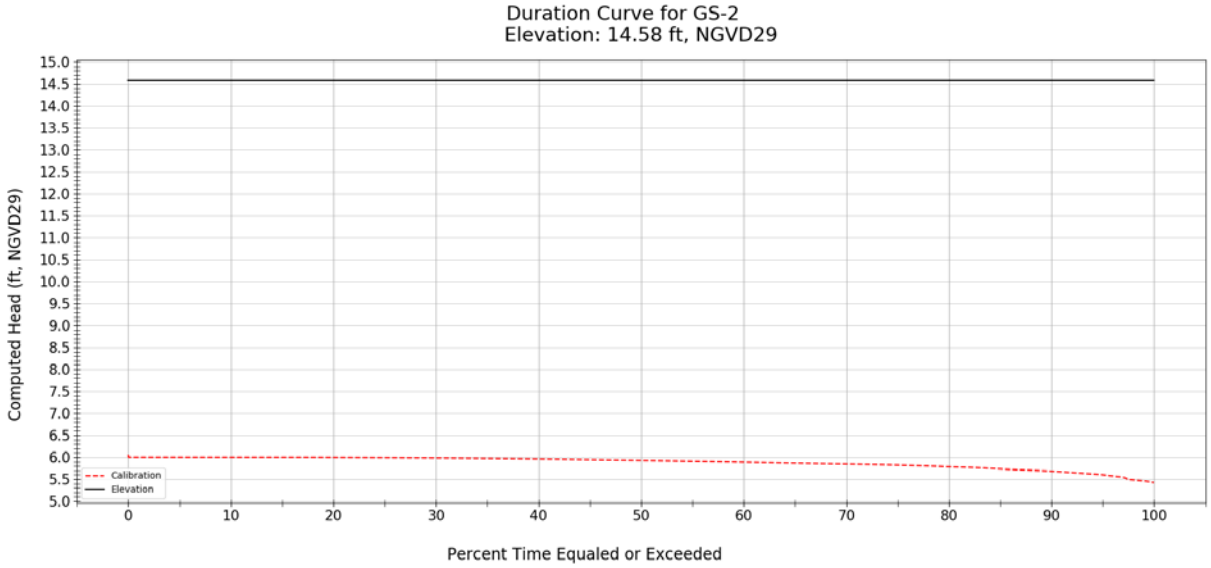

Figure C-50. Simulated stage duration curve (2006 – 2014) and model cell topography for WRAP cell GS-2.

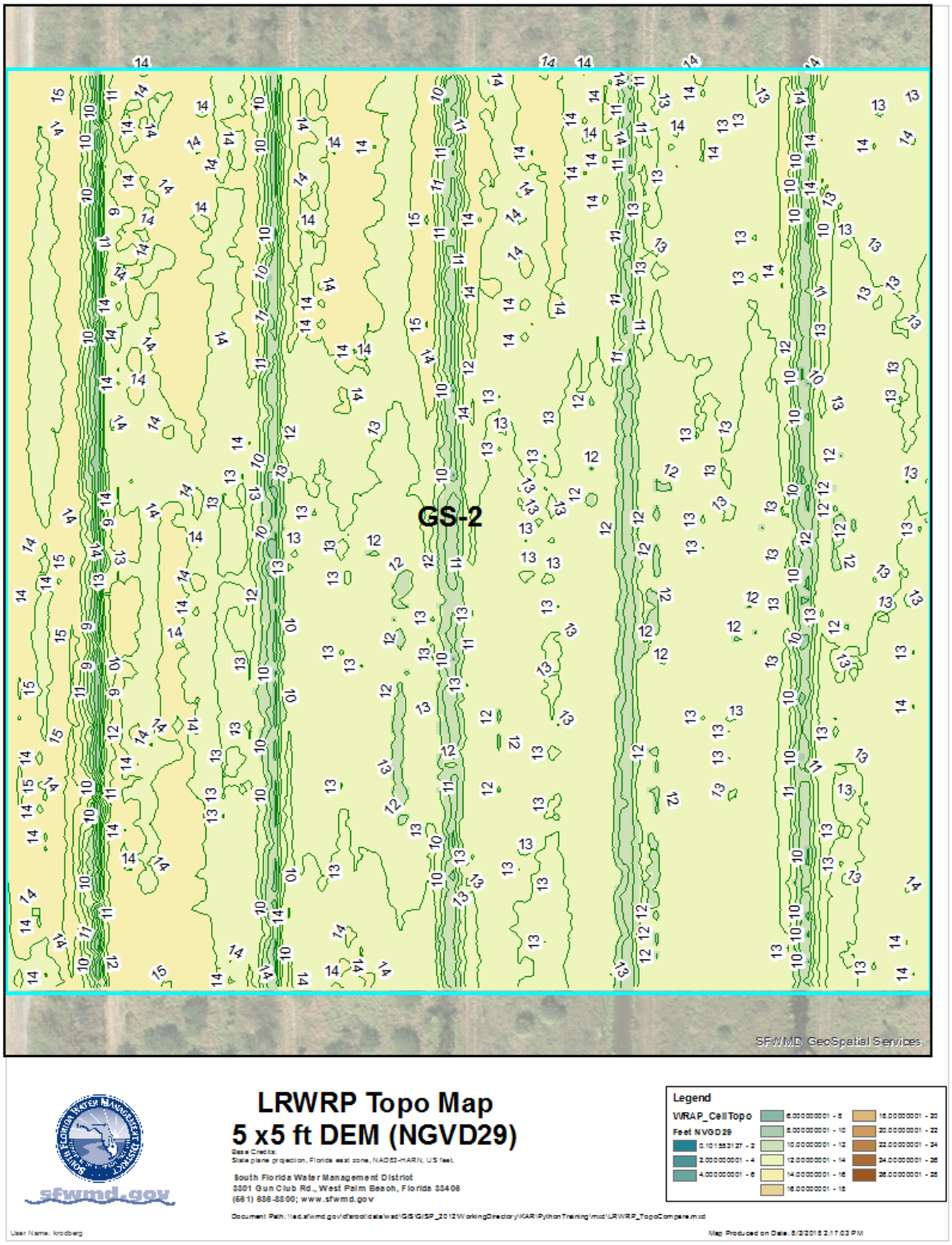

Figure C-51. Variation of model cell topography based on SFWMD's 5 ft LiDAR within WRAP cell GS-2.

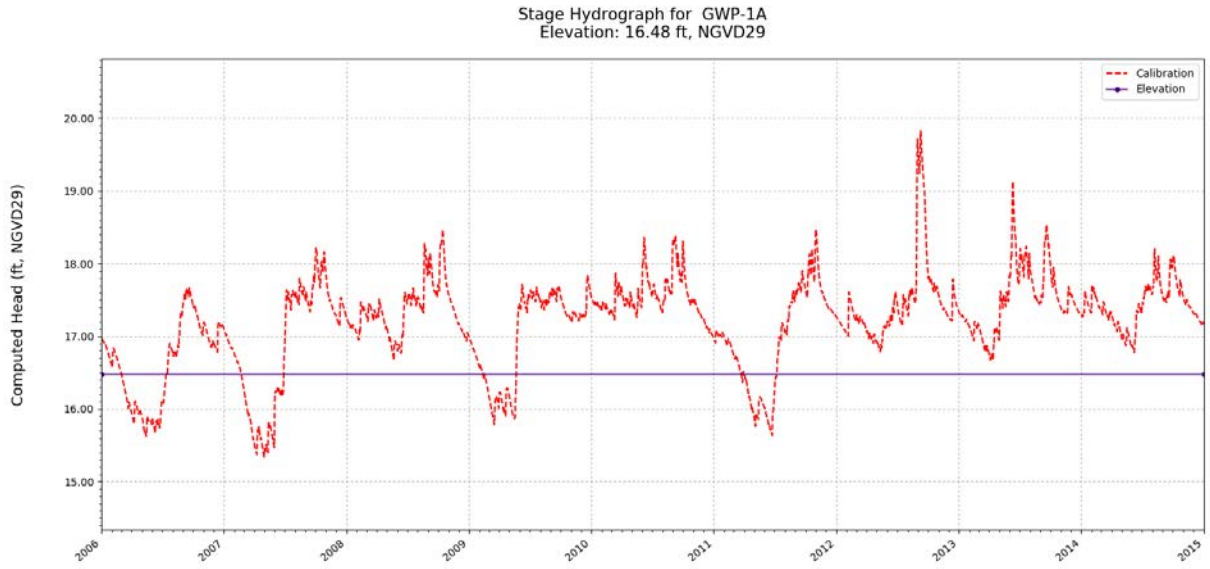

Figure C-52. Simulated stage hydrograph (2006 – 2014) and model cell topography for WRAP cell GWP-1A.

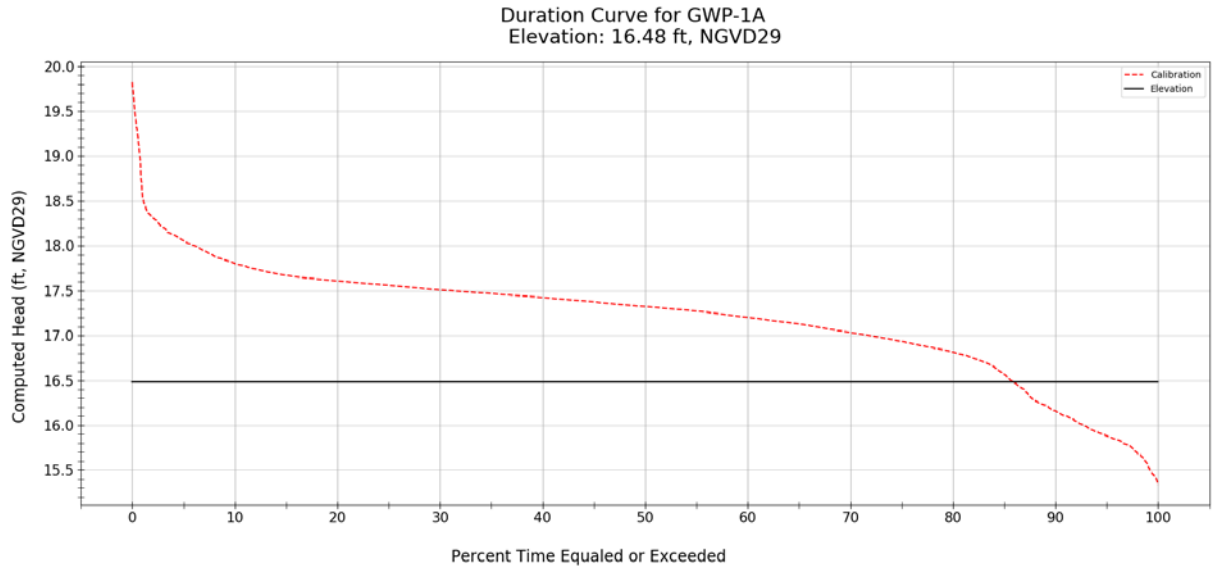

Figure C-53. Simulated stage duration curve (2006 – 2014) and model cell topography for WRAP cell GWP-1A.

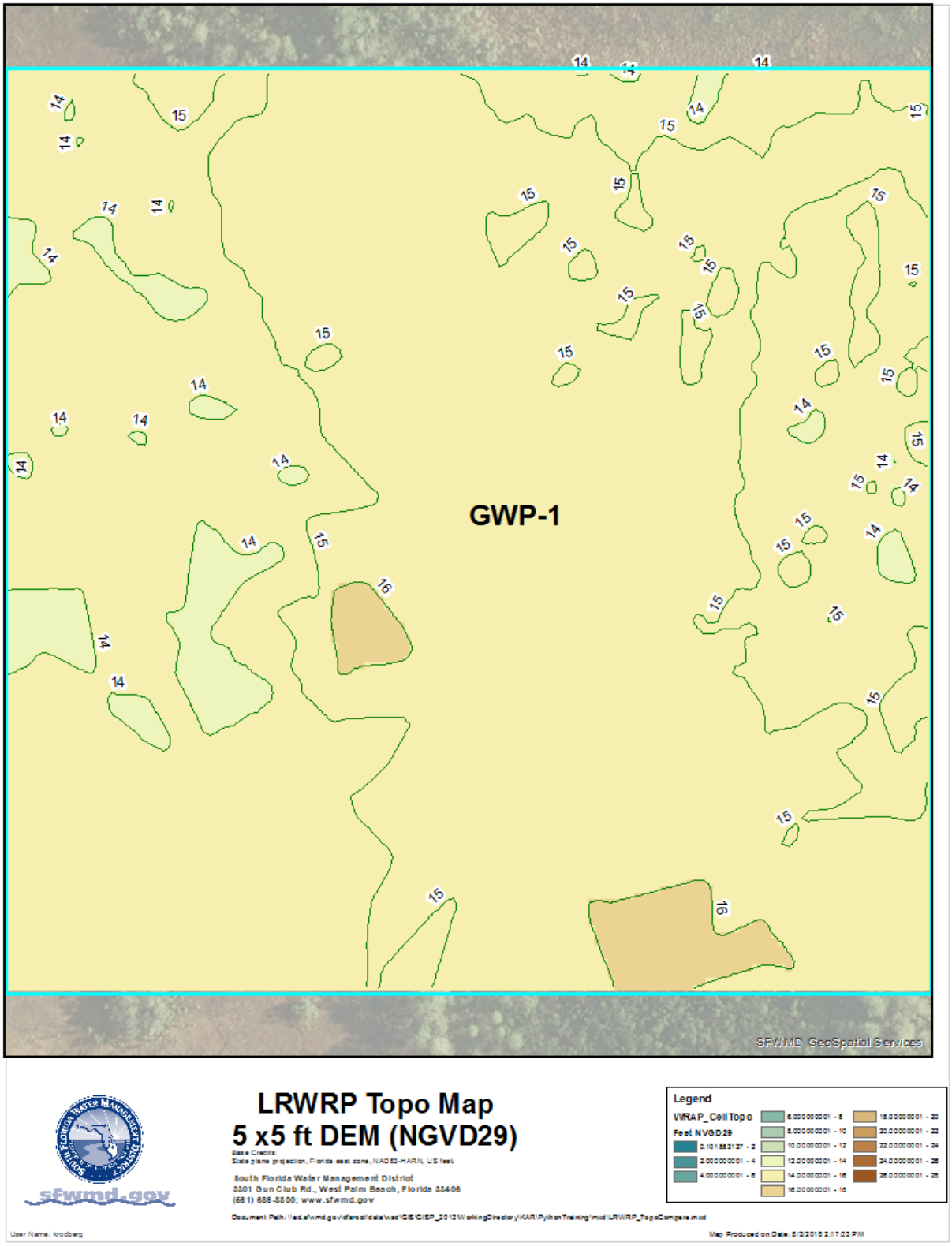

Figure C-54. Variation of model cell topography based on SFWMD's 5 ft LiDAR within WRAP cell GWP-1A.

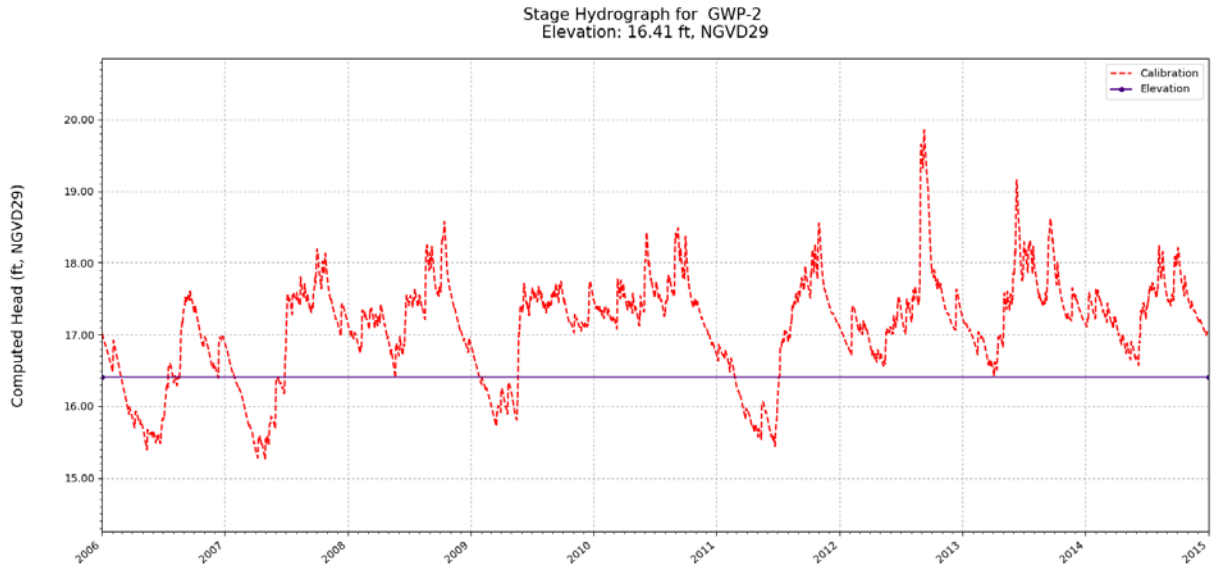

Figure C-55. Simulated stage hydrograph (2006 – 2014) and model cell topography for WRAP cell GWP-2.

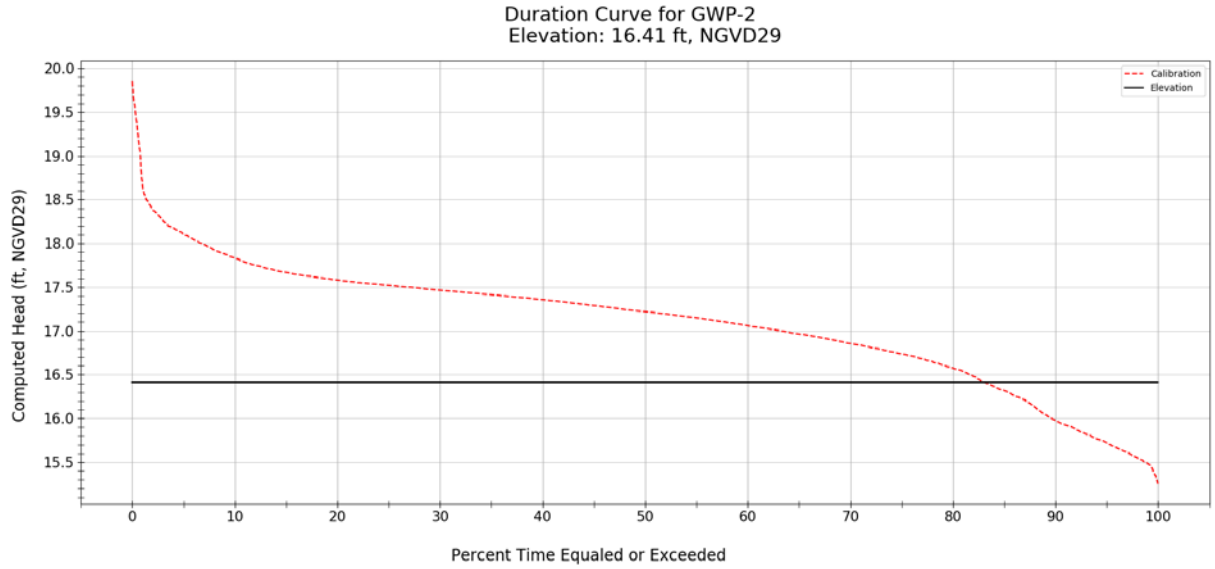

Figure C-56. Simulated stage duration curve (2006 – 2014) and model cell topography for WRAP cell GWP-2.

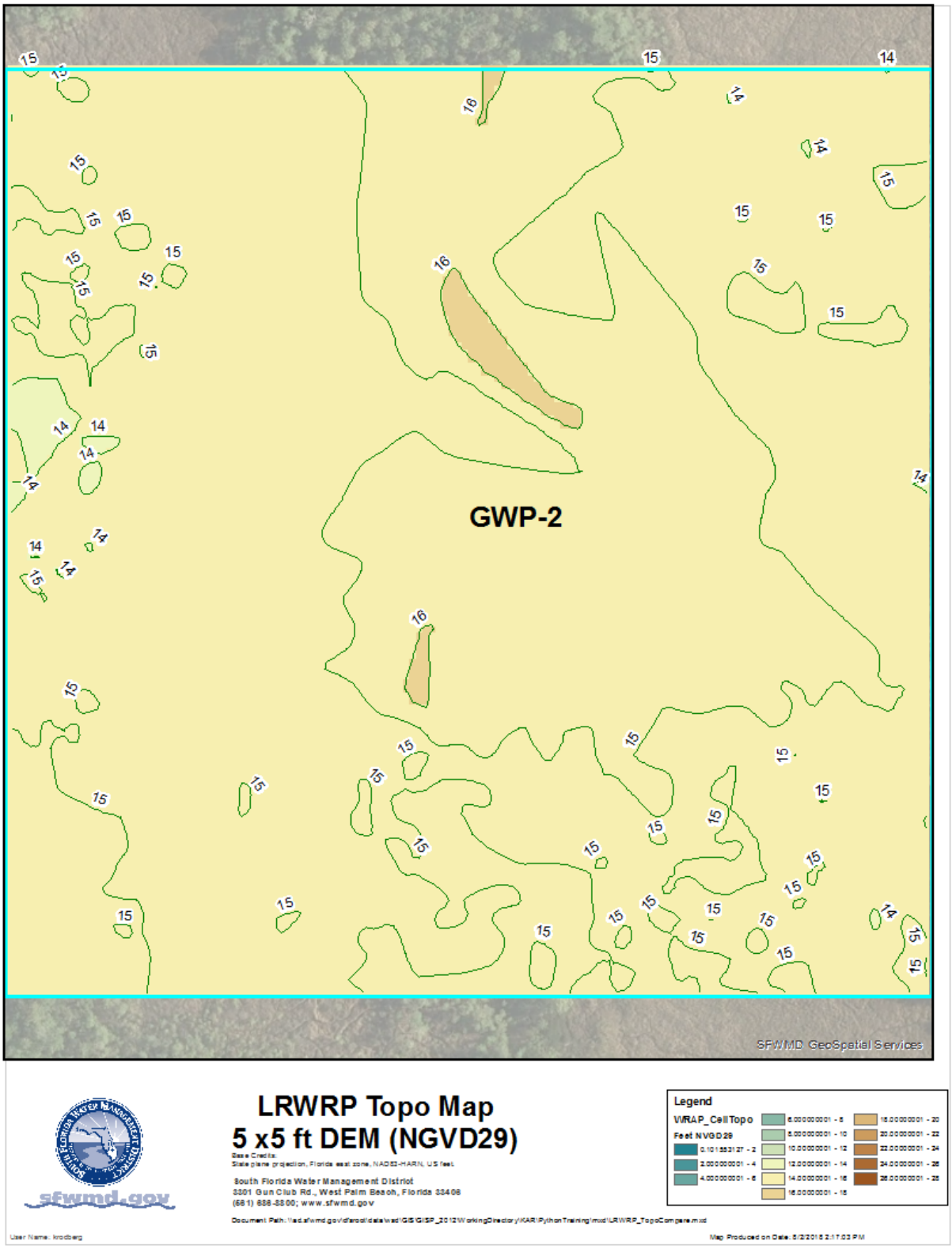

Figure C-57. Variation of model cell topography based on SFWMD's 5 ft LiDAR within WRAP cell GWP-2.

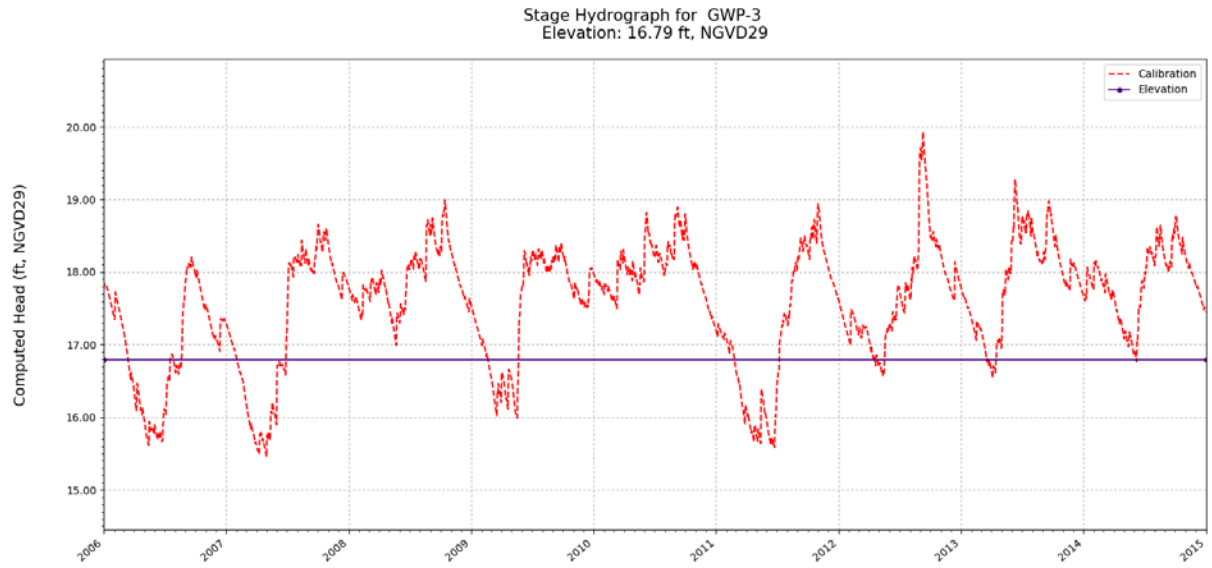

Figure C-58. Simulated stage hydrograph (2006 – 2014) and model cell topography for WRAP cell GWP-3.

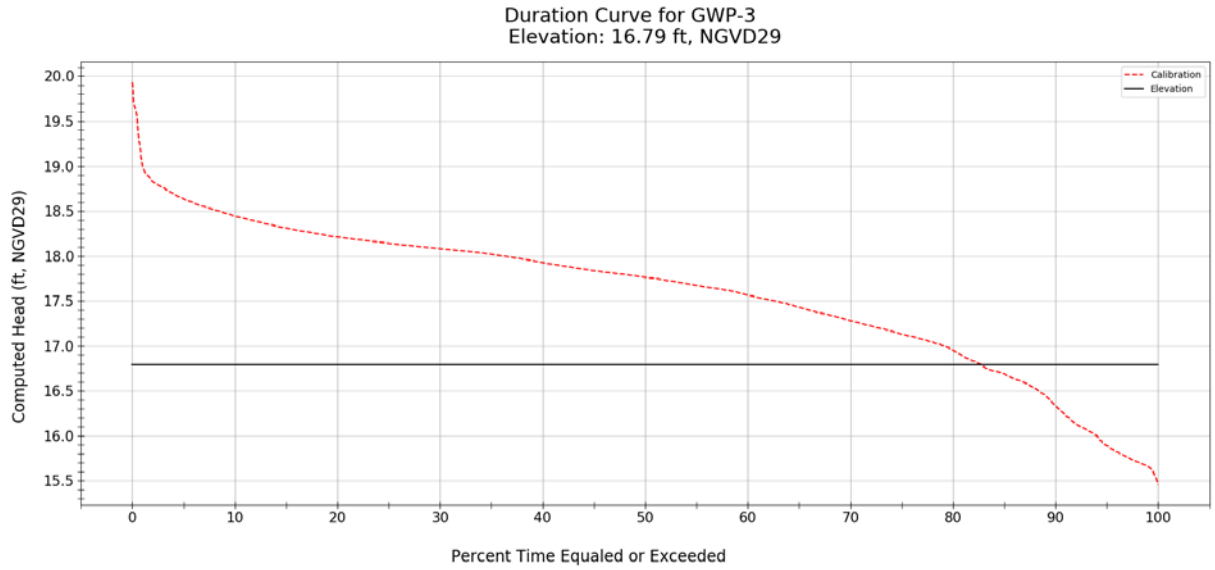

Figure C-59. Simulated stage duration curve (2006 – 2014) and model cell topography for WRAP cell GWP-3.

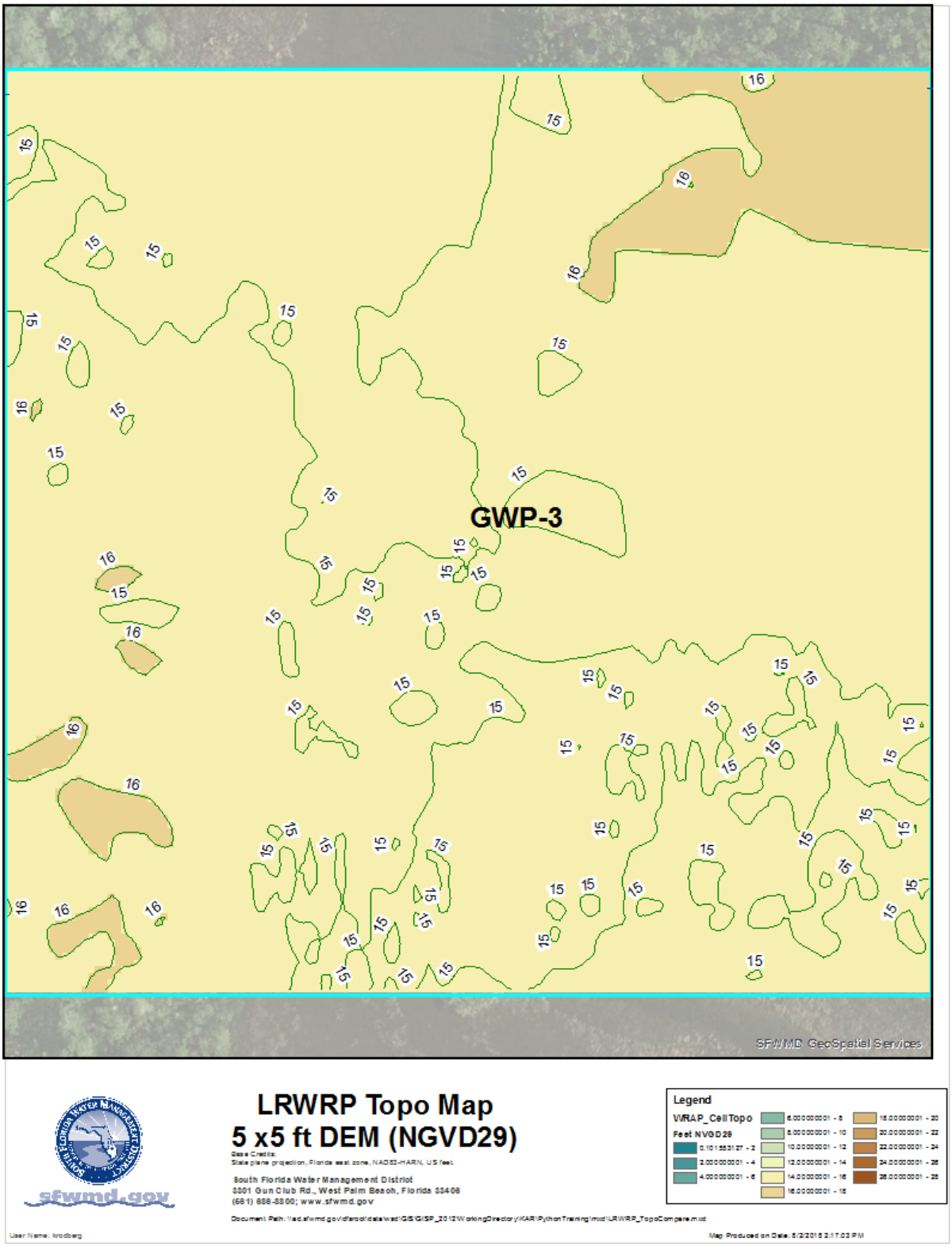

Figure C-60. Variation of model cell topography based on SFWMD's 5 ft LiDAR within WRAP cell GWP-3.

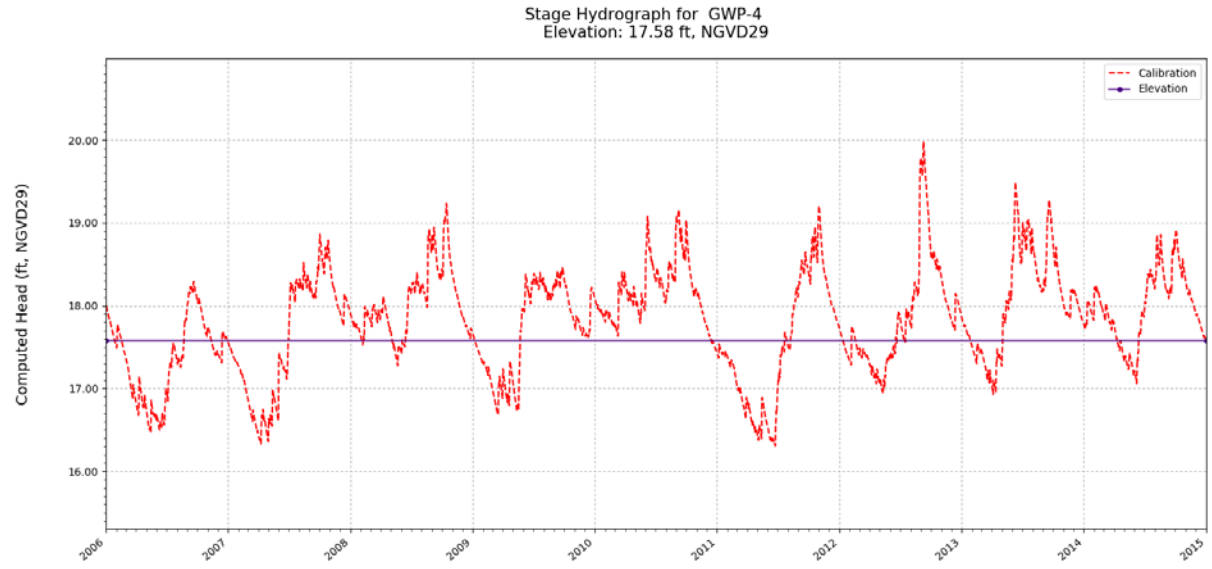

Figure C-61. Simulated stage hydrograph (2006 – 2014) and model cell topography for WRAP cell GWP-4.

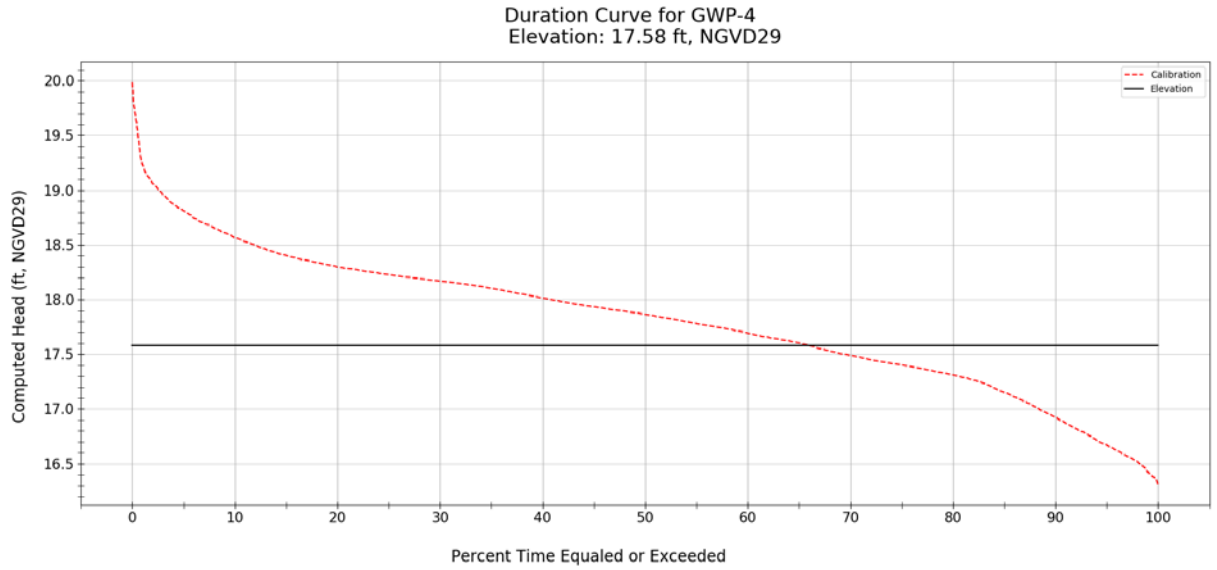

Figure C-62. Simulated stage duration curve (2006 – 2014) and model cell topography for WRAP cell GWP-4.

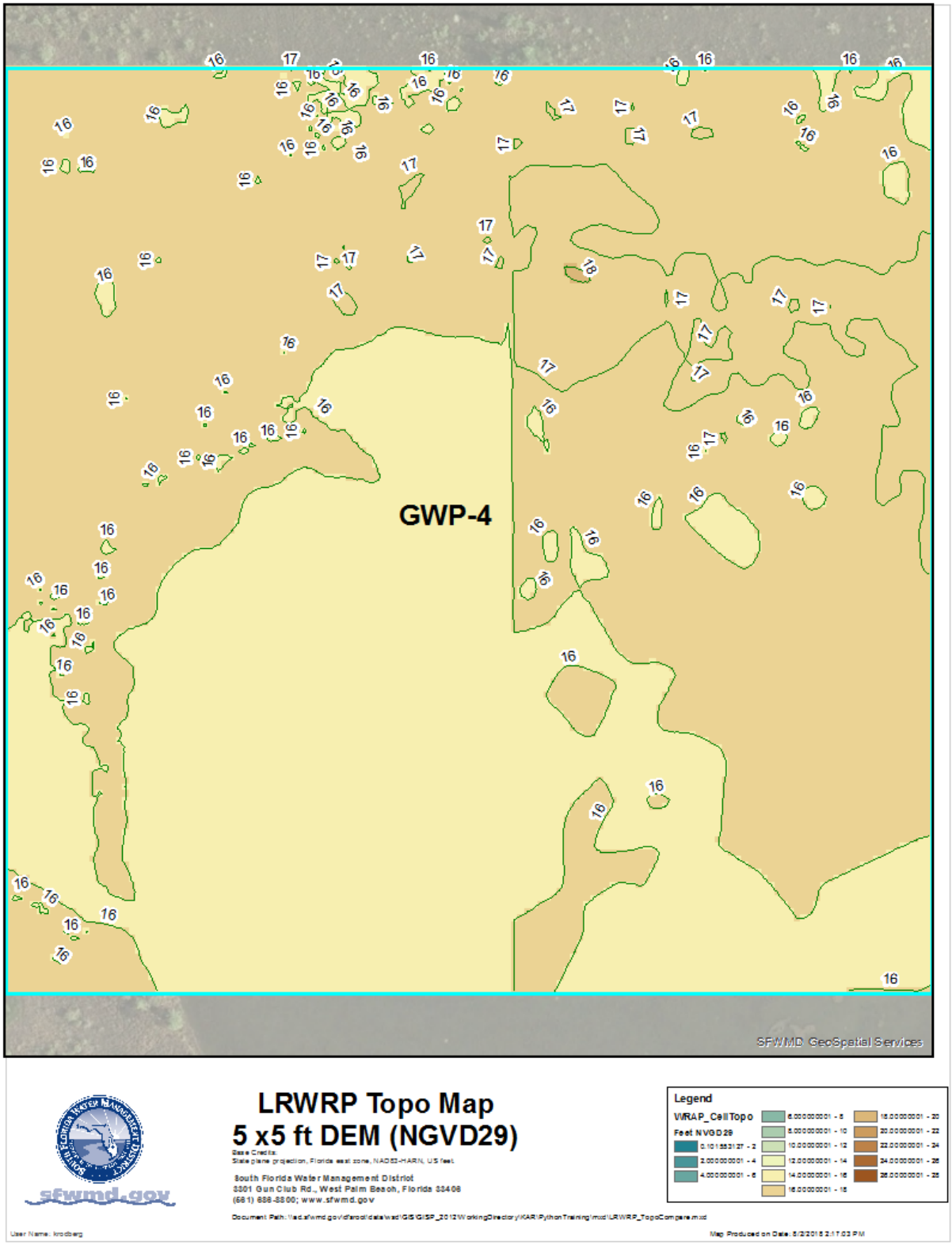

Figure C-63. Variation of model cell topography based on SFWMD's 5 ft LiDAR within WRAP cell GWP-4.

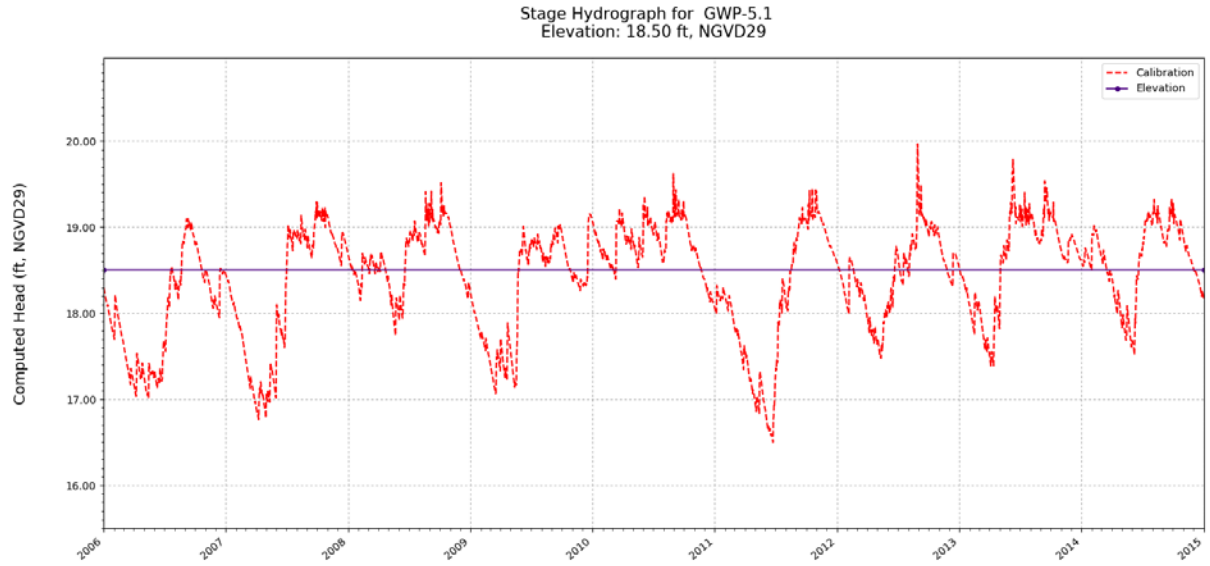

Figure C-64. Simulated stage hydrograph (2006 – 2014) and model cell topography for WRAP cell GWP-5.1.

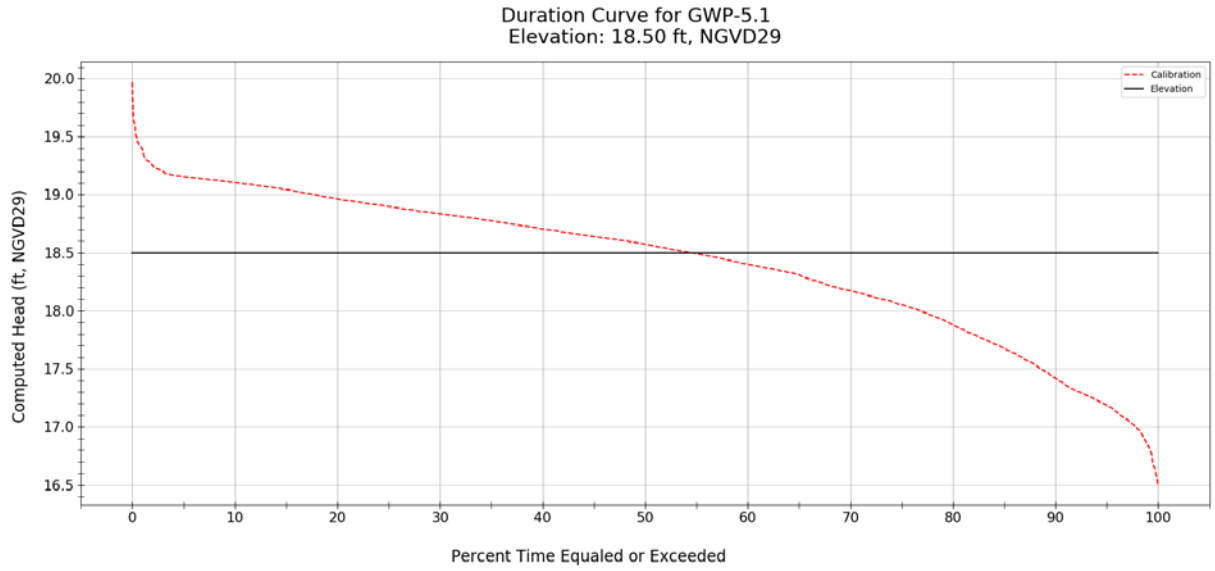

Figure C-65. Simulated stage duration curve (2006 – 2014) and model cell topography for WRAP cell GWP-5.1.

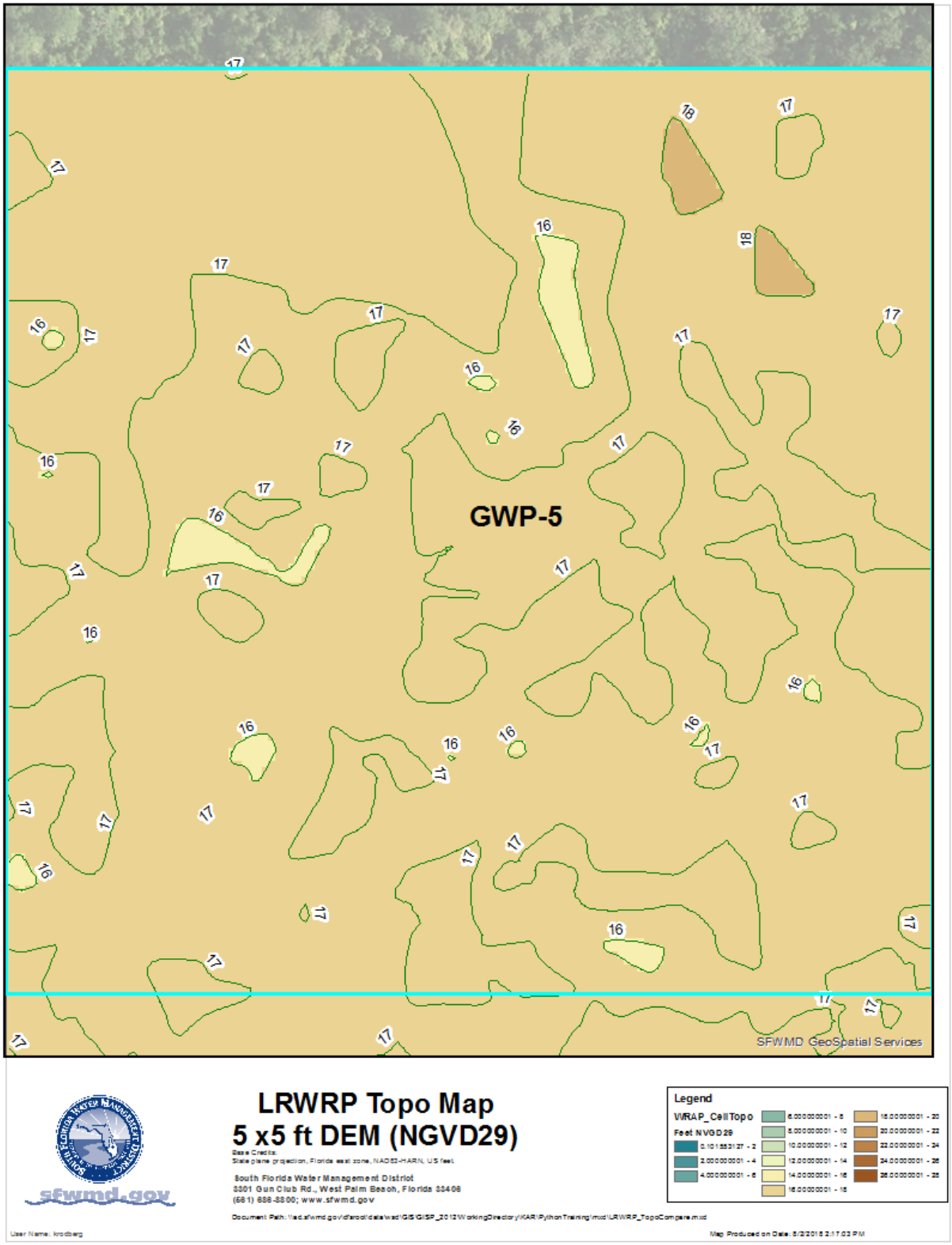

Figure C-66. Variation of model cell topography based on SFWMD's 5 ft LiDAR within WRAP cell GWP-5.1.

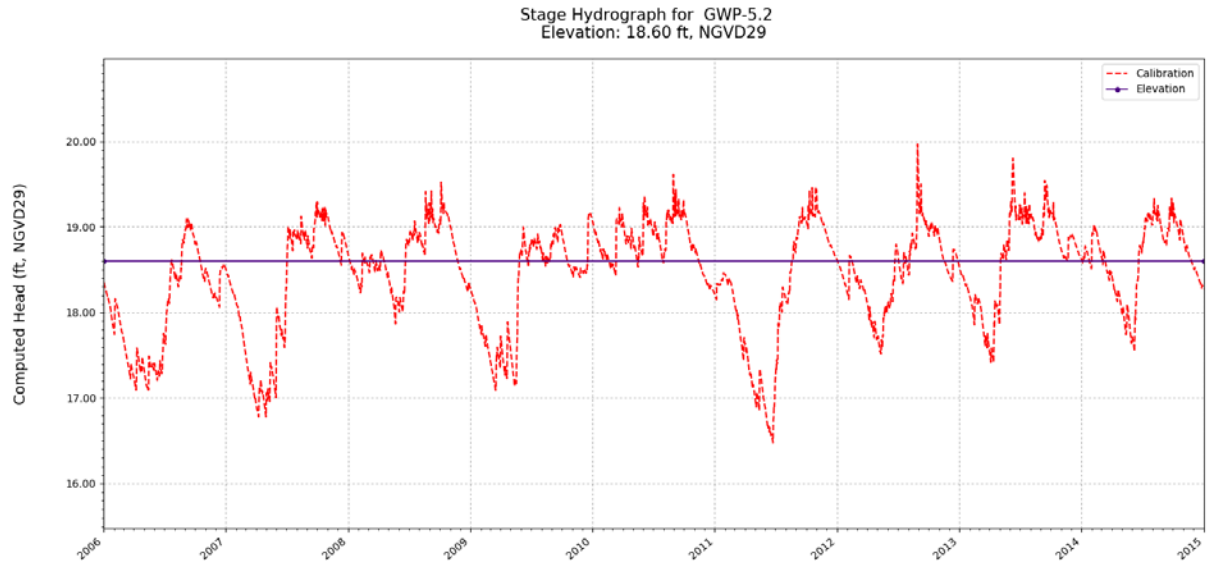

Figure C-67. Simulated stage hydrograph (2006 – 2014) and model cell topography for WRAP cell GWP-5.2.

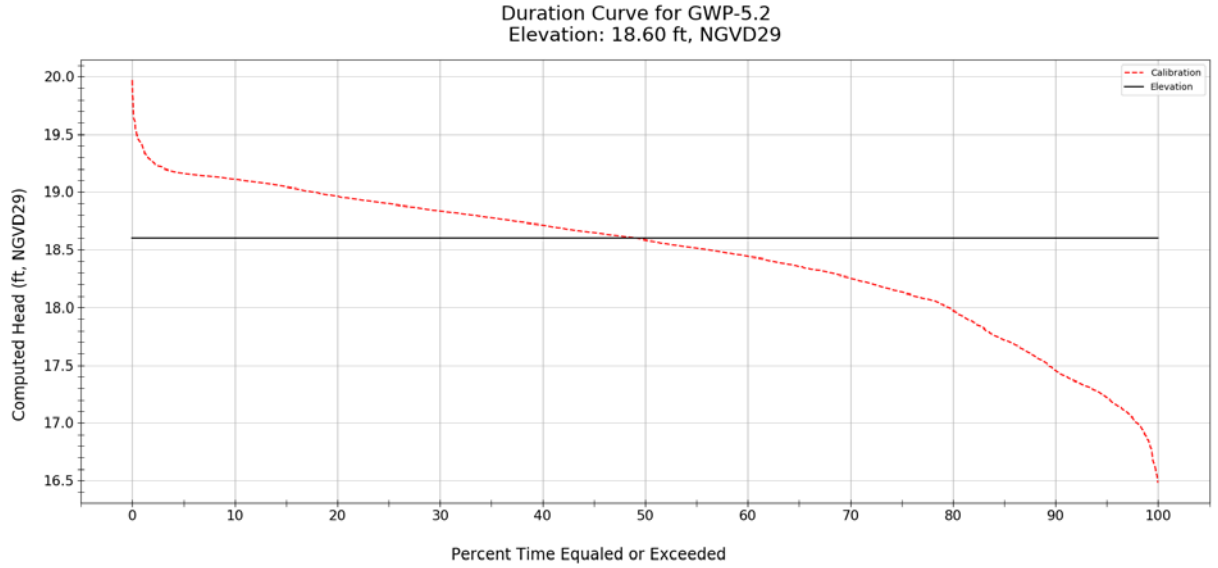

Figure C-68. Simulated stage duration curve (2006 – 2014) and model cell topography for WRAP cell GWP-5.2.

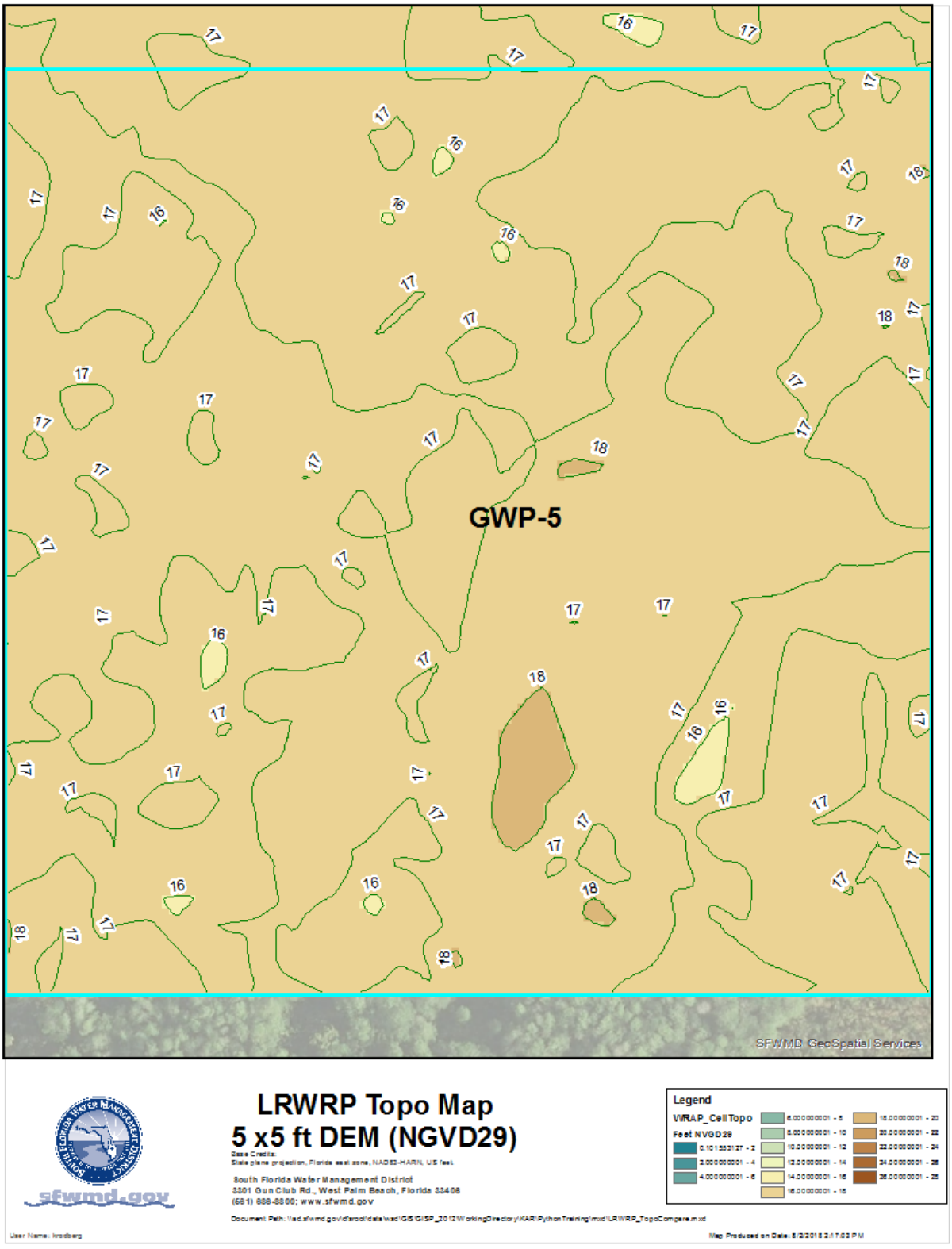

Figure C-69. Variation of model cell topography based on SFWMD's 5 ft LiDAR within WRAP cell GWP-5.2.

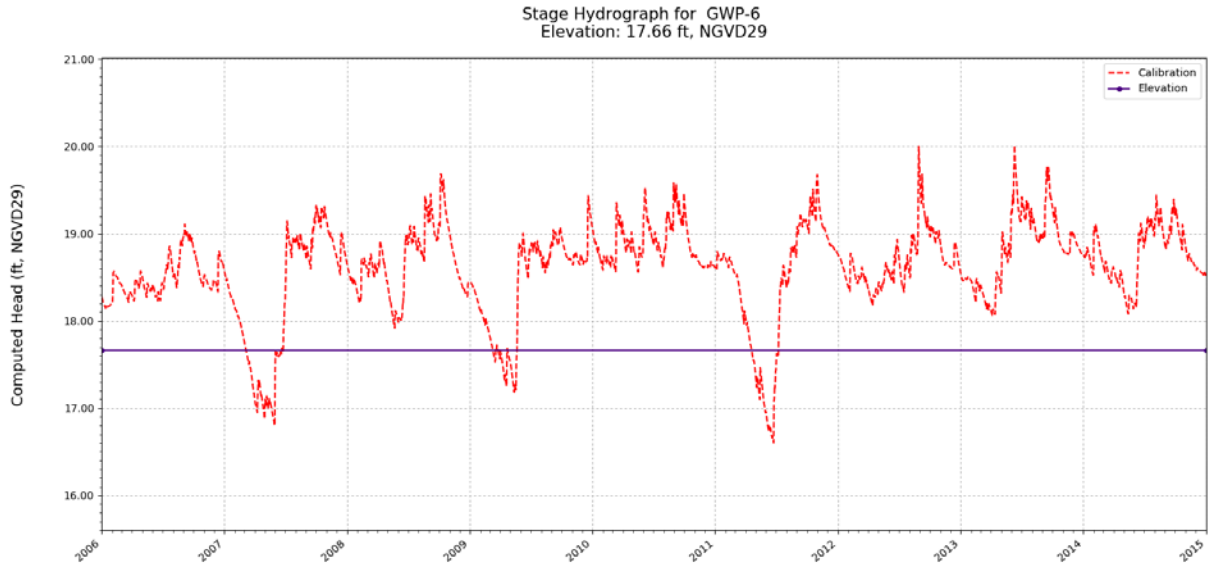

Figure C-70. Simulated stage hydrograph (2006 – 2014) and model cell topography for WRAP cell GWP-6.

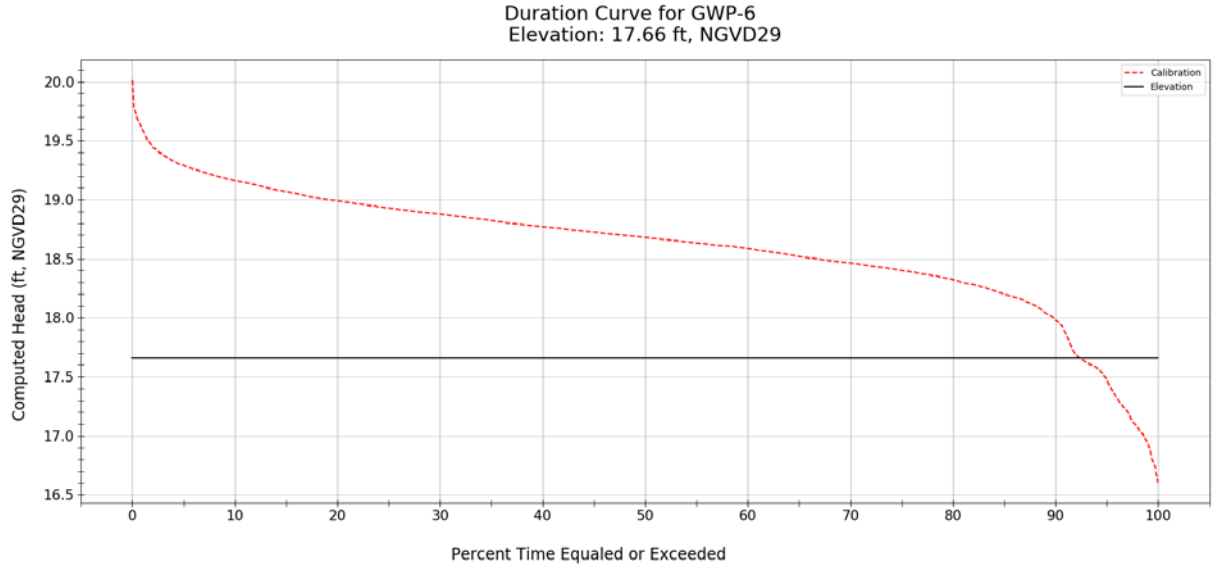

Figure C-71. Simulated stage duration curve (2006 – 2014) and model cell topography for WRAP cell GWP-6.

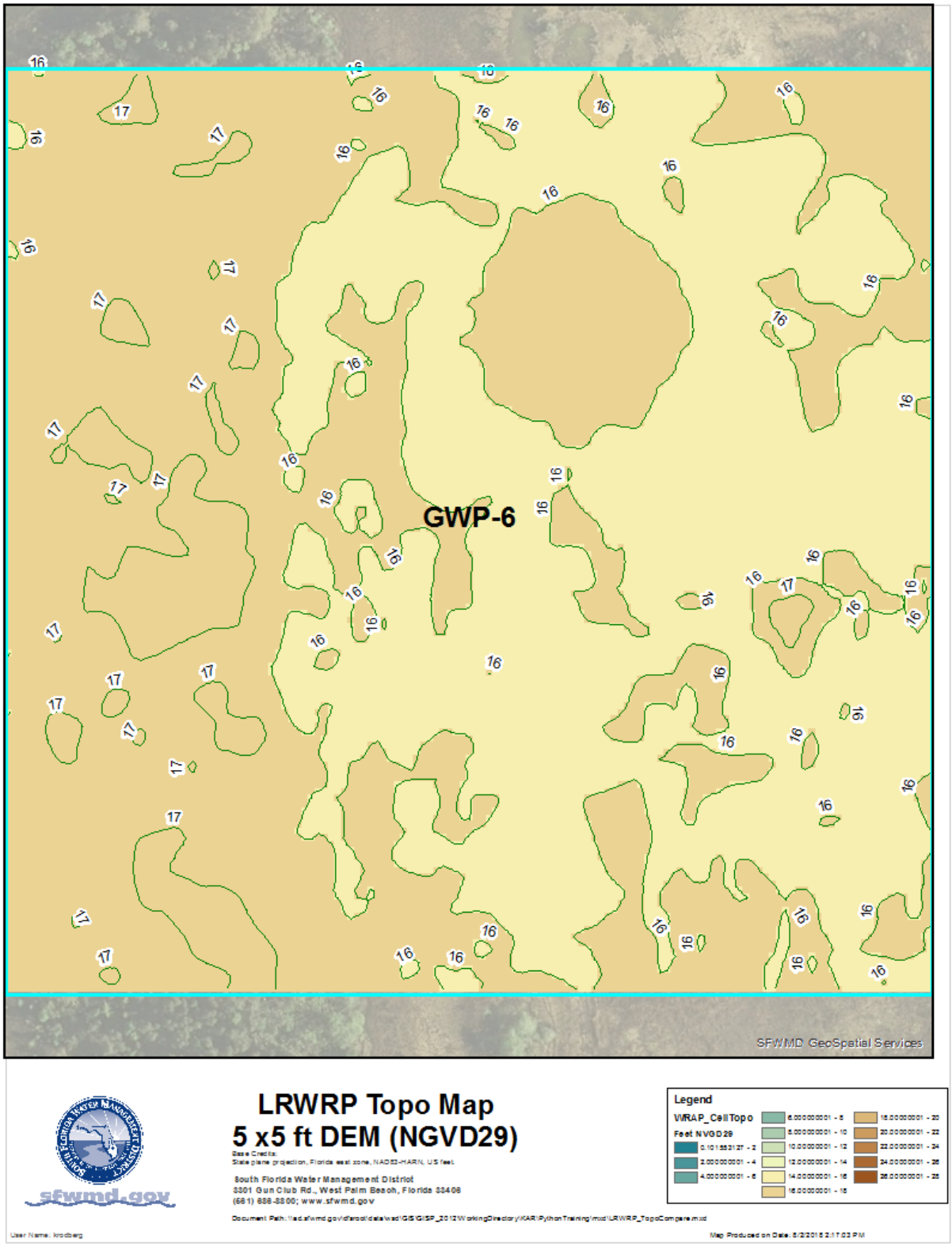

Figure C-72. Variation of model cell topography based on SFWMD's 5 ft LiDAR within WRAP cell GWP-6.

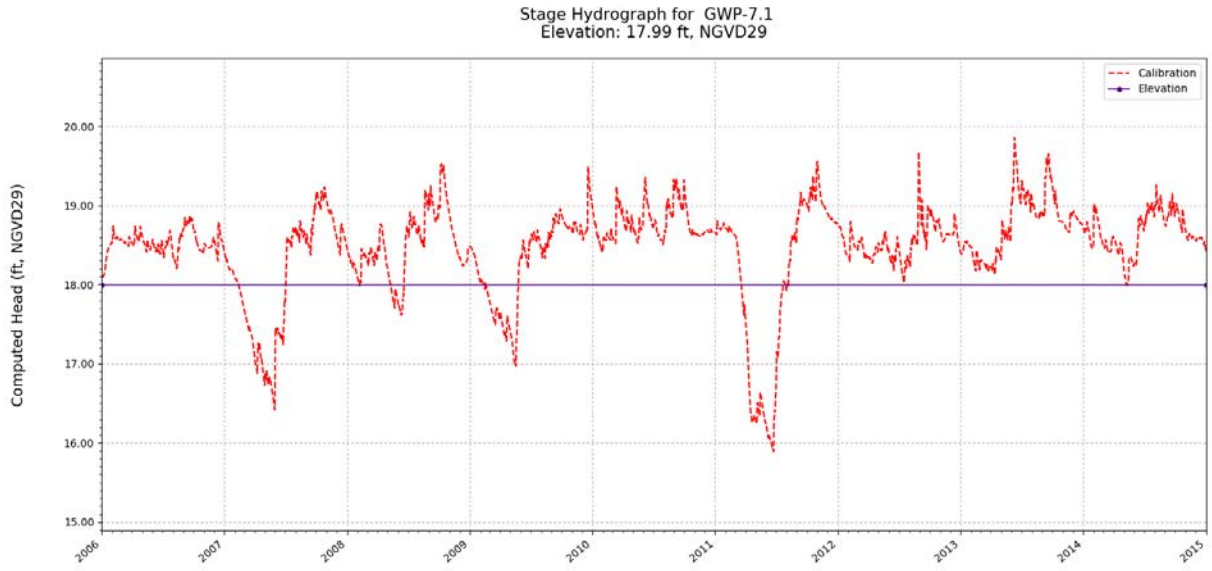

Figure C-73. Simulated stage hydrograph (2006 – 2014) and model cell topography for WRAP cell GWP-7.1.

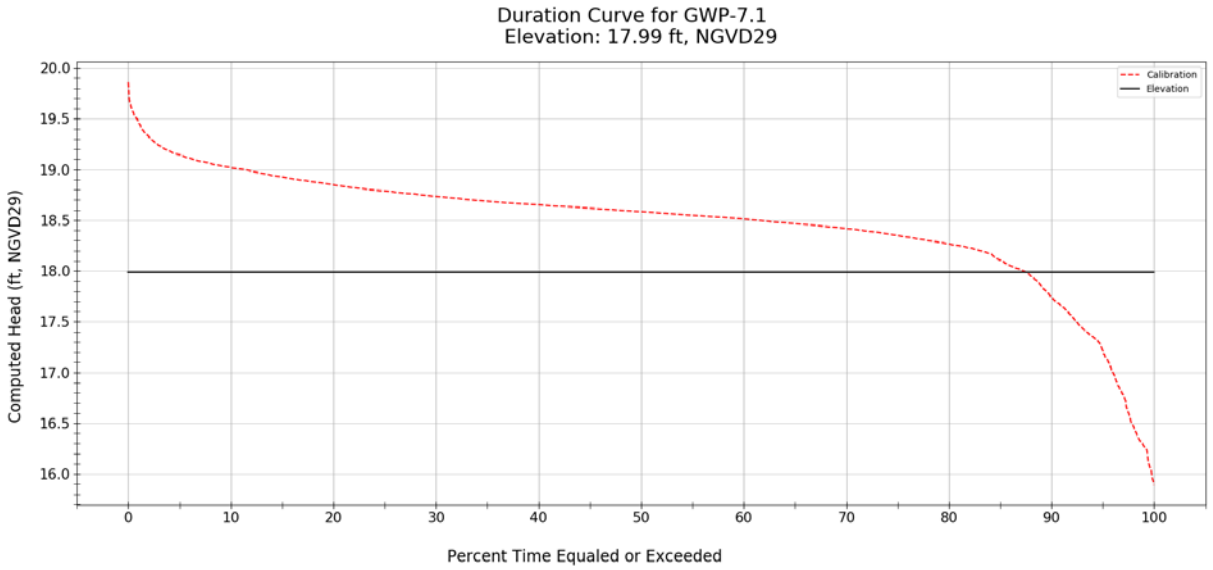

Figure C-74. Simulated stage duration curve (2006 – 2014) and model cell topography for WRAP cell GWP-7.1.

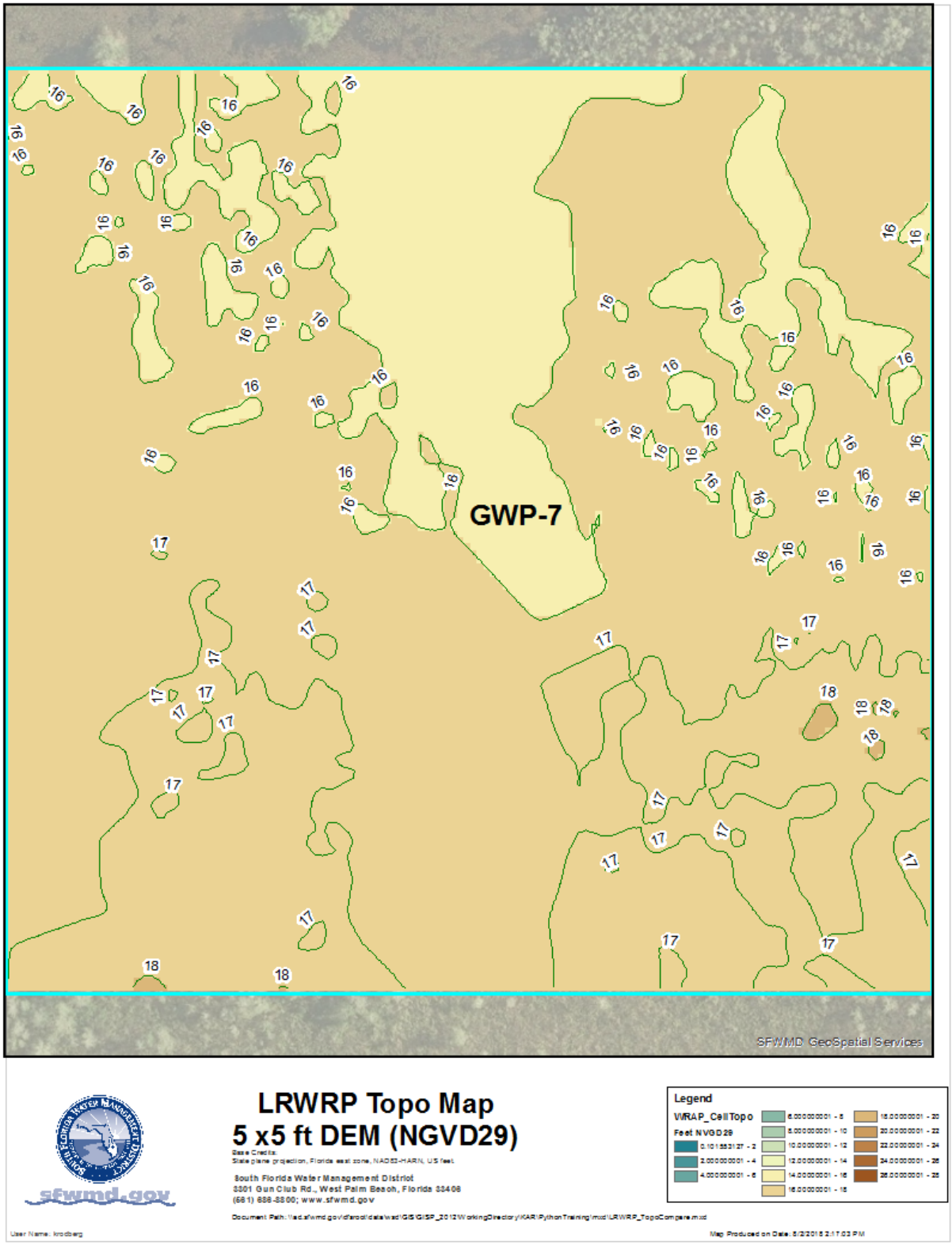

Figure C-75. Variation of model cell topography based on SFWMD's 5 ft LiDAR within WRAP cell GWP-7.1.

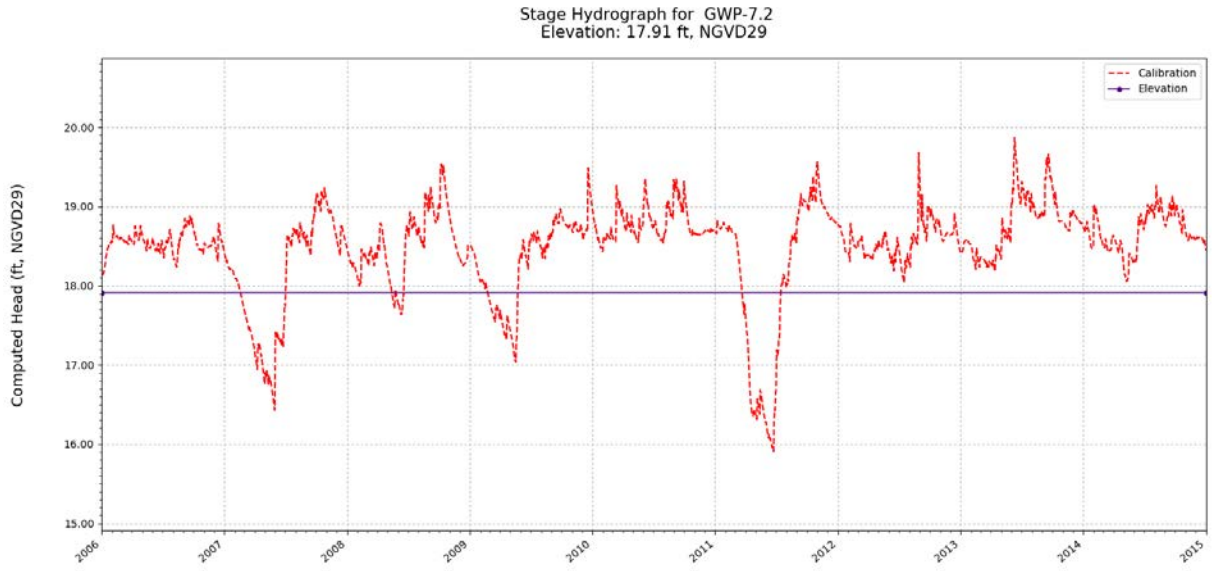

Figure C-76. Simulated stage hydrograph (2006 – 2014) and model cell topography for WRAP cell GWP-7.2.

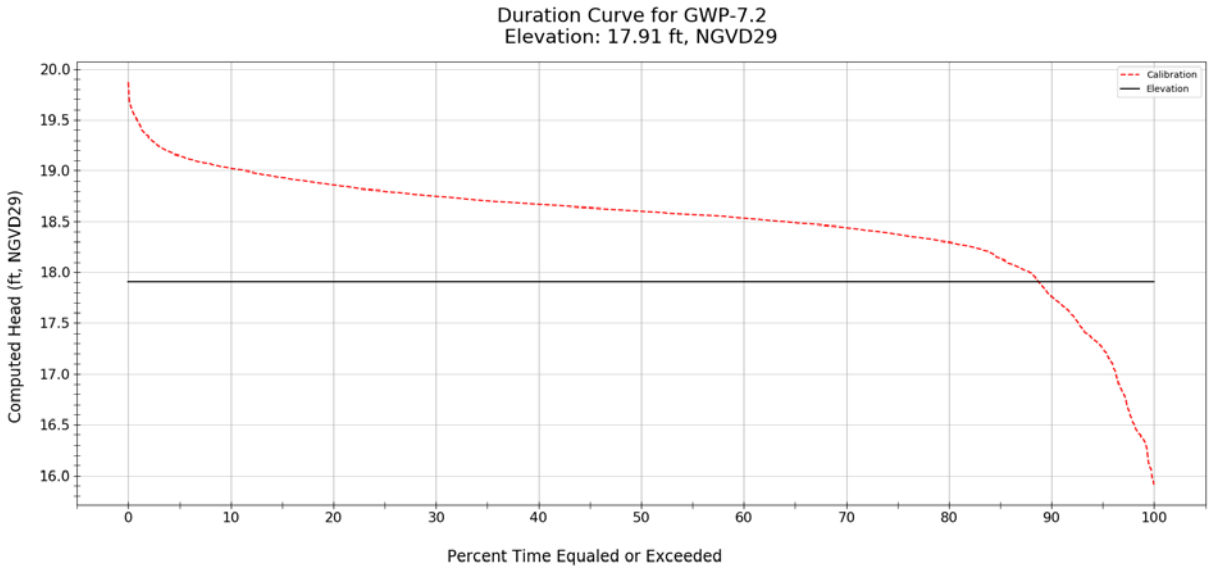

Figure C-77. Simulated stage duration curve (2006 – 2014) and model cell topography for WRAP cell GWP-7.2.

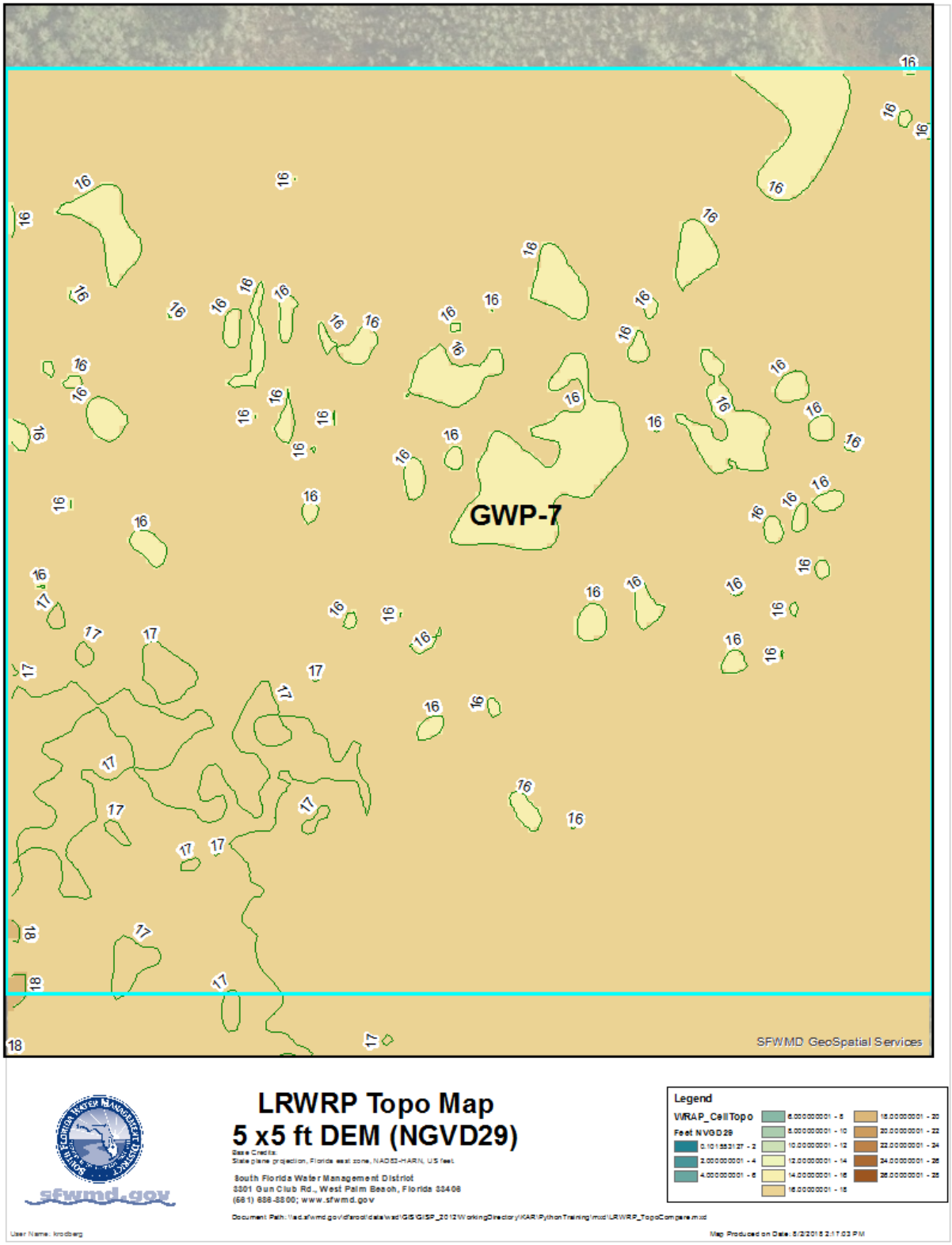

Figure C-78. Variation of model cell topography based on SFWMD's 5 ft LiDAR within WRAP cell GWP-7.2.

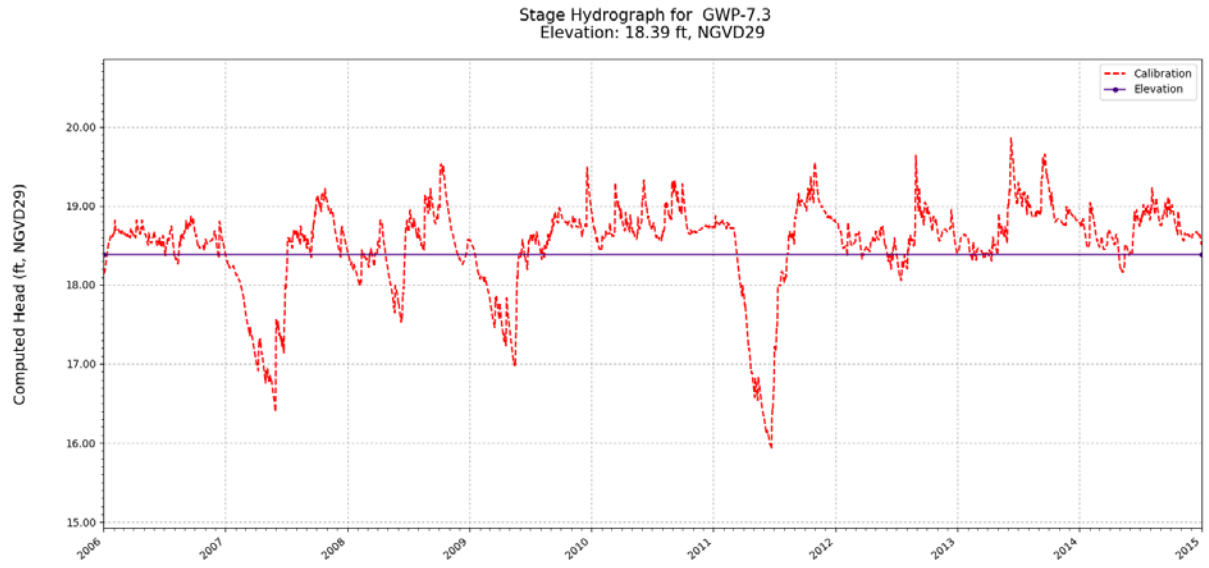

Figure C-79. Simulated stage hydrograph (2006 – 2014) and model cell topography for WRAP cell GWP-7.3.

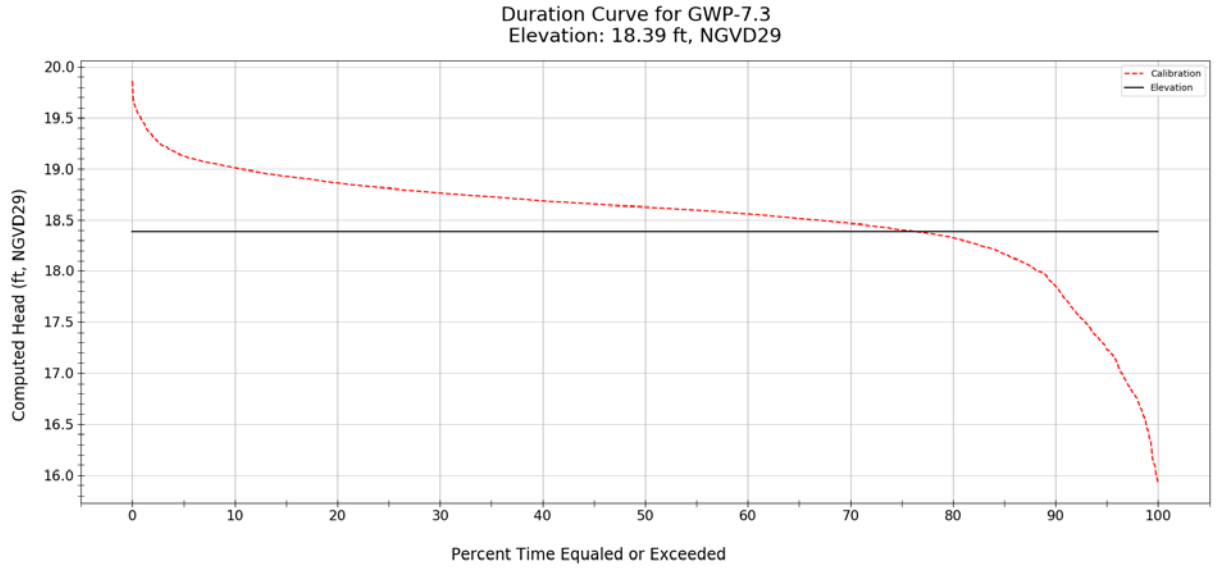

Figure C-80. Simulated stage duration curve (2006 – 2014) and model cell topography for WRAP cell GWP-7.3.

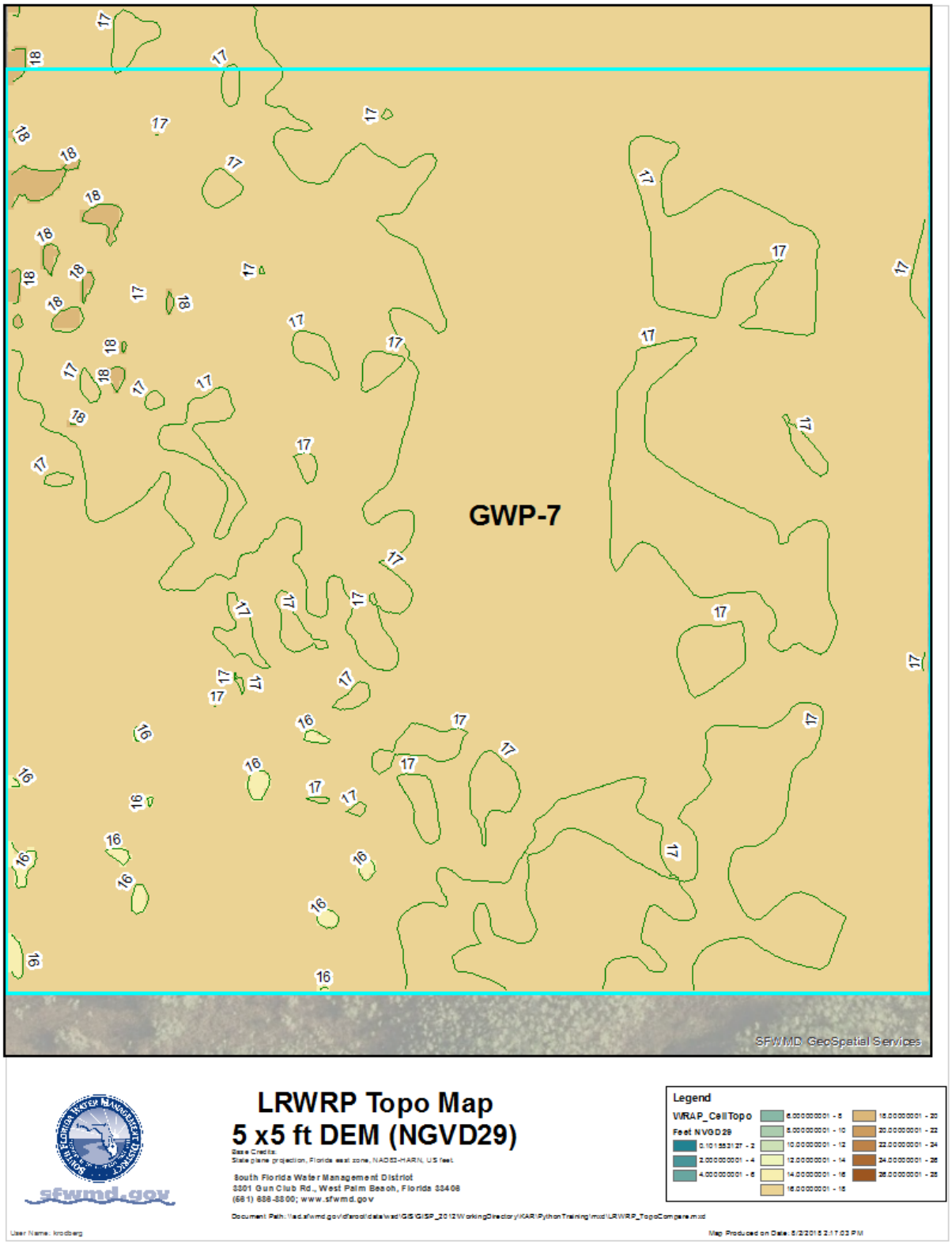

Figure C-81. Variation of model cell topography based on SFWMD's 5 ft LiDAR within WRAP cell GWP-7.3.

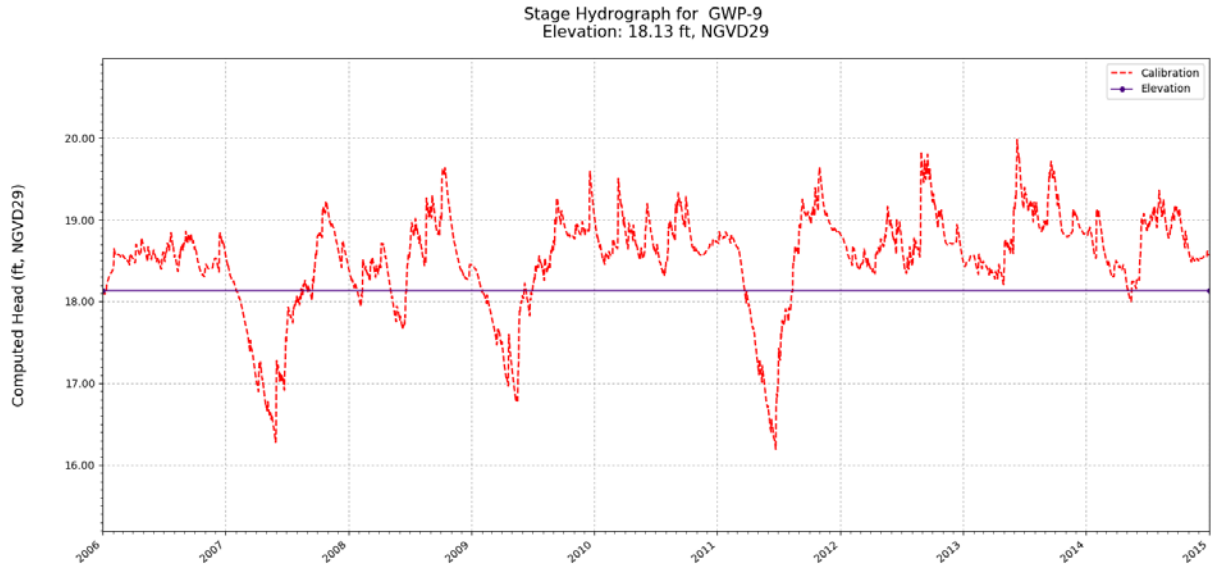

Figure C-82. Simulated stage hydrograph (2006 – 2014) and model cell topography for WRAP cell GWP-9.

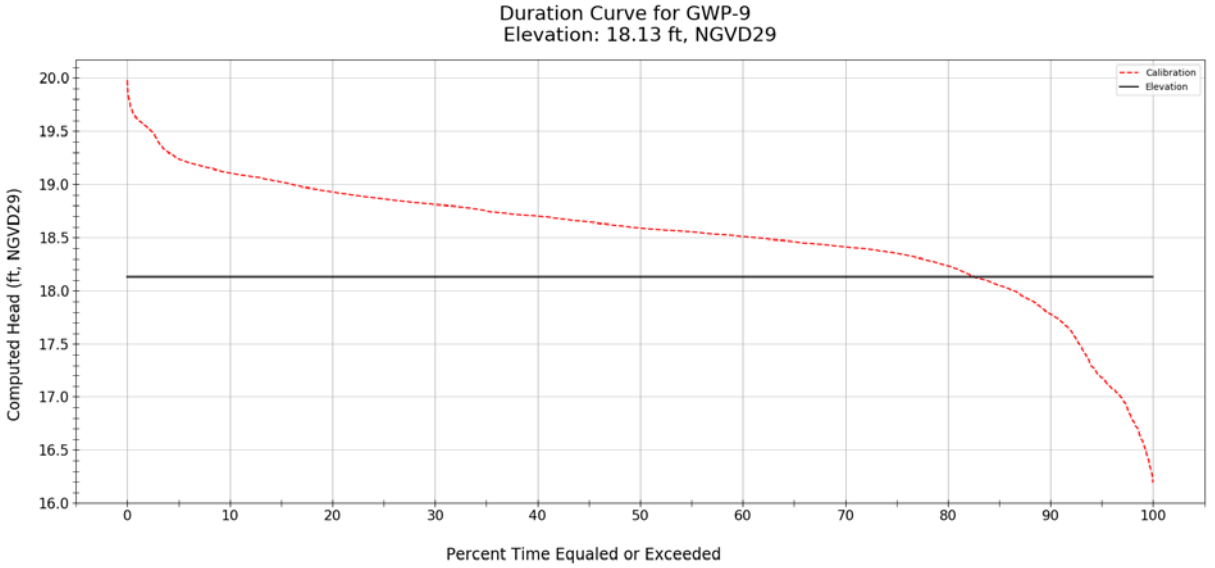

Figure C-83. Simulated stage duration curve (2006 – 2014) and model cell topography for WRAP cell GWP-9.

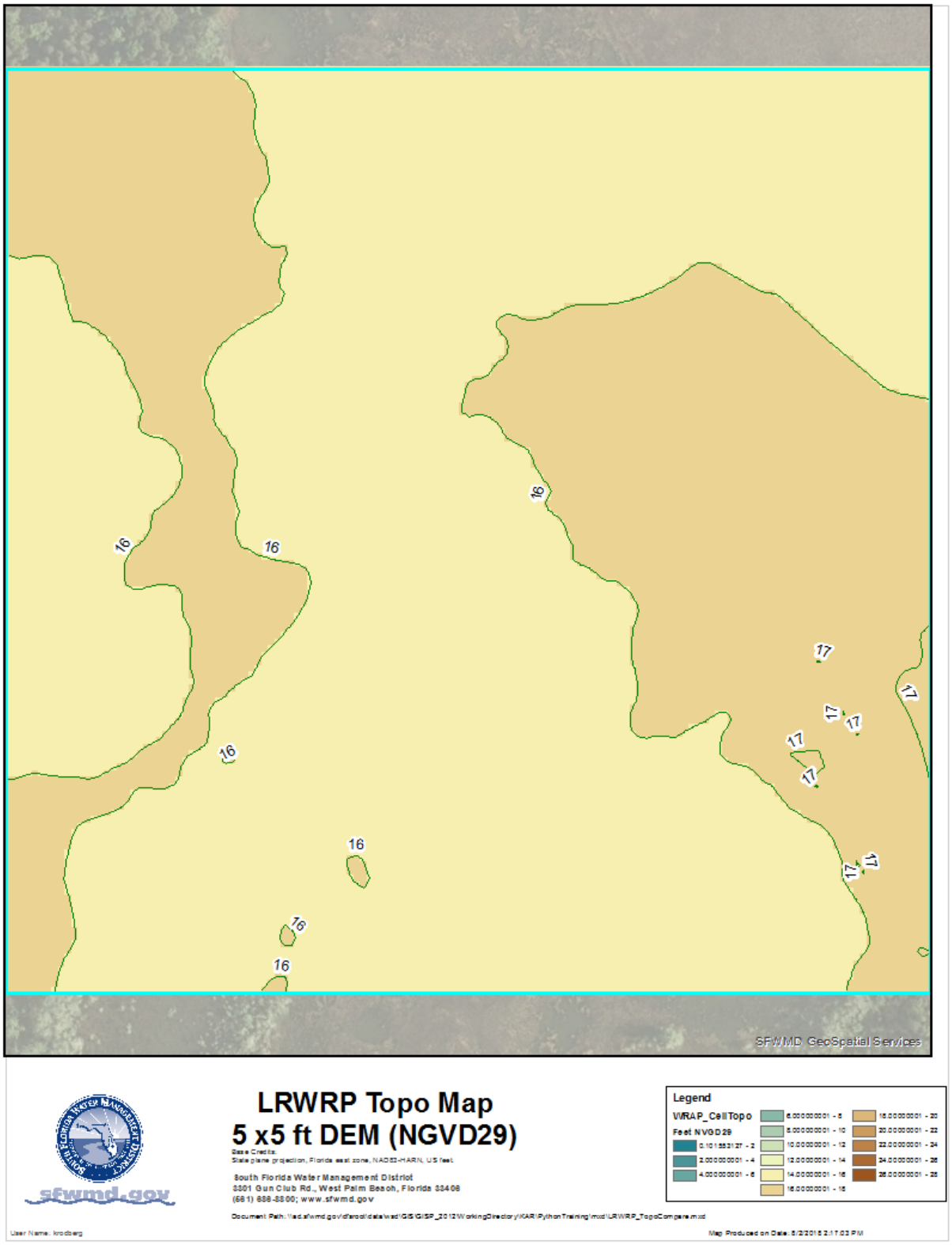

Figure C-84. Variation of model cell topography based on SFWMD's 5 ft LiDAR within WRAP cell GWP-9.

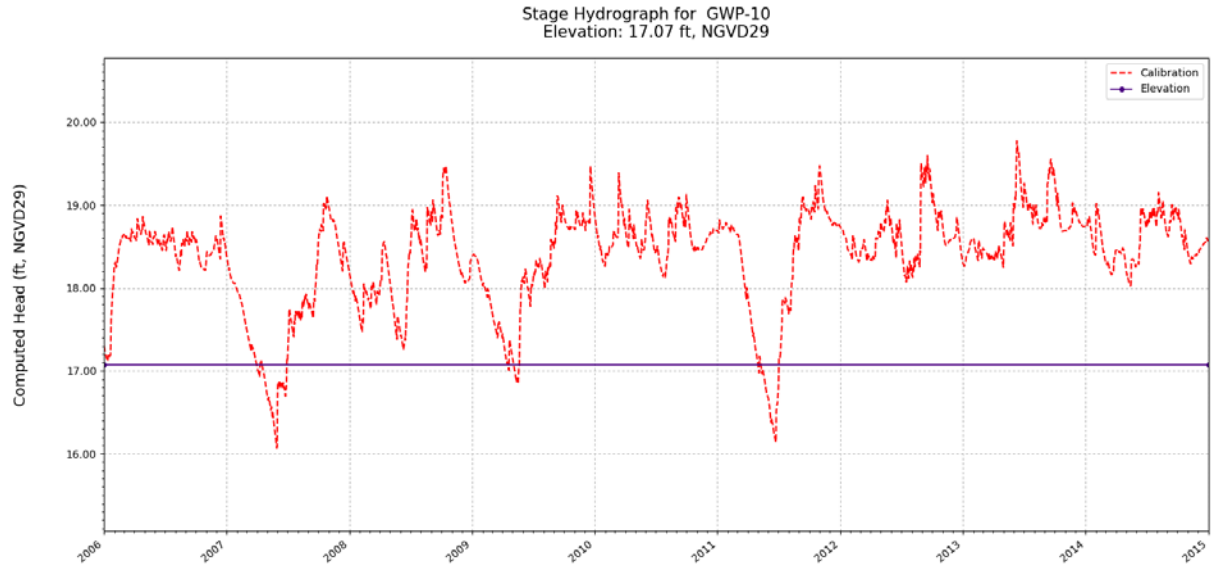

Figure C-85. Simulated stage hydrograph (2006 – 2014) and model cell topography for WRAP cell GWP-10.

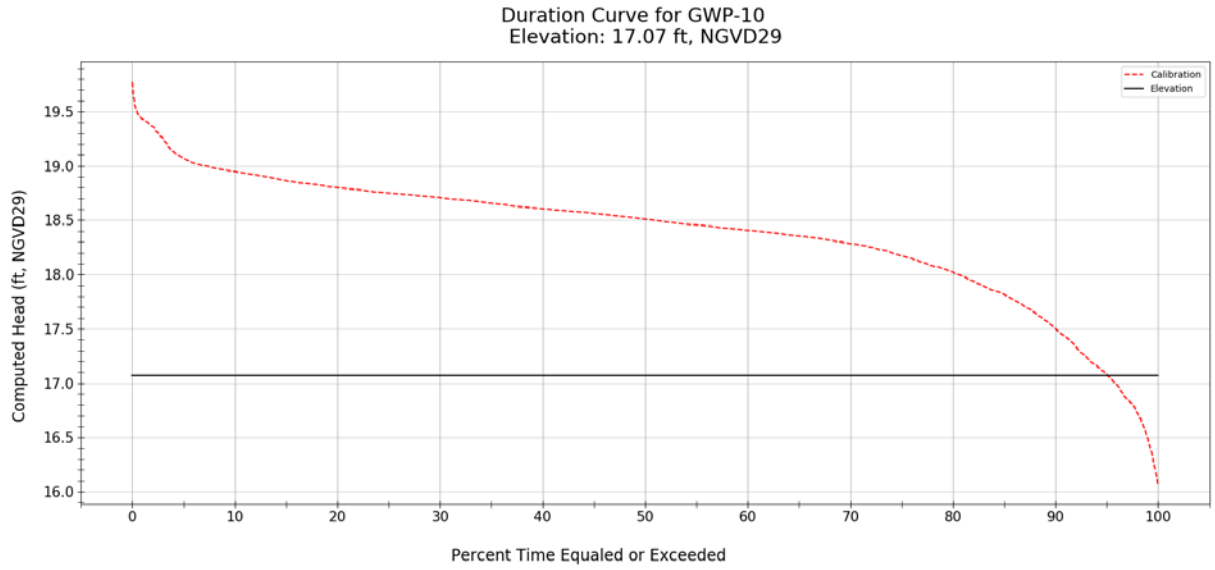

Figure C-86. Simulated stage duration curve (2006 – 2014) and model cell topography for WRAP cell GWP-10.

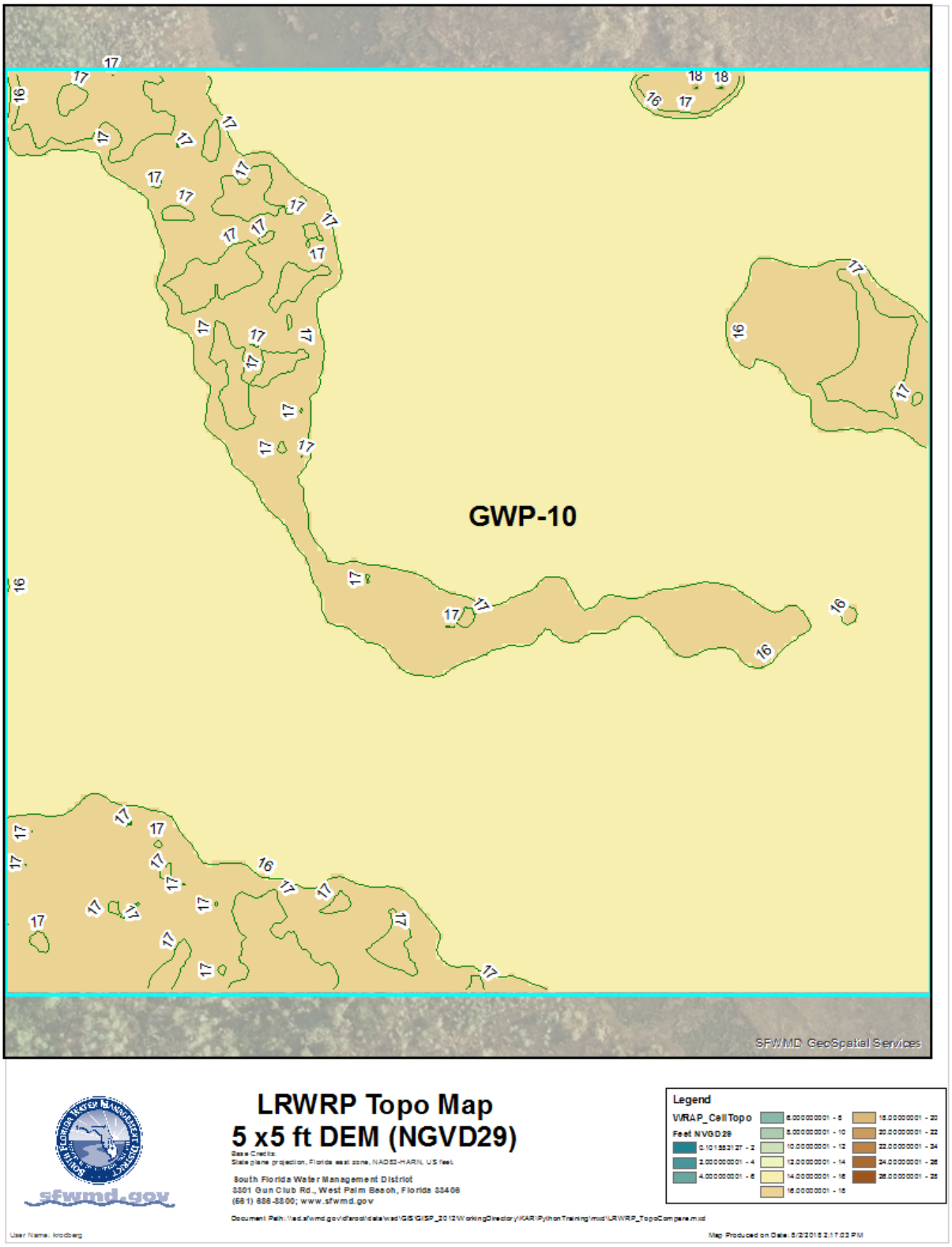

Figure C-87. Variation of model cell topography based on SFWMD's 5 ft LiDAR within WRAP cell GWP-10.

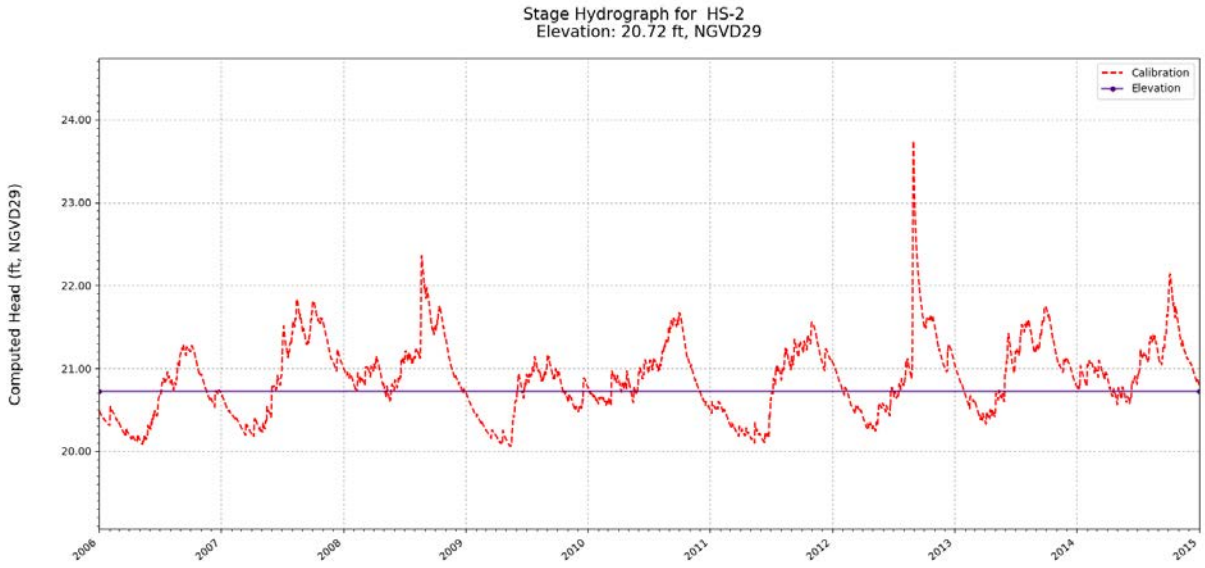

Figure C-88. Simulated stage hydrograph (2006 – 2014) and model cell topography for WRAP cell HS-2.

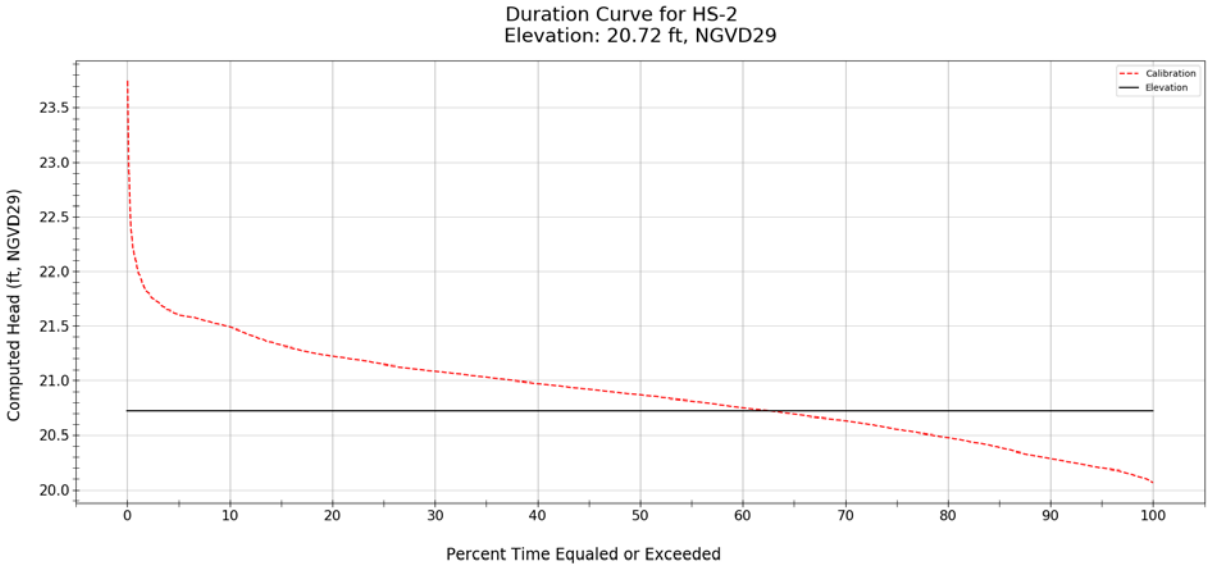

Figure C-89. Simulated stage duration curve (2006 – 2014) and model cell topography for WRAP cell HS-2.

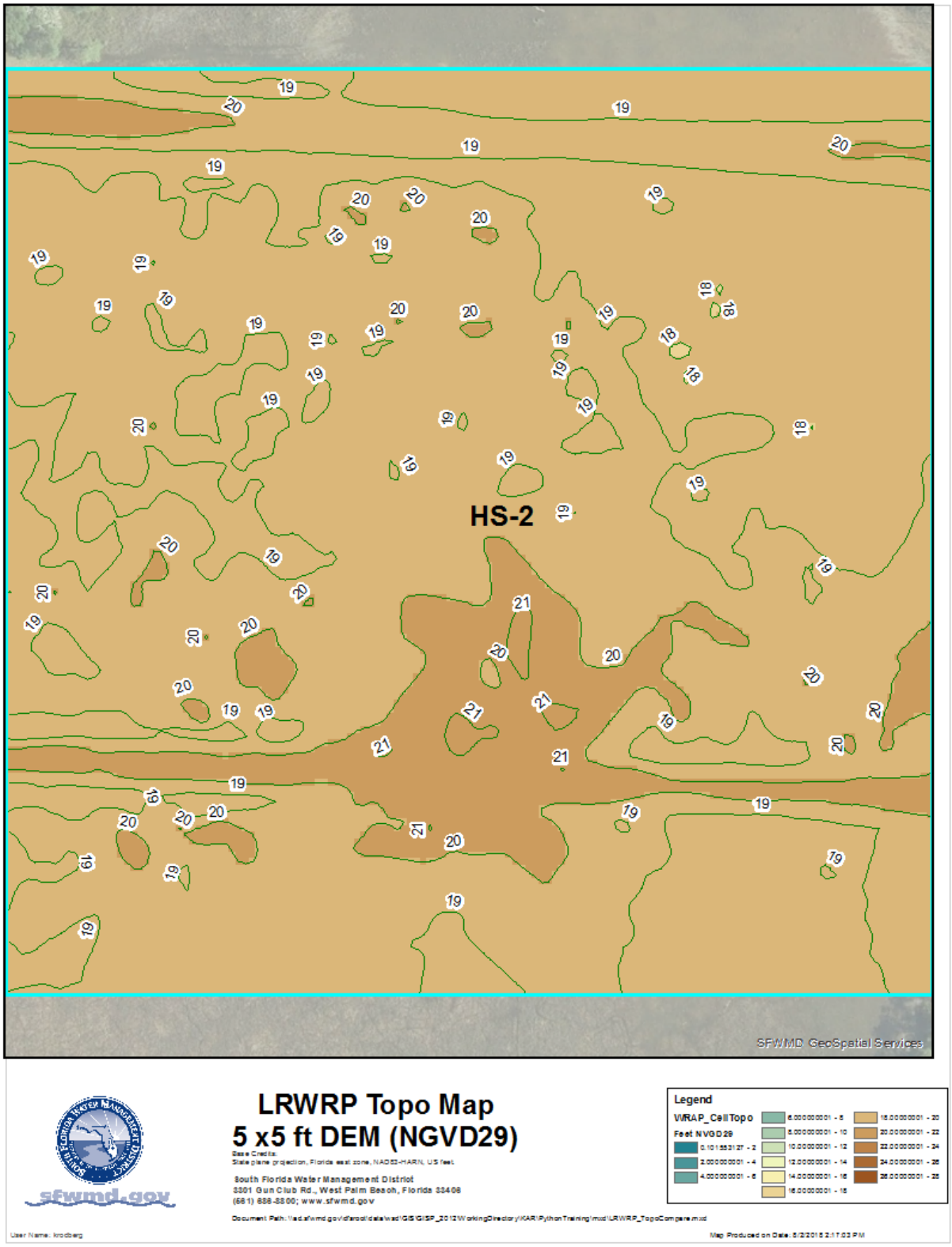

Figure C-90. Variation of model cell topography based on SFWMD's 5 ft LiDAR within WRAP cell HS-2.

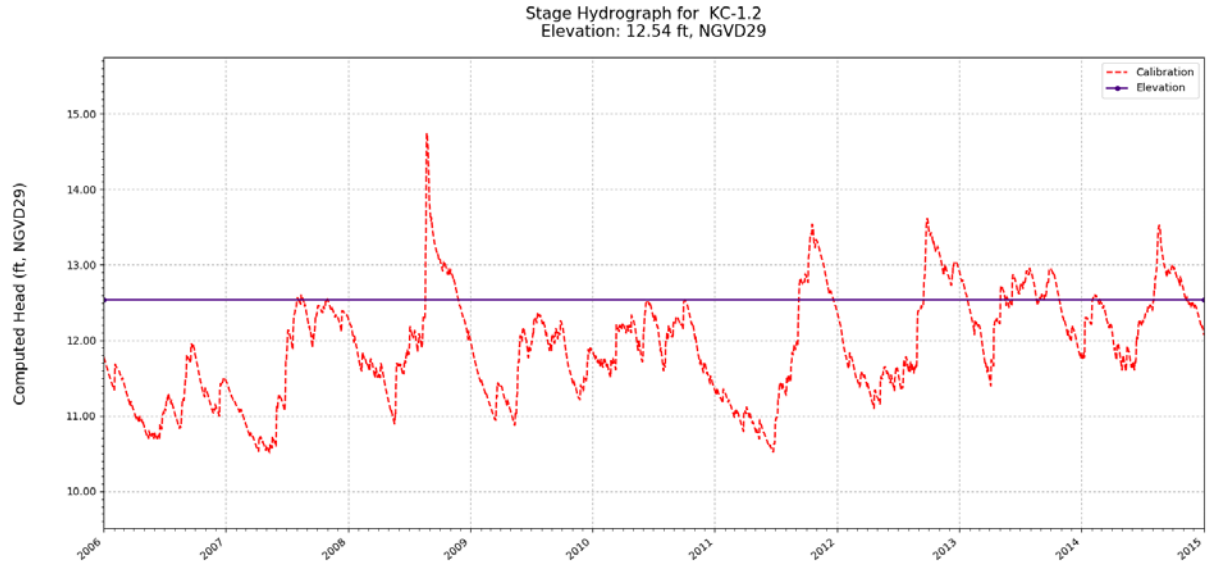

Figure C-91. Simulated stage hydrograph (2006 – 2014) and model cell topography for WRAP cell KC-1.2.

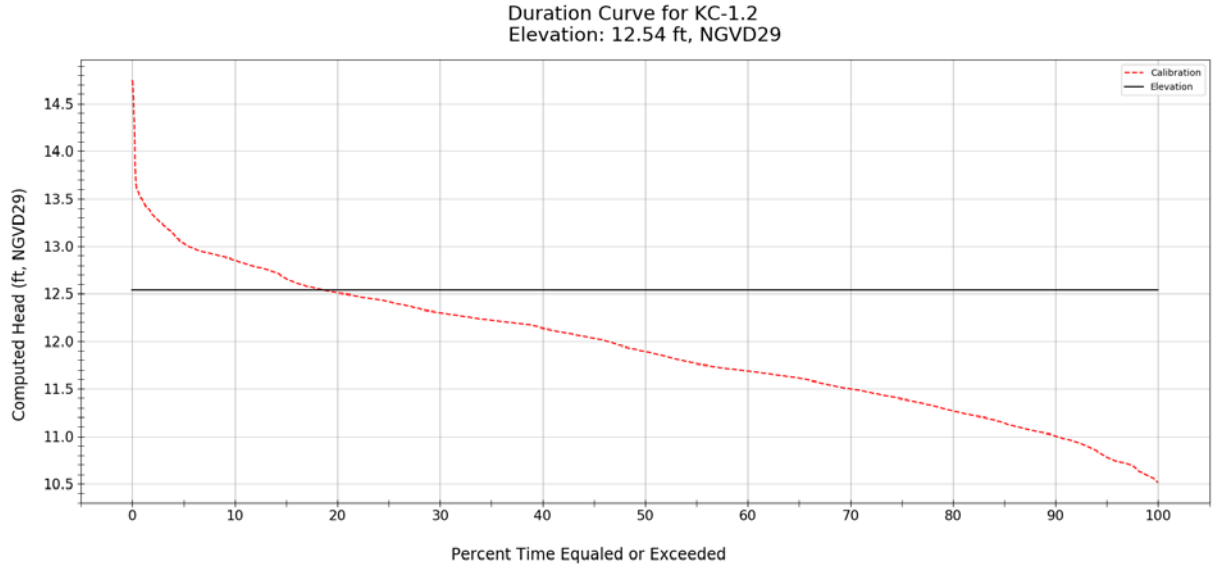

Figure C-92. Simulated stage duration curve (2006 – 2014) and model cell topography for WRAP cell KC-1.2.

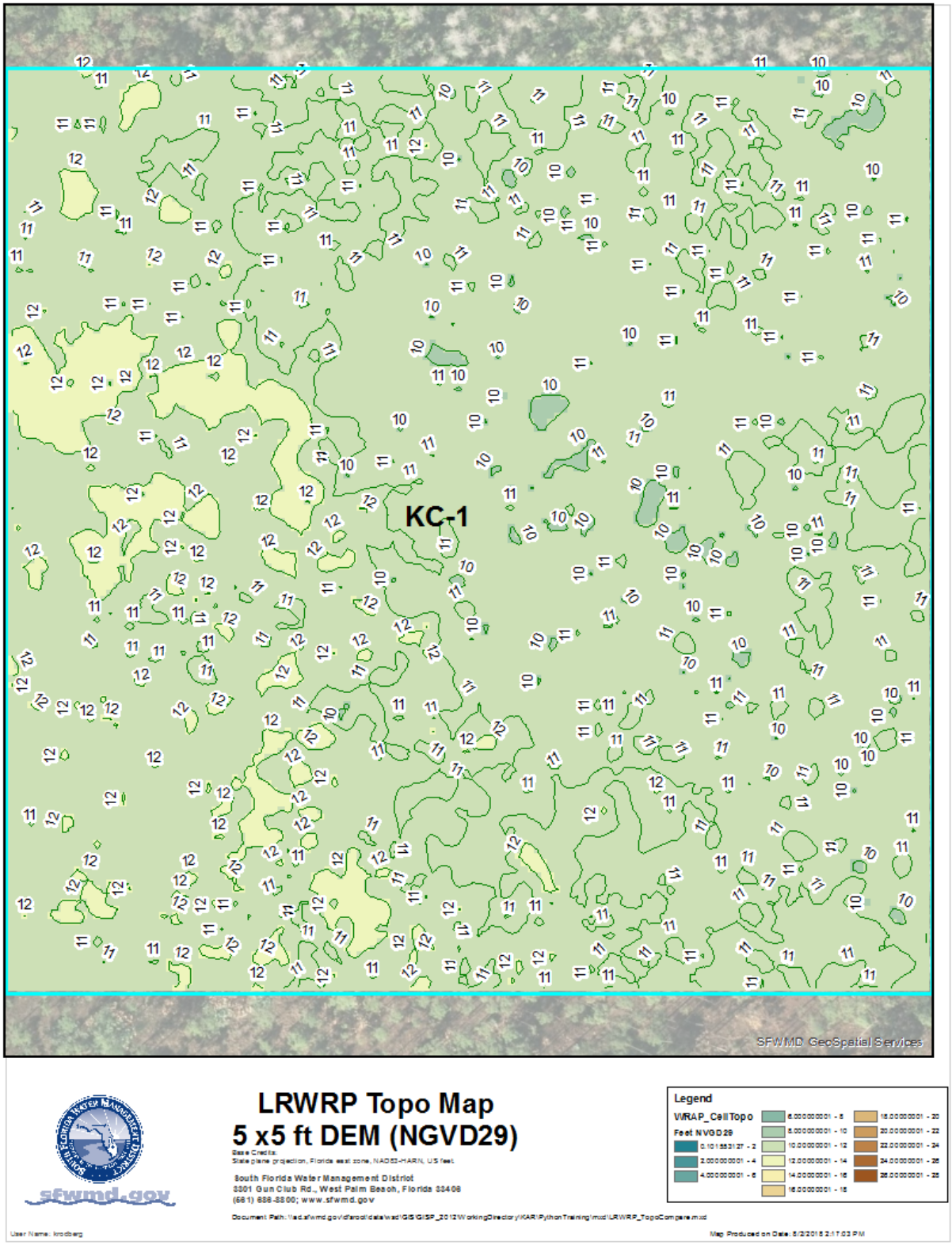

Figure C-93. Variation of model cell topography based on SFWMD's 5 ft LiDAR within WRAP cell KC-1.2.

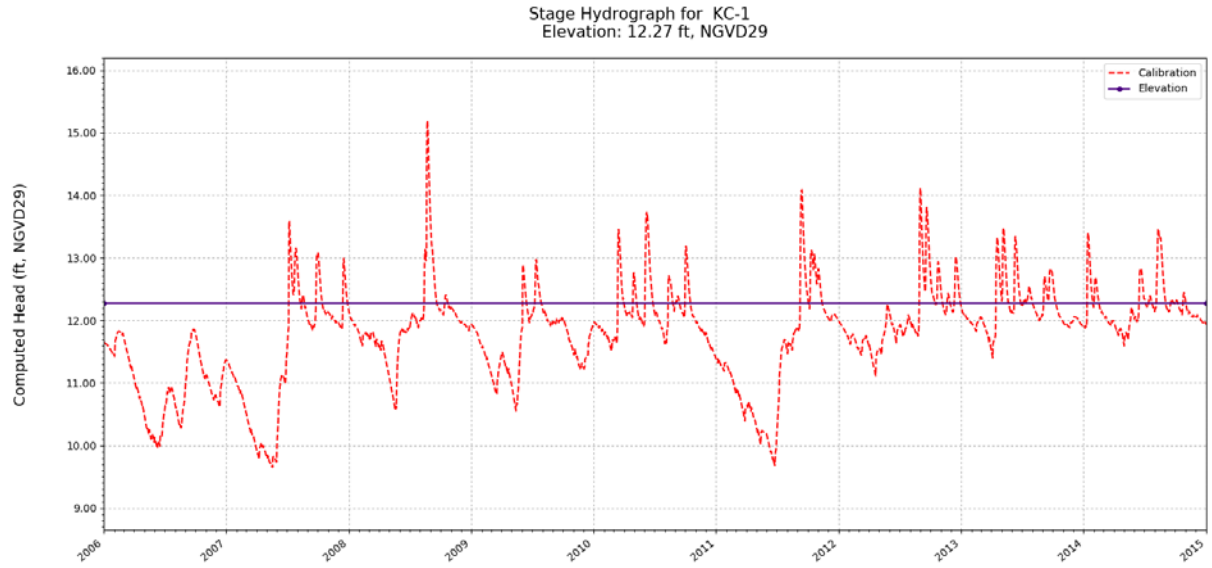

Figure C-94. Simulated stage hydrograph (2006 – 2014) and model cell topography for WRAP cell KC-1.

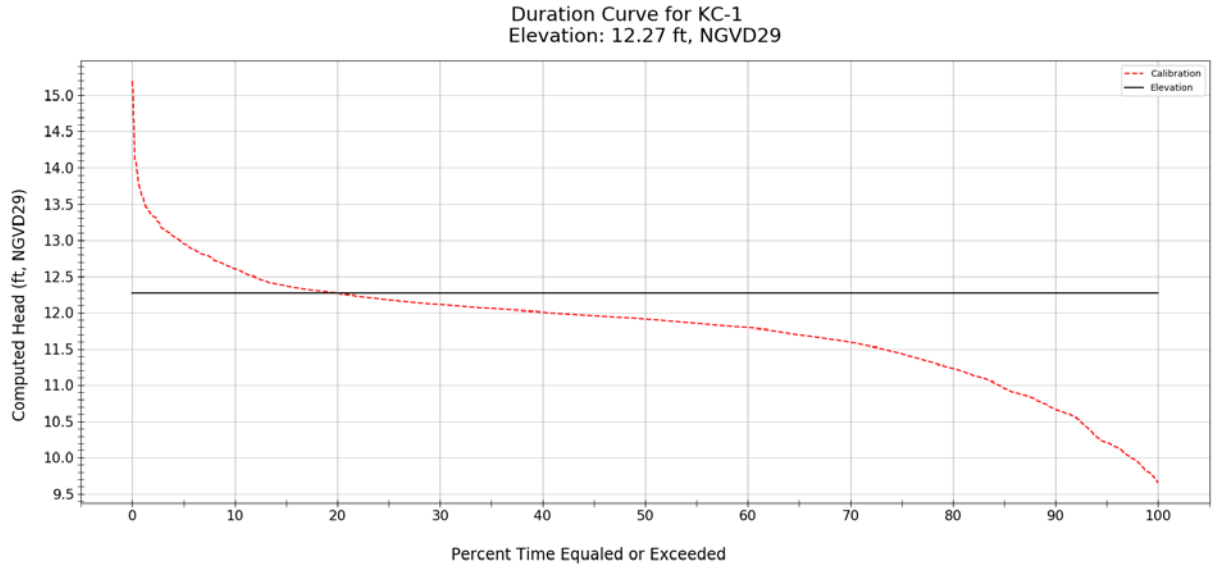

Figure C-95. Simulated stage duration curve (2006 – 2014) and model cell topography for WRAP cell KC-1.

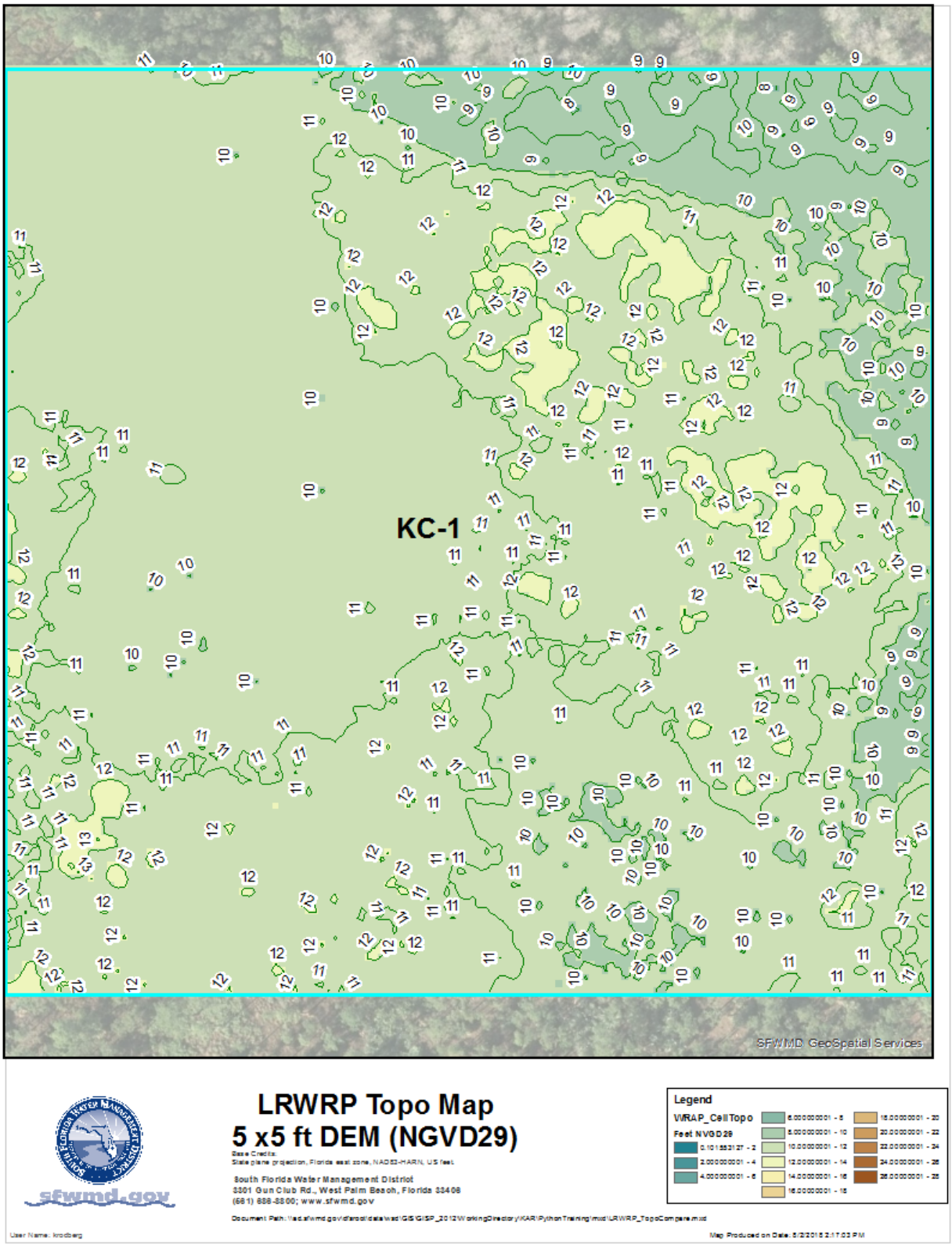

Figure C-96. Variation of model cell topography based on SFWMD's 5 ft LiDAR within WRAP cell KC-1.

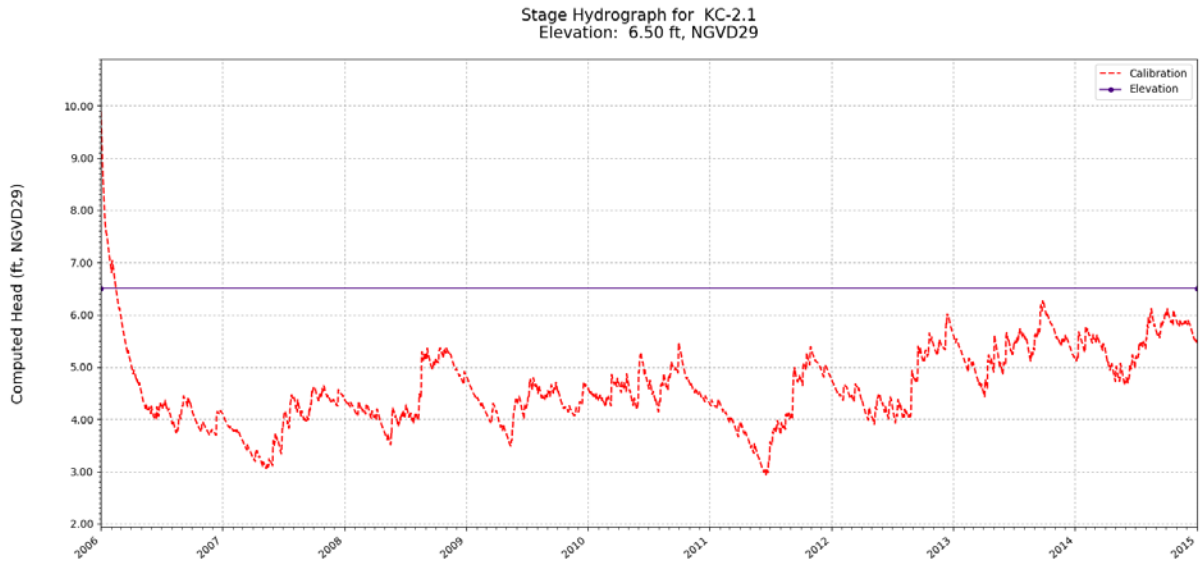

Figure C-97. Simulated stage hydrograph (2006 – 2014) and model cell topography for WRAP cell KC-2.1.

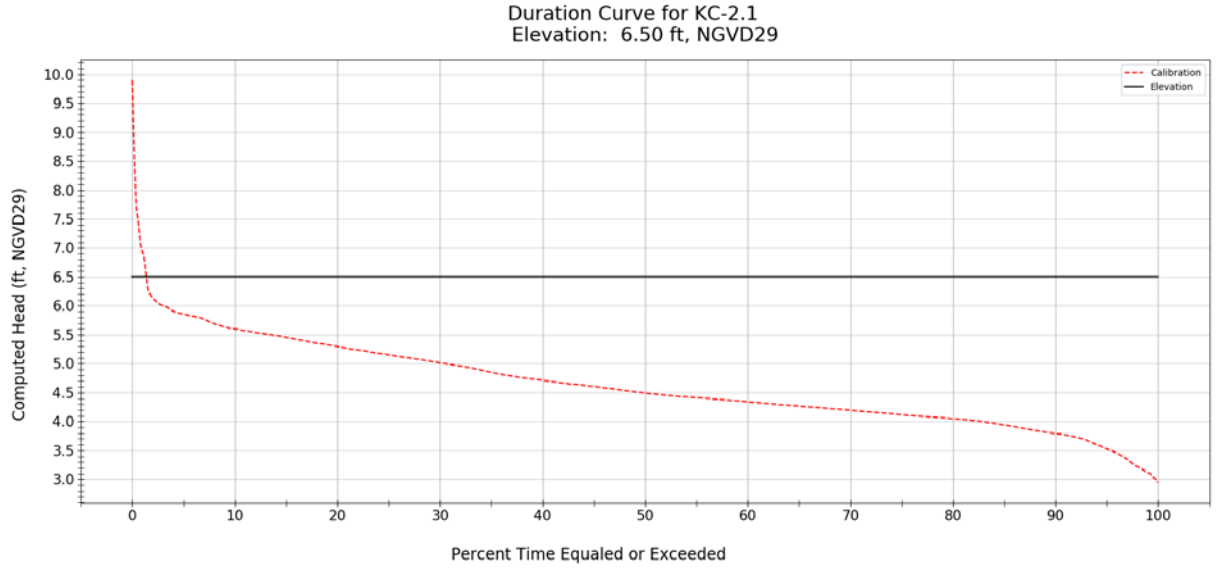

Figure C-98. Simulated stage duration curve (2006 – 2014) and model cell topography for WRAP cell KC-2.1.

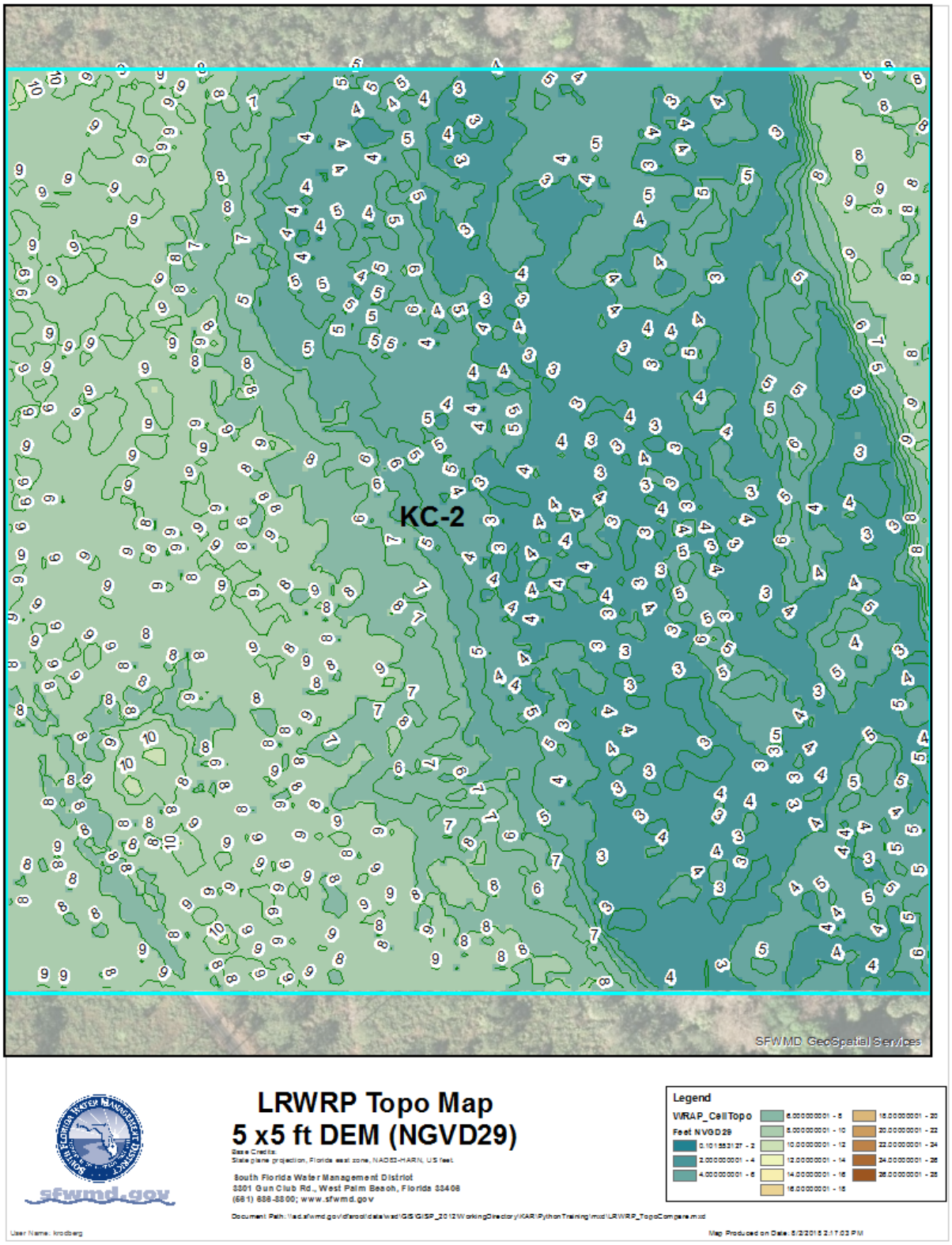

Figure C-99. Variation of model cell topography based on SFWMD's 5 ft LiDAR within WRAP cell KC-2.1.

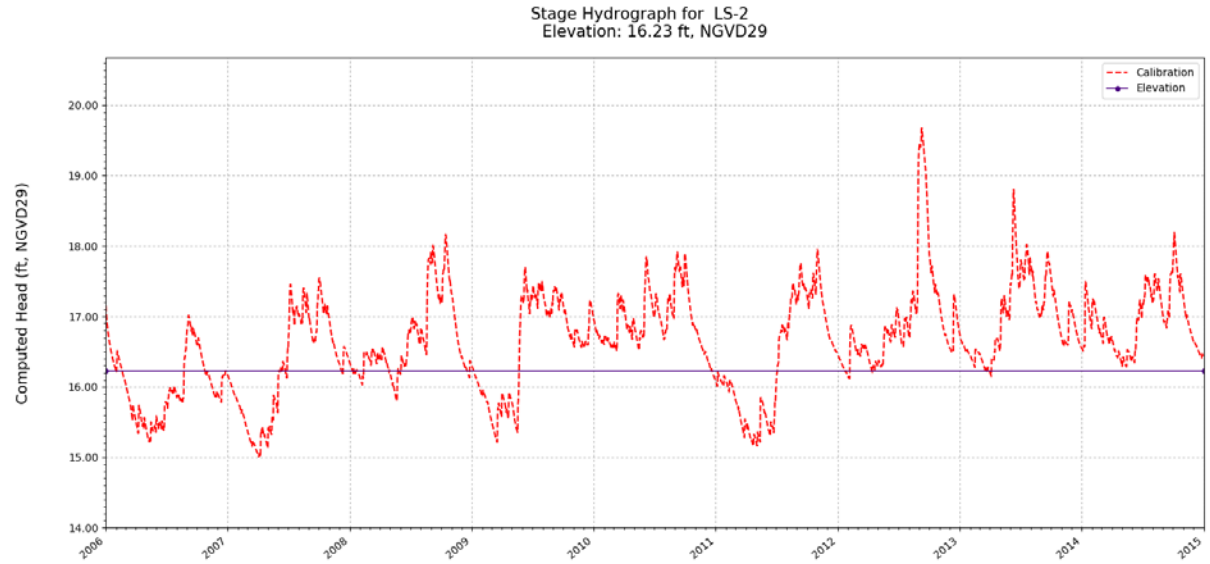

Figure C-100. Simulated stage hydrograph (2006 – 2014) and model cell topography for WRAP cell LS-2.

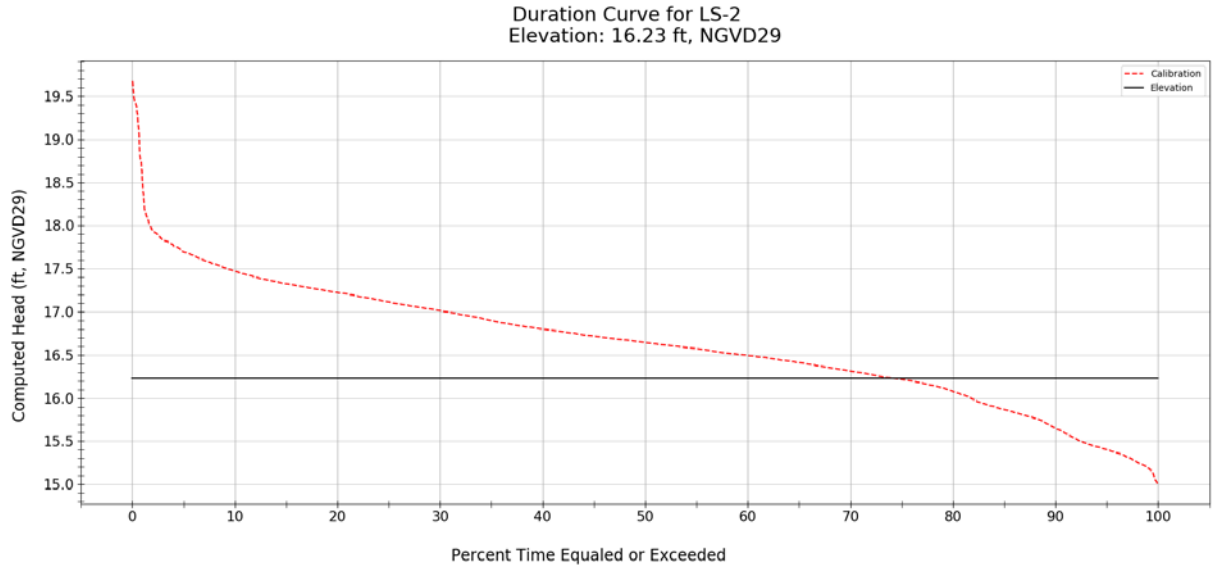

Figure C-101. Simulated stage duration curve (2006 – 2014) and model cell topography for WRAP cell LS-2.

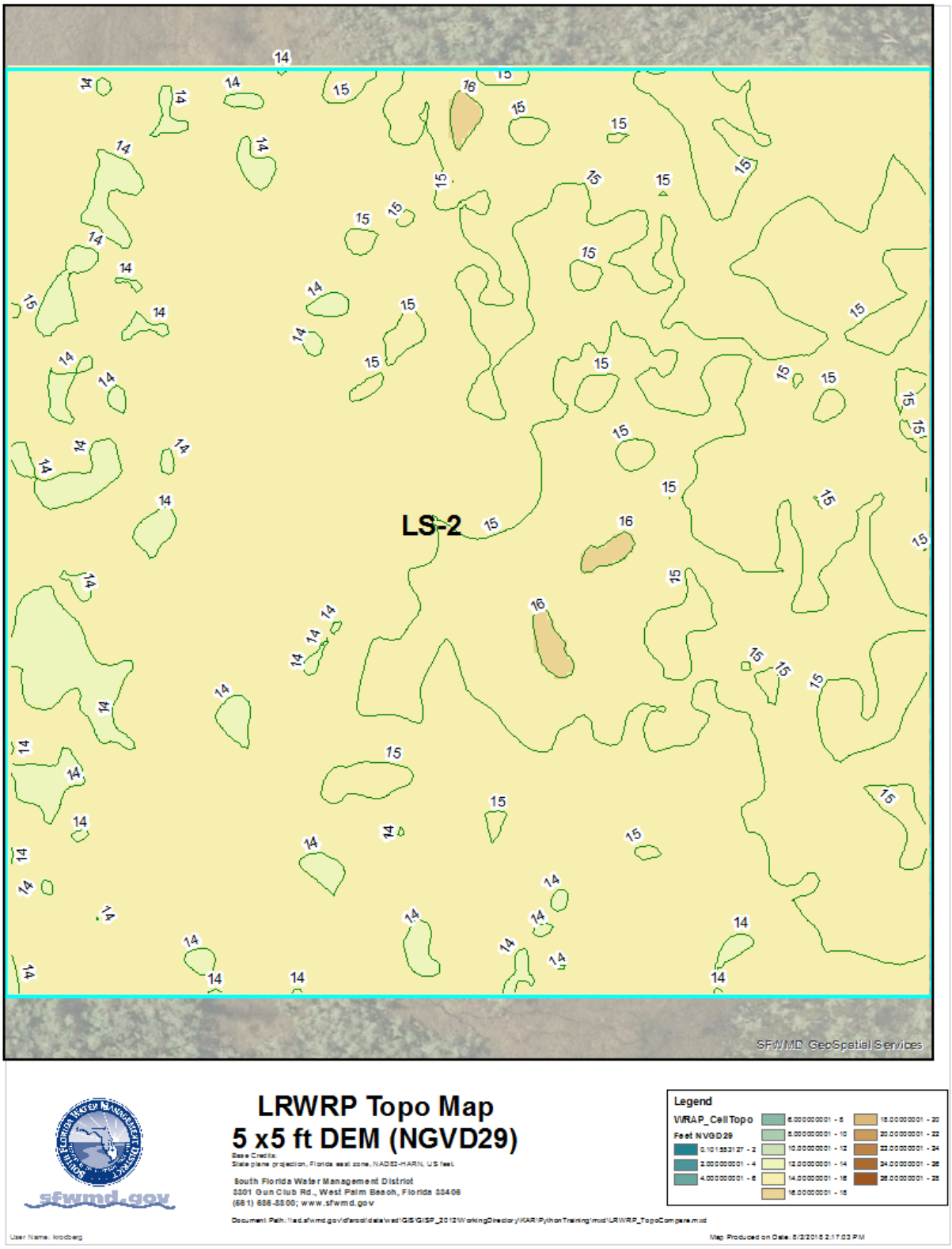

Figure C-102. Variation of model cell topography based on SFWMD's 5 ft LiDAR within WRAP cell LS-2.

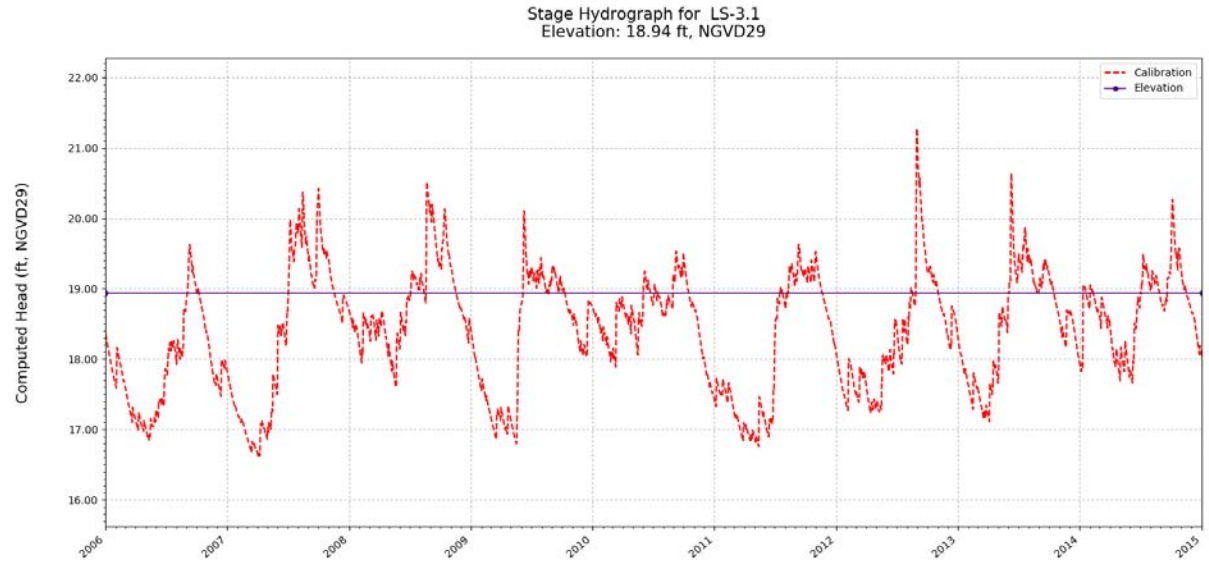

Figure C-103. Simulated stage hydrograph (2006 – 2014) and model cell topography for WRAP cell LS-3.1.

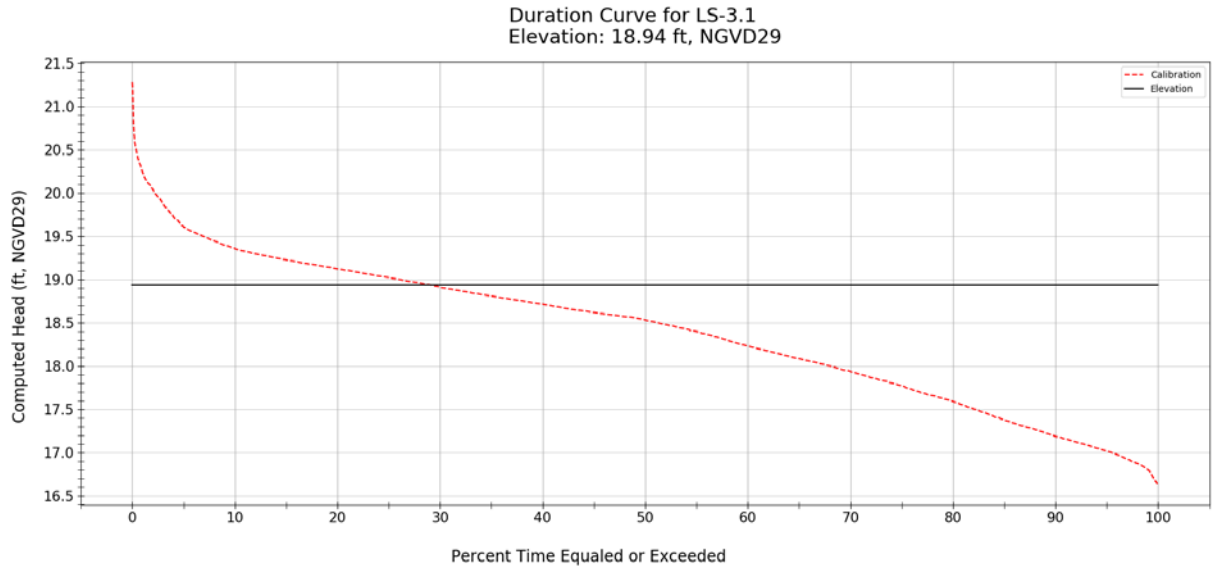

Figure C-104. Simulated stage duration curve (2006 – 2014) and model cell topography for WRAP cell LS-3.1.

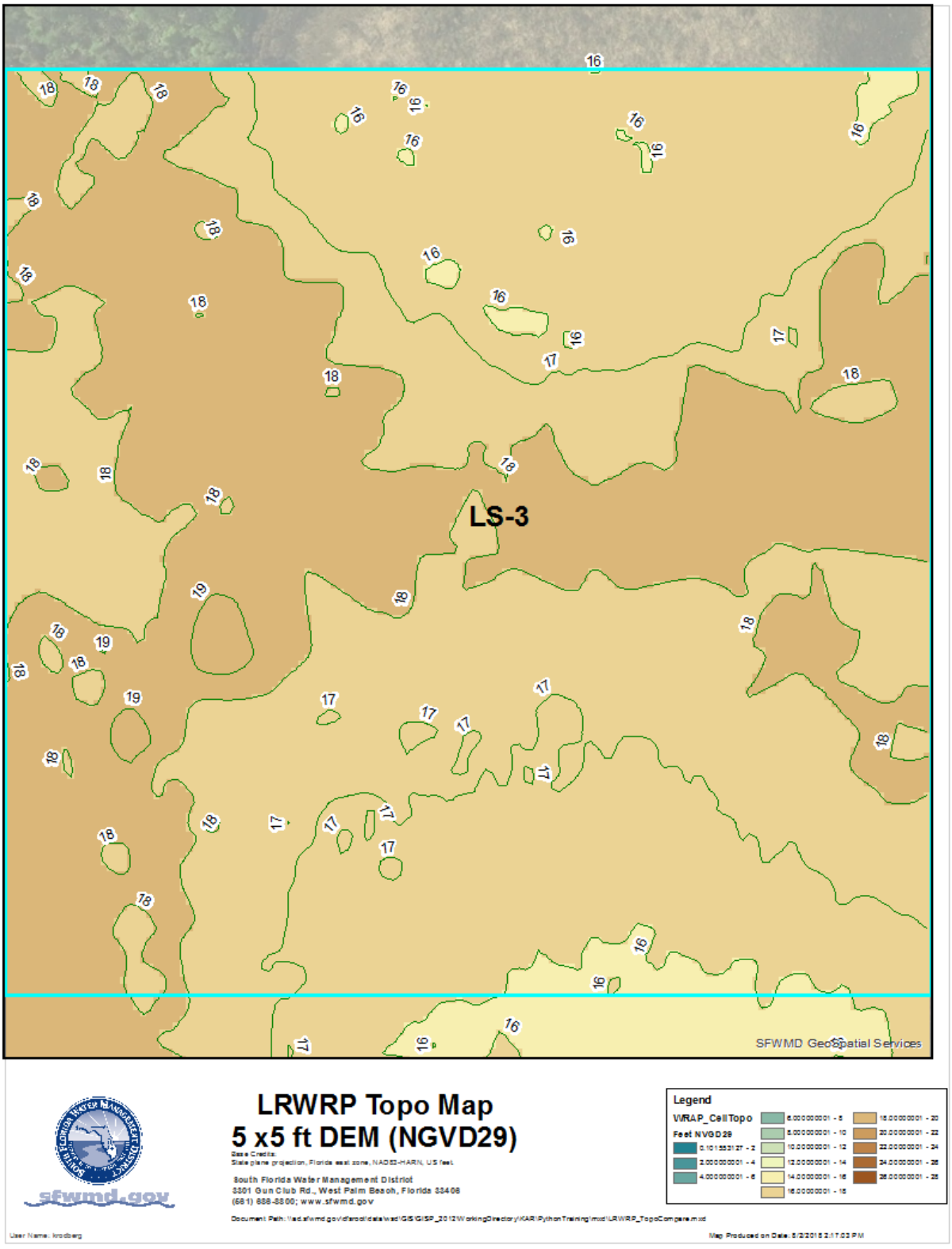

Figure C-105. Variation of model cell topography based on SFWMD's 5 ft LiDAR within WRAP cell LS-3.1.

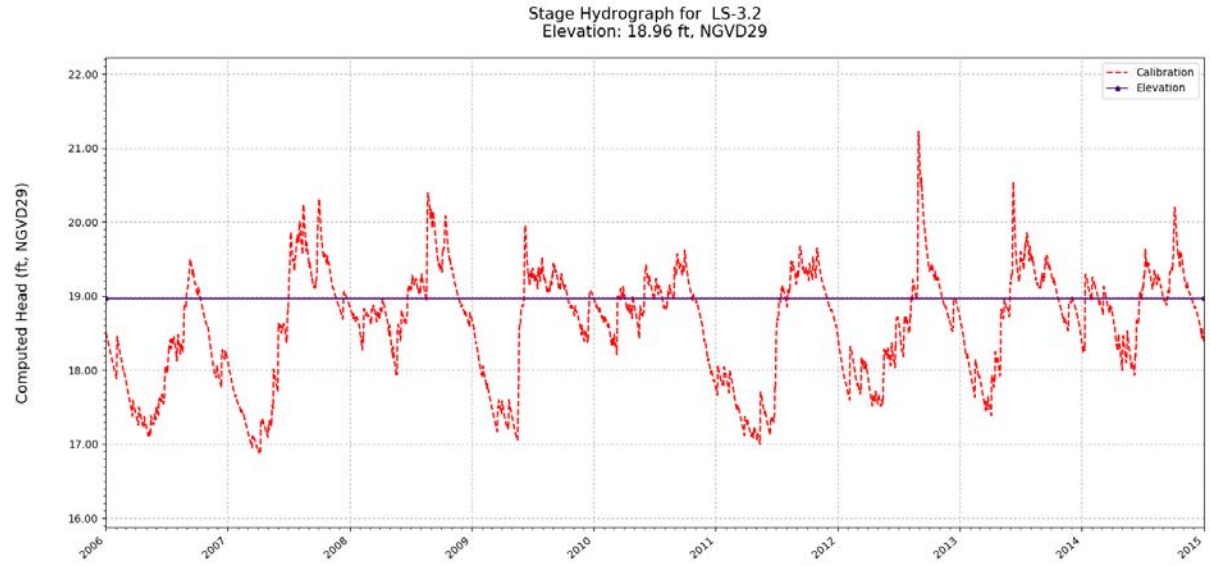

Figure C-106. Simulated stage hydrograph (2006 – 2014) and model cell topography for WRAP cell LS-3.2.

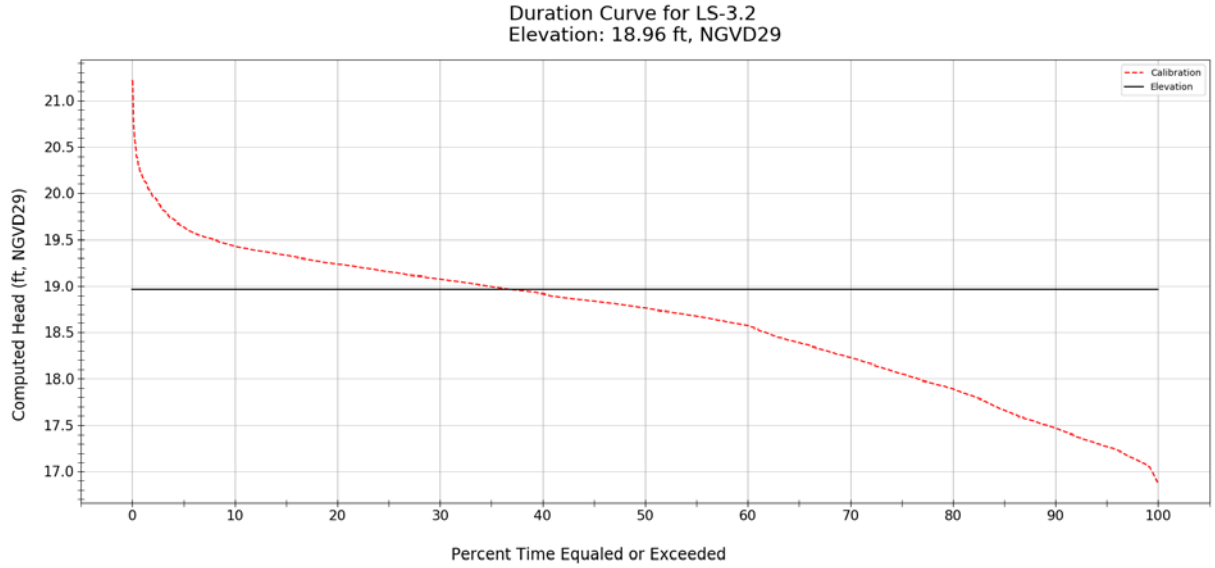

Figure C-107. Simulated stage duration curve (2006 – 2014) and model cell topography for WRAP cell LS-3.2.

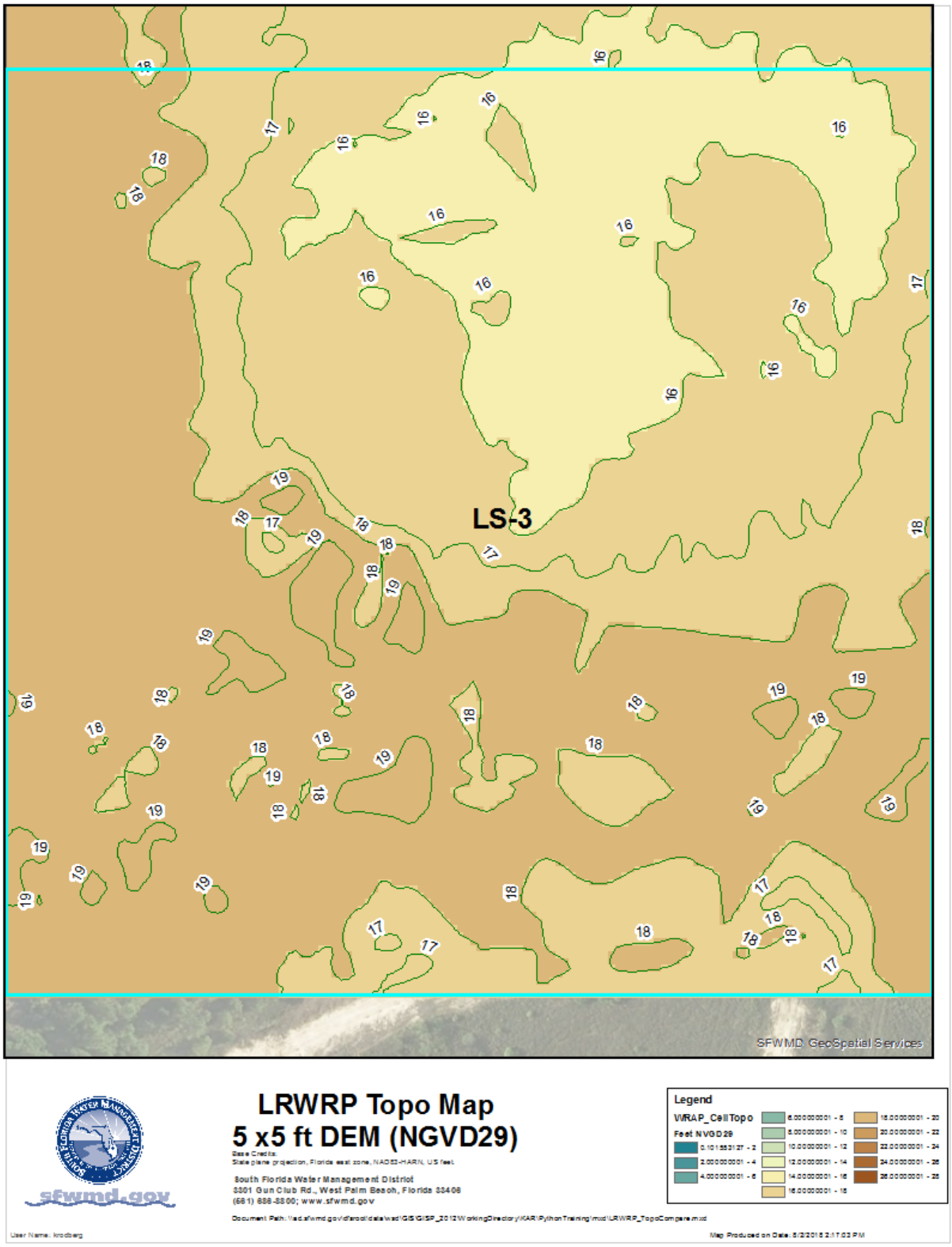

Figure C-108. Variation of model cell topography based on SFWMD's 5 ft LiDAR within WRAP cell LS-3.2.

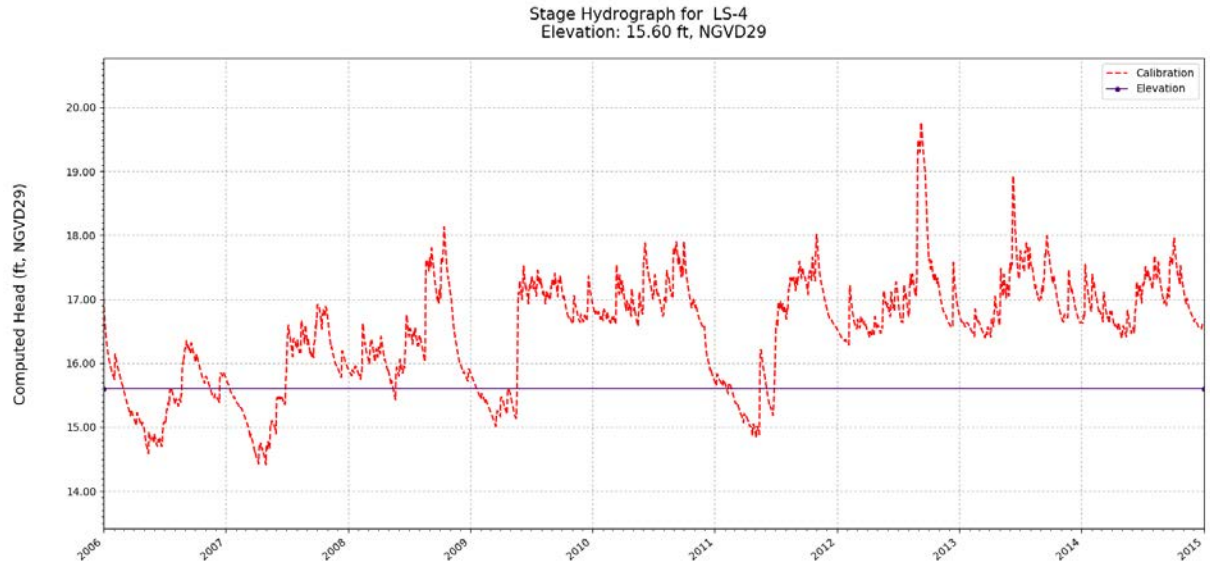

Figure C-109. Simulated stage hydrograph (2006 – 2014) and model cell topography for WRAP cell LS-4.

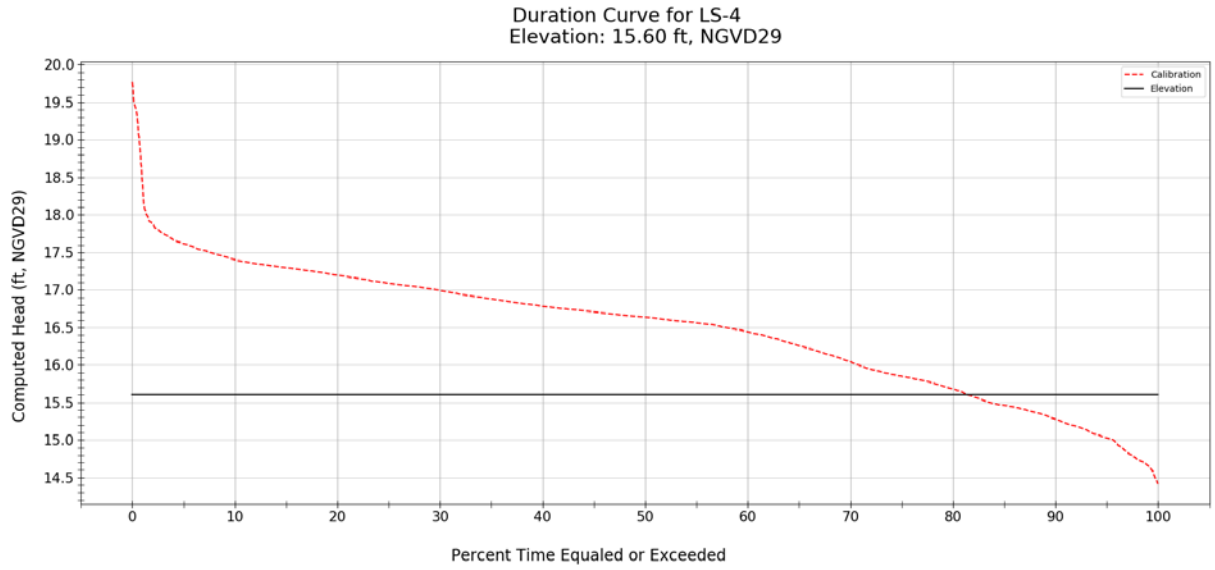

Figure C-110. Simulated stage duration curve (2006 – 2014) and model cell topography for WRAP cell LS-4.

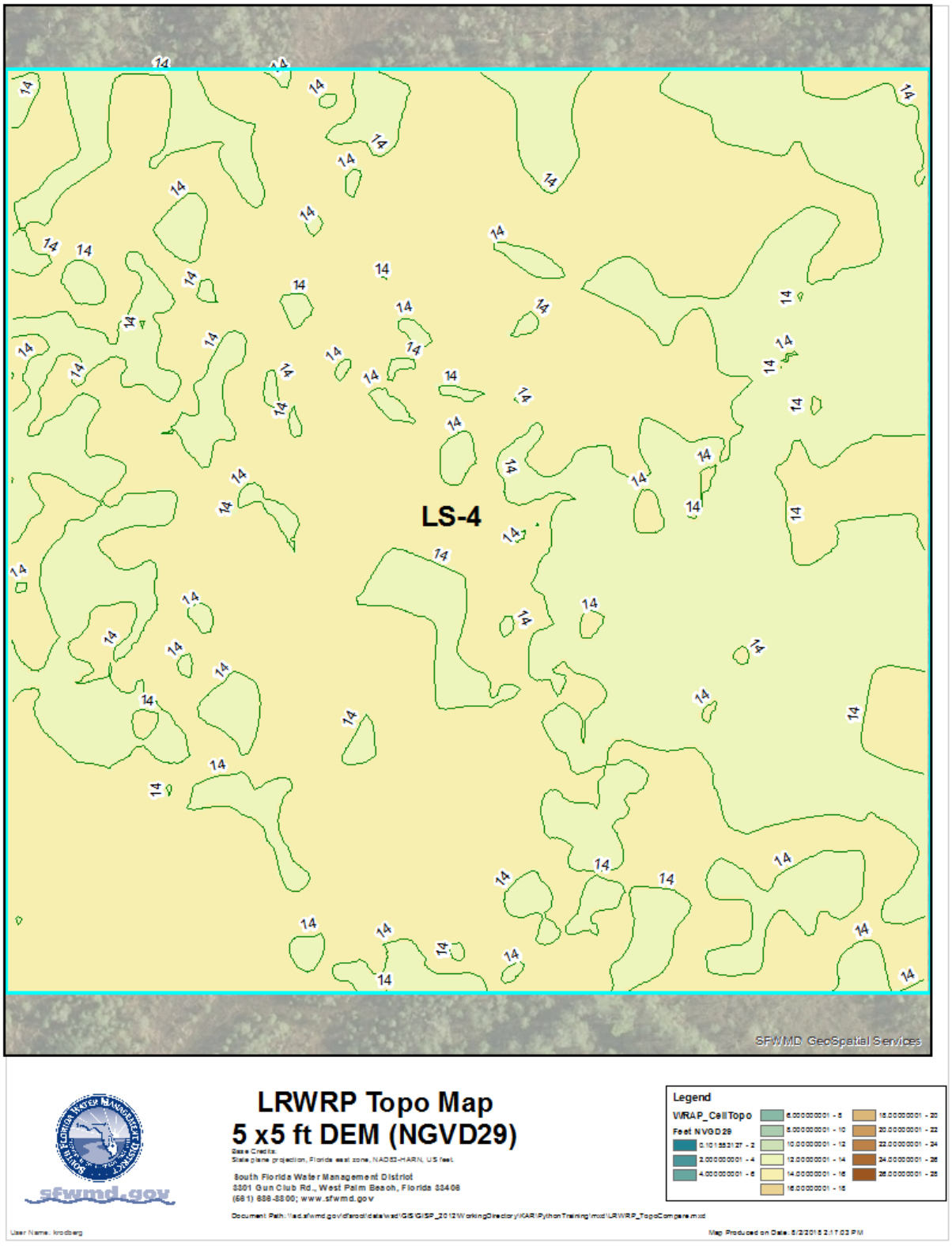

Figure C-111. Variation of model cell topography based on SFWMD's 5 ft LiDAR within WRAP cell LS-4.

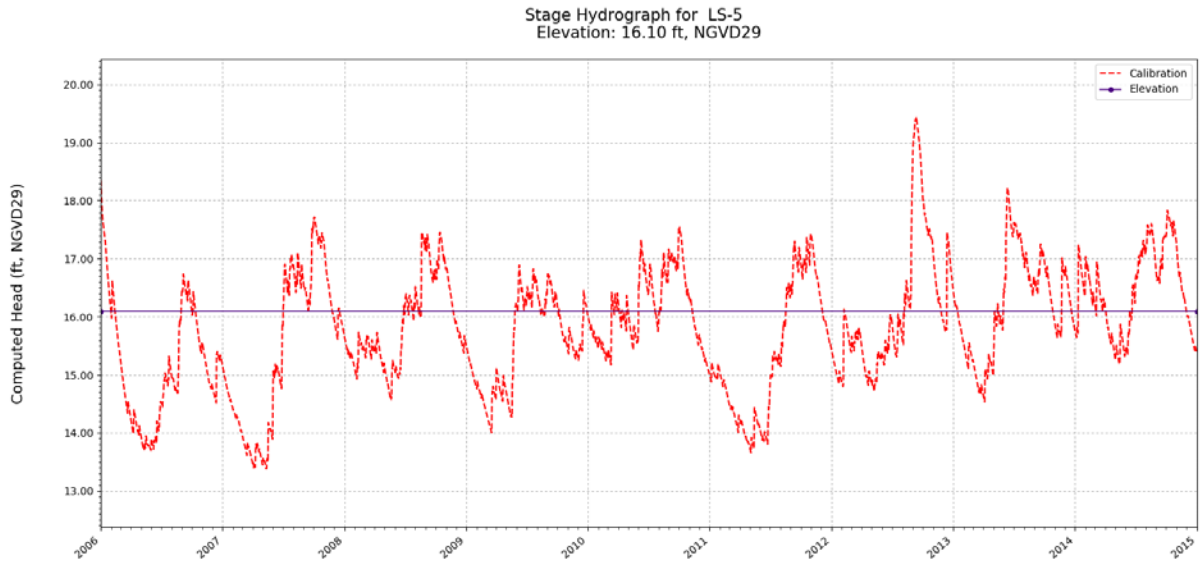

Figure C-112. Simulated stage hydrograph (2006 – 2014) and model cell topography for WRAP cell LS-5.

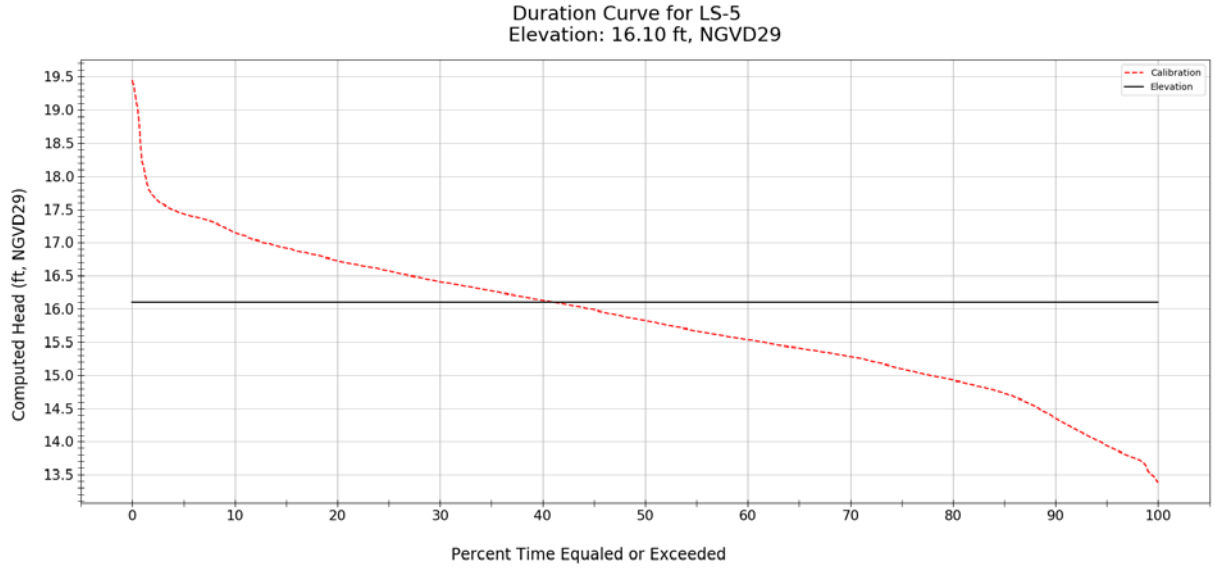

Figure C-113. Simulated stage duration curve (2006 – 2014) and model cell topography for WRAP cell LS-5.

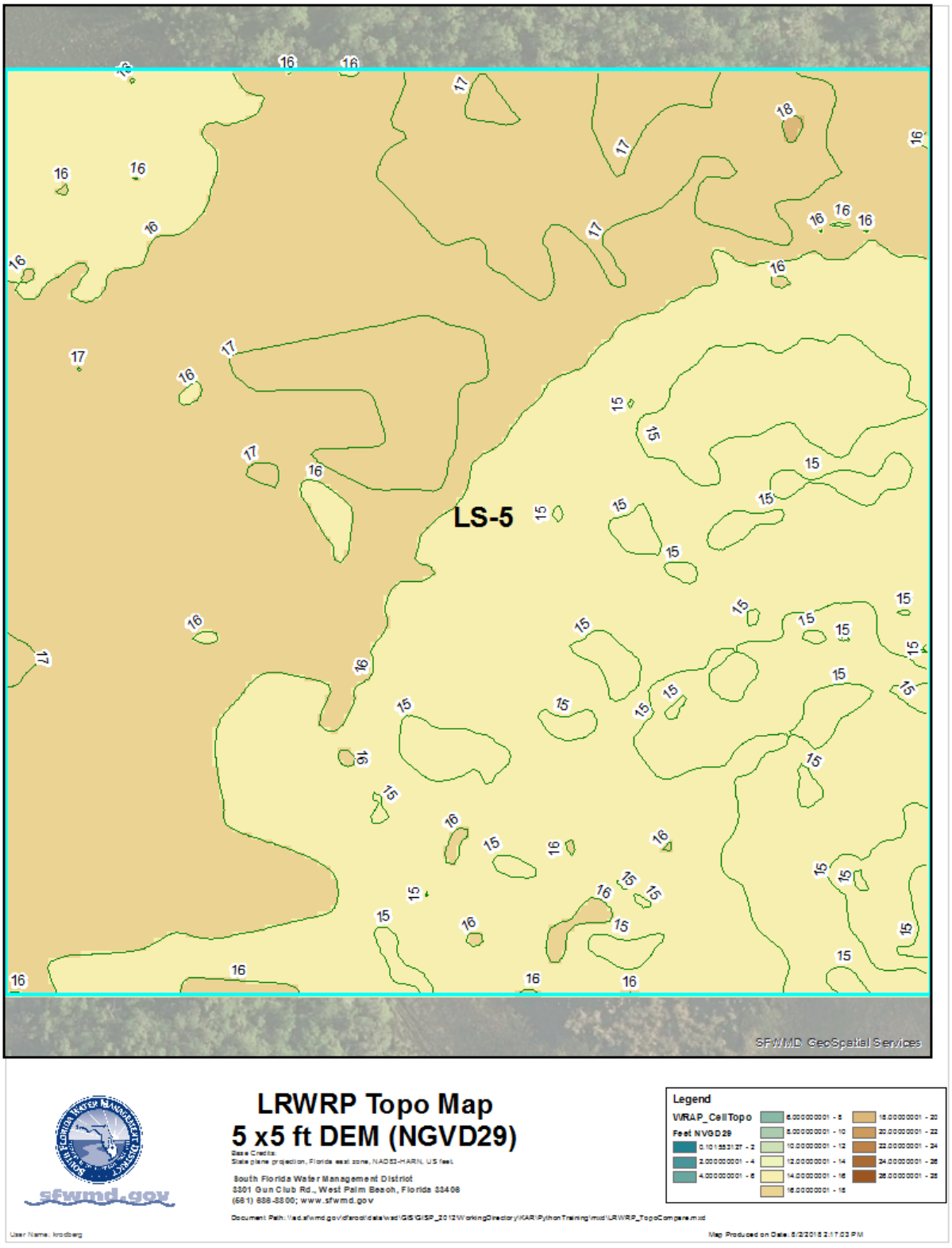

Figure C-114. Variation of model cell topography based on SFWMD's 5 ft LiDAR within WRAP cell LS-5.

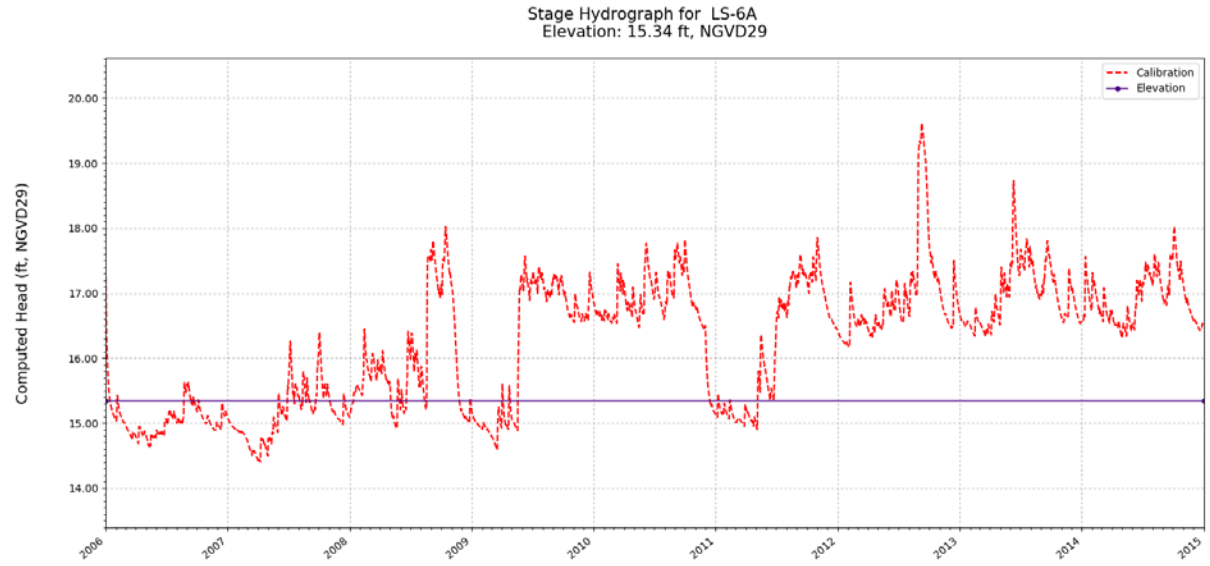

Figure C-115. Simulated stage hydrograph (2006 – 2014) and model cell topography for WRAP cell LS-6A.

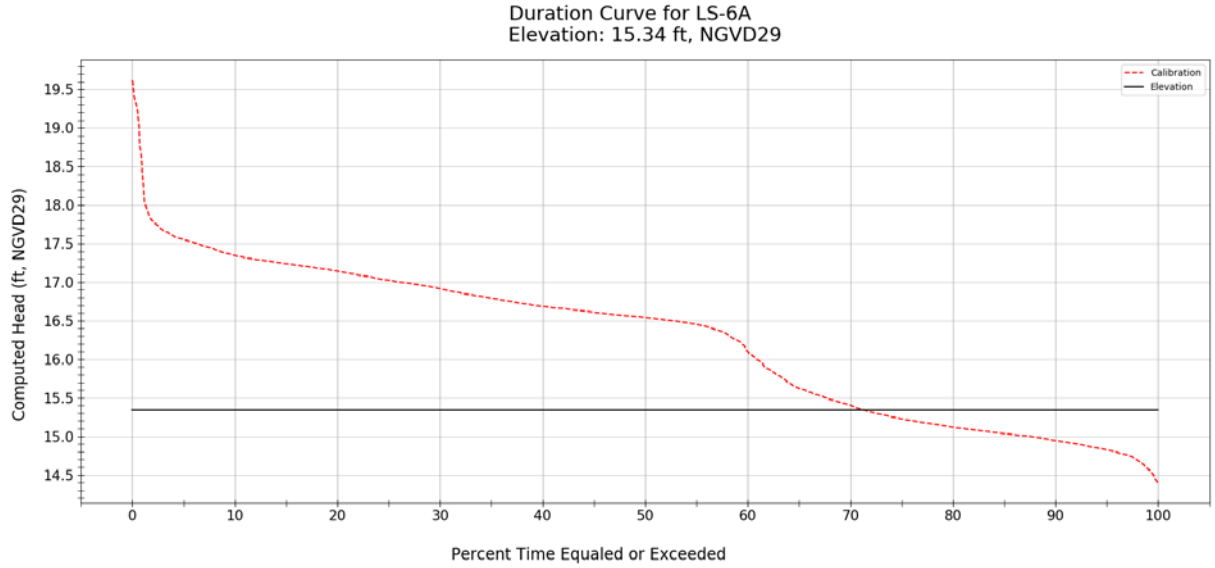

Figure C-116. Simulated stage duration curve (2006 – 2014) and model cell topography for WRAP cell LS-6A.

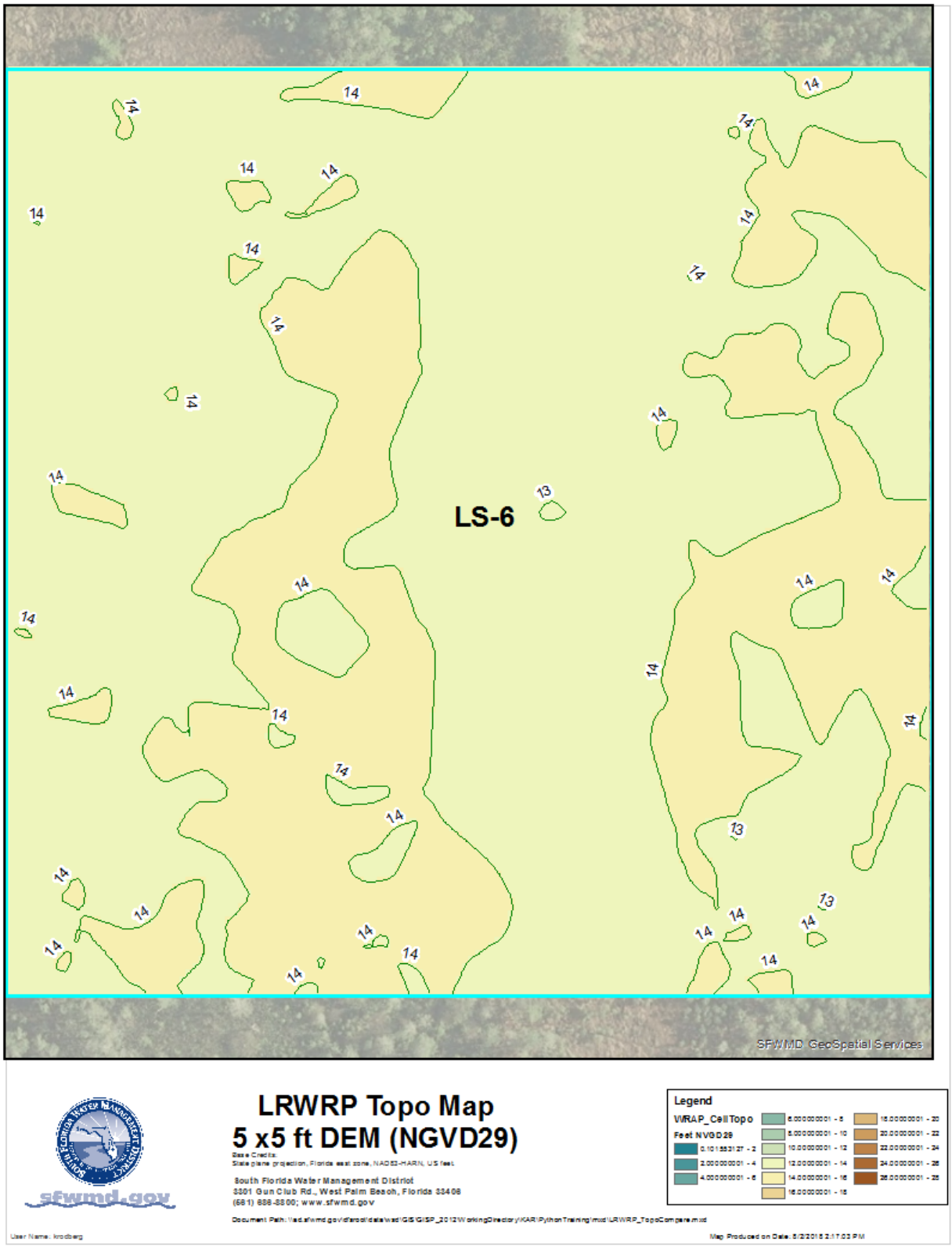

Figure C-117. Variation of model cell topography based on SFWMD's 5 ft LiDAR within WRAP cell LS-6A.

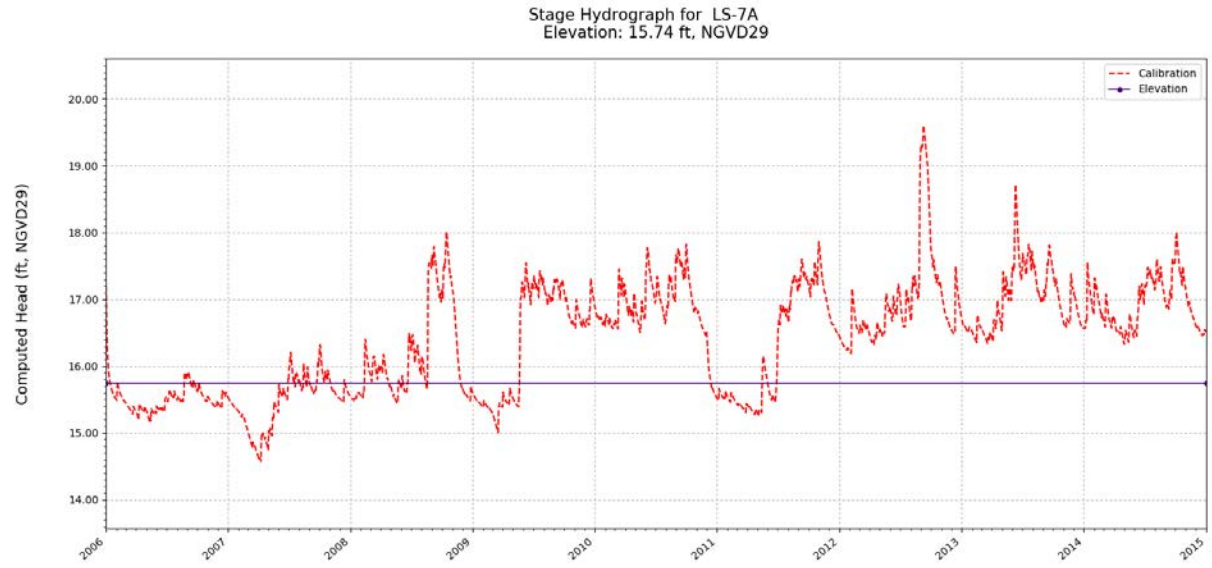

Figure C-118. Simulated stage hydrograph (2006 – 2014) and model cell topography for WRAP cell LS-7A.

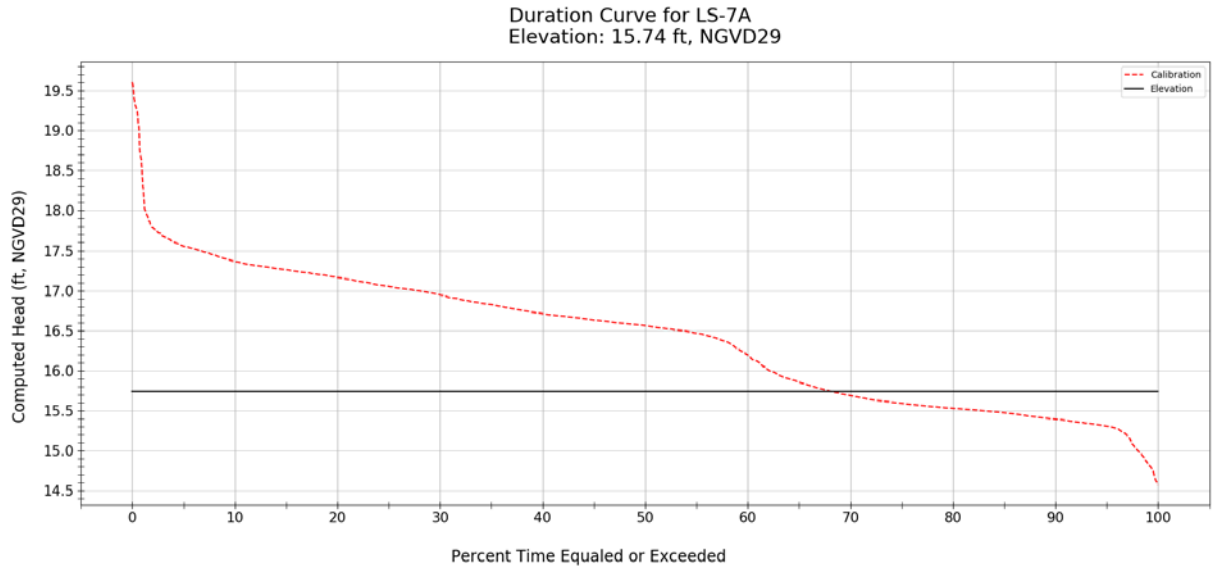

Figure C-119. Simulated stage duration curve (2006 – 2014) and model cell topography for WRAP cell LS-7A.

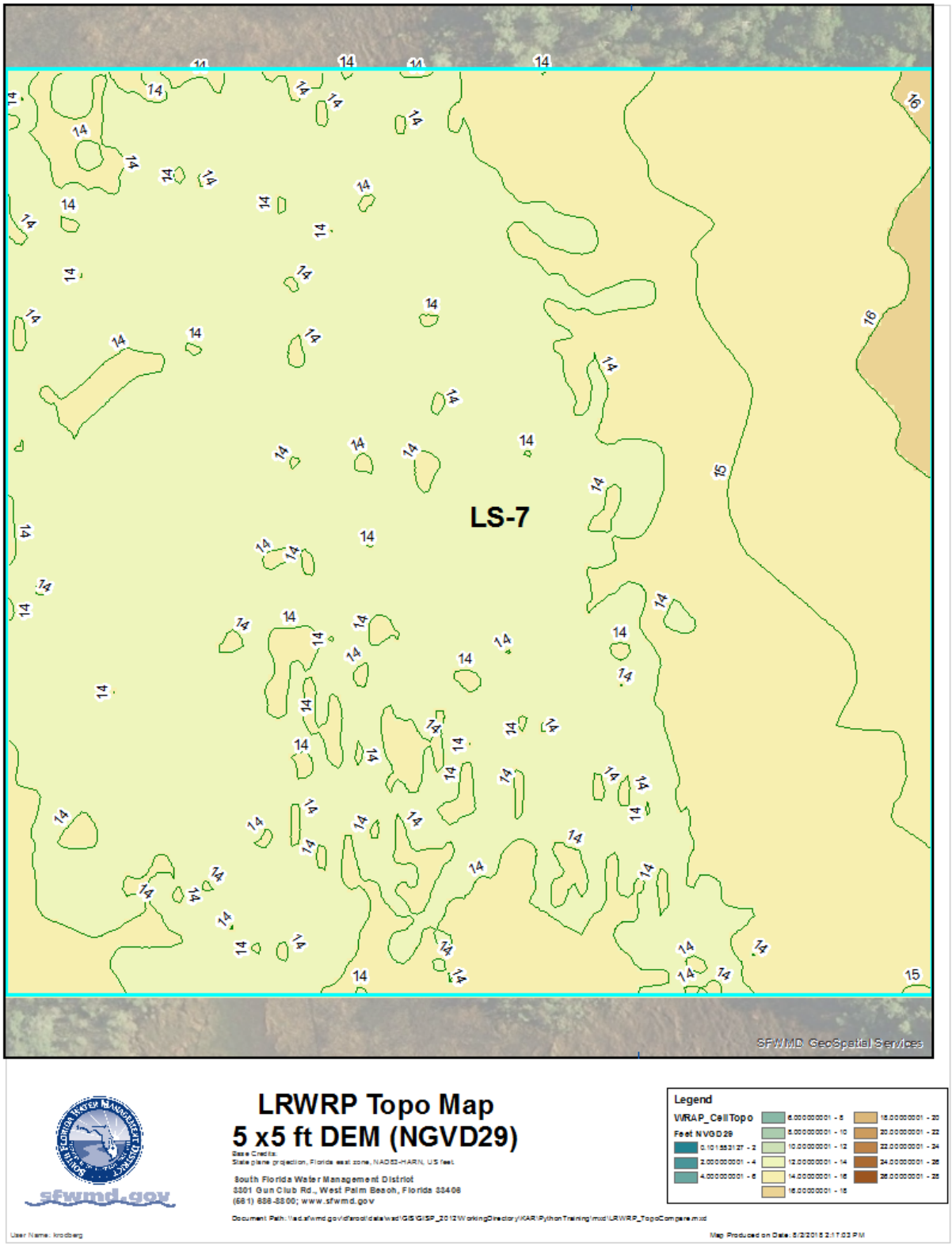

Figure C-120. Variation of model cell topography based on SFWMD's 5 ft LiDAR within WRAP cell LS-7A.

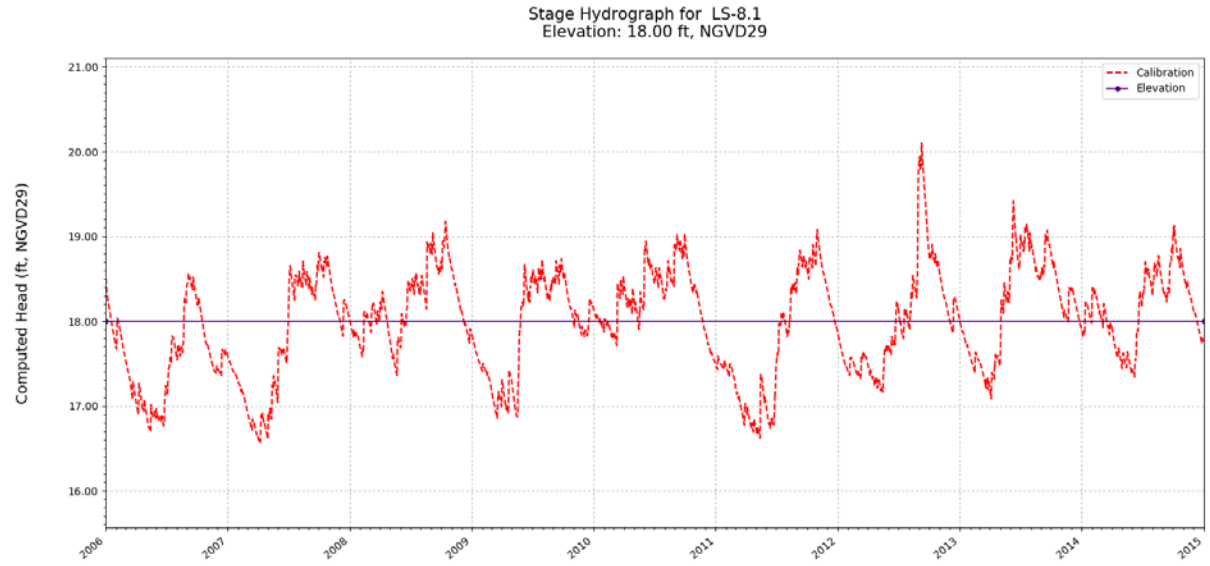

Figure C-121. Simulated stage hydrograph (2006 – 2014) and model cell topography for WRAP cell LS-8.1.

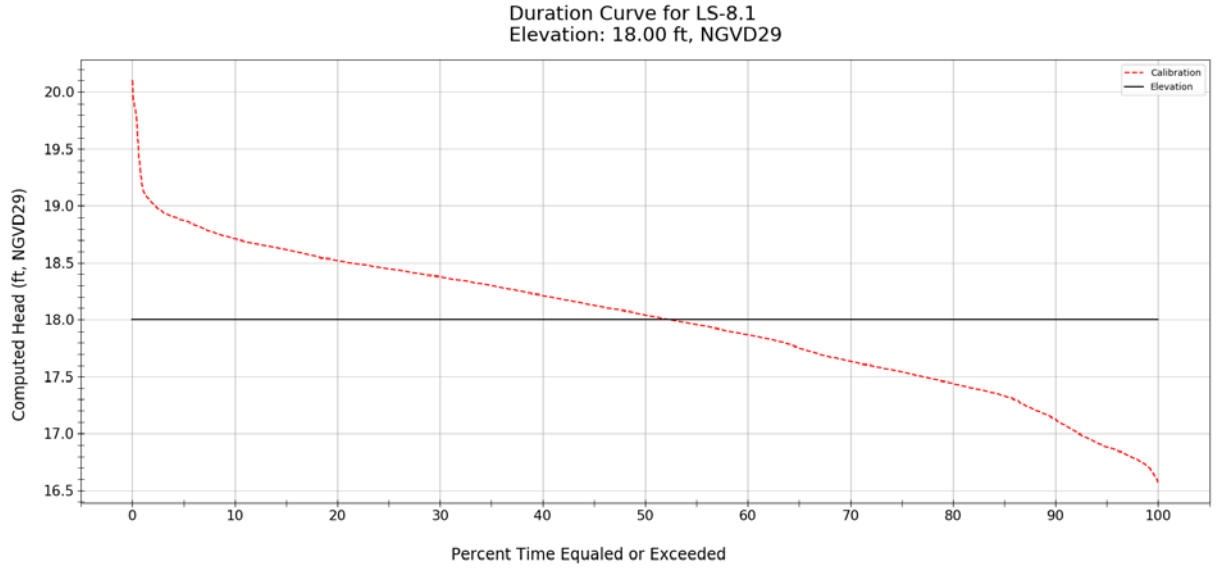

Figure C-122. Simulated stage duration curve (2006 – 2014) and model cell topography for WRAP cell LS-8.1.

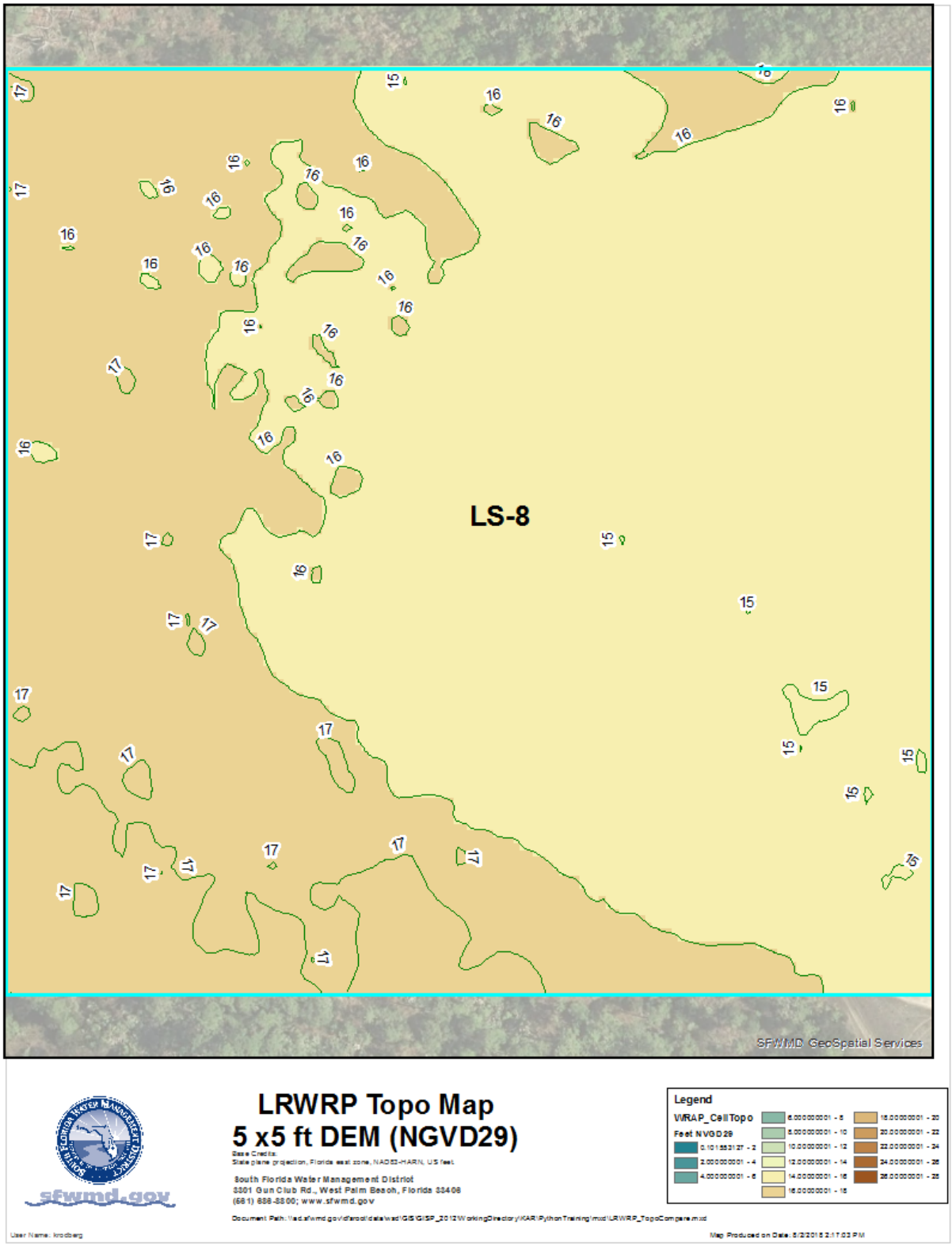

Figure C-123. Variation of model cell topography based on SFWMD's 5 ft LiDAR within WRAP cell LS-8.1.

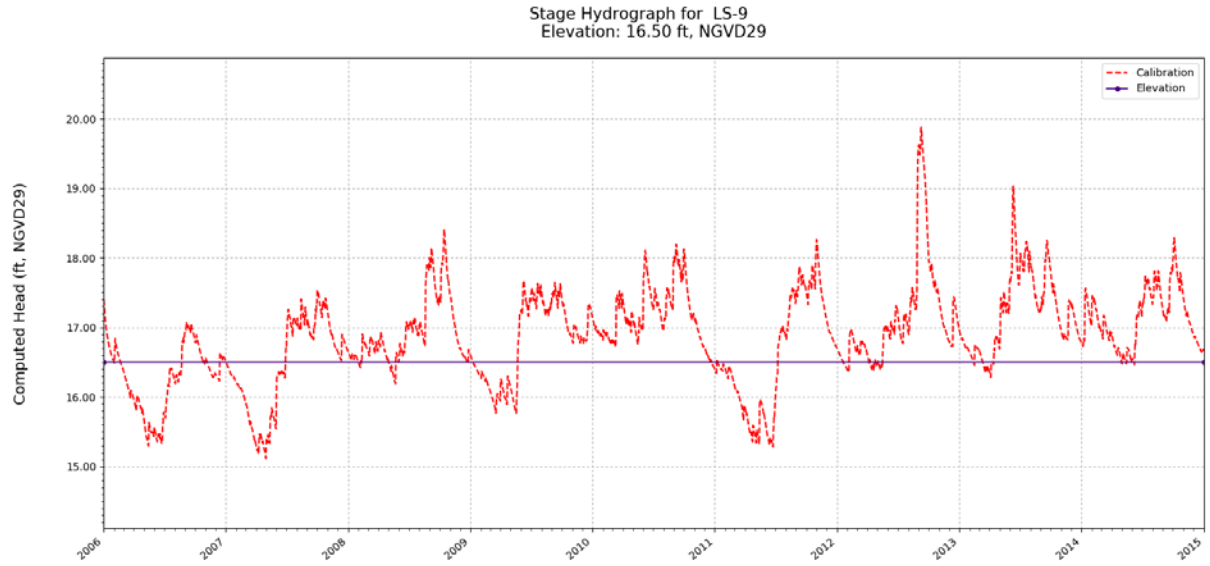

Figure C-124. Simulated stage hydrograph (2006 – 2014) and model cell topography for WRAP cell LS-9.

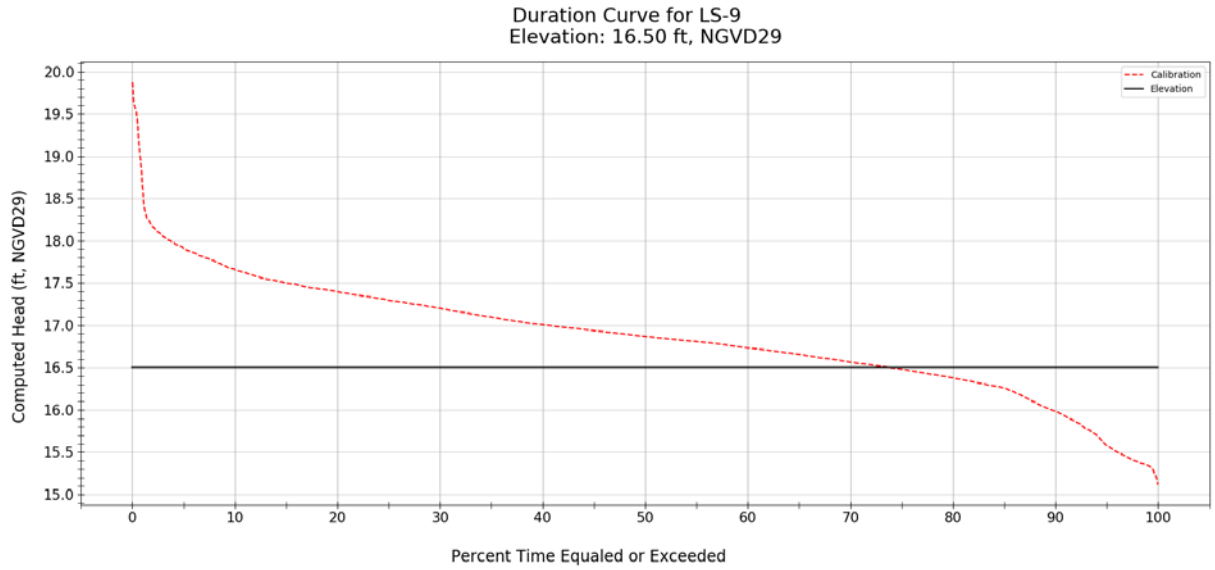

Figure C-125. Simulated stage duration curve (2006 – 2014) and model cell topography for WRAP cell LS-9.

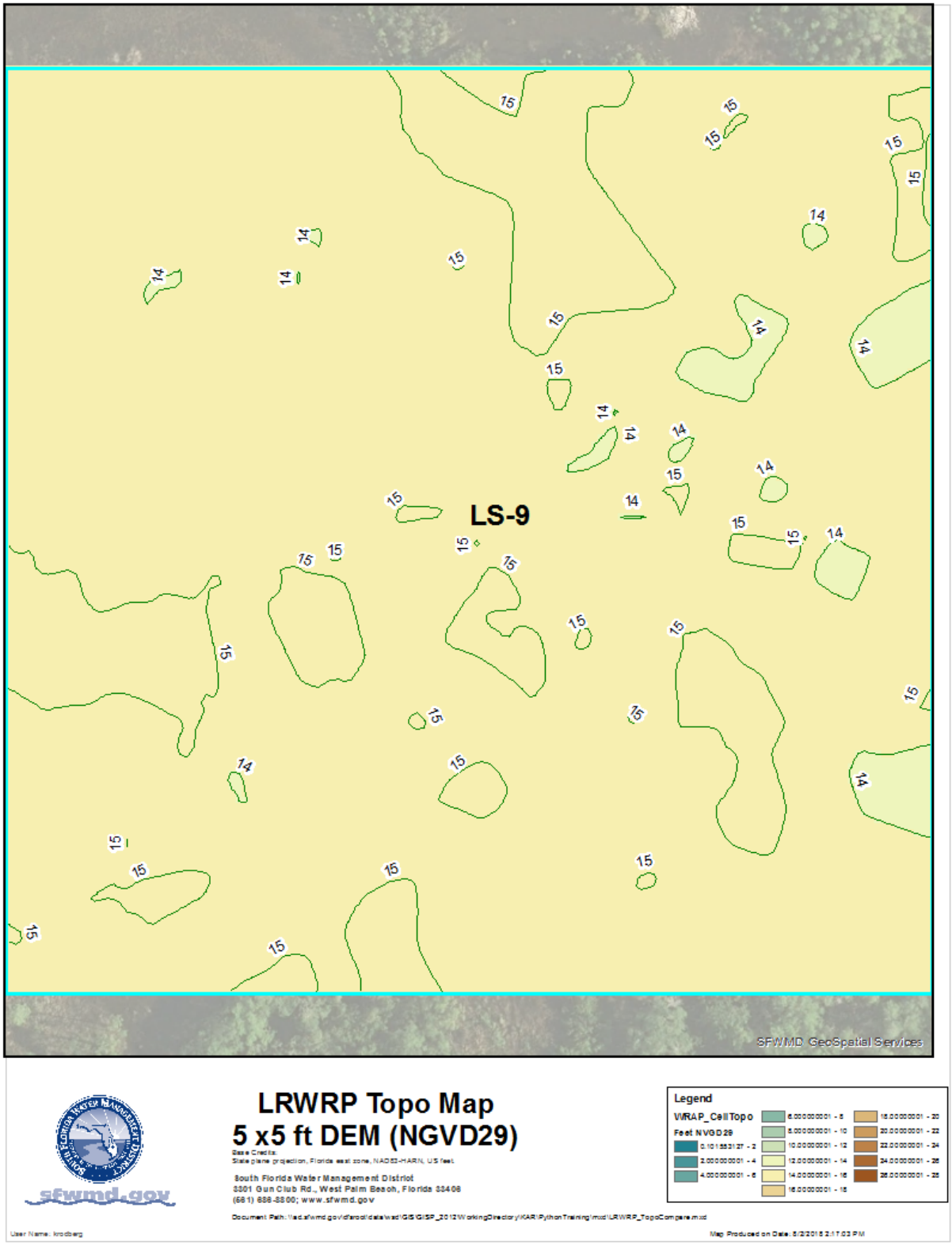

Figure C-126. Variation of model cell topography based on SFWMD's 5 ft LiDAR within WRAP cell LS-9.

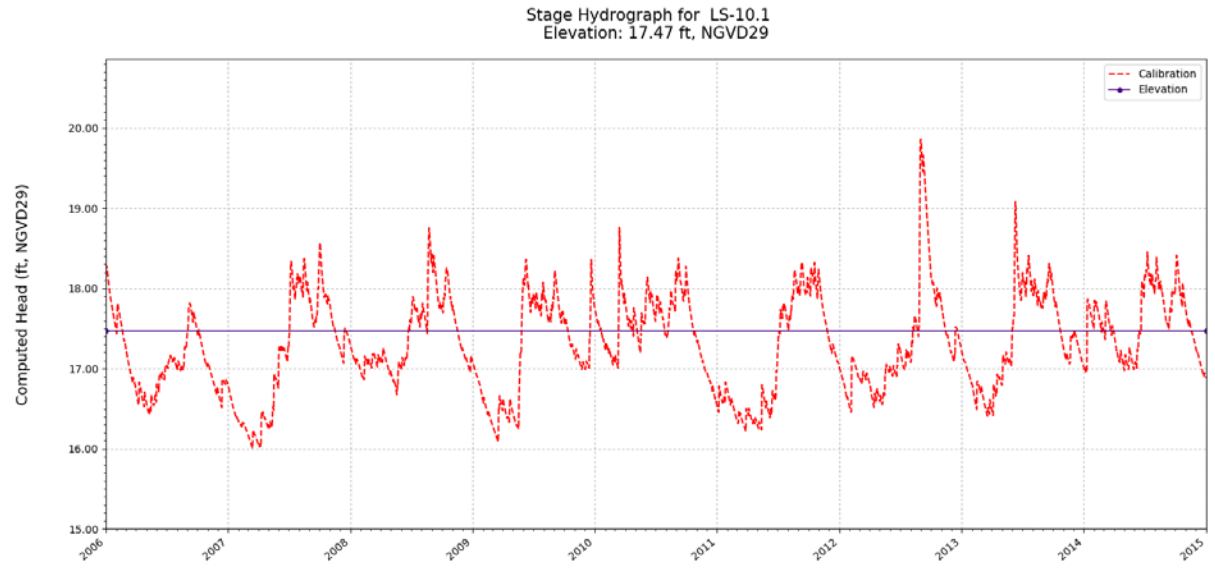

Figure C-127. Simulated stage hydrograph (2006 – 2014) and model cell topography for WRAP cell LS-10.1.

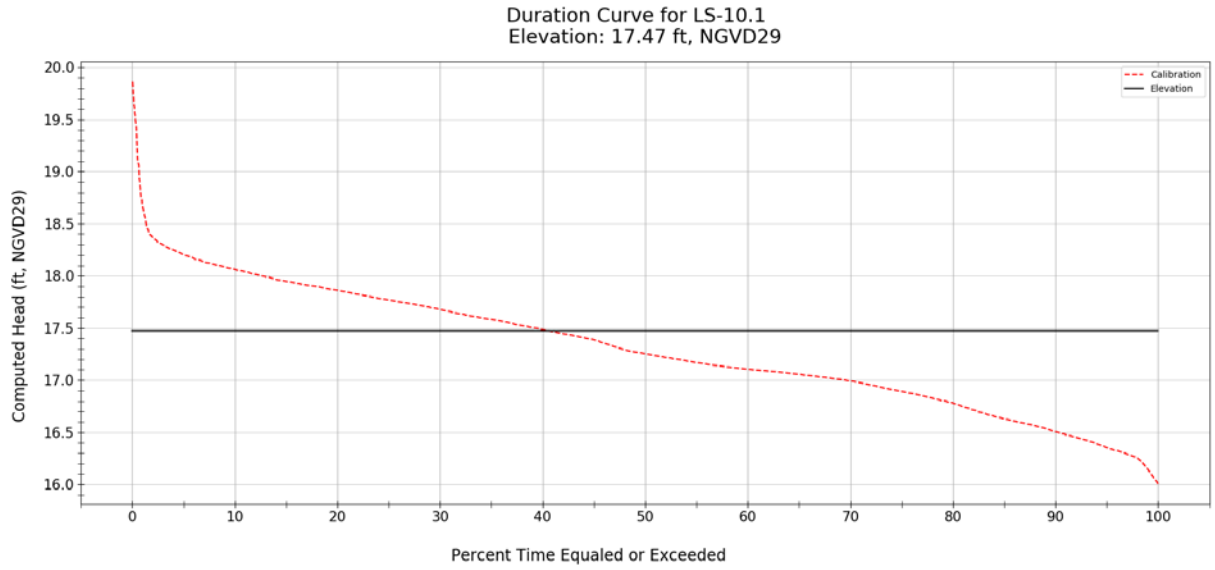

Figure C-128. Simulated stage duration curve (2006 – 2014) and model cell topography for WRAP cell LS-10.1.

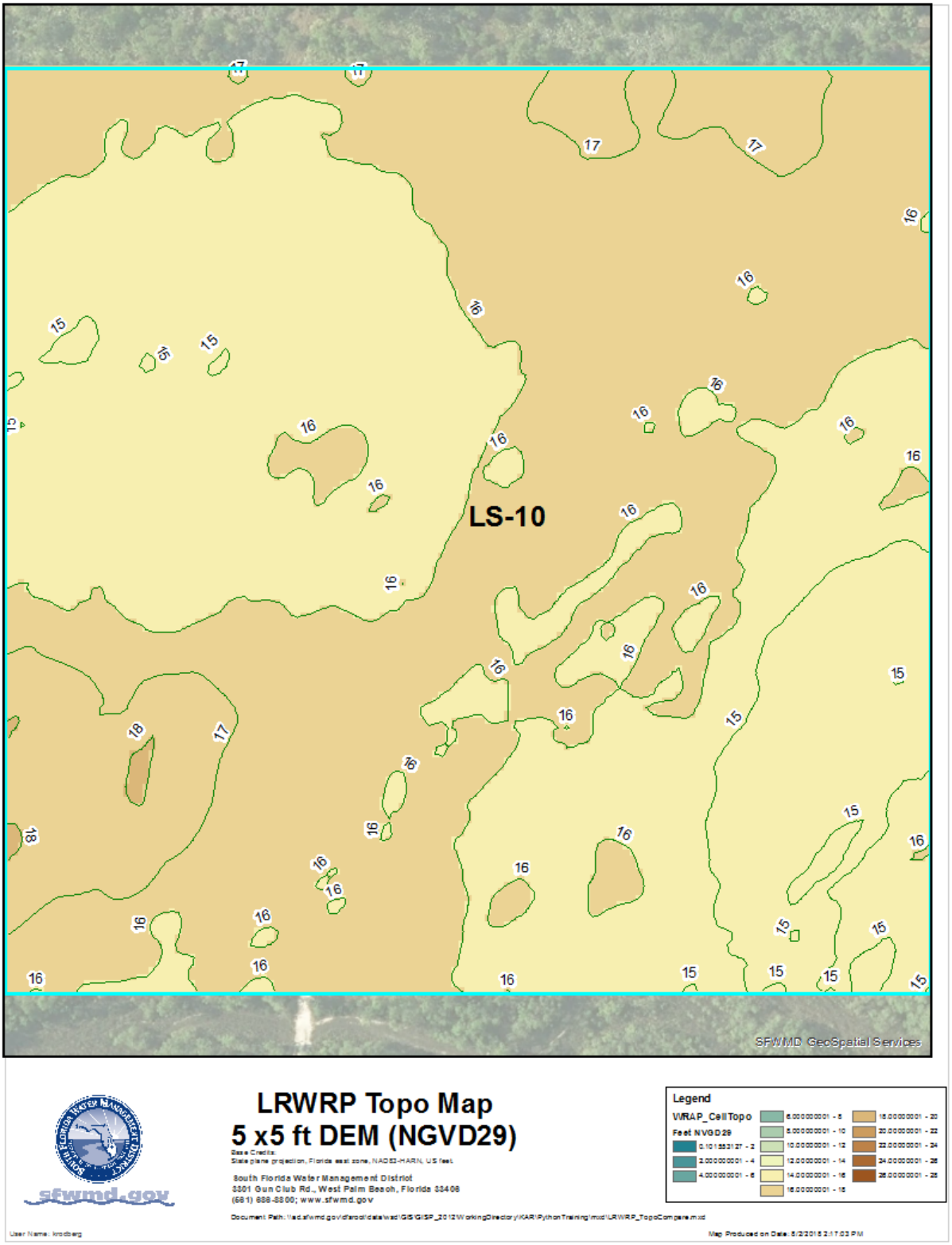

Figure C-129. Variation of model cell topography based on SFWMD's 5 ft LiDAR within WRAP cell LS-10.1.

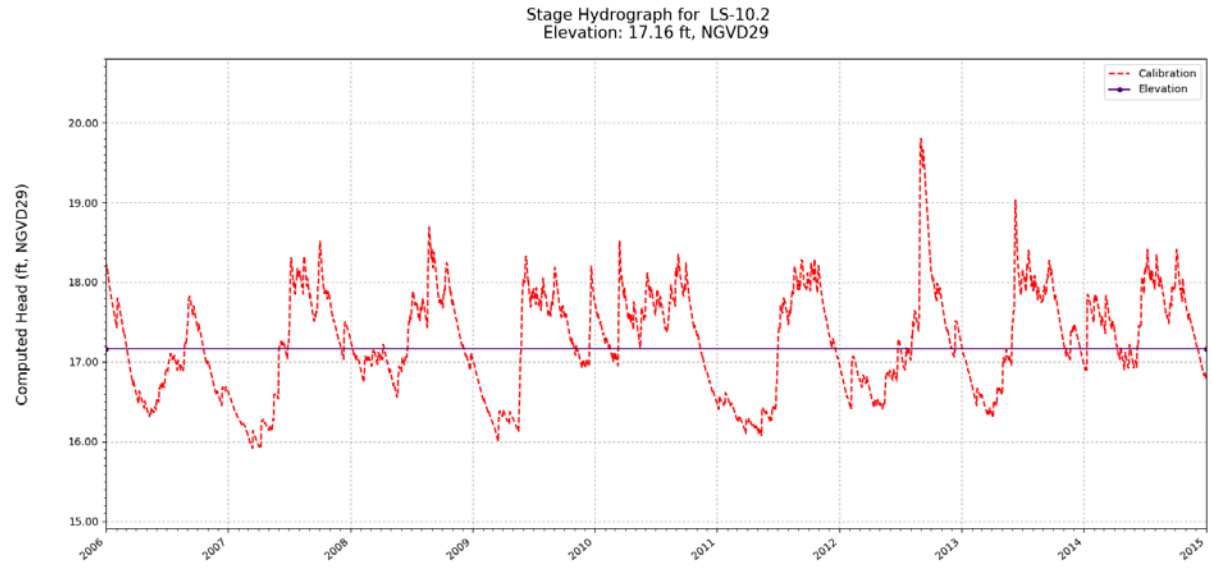

Figure C-130. Simulated stage hydrograph (2006 – 2014) and model cell topography for WRAP cell LS-10.2.

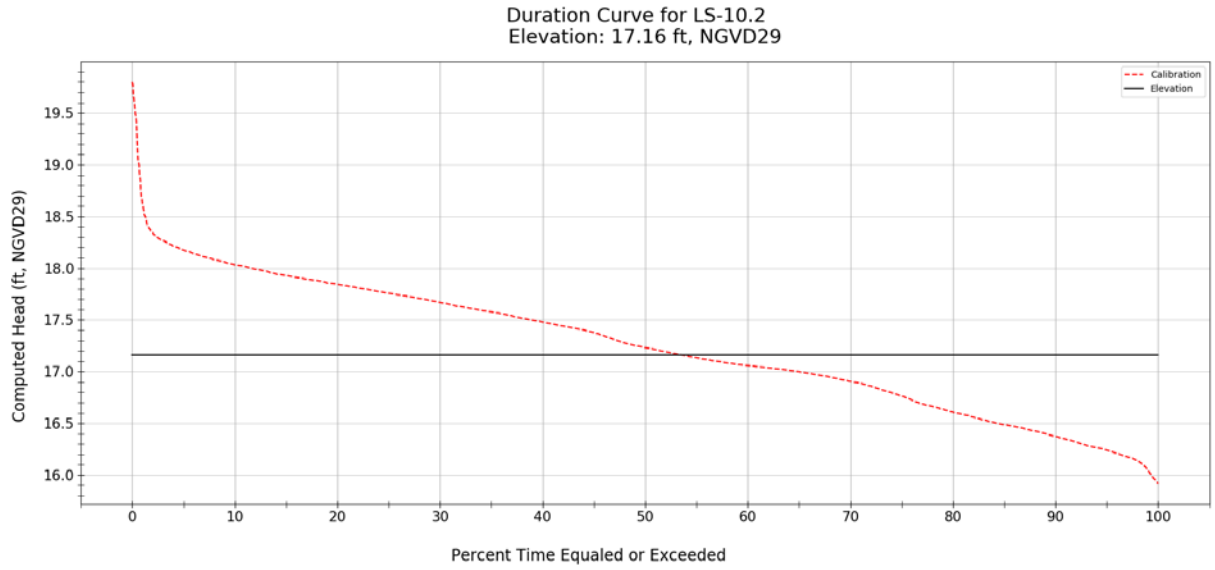

Figure C-131. Simulated stage duration curve (2006 – 2014) and model cell topography for WRAP cell LS-10.2.

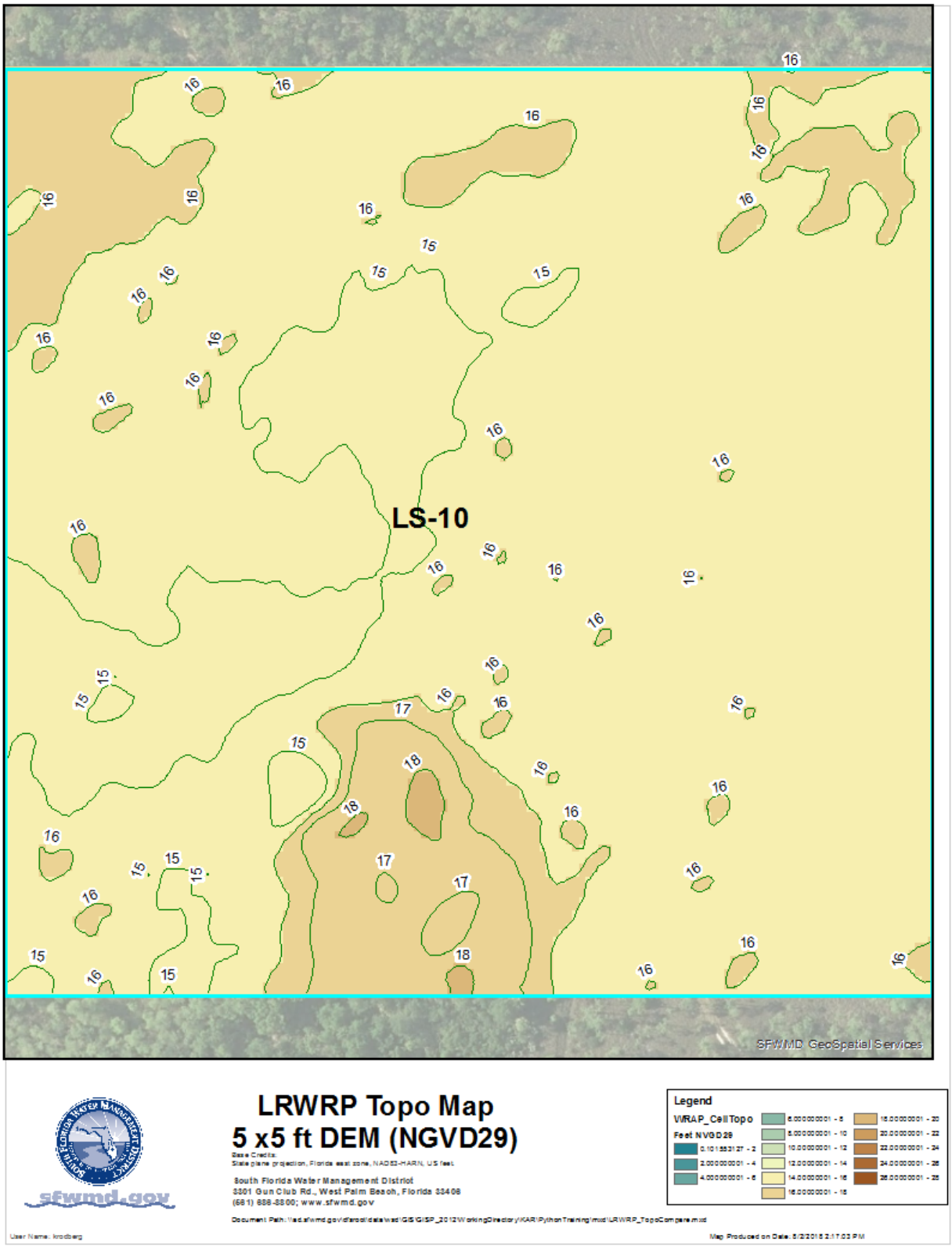

Figure C-132. Variation of model cell topography based on SFWMD's 5 ft LiDAR within WRAP cell LS-10.2.

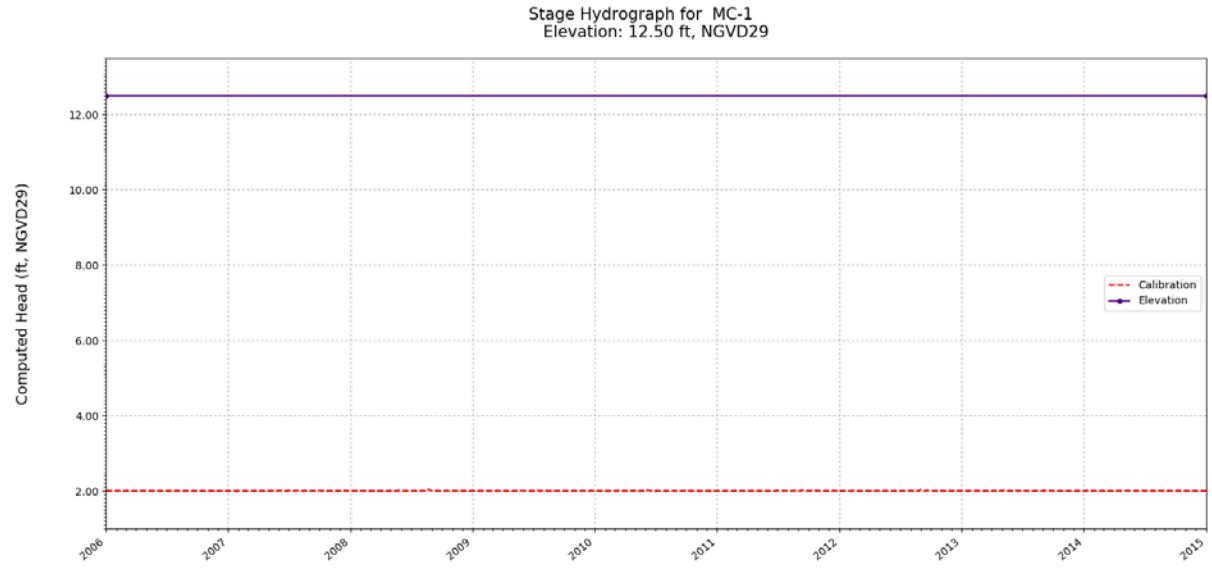

Figure C-133. Simulated stage hydrograph (2006 – 2014) and model cell topography for WRAP cell MC-1.

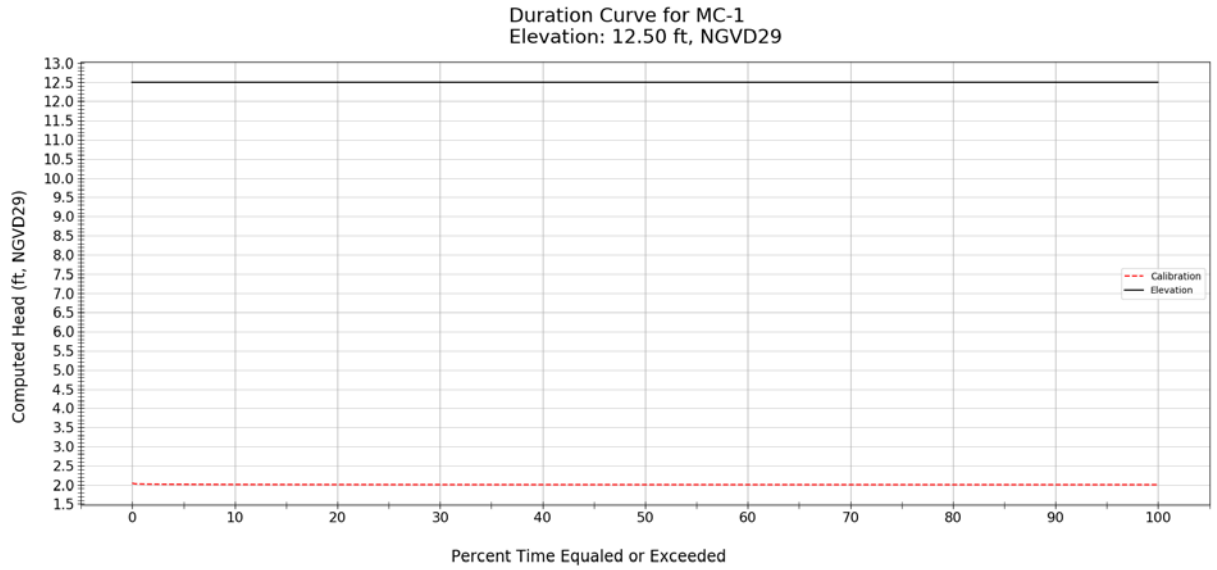

Figure C-134. Simulated stage duration curve (2006 – 2014) and model cell topography for WRAP cell MC-1.

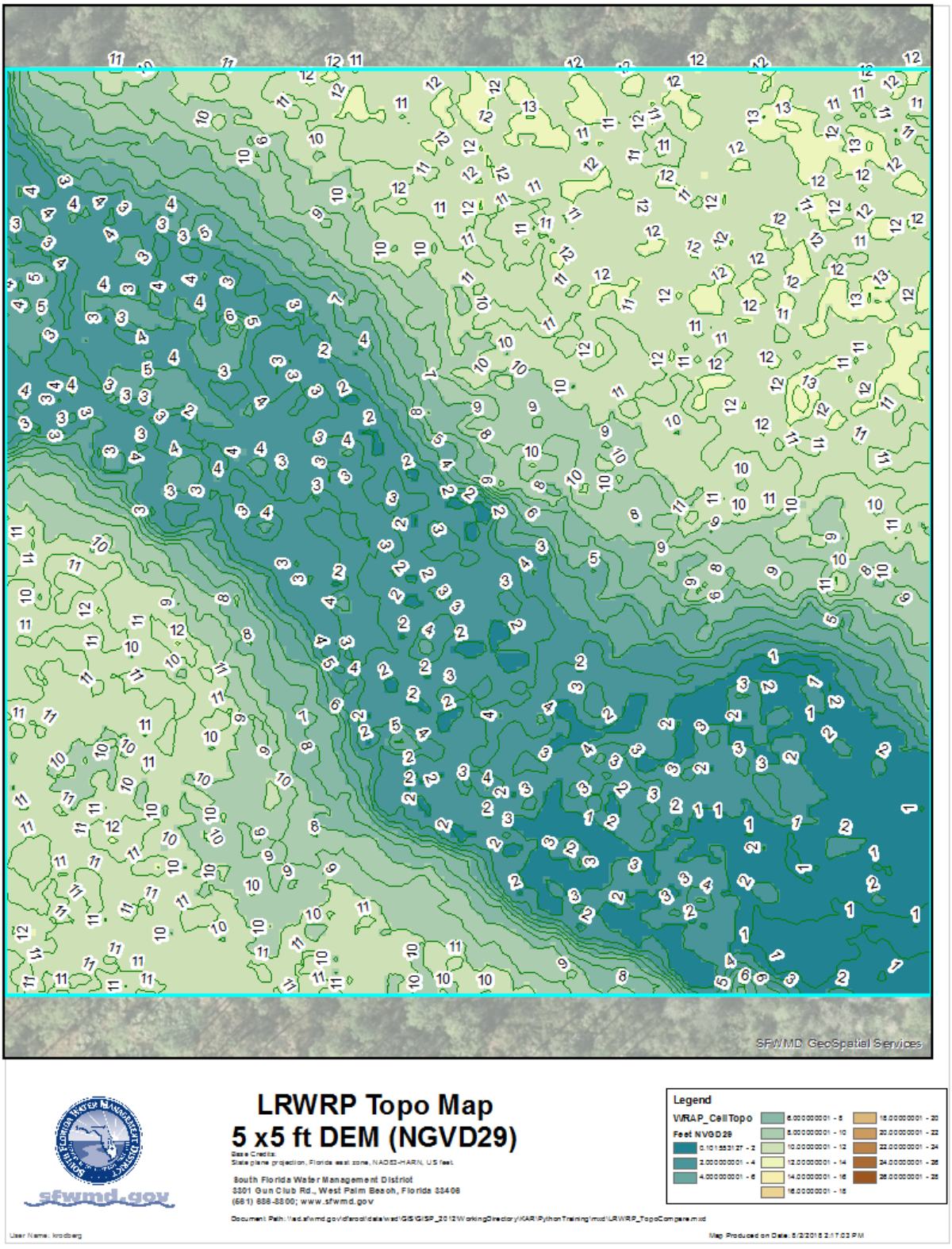

Figure C-135. Variation of model cell topography based on SFWMD's 5 ft LiDAR within WRAP cell MC-1.

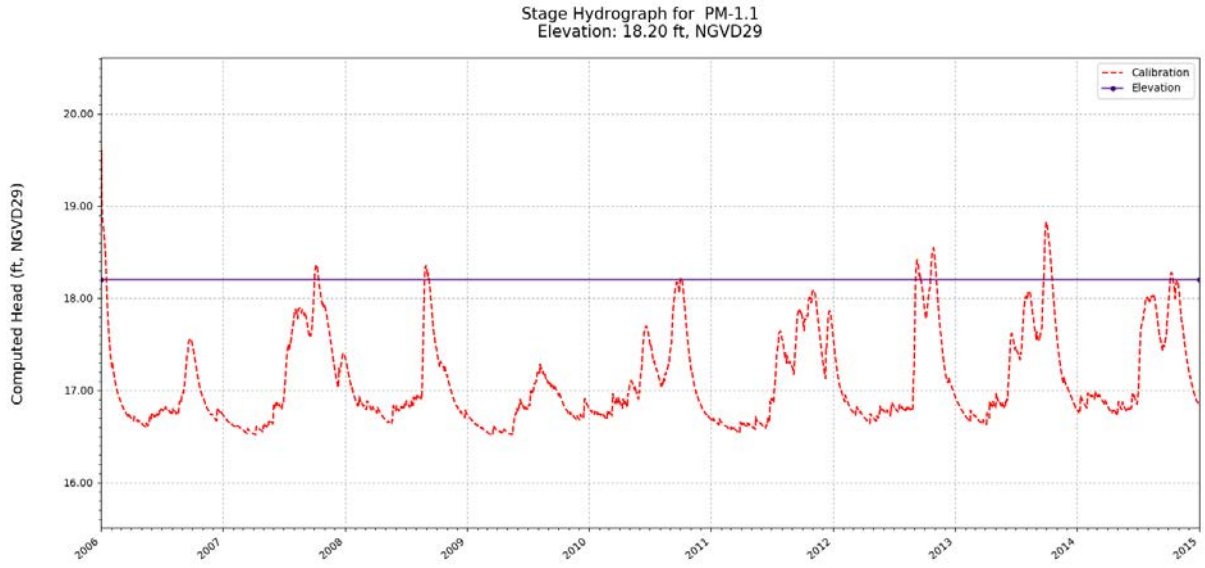

Figure C-136. Simulated stage hydrograph (2006 – 2014) and model cell topography for WRAP cell PM-1.1.

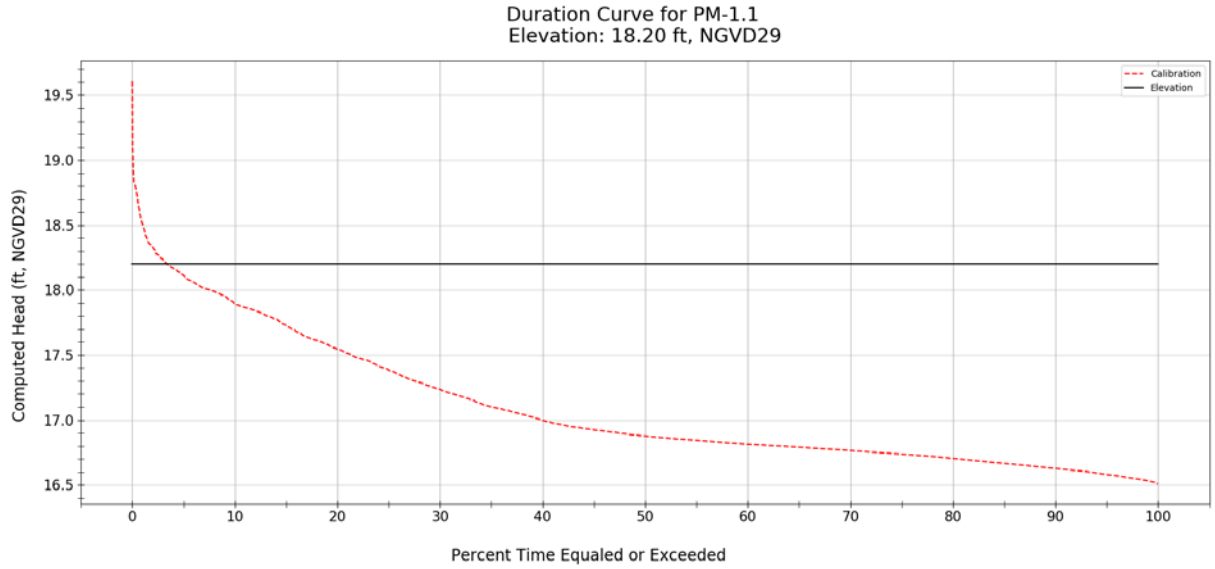

Figure C-137. Simulated stage duration curve (2006 – 2014) and model cell topography for WRAP cell PM-1.1.

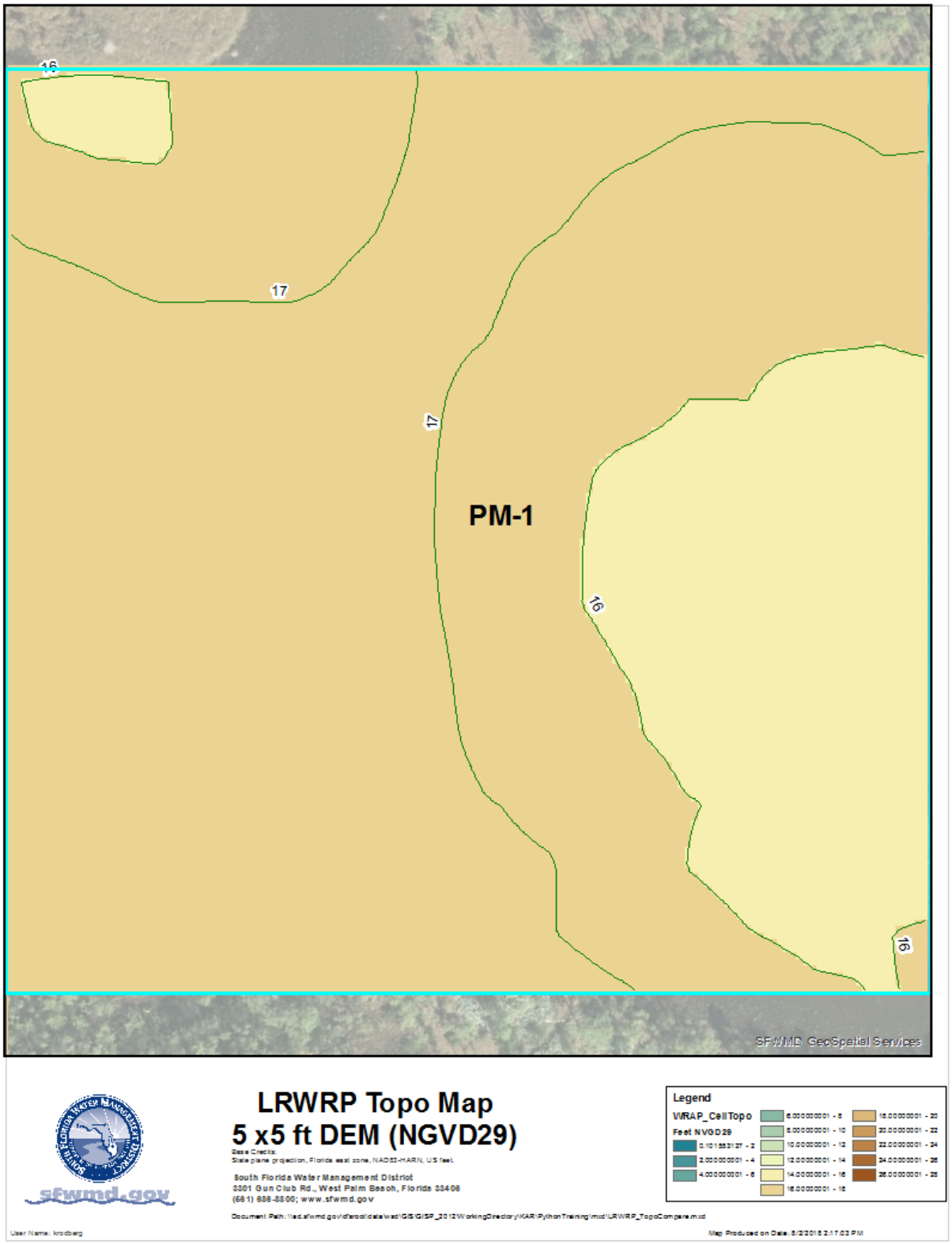

Figure C-138. Variation of model cell topography based on SFWMD's 5 ft LiDAR within WRAP cell PM-1.1.

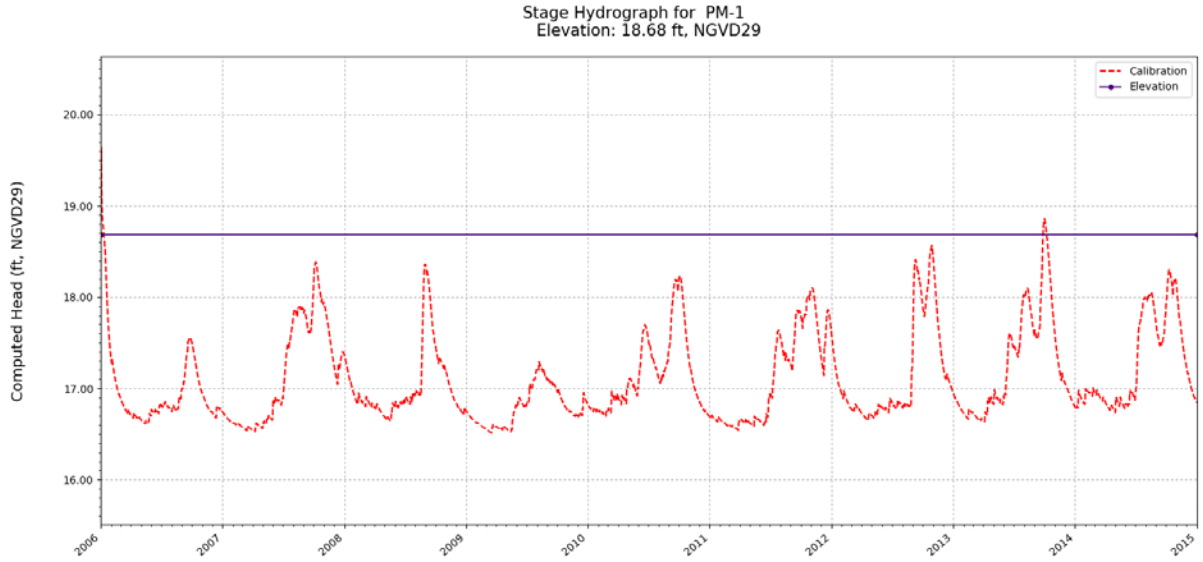

Figure C-139. Simulated stage hydrograph (2006 – 2014) and model cell topography for WRAP cell PM-1.

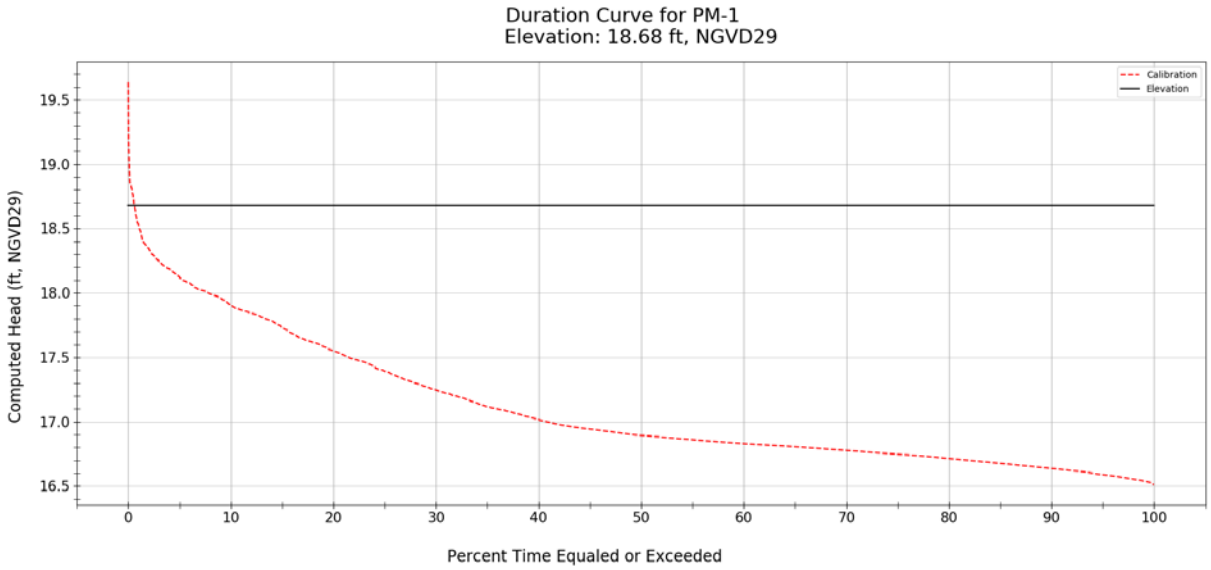

Figure C-140. Simulated stage duration curve (2006 – 2014) and model cell topography for WRAP cell PM-1.

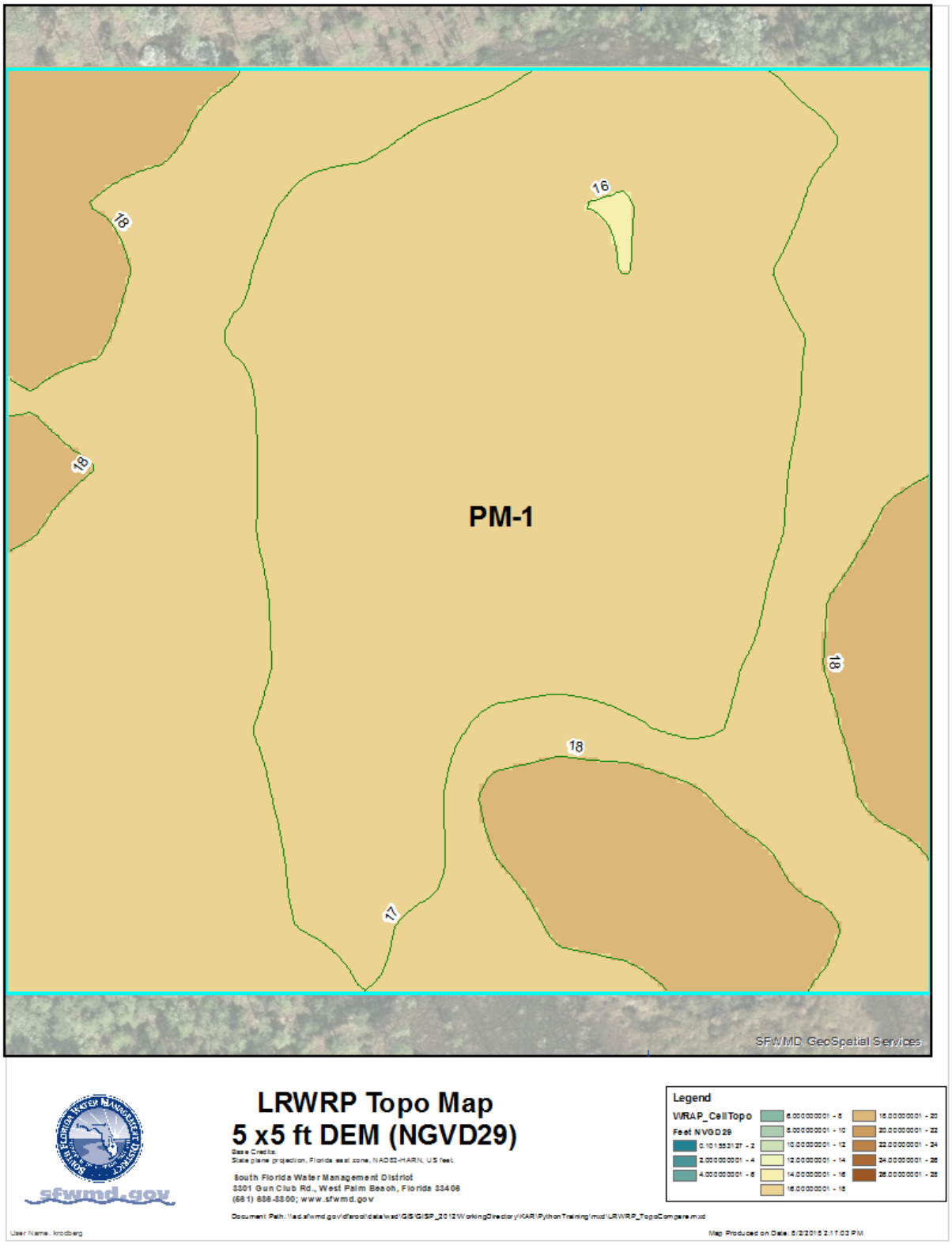

Figure C-141. Variation of model cell topography based on SFWMD's 5 ft LiDAR within WRAP cell PM-1.

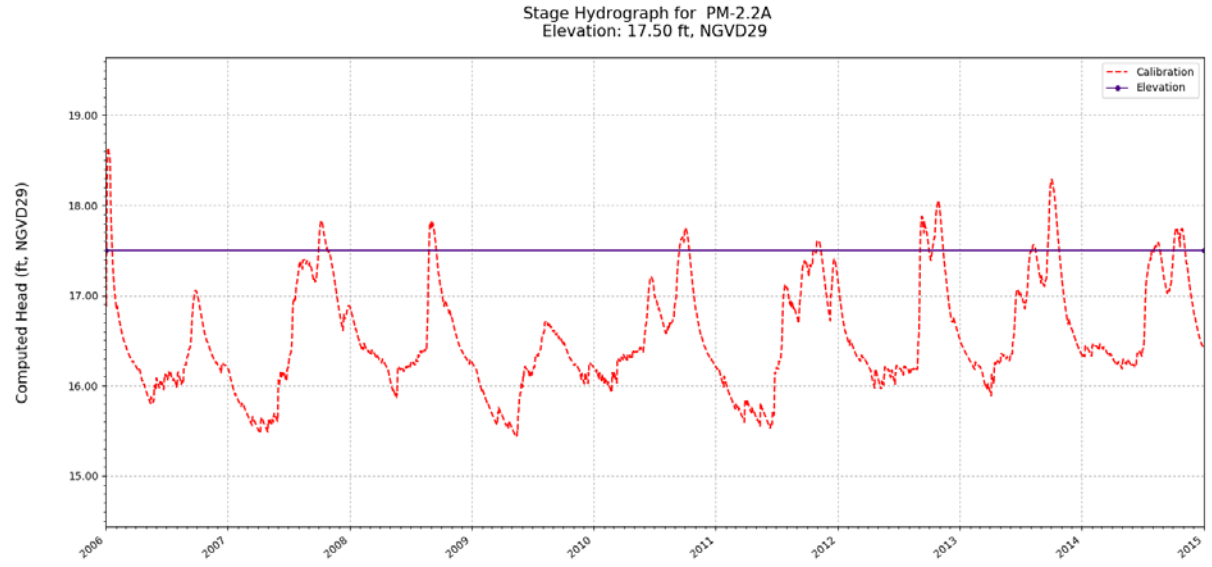

Figure C-142. Simulated stage hydrograph (2006 – 2014) and model cell topography for WRAP cell PM-2.2A.

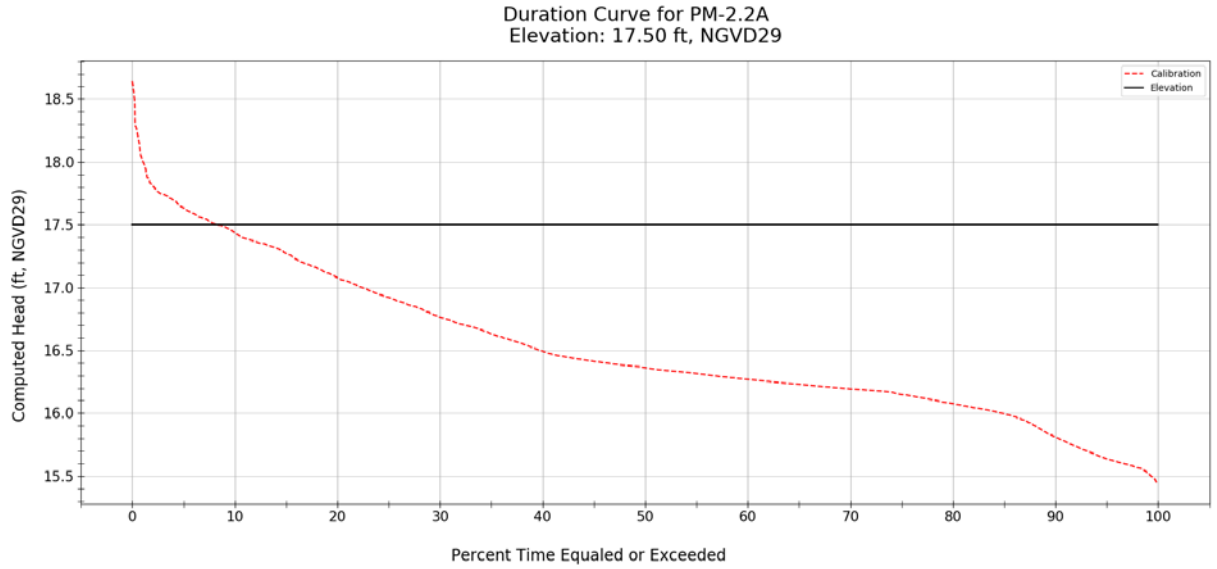

Figure C-143. Simulated stage duration curve (2006 – 2014) and model cell topography for WRAP cell PM-2.2A.

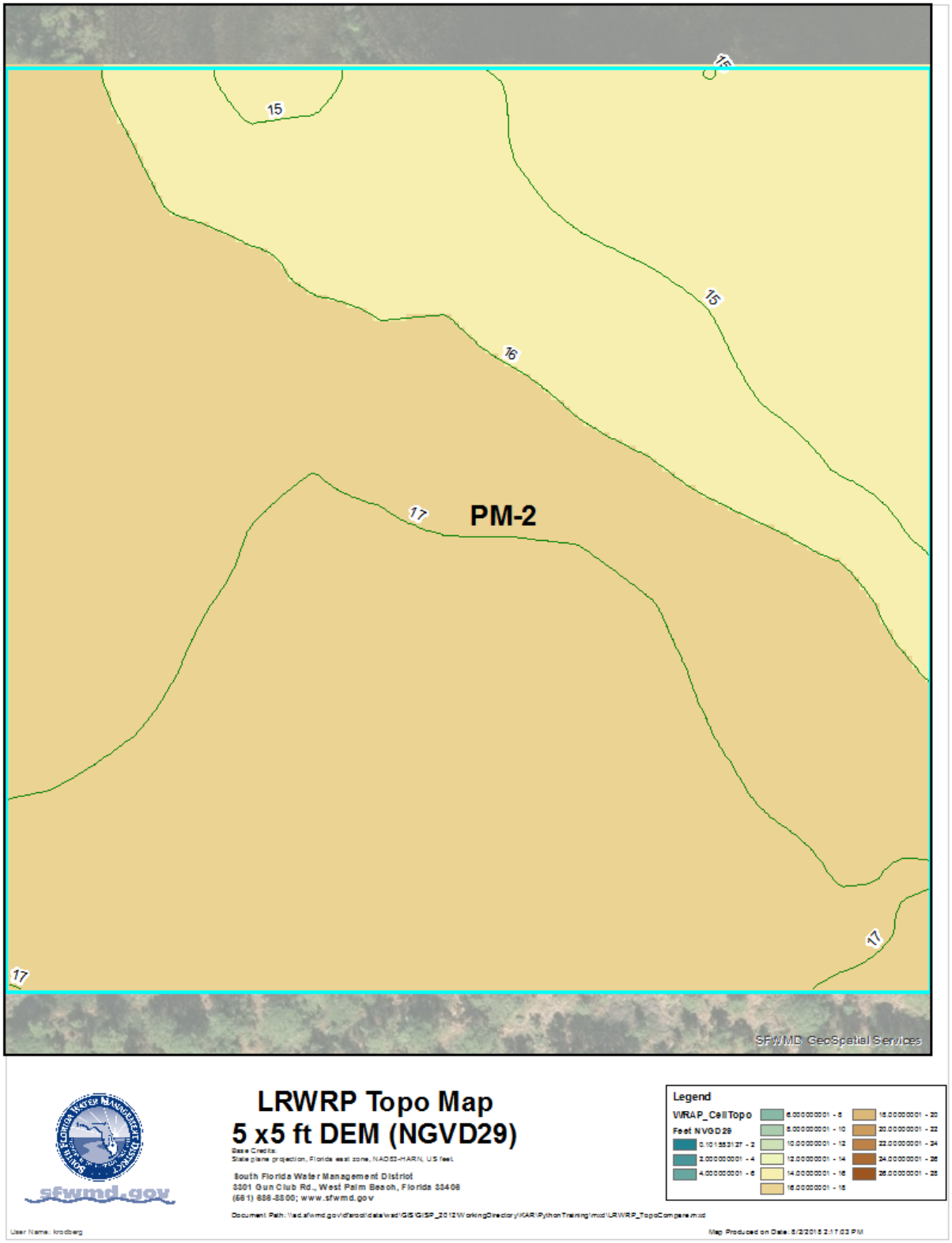

Figure C-144. Variation of model cell topography based on SFWMD's 5 ft LiDAR within WRAP cell PM-2.2A.

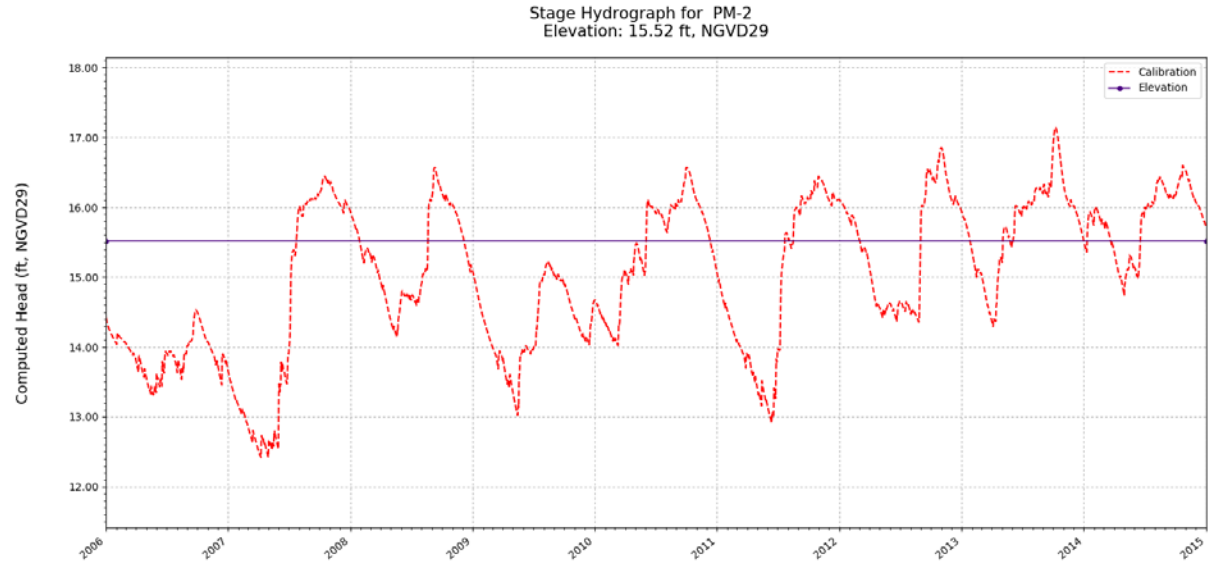

Figure C-145. Simulated stage hydrograph (2006 – 2014) and model cell topography for WRAP cell PM-2.

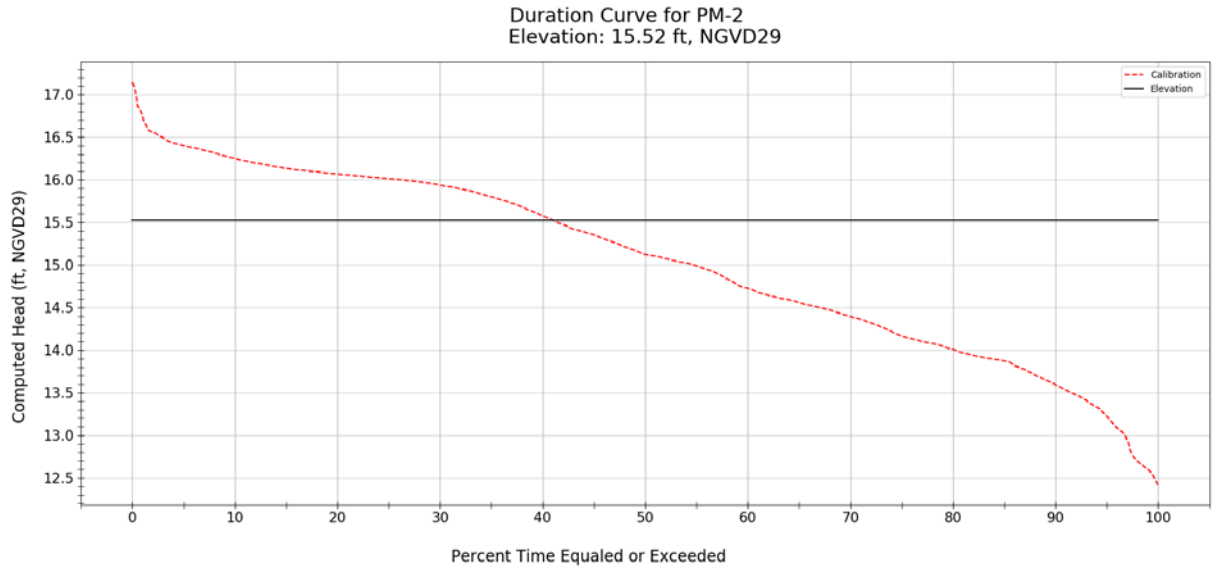

Figure C-146. Simulated stage duration curve (2006 – 2014) and model cell topography for WRAP cell PM-2.

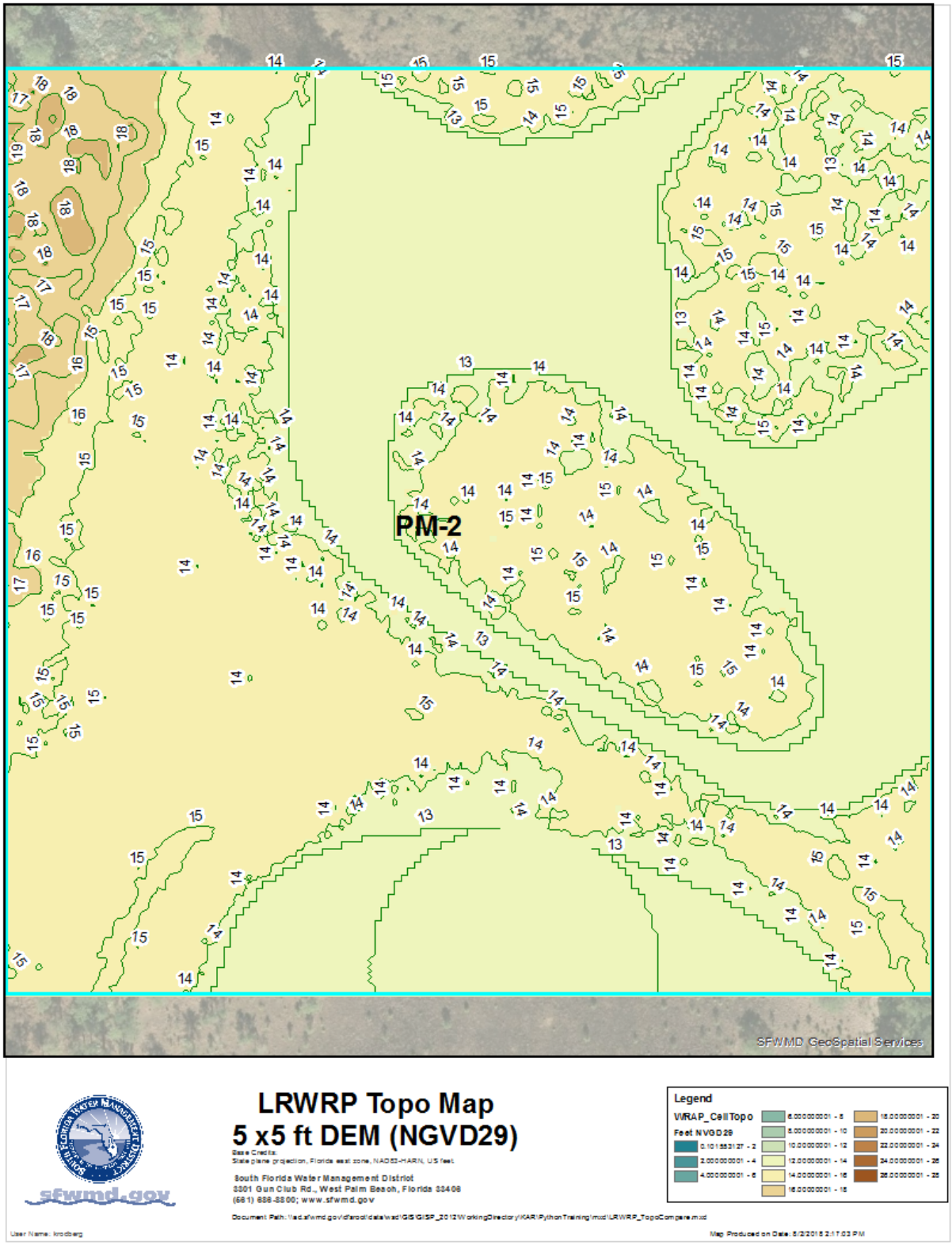

Figure C-147. Variation of model cell topography based on SFWMD's 5 ft LiDAR within WRAP cell PM-2.

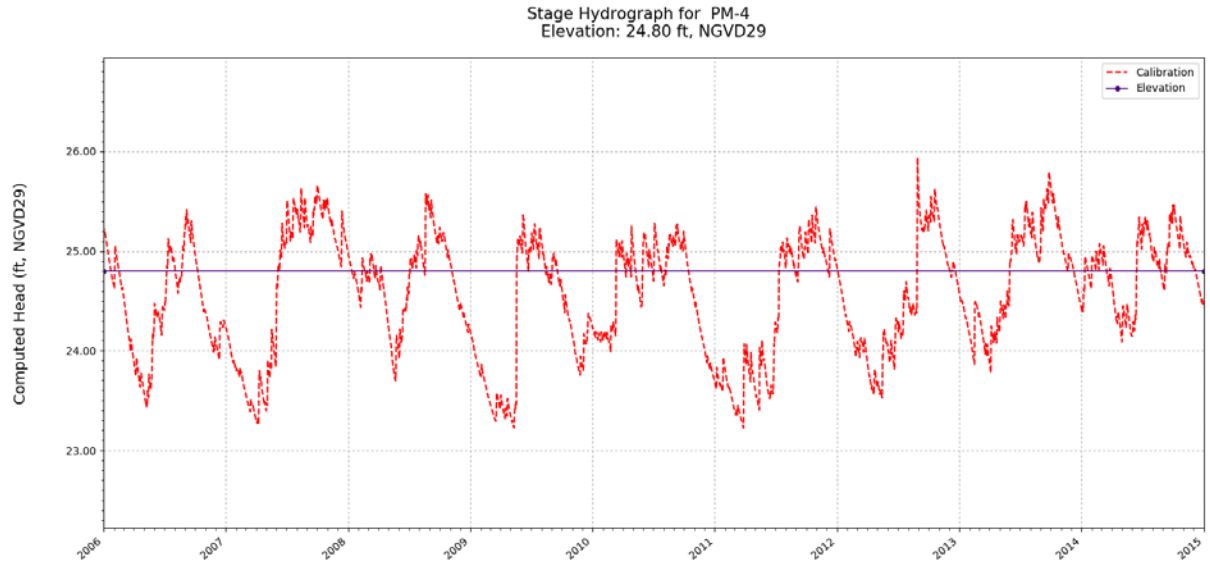

Figure C-148. Simulated stage hydrograph (2006 – 2014) and model cell topography for WRAP cell PM-4.

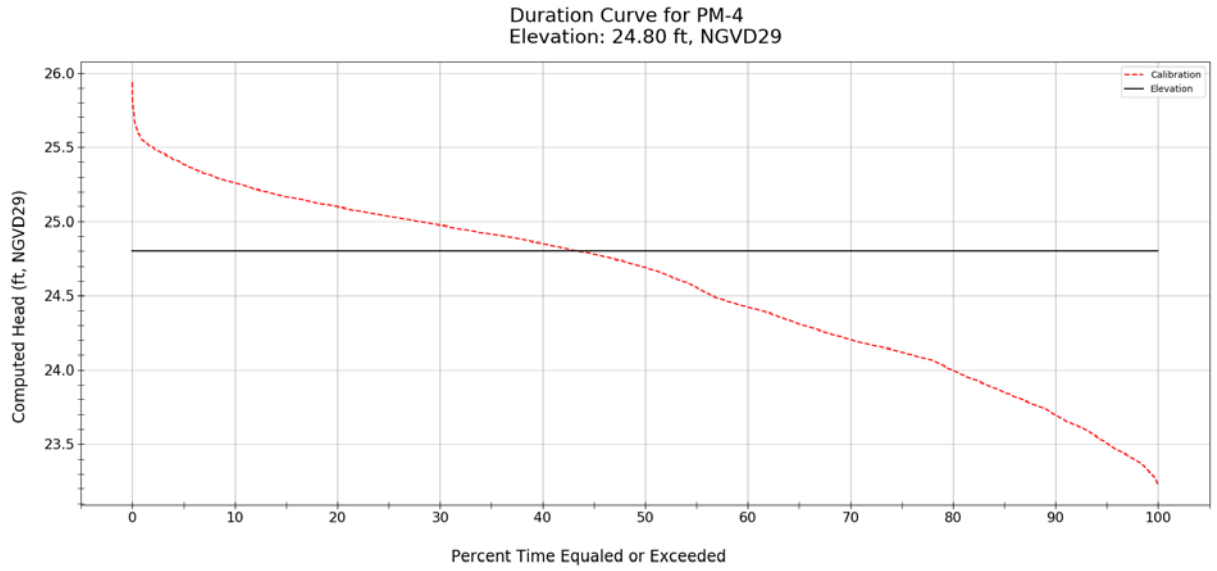

Figure C-149. Simulated stage duration curve (2006 – 2014) and model cell topography for WRAP cell PM-4.

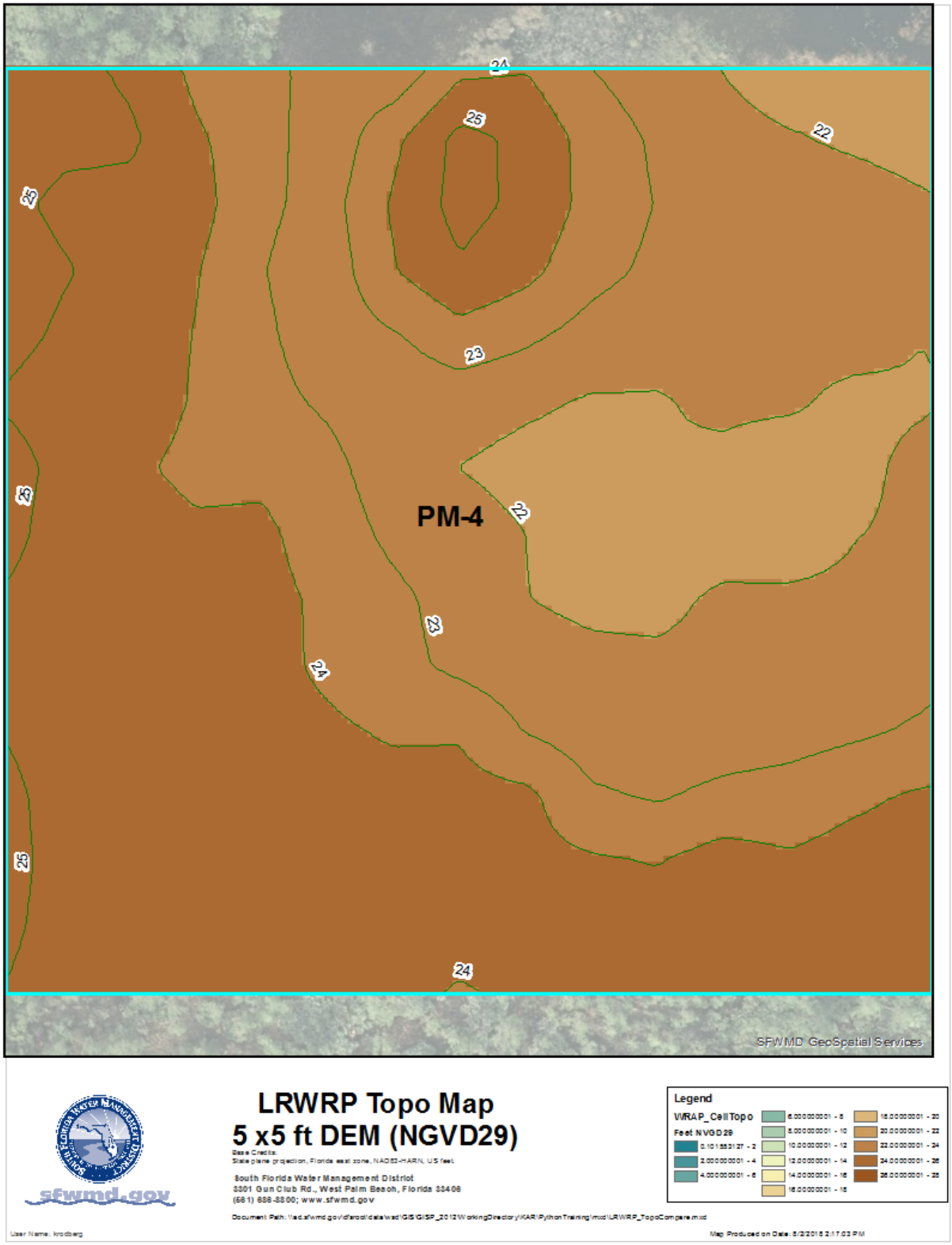

Figure C-150. Variation of model cell topography based on SFWMD's 5 ft LiDAR within WRAP cell PM-4.

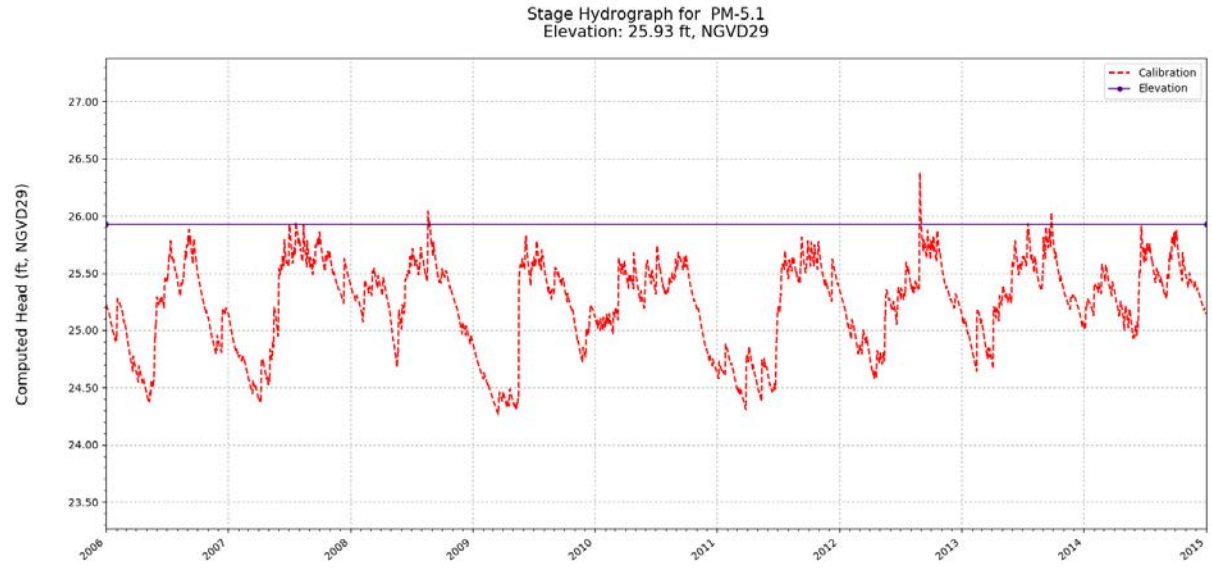

Figure C-151. Simulated stage hydrograph (2006 – 2014) and model cell topography for WRAP cell PM-5.1.

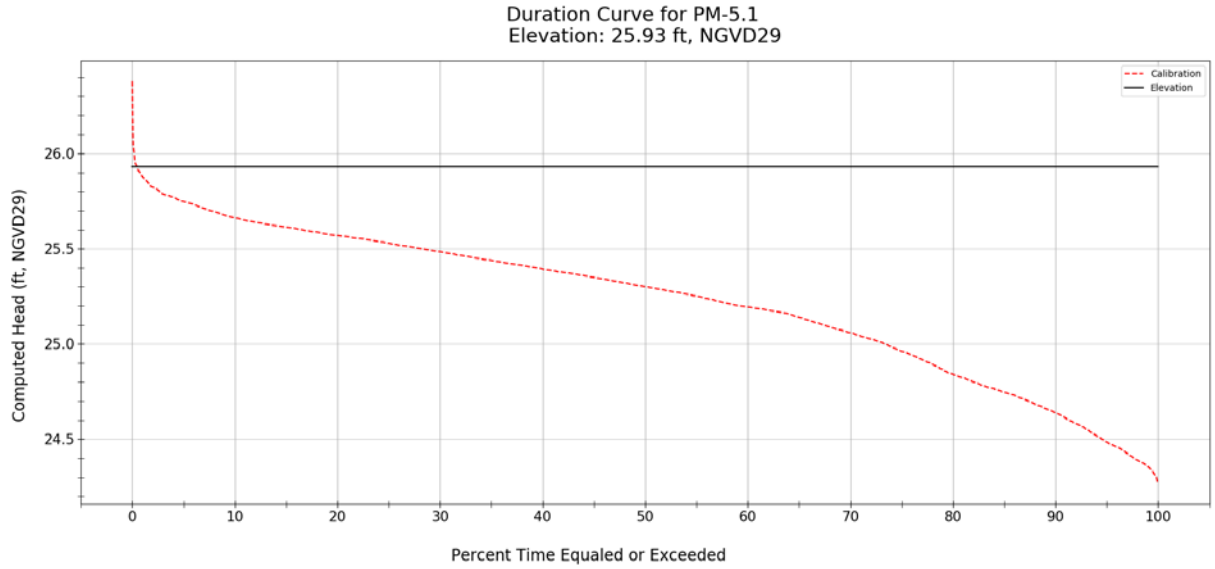

Figure C-152. Simulated stage duration curve (2006 – 2014) and model cell topography for WRAP cell PM-5.1.

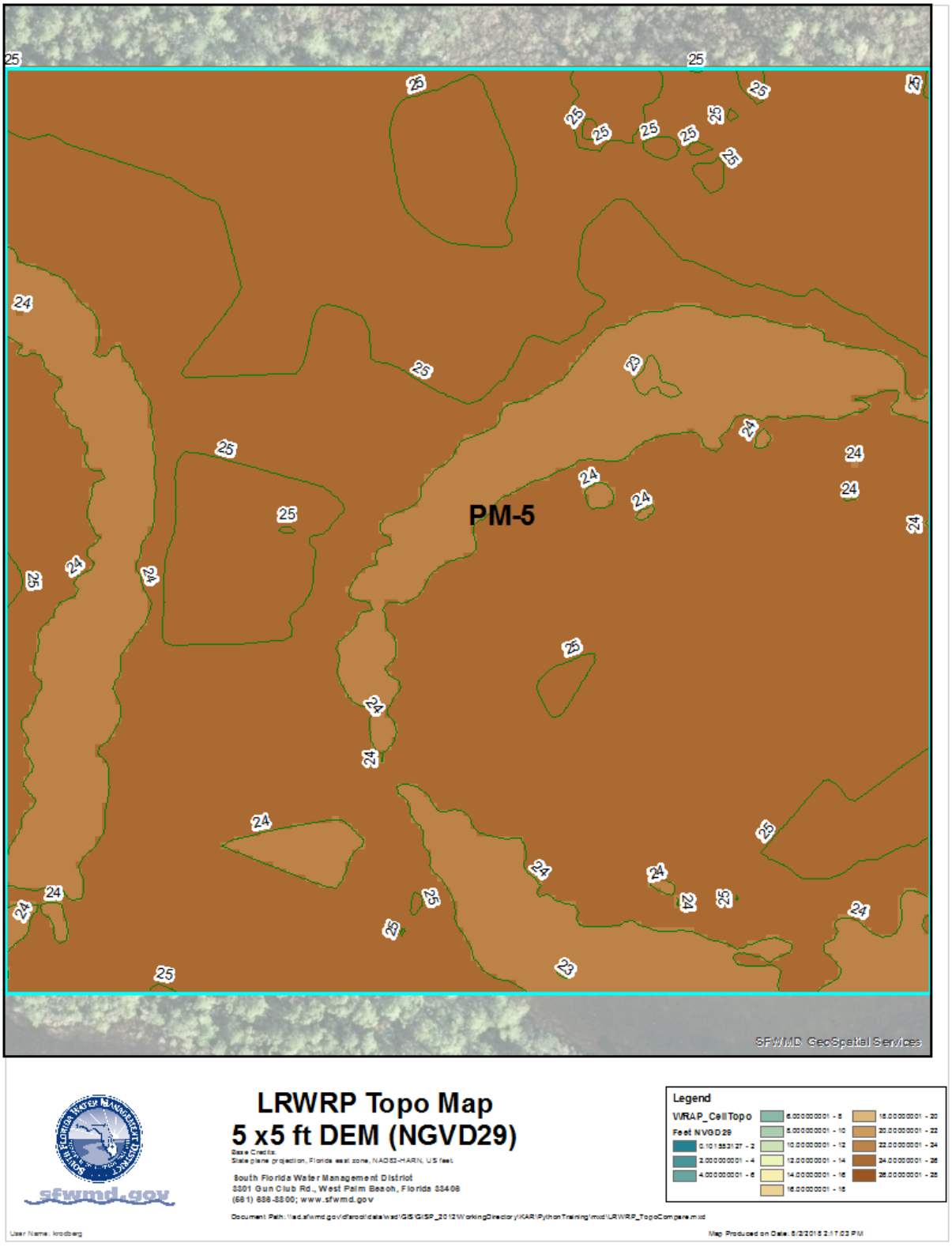

Figure C-153. Variation of model cell topography based on SFWMD's 5 ft LiDAR within WRAP cell PM-5.1.

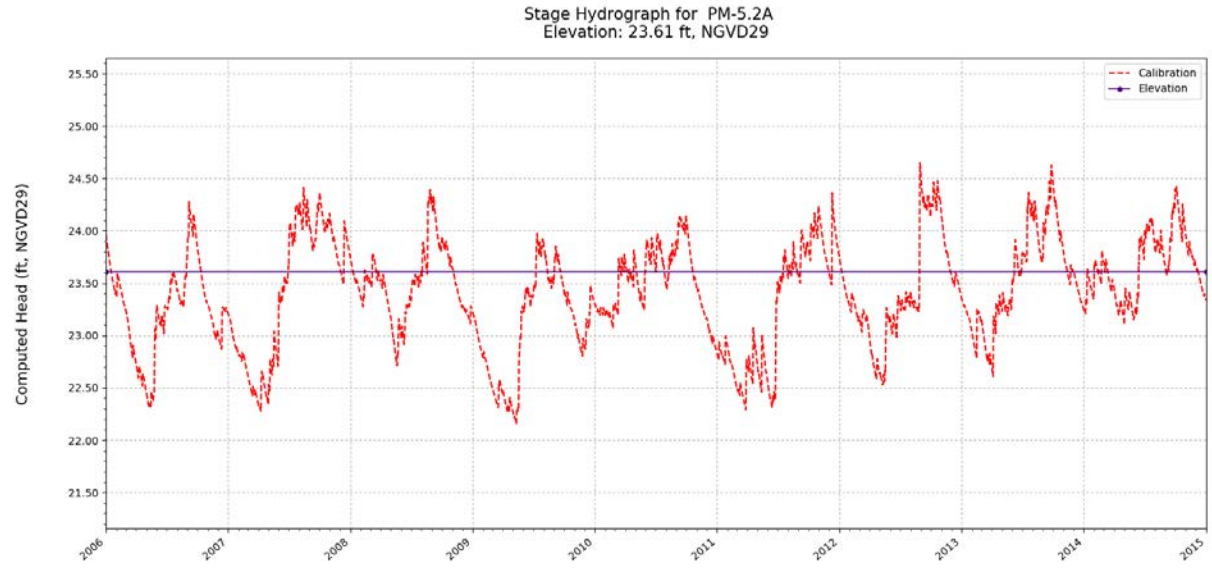

Figure C-154. Simulated stage hydrograph (2006 – 2014) and model cell topography for WRAP cell PM-5.2A.

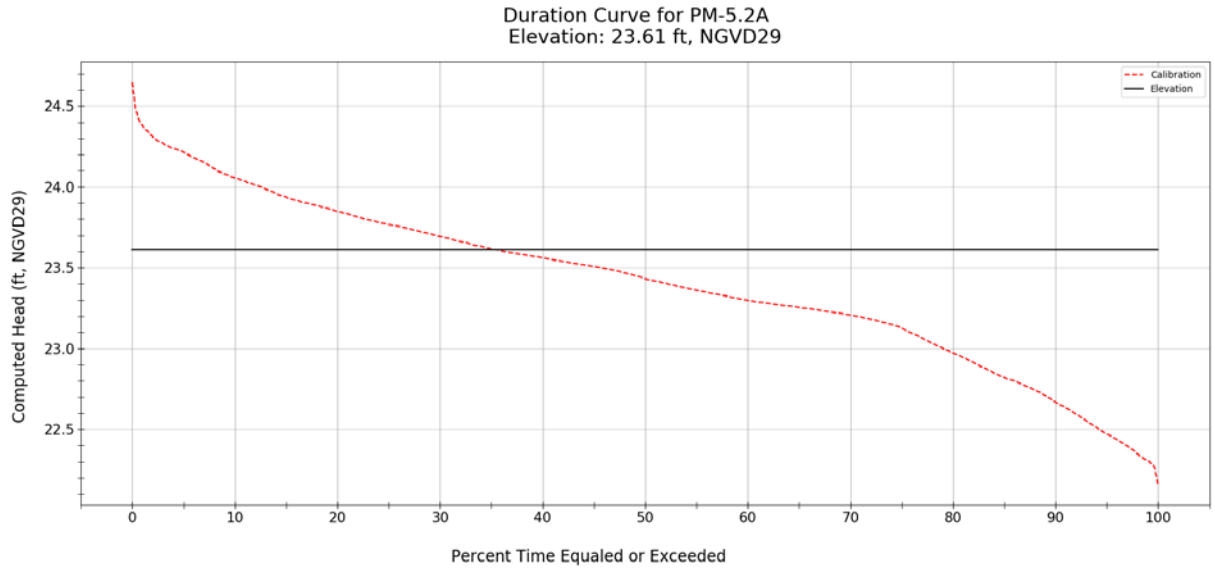

Figure C-155. Simulated stage duration curve (2006 – 2014) and model cell topography for WRAP cell PM-5.2A.

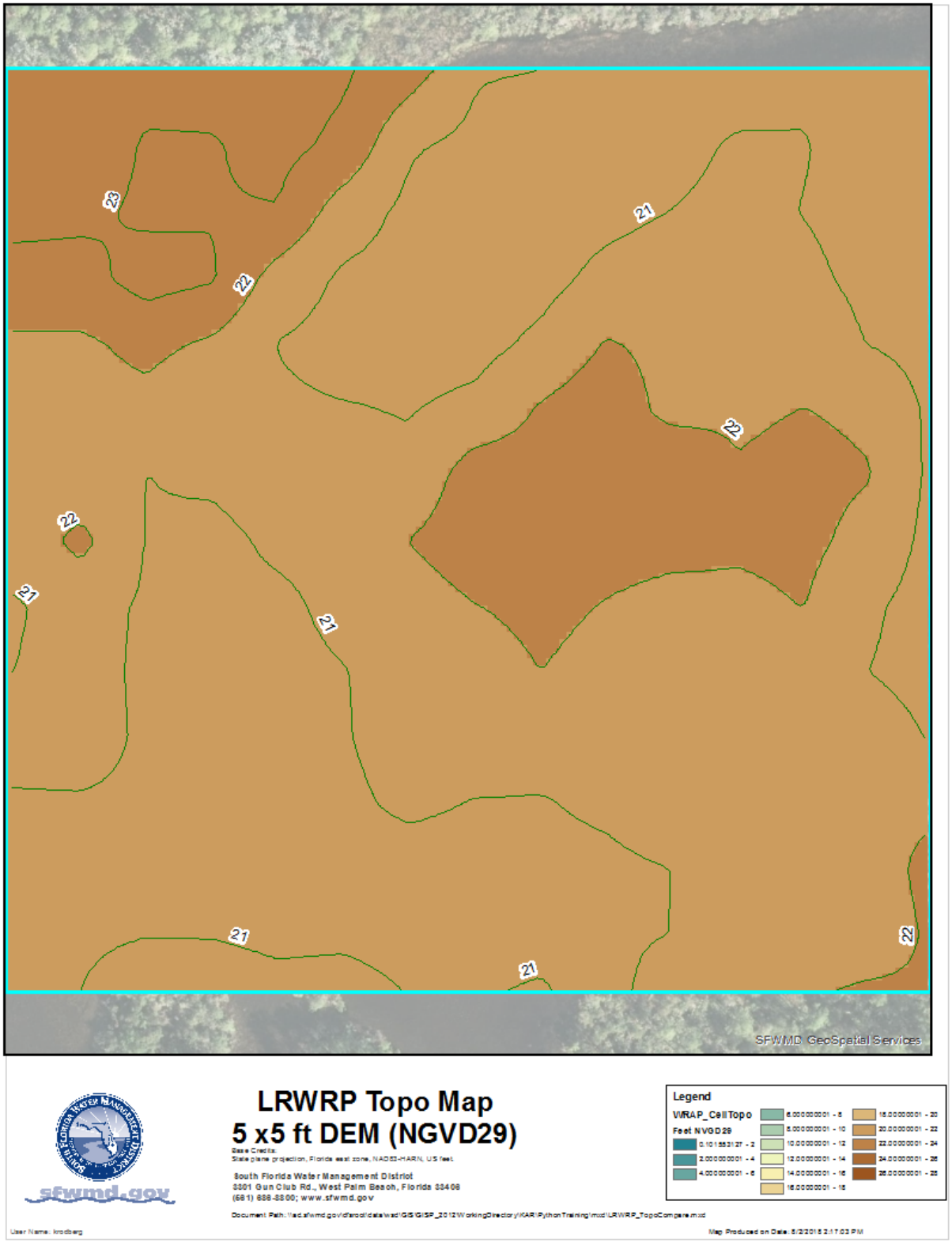

Figure C-156. Variation of model cell topography based on SFWMD's 5 ft LiDAR within WRAP cell PM-5.2A.

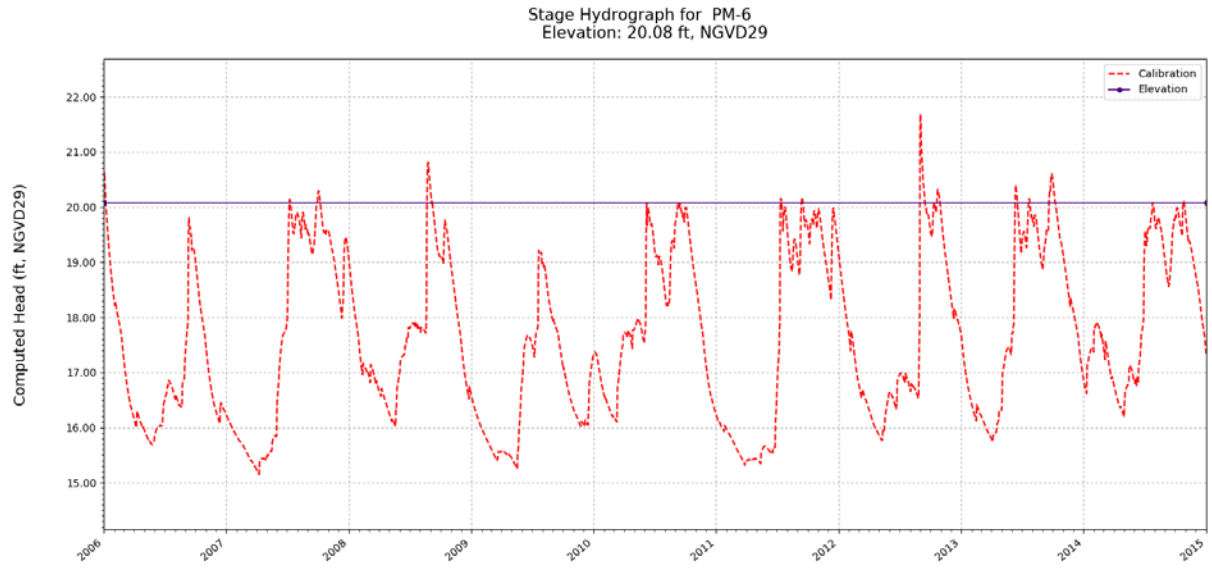

Figure C-157. Simulated stage hydrograph (2006 – 2014) and model cell topography for WRAP cell PM-6.

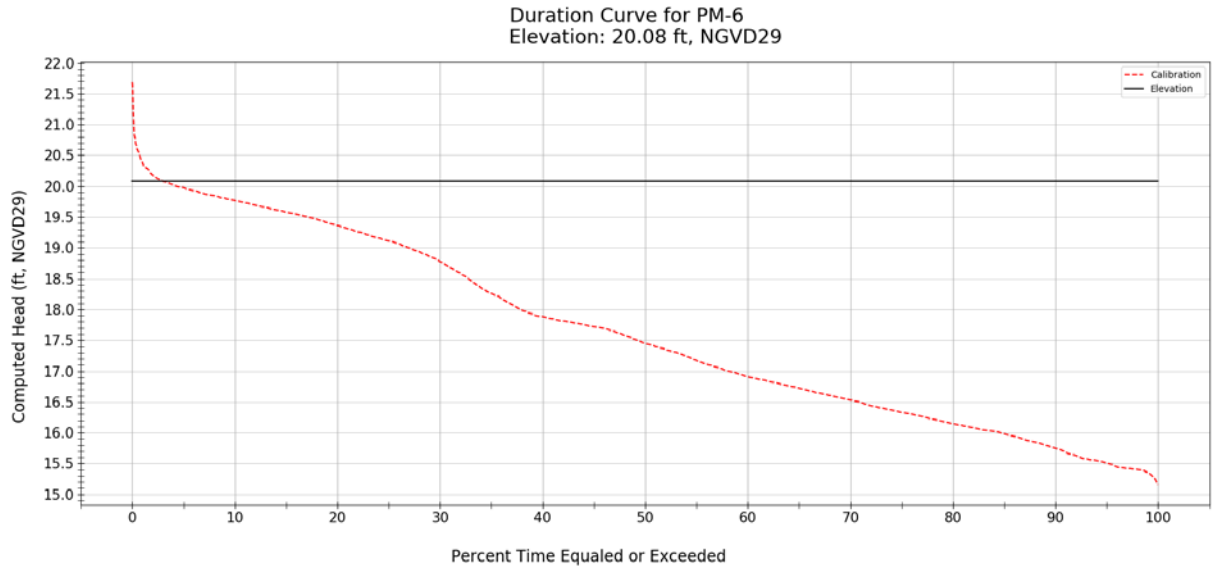

Figure C-158. Simulated stage duration curve (2006 – 2014) and model cell topography for WRAP cell PM-6.

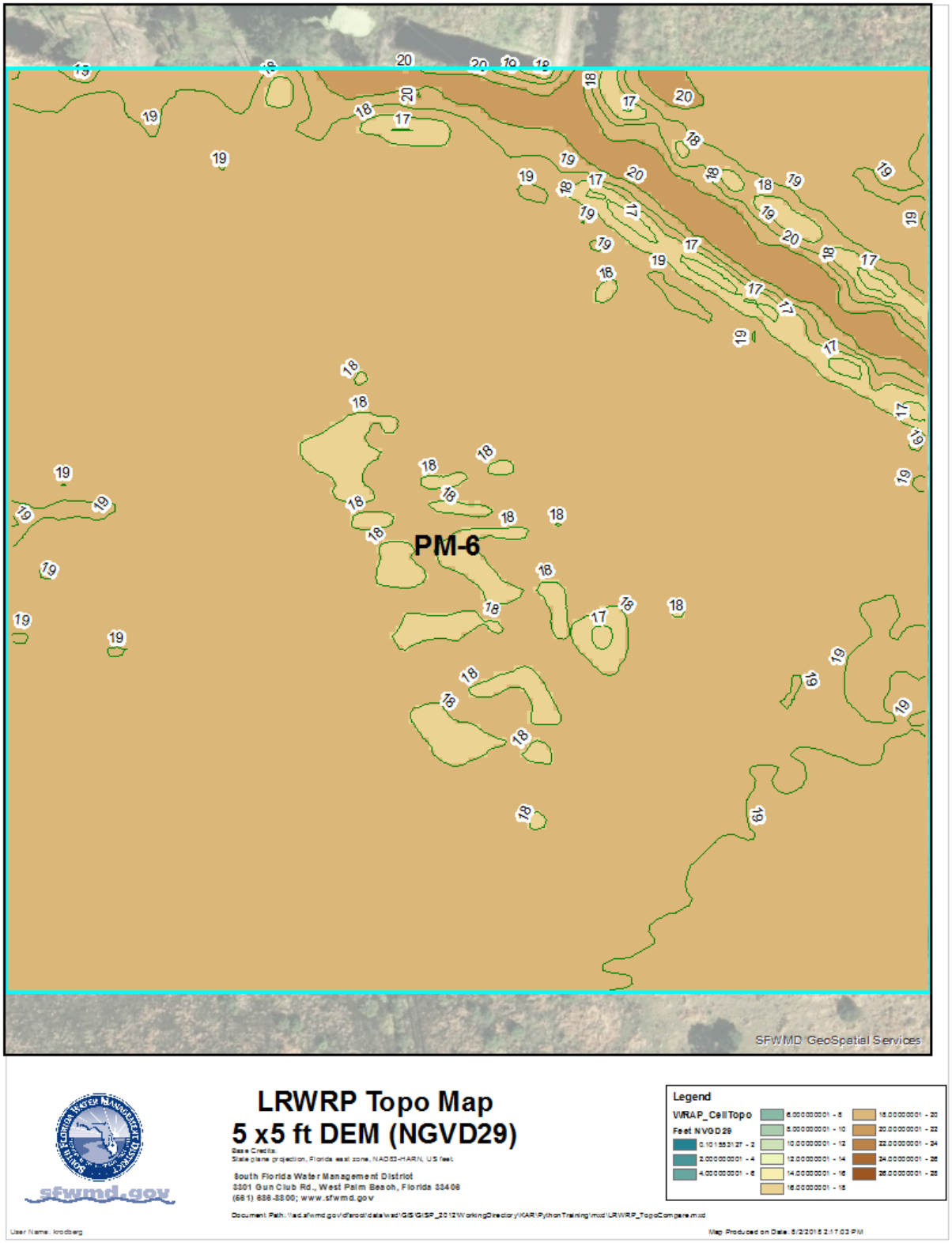

Figure C-159. Variation of model cell topography based on SFWMD's 5 ft LiDAR within WRAP cell PM-6.

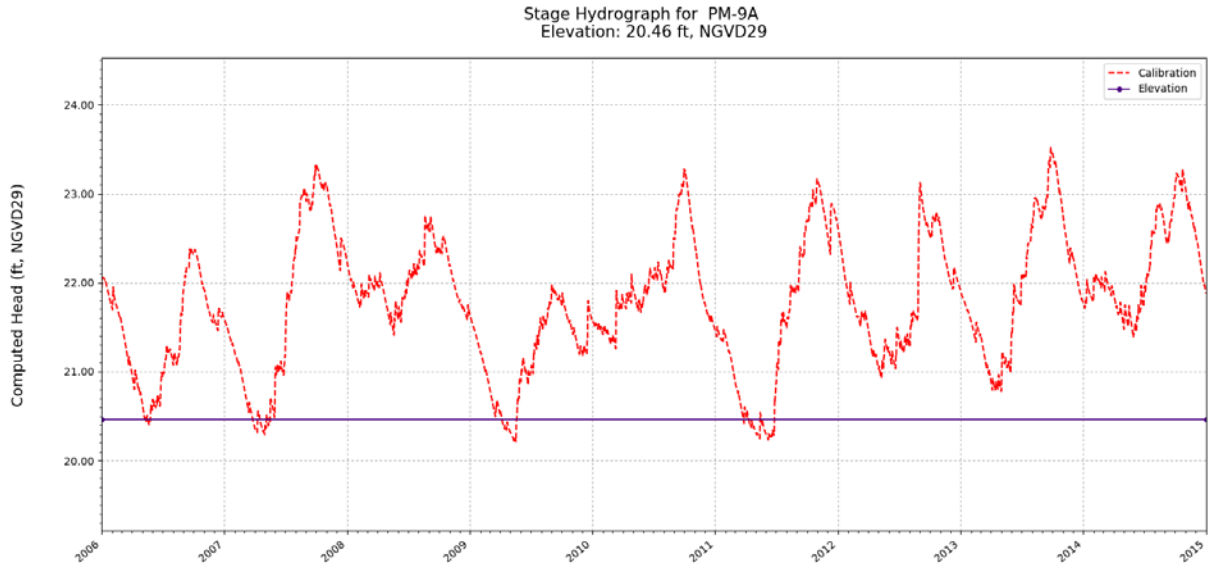

Figure C-160. Simulated stage hydrograph (2006 – 2014) and model cell topography for WRAP cell PM-9A.

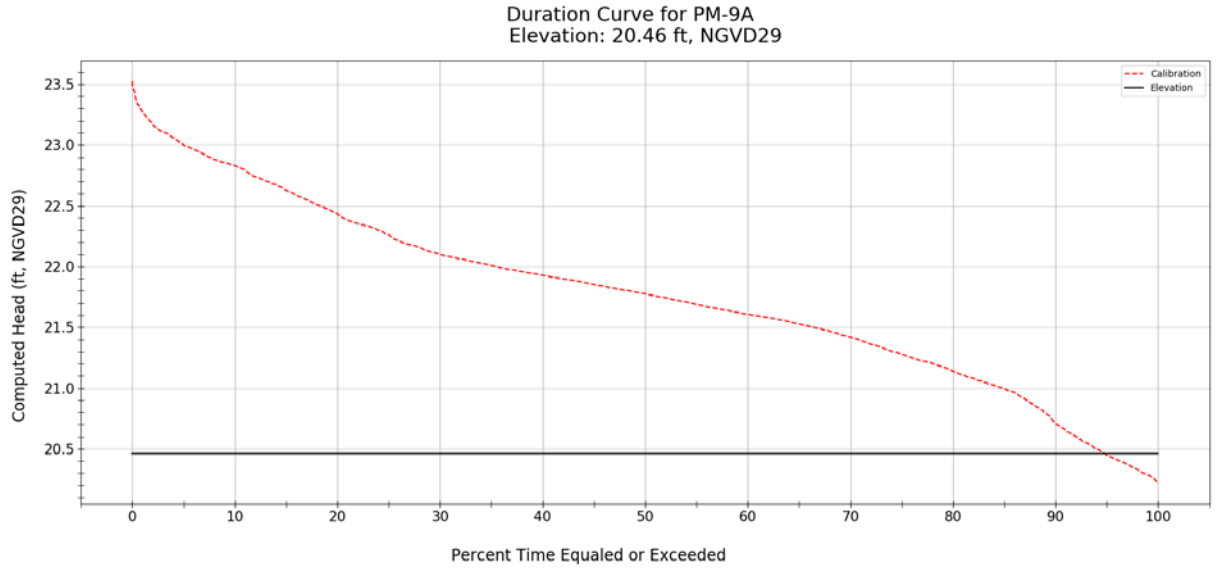

Figure C-161. Simulated stage duration curve (2006 – 2014) and model cell topography for WRAP cell PM-9A.

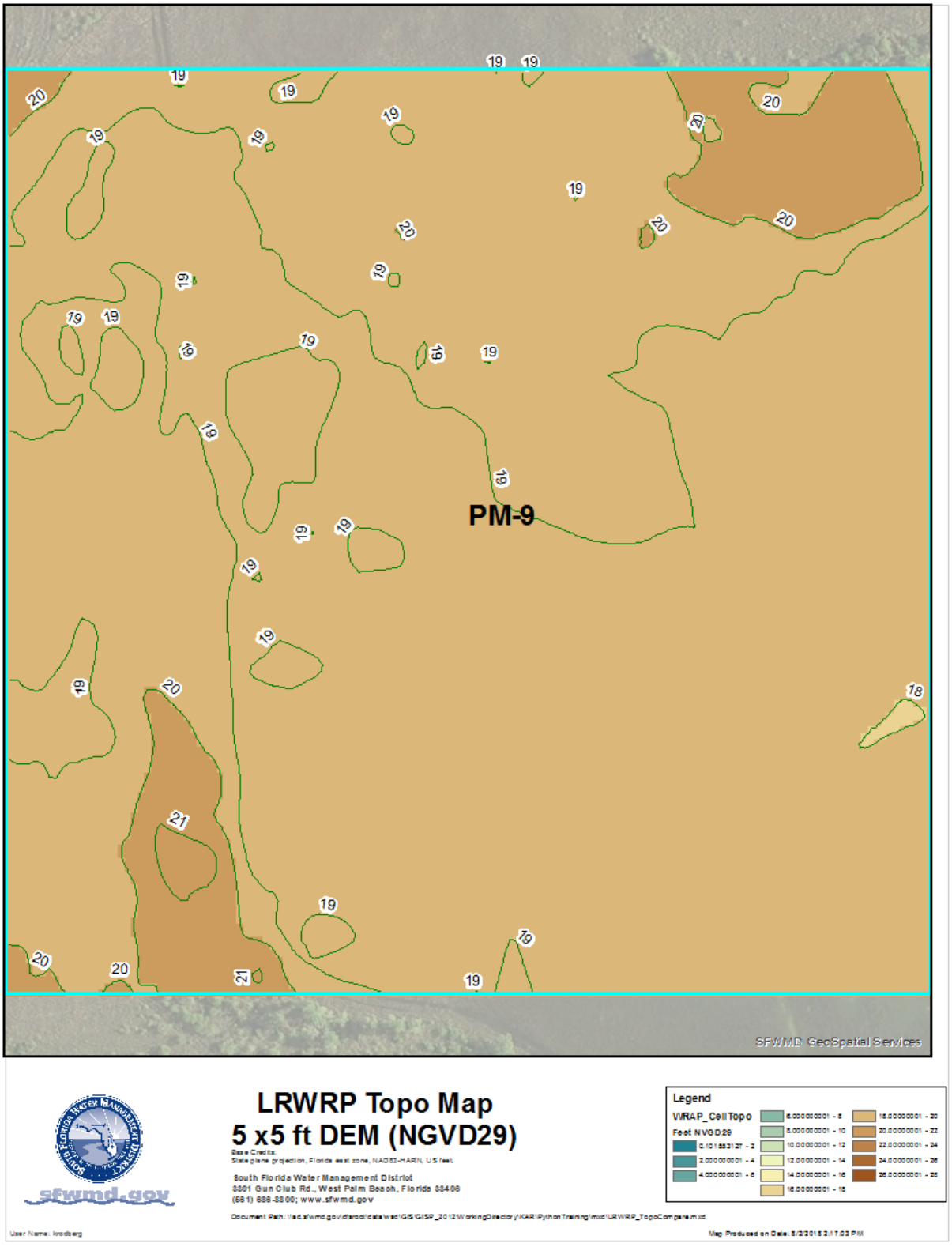

Figure C-162. Variation of model cell topography based on SFWMD's 5 ft LiDAR within WRAP cell PM-9A.

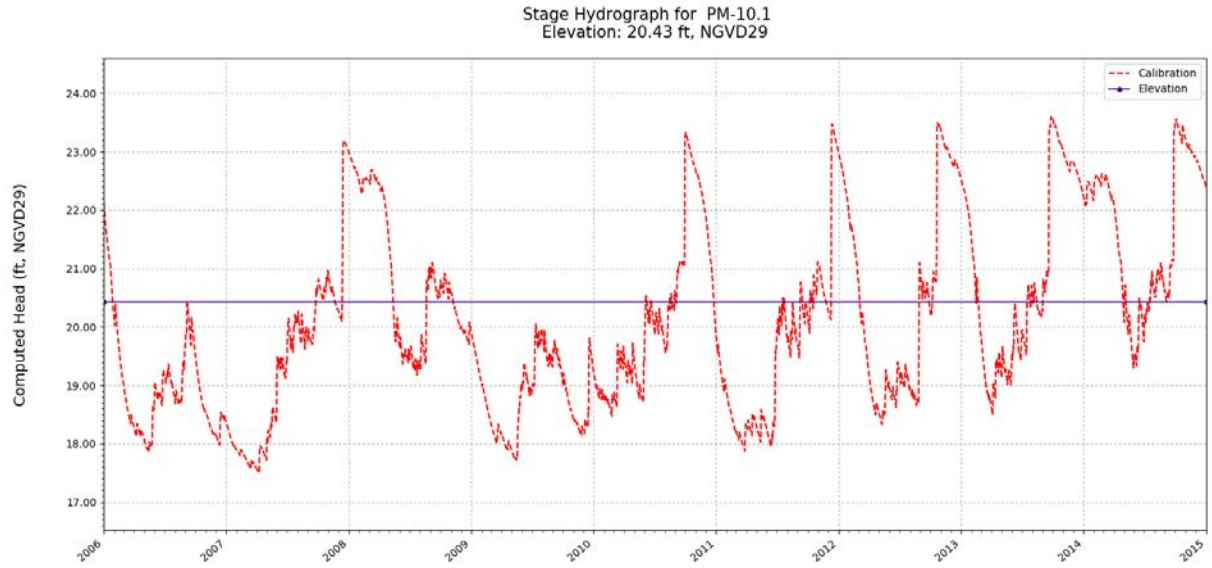

Figure C-163. Simulated stage hydrograph (2006 – 2014) and model cell topography for WRAP cell PM-10.1.

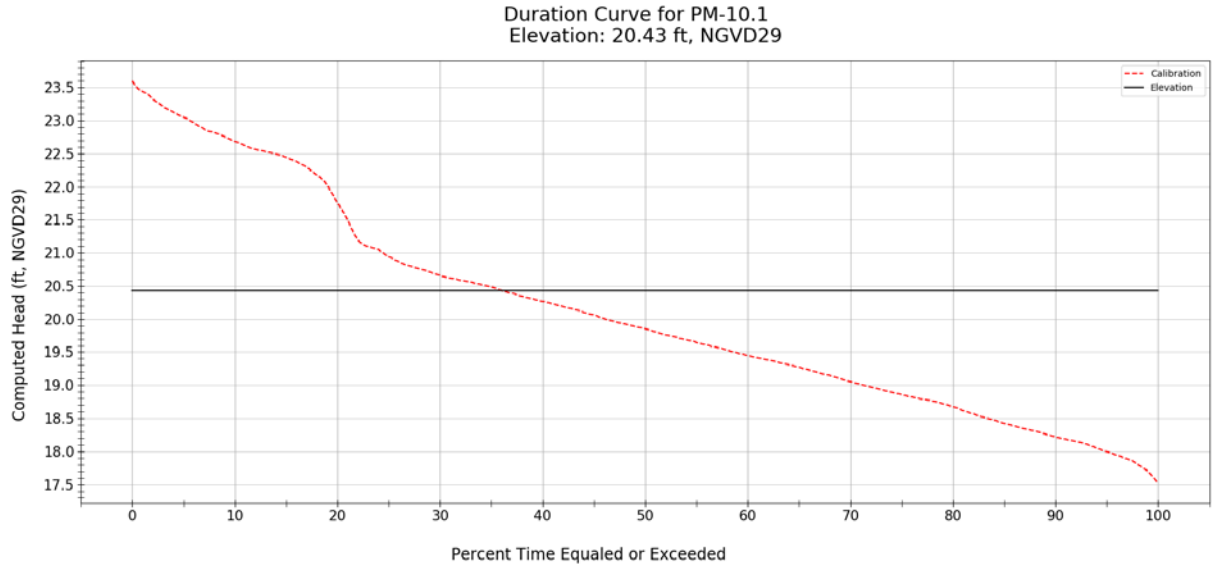

Figure C-164. Simulated stage duration curve (2006 – 2014) and model cell topography for WRAP cell PM-10.1.

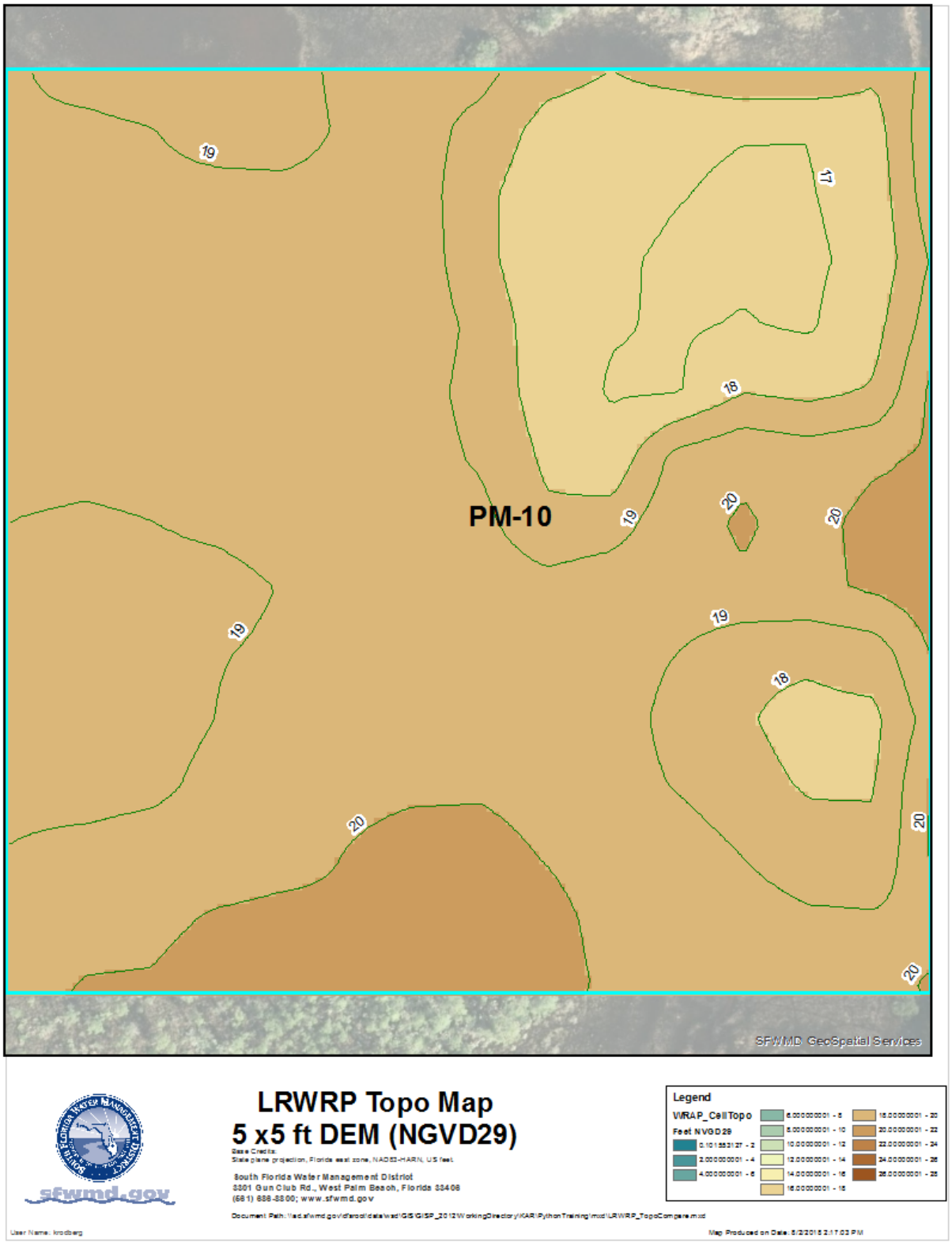

Figure C-165. Variation of model cell topography based on SFWMD's 5 ft LiDAR within WRAP cell PM-10.1.

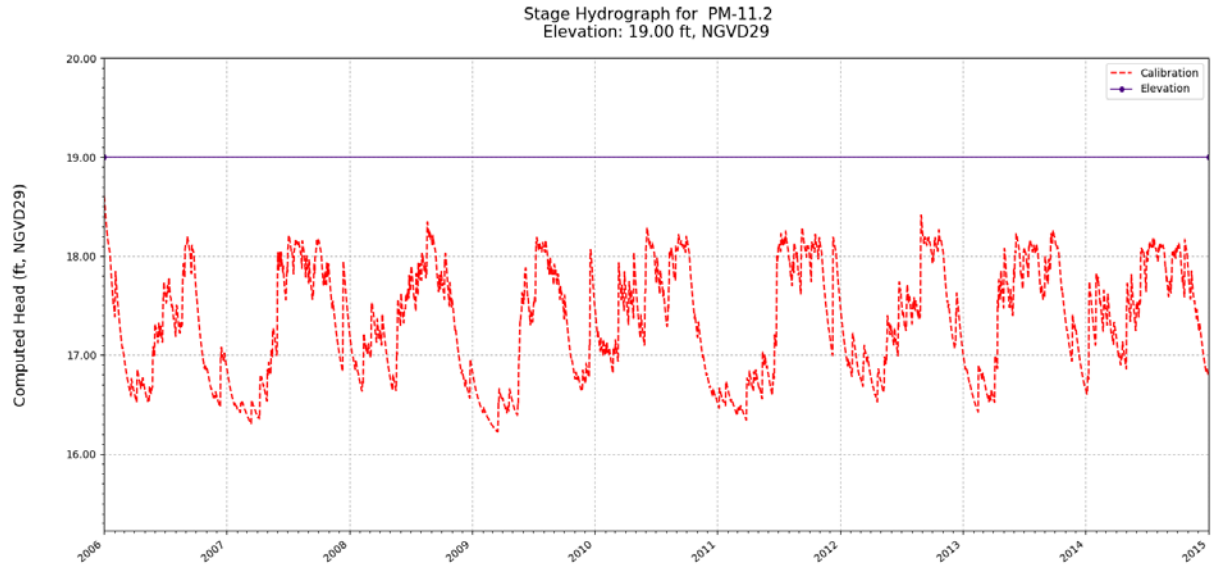

Figure C-166. Simulated stage hydrograph (2006 – 2014) and model cell topography for WRAP cell PM-11.2.

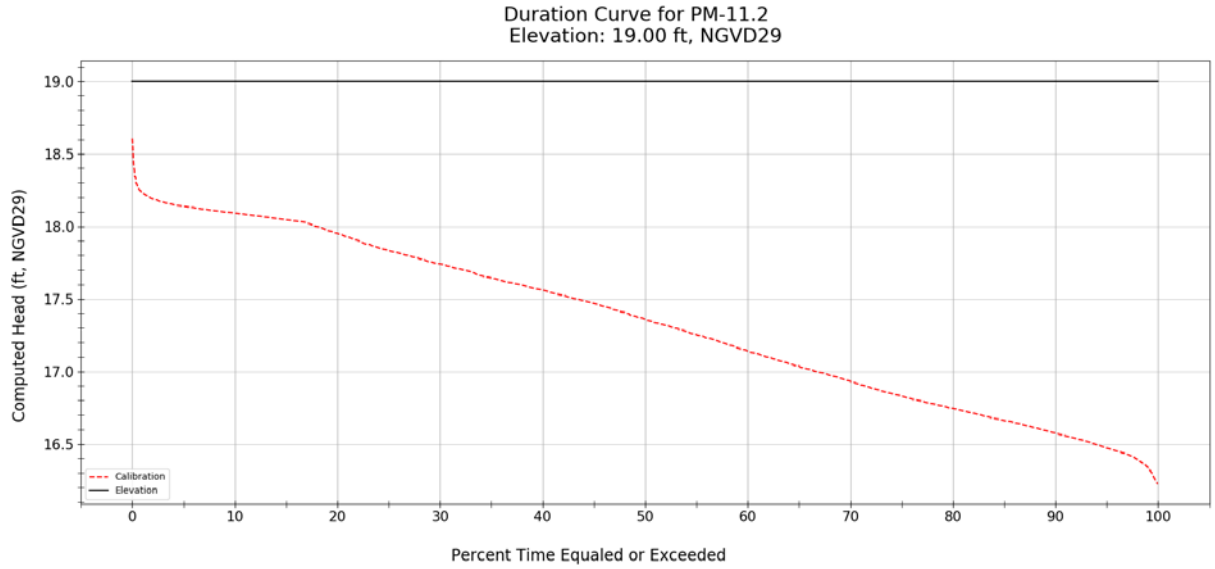

Figure C-167. Simulated stage duration curve (2006 – 2014) and model cell topography for WRAP cell PM-11.2.

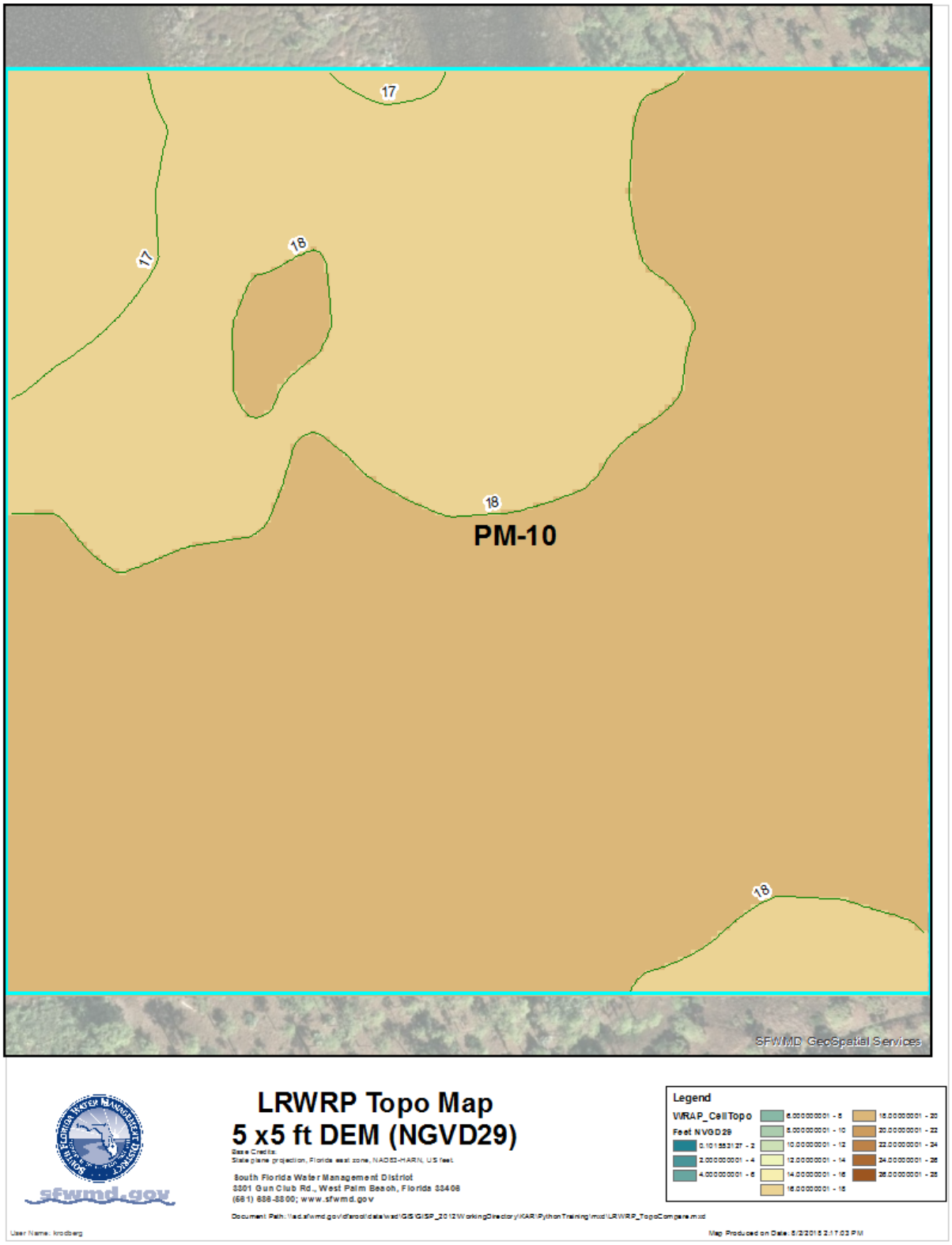

Figure C-168. Variation of model cell topography based on SFWMD's 5 ft LiDAR within WRAP cell PM-11.2.

APPENDIX D: WATER BUDGETS

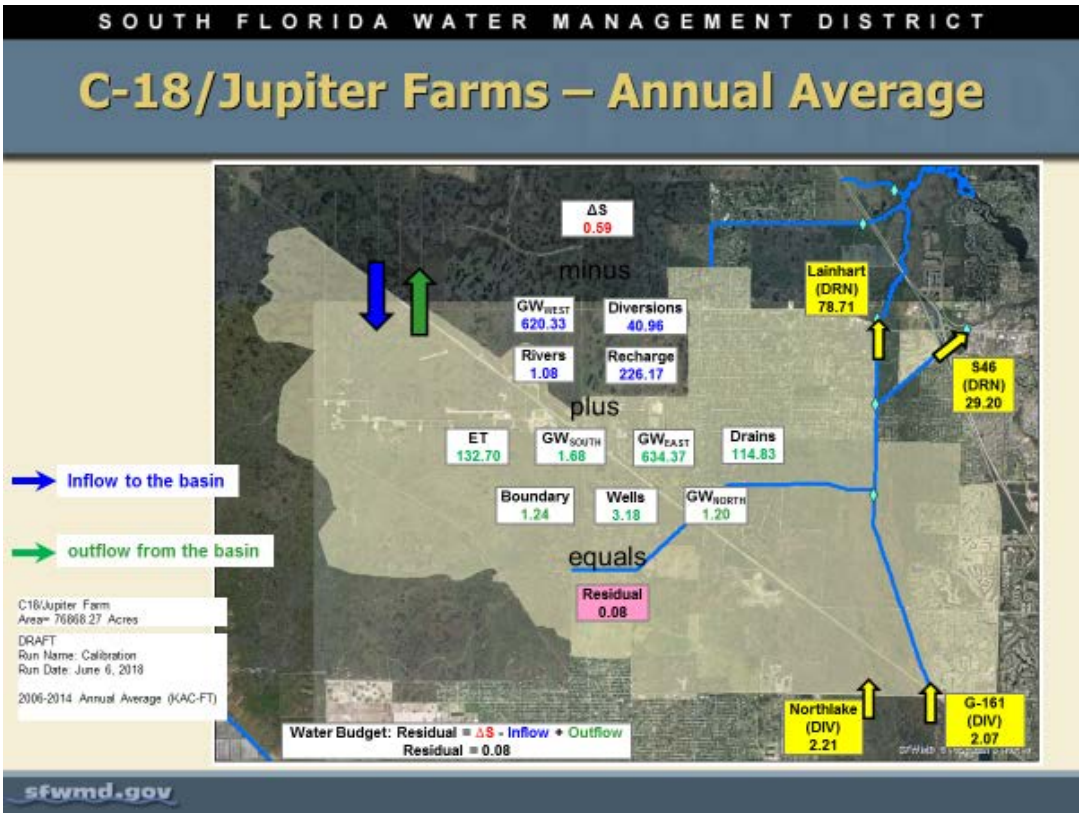

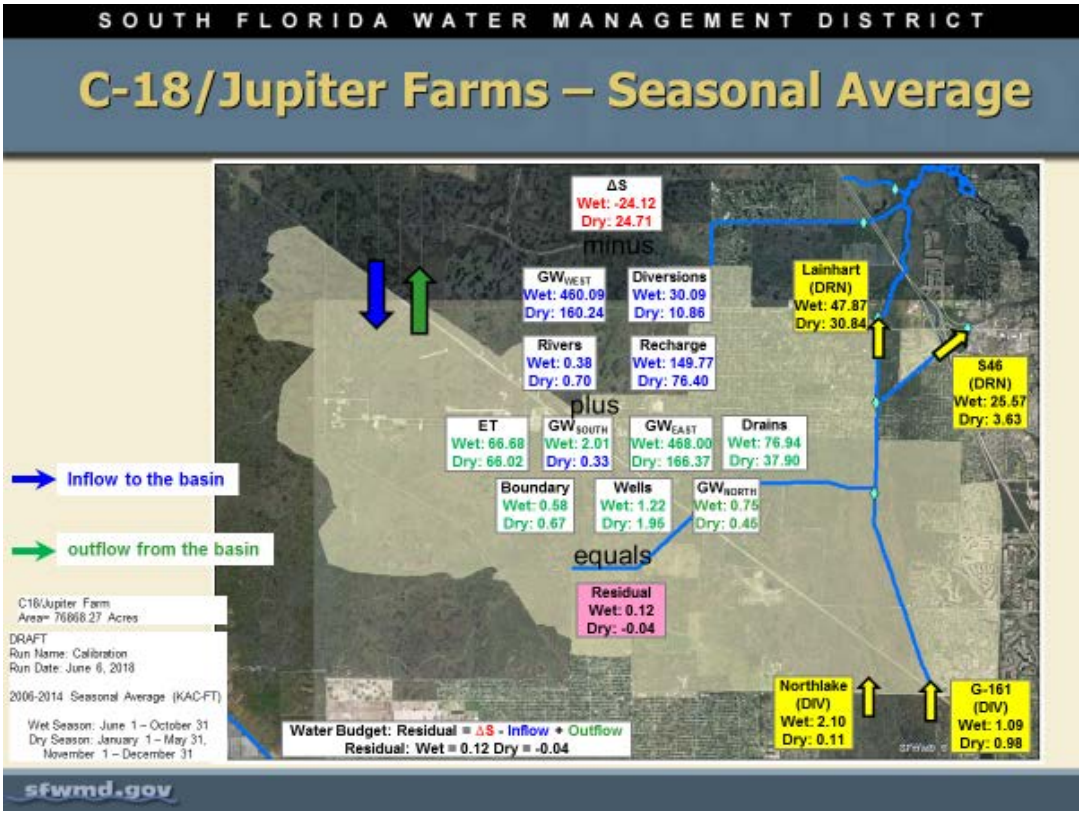

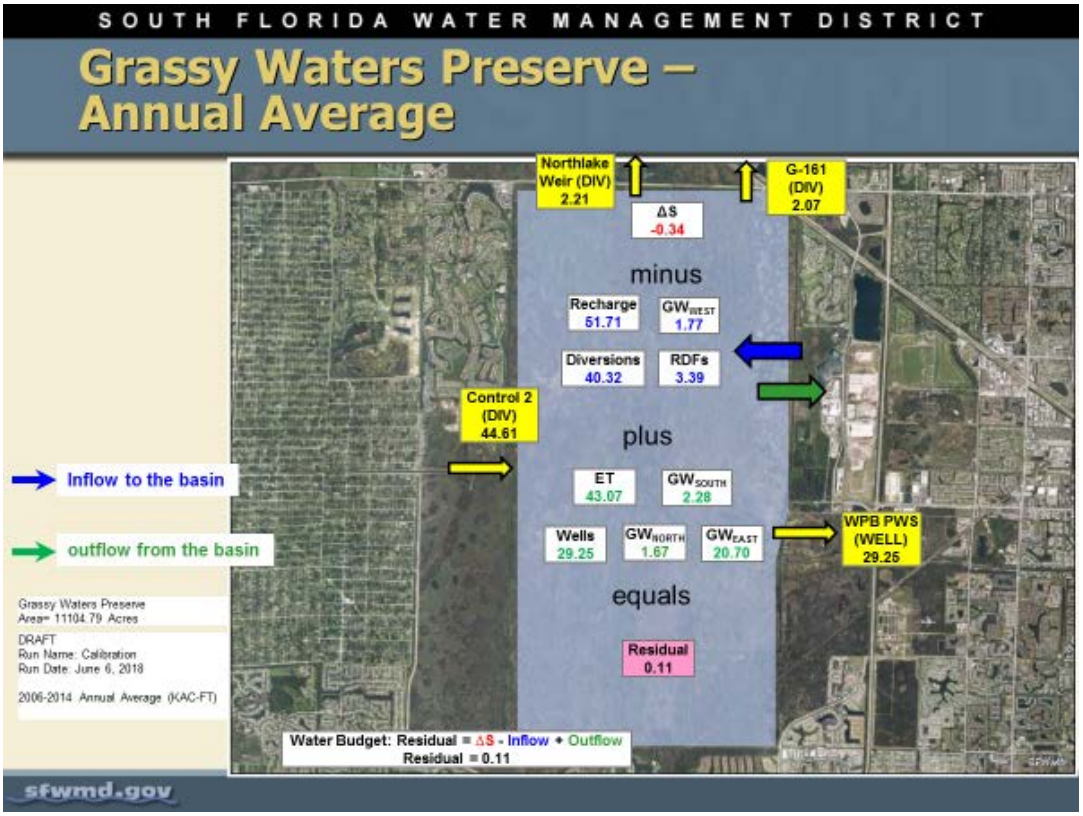
SOUTH FLORIDA WATER MANAGEMENT DISTRICT
Grassy Waters Preserve – Annual Average
Northlake Weir (DIV) 2.21
ΔS -0.34
G-161 (DIV) 2.07
minus
Recharge 51.71
GW WEST 1.77
Diversions 40.32
RDFs 3.39
Control 2 (DIV) 44.61
plus
ET 43.07
GW SOUTH 2.28
Wells 29.25
GW NORTH 1.67
GW EAST 20.70
WPB PWS (WELL) 29.25
equals
Residual 0.11
Inflow to the basin
outflow from the basin
Grassy Waters Preserve Area= 11104.79 Acres
DRAFT
Run Name: Calibration
Run Date: June 6, 2018
2006-2014 Annual Average (KAC-FT)
Water Budget: Residual = ΔS - Inflow + Outflow
Residual = 0.11
sfwmd.gov

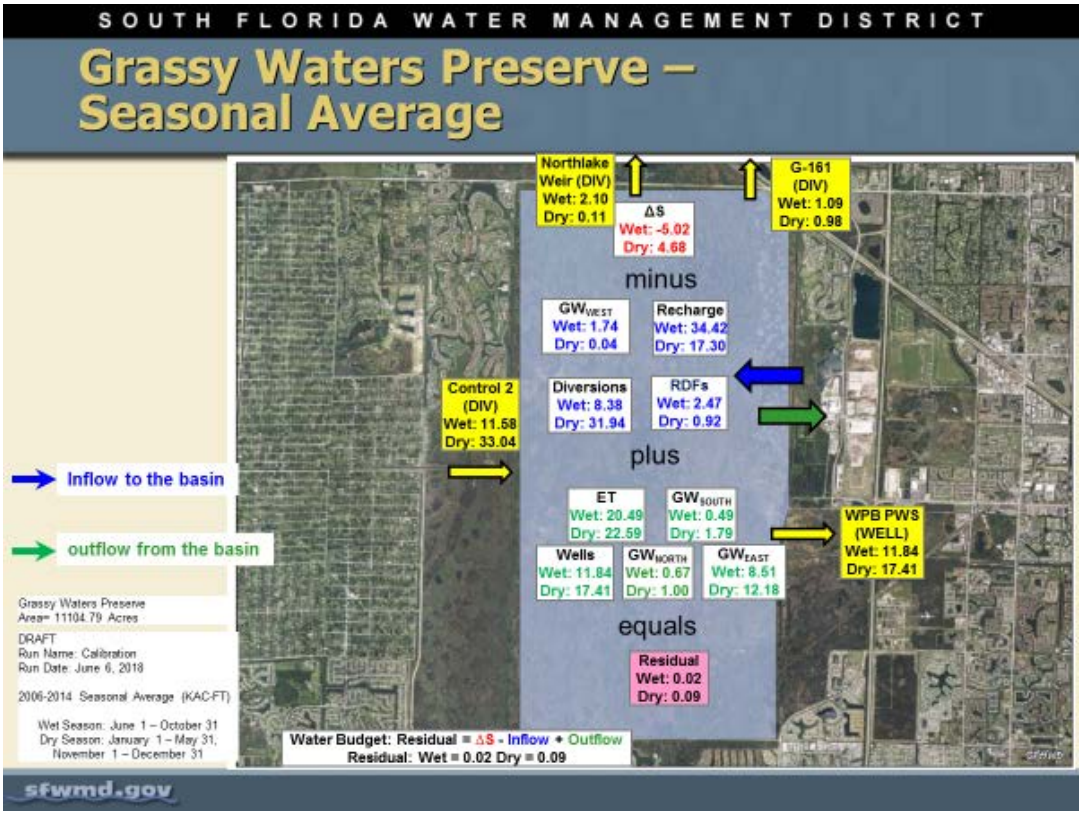
SOUTH FLORIDA WATER MANAGEMENT DISTRICT
Grassy Waters Preserve – Seasonal Average
Northlake Weir (DIV) Wet: 2.10 Dry: 0.11
ΔS Wet: -5.02 Dry: 4.68
G-161 (DIV) Wet: 1.09 Dry: 0.98
minus
GW WEST Wet: 1.74 Dry: 0.04
Recharge Wet: 34.42 Dry: 17.30
Diversions Wet: 8.38 Dry: 31.94
RDFs Wet: 2.47 Dry: 0.92
Control 2 (DIV) Wet: 11.58 Dry: 33.04
plus
ET Wet: 20.49 Dry: 22.59
GW SOUTH Wet: 0.49 Dry: 1.79
Wells Wet: 11.84 Dry: 17.41
GW NORTH Wet: 0.67 Dry: 1.00
GW EAST Wet: 8.51 Dry: 12.18
WPB PWS (WELL) Wet: 11.84 Dry: 17.41
equals
Residual Wet: 0.02 Dry: 0.09
Inflow to the basin
outflow from the basin
Grassy Waters Preserve Area= 11104.79 Acres
DRAFT
Run Name: Calibration
Run Date: June 6, 2018
2006-2014 Seasonal Average (KAC-FT)
Wet Season: June 1 – October 31
Dry Season: January 1 – May 31; November 1 – December 31
Water Budget: Residual = ΔS - Inflow + Outflow
Residual: Wet = 0.02 Dry = 0.09
sfwmd.gov

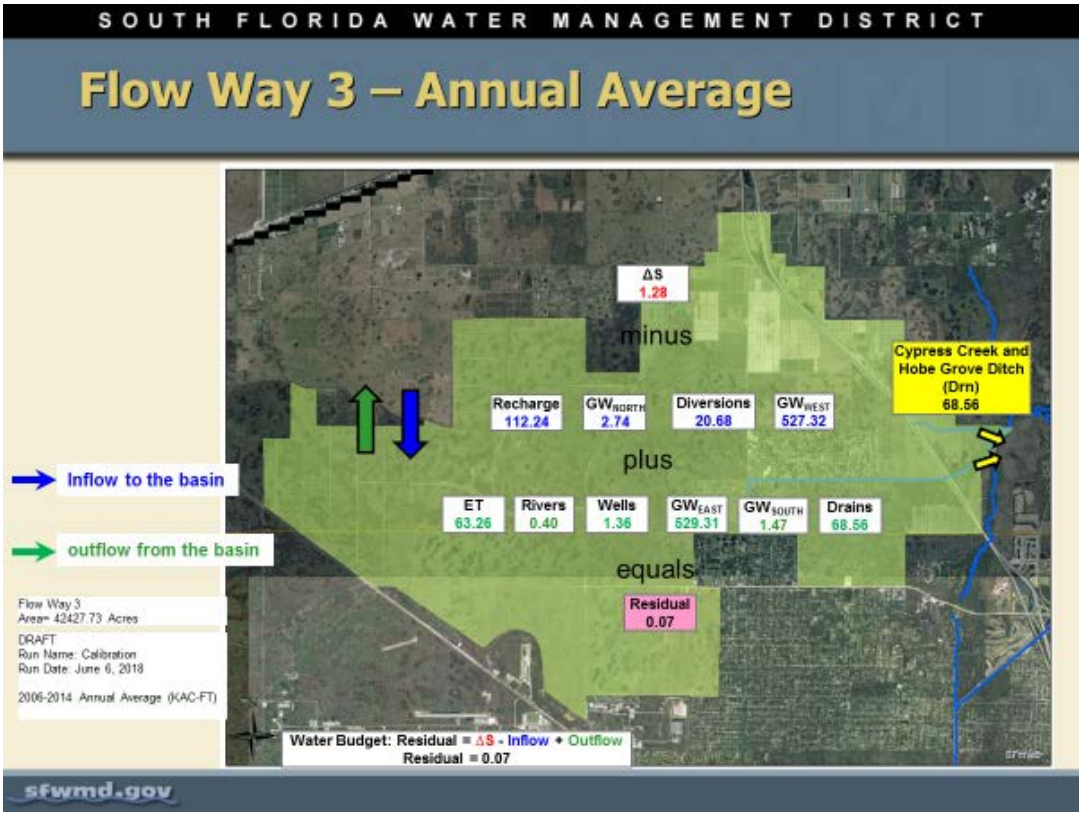
SOUTH FLORIDA WATER MANAGEMENT DISTRICT
Flow Way 3 – Annual Average
ΔS
1.28
minus
Recharge
112.24
GWNORTH
2.74
Diversions
20.68
GWWEST
527.32
Cypress Creek and Hobe Grove Ditch (Drn)
68.56
plus
ET
63.26
Rivers
0.40
Wells
1.36
GWEAST
529.31
GWSOUTH
1.47
Drains
68.56
equals
Residual
0.07
Inflow to the basin
outflow from the basin
Flow Way 3
Area= 42427.73 Acres
DRAFT
Run Name: Calibration
Run Date: June 6, 2018
2006-2014 Annual Average (KAC-FT)
Water Budget: Residual = ΔS - Inflow + Outflow
Residual = 0.07
sfwmd.gov

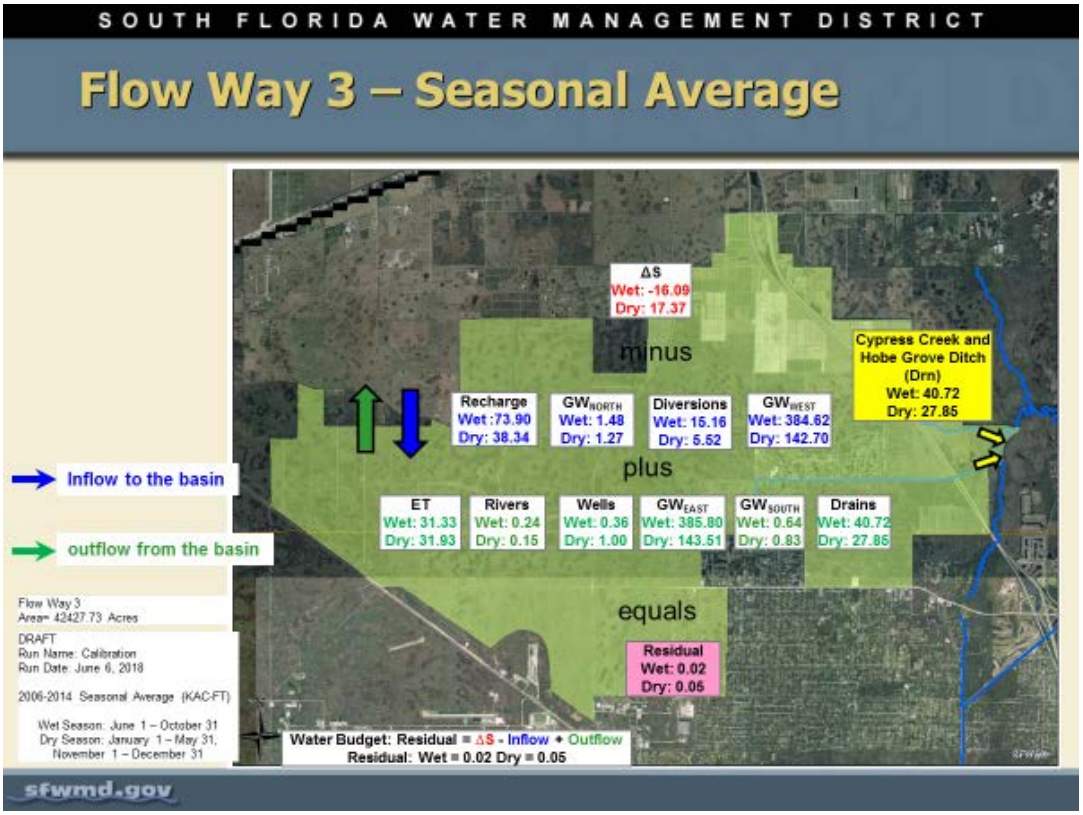
SOUTH FLORIDA WATER MANAGEMENT DISTRICT
Flow Way 3 – Seasonal Average
ΔS
Wet: -16.09
Dry: 17.37
minus
Recharge
Wet :73.90
Dry: 38.34
GWNORTH
Wet: 1.48
Dry: 1.27
Diversions
Wet: 15.16
Dry: 5.52
GWWEST
Wet: 384.62
Dry: 142.70
Cypress Creek and Hobe Grove Ditch (Drn)
Wet: 40.72
Dry: 27.85
plus
ET
Wet: 31.33
Dry: 31.93
Rivers
Wet: 0.24
Dry: 0.15
Wells
Wet: 0.36
Dry: 1.00
GWEAST
Wet: 385.80
Dry: 143.51
GWSOUTH
Wet: 0.64
Dry: 0.83
Drains
Wet: 40.72
Dry: 27.85
equals
Residual
Wet: 0.02
Dry: 0.05
Inflow to the basin
outflow from the basin
Flow Way 3
Area= 42427.73 Acres
DRAFT
Run Name: Calibration
Run Date: June 6, 2018
2006-2014 Seasonal Average (KAC-FT)
Wet Season: June 1 – October 31
Dry Season: January 1 – May 31;
November 1 – December 31
Water Budget: Residual = ΔS - Inflow + Outflow
Residual: Wet = 0.02 Dry = 0.05
sfwmd.gov

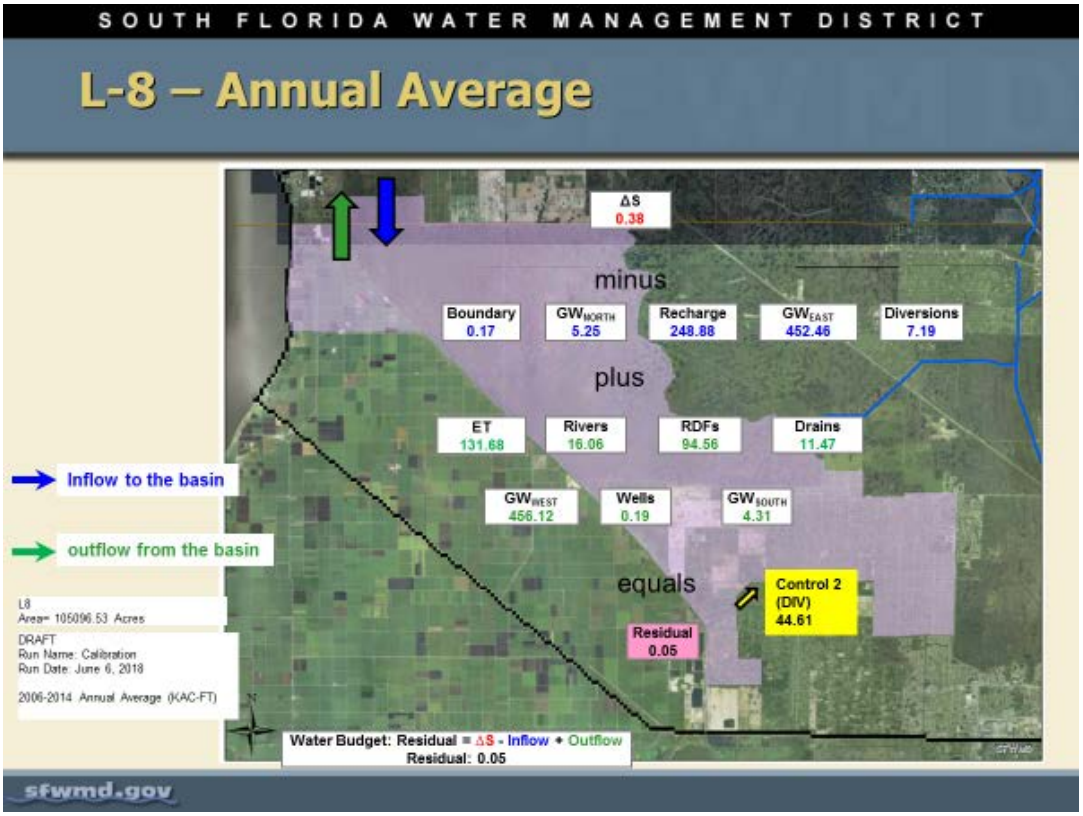
SOUTH FLORIDA WATER MANAGEMENT DISTRICT
L-8 – Annual Average
ΔS
0.38
minus
Boundary
0.17
GW NORTH
5.25
Recharge
248.88
GW EAST
452.46
Diversions
7.19
plus
ET
131.68
Rivers
16.06
RDFs
94.56
Drains
11.47
GW WEST
456.12
Wells
0.19
GW SOUTH
4.31
Inflow to the basin
outflow from the basin
equals
Control 2
(DIV)
44.61
Residual
0.05
L8
Area= 105096.53 Acres
DRAFT
Run Name: Calibration
Run Date: June 6, 2018
2006-2014 Annual Average (KAC-FT)
Water Budget: Residual = ΔS - Inflow + Outflow
Residual: 0.05
sfwmd.gov

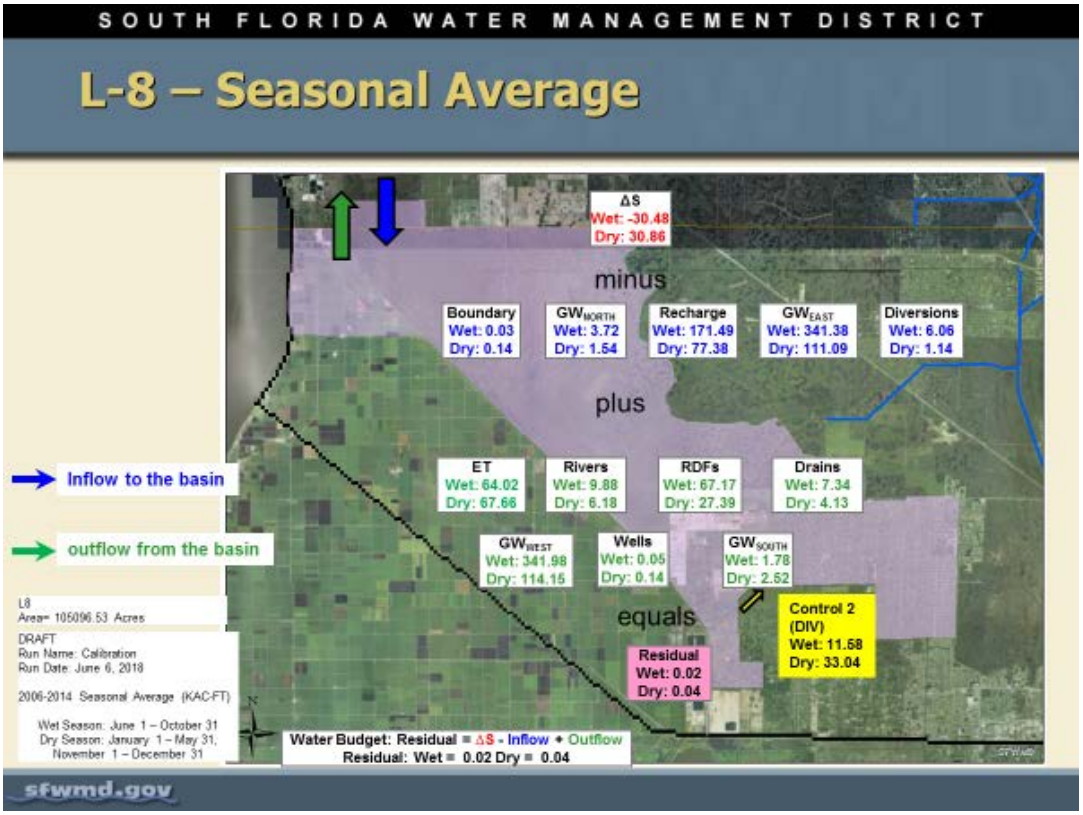
SOUTH FLORIDA WATER MANAGEMENT DISTRICT
L-8 – Seasonal Average
ΔS
Wet: -30.48
Dry: 30.86
minus
Boundary
Wet: 0.03
Dry: 0.14
GW NORTH
Wet: 3.72
Dry: 1.54
Recharge
Wet: 171.49
Dry: 77.38
GW EAST
Wet: 341.38
Dry: 111.09
Diversions
Wet: 6.06
Dry: 1.14
plus
ET
Wet: 64.02
Dry: 67.66
Rivers
Wet: 9.88
Dry: 6.18
RDFs
Wet: 67.17
Dry: 27.39
Drains
Wet: 7.34
Dry: 4.13
GW WEST
Wet: 341.98
Dry: 114.15
Wells
Wet: 0.05
Dry: 0.14
GW SOUTH
Wet: 1.78
Dry: 2.62
Inflow to the basin
outflow from the basin
equals
Control 2
(DIV)
Wet: 11.58
Dry: 33.04
Residual
Wet: 0.02
Dry: 0.04
L8
Area= 105096.53 Acres
DRAFT
Run Name: Calibration
Run Date: June 6, 2018
2006-2014 Seasonal Average (KAC-FT)
Wet Season: June 1 – October 31
Dry Season: January 1 – May 31;
November 1 – December 31
Water Budget: Residual = ΔS - Inflow + Outflow
Residual: Wet = 0.02 Dry = 0.04
sfwmd.gov

APPENDIX E: VERIFICATION RESULTS

Groundwater Monitoring Wells

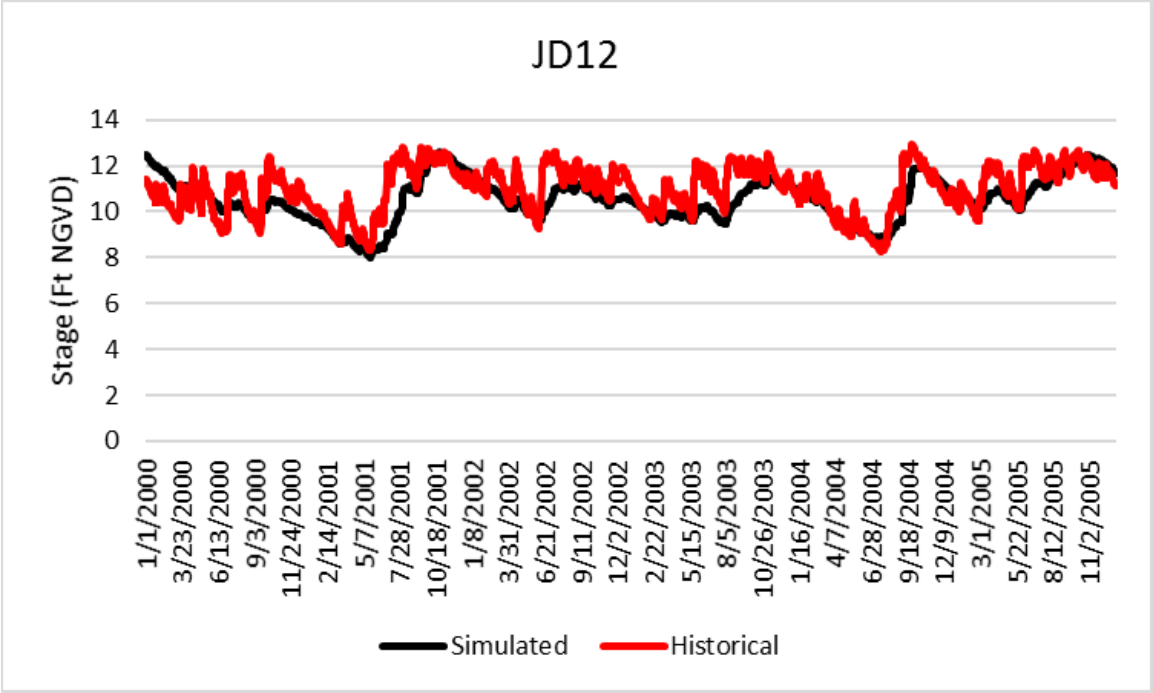

Figure E-1. Historical and simulated groundwater monitoring well stage hydrograph (2000 – 2005) for JD12.

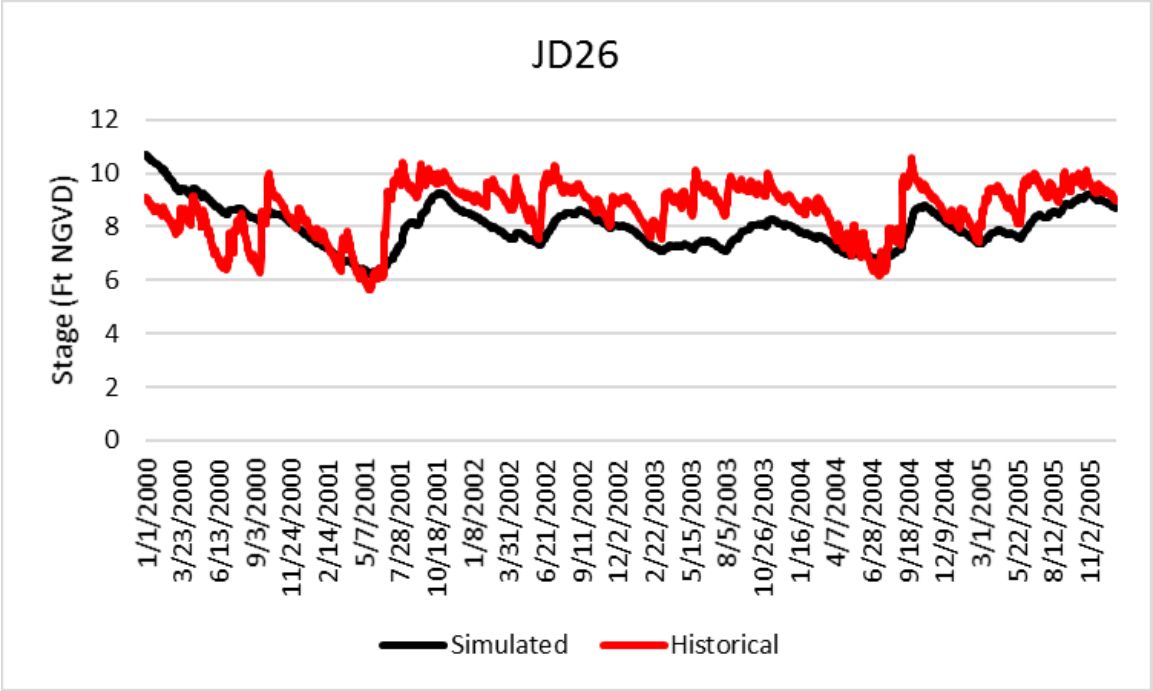

Figure E-2. Historical and simulated groundwater monitoring well stage hydrograph (2000 – 2005) for JD26.

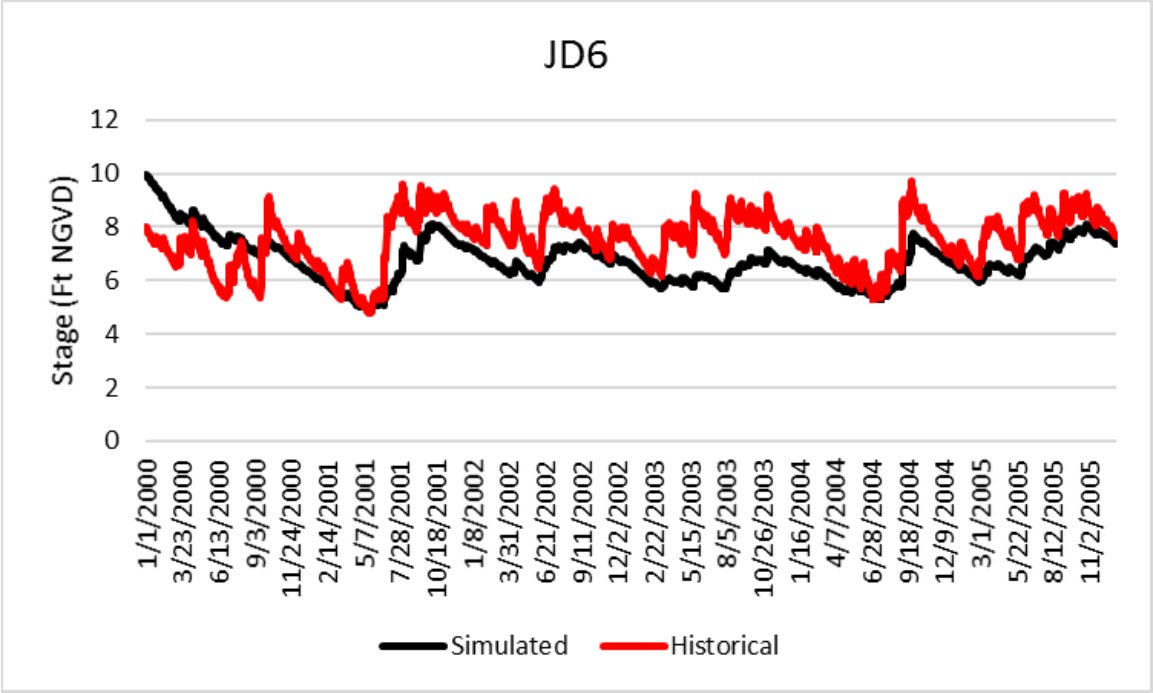

Figure E-3. Historical and simulated groundwater monitoring well stage hydrograph (2000 – 2005) for JD6.

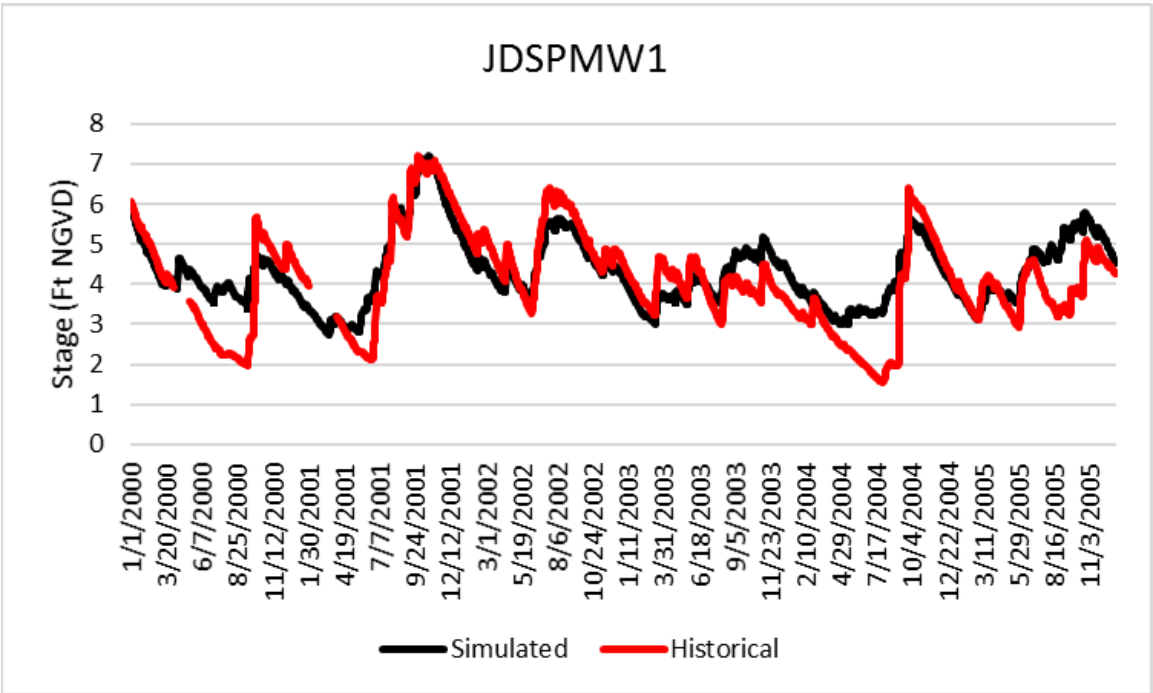

Figure E-4. Historical and simulated groundwater monitoring well stage hydrograph (2000 – 2005) for JDSPMW1.

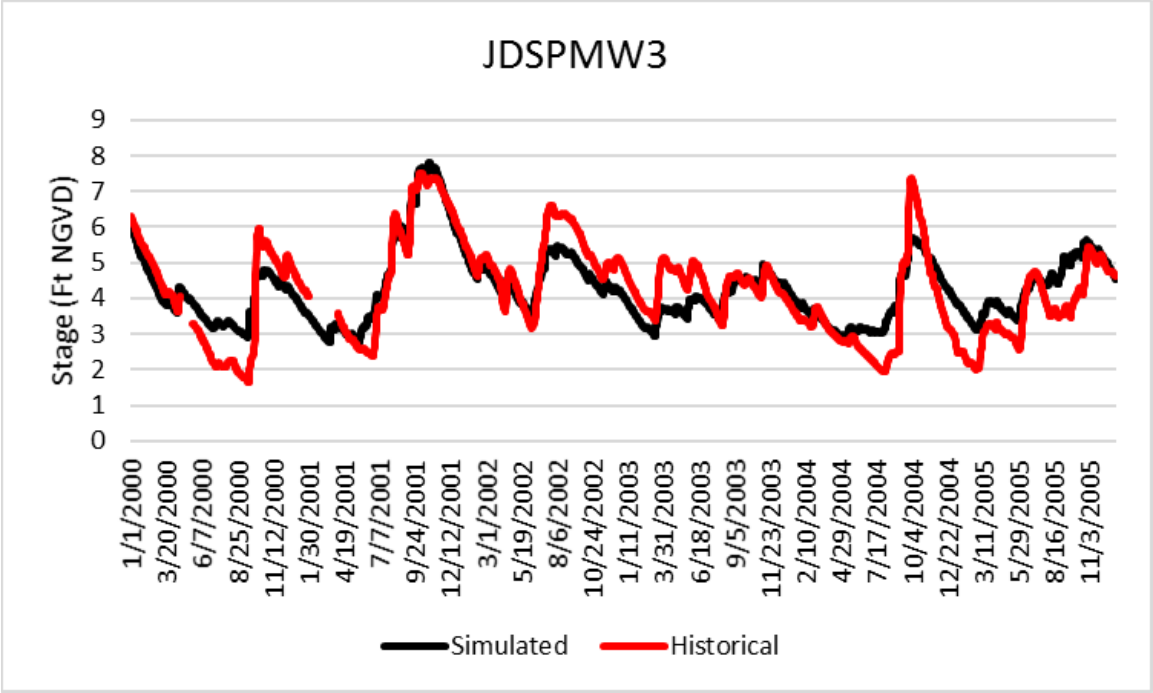

Figure E-5. Historical and simulated groundwater monitoring well stage hydrograph (2000 – 2005) for JDSPMW3.

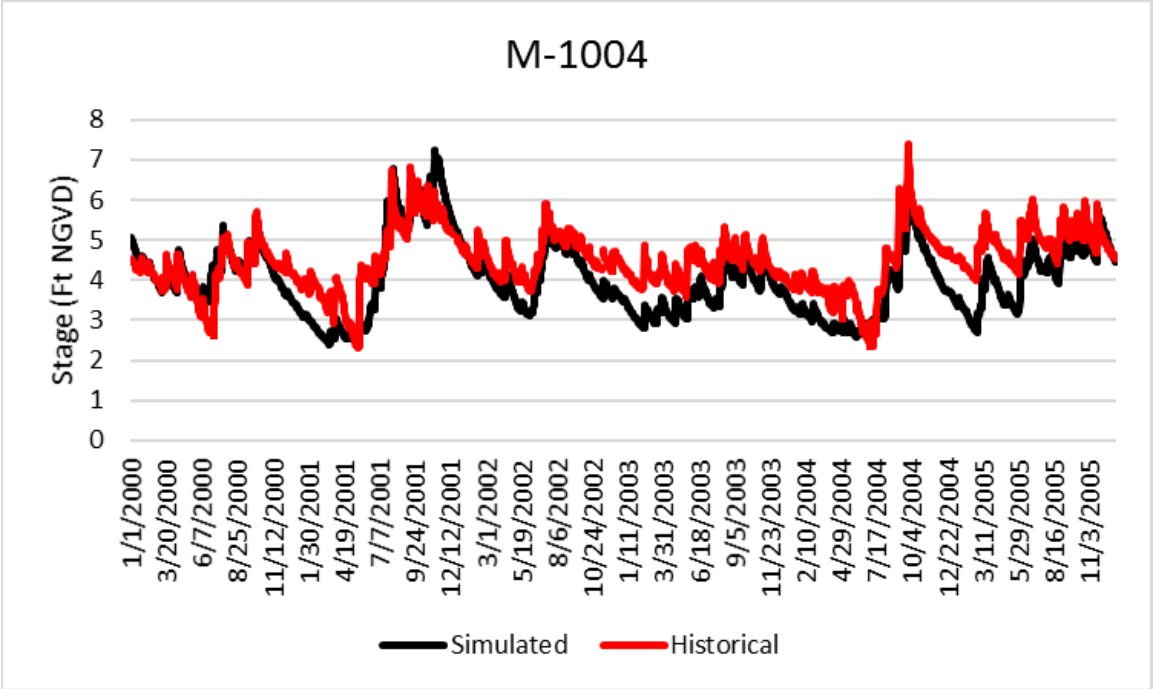

Figure E-6. Historical and simulated groundwater monitoring well stage hydrograph (2000 – 2005) for M-1004.

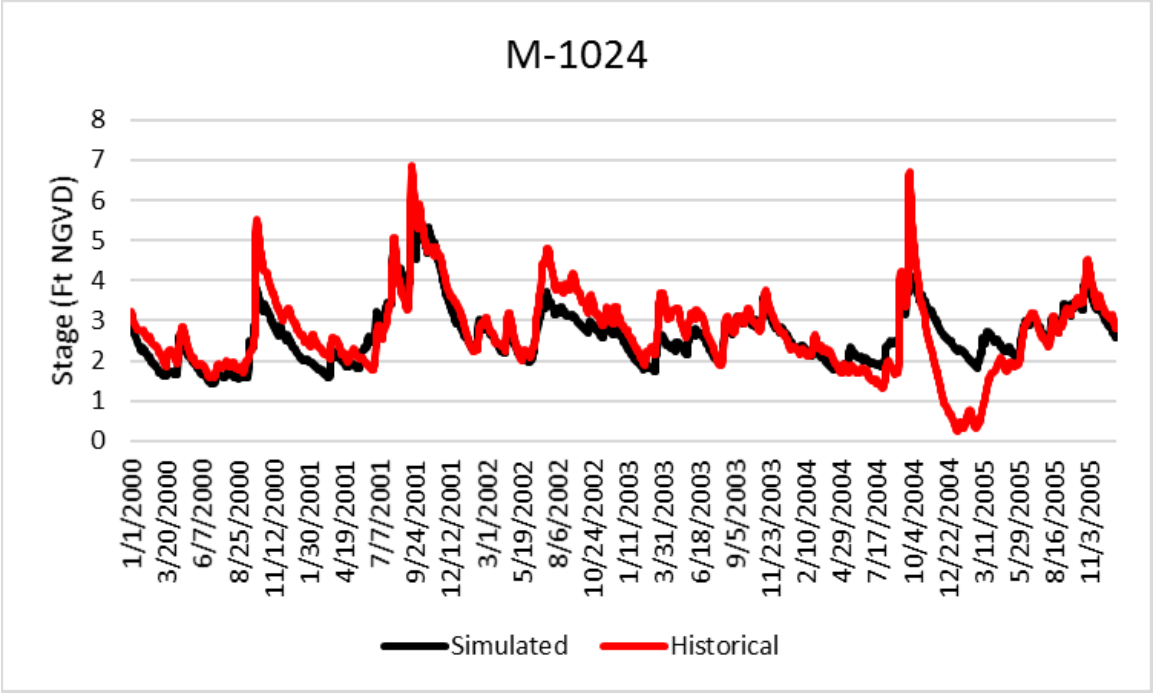

Figure E-7. Historical and simulated groundwater monitoring well stage hydrograph (2000 – 2005) for M-1024.

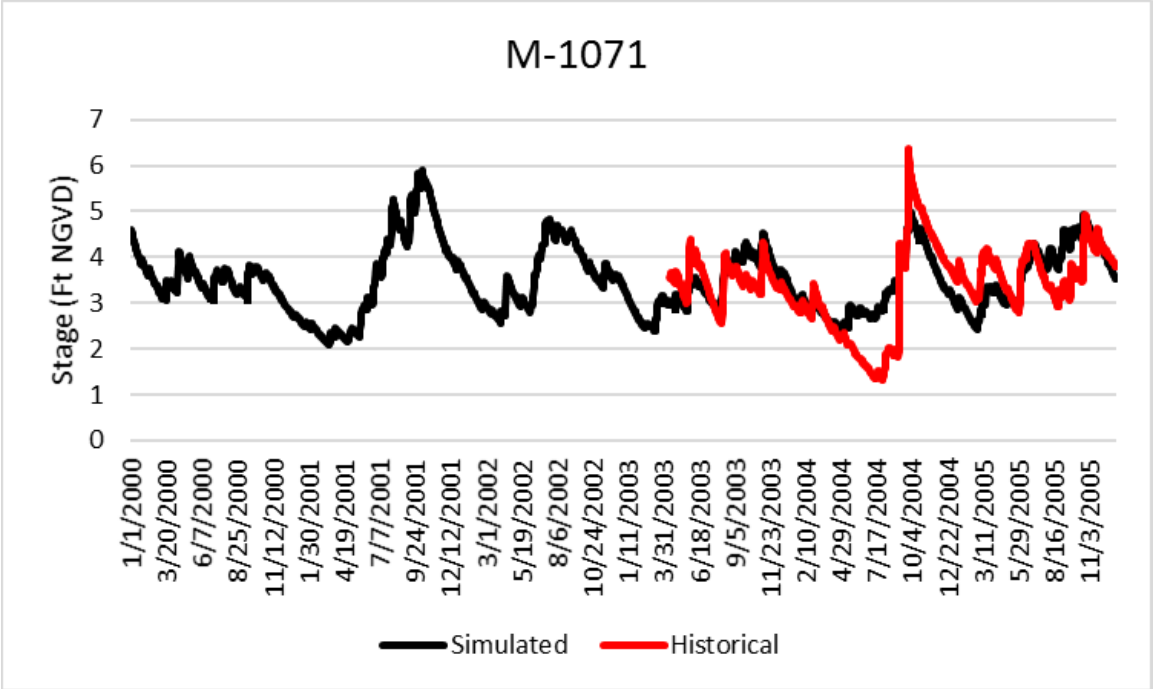

Figure E-8. Historical and simulated groundwater monitoring well stage hydrograph (2000 – 2005) for M-1071.

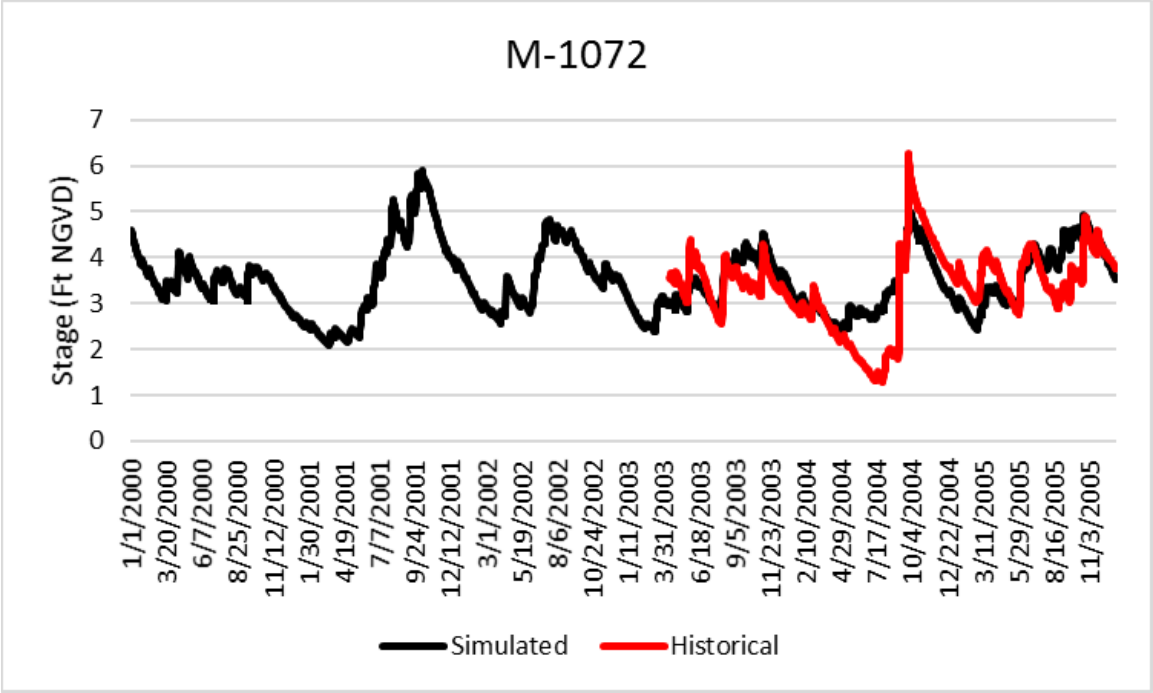

Figure E-9. Historical and simulated groundwater monitoring well stage hydrograph (2000 – 2005) for M-1072.

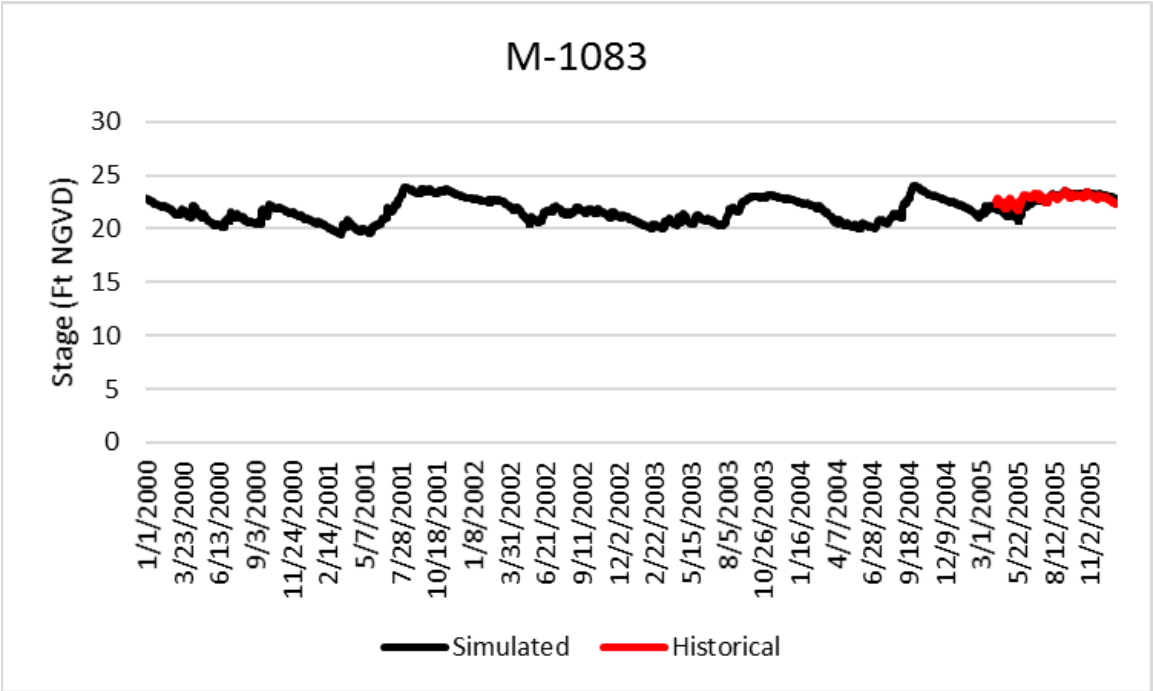

Figure E-10. Historical and simulated groundwater monitoring well stage hydrograph (2000 – 2005) for M-1083.

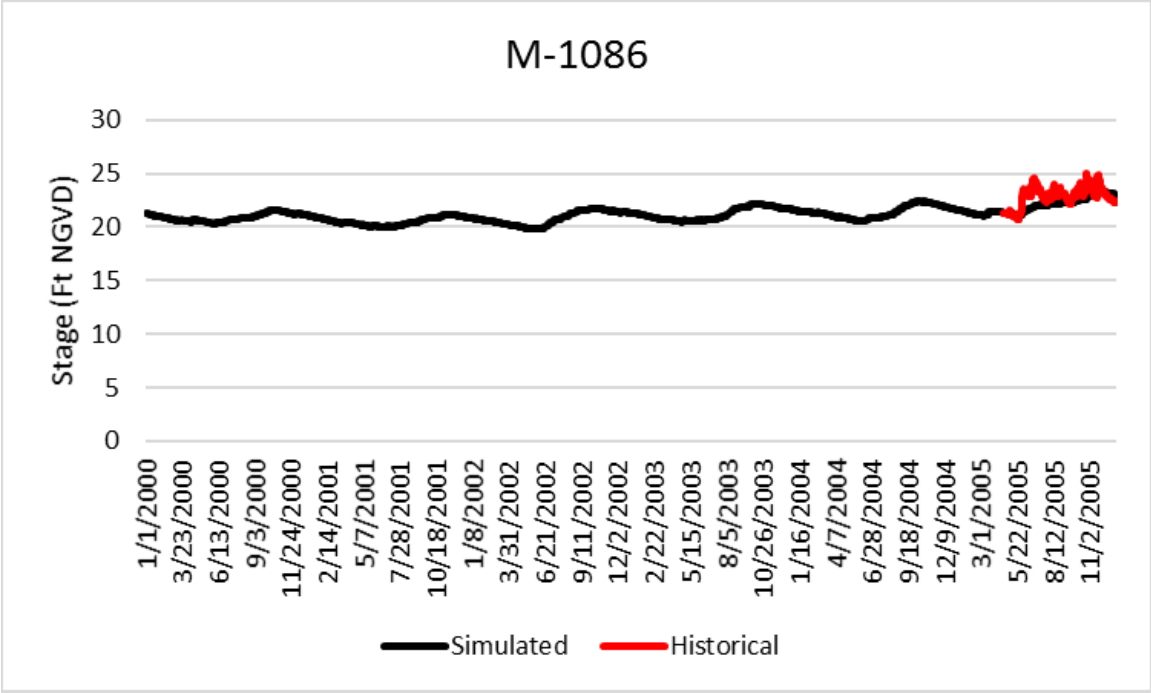

Figure E-11. Historical and simulated groundwater monitoring well stage hydrograph (2000 – 2005) for M-1086.

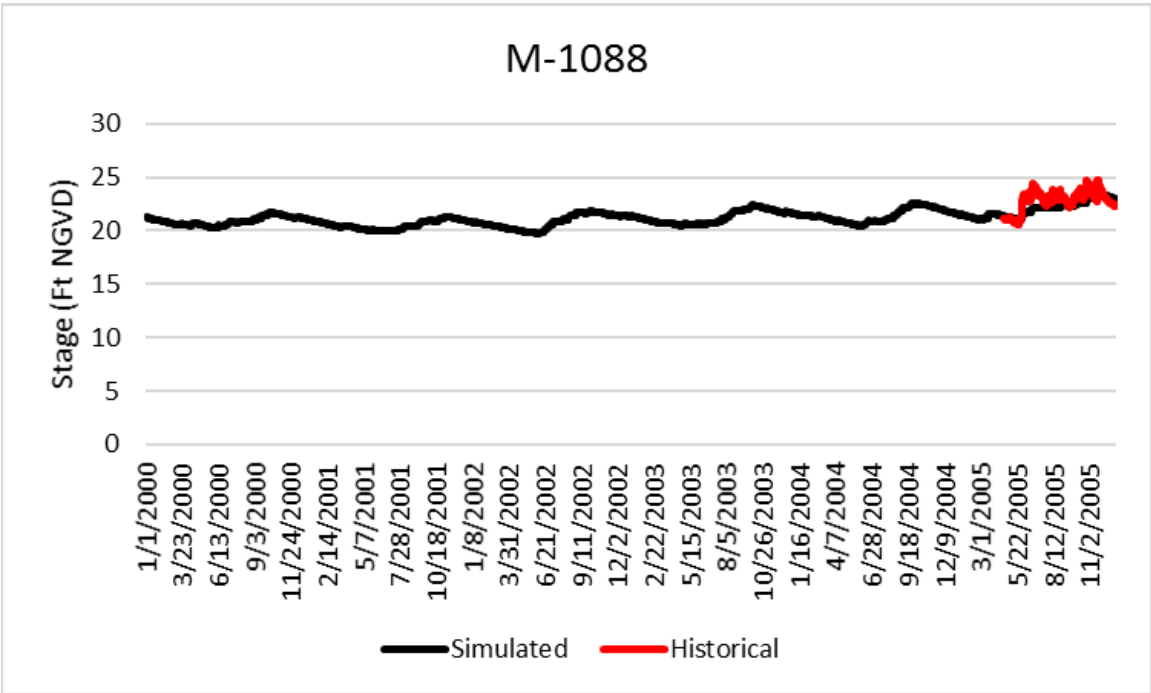

Figure E-12. Historical and simulated groundwater monitoring well stage hydrograph (2000 – 2005) for M-1088.

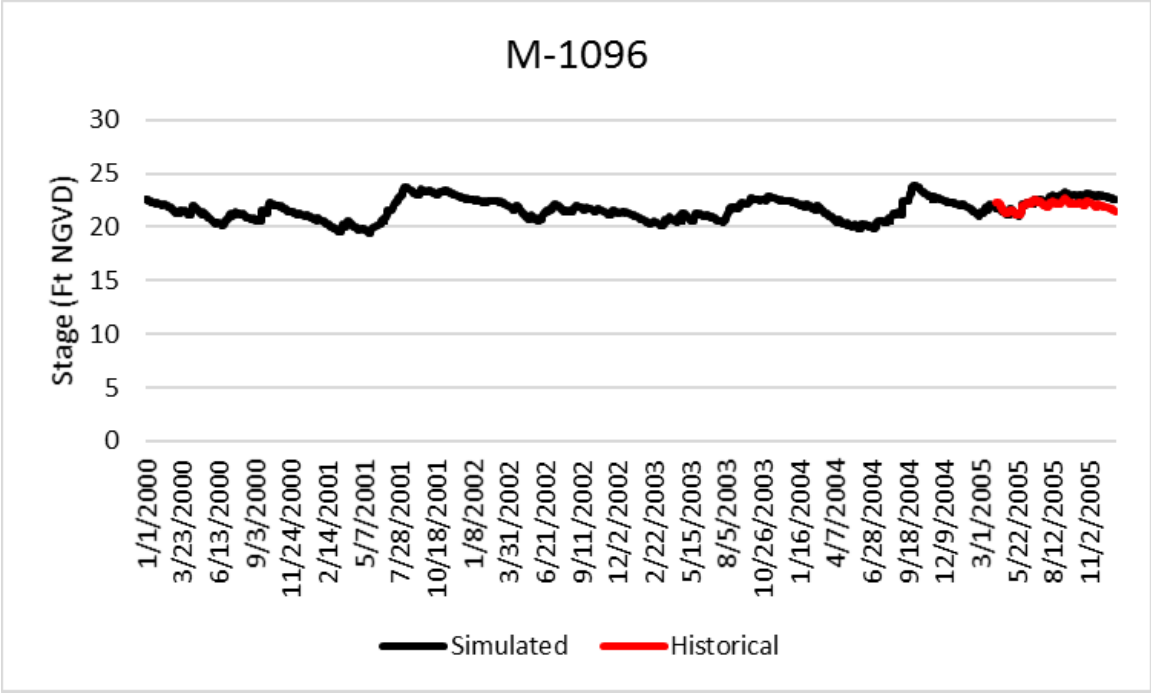

Figure E-13. Historical and simulated groundwater monitoring well stage hydrograph (2000 – 2005) for M-1096.

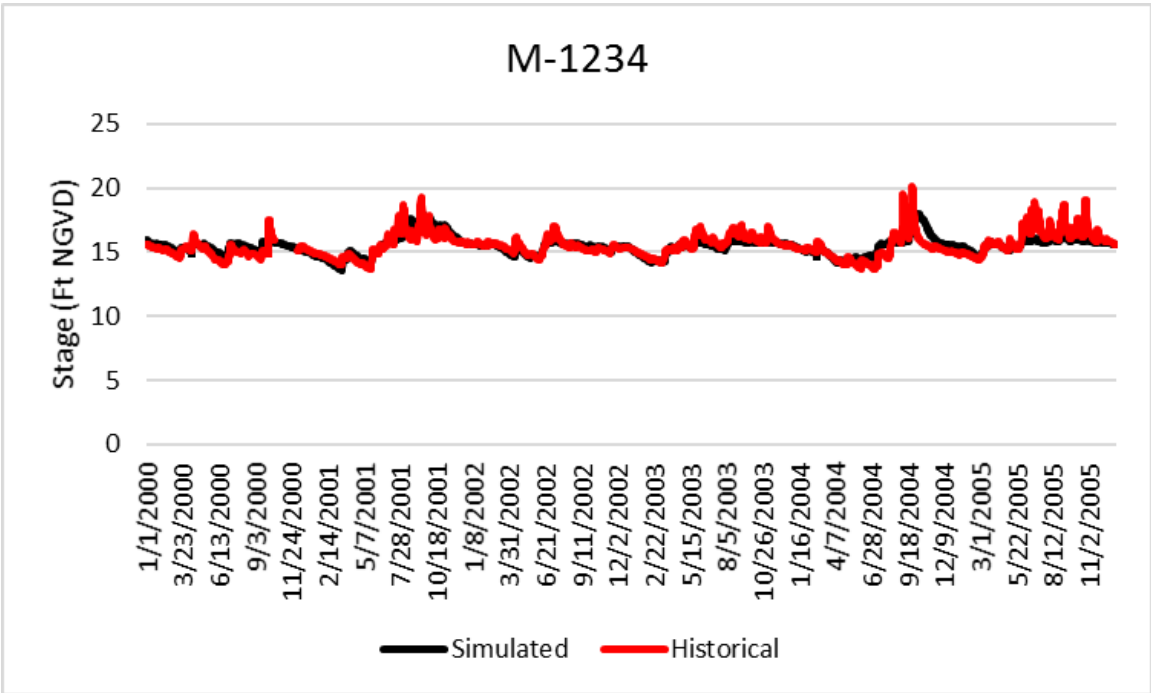

Figure E-14. Historical and simulated groundwater monitoring well stage hydrograph (2000 – 2005) for M-1234.

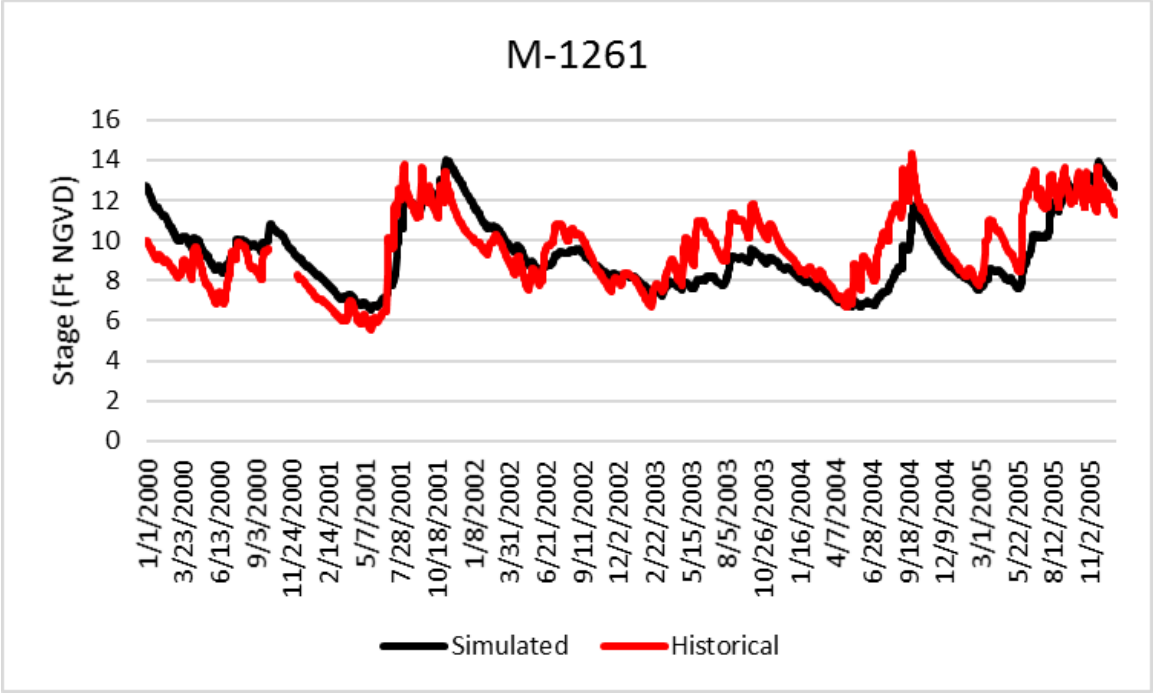

Figure E-15. Historical and simulated groundwater monitoring well stage hydrograph (2000 – 2005) for M-1261.

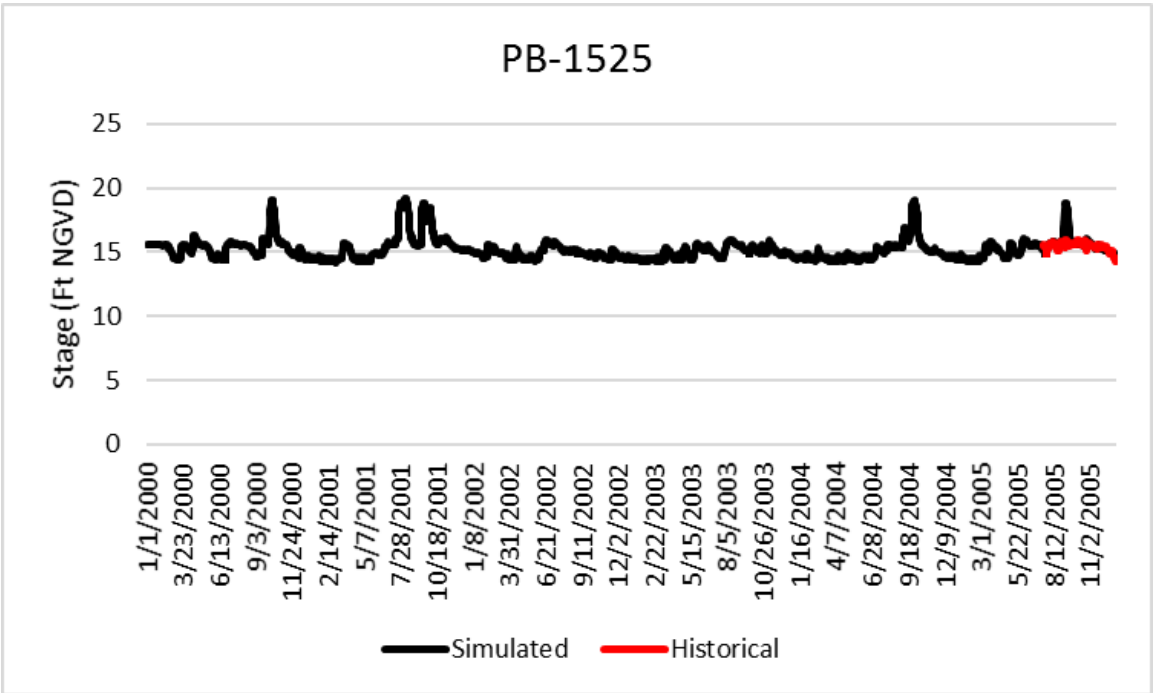

Figure E-16. Historical and simulated groundwater monitoring well stage hydrograph (2000 – 2005) for PB-1525.

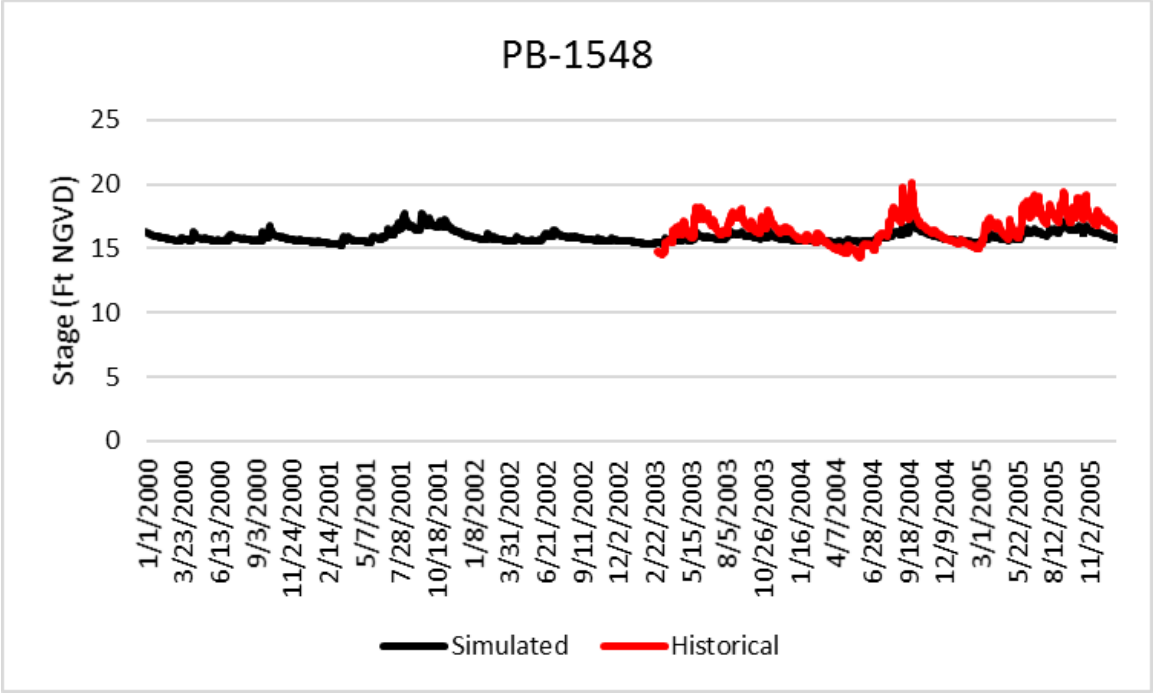

Figure E-17. Historical and simulated groundwater monitoring well stage hydrograph (2000 – 2005) for PB-1548.

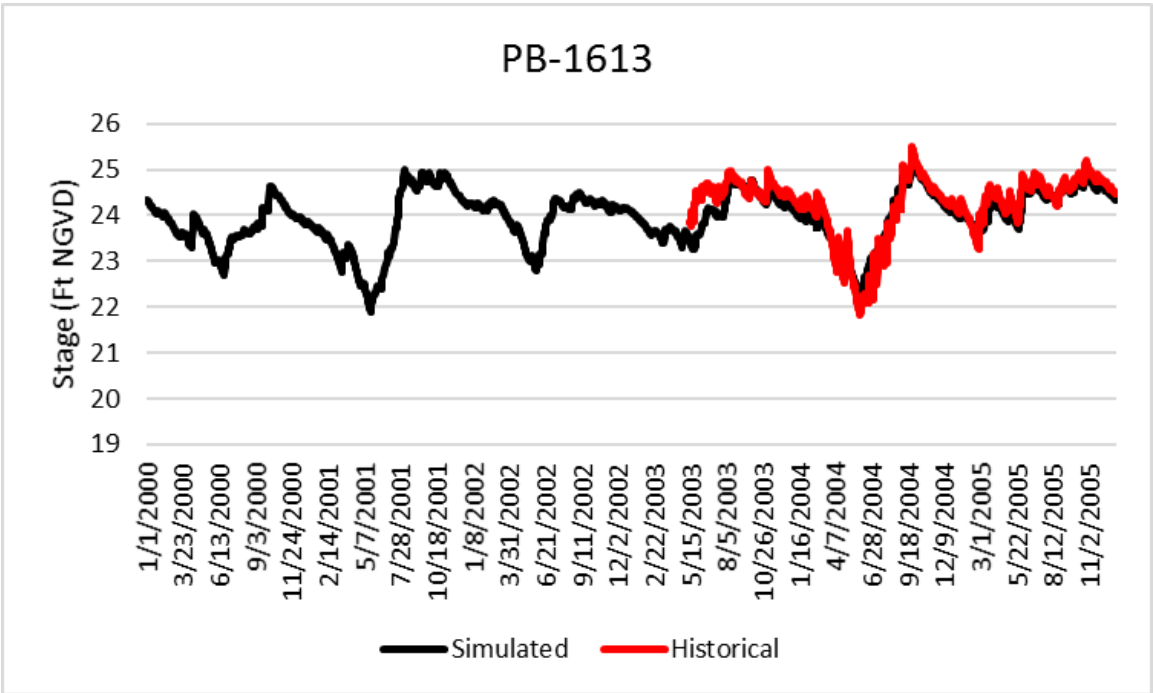

Figure E-18. Historical and simulated groundwater monitoring well stage hydrograph (2000 – 2005) for PB-1613.

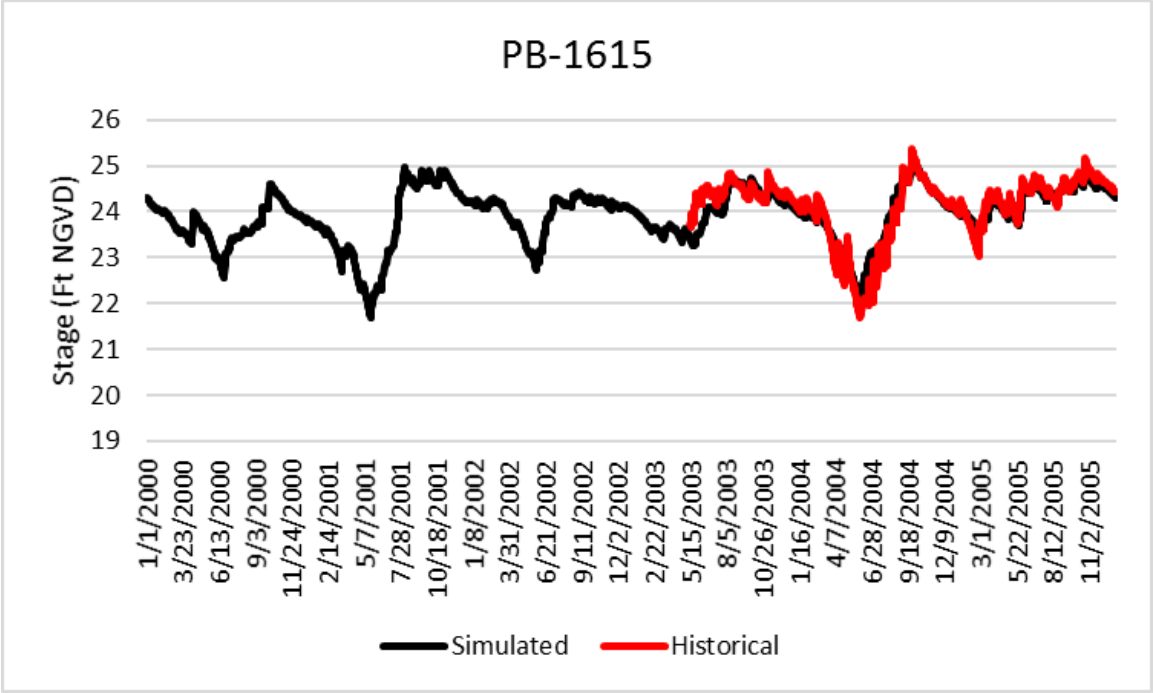

Figure E-19. Historical and simulated groundwater monitoring well stage hydrograph (2000 – 2005) for PB-1615.

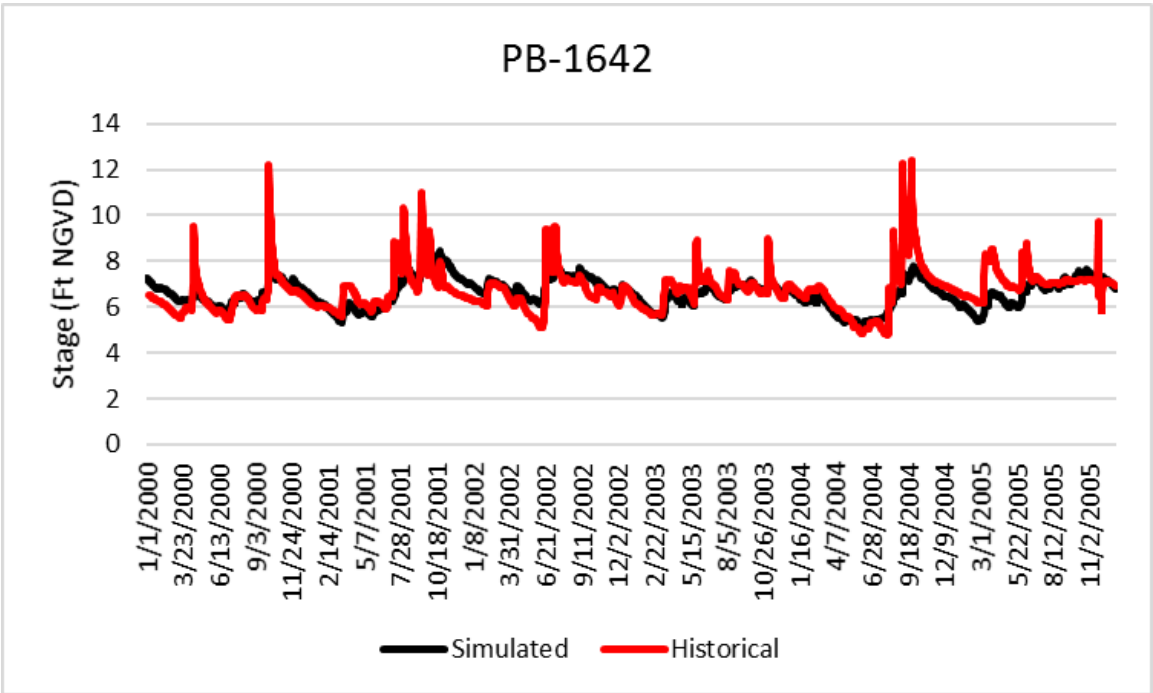

Figure E-20. Historical and simulated groundwater monitoring well stage hydrograph (2000 – 2005) for PB-1642.

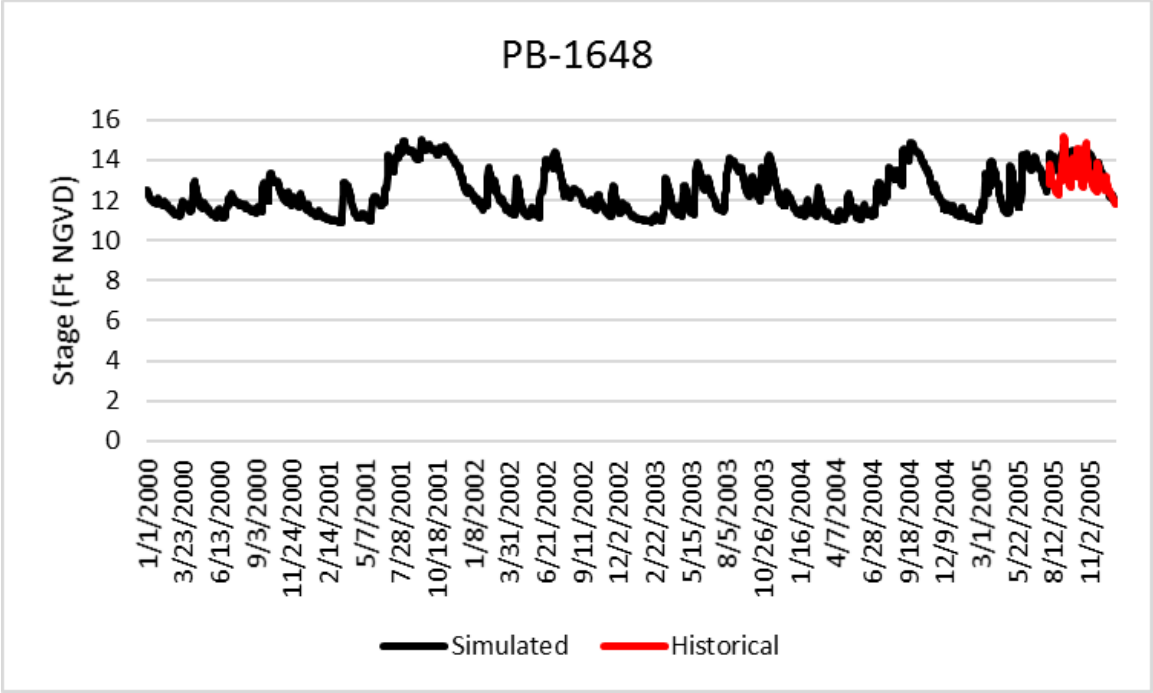

Figure E-21. Historical and simulated groundwater monitoring well stage hydrograph (2000 – 2005) for PB-1648.

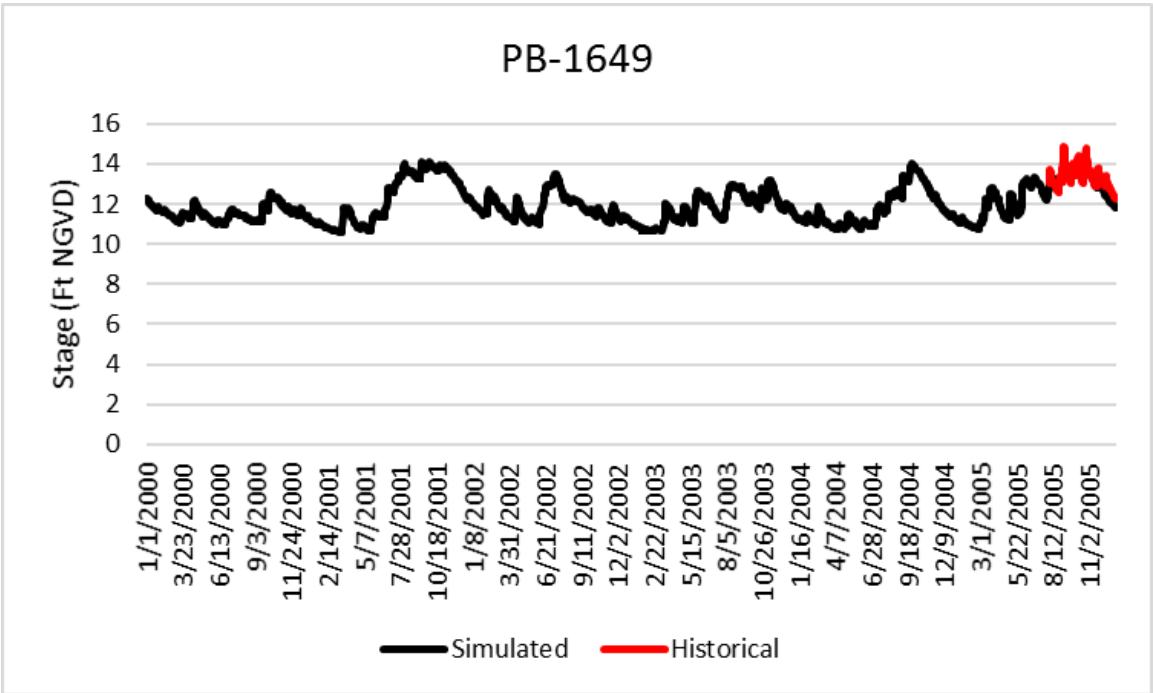

Figure E-22. Historical and simulated groundwater monitoring well stage hydrograph (2000 – 2005) for PB-1649.

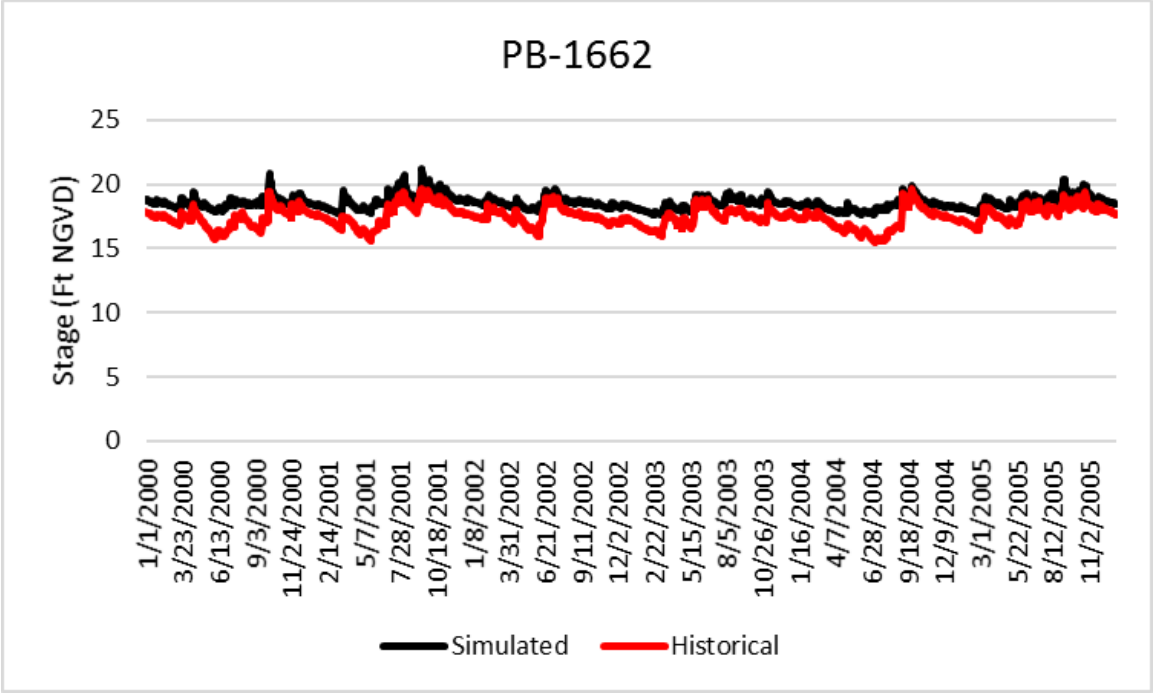

Figure E-23. Historical and simulated groundwater monitoring well stage hydrograph (2000 – 2005) for PB-1662.

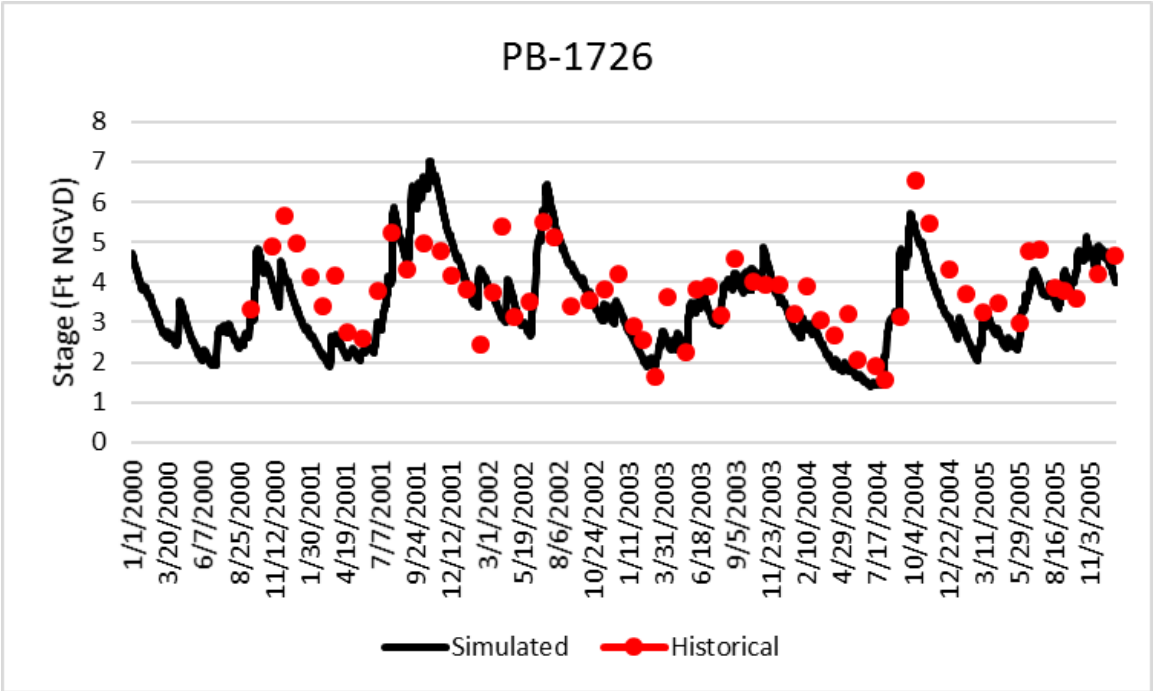

Figure E-24. Historical and simulated groundwater monitoring well stage hydrograph (2000 – 2005) for PB-1726.

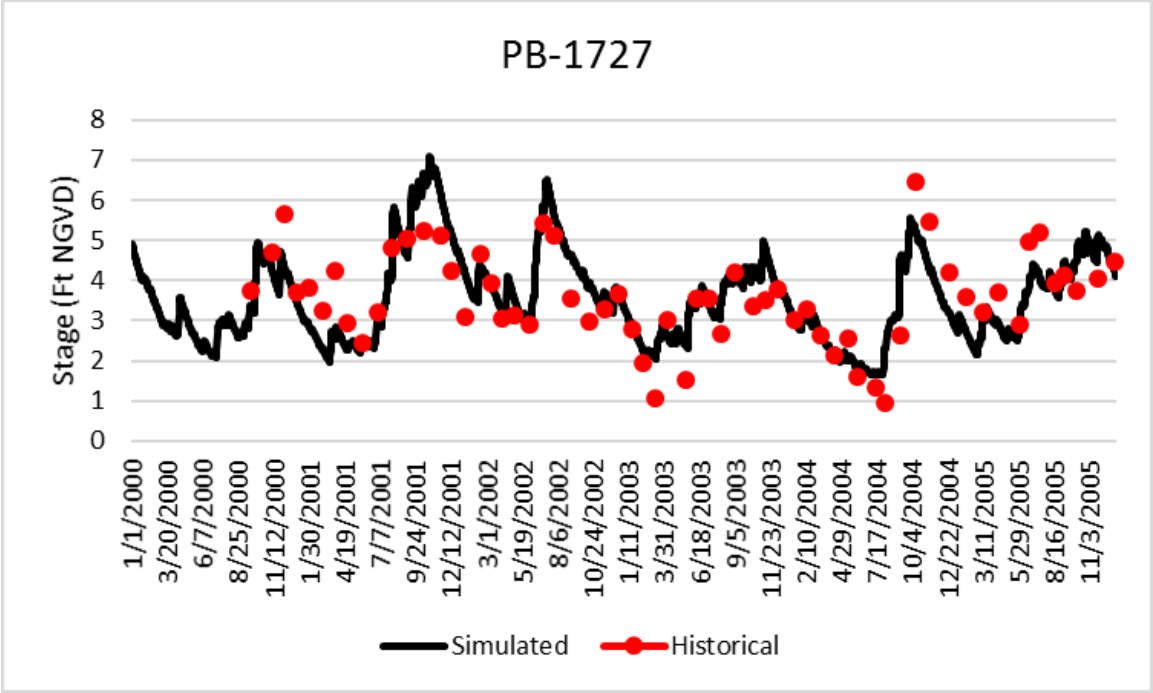

Figure E-25. Historical and simulated groundwater monitoring well stage hydrograph (2000 – 2005) for PB-1727.

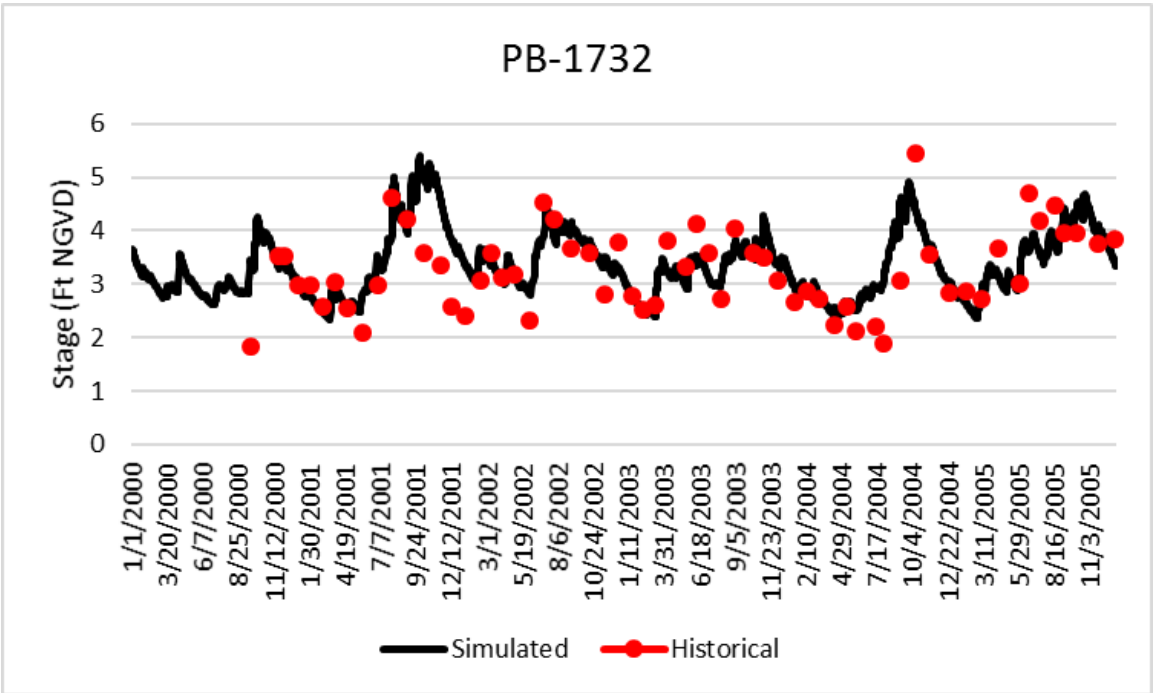

Figure E-26. Historical and simulated groundwater monitoring well stage hydrograph (2000 – 2005) for PB-1732.

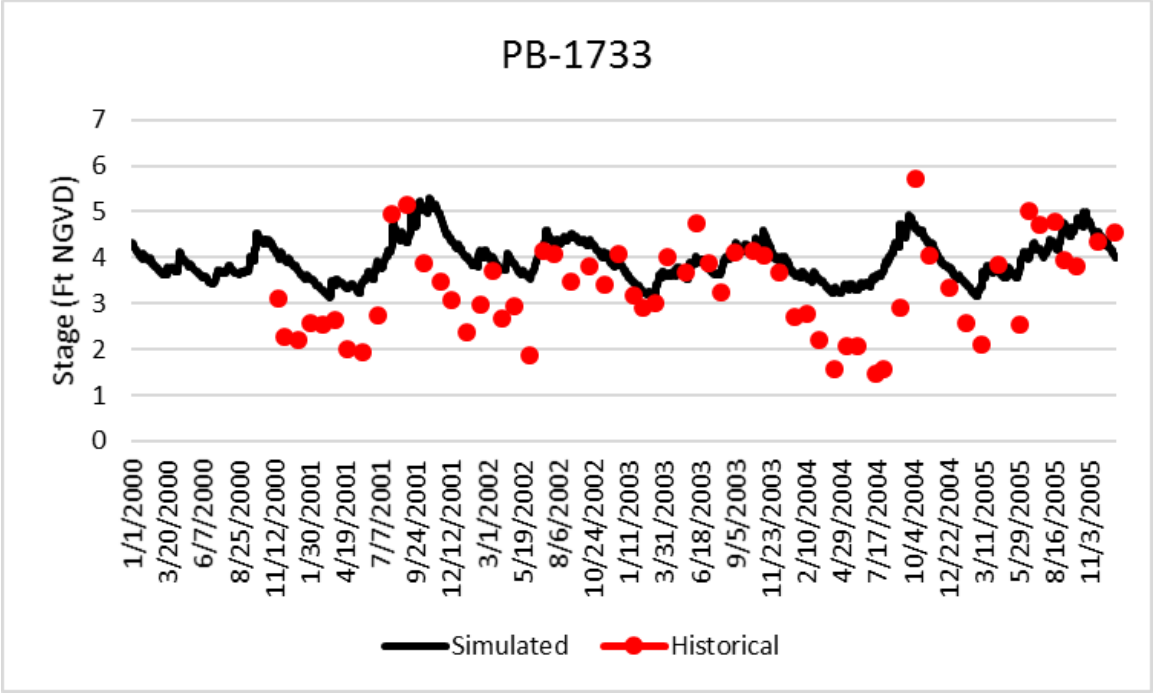

Figure E-27. Historical and simulated groundwater monitoring well stage hydrograph (2000 – 2005) for PB-1733.

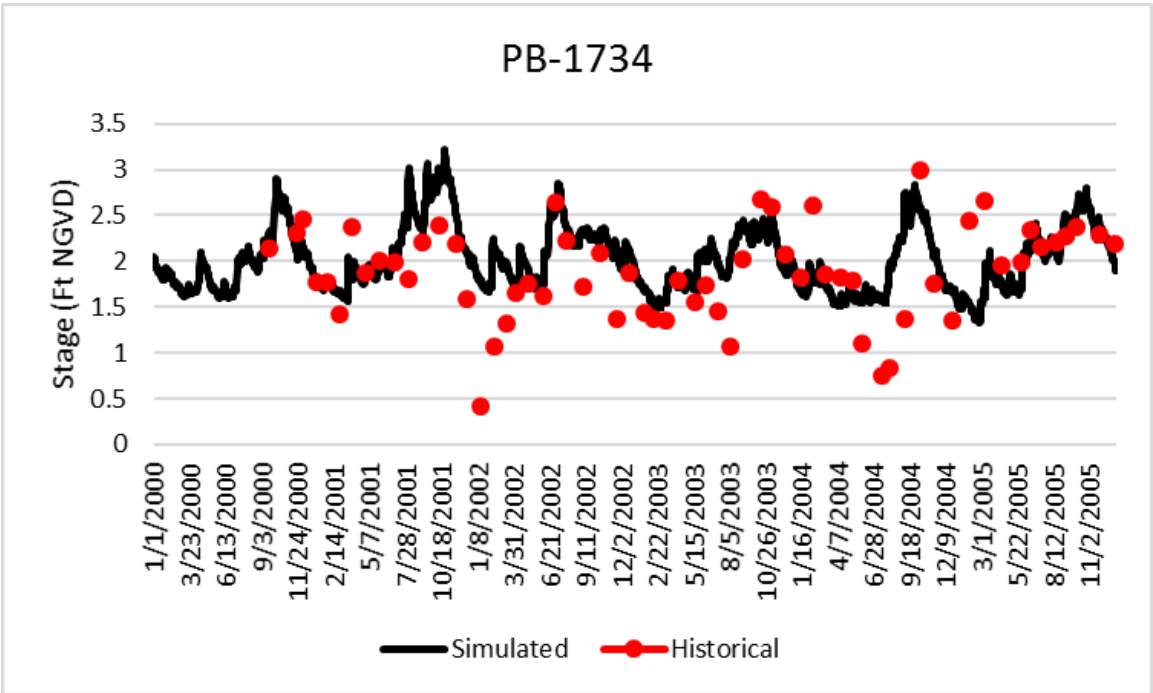

Figure E-28. Historical and simulated groundwater monitoring well stage hydrograph (2000 – 2005) for PB-1734.

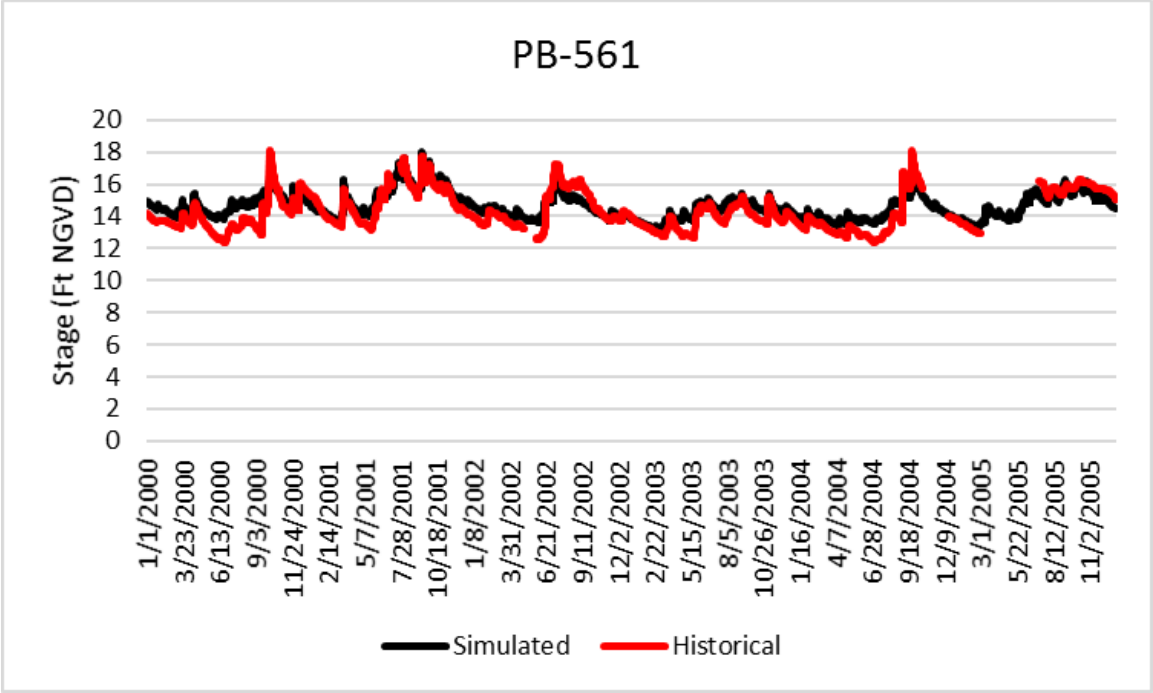

Figure E-29. Historical and simulated groundwater monitoring well stage hydrograph (2000 – 2005) for PB-561.

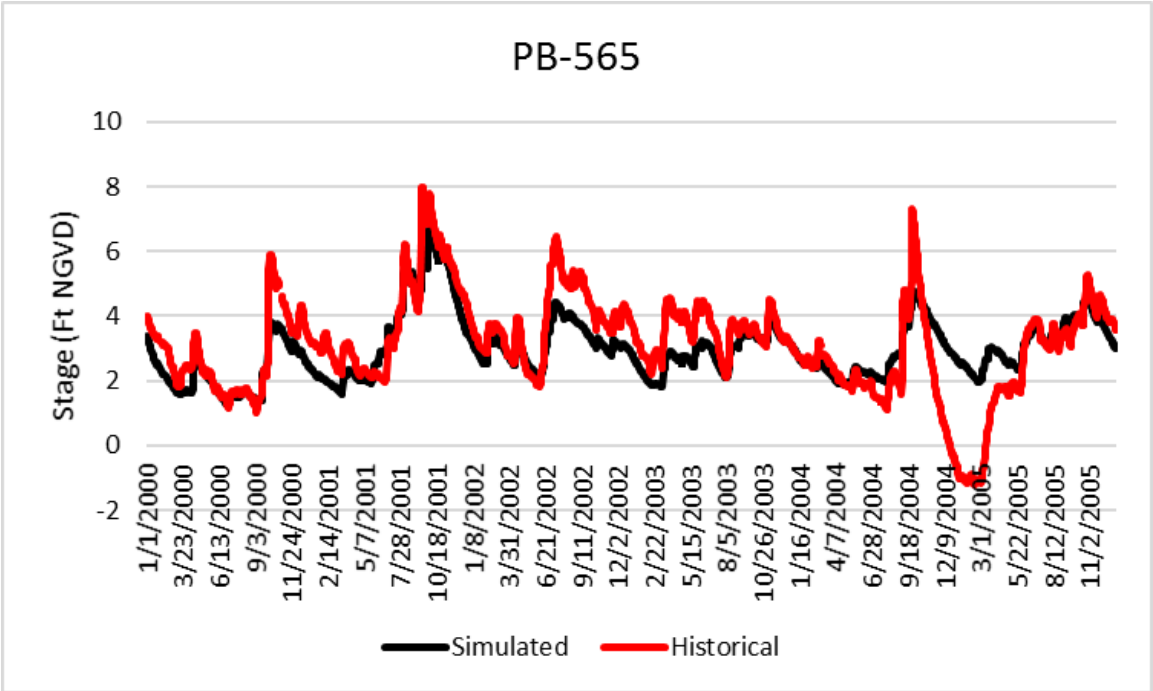

Figure E-30. Historical and simulated groundwater monitoring well stage hydrograph (2000 – 2005) for PB-565.

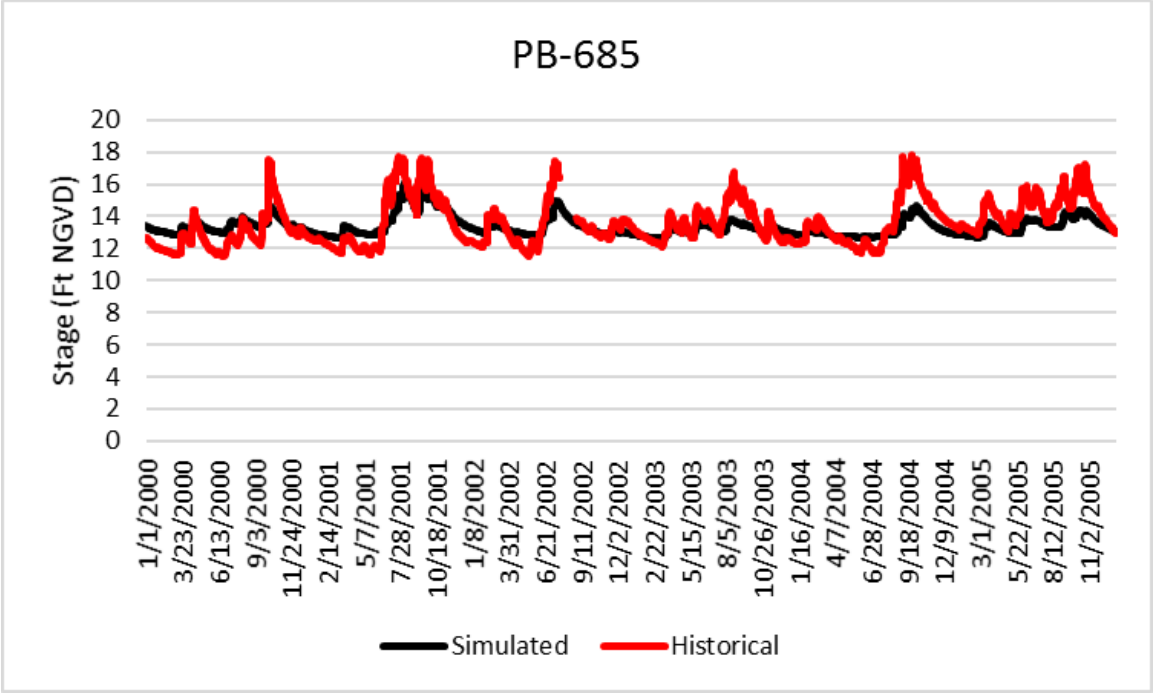

Figure E-31. Historical and simulated groundwater monitoring well stage hydrograph (2000 – 2005) for PB-685.

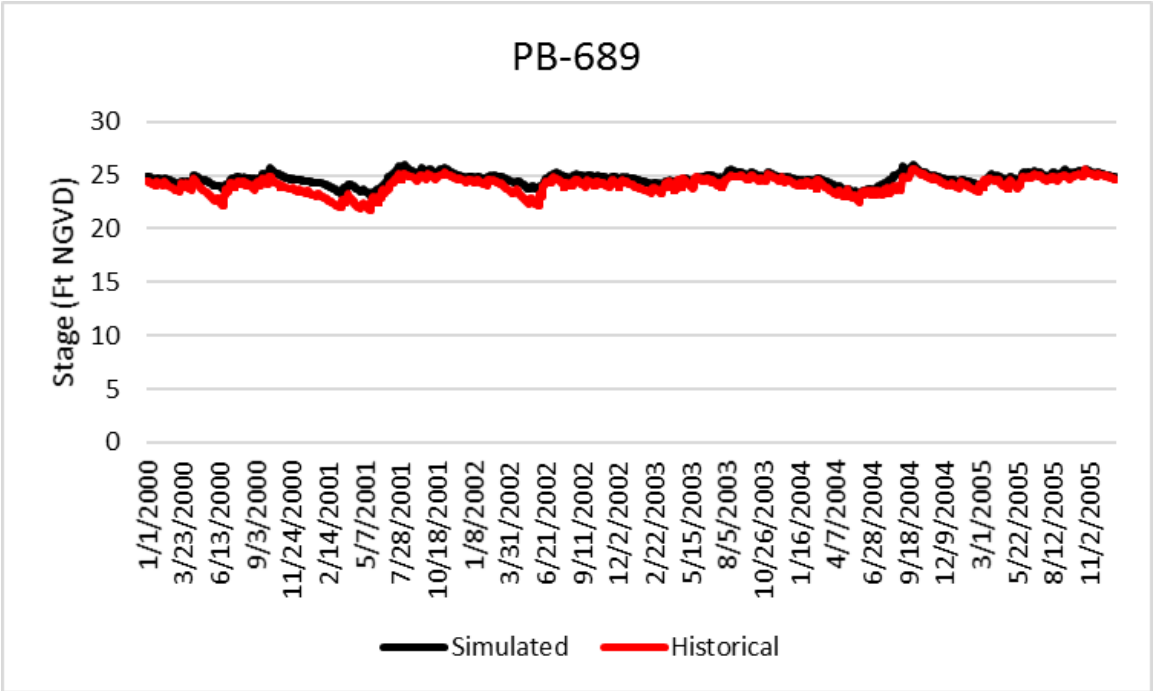

Figure E-32. Historical and simulated groundwater monitoring well stage hydrograph (2000 – 2005) for PB-689.

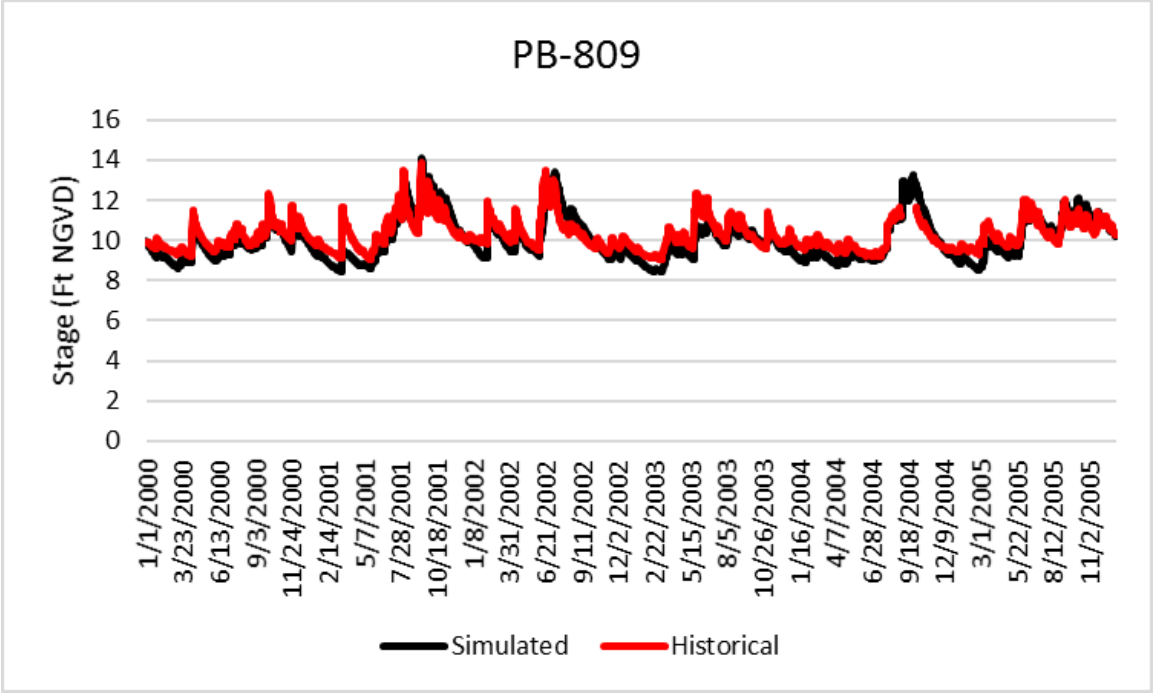

Figure E-33. Historical and simulated groundwater monitoring well stage hydrograph (2000 – 2005) for PB-809.

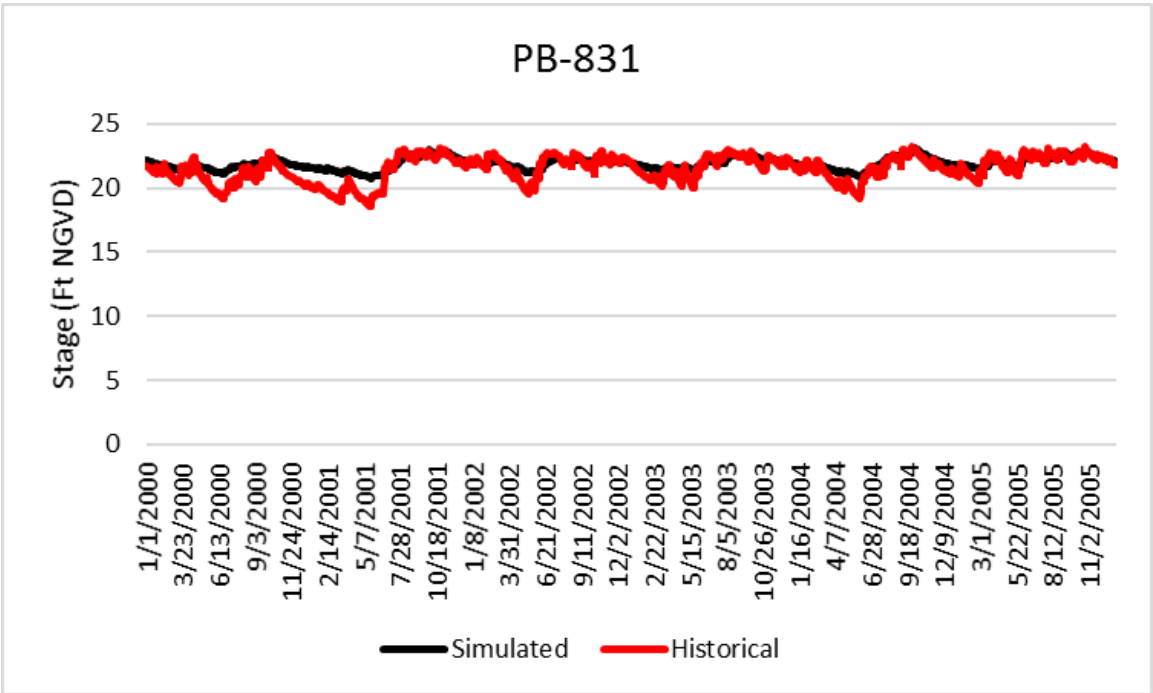

Figure E-34. Historical and simulated groundwater monitoring well stage hydrograph (2000 – 2005) for PB-831.

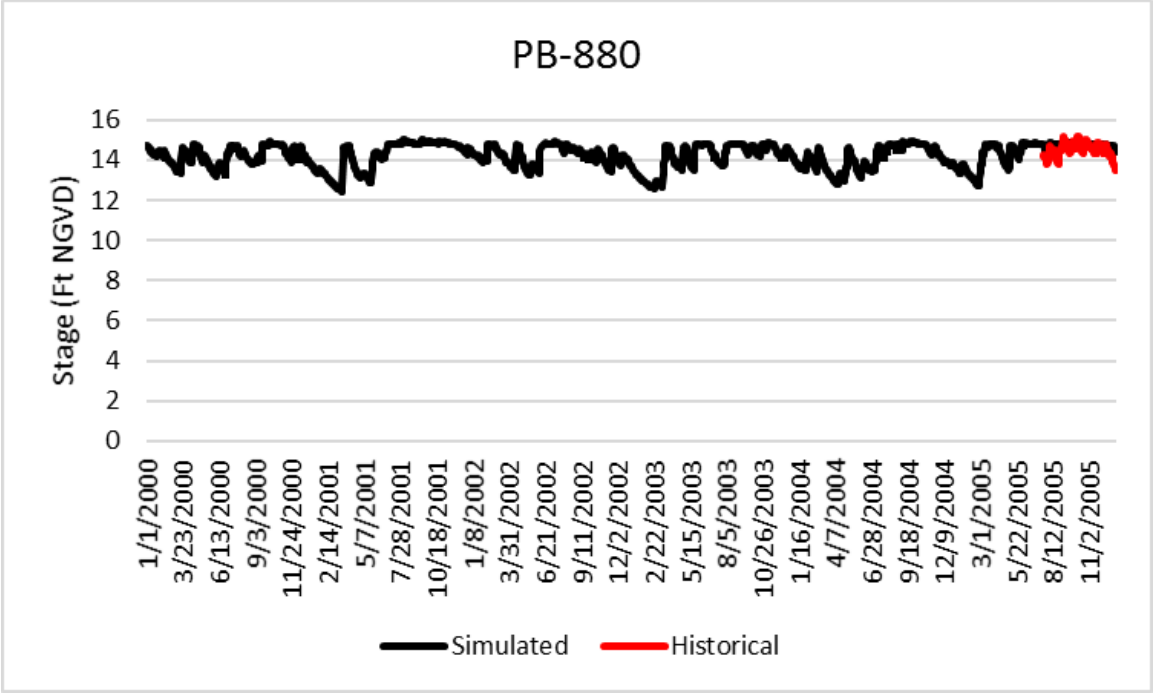

Figure E-35. Historical and simulated groundwater monitoring well stage hydrograph (2000 – 2005) for PB-880.

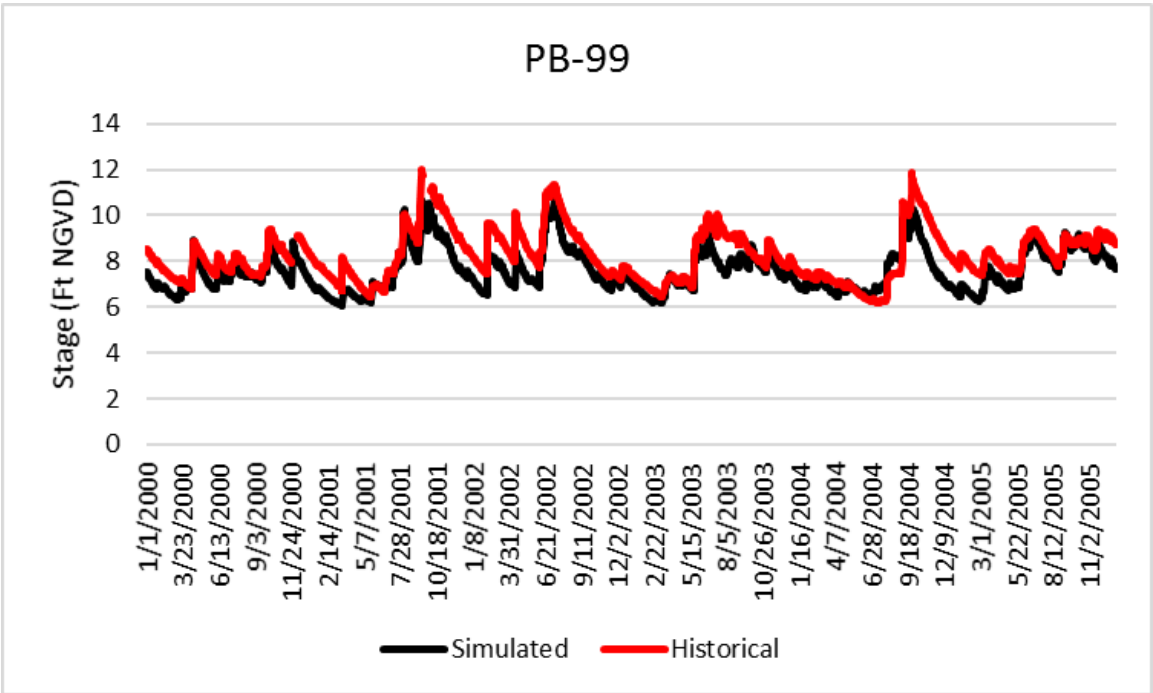

Figure E-36. Historical and simulated groundwater monitoring well stage hydrograph (2000 – 2005) for PB-99.

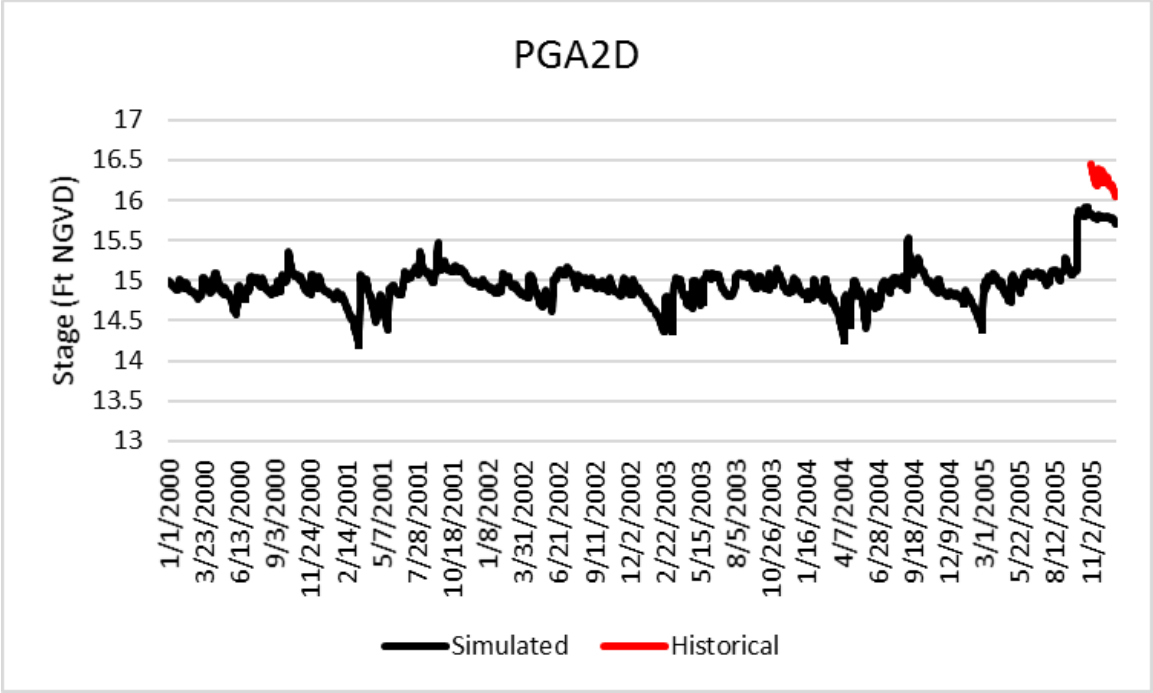

Figure E-37. Historical and simulated groundwater monitoring well stage hydrograph (2000 – 2005) for PGA2D.

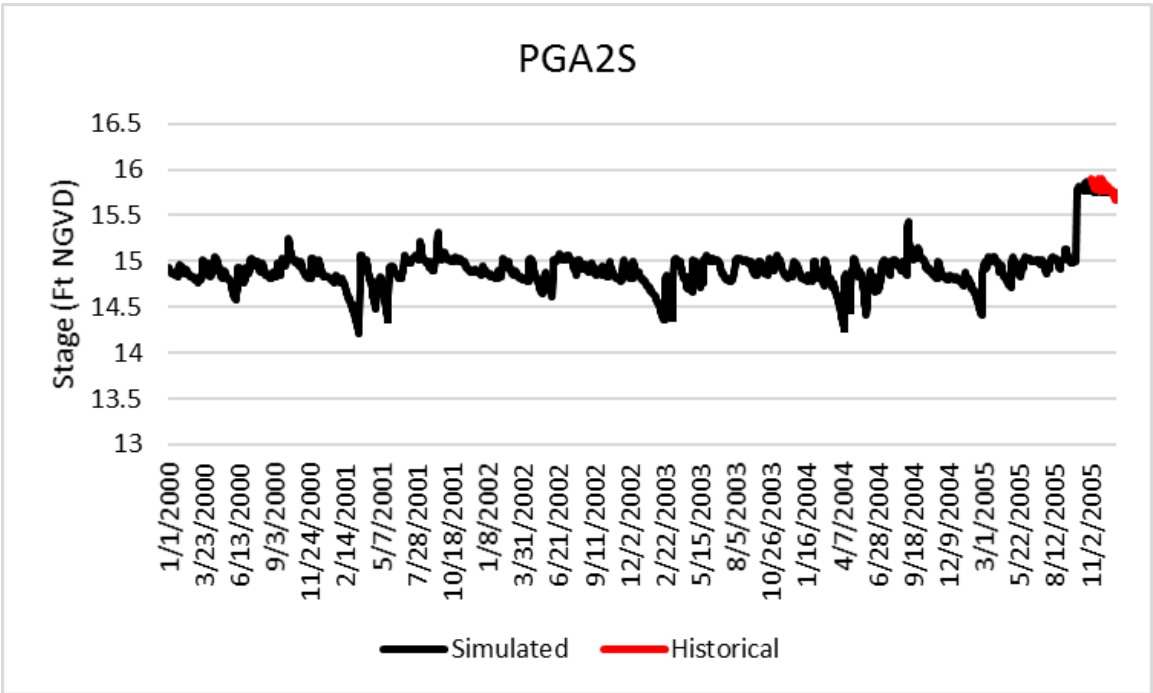

Figure E-38. Historical and simulated groundwater monitoring well stage hydrograph (2000 – 2005) for PGA2S.

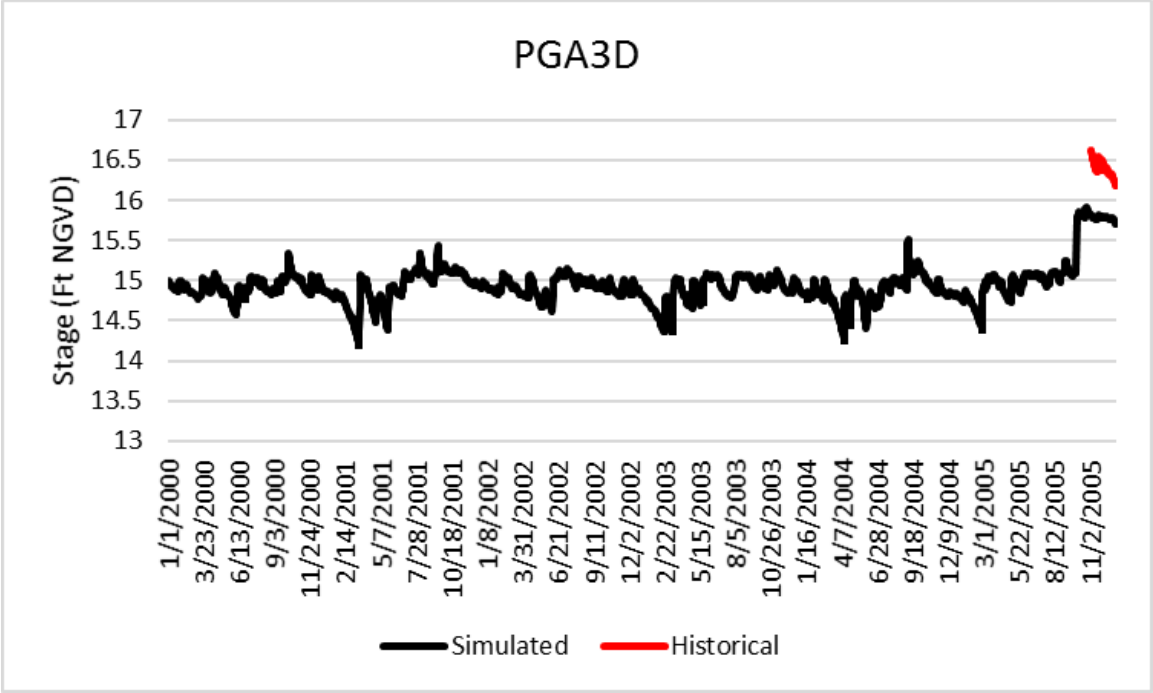

Figure E-39. Historical and simulated groundwater monitoring well stage hydrograph (2000 – 2005) for PGA3D.

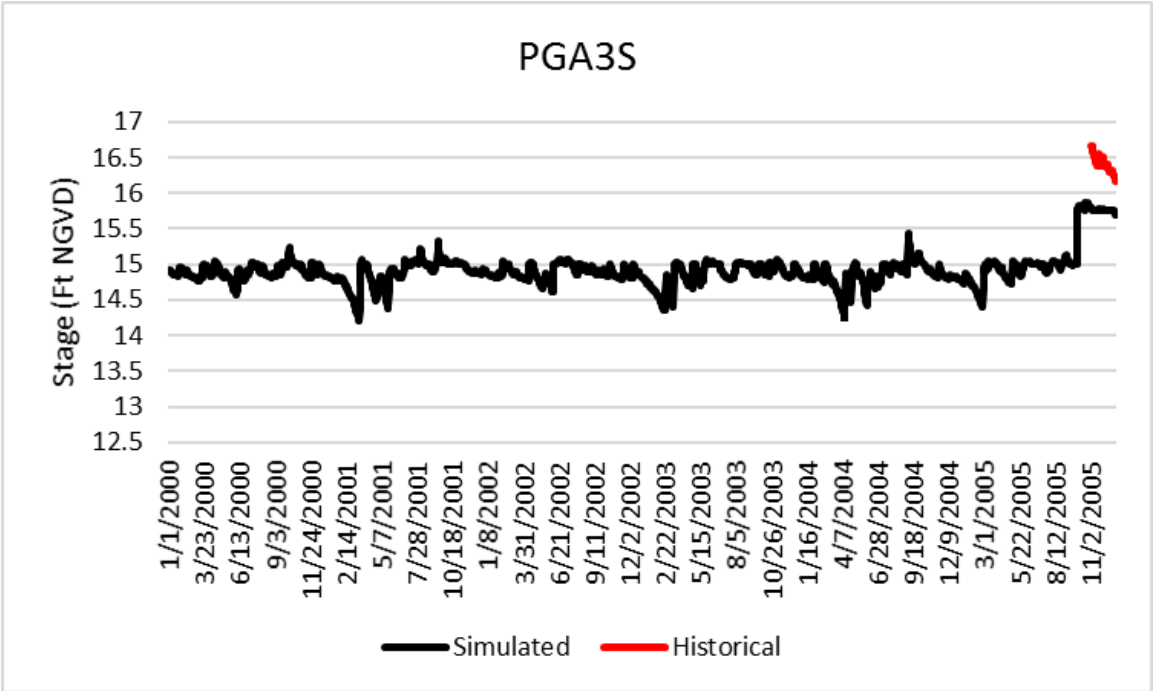

Figure E-40. Historical and simulated groundwater monitoring well stage hydrograph (2000 – 2005) for PGA3S.

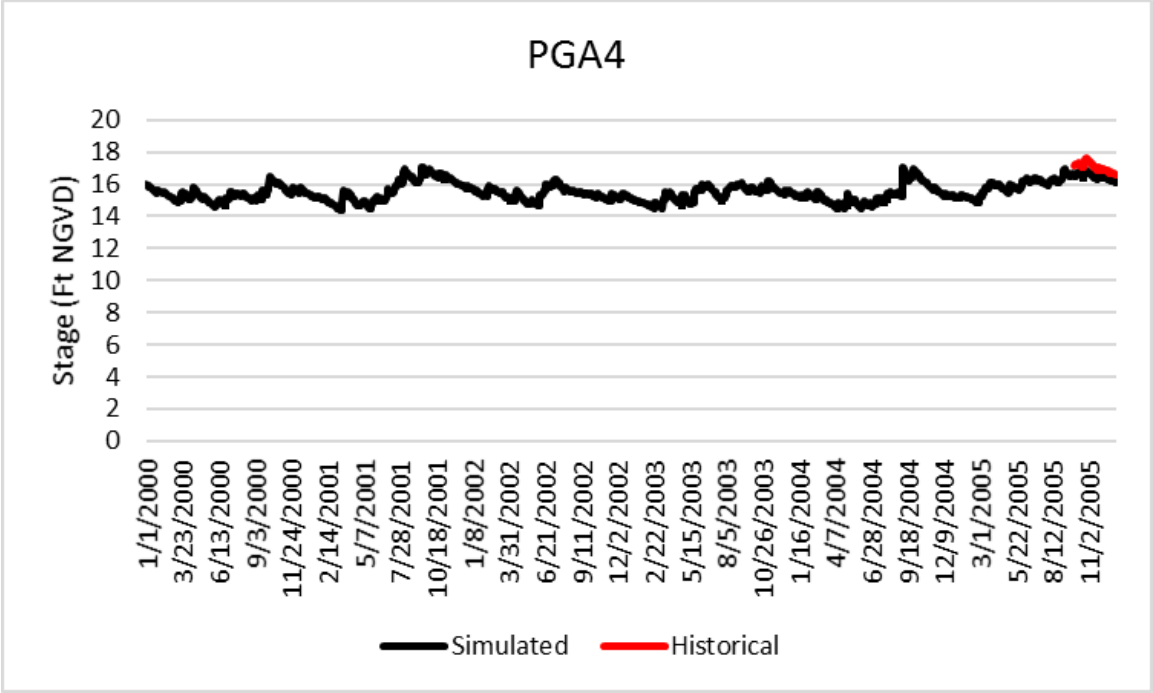

Figure E-41. Historical and simulated groundwater monitoring well stage hydrograph (2000 – 2005) for PGA4.

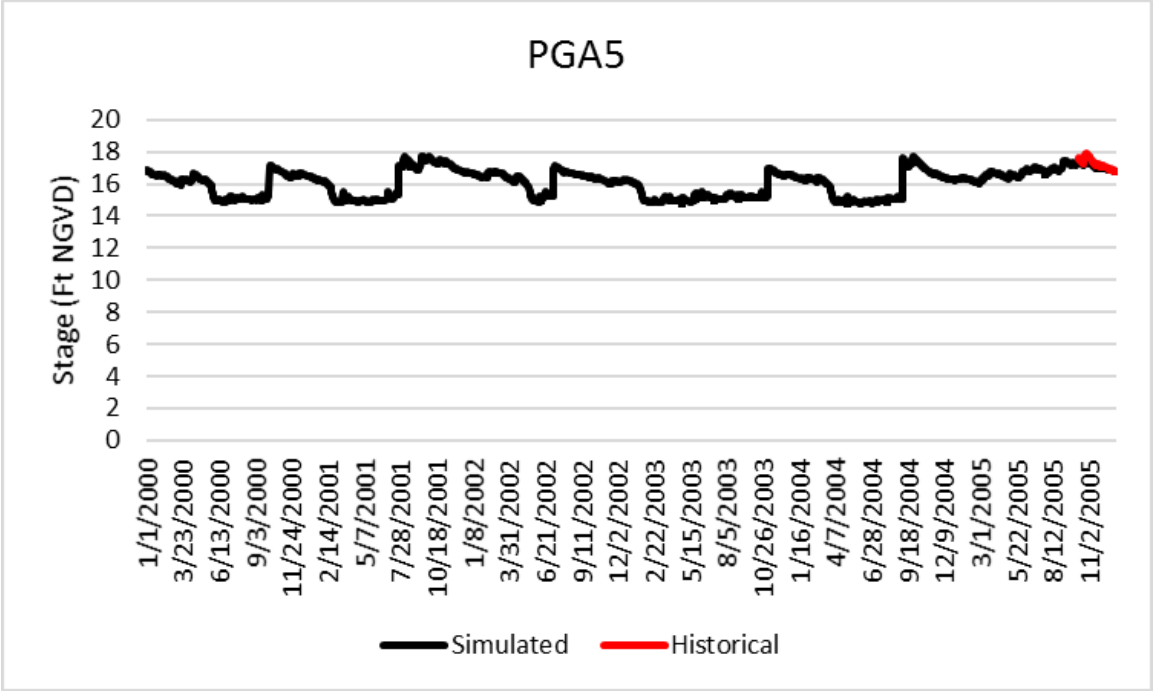

Figure E-42. Historical and simulated groundwater monitoring well stage hydrograph (2000 – 2005) for PGA5.

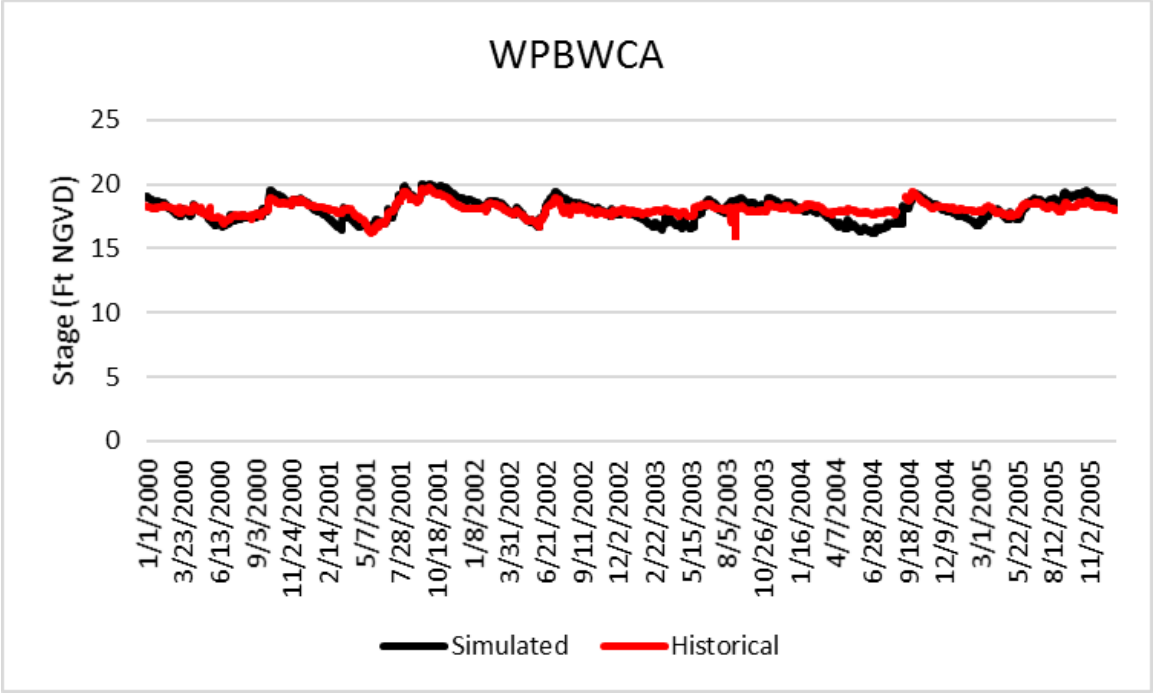

Figure E-43. Historical and simulated groundwater monitoring well stage hydrograph (2000 – 2005) for WPBWCA.

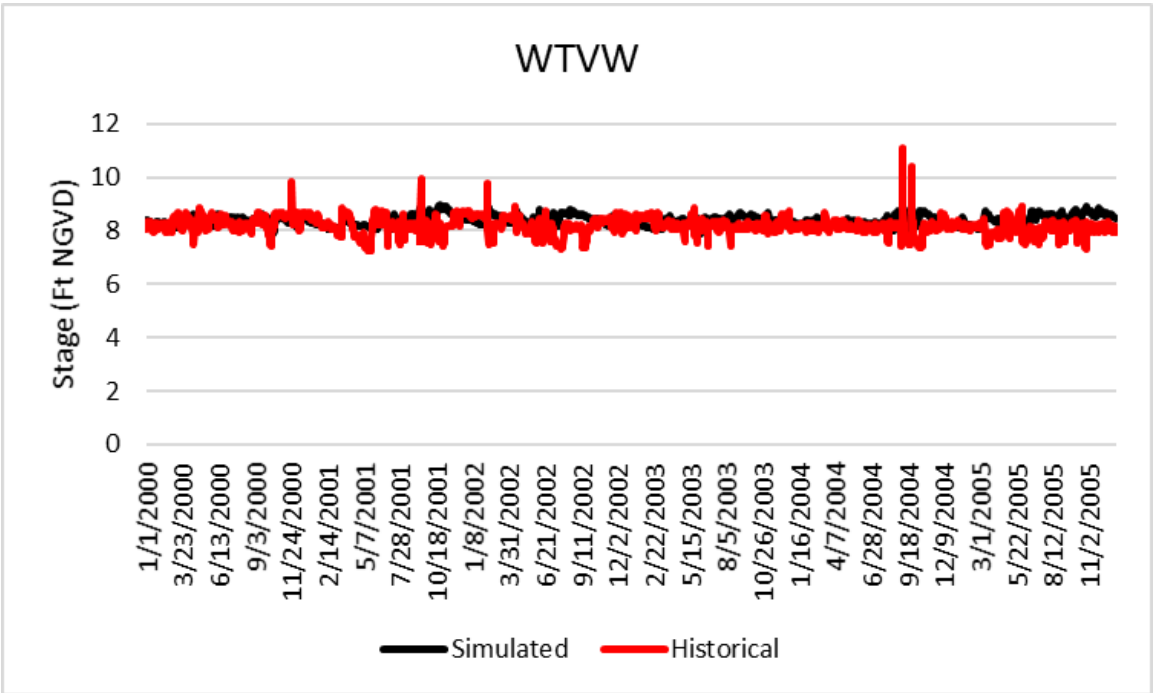

Figure E-44. Historical and simulated groundwater monitoring well stage hydrograph (2000 – 2005) for WTVW.

Wetland Gauges

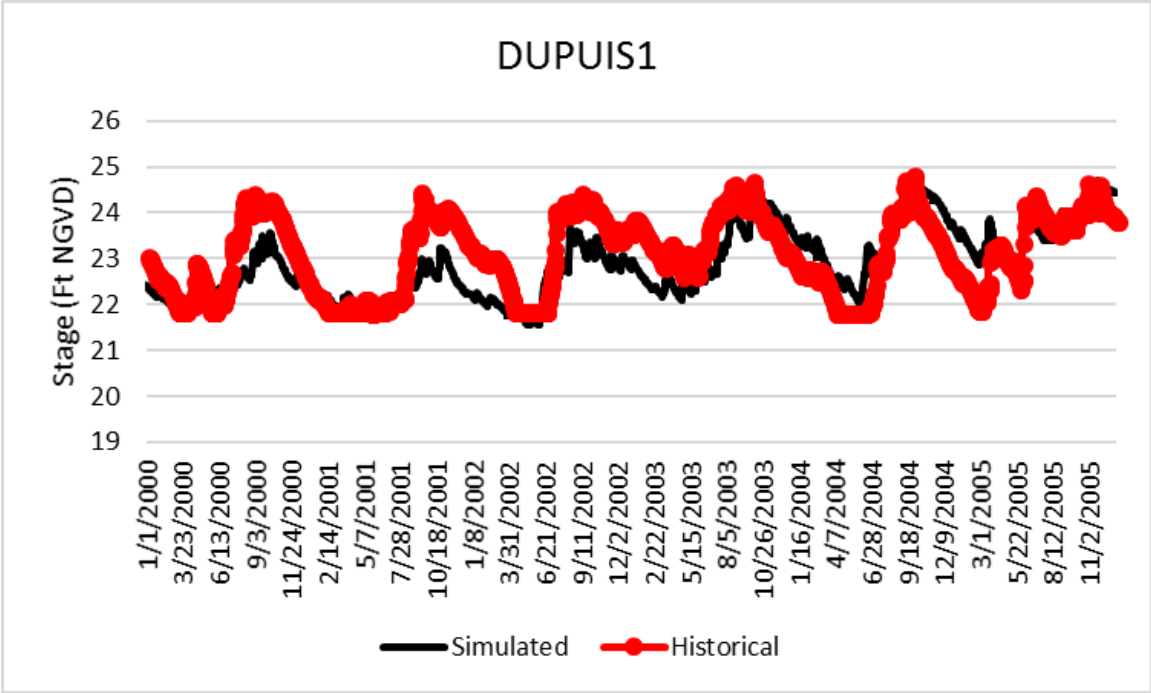

Figure E-45. Historical and simulated wetland gauge stage hydrograph (2000 – 2005) for Dupuis1.

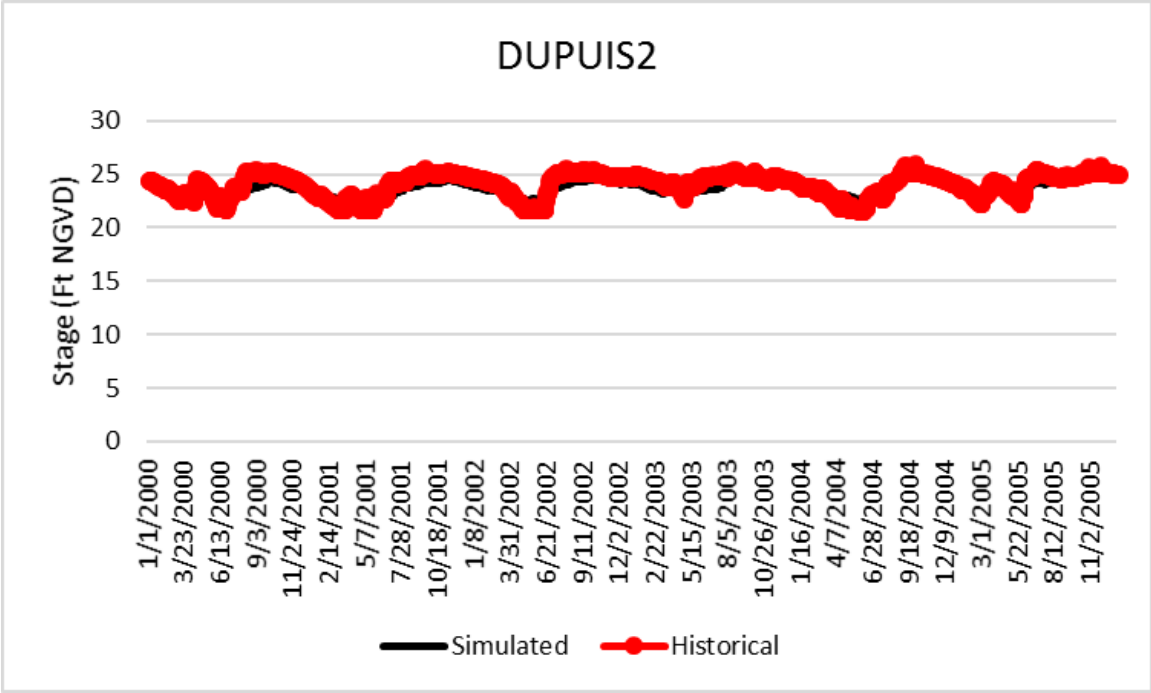

Figure E-46. Historical and simulated wetland gauge stage hydrograph (2000 – 2005) for Dupuis2.

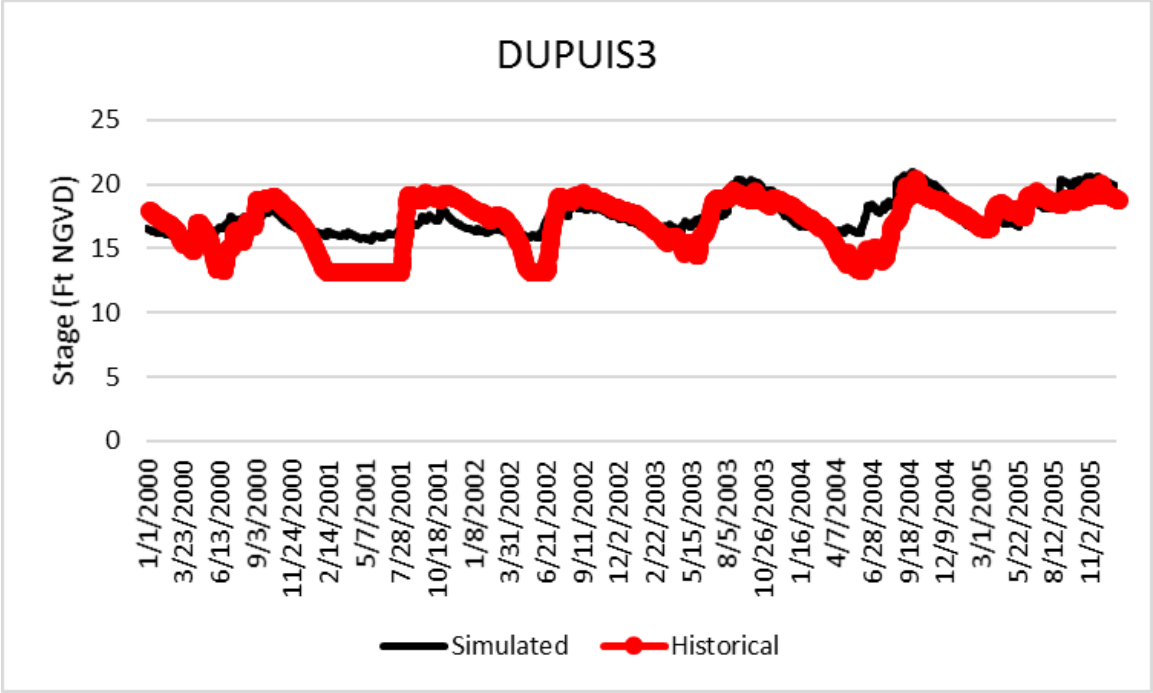

Figure E-47. Historical and simulated wetland gauge stage hydrograph (2000 – 2005) for Dupuis3.

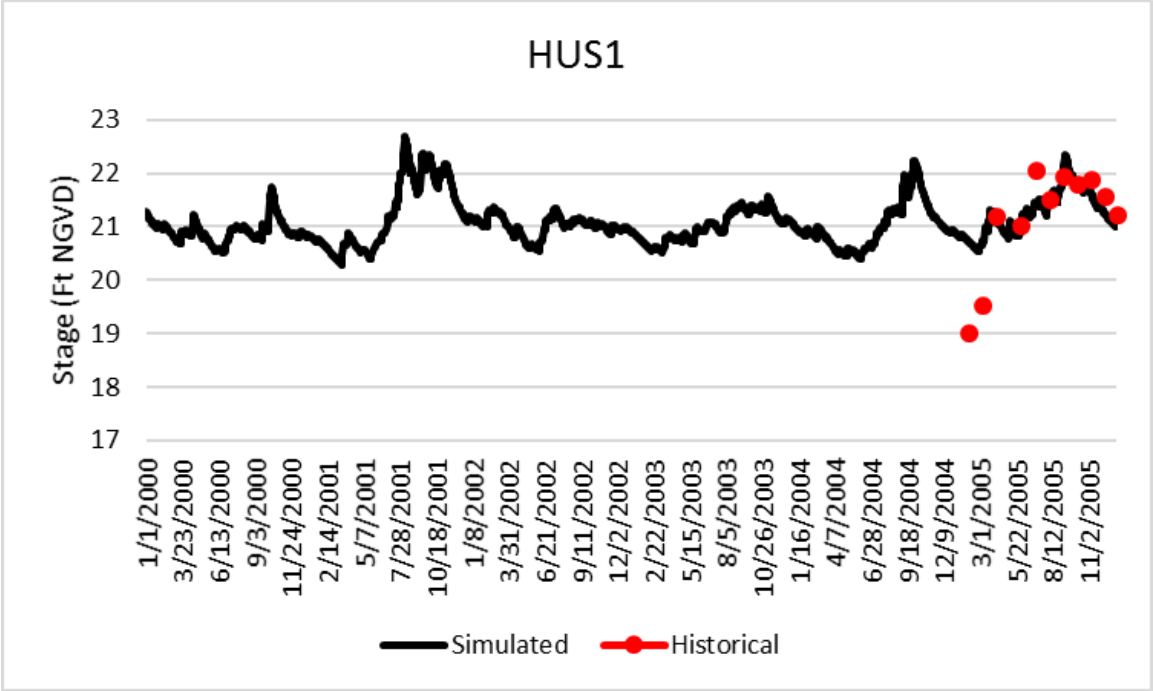

Figure E-48. Historical and simulated wetland gauge stage hydrograph (2000 – 2005) for HUS1.

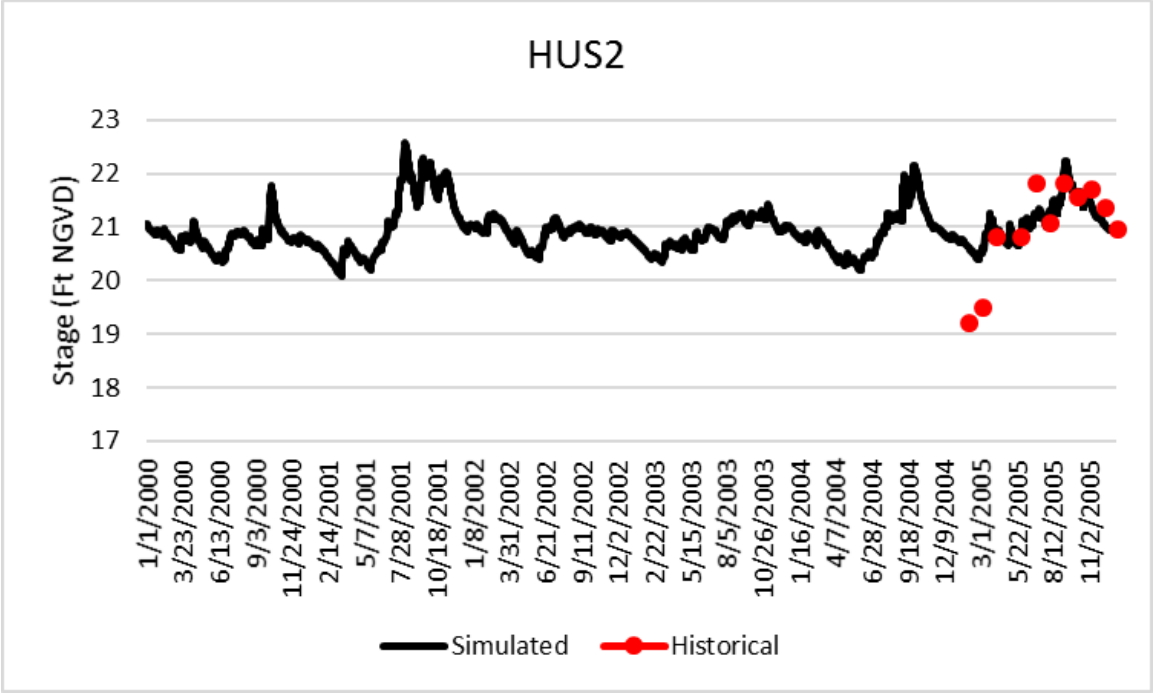

Figure E-49. Historical and simulated wetland gauge stage hydrograph (2000 – 2005) for HUS2.

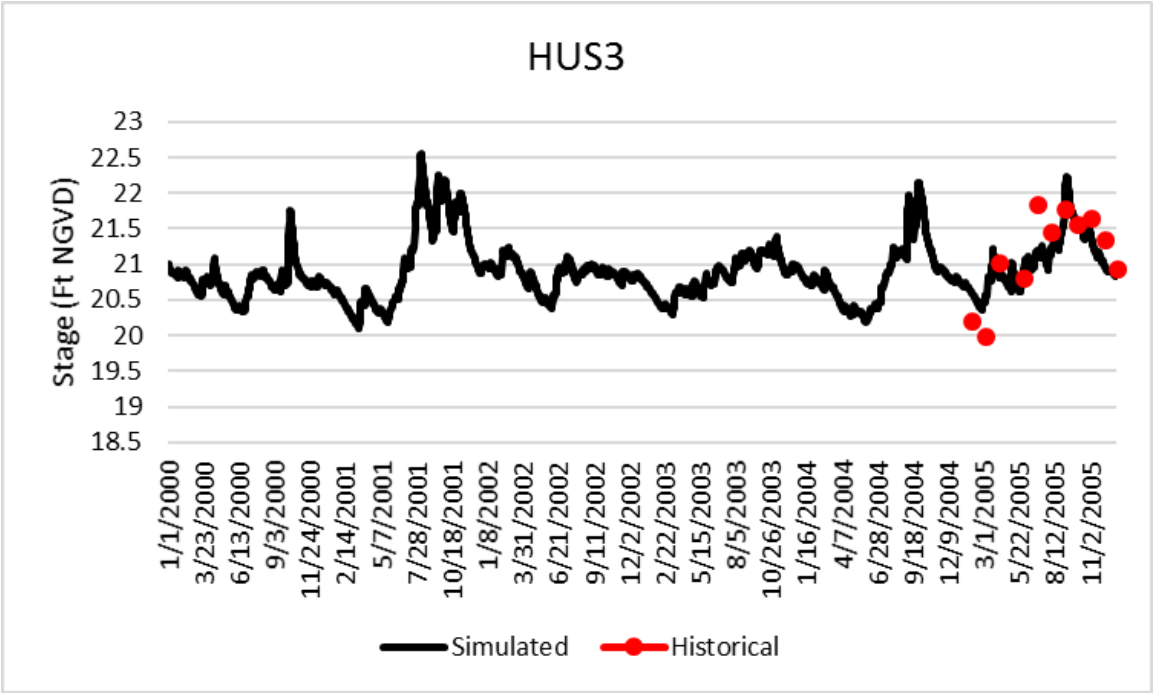

Figure E-50. Historical and simulated wetland gauge stage hydrograph (2000 – 2005) for HUS3.

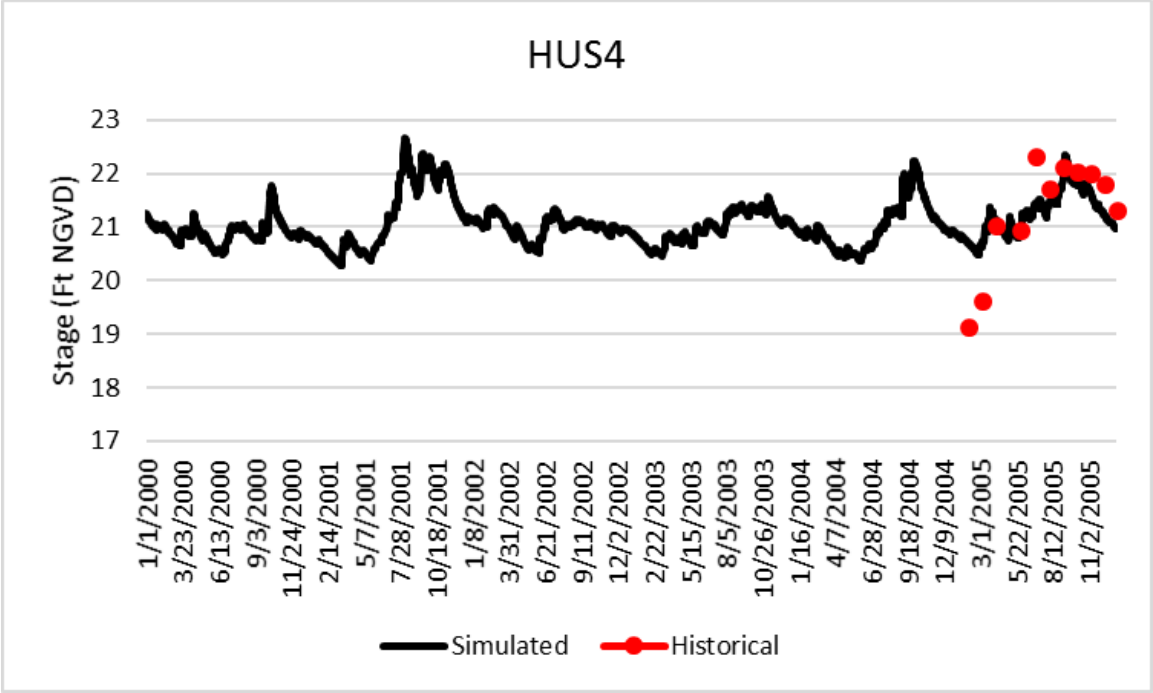

Figure E-51. Historical and simulated wetland gauge stage hydrograph (2000 – 2005) for HUS4.

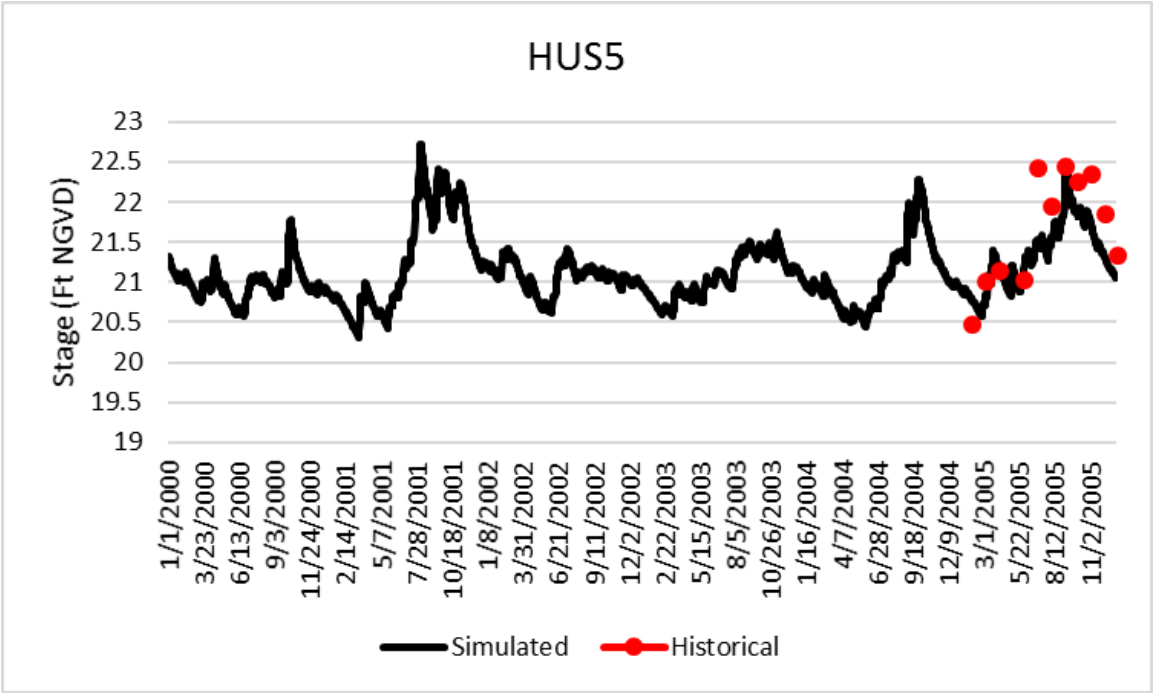

Figure E-52. Historical and simulated wetland gauge stage hydrograph (2000 – 2005) for HUS5.

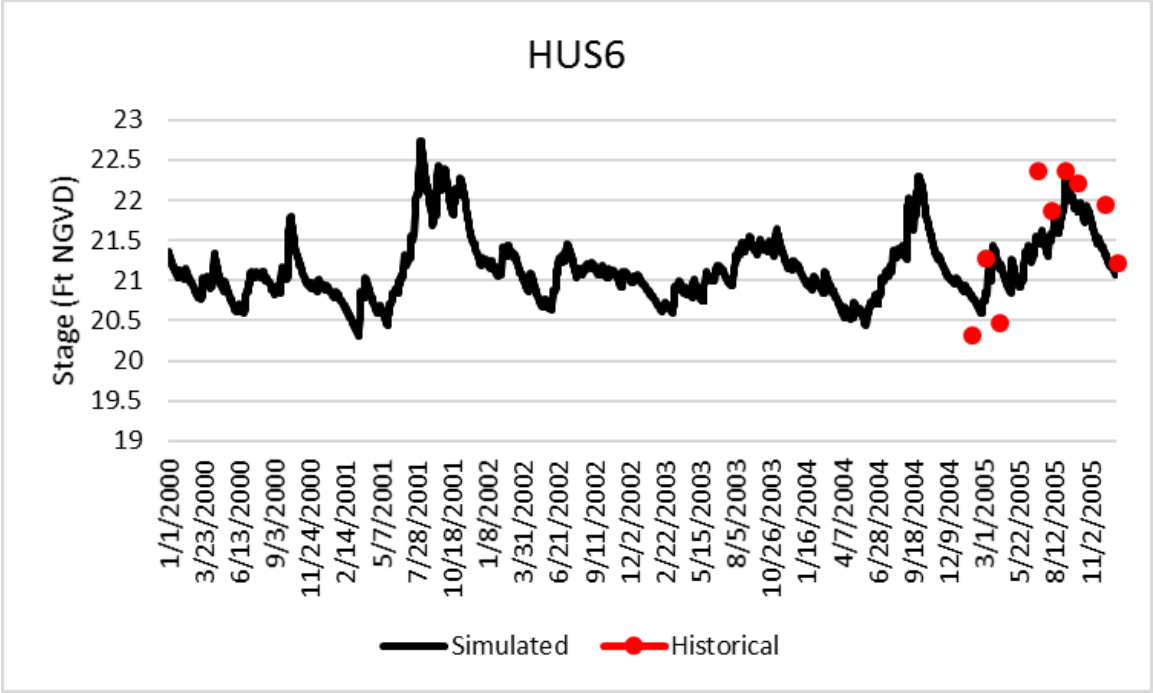

Figure E-53. Historical and simulated wetland gauge stage hydrograph (2000 – 2005) for HUS6.

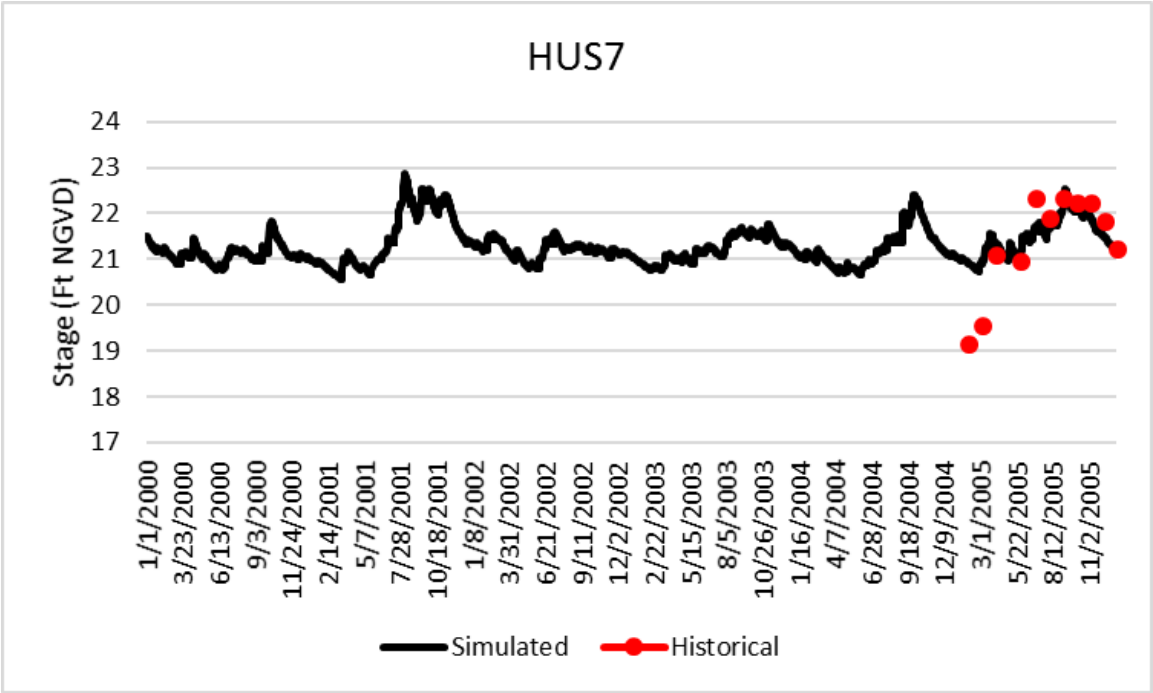

Figure E-54. Historical and simulated wetland gauge stage hydrograph (2000 – 2005) for HUS7.

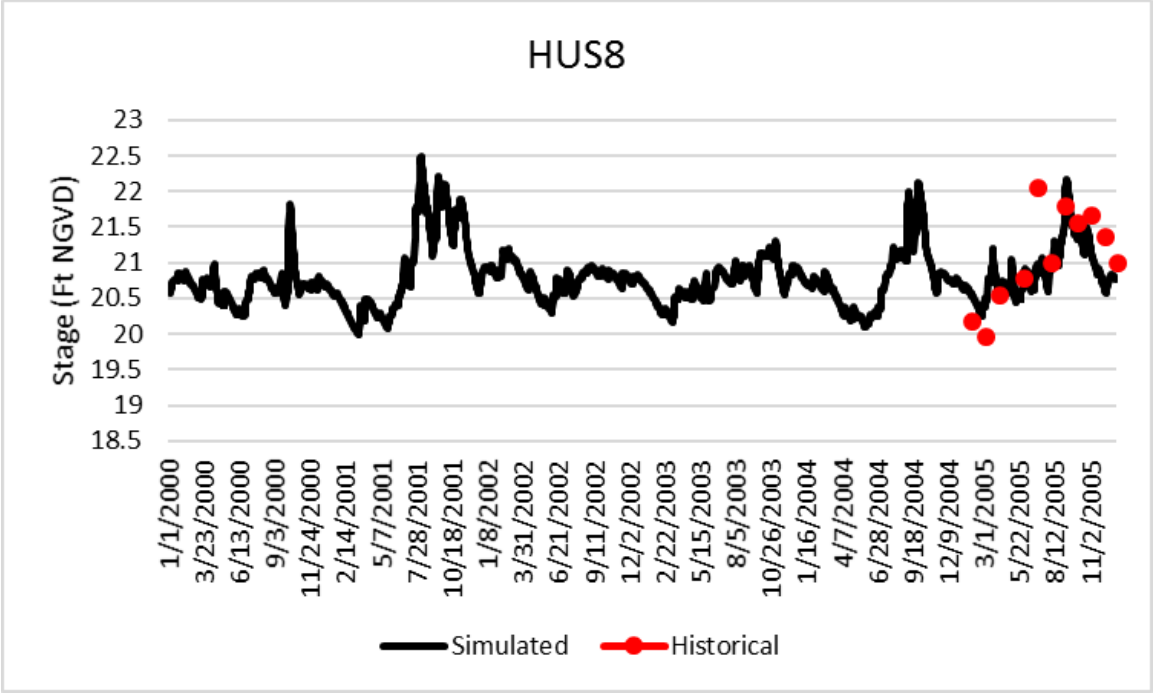

Figure E-55. Historical and simulated wetland gauge stage hydrograph (2000 – 2005) for HUS8.

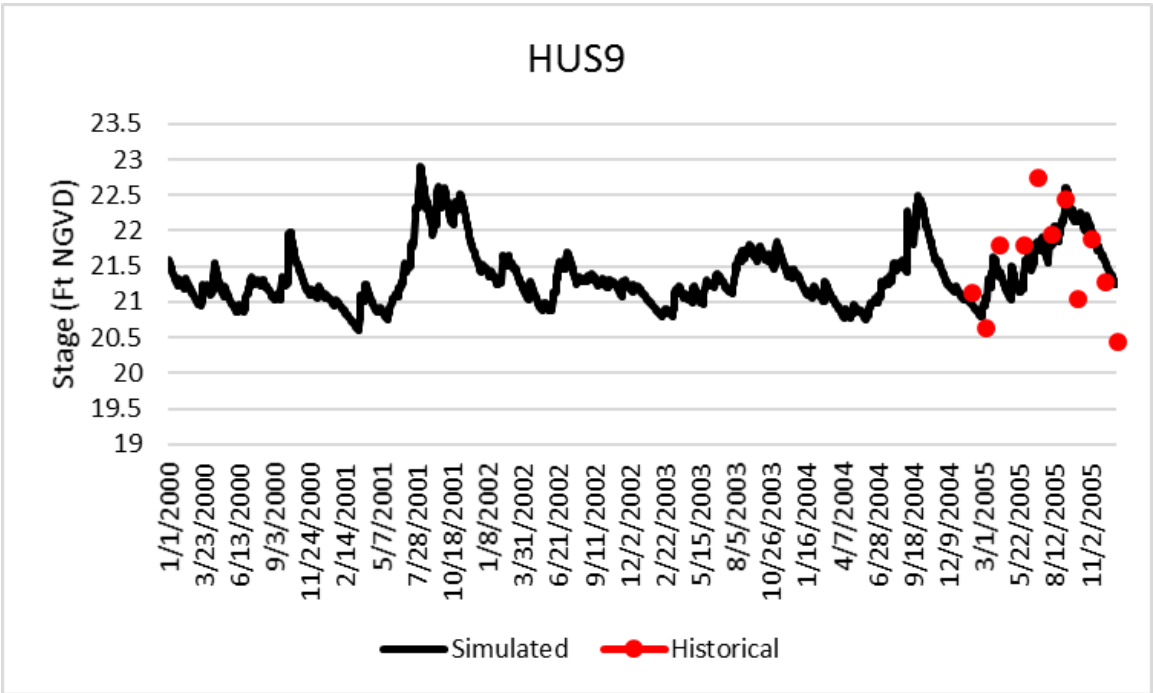

Figure E-56. Historical and simulated wetland gauge stage hydrograph (2000 – 2005) for HUS9.

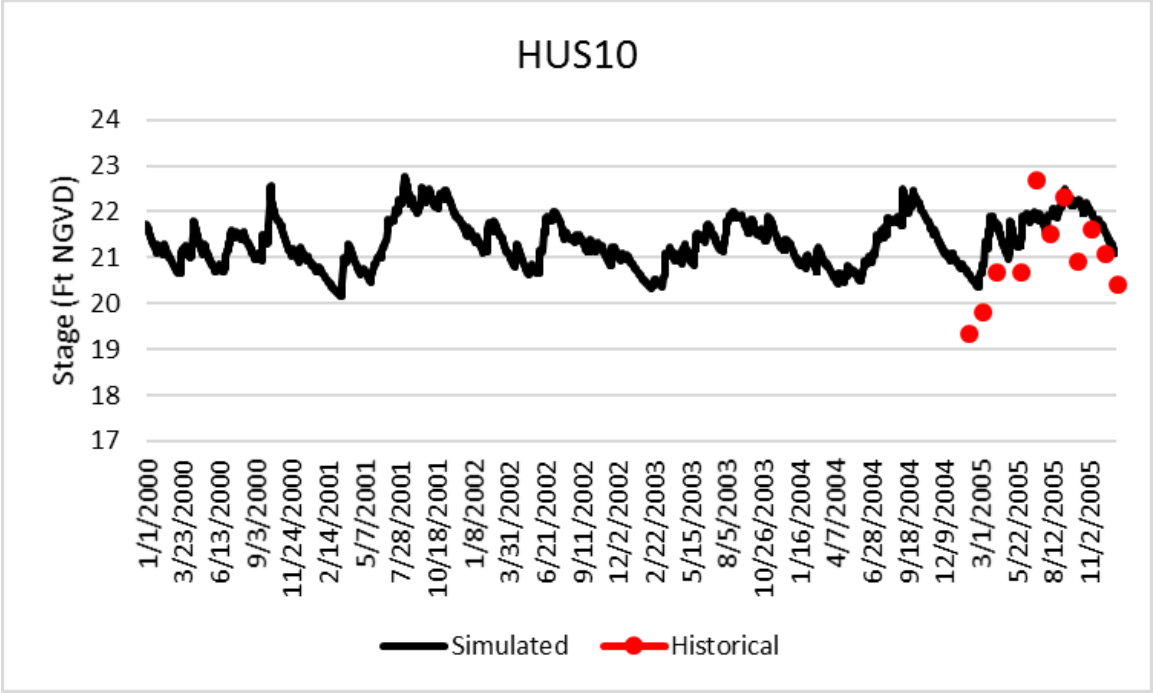

Figure E-57. Historical and simulated wetland gauge stage hydrograph (2000 – 2005) for HUS10.

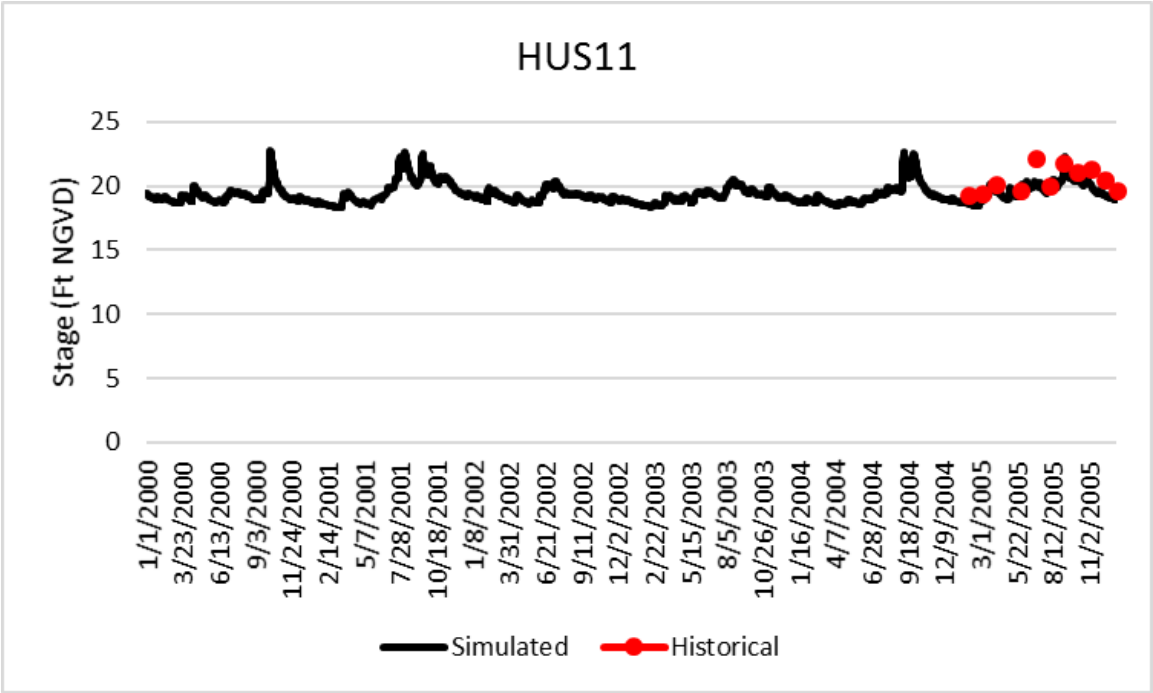

Figure E-58. Historical and simulated wetland gauge stage hydrograph (2000 – 2005) for HUS11.

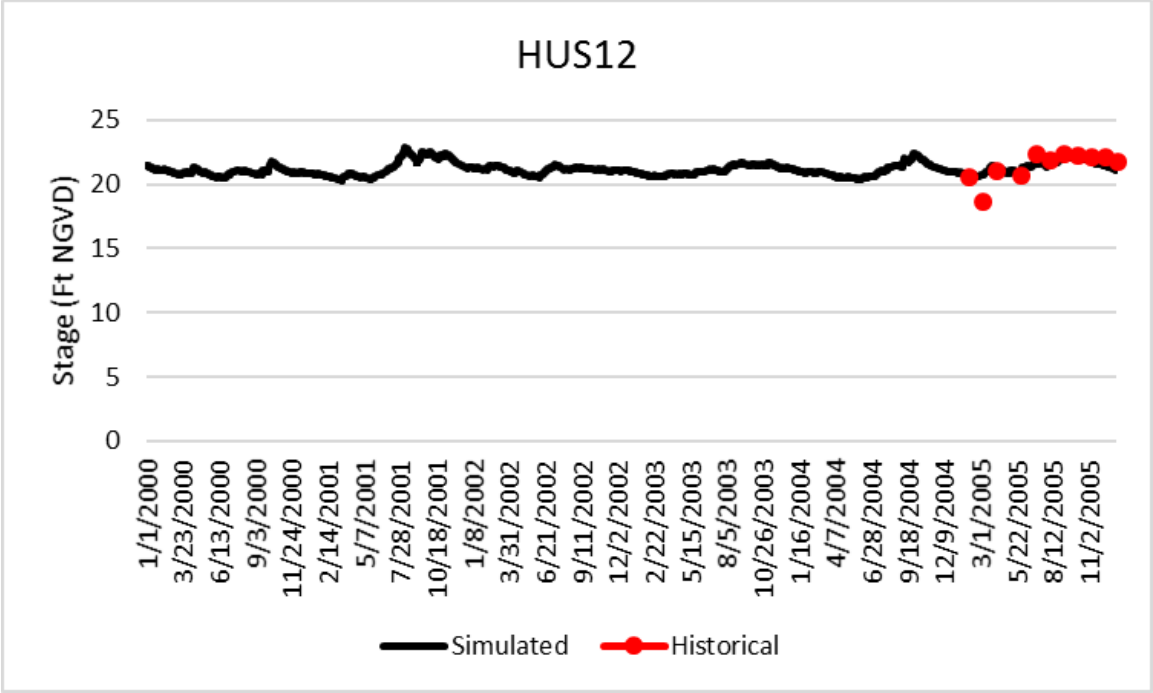

Figure E-59. Historical and simulated wetland gauge stage hydrograph (2000 – 2005) for HUS12.

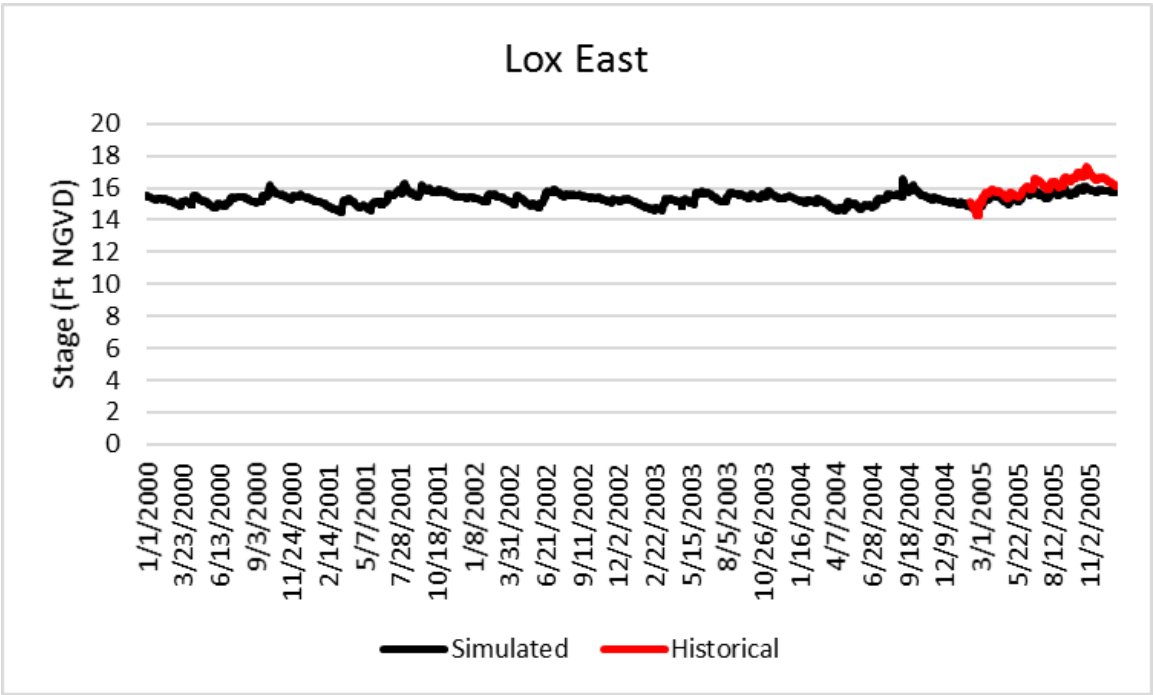

Figure E-60. Historical and simulated wetland gauge stage hydrograph (2000 – 2005) for Lox East.

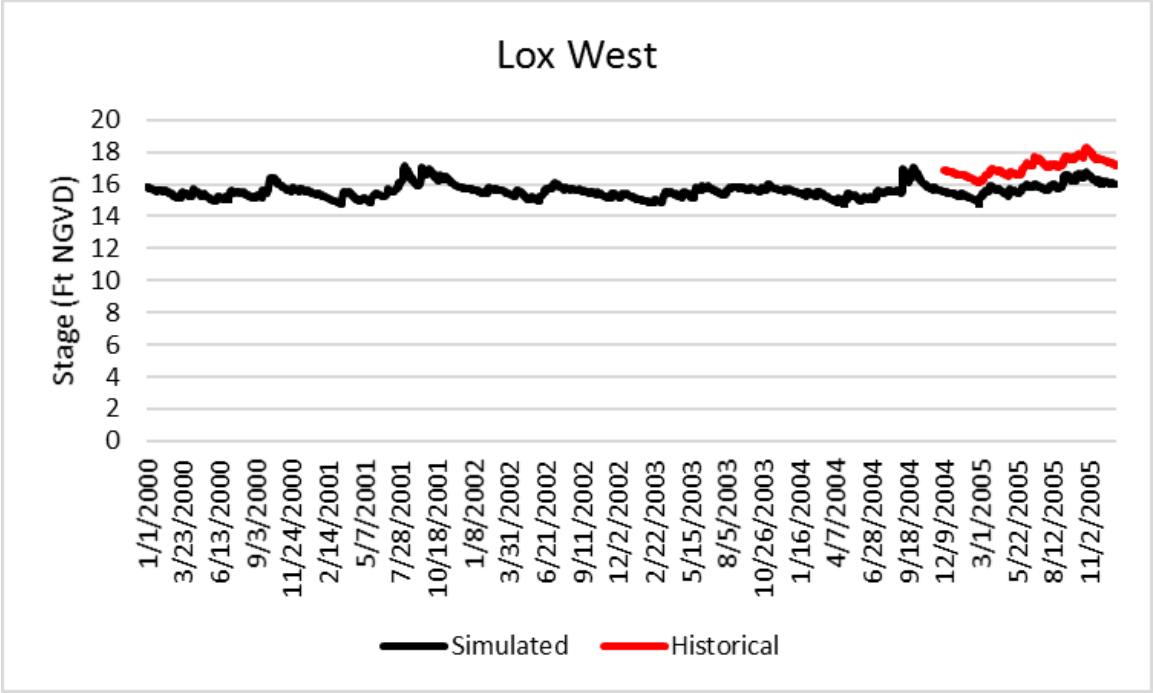

Figure E-61. Historical and simulated wetland gauge stage hydrograph (2000 – 2005) for Lox West.

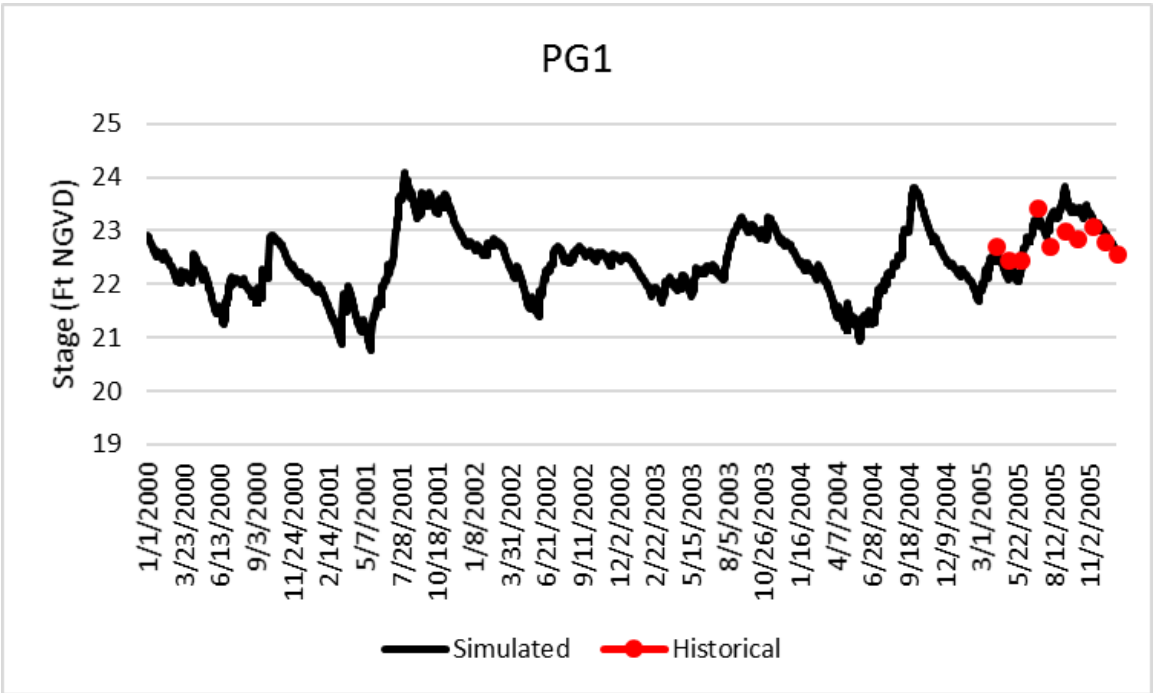

Figure E-62. Historical and simulated wetland gauge stage hydrograph (2000 – 2005) for PG1.

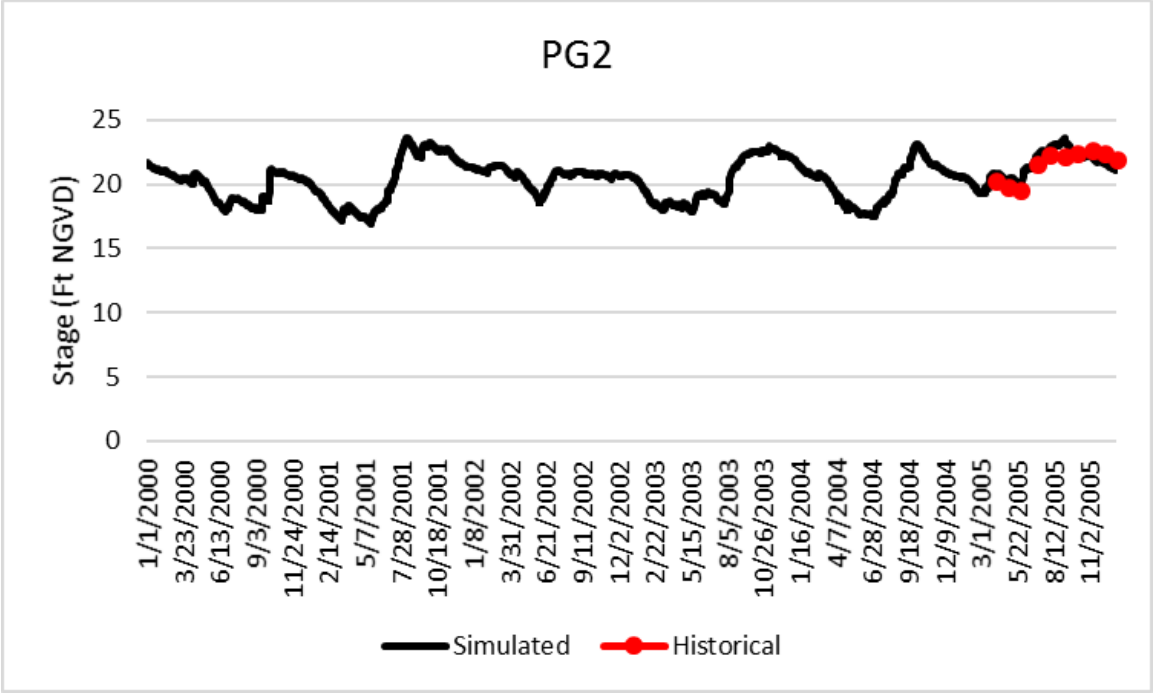

Figure E-63. Historical and simulated wetland gauge stage hydrograph (2000 – 2005) for PG2.

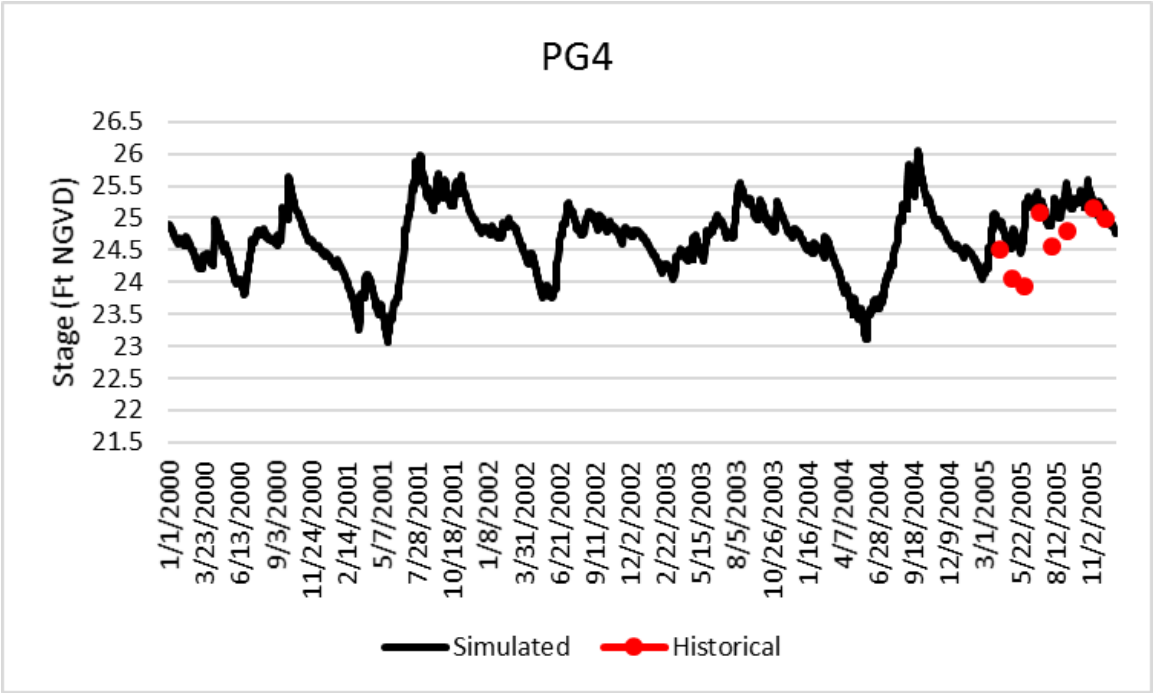

Figure E-64. Historical and simulated wetland gauge stage hydrograph (2000 – 2005) for PG4.

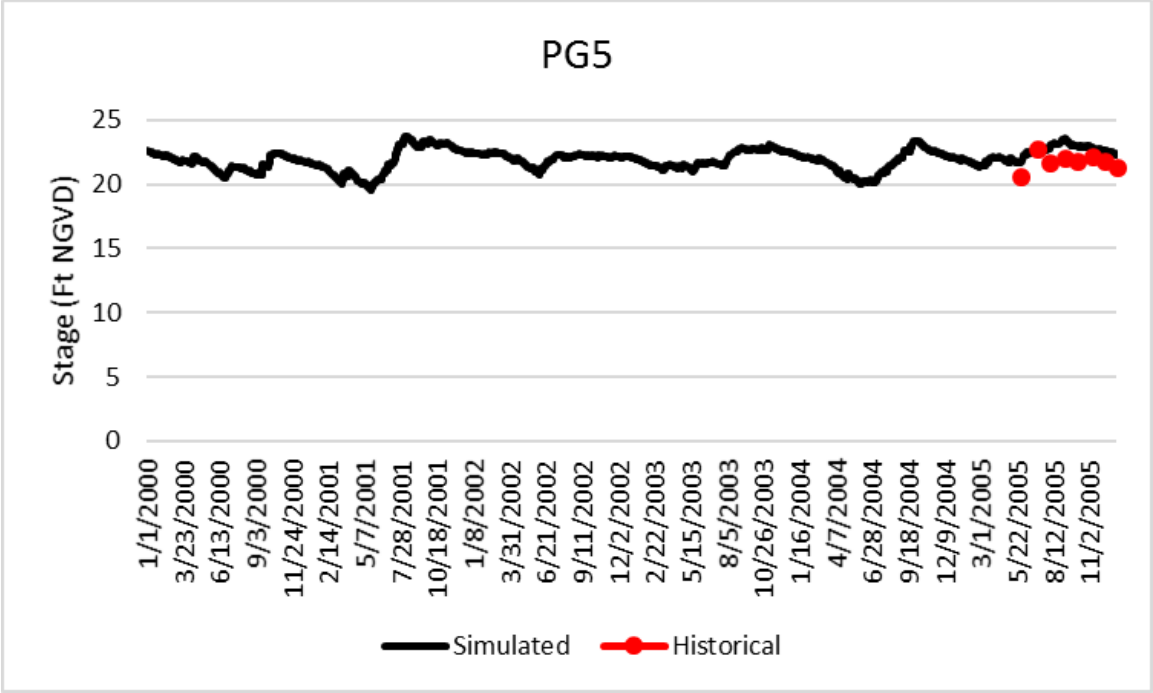

Figure E-65. Historical and simulated wetland gauge stage hydrograph (2000 – 2005) for PG5.

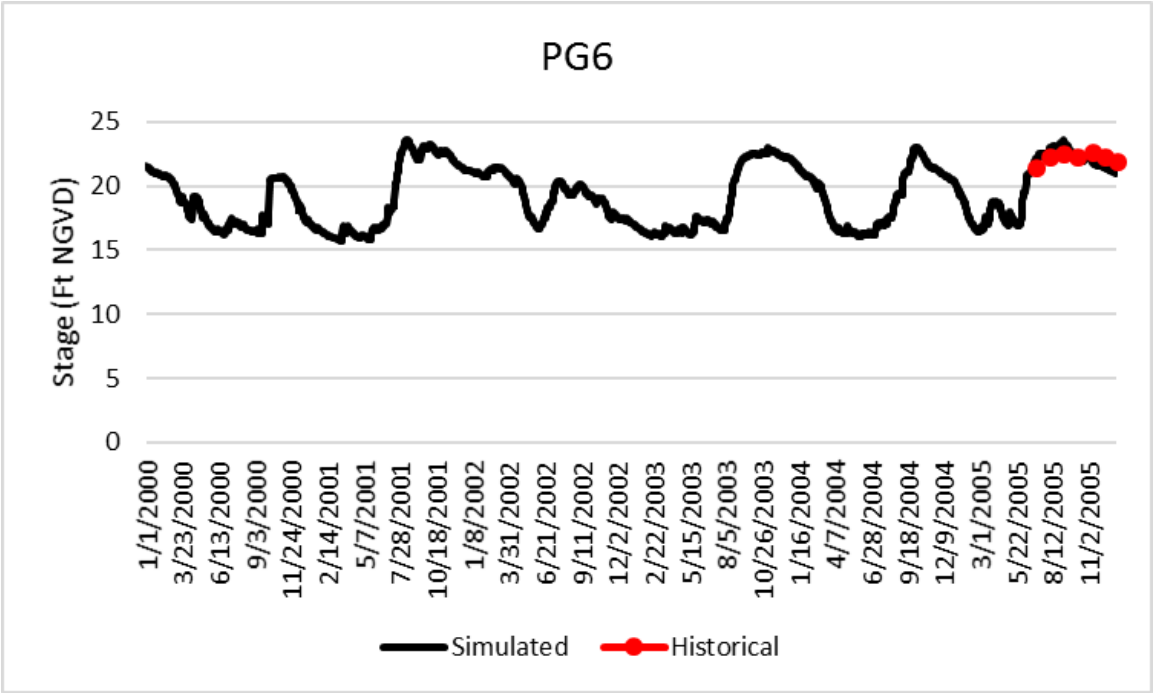

Figure E-66. Historical and simulated wetland gauge stage hydrograph (2000 – 2005) for PG6.

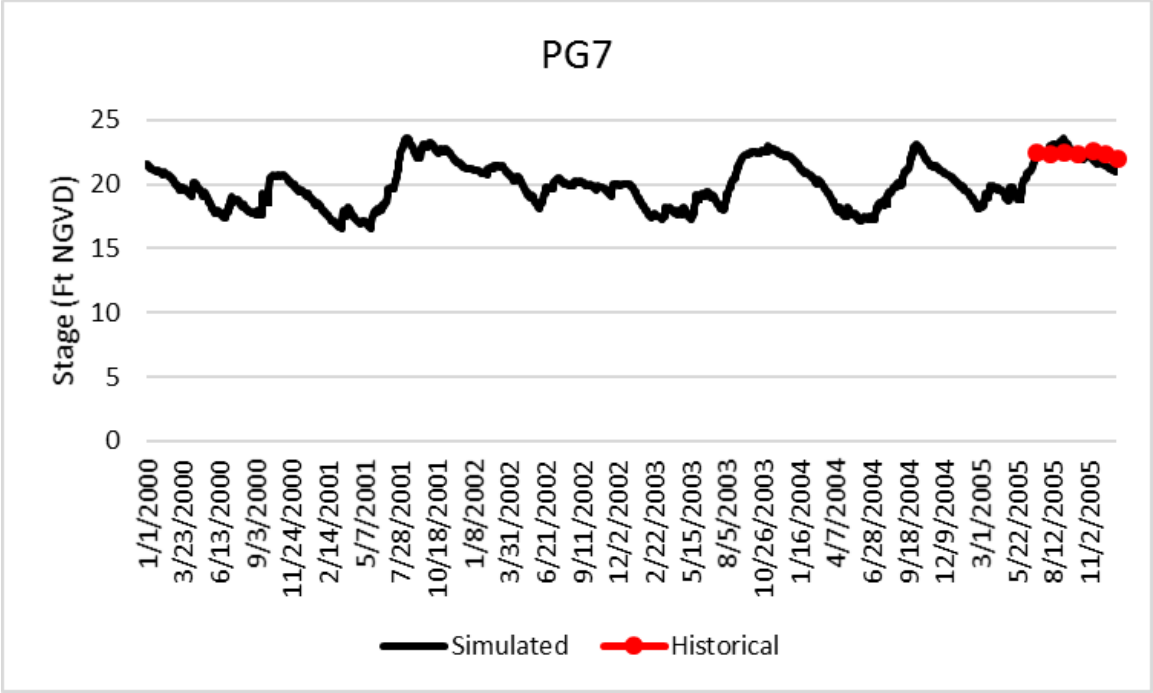

Figure E-67. Historical and simulated wetland gauge stage hydrograph (2000 – 2005) for PG7.

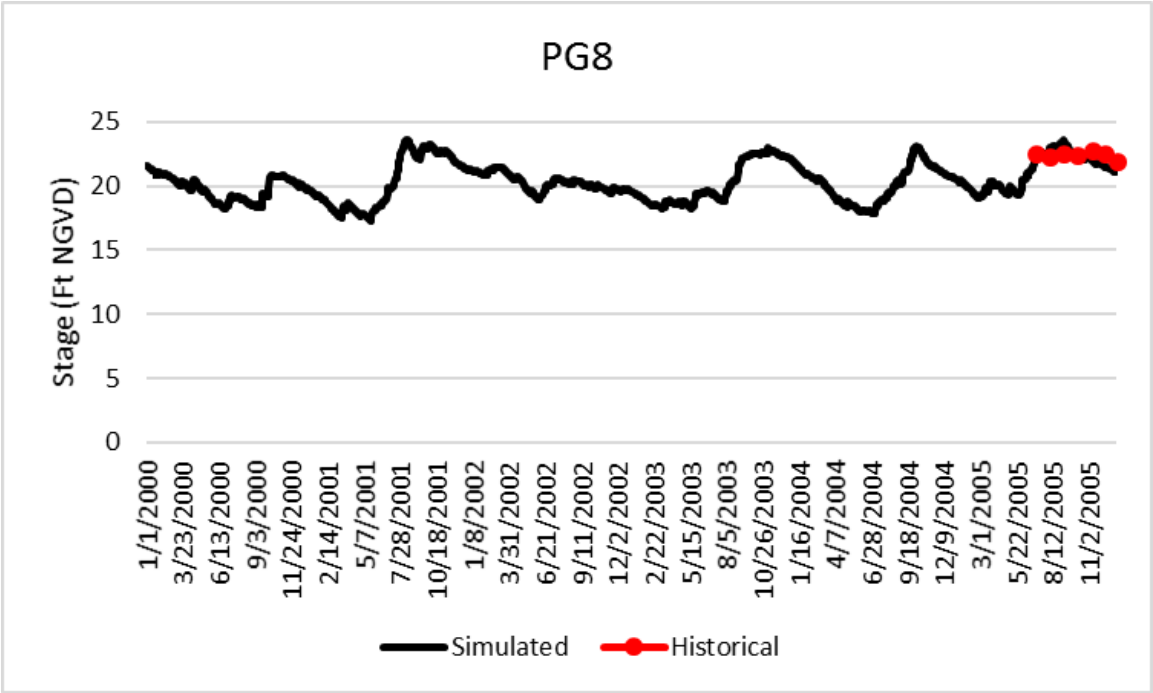

Figure E-68. Historical and simulated wetland gauge stage hydrograph (2000 – 2005) for PG8.

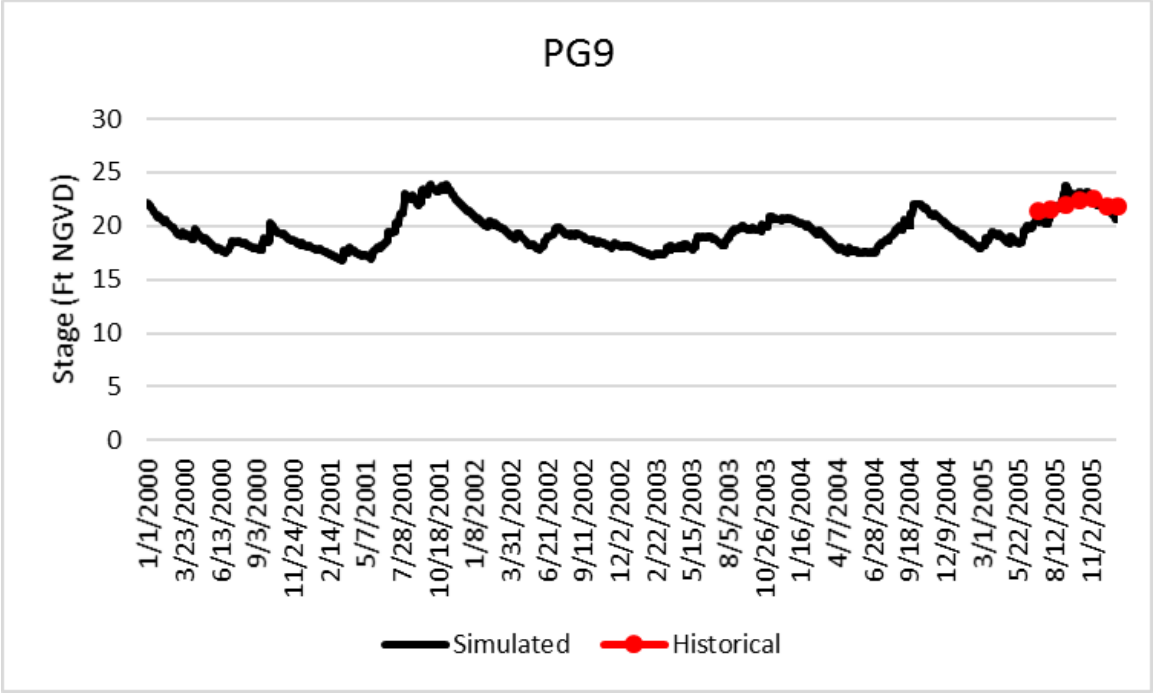

Figure E-69. Historical and simulated wetland gauge stage hydrograph (2000 – 2005) for PG9.

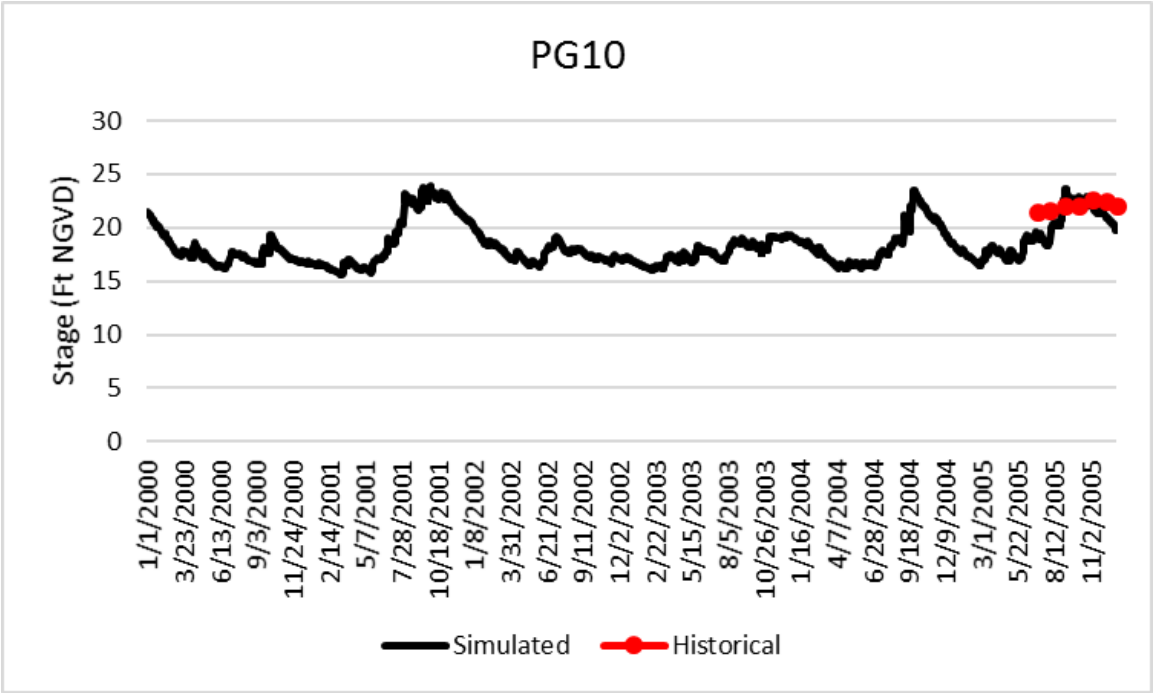

Figure E-70. Historical and simulated wetland gauge stage hydrograph (2000 – 2005) for PG10.